RADIOCHRONOLOGICAL INVESTIGATIONS OF THE POLLUTION HISTORY OF LEAD AND OTHER HEAVY METALS IN SCOTTISH FRESHWATER LOCH SEDIMENTS.

LORNA J. EADES

PhD THESIS

THE UNIVERSITY OF EDINBURGH

1999

Declaration.

The work presented in this thesis is entirely my own, except where reference is made to other sources. Some of the work has been published elsewhere, but the work has not been submitted, in part or in whole for any other degree.

Edinburgh, 12.09.99

Acknowledgements.

I would like to thank the following people to whom I am eternally grateful for their help and advice along the way:

Dr. John Farmer and Dr. Angus MacKenzie for their invaluable help and support in this research project. Thank you for your patience and for helping to unravel some of the mysteries of writing.

Alex Kirika for his boundless energy and enthusiasm and endless supply of cakes and herbal teas.

Dr A.E. Bailey-Watts for the use of the IFE facilities.

The University of Edinburgh for funding the research.

Fieldwork: Glasgow University Field Centre, Rowardennan, Firbush Point Outdoor Centre, Charlotte Bryant, Carol Sugden, Tim Brand, Keith Gavin, Malcolm Sangster, Denise Kesterton, Nicola Paterson, Andrea Lancaster, Euan Brechin, Jennifer Whitehead and Colin Eades.

Analysis: SURRC, Dr Tracey Shimmield, Caroline Gray, Alison Stewart and Geoff Angell.

Thesis: Jon Musgrave (Deeside Orienteering and Leisure Mapping, LTD), Graphics workshop and Dr. Steven Henderson for help with preparing the diagrams. I would also like to thank the following friends whose advice and help were greatly appreciated: Colin Eades (proof reading and loving support), Robert Lee (statistics), Dr. Paul Caban (proof reading, computing and feeding), Fiona Weir (proof reading), and David Peel (diagrams).

" don't die not knowing how good you could have been…."

Peter Snow, 1998.

Abstract

Vertical profiles of Pb, other heavy metals (Cd, Cu, Zn, Mn and Fe), stable Pb isotopes (^{206}Pb, ^{207}Pb and ^{208}Pb) and radionuclides (^{134}Cs, ^{137}Cs, ^{210}Pb, and ^{226}Ra) were investigated in sediment cores from four contrasting freshwater lochs in Scotland. Loch Lomond and Lake of Menteith are close to the heart of Scotland's heavily populated industrial belt, while Loch Tay lies within a region of high mineralisation and consequent Pb/Zn/Cu mining. Loch Ness, in contrast, is remote from any heavy industry.

^{210}Pb dating models (CIC and CRS) were used to determine chronologies for each core. In all of the lochs, except for Lake of Menteith, distinguishable peaks for radiocaesium relating to deposition of Chernobyl and nuclear weapons testing fallout were evident. This enabled sedimentation rates to be calculated and the reliability of the ^{210}Pb dating to be assessed. In the Lake of Menteith, post-depositional mobility has led to a smearing of the two ^{137}Cs peaks. The sedimentary radiocaesium inventories for Chernobyl and weapons testing fallout varied considerably for the different lochs, with Loch Lomond (south) in closest agreement with estimated atmospheric deposition values.

The stable Pb isotope trends were very similar for Loch Lomond (north and south), Lake of Menteith and Loch Ness. The ^{206}Pb/^{207}Pb atom ratio of anthropogenic Pb during the Industrial Revolution was in the range 1.170-1.177, reflecting inputs of Pb from the smelting of indigenous Pb ores and coal burning. From ~ 1910-1985 the ratio declined, initially due to the influence of comparatively ^{206}Pb-depleted Pb ores from Australia, and then from the 1920s until the mid-1980s due to car-exhaust emissions of Pb arising from the use of ^{206}Pb-depleted alkyl Pb additives in petrol (^{206}Pb/^{207}Pb atom ratio 1.06-1.09). Pb in Loch Tay (east and west) has been largely dominated by the Pb-ore deposits at Tyndrum and Kepranich (1.144 ± 0.004). Despite its remoteness, Loch Ness still reflects the changing contributions of Pb and

other pollutants from varying sources, highlighting the long-range transport of aerosols.

The pollutant heavy metal profiles (Pb, Cd, and Zn) in the sediment column of all of the lochs reflected the historical input from atmospheric deposition and catchment run-off. There was, however, evidence for remobilisation and possible loss of Cu from the surficial sediments, casting doubt on the validity of the apparent historical record for Cu. In contrast to Pb, Cd and Zn, classic diagenetic profiles were observed for Mn and Fe at all of the sites, a consequence of the redox-related cycling induced by the microbiological decomposition of organic matter.

The excess metal inventories for Pb, Cd, Cu and Zn were highest in Loch Tay due to the mineralisation of the area, and in Loch Lomond (north) due primarily to a high flux of sediment. Inventories for Loch Lomond (south) and Lake of Menteith were similar as a result of their proximity to the central industrial belt of Scotland. In contrast, the excess inventories for Loch Ness were much lower due to its remoteness from industry.

Contents. Page

List of Tables.

Chapter 1 Introduction

Chapter 2 Materials and methods.

Chapter 3 Loch Lomond

List of Figures. Page

Chapter 1 Introduction

Chapter 2 Materials and methods

Chapter 3 Loch Lomond.

Chapter 4 Lake of Menteith

Chapter 5 Loch Tay.

Chapter 1 Introduction.

1.1 Background to study.

The monitoring of environmental change and pollution is an increasingly important area of research. Concern over the fate of heavy metals released into the environment, as a legacy of past and present heavy industrialisation, has led to a growing number of studies on their impact and fate in the environment. Scotland in particular was involved at the outset in the industrialisation of Great Britain with large coal fields and steel works, a centre of shipbuilding and heavy industry (SEPA, 1996). Even now it continues to have a significant industrial presence.

Heavy metals in high concentrations are very toxic to living organisms, but are often required in trace amounts for normal functioning. They often feature prominently in public debates over the perceived state of the environment and their risk to public health. In particular, Pb, a known neurotoxin, is of much interest as concentrations of Pb have been anthropogenically elevated over natural levels to a far greater extent than for most other heavy metals (Nriagu, 1978).

Many natural processes (e.g. erosion, weathering of rock deposits and forest fires) and human activities (e.g. burning of fossil fuels, mining and smelting) can give rise to atmospheric emissions of heavy metals. Emissions of pollutants to the environment are often observed considerable distances from their sources due to long-range transport. Freshwater loch sediments are among the useful media for examining temporal trends of anthropogenic input of heavy metals to the environment (Farmer, 1991). Stable Pb isotopes are proving to be a useful tool in sourcing the input of Pb, but, until relatively recently, few sets of data on Pb concentrations have included isotopic data.

Radioactive releases to the environment are another public concern, although anthropogenic sources of radioactivity only account for 15 % of the UK annual dose of radiation (SEPA, 1996). Both anthropogenic emissions (e.g. $^{134,137}Cs$) and natural emission (e.g. ^{210}Pb from ^{222}Rn decay) are, however, useful in the calculation of time scales that are essential if historical information is to be gleaned from sedimentary cores (Farmer, 1991; Appleby *et al.*, 1993).

The use of sedimentary cores to furnish historical records of metal pollution depends on several pre-requisites, the most important being that, following deposition, no degradation, mobilisation and physical disturbance occurs. Many studies have shown that, for certain elements (e.g. Mn, Fe and As), remobilisation may occur, leading to discrete bands of enhanced concentrations in the top few centimetres (Farmer, 1991). The majority of work on sediments has involved sectioning the cores at 1-5 cm increments. Recent work, however, on pore-water samples suggests that controlling processes and enrichments may occur on the sub-centimetre scale in the sediment column (Davison *et al.*, 1991).

Freshwater lochs are highly sensitive to change and there are many factors which influence the removal of heavy metals and their subsequent incorporation into the bottom sediments. The remaining sections of the introduction include an overview of some of the many limnological factors influencing sediment formation and a review of sources and emissions of heavy metals to the environment.

1.2 Overview of factors influencing the accumulation of radionuclides and heavy metals in freshwater sediments.

1.2.1 Lake structure.

All lakes have a distinctive structure which is determined by their basin morphometry (Horne and Goldman, 1994), e.g. deep sided lakes behave very differently to shallow ones. Once the basin is formed, the physical, chemical and

biological factors interact to form a discernible structure within the water. There are four main factors that together define the overall structure within a lake system: (i) the position in the lake relative to the lake edge (ii) light and temperature (iii) distribution of chemicals and biota and (iv) the lake bottom sediments. These structures are summarised in Figures 1.1 and 1.2.

In the centre of a lake, the area of water not in contact with the sides or the bottom of the lake is known as the *pelagic zone*. Water in contact with the lake sides is known as the *littoral zone*, and is the part of the system most subject to wave action.

The components of light and temperature have the largest impact on the structure of a lake, particularly in determining the distribution of dissolved oxygen. If a lake is deep enough there are two light zones; the *photic* and *aphotic zones*, the position of which will vary both daily and seasonally. In the photic zone, which extends from the surface to a depth where the light dims to ~1 % of the surface incident light, there is oxygen production by photosynthesis from plants but also some removal by respiration of animals. In the aphotic zone there is insufficient light for photosynthesis; therefore, only respiration occurs, resulting in a net depletion in oxygen levels.

The temperature of the water in a lake varies seasonally to give periods of vertical thermal stratification and periods of vertically uniform temperature. In the winter the water temperature is constant throughout and is often close to that of its maximum density, i.e. 4°C. During the spring the water temperature at the surface increases, leading to a reduction in the density of the top waters and thus setting up three layers of different density. These layers are termed the *epilimnion, metalimnion and the hypolimnion.* The upper epilimnion is the warmest layer of water and is situated at the top of the lake. The hypolimnion is the deepest layer and is a layer of colder water. The layer separating them is the metalimnion where the rate of change with depth is greatest. The gradient of water temperature change is called the *thermocline.* Throughout the summer the position of the thermocline moves downwards and the

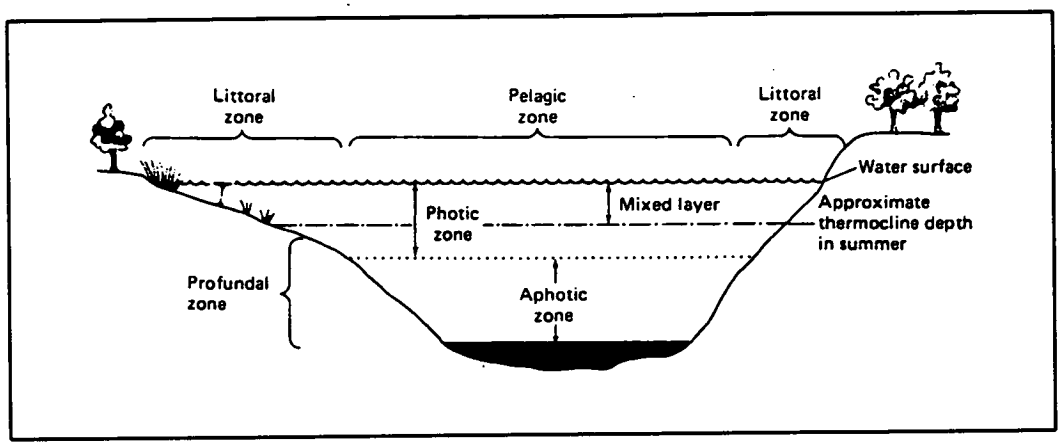

Figure 1.1 The influence of the distribution of light and temperature on the physical structure of a lake. (Horne and Goldman, 1994).

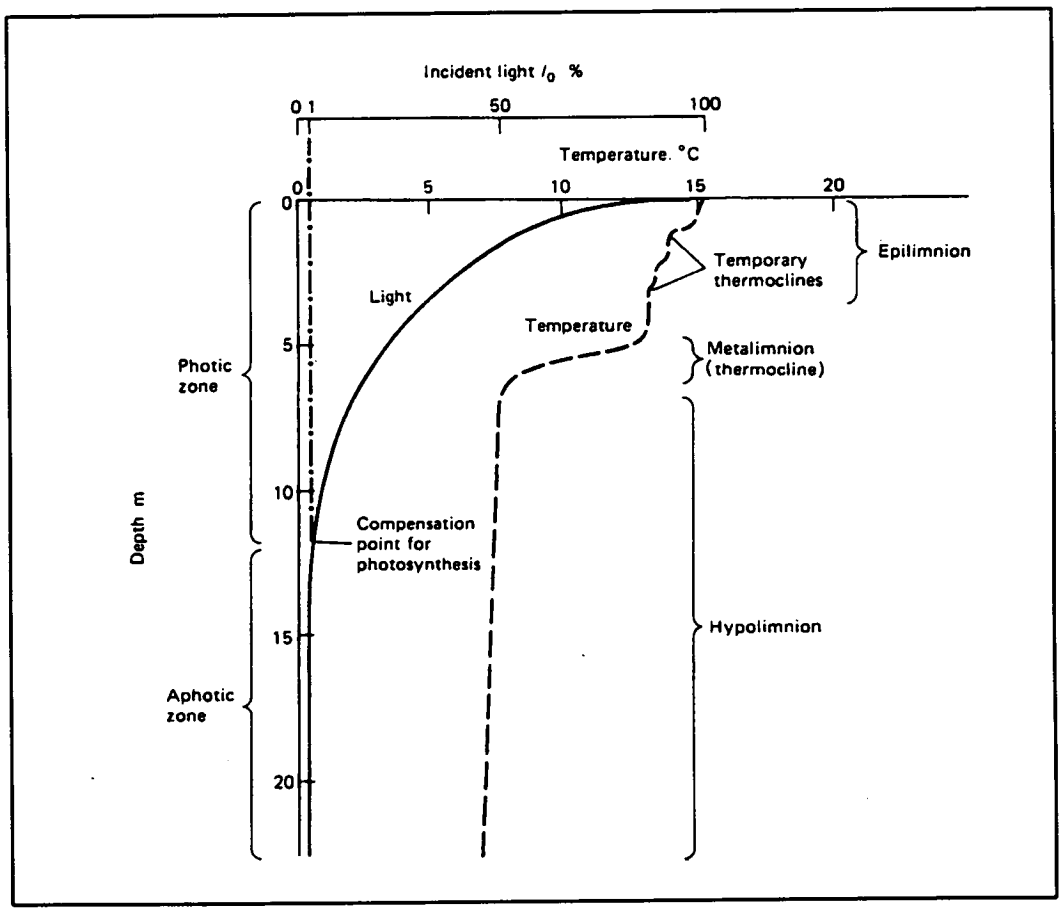

Figure 1.2 The thermal and optical structure of a lake with depth during period of summer thermal stratification. (Horne and Goldman, 1994).

lake becomes fully stratified. The upper epilimnion is a well mixed region. In the autumn the epilimnion water begins to cool and increases in density, causing the water to sink. This in turn sets up currents which mix the entire water column.

The third component of a lake's structure is the distribution of chemicals, biota and particles. The chemicals are often distributed in a similar fashion to the temperature gradients, and the chemical gradient is termed the *chemocline*. The distribution of chemicals (and nutrients) gives rise to a further classification where a lake can be said to be either *eutrophic* (nutrient rich) or *oligotrophic* (nutrient poor). In the summer the hypolimnion of an eutrophic lake can become very depleted in oxygen and is termed *anoxic*. Once the water becomes suitably anoxic (or reducing) other electron acceptors are utilised for oxidation, e.g. SO_4^{2-} (sulphate) and NO_3^- (nitrate).

1.2.2 Formation of the bottom sediments and removal of metals.

The formation of bottom sediments in a lake's system is the result of a variety of physical, chemical and biological processes, e.g. shoreline erosion, precipitation reactions and bacterial activity (Manahan, 1990). Sedimentation rates of 4-80 mg cm^{-2} y^{-1} are typically observed in lakes, although higher values are often found in highly eutrophic lakes (Stumm and Morgan, 1996).

Although sediments constitute the final repository for trace metals, they can be recycled many times across the sediment-water boundary before being permanently buried (Santschi *et al.*, 1990). In the water column trace metals interact with solutes (complex formation), inorganic particles (adsorption) and organic matter (assimilation), and their removal is a highly efficient process (Stumm and Morgan, 1996). The affinity of the trace metals for the particles, which settle through the water column, determines their relative residence time and their ultimate fate. Figure 1.3 is a schematic representation of the cycling of trace metals in a lake (Sigg and Stumm, 1994)

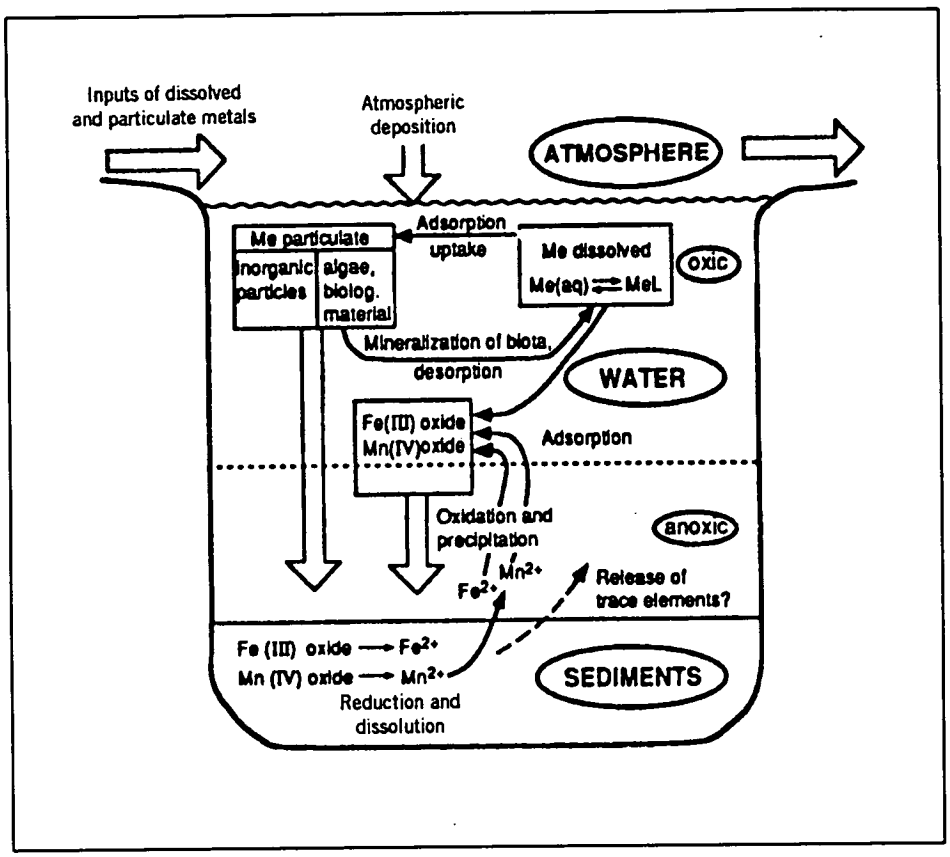

Figure 1.3 Schematic representation of the cycling of trace elements in a lake. (Sigg and Stumm, 1994).

The most common processes taking place are the removal of colloidal particles by adsorption, flocculation and coagulation to form aggregated particles large enough to settle out onto the lake bottom (Stumm and Morgan, 1996). Colloids are particles, with a size range of 0.001-1 μm, that would normally remain suspended in solution. They can be mineral, clays, organics, macromolecules, oxides, organisms or biological debris. Of the processes which bring about aggregation of colloids, adsorption is the most significant.

Adsorption is defined as "the accumulation of matter at a solid-water interface". It influences the distribution of substances between the aqueous phase and the solid phase particulate matter. Surfaces can be inorganic or organic in nature and may have extending structures bearing functional groups, e.g. -OH, -SH or -COOH. Adsorption is a competitive process (Oakley *et al.*, 1981; Luoma and Davies, 1983) and cations and anions show varying tendencies to become sorbed on a surface. Alkali and alkaline earth cations are ionic radius dependent, and tend to follow the following order of adsorption preference: Cs^{+}> Rb^{+}> K^{+}> Na^{+}> Li^{+}. The transition elements are affected by their electron configuration, e.g. Cu^{2+}> Ni^{2+}> Co^{2+}> Fe^{2+}> Mn^{2+} is often observed.

The adsorption and binding of metals is highly pH dependent and the residual concentrations of these metals in the water column tends to decrease with increasing pH (Salomons, 1985; Stumm and Morgan, 1996). Figure 1.4 illustrates the sorption of various metal ions on hydrous ferric oxide and shows that for each metal ion there is a narrow interval of 1-2 pH units where the extent of sorption rises from zero to almost 100 % (Stumm and Morgan, 1996).

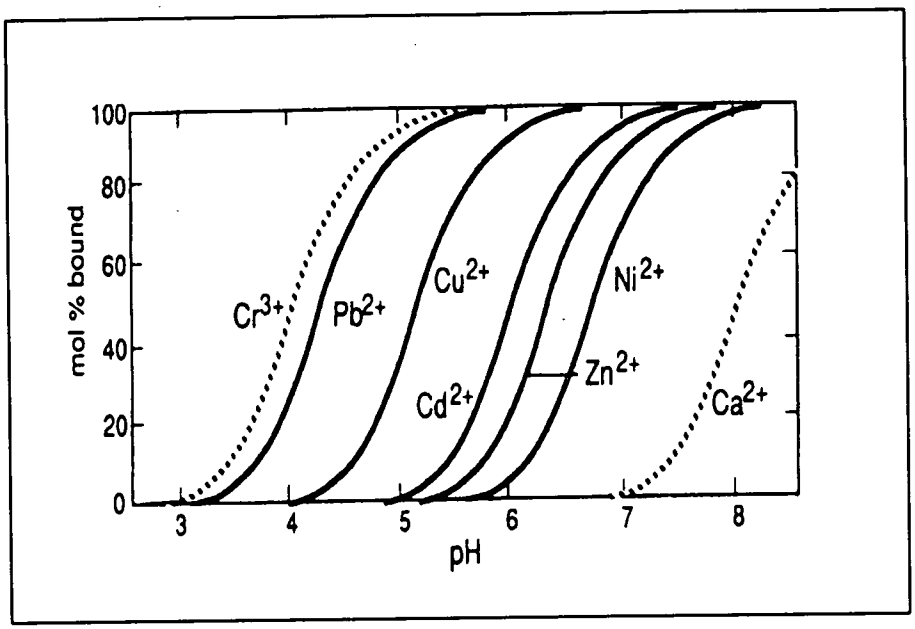

Figure 1.4 Extent of surface complex formation as a function of pH. (Dzombak and Morel, 1990).

Of the inorganic surfaces, oxides play a prominent role in most lake systems. Two of the processes which lead to binding on oxides are surface complex formation and ligand exchange.

1. Surface complex formation involves the coordination of the metal ions with the oxygen donor atoms and the release of protons from the surface.
   For example,

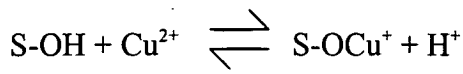

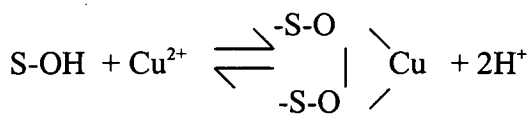

2. Ligand exchange is a surface complex formation of anions and weak acids where one surface ligand is replaced by another. For example,

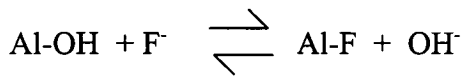

Clay minerals are effective adsorbents with metals and ligands being sorbed by ion-exchange mechanisms onto flat planar surfaces and frayed edge sites or, depending on the cation size, incorporated into the clay lattice. Another important adsorption surface is provided by *humic substances*. Humic substances account for almost all of the organic carbon in fresh waters (Killops and Killops, 1993). They are a complex mixture of different sized molecules but can be divided essentially into three fractions; fulvic acid, humic acid and humin (Stevenson, 1994). These fractions are defined in terms of their solubility characteristics. Humin is insoluble in alkali, humic acid and fulvic acid are both soluble in alkali, but humic acid can precipitate in acid whereas fulvic acid cannot. In general, humic substances contain a wide array of acidic functional groups (e.g. COOH, phenolic, enolic and alcoholic OH) and exhibit a large buffering capacity over a wide pH range. They carry a net negative charge and hence have the ability to form both soluble and insoluble complexes with

metal ions. Monovalent cations (Na^+, and K^+) are held by the simple formation of salts with the carbonyl groups. Multivalent cations (Cu^{2+}, Zn^{2+}, Fe^{3+} and Pb^{2+}) have the potential to form coordinate linkages with the molecules.

As with the clay minerals, humic substances are effective cation exchangers. The charge on the humics arises largely from ionisation of COOH groups although some contribution from phenolic OH is suspected. Clay and oxide particles can obtain an organic coating (Davis, 1982, 1984) which can mask the adsorption properties of the underlying particle (Hunter, 1980) and create a new surface with very different properties.

Chemical reactions occurring in the water column can result in the chemical precipitation of dissolved species, depending upon the availability of oxygen. For example, Fe is soluble as Fe(II) bicarbonate but precipitates out as Fe(III) hydroxide if oxygen is present. Hence in an oligotrophic lake (with a high level of oxygen throughout its depths) Fe(III) hydroxide will be precipitated onto the bottom sediments. In an eutrophic lake, however, the bottom waters can become sufficiently anoxic that the Fe(III) will be reduced to Fe(II) and go back into solution, thus re-entering the water column (Ruttner, 1969). Mn behaves in a very similar fashion to Fe and these reactions that they undergo are termed *redox reactions*.

1.2.3 Post-depositional reactions of metals in the bottom sediments.

Once on the lake bottom the sediments can undergo further change either whilst still on the surface or, later, once they have been buried by continuing accumulation of sediment. The first major process to occur in the sediment following deposition is the microbial decomposition of organic matter. Bacteria and other micro-organisms obtain energy by oxidising organic compounds. In aerobic conditions O_2 is used via the following reaction:

$$CH_2O + O_2 \rightarrow CO_2 + H_2O$$

When free O_2 becomes scarce (at some depth in the sediment the conditions will become anoxic), other electron acceptors (e.g, NO_3^-) are used instead in the following thermodynamically favourable order, catalysed by bacteria (Berner, 1980):

Reaction	ΔG^o (kJ mol^{-1} of CH_2O)
$CH_2O + O_2 \rightarrow CO_2 + H_2O$	-475
$5CH_2O + 4NO_3^- \rightarrow 2N_2 + 4HCO_3^- + CO_2 + 3H_2O$	-448
$CH_2O + 3CO_2 + H_2O + 2MnO_2 \rightarrow 2Mn^{2+} + 4HCO_3^-$	-349
$CH_2O + 7CO_2 + 4Fe(OH)_3 \rightarrow 4Fe^{2+} + 8HCO_3^- + 3H_2O$	-114
$2CH_2O + SO_4^{2-} \rightarrow H_2S + 2HCO_3$	-77
$2CH_2O \rightarrow CH_4 + CO_2$	-58

where ΔG^o is the standard free energy change for the bacterially-mediated reactions and data for CH_2O and MnO_2 are for sucrose and birnessite, respectively.

One of the later steps in the bacterially mediated decomposition of organic material in the sediment is the reaction of sulphate-reducing bacteria to produce H_2S. This diagenetic process does not occur near the sediment-water interface and only occurs when all other electron acceptors have been utilised. It leads to subsequent reactions with FeS and other metals present to produce insoluble metal sulphides which are retained in the sediment (Förstner and Salomons, 1983,1991).

$$2Fe(OH)_{3(s)} + 3H_2S \rightarrow 2FeS + S + 3H_2O$$

$$FeS + S \rightarrow FeS_2 \text{ (pyrite, black insoluble solid)}$$

In fresh water sediments this reaction can take place at relatively shallow depths as levels of SO_4^{2-} are generally quite low due to low salinity. Therefore not enough H_2S is produced to "titrate" all the available Fe. As a result, once all the SO_4^{2-} is depleted and all remaining H_2S is precipitated to form highly insoluble FeS_2 minerals, the

concentration of dissolved Fe(II) can increase by continued bacterial reduction of Fe oxides (Berner, 1980). Where this has occurred it can be observed as bands of black FeS_2 and red Fe(III) oxide in the top few cm of the sediment.

The release of metals to solution by degradation of organic matter, or the re-solubilisation of metals by reduction may lead to upward or downward diffusion along concentration gradients until they find new adsorption sites. The most common and well researched example of post-depositional mobility is that of Fe and Mn. The transport of these redox-sensitive species can be described by a simple conceptual model developed by Burdige and Gieskes (1983). Their model is a steady-state diagenetic model which accounts for changes in pore-water and solid phase Mn profiles in sediments due to advection, diffusion and redox reactions. The model, which uses the concept of a *redox-boundary,* is generally accepted. Manganese is deposited on the surface of the sediments as oxidised Mn(IV), in the form of MnO_2. As the sediment becomes reducing with depth the Mn is reduced to Mn(II), which is soluble and can enter the porewaters. It can now migrate upwards until the presence of free oxygen at the redox boundary re-oxidises Mn(II) to solid phase $Mn(IV)O_2$. With time, therefore, there is an enhancement of the Mn concentration at this depth in the sediment column.

The control of redox-related processes in freshwater sediments is well established. Farmer and Lovell (1984, 1986) reported very high levels of Mn in the surface and near surface sediments of Loch Lomond. There can exist, however, a wide variety of Mn concentration profile shapes (Davison, 1985) due to the dependence of Mn on pH-Eh equilibria. In acidic lochs the formation of Mn particulates decreases with decreasing pH, resulting in a low input of Mn particulates to the sediments (White and Driscoll, 1987a). Bryant *et al.* (1997) found this to be the case in the acidic Round Loch of Glenhead, which showed an increasing concentration of Mn with depth in the sediment.

In Loch Lomond, an area in which there had been no recent significant sources of environmental As contamination, sharp sub-surface peaks were also observed for Fe and As (Farmer and Cross, 1979; Farmer and Lovell, 1986). Trace element As is released (as an anion) from association with $Fe(OH)_3$ into the porewaters, as a result of the dissolution of $Fe(OH)_3$ under sufficiently reducing conditions. It subsequently re-adsorbs onto the Fe oxides and hydroxides in the aerobic layers. The positions of the diagenetic peaks of Mn and Fe/As in the sediment are slightly different due to differences in the kinetics and thermodynamics of the redox process. In Loch Lomond and Lake Washington sediments the Mn peak was displaced upwards relative to the Fe and As peaks (Farmer and Lovell, 1986; Peterson and Carpenter, 1986).

Redox-controlled diagenetic mobility and enrichment of trace metals (such as Pb and Zn) have not been shown to occur after deposition. It is therefore possible in many freshwater lakes to construct a contamination history for these metals. However, the solubility of Zn can be shown to be affected by changes towards lower pH (White and Driscoll, 1987a), thus affecting Zn deposition in acidic lakes. Copper has been reported as being associated with organic matter diagenesis (Boyle *et al.*, 1977; Graybeal and Heath, 1984; Ridgway and Price, 1987).

Biological processes which occur in the bottom sediments of lakes not markedly depleted in oxygen are collectively termed *bioturbation*, i.e. the effect of all biological activities on particle and porewater dynamics at the sediment-water interface (Santschi *et al.*, 1990). The effect of bioturbation is to effectively mix the sediment and can produce an increase in the penetration depth of oxygen, thus increasing the oxidised surface layer (Salomons, 1985). Robbins *et al.* (1977), in a study of ^{137}Cs and ^{210}Pb in some of the Great Lakes (Superior, Michigan and Huron), reported that actual distributions of the radionuclides in the lake sediment often exhibited a reduced or constant activity within a zone of varying depth at the sediment-water interface. As these distributions are usually found in deposits known to support populations of mobile benthic organisms, then this near surface activity

must be due to bioturbation. Similarly, Kershaw *et al.* (1983) considered the possibility that upward and downward movement of Pu in sediments of the Irish Sea was due to bioturbation, rather than to pore-water advection.

Exact mathematical modelling of bioturbation is very difficult because of the variety, irregularity and complexity of the various bioturbational processes. The usual approach is to combine all the processes together and describe bioturbation simply as a random mixing process (Goldberg and Koide, 1962). This can be done in two ways, either by a simple box model (Berger and Heath, 1968) or by treating the process as molecular diffusion (Goldberg and Koide, 1962).

There are many different physical processes occurring in lakes affecting the distribution of sediment on the lake bed, e.g. slumping and sliding on slopes, peripheral wave attack and sediment focusing. In a study of the dominant process of sediment redistribution, Hilton *et al.* (1986) concluded that four processes had the greatest effect on the accumulation of sediment. Of these, sediment focusing had the largest effect followed by peripheral wave action. The phenomenon of sediment focusing was first described by Likens and Davis (1975) to describe the resuspension of sediment from shallow zones by waves and water currents followed by redistribution to deeper zones of the lake. They also found that there was an apparent decrease in sedimentation rate as the sediments became more recent. Their observation, that focusing appeared to be a function of lake form rather than depth of water, was corroborated by Blais and Kalff (1995). Their study, on the influence of lake morphology on sediment focusing, demonstrated a link between the accumulation zone and basin slope and explained the change in sedimentation rate with time. Early on in a lake's formation it will have a steeper basin, giving rise to a higher degree of focusing. As the basin fills, the accumulation zone and basin slope widen, causing the focusing to decrease, thus causing an apparent decrease in the sedimentation rate.

1.3 Radionuclides in the sedimentary environment.

1.3.1 ^{210}Pb.

In the absence of known marker horizons such as ashfalls, recorded slumps or industrial pollutants, the determination of sedimentation rates and thus the dating of sediment cores can be difficult. Radionuclides, as radiotracers, are a useful tool in the determination of chronological scales in aquatic sediments (Christiensen and Bhunia, 1986).

One of the most widely studied radionuclides is ^{210}Pb, a member of the ^{238}U series with a half-life of 22.35 years. As a particle-reactive radionuclide, it is readily scavenged from the water column by particulates, forming an unsupported or excess activity at the sediment surface, additional to the *in situ* production from ^{226}Ra[♦]. The use of ^{210}Pb for dating was initially carried out by Goldberg (1963), who dated an ice-core from the Greenland ice-sheet. Krishnaswamy *et al.* (1971) and Koide *et al.* (1973) adapted the method for dating freshwater and marine sediments.

Of the many models developed for calculating sedimentation rates using radionuclides, the majority stem from two basic conceptual models; the constant initial concentration (CIC) model and the constant rate of supply (CRS) model. Both models require that: (a) no grossly discontinuous (episodic) sedimentation or resuspension processes occur and (b) no post-depositional mobility of ^{210}Pb or redistribution of the sediments occur (Goldberg, 1963; Robbins and Herche, 1993).

The CIC model assumes a constant initial concentration of 'unsupported' ^{210}Pb at the sediment-water interface. Once buried it is cut off from new sources and decays by 1st order kinetics according to the following equation (Faure, 1986):

♦ ^{210}Pb is the decay product of ^{226}Ra which decays via ^{222}Rn.

$$^{210}Pb_d = {}^{210}Pb_s \cdot e^{-\lambda t}$$

Where: $^{210}Pb_d$ is the activity of $^{210}Pb_{(unsupp)}$ at depth d, $^{210}Pb_s$ is the activity of $^{210}Pb_{(unsupp)}$ at the surface, t is the age of the sediment, and λ is the decay constant of ^{210}Pb (i.e. = $\ln 2/t_{1/2}$)

Any ^{226}Ra present in the sediment will decay to give some 'supported' ^{210}Pb. Its activity is a constant, non-zero value, which, when subtracted from the total activity, gives the true 'unsupported' ^{210}Pb value. If the rate of accumulation is constant, t is given by d/a where a is the annual rate of accumulation, and it follows that:

$$\ln {}^{210}Pb_d = \ln {}^{210}Pb_s - \lambda d/a,$$

which is the equation of a straight line. Therefore, a plot of ln ($^{210}Pb_d$) vs. depth should give a straight line of gradient m = $-\lambda/a$, where a is the sedimentation rate and λ is a constant = $\ln 2/t_{1/2}$, where $t_{1/2}$ is the half life of ^{210}Pb (22.35 y).

The CRS model assumes that there is a constant rate of supply of unsupported ^{210}Pb, no mixing and no post-depositional mobility of ^{210}Pb, but allows for the possibility of a change in sedimentation rate (Goldberg, 1963; Appleby and Oldfield, 1978). The total inventory of unsupported ^{210}Pb (Bq m^{-2}) in the core and the inventories below the base of each section are calculated. The age of any individual section is then given by:

$$t_i = \frac{1}{\lambda} \ln \frac{I}{I_i}$$

Where: t_i is the age of the i^{th} layer, λ is the ^{210}Pb decay constant, I is the total unsupported ^{210}Pb inventory and I_i is the unsupported ^{210}Pb inventory below the i^{th} layer.

These models have been adapted by many workers to allow for problems of mixing by physical or bioturbation processes in the sediment (Robbins *et al.*, 1977; Brand and Shimmield, 1990; Appleby and Oldfield, 1992; Dukat and Kuehl, 1995).

1.3.2 ^{134}Cs and ^{137}Cs.

These anthropogenic radionuclides are present in the atmosphere as a result of nuclear weapons testing and releases from nuclear power installations. Both ^{134}Cs and ^{137}Cs are gamma-emitting, with half-lives of 2.05 and 30.23 years respectively. Radiocaesium is a potential hazard to living organisms as it is readily taken up into body tissues. ^{134}Cs differs in source from ^{137}Cs in that, whilst it is produced in small quantities in nuclear power waste, it is not present in any detectable amounts in weapons testing fallout. This is due to the mechanism by which it is formed. ^{134}Cs results from neutron capture by stable ^{133}Cs, which is a fission product. The direct production of ^{133}Cs is, however, small and the concentration builds up as a consequence of a succession of beta-decays in the mass 133 chain. Therefore ^{134}Cs is not produced in weapons testing since the irradiation time during the detonation is too short in comparison with the ^{133}Xe half-life. However, it is often found in varying amounts in spent fuel waste depending on the irradiation and cooling times (MacKenzie and Scott, 1984).

^{137}Cs is found in both weapons testing and nuclear power waste. The relative amounts of ^{134}Cs and ^{137}Cs found in nuclear power waste are characteristic of the reactor in which they are produced. This information is useful in attributing a release to a particular incident. For example, the ^{134}Cs:^{137}Cs ratio in releases from the Chernobyl accident in 1986 was 0.55 (Clark and Smith, 1988; Horrill *et al.*, 1988).

The major input of radiocaesium into the atmospheric environment occurred between 1954-1968 as a result of nuclear weapons testing. A plot of the annual global deposition of ^{137}Cs fallout shows a bimodal trend with the major peak of deposition

occurring in 1963 (Cambray *et al.* 1982). The total inventory of ^{137}Cs released is estimated at 242 kg of ^{137}Cs, representing an initial activity of 7.8 TBq. This fallout has been distributed globally.

The second major input of both ^{134}Cs and ^{137}Cs into the atmosphere occurred on 26th April 1986 as a direct result of the accident at the Chernobyl nuclear power station. An estimated $2x10^6$ TBq of fission and activation products were released over a period of about ten days (Clark and Smith, 1988). A large proportion of the volatile species ($^{134,137}Cs$, ^{131}I and ^{132}Te) were transported over a wide area of Europe. The 'cloud' passed over the UK between 2nd and 8th May 1986 and deposited, as both wet and dry deposition, an average of 1.3 kBq m^{-2} over the UK. Of this ~$3x10^{14}$ Bq was estimated to be ^{137}Cs and $1.65x10^{14}$ Bq to be ^{134}Cs. Some areas, for example, SW Scotland (> 20 kBq m^{-2}) and Cumbria (10-20 kBq m^{-2}) received very high deposition in comparison with the rest of the country. The characteristic ratio of the ^{134}Cs:^{137}Cs was measured at 0.55 at the time of the accident, providing a potentially useful signature for resolution of weapons Cs from Chernobyl Cs. Other smaller scale releases of ^{134}Cs and ^{137}Cs come from low level liquid radioactive waste, e.g. from the BNFL Reprocessing Plant at Sellafield, West Cumbria, but are released into the marine aquatic environment.

The generally accepted removal mechanism of Cs from the environment is by uptake by clay minerals via ion-exchange. Much of the early research in the 1960s was centred on assessing the sorption and fixation of cations by clay minerals in soils and their exchangeability. It is well accepted that the sorption of cations from solution by clay minerals is an ion-exchange process (Sawhney, 1972). Two types of sorption occur: (a) non-selective sorption where the amounts of cations adsorbed are proportional to their relative concentrations in solution and can be described in terms of the law of mass action and (b) selective sorption, originally thought to be due to the close fit into hexagonal cavities, but was later shown to be due to low hydration energies of the cations (Coleman *et al.*, 1963a, b).

It has also been shown that there are three different types of site for binding Cs to clay minerals which produce different levels of exchangeability with other cations (Evans *et al.*, 1983). These sites are: (a) surface planar sites from which ^{137}Cs is generally exchanged by a large number of cations (e.g. Na^+, NH_4^+, H^+, Cs^+, Ca^{2+} Mn^{2+}), (b) wedge sites where ^{137}Cs exchange is sterically limited to cations of similar size and charge (e.g. NH_4^+, K^+, H^+, Cs^+ and possibly H_3O^+) and (c) interlayer sites from which ^{137}Cs is not readily exchanged by any cations.

The types of clay minerals which have an abundance of these interlayer and wedge sites are the interlayered micas (illite), vermicullite, and to a lesser extent some smectites (e.g. montmorillonite). When cations of low hydration are sorbed into the frayed edges it causes interlayer dehydration and the layers collapse, fixing the cations. The amount of collapse of the lattice is governed by the hydration energy of the cation involved and, to a lesser extent, the interlayer charge. For example, vermicullite collapses to a spacing of ~10.8 Å, which is too small for most cations to 'get in' to displace the Cs, thus effectively fixing it. Montmorillonite on the other hand only collapses to ~12 Å spacing. Cations such as Ca^{2+} with higher hydration energies are able to get in to this spacing and cause a re-expansion of the layers.

The interest in radioactive fallout, the disposal of low level radioactive effluent and the results from studies on clay minerals have prompted many studies on the removal of radiocaesium to the sediments and its mobility after burial (Lomenick and Tamura, 1965; Francis and Brinkley, 1976; Evans *et al.* 1983).

Much use has been made of ^{137}Cs to assess the reliability of ^{210}Pb dating methods and to investigate mixing in sediments (Appleby *et al.* 1993). The use of ^{137}Cs as a dating tool is only viable, however, where there is little or no post-depositional mobility. In lake sediments of low clay content a relatively high degree of ^{137}Cs mobility has been observed. In these lakes the ^{137}Cs is taken up by organic matter which decomposes after burial, releasing the ^{137}Cs into the pore-waters (Davies *et al.* 1984). Similarly Bryant *et al.* (1993) showed that there has been considerable downward diffusion in

the sediments of the Round Loch of Glenhead (SW Scotland), an acidified loch with organic-rich sediments. As the record of input has been obscured, no measurement of sedimentation rate and chronological scale can be made. In contrast, a clay-rich sediment core taken from Loch Lomond exhibited good resolution of the two peaks from the Chernobyl accident and weapons testing. This enabled a measure of the sedimentation rate which compared favorably with that obtained by ^{210}Pb dating (Bryant *et al.*, 1993).

Other researchers have used Chernobyl Cs to look at the scavenging of radionuclides from the water column (Robbins *et al.*, 1992), residence times (Edgington *et al.*, 1991), and to construct models to account for mixing in the sediments (Christiensen and Klein, 1991; Abril *et al.*, 1992).

1.4 Heavy metals in the sedimentary environment.

1.4.1 Lead.

Lead is present as a trace constituent in soil, water, animal life and air. The use and knowledge of Pb extends as far back as 5000 B.C. to the ancient Egyptians (Fig 1.5). As a metal it was used extensively by the Phoenicians, Romans, Indians and Chinese (Habashi, 1997). In ancient civilisations it was used for decorative objects, fishing weights, water pipes, coins etc. (Nriagu, 1978). Pb occurs in several mineral forms in the geosphere but it is usually deposits of galena (PbS) that are mined. Pb has been extensively mined by man for several millennia and the first known mines were in Spain in 2000 B.C. It is relatively easily extracted from ores. During the Industrial Revolution the use of Pb escalated and it is now used in a diverse range of products, e.g. batteries, radiation insulation and petrol additives. In recent times the main source of Pb in the environment has come from Pb-smelting and Pb-additives in petrol (Table 1.1) and it is estimated that some 47 % of the annual production of Pb is lost to the environment.

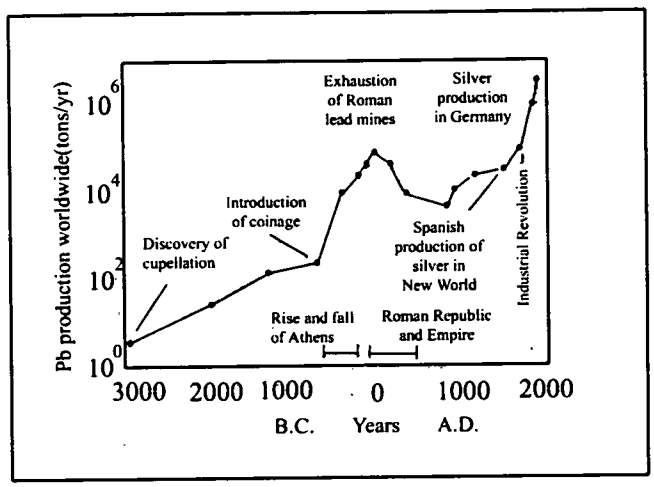

Figure 1.5 Pb production over the past 5000 years. (Settle and Patterson, 1980).

Table 1.1 Worldwide emissions of Pb, Cu, Zn and Cd (10^3 kg y^{-1}) to the atmosphere from anthropogenic and natural sources in 1988.

Anthropogenic Emissions	(Nriagu and Pacyna, 1988)	Pb	Cu	Zn	Cd
Coal Combustion	Electric utilities	775-4650	930-3100	1085-7750	77-387
	Industry and domestic	990-9900	1390-4950	1485-11880	99-495
Oil	Electric utilities	232-1740	348-2320	174-1280	23-174
	Industry and domestic	716-2150	179-1070	358-2506	18-72
Nonferrous metal production	Mining	1700-3400	160-800	310-620	0.6-3
	Pb production	11700-31200	234-312	195-468	39-195
	Cu/Ni	10050-22100	14450-30600	4250-8500	1700-3400
	Zn/Cd	5520-11500	230-690	4600-82800	920-4600
Secondary nonferrous metal production			55-165		2.3-3.6
Steel and iron production		1065-14200	142-2840	7100-31950	28-284
Refuse incineration	Municipal	1400-2800	980-1960	2800-8400	56-1400
	Sewage sludge	240-300	30-180	150-450	3-36
Phosphate fertilisers				1370-6850	68-274
Cement production		18-14240	137-685	1780-17800	8.9-534
Wood combustion		1200-3000	600-1200	1200-6000	60-180
Mobile sources		*248030			
Total emissions		288700-376000	19860-50870	30150-141860	3100-12040

*assuming a value of 45% of the world's petrol has a Pb content of 0.15 g l^{-1}

Natural Emissions	(Nriagu, 1989a)				
Windborne soil		300-7500	900-15000	3000-35000	10-400
Sea salt spray		20-2800	230-6900	20-860	0-110
Volcanoes		5400-6000	900-18000	3100-19000	140-1500
Wild forest fires		60-3800	100-7500	300-15000	0-220
Total emissions		970-23000	2300-54000	4000-86000	1500-26000
Ratio Anthropogenic:Natural		0.003-0.6	0.12-1.1	0.1-0.6	0.5-2

The discovery in 1921 that organo-lead compounds made excellent antiknock agents for petrol led to a revolution in the automobile industry (Nriagu, 1990). Pb-alkyl antiknock additives were soon commercially produced. By 1970 it is estimated that some 375 000 tonnes of petrol Pb had been consumed world wide (assuming an average Pb content of 0.52 g l^{-1}).

The adverse health effects of Pb exposure have been known since as early as the 2nd Century B.C. (Landrigan, 1990) and Pb poisoning has been a reportable disease since 1899 (Lippmann, 1990). However, mounting public concern, aroused by publications by Patterson (1965), led to many new studies into the subclinical effects of long term exposure to Pb and the elevation of Pb in the environment. As a result, leaded petrol has become one of the first "environmentally unsafe" products to be forced out of the market place (Nriagu, 1990). Japan, the USA and Canada were the first to start the gradual phasing out of Pb-additives from petrol from 1975 until 1989 when the maximum permitted Pb content of petrol was dropped to 0.026 g l^{-1} (effectively "Pb free"). In other countries the phasing out has lagged 10 years behind that of the USA, but the majority of countries now have a programme of reduction. In the UK the maximum permitted concentration of Pb was reduced from 0.4 to 0.15 g l^{-1} in 1986 and unleaded petrol was phased in from 1989. By 1996, unleaded petrol accounted for 67.6 % of the UK consumption of petrol (DETR, 1997). Most other European countries have followed a similar pattern to the UK The United States has also banned the use of Pb in paint since 1971.

1.4.2 The use of stable lead isotopes to distinguish sources of pollution.

Pb has four stable isotopes, ^{204}Pb, ^{206}Pb, ^{207}Pb and ^{208}Pb. ^{204}Pb is non-radiogenic and is therefore present in the same quantities as when the Earth was formed. The other three isotopes (Fig. 1.6), however, are the end products of the natural decay series of

^{238}U, ^{235}U and ^{232}Th, respectively[♦], and have therefore increased in concentration since the Earth's formation. Hence variations in the relative abundances of the isotopes in a Pb-ore are characteristic of the original U:Th ratio and the age of formation of the ore. The isotopic ratios are retained during smelting and refining (Sturges and Barrie, 1987; Settle and Patterson, 1982). Hence environmental releases from Pb smelting or from products of refined Pb (e.g. alkyl Pb additives which give rise to car-exhaust emissions) retain the original isotopic ratio. Other materials containing Pb can give rise to emissions during processing or burning (e.g. wood, coal and other metal refining), and these in turn will also have a characteristic ratio. When different sources of Pb are mixed, the ratio is altered and, in principle, it is possible to use the ratios to study changes in the environment resulting from different emissions. Pb ores from around the world have a wide range of $^{206}Pb/^{207}Pb$ atom ratios from 1.037-1.390 (Chow *et al.*, 1975). In Scotland the $^{206}Pb/^{207}Pb$ atom ratios in galenas are in the range of 1.110-1.186 (Moorbath, 1962).

The ability to determine quantitatively the ratios of the isotopes using thermal ionisation mass spectrometry (TIMS) and inductively coupled plasma mass spectrometry (ICP-MS) (Fig. 1.7) has led to a wide body of research into the study of sources, deposition and accumulation of Pb in the environment in a wide range of different environmental materials. The most commonly quoted atom ratio is $^{206}Pb/^{207}Pb$ and, less commonly, $^{208}Pb/^{206}Pb$ and $^{208}Pb/^{207}Pb$. Until recently, however, comparatively few of the many records of environmental Pb pollution from sediments, ice-cores and peat bogs have been accompanied by stable Pb isotope data (Farmer *et al.*, 1996).

[♦] With half-lives of 4.5×10^9, 0.7×10^9 and 14.1×10^9 y, respectively.

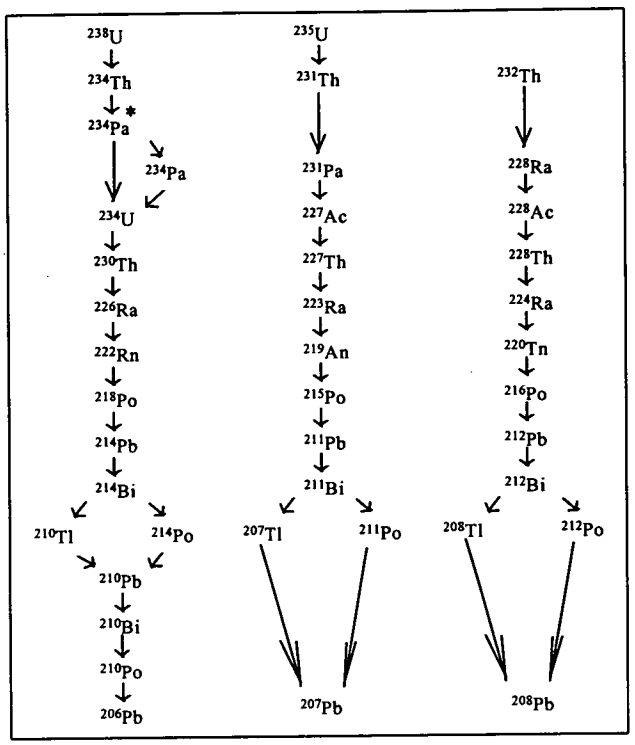

Figure 1.6 Uranium and thorium natural decay series. (Habashi, 1997).

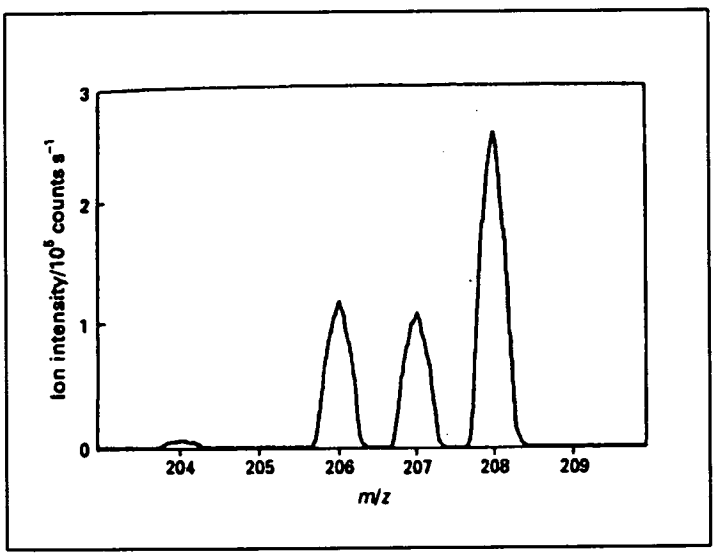

Figure 1.7 Mass spectra of position of ^{204}Pb, ^{206}Pb, ^{207}Pb and ^{208}Pb, obtainable using TIMS and ICP-MS. (Date and Cheung, 1987).

Table 1.2 shows a selection of values of $^{206}Pb/^{207}Pb$ and $^{208}Pb/^{206}Pb$ atom ratios for different environmental samples from different countries of origin. Figure 1.8 is a plot of $^{206}Pb/^{207}Pb$ against $^{208}Pb/^{206}Pb$ which demonstrates that the ratios of different sources are often isotopically distinct (Monna *et al.*, 1997). In Britain non-indigenous ores were introduced towards the end of the 19th Century, and had become the main source of Pb in England by the mid 20th Century once the mining of British ore had become uneconomic (Shotyk *et al.*, 1998). The main sources of Pb used in the manufacture of Pb-additives added to British and French petrol are Australian ($^{206}Pb/^{207}Pb$ atom ratio 1.04) and Canadian ($^{206}Pb/^{207}Pb$ atom ratio 1.16). A combination of these ores, in an approximate ratio of 70:30, has given rise to an average $^{206}Pb/^{207}Pb$ atom ratio of 1.067 in leaded petrol in Britain and 1.084 in France (Sugden, 1993; Monna *et al.*, 1997).

The addition of this source of Pb to the environment has had a marked effect on the $^{206}Pb/^{207}Pb$ atom ratio in soil, aquatic sediments and airborne particulates. Natural Pb in Britain is more radiogenic than that in alkyl Pb additives, and pre-industrial values have been measured at 1.190-1.200 for $^{206}Pb/^{207}Pb$ in sediments and peat cores (Sugden *et al.*, 1991a,b). They reported that once the Industrial Revolution had begun, the $^{206}Pb/^{207}Pb$ atom ratio of excess Pb dropped markedly in Loch Lomond sediments to 1.170 (Fig. 1.9) where it remained constant until 1930. After 1930 there was a marked drop to 1.149 by 1937, followed by a more steady decline to 1.110 by 1980 caused by the introduction of leaded petrol.

Ombrotrophic peat bogs have also been used to establish records of atmospheric pollution. Receiving all of their water and nutrients from the air by wet and dry deposition, these bogs have a high capacity to retain a number of trace elements, especially Pb (Rosman *et al.*, 1998; Shotyk *et al.*, 1998). In Scotland similar profiles to those observed in Loch Lomond sediments, have been observed in ombrotrophic peat bogs (Farmer *et al.*, 1997b; MacKenzie *et al.*, 1998b). In a recent study of archived herbage samples from a site in southern England (Fig. 1.10) it was shown that the $^{206}Pb/^{207}Pb$ atom ratio had already started to decrease before the use of

Table 1.2 Stable Pb isotope ratios in different environmental materials and current aerosol values: (a) UK (b) Worldwide.

Environmental Material	Origin	$^{206}Pb/^{207}Pb$	$^{208}Pb/^{206}Pb$	Reference
(a) UK.				
Lead Mines	Leadhills	1.170	2.090	Moorbath, 1962
	Strontian	1.172	2.081	Moorbath, 1962
	Tyndrum	1.144	2.121	Moorbath, 1962
	Minnigaff	1.170	2.096	Moorbath, 1962
	Islay (Mulreesh)	1.162	2.095	Moorbath, 1962
	Islay (Ballygrant)	1.168	2.088	Moorbath, 1962
Leaded Petrol	UK	1.067	2.193	Monna *et al*., 1997
Coal	Edinburgh	1.184	2.472	Sugden, 1993
	Edinburgh, East	1.187	2.464	Sugden, 1993
(b) World wide				
Lead Mines	Australia	1.04		Doe, 1970
	Canada	1.15		Doe, 1970
Leaded Petrol	France	1.084	2.182	Monna *et al*., 1997
	Israel, 91 octane	1.105	2.154	Erel *et al*., 1997
	Israel, 96 octane	1.114	2.145	Erel *et al*., 1997
	Switzerland	1.14		Shotyk *et al*., 1998
Fly Ash	Israel	1.209	2.051	Chow *et al*., 1975
Urban Incinerator	France	1.150	2.114	Chow *et al*., 1975
Aerosols	Edinburgh	1.094	2.166	Sugden *et al*., 1993
	London	1.117	2.141	Monna *et al*., 1997
	Israel	1.126	2.133	Erel *et al*., 1997
	Paris	1.121	2.138	Monna *et al*., 1997
	USA, North	1.161	2.097	Hamelin *et al*., 1997
	Switzerland	1.131		Shotyk *et al*., 1998

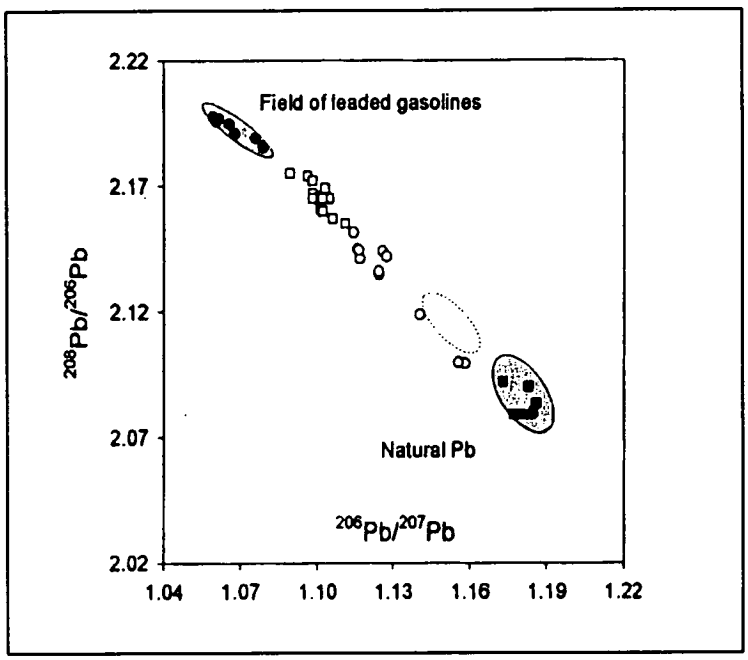

Figure 1.8 Plot of $^{206}Pb/^{207}Pb$ vs $^{208}Pb/^{206}Pb$ in environmental samples from the UK. (●) leaded gasoline, (■) pre-industrial, (□) airborne particulate matter from Southampton and (○)airborne matter from London. (Monna *et al.*, 1997).

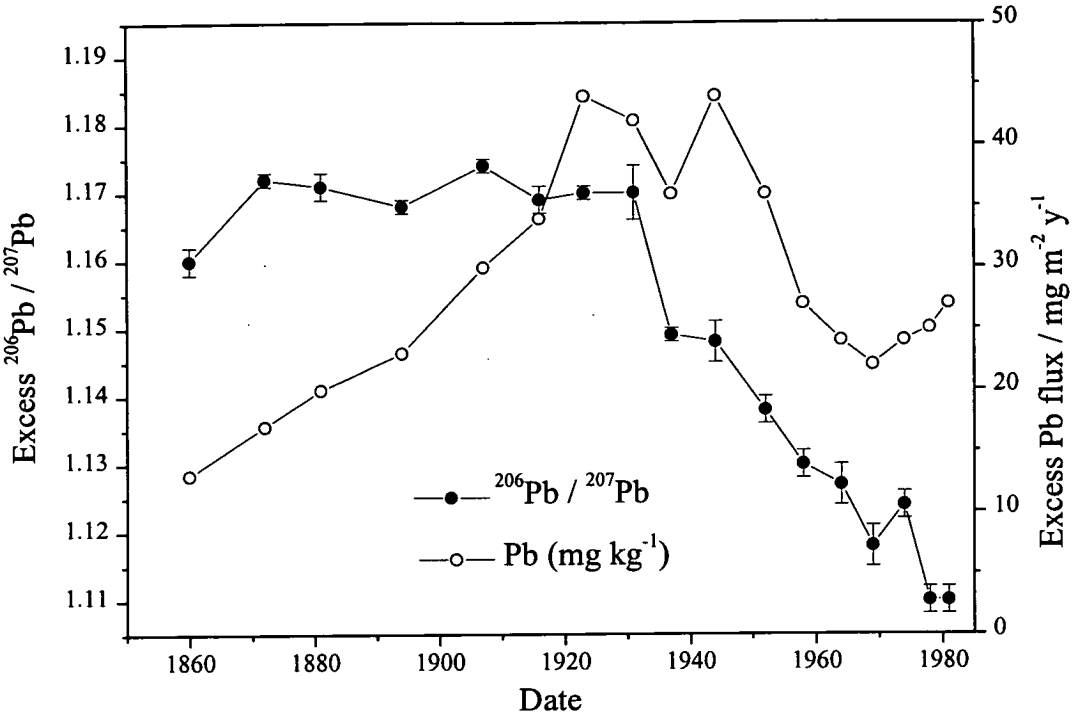

Figure 1.9 Post-1800 trends in excess Pb flux and associated $^{206}Pb/^{207}Pb$ ratio in core LL-10L from the northern basin of Loch Lomond. (Reproduced from Sugden, 1993).

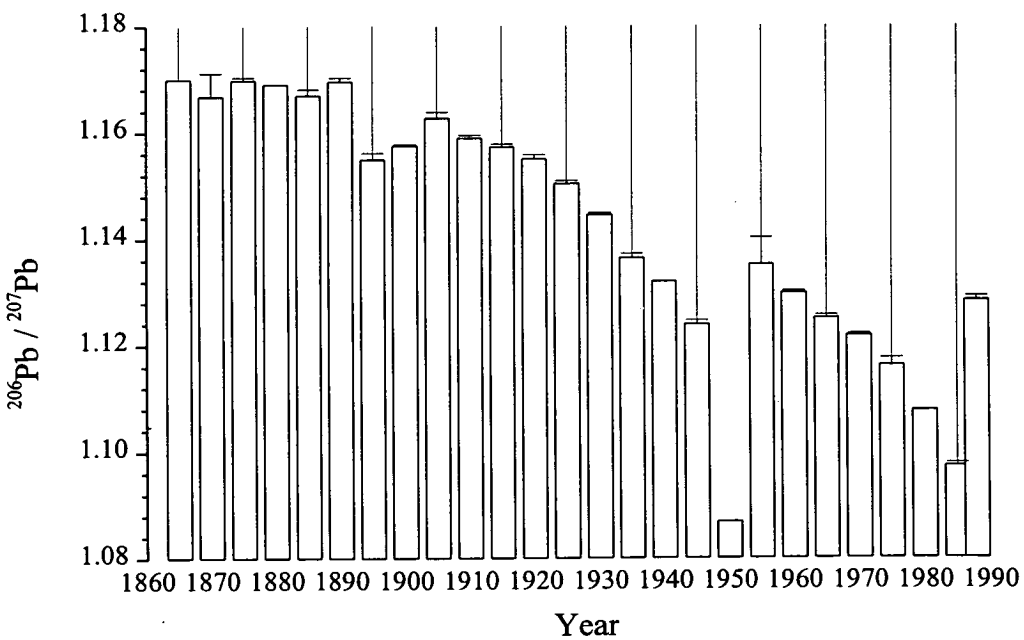

Figure 1.10 Changes of $^{206}Pb/^{207}Pb$ in 5-year bulked samples of herbage. Error bars are three standard deviations of duplicate analyses. (Reproduced from Bacon et al., 1996).

alkyl Pb-additives in petrol (Bacon *et al.*, 1996) and that recently the trend has reversed as a result of the declining use of such additives.

In western Europe similar changes in $^{206}Pb/^{207}Pb$ atom ratios have been observed, showing the anthropogenic influence of changes in emissions. Shotyk *et al.* (1998) reported results from a peat bog core from the Jura Mountains in Switzerland dating from 12 370 ^{14}C yr. BP (Fig. 1.11). The core shows 10 main regions of change in the $^{206}Pb/^{207}Pb$ atom ratio which relate to changes in atmospheric input. It shows that the $^{206}Pb/^{207}Pb$ atom ratio has changed from 1.204 in the early Holocene (10 500 ^{14}C yr. BP) to 1.130 at present. Of these changes, three have had the most significant effect in changing what was originally Pb deposition arising primarily from soil erosion of the earth's crust. The first of these changes occurred at about 3000 yr. BP when Pb mining started. The industrial revolution in 1850 AD prompted the second major decline in the ratio then finally the introduction of leaded petrol initiated the steepest decline from 1930 AD. These results are in good agreement with ice-core records taken from Greenland (Hong *et al.*, 1994). Recent studies are also beginning to show a "recovery" of the $^{206}Pb/^{207}Pb$ atom ratio towards a more geogenic ratio (~1.20), similar to that observed in the UK, and coincident with the reduction of the use of petrol Pb-additives. Moor *et al.* (1996), in a study of stable Pb isotope ratios in Lake Zug, Switzerland, report a sharp increase towards a more natural ratio in the top layer. Rosman *et al.* (1998) similarly showed changes in $^{206}Pb/^{207}Pb$ atom ratios measured in moss and aerosol samples in Norway.

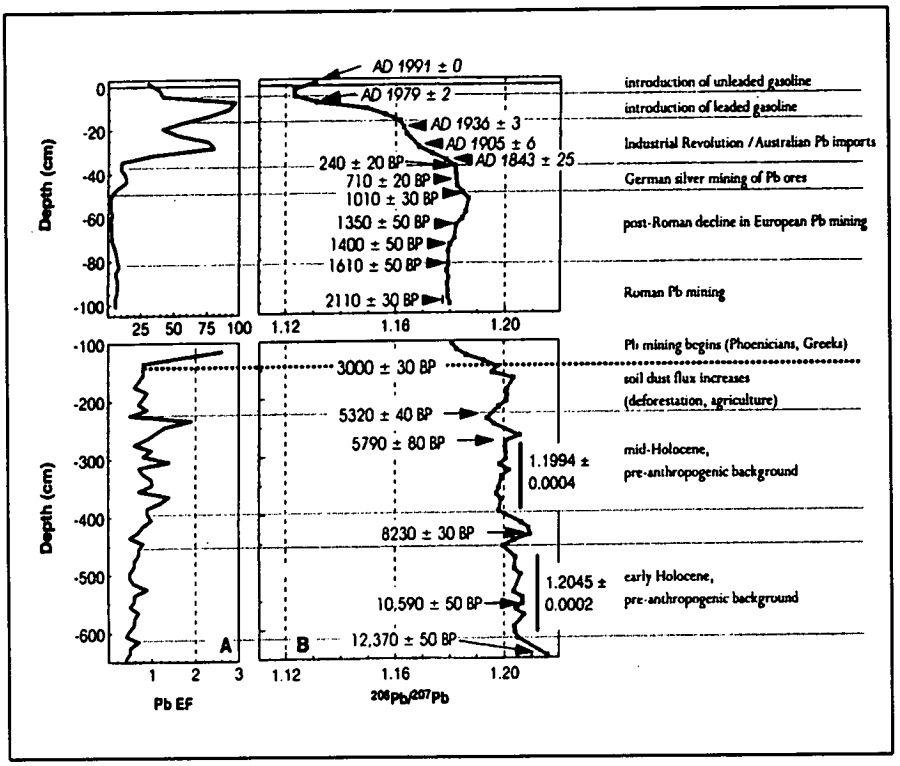

Figure 1.11 History of atmospheric Pb deposition in Europe since 12,370 ^{14}C yr BP. (Weiss *et al.*, 1997; Shotyk *et al.*, 1998).

1.4.3 Other heavy metals.

1.4.3.1 Copper.

The first metals found by Neolithic man were Au and Cu. Copper has been mined and used since approximately 7000 B.C. (Habashi, 1997), and in the UK has been mined since 2000 B.C. A Greenland ice-core, dating back ~2500 years, shows the levels of Cu in the atmosphere have been above natural levels since ~1800 years ago (Hong *et al.*, 1996).

Copper emissions are mainly due to mining and smelting of ores. Table 1.1 is a summary of the worldwide emission to the atmosphere from natural and anthropogenic sources and Figure 1.12 shows a summary of the variations in Cu production over the past 500 yr. (Hong *et al.*, 1996). It shows three major peaks in production from Roman mining, the Sung Dynasty of China and the Industrial Revolution. Emissions of Cu in real terms have actually fallen due to improvements in metallurgical and extraction techniques. The world mine production of Cu has increased dramatically from 9×10^3 t in 1700 to 8100×10^3 t in 1984 (Habashi, 1997).

In the environment Cu is exceedingly toxic to lower forms of life (algae and fungi) but is an essential nutrient in higher plants and animals. In larger doses it can be lethal but the question of chronic poisoning, unlike in the case of Pb, is still open to debate. Cu is used primarily as a conductor material with about 50 % of the world's consumption of Cu being used for electrical purposes. Other areas of application are in the fabrication of household articles, decorative objects and coins. Cu compounds are regularly added as an agricultural crop nutrient, e.g. in the form of copper sulphate pentahyrdrate (Monna *et al.*, 1995), and are also gaining popularity as a nutritional feed additive (Habashi, 1997).

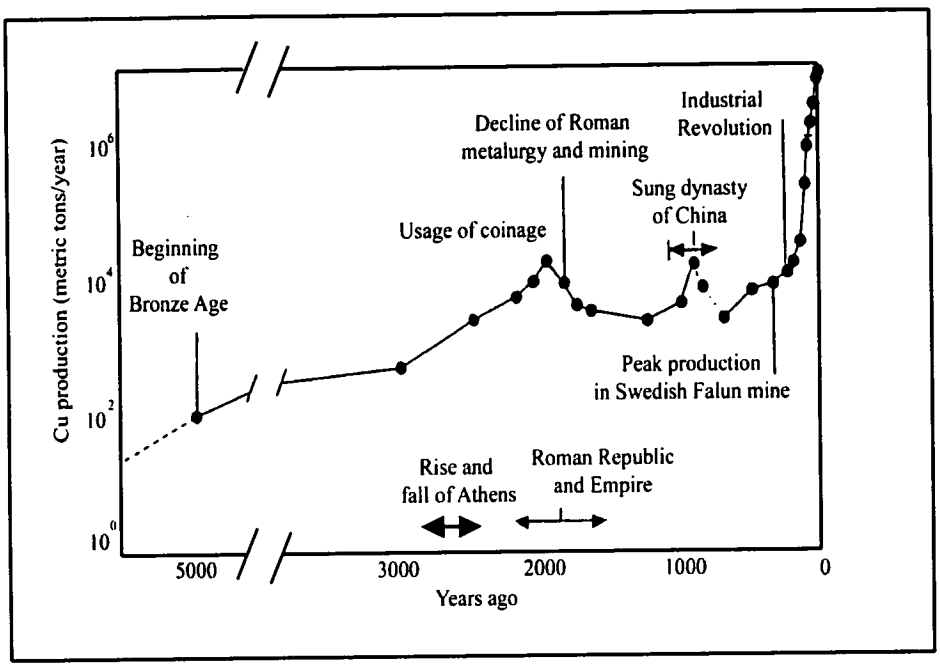

Figure 1.12 Variations in copper production rate over the past 5000 years. (Hong *et al.*, 1996).

1.4.3.2 Zinc.

The Chinese and Indians were the first known users of metallic Zn (Habashi, 1997). In India, remains of Zn smelting operations showed that it was produced prior to 1300 A.D. and in China, coins containing 99 % Zn, were cast during the Ming Dynasty (1368-1644 A.D.). In the western world brass (smelting of Cu and Zn ore together) was produced as early as 8000 B.C., but metallic Zn was unknown until about the 17th Century B.C. The use of Zn in industry did not start to expand until the end of the 19th Century. Its main use is the galvanising of Fe and other metals and more recently in the manufacture of special steels (Gilbertson *et al.*, 1997). Table 1.1 is a summary of the world wide emissions of Zn from anthropogenic and natural sources. Prior to 1900 Zn was used in coins and decorative items. The other main user of Zn is the rubber industry giving rise to Zn and Cd emissions due to wear of car tyres (Akhter and Madany, 1993).

In the environment Zn is an essential element for humans and all other forms of plant life. It is required by a large variety of functions, e.g. growth and skin integrity and function. As a result it has a relatively low acute toxicity, when compared with other heavy metals. Chronic effects have been reported in cases where continuous uptake of Zn by humans from water of concentrations greater than 40 mg kg^{-1} occurred (Habashi, 1997).

1.4.3.3 Cadmium.

Pure deposits of Cd are very rare. As a result it was not discovered until 1817, and then was not used for at least a full century after its discovery. Therefore, unlike Pb and Cu which have been used since ancient times, its use is comparatively new. Cadmium is usually present as an impurity in Zn ores (plus to a lesser extent in Pb and Cu ores) (Habashi, 1997) and will therefore tend to be from the same source. Cd is usually refined from one of the steps in the Zn smelting process. A summary of

the world wide emissions in 1988 of Cd from anthropogenic and natural sources is shown in Table 1.1.

In the environment Cd is not particularly toxic to animals but in larger doses it can be lethal to humans. Acute and chronic poisoning lead to long-term damage to the lungs and kidneys and can cause renal tubular dysfunction. There have been reports of Cd poisoning due to plant uptake, e.g. in Japan, where a contaminated area led to poisoning from high levels of Cd in rice (Habashi, 1997). Cadmium has a limited use due to public concern over its toxicity and is currently only used as plastic stabilisers and Cd-Ni batteries.

1.5 Aims, objectives and structure of Thesis.

1.5.1 Aims.

The overall aim of the research presented here is to investigate and compare the potential high-resolution historical record of heavy metal pollution, in particular that of Pb, contained within the sediment column of several Scottish freshwater lochs. The lochs were selected on the basis of geographical location (Fig 1.13) and were:

- Loch Lomond, situated close to Scotland's main west-central industrial belt, the area of highest population density, and the location of previous, lower-resolution studies.
- Lake of Menteith, east of Loch Lomond but again close to the central belt and, indeed, to the ombrotrophic peat bog of Flanders Moss, a potential historical archive of atmospheric deposition and under concomitant investigation.
- Loch Tay, situated in a highly mineralised area further to the north and subject to Pb mining and smelting activity in the past.
- Loch Ness, in the north of Scotland, remote from heavy industry and in a relatively sparsely populated region.

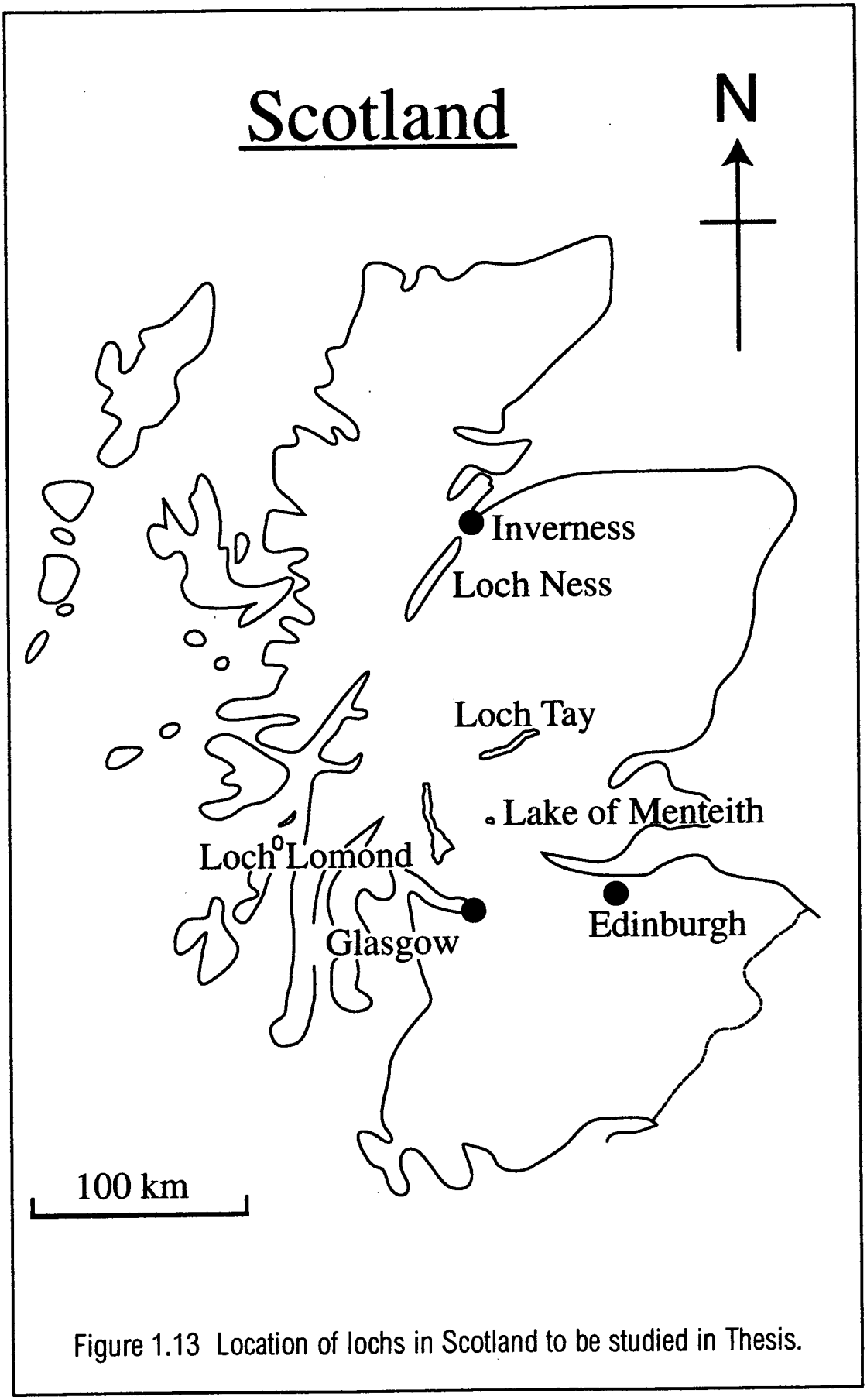

Figure 1.13 Location of lochs in Scotland to be studied in Thesis.

1.5.2 Objectives and structure of Thesis.

The specific objectives were as follows.

1. To develop and apply appropriate high-resolution sampling methods for the collection and slicing of sediment cores from the four freshwater lochs (Chapter 2).
2. To develop appropriate procedures for the determination of radionuclides ^{210}Pb, ^{134}Cs and ^{137}Cs in collected material, in order to obtain accurate sedimentation rates, chronologies and any other relevant perturbatory information, for the sediment columns of the freshwater lochs (Chapter 2).
3. To develop appropriate procedures for the determination of heavy metals (Mn, Fe, Pb, Zn, Cu and Cd) and stable Pb isotopes in collected material, in order to obtain accurate, high-resolution profiles in the freshwater loch sediments, for historical or other perturbatory interpretation (Chapter 2).
4. To apply procedures developed in 1, 2 and 3 to the detailed investigation of radionuclide and heavy metal profiles in the bottom sediments of Loch Lomond (Chapter 3), Lake of Menteith (Chapter 4), Loch Tay (Chapter 5) and Loch Ness (Chapter 6). This enables an inter-loch comparison of the historical records of heavy metal pollution, in particular that of Pb and its contributory sources, across Scotland (Chapter 7).

A brief summary of the main findings of this research is presented in Chapter 8.

Chapter 2. Materials and methods.

The following chapter is an account of the procedures and techniques used in the collection and preparation of samples.

2.1 Sediment core collection and sectioning.

2.1.1 Sampling techniques.

Sediment cores were taken from selected sites on Loch Lomond, Lake of Menteith, Loch Tay and Loch Ness using two different coring devices: (a) Mini-Mackereth corer (Mackereth, 1969) and (b) Jenkin surface mud corer (Ohnstad and Jones, 1982).

(a) Mini-Mackereth corer: this sampler was used to obtain cores of 60-100 cm in length for the determination of heavy metal concentrations and stable lead isotope ratios (Fig. 2.1.1). The corer is operated by attaching a perspex core tube (internal diameter = 65 mm) to a piston inside the corer housing. The corer is then lowered slowly into the water and allowed to steady about 5 m above the sediment surface, (downward progress can be monitored using an echo-sounder) before gently easing it into the surface sediment. Compressed air, to about 6-7 atm above hydrostatic pressure, is introduced via an air line to the corer piston causing it to push the core tube down into the sediment. The stationary inner piston ensures that the sediment material enters the tube due to the external pressure. When some air bubbles have appeared at the surface, the corer is carefully pulled up to the surface and a rubber bung placed in the bottom of the tube just before it is pulled out fully from the water and also at the top once the tube has been disengaged from the corer.

(b) Jenkin surface mud sampler: this sampler was used to obtain cores of 10-30 cm in length, with the retention of the overlying water in a relatively undisturbed state, for the radiometric determination of sediment accumulation rates. As with the Mini-

Mackereth corer, the sampler (Fig. 2.1.2) is lowered from the boat into the sediment surface. The weight of the corer causes the corer tube (internal diameter = 69 mm) to sink down into the sediment. Once the corer has sunk in as far as it can, and is at rest, the tube is sealed at both ends by a spring mechanism which automatically releases when the rope tension relaxes. The sampler is then raised carefully to the surface.

After collection, the cores were taken back to the onshore field stations for sectioning at different vertical depth increments ranging from 2 mm to 5 cm. The exact sectioning ranges for each core are detailed in section 2.1.2. The cores were extruded using a simple hydraulic water pump which allowed very fine control of the upward movement of the sediment (Fig. 2.2.1). The following modifications were made for the 2-3 mm sections in order to minimise the amount of sample lost on sectioning, and to give a high degree of accuracy:

- A section of camera film was taped to the outside of a 2 cm perspex sectioning ring (Fig. 2.2.2). The distance from the bottom of the ring to the bottom of the two holes was 2-3 mm, i.e. the sediment is extruded up into the ring until the surface of the core is just visible in the holes of the camera film, at which point there should be 2-3 mm of sediment present and the section can be taken. This technique was later improved by etching a 2 mm mark onto a 1 cm ring, thereby yielding a more accurate measurement of 2 mm.
- A 0.3 mm thick sheet of perspex was used to slice the section, thus minimising the amount of sample lost per section.
- The 1, 2 and 5 cm thick sections were taken using appropriate sized perspex rings.

Each section was placed in a numbered, tapered polythene bag and sealed, ready for transport back to the laboratory.

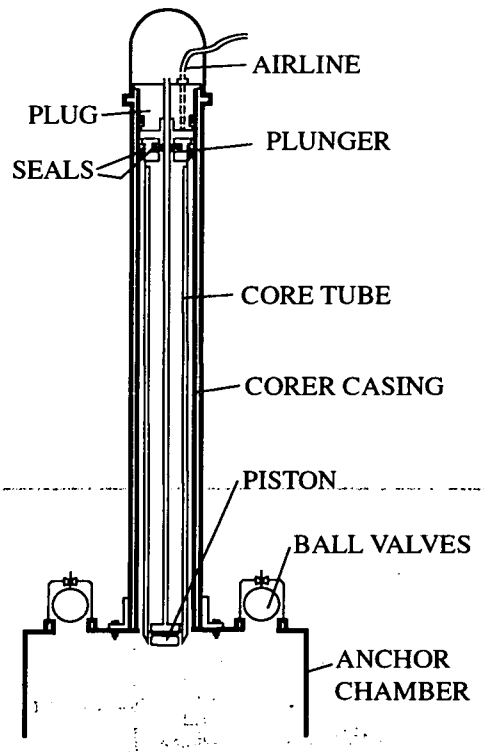

Figure 2.1.1 Mini-Mackereth corer.

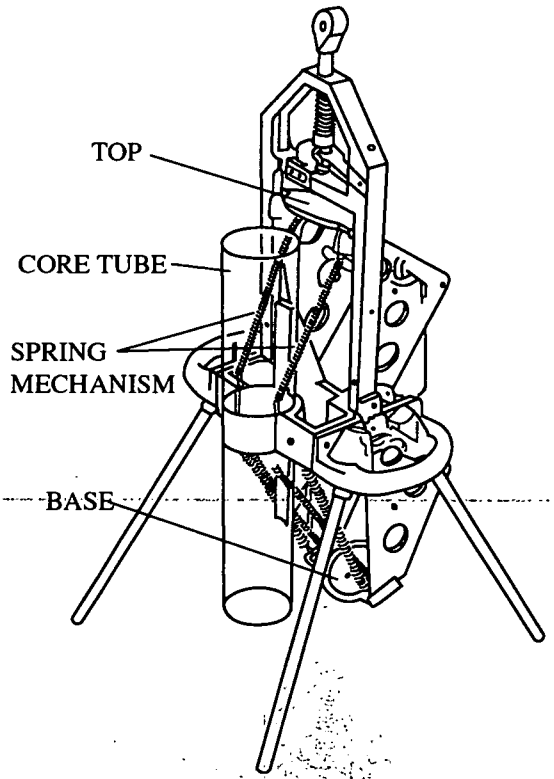

Figure 2.1.2 Jenkin corer.

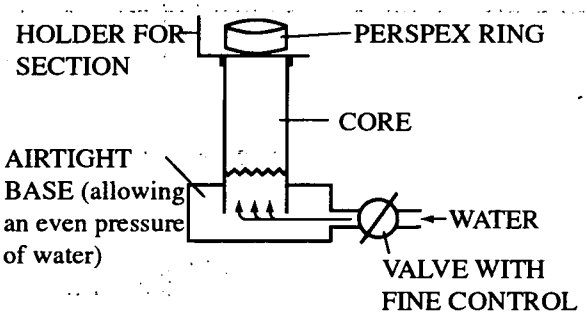

Figure 2.2.1 Extrusion Apparatus set up.

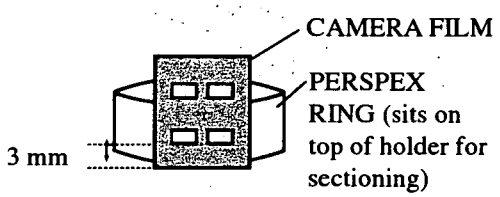

Figure 2.2.2 Sectioning Apparatus for 3 mm sections.

2.1.2 Cores taken at sampling sites.

The location and position of the sample sites for the cores and stream sediment samples are shown in Figure 2.3.

2.1.2.1 Loch Lomond.

Two sites were chosen in Loch Lomond. The first was in the southern basin (LL/South, Grid Ref. NS391884). This site lies in the middle of a channel between the two islands of Inchmurrin and Creinich. These islands are part of a chain of islands which lie parallel to the Highland Boundary fault. The channels between the islands are approximately 20 m in depth and allow water to move into the most southerly section of the southern Loch Lomond basin. Two cores were taken on 26/11/91 from the site at a depth of 18 m. (a) The Mini-Mackereth corer was used to obtain a core of 80 cm length, which was sectioned into 3 mm increments from 0-30 cm, 2 cm increments from 30-50 cm and 5 cm from 50 cm to the base. (b) The Jenkin surface mud corer was used to obtain a core of length 14.4 cm which was sectioned into 3 mm intervals over the entire length of the core.

The second site was in the centre of the northern-most basin, known as the Ardlui basin (LL/North, Grid Ref. NN327145), which has a maximum depth of 60 m. Sampling at this site proved to be difficult due to the production of air bubbles in the core once removed from the water. This had the effect of expanding the core during sectioning, causing it to split into sections as it was extruded. A Mini-Mackereth core of 70 cm length was obtained on 16/07/95 and sectioned into 2 mm increments from 0-5 cm, 1 cm increments from 5-20 cm and 2 cm increments from 20-70 cm.

2.1.2.2 Lake of Menteith.

Two cores were taken from the deepest part of the lake using the two corers used on Loch Lomond (LMM, Grid Ref. NN580004). The Mini-Mackereth core obtained on

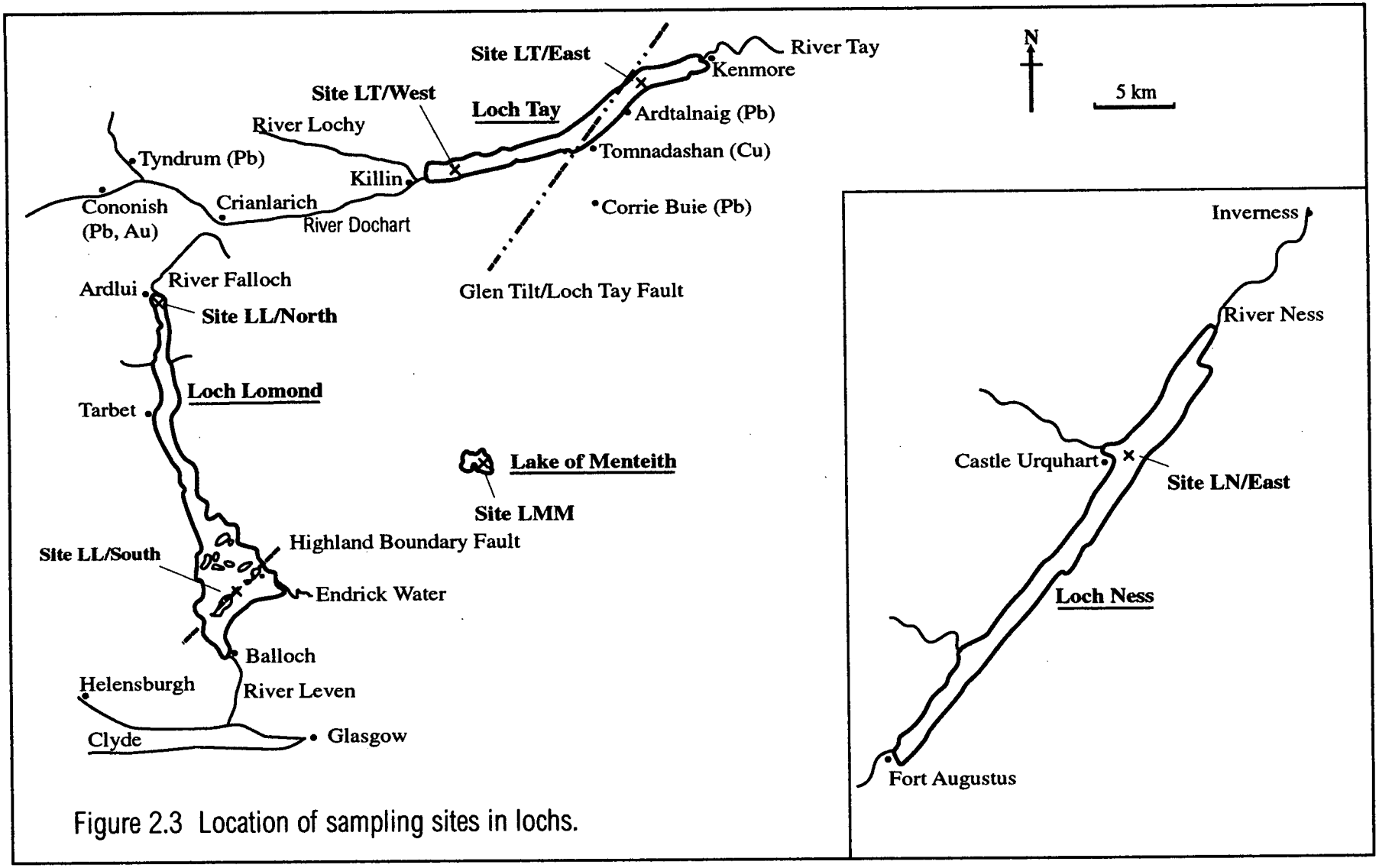

Figure 2.3 Location of sampling sites in lochs.

13/11/96 (Paterson, 1997) at a depth of 13 m was 56 cm in length and was sectioned into 2 mm increments from 0-5 cm, 0.5 cm increments from 5-50 cm and 1 cm increments from 50-56 cm. The Jenkin core obtained was 22 cm in length and was sectioned into 1 cm increments over the entire core.

2.1.2.3 Loch Tay.

Two sites were used in Loch Tay. The first was in the western end of the loch where the water depth is ~50 m and lies to the west of the Loch Tay-Glen Tilt Fault. Two cores were taken from this western site (LT/West, Grid Ref. NN715335) on 17/11/92 using the two different corers as used on Loch Lomond (Kesterton, 1993). A Mini-Mackereth core, obtained from a depth of 48 m, was 90 cm in length and was sectioned at 1 cm intervals from 0-20 cm, 2 cm intervals from 20-40 cm and 5 cm intervals from 40 cm to the base. A Jenkin core of 16 cm length, obtained from the same site, was sectioned at 1 cm intervals throughout the core.

The second site lies to the east of the Loch Tay-Glen Tilt fault in the eastern basin, in which the water depth varies from 50-150 m. Two cores were taken from the eastern site (LT/East, Grid Ref. NN709426), again using the two different corers as used on Loch Lomond. The Mackereth core, obtained on 18/06/96 at a water depth of 120 m, was 100 cm in length and was sectioned into 2 mm increments from 0-20 cm, 1 cm increments from 20-40 cm and 2 cm increments from 40-80 cm, plus a bottom section of 13 cm. The Jenkin core obtained was 32.5 cm long and was sectioned into 2 mm increments from 0-20 cm and 1 cm increments from 20 cm to the base.

2.1.2.4 Loch Ness.

A Mini-Mackereth core was taken from Urquhart Bay (LN/East), Loch Ness, as part of a project run by the Institute of Freshwater Ecology (Whiteford, 1996). The core, taken on 19/11/90 at a depth of 170 m, was 128 cm in length and was sectioned at 2

cm increments throughout. It is thought that a section from the top of the core may have been lost during sampling.

2.1.3 Stream sediment samples.

Samples of sediment were collected in August 1997 from rivers and streams flowing into Loch Lomond (via the River Falloch) and Loch Tay (northern shore). The samples were collected using a trowel to scoop out fine-grained material which had been deposited at the edges of the rivers and streams. The samples were placed in polythene bags and sealed for transport back to the laboratory. These samples were taken in order to characterise the stable Pb isotope signature of different sources to the lochs. Sediment samples from the inflowing rivers and streams on the southern shore of Loch Tay were previously collected in 1995/6 (Lancaster, 1996).

2.1.4 Physical parameters at some of the coring sites.

For some of the lochs, measurements of the temperature, pH, conductivity, dissolved oxygen and total dissolved solids of the overlying surface water were made using portable meters. A summary of this information is shown in Table 2.1.

2.2 Drying and milling of samples.

2.2.1 Loch sediments.

Each sample was placed in a pre-weighed, acid-washed plastic boat and dried for 48 hours at 35-40 ^{o}C. Both the wet and dry weights were recorded. In order to ensure complete homogeneity, the samples were finely ground. For the 3 mm sections this was achieved by placing each sample in the polythene bag in which it was to be stored and, after carefully sealing, gently rolling it with a "rolling-pin" until finely ground. This *in situ* method prevented loss of sample as a result of transfer to and from a mortar. The 1-, 2- and 5- cm sections were too large and solid for this method and were therefore ground using the traditional mortar and pestle method.

Table 2.1 Physical parameters measured in the water overlying some of the sediment cores collected.

	Loch Lomond (LL/South) 26/11/91	Lake of Menteith (LMM) 13/11/96
Temperature / °C	8.25	7.5
Conductivity / μs	72.8	114.6
Dissolved Oxygen / %	102.0	86
pH	6.15	7.5
TDS / mg l^{-1}	36.4	not analysed

2.2.2 Stream sediment.

Each sample was dried at 35-40 °C before sieving through a 100 mesh sieve (150 μm).

2.2.3 Reference standards.

Two large samples, made up from unused core material at each of the Loch Lomond north and Loch Tay east sites, were dried separately at 35-40 °C. The samples were ground using a mortar and pestle and thoroughly homogenised to give two 'in-house' reference standards labelled LL/REF and LT/REF. A certified reference material (Lake sediment SL-1) obtained from the International Atomic Energy Agency (IAEA).

2.3 Preparation and analysis of sediment samples for γ-spectrometry.

2.3.1 Preparation of sediment samples.

The Jenkin cores were used for Loch Lomond south, Lake of Menteith, Loch Tay east and west. For Loch Lomond north and Loch Ness the Mini-Mackereth core was used. (Ref. S3001A-048A, EJ001-110, LTJ001-016, NM001-075 and Ntop-N63). A sample of each section was accurately weighed out and placed into a labelled polypropylene sample container and sealed. Where the sample weight was greater than 5 g the sample was pressed into a disc using a 20 tonne hydraulic press, to give a uniform geometry and to minimise the sample height, thereby maximising the detection efficiency. The weights taken corresponded to one of the following and were accurate to within +/- 0.005g: 0.500, 1.000, 1.5000, 2.000 or 2.500g.

A series of standards were prepared by "spiking" appropriate weights of sediment with solutions of known activity of the radionuclides being analysed. The spike solutions were traceable to primary standards purchased from Amersham

International plc. The standards prepared corresponded to each of the sample weight categories and were used to calculate the detection efficiency of the spectrometer. The spiking was carried out by adding the required radionuclide, as a small volume of solution (typically 0.5 ml), to a known mass of dry sediment. The sediment used was taken from the base of the core where no ^{137}Cs was present or, in the case of ^{210}Pb, where it was at background levels and allowance was made for this. This minimises the possibility of systematic errors introduced by density or average z-value variations between samples and standards. The spiked sediment was then dried at 40 °C and thoroughly homogenised before being pressed into discs as described for the samples.

2.3.2 Analysis of sediment samples by γ-spectrometry.

For γ-spectrometry analysis, the sample containers were placed in a reproducible position on the protective Al outer container of a High Purity n-type Germanium (HPGe) gamma photon detector, which was covered by a plastic film to avoid contamination. A graded Pb-Cd-Cu shield (10 cm Pb) was used to reduce the background count rate (the Cd/Cu lining absorb any x-rays induced in the shield). The detector used was a Tennelec 35 % relative efficiency crystal with a resolution (FWHM) of 1.91 keV at 1.33 MeV and 652 eV at 22 keV. The spectra were recorded using an EG & G Ortec multi channel buffer (MCB), which records spectra from 4 detectors simultaneously, storing the data in 4 memory segments. The spectra produced were analysed using the EG & G Ortec peak search and analysis programme Gamm Vision.

2.4 Preparation and analysis of sediment samples for α-spectrometry.

The 2- and 3-mm sections for the Loch Lomond (north and south) and Loch Tay east cores were found to be too small to yield ^{210}Pb data of acceptable precision using γ-spectrometry. These samples were therefore analysed by α-spectrometry of ^{210}Po,

and ^{210}Pb activities inferred with the assumption that a state of secular equilibrium exists between ^{210}Pb and ^{210}Po.

2.4.1 Preparation of sediment samples for α-spectrometry.

The samples were accurately weighed into a beaker, wetted with 6M HCl (Analar), spiked with 1 ml of a known activity of $^{208,209}Po$ (traceable to a primary standard from Amersham International plc), then made up to 50 ml with 6M HCl (Analar). This solution was taken to dryness by heating gently on a hotplate for 3-4 hours. About 50 ml of aqua regia was added then dried by heating for 2-3 hours. 10-20 ml of H_2O_2 was added and again heated to dryness for 1-2 hours. The resulting residue was taken up in 6M HCl (Analar), heated for 30 minutes to leach out the soluble material, then allowed to cool and settle before filtering through a Whatman 540 filter paper. The solution was extracted with diisopropyl ether until the aqueous phase became clear (to remove Fe). After the removal of the organic phase, the sample was taken to dryness to remove any residual diisopropyl ether. Finally the residue was taken up in about 40 ml of water (pre-treated by reverse osmosis) and 5 ml of 30 % hydroxylammonium chloride solution. A thin source was prepared by spontaneous deposition of the polonium isotopes onto a copper foil (1 cm^2) which was placed in the solution and stirred (using a magnetic stirrer) for 1 hour at 95 °C (the volume was maintained during this stage). The Cu foil was removed from the plating solution, rinsed with cold water and dried under a heat lamp (MacKenzie and Scott, 1979).

2.4.2 Analysis of sediment samples by α-spectrometry.

α-spectrometry was performed by fixing the Cu foil to a planchette and placing this on the sample holder platform in the counting chamber of a Canberra Instruments Quad Alpha detector. This detector is a passivated ion-implanted planar silicon detector with a resolution (FWHM) of 22 keV and a depletion depth of 100 μm. The chamber was evacuated and a voltage of 30 V applied to the detector. The α-

spectrum was recorded using a 16 input mixer-router coupled to a PC based Canberra Instruments multi channel analyser. The spectra produced were analysed by printing out "regions of interest" followed by manual calculation of peak areas. Backgrounds were recorded before and after each analysis and appropriate corrections were made to the observed count rates. Blank analyses were also performed but these gave insignificant count rates above background.

2.5 Preparation and analysis of samples for the determination of heavy metals by flame atomic absorption spectrometry.

2.5.1 Acid digestion procedure for samples.

The following method was used to digest and prepare each of the samples from the Mini-Mackereth cores from Loch Lomond south (ref. S3B 001-116), Loch Lomond north (ref. NM001-075), Loch Tay east (ref. EM001-141), Loch Tay west (ref. LTM001-090), Lake of Menteith (ref. LMM001-121) and Loch Ness (ref. NTop-N63) for the determination of heavy metals by FAAS:

0.3-0.5 g of sample was placed in a 100 ml pyrex-glass beaker. After the addition of 8M HNO_3 (20 ml Analar), each sample was gently refluxed at ~90 °C for 2 hours on a hot-plate (covered with a watch glass). Concentrated HCl (10 ml Analar, 12M) was then carefully added and the samples refluxed for a further 1 hour before leaving to cool.

After cooling, the samples were filtered through Whatman No.40 ashless filter papers into clean 100 ml pyrex-glass beakers, washing through with 1M HCl. The samples were reheated and 5-10 ml portions of the concentrated HC1 (12M) were added until brown fumes of $NO_{2(g)}$ had ceased to appear (this took 3-4 hours on average).

At this point the solutions were evaporated down to 1 ml and transferred to 25 ml volumetric flasks, making up to the mark with 1M HCl. Finally the solutions were transferred into 30 ml polypropylene tubes for storage. The samples at this stage were usually a pale yellow colour.

Comments about method:

- All glassware was acid washed (4 hours heated in 5M HNO_3 followed by 4 hours heating in Milli-Q, 18 MΩ (0.06μS cm^{-1}), deionised water).
- 1M HCl was prepared by taking 83 ml of concentrated HCl (11.6M, Analar) and making up to 1000 ml with deionised water.
- 8M HNO_3 was prepared by a 1:1 dilution of concentrated HNO_3 (15.9M, Analar) with deionised water.
- If any of the samples accidentally evaporated to dryness, it was redissolved in 3-4 ml of concentrated HCl (11.6M, Analar) then evaporated to 1 ml.
- A blank and an aliquot of one of the 'in-house' reference standard LL/REF were taken through the complete digestion procedure with each batch of samples prepared.

2.5.2 Determination of heavy metals by FAAS.

Concentrations of Fe, Mn, Pb, Cu and Zn were determined for each sample solution using FAAS. A Pye Unicam SP9-800 (with D_2 background correction) was used for Loch Lomond south, Lake of Menteith, Loch Tay west and Loch Ness. An ATI Unicam Solaar 929, (with D_2 background correction) was used for Loch Lomond north and Loch Tay east. Cd was also determined in the Loch Lomond north, Lake of Menteith, Loch Tay east and west and Loch Ness cores. An air-acetylene flame was employed in all cases. Table 2.2 shows a summary of the instrumental conditions required for each element.

Table 2.2 Instrumental parameters required for FAAS.

Element	Wavelength	Bandpass	Burner Rot.	Background	Burner Type
Fe	346.6 nm	0.2 nm	30°	No	100 mm
Mn	403.1 nm	0.2 nm	20°	No	100 mm
Pb	217.0 nm	0.5 nm		Yes	100 mm
Cu	324.8 nm	0.5 nm		No	100 mm
Zn	213.9 nm	0.5 nm	10°	Yes	100 mm
Cd	228.8 nm	0.5 nm		Yes	50 mm STAT Tube

Standard solutions for each element were made up immediately prior to analysis, by diluting the appropriate 1000 mg l^{-1} Spectrosol (Fisons) stock solution with 1M HCl. The standards prepared covered the concentration range expected in the samples and were within the linear concentration range for each metal. Hence the absorbances obtained were used to prepare a calibration graph using a linear regression fit; from this, the concentrations of the unknown samples were calculated. The results were corrected for weight and volume and expressed in mg kg^{-1} using the following equation:

$$[\text{metal}]\ \text{mg kg}^{-1} = [\text{metal}]\ (\text{mg l}^{-1}) \times \text{volume (ml)} / \text{weight (g)}$$

Before the analysis of Fe, all samples required a 3-fold dilution with 1M HCl in order to bring them into a suitable linear range for the highest concentration standard available.

During the analysis of any set, a sample from a previously analysed set was re-run in order to check for reproducibility of results. The precision for these re-runs is typically < 4 % RSD.

The within set reproducibility was examined by analysing 2 sets of the 'in-house' reference sample LL/REF, the results of which are shown in Table 2.3. The precision for the within set reproducibility was better than 3 % RSD for Fe, Mn, Pb, Cu and Zn and 7% RSD for Cd. The reference samples analysed with each set of samples served as a measure of the long-term reproducibility of the digestion and analysis procedures. The results from these samples are given in Table 2.4. The precision for the long-term stability was < 5.6 % RSD.

Table 2.3 Within set reproducibility for the determination of heavy metals in reference material LL/REF.

Sample Code	Wt /g	Fe / %	Mn / %	Pb / mg kg^{-1}	Cu / mg kg^{-1}	Zn / mg kg^{-1}
96/001/1	0.49	7.39	0.19	127.5	52.74	336.6
96/001/2	0.499	7.38	0.192	127.1	54.14	343.8
96/001/3	0.505	7.25	0.186	124.4	52.07	331.9
96/001/4	0.507	6.95	0.184	128.2	52.12	331.2
96/001/5	0.495	7.34	0.195	123.5	53.46	340.9
96/001/6	0.507	6.99	0.191	122.6	52.88	332.0
96/001/7	0.496	7.23	0.193	125.7	54.10	341.4
96/001/8	0.496	7.23	0.196	125.0	53.79	339.2
Mean (x)		7.22	0.191	125.5	53.16	337.1
STDEV		0.17	0.004	1.99	0.83	4.93
% RSD		2.32	2.18	1.59	1.57	1.46
96/002/09	0.498	6.81	0.186	120.3	50.92	327.7
96/002/10	0.497	7.15	0.196	124.8	53.00	334.9
96/002/11	0.501	6.85	0.188	118.3	51.58	329.0
96/002/12	0.502	6.88	0.193	122.9	52.32	328.0
96/002/13	0.509	7.02	0.191	125.4	52.69	333.8
96/002/14	0.501	6.85	0.187	122.5	52.02	333.1
96/002/15	0.502	6.88	0.187	121.3	51.24	323.9
96/002/16	0.506	6.78	0.185	118.6	50.13	322.9
Mean (x)		6.90	0.189	121.8	51.74	329.2
STDEV		0.12	0.004	2.64	0.96	4.48
% RSD		1.78	2.027	2.16	1.85	1.36

Table 2.4 Long-term reproducibility of heavy metal analysis for reference material LL/REF.

Sample Code	Wt / g	Fe / %	Mn / %	Pb / mg kg^{-1}	Cu / mg kg^{-1}	Zn / mg kg^{-1}	Cd / mg kg^{-1}
96/001	0.496	7.23	0.196	125.0	53.8	339.2	2.56
96/002	0.506	6.78	0.185	118.6	50.1	322.9	2.43
96/003	0.505	6.70	0.188	121.3	50.9	329.3	2.36
96/004	0.501	6.92	0.192	118.6	51.5	319.4	2.42
96/005	0.504	6.60	0.182	113.6	49.5	318.5	2.32
96/006	0.502	6.55	0.187	120.1	49.1	339.4	2.44
96/007	0.503	6.95	0.194	120.9	n/a	326.9	2.35
96/008	0.504	7.00	0.191	124.4	49.8	328.9	2.30
96/009	0.503	6.65	0.189	129.9	56.6	372.3	2.40
96/010	0.509	7.09	0.191	128.4	53.8	n/a	2.35
96/011	0.505	6.97	0.194	127.1	52.7	328.5	2.43
96/012	0.506	6.62	0.186	119.2	50.3	321.3	2.26
96/013	0.505	6.92	0.193	121.9	51.9	339.4	2.27
96/014	0.494	6.24	0.186	125.5	52.5	327.9	2.37
96/015	0.508	6.17	0.198	127.5	55.1	330.9	2.15
96/016	0.504	6.17	0.195	132.8	52.4	327.8	2.26
96/017	0.499	6.28	0.195	125.1	50.6	339.2	2.39
96/018	0.300	6.58	0.191	131.4	50.3	314.5	2.47
96/019	0.302	6.41	0.202	125.6	51.9	374.0	2.27
96/020	0.255	6.35	0.216	128.6	50.6	323.2	2.37
96/021	0.251	6.20	0.201	133.7	48.6	333.7	2.23
96/022	0.256	6.42	0.204	125.6	51.5	319.1	2.25
96/023	0.303	6.32	0.186	120.0	49.5	321.4	2.19
96/024	0.500	6.21	0.181	122.0	48.7	304.9	2.17
96/025	0.255	5.82	0.191	119.1	50.1	323.1	2.24
96/026	0.249	6.49	0.195	123.0	49.8	315.8	2.26
96/027	0.248	5.75	0.184	124.8	49.8	342.7	2.07
96/028	0.248	6.16	0.188	114.8	47.1	320.4	2.48
96/029	0.248	6.68	0.178	117.4	48.1	301.9	2.30
96/030	0.252	6.75	0.187	115.0	48.4	332.4	2.28
96/031	0.252	6.72	0.184	129.5	50.7	303.5	2.35
96/032	0.249	6.58	0.190	121.4	49.7	340.2	2.41
96/033	0.251	6.90	0.191	126.5	57.8	329.9	2.26
96/034	0.253	6.77	0.187	127.6	50.8	331.1	2.31
96/035	0.249	6.50	0.184	116.3	50.9	321.7	2.00
97/036	0.253	6.44	0.190	139.6	56.0	341.2	2.16
97/038	0.252	6.46	0.180	104.2	56.2	356.0	2.14
97/039	0.248	6.11	0.200	105.7	50.6	359.0	2.10
97/040	0.253	6.22	0.190	105.0	51.5	355.4	2.08
97/040b	0.253	6.13	0.180	107.0	51.8	345.0	2.08
Mean (x)		6.54	0.191	123.5	50.8	328.5	2.29
STDEV		0.35	0.008	5.2	2.1	15.9	0.13
% RSD		5.4	4.0	4.2	4.1	4.9	5.6

2.6 Preparation and analysis of samples for determination of stable lead isotopes by inductively coupled mass spectrometry.

2.6. Acid digestion procedure for samples.

The following method was used for the preparation of samples for the ICP-MS determination of stable Pb isotope ratios. The following sediment samples were used: Loch Lomond south (ref. LL/S3B 001-116), Loch Lomond north (ref. LL/NM001-075) and Loch Tay east (ref. LT/EM001-141), Loch Tay west (ref. LTM001-090) Lake of Menteith (ref. LMM1-121), Loch Ness (ref. Ntop-N63) and all stream sediment samples.

0.09-0.11 g of sample was placed in a 100 ml pyrex-glass beaker, dried at 100 ^{o}C for 1 hour then ashed at 450 ^{o}C for 4 hours. After cooling, 8M HNO_3 (30 ml Aristar) was added to each sample then gently refluxed at ~90°C for 2 hours, covered with a watch-glass, on a hot-plate. The samples were allowed to cool, before filtering through Whatman No. 40 ashless filter papers, into clean 100 ml pyrex-glass beakers.

The samples were placed back on the hot-plate and evaporated down to 1 ml before transferring to either 100, 50 or 25 ml volumetric flasks and making up to the mark with 2% v/v HNO_3 (Aristar).

With each set of samples a standard reference material (Lake sediment SL-1, International Atomic Energy Agency), an 'in-house' reference standard (LL/REF or LT/REF) and a sample blank were also prepared.

Comments about the method:

- The 2 % v/v HNO_3 was made up by diluting 20 ml HNO_3 (15.9M, Aristar) to 1000 ml with deionised water (18 MΩ (0.06μS cm^{-1})).
- If the samples accidentally went to dryness during evaporation, they were redissolved with 3-4 ml HNO_3 (15.9M, Aristar) and evaporated down to 1 ml.

2.6.2 Determination of lead by FAAS.

The elemental Pb concentration in each sample was initially determined using FAAS (ATI Unicam Solaar 929, with D_2 background correction). The instrumental conditions were as shown in Table 2.2, with the exception that the burner used had a 50 mm slot, fitted with a slotted atom trap tube (STAT-Tube) for increased sensitivity. Standards were prepared immediately prior to analysis by diluting 1000 mg l^{-1} Pb standard solution (Spectrosol, Fisons) with 2 % v/v HNO_3.

The samples were then diluted with 2 % v/v HNO_3 to the optimum range (30-60 µg l^{-1}) for isotopic analysis by ICP-MS.

2.6.3 Determination of stable lead isotopes by ICP-MS.

The pre-diluted samples were analysed for stable Pb isotopes ^{206}Pb, ^{207}Pb and ^{208}Pb using a VG PlasmaQuad2 (based at SURRC, East Kilbride) for Loch Lomond south and Loch Tay west. A VG PlasmaQuad3 (based at The University of Edinburgh Chemistry Department) was used for Loch Lomond north, Loch Tay east, Lake of Menteith and Loch Ness. Both the PlasmaQuad2 and the PlasmaQuad3 use a Gilson Minipuls3 peristaltic pump to introduce the samples into the instrument via a Meinhard nebuliser. The parameters for the set up of the two instruments are shown in Table 2.5. The initial raw data produced by each instrument are in the form of total counts.

The instrument was calibrated at the beginning of each run using a standard reference solution SRM 981 (NIST). The reference material is initially provided as a piece of solid, pure lead which required to be dissolved. The method of dissolution used was as follows:

Table 2.5 Parameters for ICP-MS analysis.

PQ2	PQ3
Scanning Mode	Peak jumping mode
Dwell time: 80 μs	Dwell time: 2.0 ms
Channels: 19 per amu.	Points/peak: 1
Mass range: 201.6 to 211.4 amu.	DAC step: 5
Reflected power: 1-3 W	Mode: Pulse counting
Argon flow: 0.76-0.84 l min^{-1}	Mass range: 203.6 to 209.4 amu.
Uptake rate 0.55 ml min^{-1}	Reflected power: 1-3 W
	Argon flow: 0.76-0.84 l min^{-1}
	Uptake rate 0.55 ml min^{-1}
Method:	Method:
Auto sampler (Gilson)	Auto sampler (Gilson)
No. of repeats: 5	No. of repeats: 5
Settle time: 30 s	Settle time: 30 s
Uptake time: 120 s	Uptake time: 150 s
Acquisition time: 30 s	Acquisition time: 60 s
Wash out time: 180 s	Wash out time: 30 s

The total sample (1.272 g) was placed in an acid washed pyrex beaker along with 20 ml of 4M HNO_3 (Aristar). The sample was heated until dissolved, whereupon an excess of 2 % v/v HNO_3 (Aristar) was added to the still hot solution before being left to cool. If the solution was left to cool or evaporate before addition of 2 % v/v HNO_3, it was found that the lead precipitated out as a white powder of the oxide. Once the solution had cooled to room temperature, it was decanted into a 1 l volumetric flask and made up to the mark with 2 % v/v HNO_3 to give a primary standard of 1272 mg kg^{-1}. A 12.7 mg kg^{-1} secondary stock solution was prepared from the primary standard by diluting 1 ml of the primary standard to 100 ml with 2 % v/v HNO_3 (Aristar). The final working solution of approximately 60 μg l^{-1} was freshly prepared on each instrumental analysis day by diluting 500 μl of the secondary stock solution to 100 ml with 2 % v/v HNO_3 (Aristar).

The reference material SRM 981 has the following certified isotope abundance and ratios:

Isotope Abundance / % :		Atom Ratios:	
206	24.1442 +/- 0.0057	$^{206}Pb/^{207}Pb$	1.093
207	22.0833 +/- 0.0027	$^{208}Pb/^{207}Pb$	2.370
208	52.3470 +/- 0.0086	$^{208}Pb/^{206}Pb$	2.168

A blank solution of 2 % v/v HNO_3 (Aristar) was analysed at the beginning of the run and the counts obtained for each isotope were subtracted from the counts obtained for each of the SRM 981 standard results. The PQVision software then uses the counts obtained to calculate the ratios of the standard and to calculate a bias factor to take into account any deviation from the certified values caused by mass fractionation. Mass fractionation is caused by the mass spectrometer having different sensitivities to different isotopes. The mass bias for the ratios $^{206}Pb/^{207}Pb$, $^{208}Pb/^{207}Pb$ and $^{208}Pb/^{206}Pb$ were typically 1.000, 1.050 and 1.050, respectively. The samples were blank corrected using the blank that was prepared with each set. The PQVision

software then calculates the ratios and corrects for mass bias. The standard deviation of the 5 readings for each sample provides a measure of the internal precision.

The standard reference material SL-1 analysed with every set, along with the 'in-house' reference materials LL/REF and LT/REF, gave a measure of the long-term stability and precision of the digestion and analysis procedures. The stable lead isotope ratio data for these samples are given in Tables 2.6, 2.7, and 2.8, respectively, and are shown graphically in Figures 2.4, 2.5 and 2.6, respectively.

Table 2.6 Stable lead isotope ratios for IAEA reference material Lake Sediment SL-1.

Set Code	Wt / g	Pb/mgkg^{-1}	$^{206}Pb/^{207}Pb$	σ_{n-1}	$^{208}Pb/^{207}Pb$	σ_{n-1}	$^{208}Pb/^{206}Pb$	σ_{n-1}
97/046a	0.108	34.5	1.215	0.0012	2.467	0.0018	2.031	0.0032
97/046b	0.106	34.2	1.215	0.0015	2.470	0.0061	2.032	0.0026
97/047a	0.110	27.4	1.217	0.0024	2.479	0.0036	2.036	0.0023
97/047b	0.109	23.4	1.222	0.0015	2.495	0.0046	2.042	0.0019
97/048	0.104	28.4	1.216	0.0006	2.477	0.0047	2.037	0.0031
97/049	0.106	28.4	1.213	0.0014	2.472	0.0003	2.038	0.0013
97/050	0.107	29.2	1.219	0.0011	2.483	0.0036	2.037	0.0021
97/051	0.092	38.5	1.219	0.0010	2.486	0.0015	2.040	0.0025
97/052	0.093	44.6	1.220	0.0030	2.494	0.0028	2.045	0.0040
97/054	0.099	56.8	1.219	0.0012	2.485	0.0009	2.038	0.0023
97/055	0.107	30.0	1.220	0.0013	2.490	0.0026	2.041	0.0018
97/057	0.099	31.9	1.220	0.0018	2.499	0.0021	2.046	0.0021
97/058	0.108	33.2	1.215	0.0006	2.469	0.0029	2.032	0.0016
97/060	0.106	27.2	1.217	0.0023	2.480	0.0049	2.038	0.0027
97/061	0.096	33.2	1.216	0.0017	2.478	0.0025	2.039	0.0028
97/062	0.094	31.7	1.215	0.0009	2.471	0.0017	2.034	0.0029
97/064	0.098	27.0	1.209	0.0012	2.473	0.0041	2.046	0.0027
97/065	0.096	42.2	1.215	0.0021	2.484	0.0035	2.044	0.0034
97/067	0.099	31.7	1.215	0.0028	2.477	0.0045	2.038	0.0018
97/068	0.100	33.0	1.221	0.0020	2.511	0.0061	2.057	0.0035
97/070	0.103	32.0	1.215	0.0014	2.498	0.0032	2.056	0.0016
97/071	0.101	28.9	1.218	0.0014	2.500	0.0031	2.053	0.0033
97/073	0.093	26.4	1.218	0.0013	2.495	0.0041	2.049	0.0027
97/074	0.097	27.9	1.216	0.0009	2.483	0.0028	2.041	0.0024
97/075	0.104	25.8	1.215	0.0010	2.482	0.0035	2.043	0.0015
97/076	0.104	34.8	1.212	0.0013	2.470	0.0040	2.038	0.0032
97/077	0.097	39.0	1.214	0.0015	2.472	0.0013	2.037	0.0026
97/078	0.098	21.5	1.211	0.0018	2.471	0.0039	2.040	0.0038
97/079	0.110	36.1	1.211	0.0016	2.461	0.0027	2.032	0.0036
97/080	0.106	29.4	1.212	0.0013	2.481	0.0017	2.048	0.0019
97/081	0.103	31.3	1.213	0.0007	2.494	0.0033	2.055	0.0035
97/082	0.097	21.4	1.214	0.0018	2.484	0.0022	2.046	0.0021
97/083	0.102	27.4	1.211	0.0023	2.477	0.0046	2.045	0.0017
97/084	0.107	35.7	1.212	0.0019	2.459	0.0032	2.028	0.0014
97/087	0.099	32.8	1.214	0.0012	2.474	0.0016	2.038	0.0016
97/088	0.111	27.9	1.218	0.0015	2.466	0.0048	2.025	0.0029
97/089	0.098	31.9	1.214	0.0034	2.478	0.0039	2.041	0.0040
97/090	0.095	30.1	1.216	0.0010	2.478	0.0030	2.038	0.0024
97/091	0.099	26.9	1.222	0.0016	2.494	0.0047	2.041	0.0029
97/093	0.102	28.8	1.210	0.0010	2.459	0.0032	2.033	0.0024
97/094	0.103	24.6	1.215	0.0011	2.498	0.0050	2.057	0.0026
97/095	0.101	28.2	1.214	0.0018	2.507	0.0038	2.064	0.0016
97/098	0.103	34.5	1.215	0.0017	2.514	0.0077	2.069	0.0042
97/099	0.107	29.6	1.214	0.0027	2.478	0.0051	2.041	0.0060
97/100	0.109	26.0	1.218	0.0018	2.476	0.0049	2.032	0.0033

Table 2.6 Stable lead isotope ratios for IAEA reference material Lake Sediment SL-1, continued.

Set Code	Wt / g	Pb/mgkg^{-1}	$^{206}Pb/^{207}Pb$	σ_{n-1}	$^{208}Pb/^{207}Pb$	σ_{n-1}	$^{208}Pb/^{206}Pb$	σ_{n-1}
97/101	0.098	31.5	1.215	0.0022	2.480	0.0041	2.041	0.0044
97/103	0.097	27.3	1.216	0.0021	2.467	0.0041	2.028	0.0017
97/104	0.093	36.8	1.221	0.0019	2.483	0.0047	2.034	0.0011
97/105	0.153	29.9	1.219	0.0040	2.490	0.0077	2.044	0.0056
97/106	0.146	29.6	1.215	0.0023	2.477	0.0036	2.038	0.0025
97/107	0.146	30.1	1.216	0.0018	2.461	0.0027	2.023	0.0040
97/108	0.105	38.1	1.202	0.0013	2.463	0.0029	2.049	0.0028
97/109	0.096	12.3	1.216	0.0003	2.487	0.0048	2.044	0.0036
97/110	0.096	28.9	1.217	0.0018	2.485	0.0035	2.042	0.0024
97/111	0.103	19.0	1.222	0.0015	2.476	0.0038	2.026	0.0036
Mean (x)		30.7	1.216		2.481		2.041	
STDEV		6.5	0.004		0.013		0.009	
% RSD		21.2	0.3		0.5		0.5	
Certified Values		37.7 +/- 7.4	1.215		2.469		2.032	
Viczian et al., 1990		33.1 +/- 4.0	1.214	0.012			2.035	0.02

Figure. 2.4 Mean data for standard SL-1 (a) Pb, (b) $^{206}Pb/^{207}Pb$, (c) $^{208}Pb/^{207}Pb$ and $^{208}Pb/^{206}Pb$.

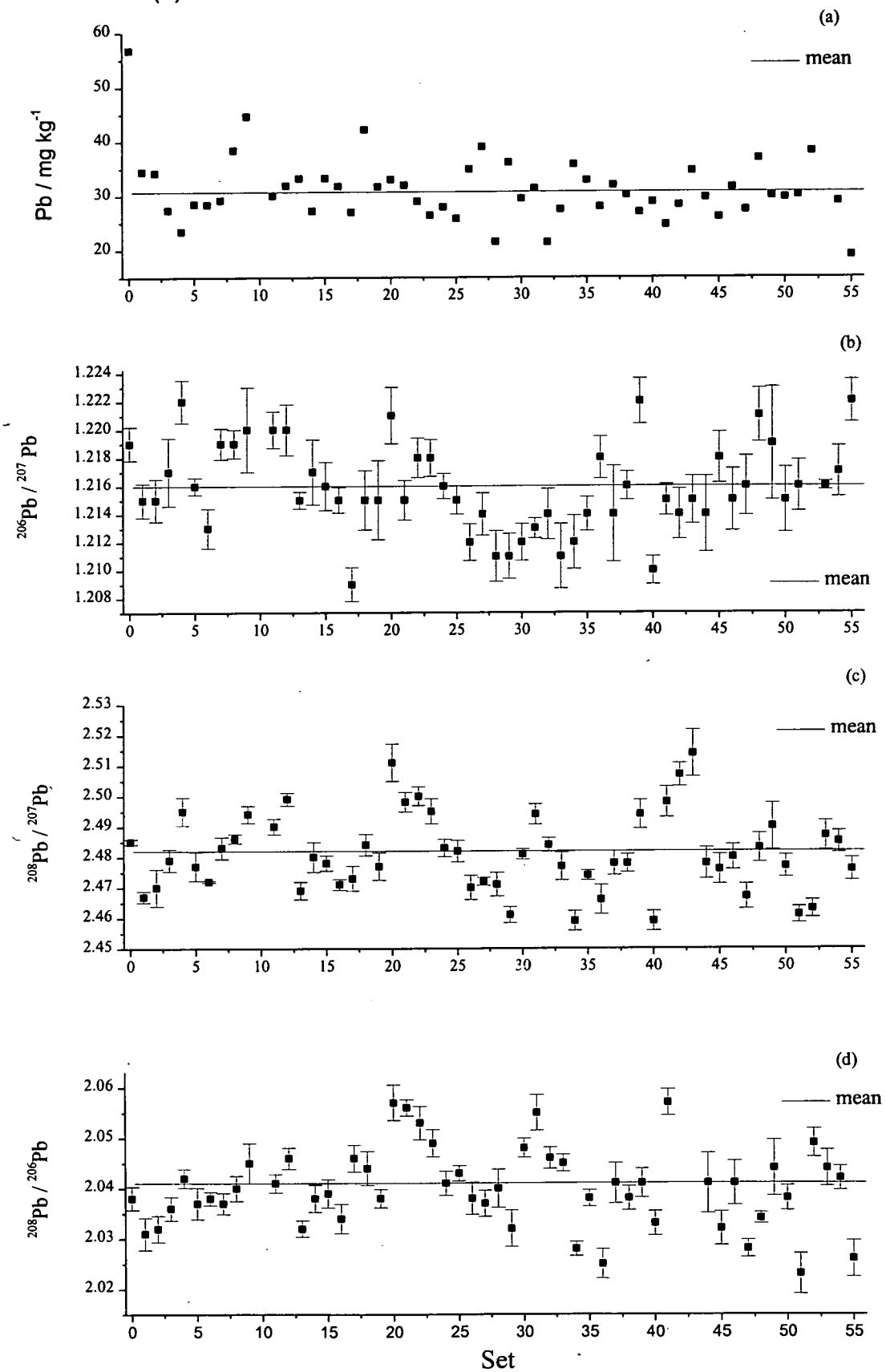

Table 2.7 Stable Pb isotope results for reference material LL/REF.

Set Code	Wt / g	Pb/ mg kg^{-1}	$^{206}Pb/^{207}Pb$	σ_{n-1}	$^{208}Pb/^{207}Pb$	σ_{n-1}	$^{208}Pb/^{206}Pb$	σ_{n-1}
97/046	0.104	105.9	1.141	0.0010	2.435	0.0019	2.134	0.0033
97/046	0.102	127.0	1.140	0.0014	2.432	0.0052	2.133	0.0027
97/047	0.101	118.2	1.142	0.0013	2.443	0.0055	2.139	0.0050
97/047	0.105	118.3	1.141	0.0013	2.440	0.0021	2.139	0.0035
97/048	0.102	113.6	1.141	0.0023	2.440	0.0049	2.139	0.0064
97/049	0.106	113.5	1.141	0.0018	2.441	0.0022	2.140	0.0031
97/050	0.110	112.9	1.136	0.0023	2.423	0.0066	2.132	0.0028
97/052	0.107	131.0	1.137	0.0019	2.433	0.0063	2.139	0.0080
97/054	0.107	149.0	1.140	0.0010	2.432	0.0133	2.134	0.0112
97/055	0.098	108.9	1.142	0.0007	2.436	0.0027	2.132	0.0026
97/057	0.102	112.7	1.142	0.0017	2.446	0.0061	2.142	0.0024
97/061	0.117	120.5	1.140	0.0016	2.434	0.0062	2.136	0.0065
97/065	0.095	120.9	1.140	0.0020	2.464	0.0029	2.162	0.0024
97/067	0.097	121.2	1.139	0.0010	2.433	0.0039	2.136	0.0040
97/068	0.098	150.9	1.144	0.0019	2.421	0.0071	2.166	0.0041
97/070	0.106	111.6	1.141	0.0007	2.458	0.0046	2.155	0.0047
97/071	0.094	123.7	1.142	0.0020	2.469	0.0084	2.162	0.0053
97/073	0.102	124.3	1.141	0.0015	2.449	0.0052	2.147	0.0019
97/074	0.100	112.1	1.143	0.0015	2.449	0.0075	2.143	0.0047
97/075	0.100	108.2	1.139	0.0020	2.442	0.0064	2.145	0.0033
97/076	0.098	112.3	1.140	0.0028	2.442	0.0102	2.143	0.0057
97/077	0.096	126.4	1.140	0.0023	2.446	0.0067	2.145	0.0056
97/078	0.105	115.4	1.137	0.0023	2.436	0.0116	2.143	0.0064
97/079	0.107	117.7	1.138	0.0017	2.434	0.0051	2.139	0.0046
97/080	0.102	128.0	1.142	0.0005	2.461	0.0014	2.155	0.0020
97/081	0.094	125.2	1.141	0.0017	2.477	0.0052	2.172	0.0052
Mean (x)		120.4	1.140		2.443		2.144	
STDEV		11.0	0.002		0.014		0.011	
% RSD		9.1	0.16		0.55		0.01	

Figure. 2.5 Mean data for standard LL/REF (a) Pb, (b) $^{206}Pb/^{207}Pb$, (c) $^{208}Pb/^{207}Pb$ and $^{208}Pb/^{206}Pb$.

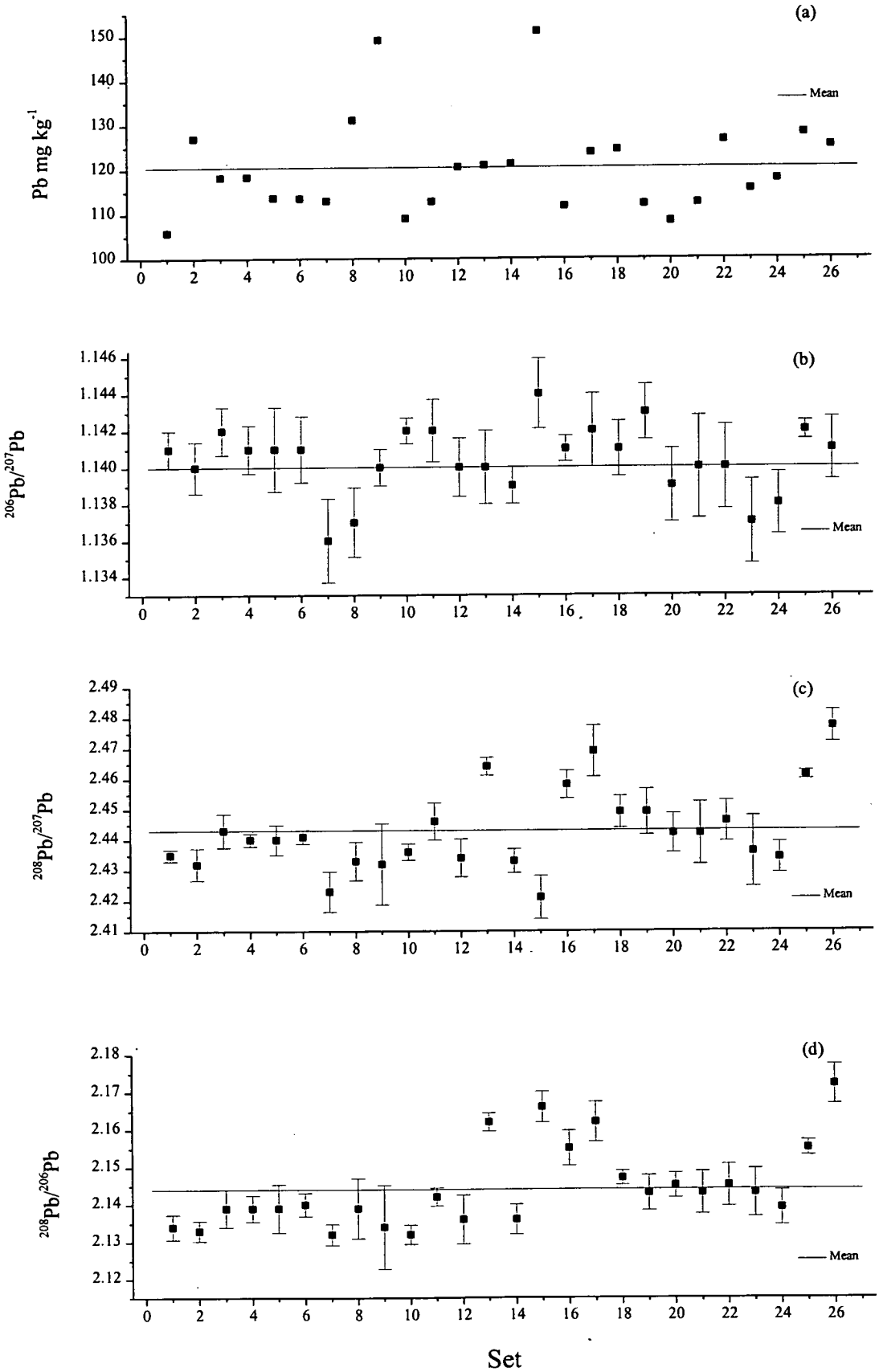

Table 2.8 Stable Pb isotope results for reference material LT/REF.

Set Code	Wt / g	Pb / mg kg^{-1}	$^{206}Pb/^{207}Pb$	σ_{n-1}	$^{208}Pb/^{207}Pb$	σ_{n-1}	$^{208}Pb/^{206}Pb$	σ_{n-1}
97/046	0.109	445	1.150	0.0026	2.449	0.0050	2.130	0.0013
97/046	0.109	462	1.150	0.0019	2.441	0.0038	2.124	0.0030
97/047	0.104	443	1.150	0.0016	2.449	0.0028	2.130	0.0043
97/047	0.100	486	1.150	0.0014	2.448	0.0020	2.129	0.0023
97/048	0.097	421	1.152	0.0012	2.455	0.0036	2.132	0.0022
97/049	0.109	414	1.148	0.0014	2.442	0.0028	2.127	0.0025
97/050	0.116	446	1.145	0.0007	2.439	0.0022	2.130	0.0018
97/051	0.100	498	1.147	0.0017	2.430	0.0139	2.119	0.0095
97/058	0.099	454	1.150	0.0016	2.456	0.0017	2.136	0.0035
97/060	0.102	422	1.149	0.0015	2.452	0.0048	2.135	0.0030
97/062	0.105	475	1.147	0.0020	2.428	0.0134	2.117	0.0104
97/064	0.097	362	1.149	0.0019	2.433	0.0204	2.117	0.0149
97/082	0.109	471	1.147	0.0018	2.455	0.0132	2.14	0.0125
97/083	0.100	455	1.149	0.0005	2.457	0.0032	2.138	0.0023
97/084	0.097	483	1.149	0.0016	2.449	0.0047	2.131	0.0042
97/086	0.106	455	1.149	0.0021	2.447	0.0159	2.129	0.0104
97/087	0.105	480	1.148	0.0011	2.447	0.0055	2.132	0.0031
97/088	0.105	462	1.149	0.0015	2.438	0.0051	2.139	0.0036
97/089	0.099	470	1.148	0.0022	2.441	0.0116	2.126	0.0106
97/090	0.102	432	1.149	0.0025	2.452	0.0063	2.134	0.0024
97/091	0.101	434	1.156	0.0030	2.468	0.0142	2.135	0.0088
97/093	0.099	416	1.150	0.0018	2.454	0.0021	2.133	0.0023
97/094	0.100	414	1.150	0.0011	2.468	0.0064	2.162	0.0056
97/095	0.110	446	1.149	0.0017	2.473	0.0065	2.153	0.0031
Mean (x)		448	1.149		2.449		2.132	
STDEV		30	0.002		0.011		0.010	
% RSD		6.7	0.18		0.47		0.47	

Figure. 2.6 Mean data for standard LT/REF (a) Pb, (b) $^{206}Pb/^{207}Pb$, (c) $^{208}Pb/^{207}Pb$ and $^{208}Pb/^{206}Pb$.

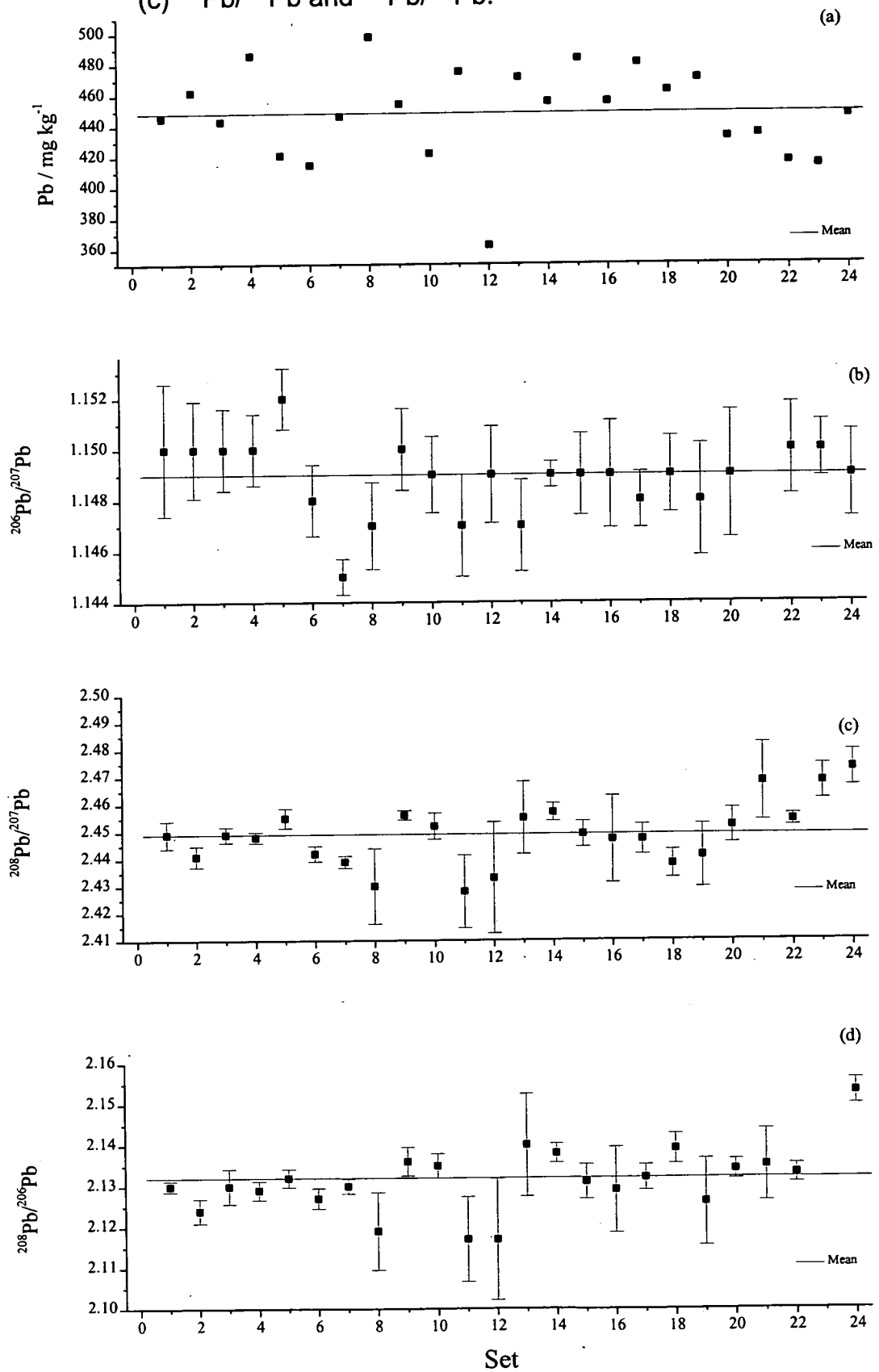

2.7 CHN Elemental analysis.

Selected samples from the Mini-Mackereth cores for each of the study sites were analysed for total carbon and nitrogen using a Perkin Elmer 2400 CHN analyser. 2 mg of sample were accurately weighed out into ultra-clean tin capsules (8x5 mm). The capsules were sealed, taking care to exclude as much air as possible. The samples were then sequentially placed into the analyser which had previously been calibrated against cyclohexanone-2,4-dinitrophenylhydrazone and acetanilide. The precision of the instrument is ± 0.3 %.

2.8 X-Ray diffraction.

Samples from each of the cores from Loch Lomond north and south, Lake of Menteith, Loch Tay east and Loch Ness were selected for XRD. Approximately 0.3 g of sediment was placed in an agate mortar along with approximately 2 ml of acetone and ground to a paste with an agate pestle. Five drops of the sediment paste were dropped onto a glass disc then left to dry. As the acetone evaporates off, it leaves behind a thin film of the sediment on the disc. The disc was placed on a metal holder and loaded into the X-Ray diffractometer (Philips PW 1800 X-Ray diffractometer). The identification of a species from its powder diffraction pattern is based upon the position of the lines (in terms of θ or 2θ) and their relative intensities (Skoog, 1985). The identification of the crystals is empirical. Samples containing more than one crystalline compound are quite complicated to characterise, and in these situations various combinations of the more intense lines are required to be used until a match for individual compounds can be found.

2.9 Conclusions.

This chapter has described and validated the methods and techniques for sample collection and treatment and the determination of radionuclides, heavy metals, Pb isotopes and other relevant entities. The data for each of the lochs will be presented, discussed and compared in the following chapters.

Chapter 3 Loch Lomond.

3.1 Location.

Loch Lomond is situated 30 km north-west of Glasgow and lies some 8 km from the estuary of the River Clyde (Figs. 1.13 and 2.3).

3.2 Topography.

Loch Lomond (Fig 3.1) was formed by a glacier that moved southward from the Ben Lui area and deposited eroded material as a terminal moraine in the southern part of the loch near Balloch (Best and Traill, 1994). Its dimensions (Murray and Pullar, 1910) are 36.4 km in length, 8 km in breadth at its widest point and an area of 71 km^2, with its long axis lying north to south. Loch Lomond is the largest fresh water loch by area in Scotland.

The loch can be divided into two main areas, upper and lower, or northern and southern (Slack, 1954), the two being divided by a shallow bar consisting of Ben Ledi Grits. The bar runs east to west from Rowardennan to Inverbeg. Geologically the loch is split by one of Scotland's major faults, the Highland Boundary Fault, which runs south-westerly from Balmaha to Arden (MacDonald, 1994).

The northern end of the loch is a deep narrow trough containing no islands and can be split into two subsidiary basins; the Ardlui basin (50 m depth) and the Tarbet basin (190 m depth). Both of the basins consist of metamorphosed mica-schists and shales derived from the Dalradian Series (Farmer, 1994). The southern, or lower, end of the loch consists of three basins and contains several groups of islands. This section of the loch overlies sedimentary rocks of Devonian and Lower Carboniferous ages including Lower and Upper Old Red sandstone, basal Carboniferous sediments of the Inverclyde Group and the overlying volcanic rocks of the Clyde Plateau (MacDonald, 1994). The first basin runs south from the bar at Inverbeg to the first

group of islands and is termed the Luss Basin and has a maximum depth of 60 m. The second, the Strathcasheil Basin, covers the U-shaped island group and has a maximum depth of about 40 m. The third basin, the Fault Basin (20-30 m in depth), covers the remaining wider end of the loch and is traversed by the Highland Boundary Fault. A line of outcropping islands consisting of Old Red Conglomerates follows the fault. The fault itself is characterised by extensive marginal terraces of pebbles, gravel or sand (Slack, 1954).

The southern basins are less oligotrophic than the northern basin and are more biologically productive (Farmer and Lovell, 1986). The Luss Basin is thermally stratified from June until November (Slack, 1954) in the range of 7.4-8.5 °C. Stratification of the Fault Basin is of a much shorter duration due to the prevailing winds having a mixing effect in this, the shallower part of the loch, thus the thermal gradients are easily broken down. The bottom sediments range from brown muds, with a thin near-surface rust-red layer, in the south, to black micaceous oozes, overlain by thin dark-brown unconsolidated material, in the north.

The main inflows to the loch are from the Douglas Water and the River Endrick to the southern section, and the River Falloch to the northern section. The main outflow from the loch is to the Clyde Estuary via the River Leven.

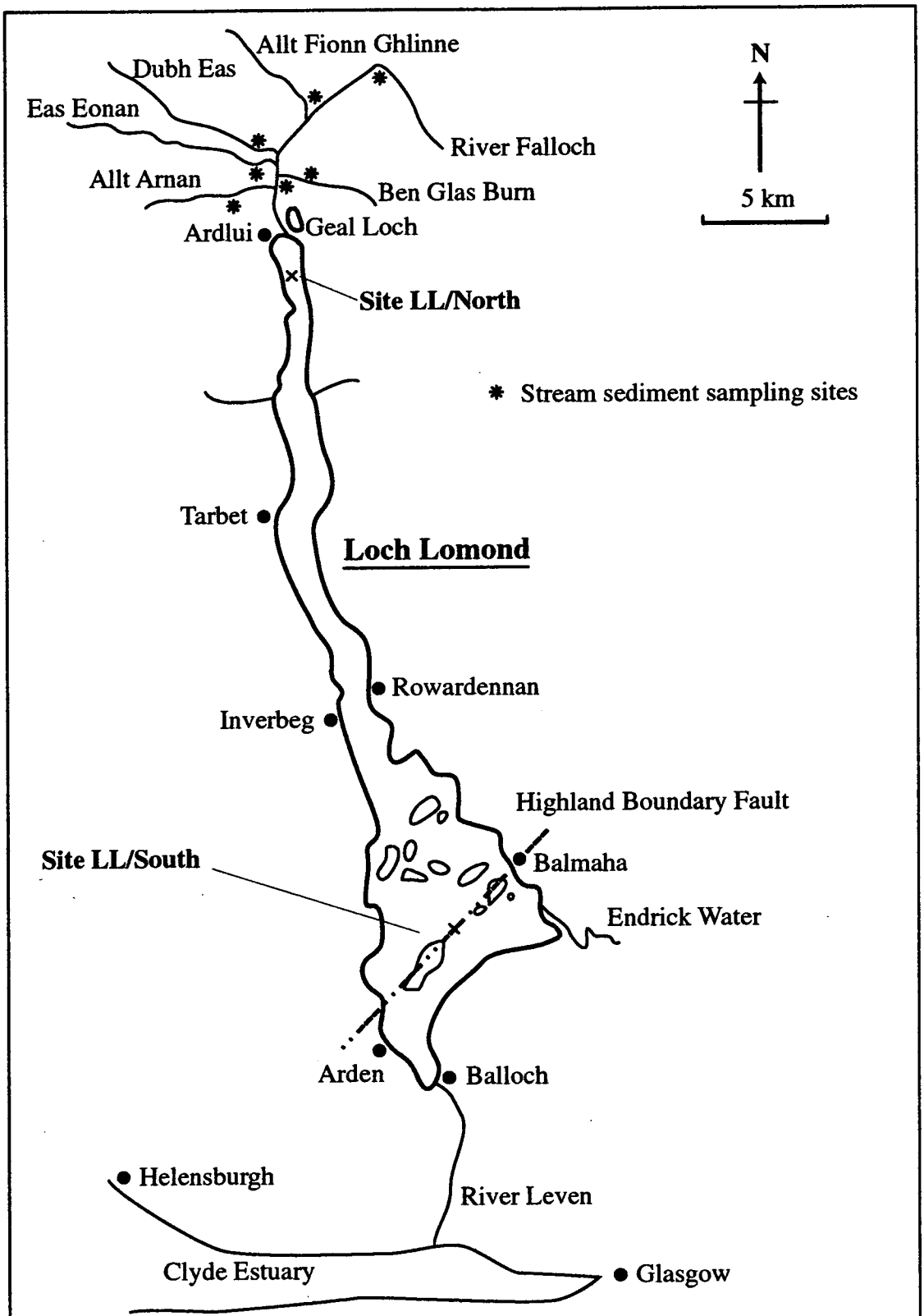

Figure 3.1 Location of core and stream sediment sites for Loch Lomond.

3.3 Contamination and pollution sources.

Due to its proximity to the west-central Scotland industrial belt, Loch Lomond received contaminants emanating from the heavy industry once present in the area. Industrialisation began in the middle of the 17th Century and underwent a rapid growth in the 18th Century which was carried through to the mid 20th Century (Farmer, 1994). In the immediate vicinity of the loch there have been a number of small industries, e.g. Fe-smelting bloomeries until the mid 18th Century and bleaching, dying and printing works from the early 18th Century to mid 20th Century (Farmer, 1994). To the north of Loch Lomond, Pb from Tyndrum was smelted at the foot of Glen Falloch for a short period of time in the middle of the 18th Century until a plant was erected closer to the mines. These local sources of contamination were however, small in comparison with the heavy industrialisation in the Clyde valley and surrounding areas (e.g. Lanarkshire, Dunbartonshire, North Ayrshire.). The majority of the heavy metal contaminants were released as a result of coal burning and Fe smelting, then later from chemical plants. A new source of Pb was introduced to the environment in about 1930 with the advent of alkyl Pb additives in petrol. Today the heavy industry is no longer present and lead additives are being phased out.

Radiocaesium has been released into the environment since 1945. Initial sources were from the atmospheric nuclear weapons testing programmes which started in 1945 and were at a peak in 1963. Radiocaesium from a second major source was introduced from the Chernobyl accident in April 1986, with atmospheric deposition in the UK occurring dominantly over a two week period in early May of that year. There will still be a contribution of radiocaesium and other heavy metals to the loch from the erosion of contaminated catchment soil.

3.4 Loch Lomond (South).

Two cores, one Jenkin (LL/S3A) and one Mini-Mackereth (LL/S3B), were collected on 26/11/91 from site LL/South (Fig. 3.1) as described in section 2.1.2.1. The Jenkin core was analysed for ^{134}Cs, ^{137}Cs and ^{210}Pb and the Mackereth core for Pb, Zn, Cu, Fe, Mn and stable Pb isotopes.

3.4.1 Results.

An initial inspection of the cores (LL/S3A and S3B) showed a series of bands of different coloured silts. The top 2 cm sections of the cores were brown/orange in colour, loosely packed and had a grainy texture, with a wet:dry ratio of 13-18. The next 2.5 cm had a black/brown mottled pattern, and appeared finer grained than the top layer with a lower wet:dry ratio of 5-6. From 4.5 cm to the base of the cores, the sediment appeared very fine grained and exhibited a series of transitions of different black and grey coloured bands. There was a micaceous component throughout the cores.

3.4.1.1 Radiocaesium.

Table 3.1 is a summary of the results for ^{134}Cs and ^{137}Cs activities in core LL/S3A. The errors are based on the counting error and a 1 % uncertainty from the spike. Figure 3.2 is a plot of the specific activities of ^{134}Cs and ^{137}Cs (Bq kg^{-1}) against depth (cm). ^{137}Cs was detectable to a depth of 11.4 cm (below 11.4 cm ^{137}Cs is less than twice σ_{n-1} and is therefore not significant) and the profile has two peaks at 1.95 and 5.85 cm. The peak at 1.95 cm is sharp, covering only 1.20 cm, with a maximum specific activity of 2000 ± 31 Bq kg^{-1}. The lower peak at 5.85 cm is broader, covering ~6 cm, and has a maximum specific activity of 1084 ± 17 Bq kg^{-1}. The ^{134}Cs penetrates to a depth of only 2.85 cm and forms a sharp peak at 1.95 cm coincident with the upper ^{137}Cs peak and with a maximum specific activity of 193 ± 12 Bq kg^{-1}.

Table 3.1 Radiocaesium results for Loch Lomond (south) core LL/S3A.

Sample Code	Depth /cm	Wet wt /g	Dry wt /g	Mid cum. wt / g cm^{-2}	^{137}Cs / Bq kg^{-1}	σ_{n-1} ^{137}Cs	^{134}Cs / Bq kg^{-1}	σ_{n-1} ^{134}Cs
S3001A	0.0-0.3	20.816	0.711	0.010	628	33	54	27
S3002A	0.3-0.6	8.182	0.570	0.027	712	35	22	23
S3003A	0.6-0.9	10.196	0.848	0.046	758	44	54	31
S3004A	0.9-1.2	10.237	0.979	0.070	755	37	39	25
S3005A	1.2-1.5	12.059	1.137	0.098	1037	25	86	20
S3006A	1.5-1.8	13.085	1.432	0.133	1572	33	147	17
S3007A	1.8-2.1	14.862	1.878	0.177	2000	31	193	12
S3008A	2.1-2.4	12.916	1.926	0.228	1228	20	114	13
S3009A	2.4-2.7	12.621	1.932	0.279	634	17	38	9
S3010A	2.7-3.0	15.322	2.553	0.339	559	14	6	8
S3011A	3.0-3.3	12.334	1.796	0.398	423	18	not detected	n/d
S3012A	3.3-3.6	12.542	1.686	0.444	437	17	n/d	n/d
S3013A	3.6-3.9	6.627	1.081	0.481	500	24	n/d	n/d
S3014A	3.9-4.2	9.275	1.648	0.518	561	18	n/d	n/d
S3015A	4.2-4.5	9.034	1.547	0.560	568	19	n/d	n/d
S3016A	4.5-4.8	9.892	1.838	0.606	644	20	n/d	n/d
S3017A	4.8-5.1	7.908	1.599	0.652	741	19	n/d	n/d
S3018A	5.1-5.4	9.059	1.907	0.698	777	20	n/d	n/d
S3019A	5.4-5.7	16.750	3.907	0.776	880	14	n/d	n/d
S3020A	5.7-6.0	9.716	2.188	0.858	1084	17	n/d	n/d
S3021A	6.0-6.3	7.694	1.845	0.912	1004	21	n/d	n/d
S3022A	6.3-6.6	11.277	2.707	0.972	857	14	n/d	n/d
S3023A	6.6-6.9	15.293	4.245	1.065	655	13	n/d	n/d
S3024A	6.9-7.2	12.816	3.211	1.165	447	11	n/d	n/d
S3025A	7.2-7.5	11.084	2.862	1.246	350	9	n/d	n/d

Table 3.1 Radiocaesium results for Loch Lomond (south) core LL/S3A, continued.

Sample Code	Depth /cm	Wet wt /g	Dry wt /g	Mid cum. wt / g cm^{-2}	^{137}Cs / Bq kg^{-1}	σ_{n-1} ^{137}Cs	^{134}Cs / Bq kg^{-1}	σ_{n-1} ^{134}Cs
S3026A	7.5-7.8	11.989	3.002	1.325	256	9	n/d	n/d
S3027A	7.8-8.1	12.754	3.113	1.407	186	11	n/d	n/d
S3028A	8.1-8.4	12.112	2.980	1.488	133	7	n/d	n/d
S3029A	8.4-8.7	13.783	3.367	1.573	85	8	n/d	n/d
S3030A	8.7-9.0	9.750	2.268	1.648	56	10	n/d	n/d
S3031A	9.0-9.3	12.845	3.155	1.721	43	7	n/d	n/d
S3032A	9.3-9.6	10.295	2.513	1.797	29	9	n/d	n/d
S3033A	9.6-9.9	11.410	2.920	1.869	25	6	n/d	n/d
S3034A	9.9-10.2	12.492	3.369	1.953	19	7	n/d	n/d
S3035A	10.2-10.5	10.290	2.820	2.036	16	8	n/d	n/d
S3036A	10.5-10.8	6.239	1.675	2.096	18	9	n/d	n/d
S3037A	10.8-11.1	10.175	2.665	2.154	48	13	n/d	n/d
S3038A	11.1-11.4	8.807	2.365	2.222	34	13	n/d	n/d
S3039A	11.4-11.7	14.950	4.279	2.310	14	7	n/d	n/d
S3040A	11.7-12.0	7.049	2.072	2.395	14	8	n/d	n/d
S3041A	12.0-12.3	8.843	2.620	2.458	12	6	n/d	n/d
S3042A	12.3-12.6	8.880	2.629	2.528	10	7	n/d	n/d
S3043A	12.6-12.9	11.873	3.665	2.612	8	7	n/d	n/d
S3044A	12.9-13.2	10.980	3.446	2.707	4	7	n/d	n/d
S3045A	13.2-13.5	10.162	3.201	2.796	5	7	n/d	n/d
S3046A	13.5-13.8	12.961	4.329	2.897	3	7	n/d	n/d
S3047A	13.8-14.1	5.779	1.943	2.981	1	9	n/d	n/d
S3048A	14.1-14.4	5.745	1.924	3.033	18	12	n/d	n/d

3.4.1.2 ^{210}Pb.

The ^{210}Pb results for shown for LL/S3A in Table 3.2 are based on the determination of ^{210}Po by α-spectrometry. It is assumed that there is secular equilibrium between ^{210}Pb and ^{210}Po. Figure 3.3 is a plot of the specific activity of total ^{210}Pb (Bq kg^{-1}) against depth (cm). The profile is approximately exponential in shape with an extremely high surface activity of 3161 Bq kg^{-1}, tailing off to give a value of 72.4 ± 21.5 Bq kg^{-1} below 11 cm. There are two small peaks in the upper part of the core at 3.5 cm and 5 cm, with specific activities of 413 and 365 Bq kg^{-1}, respectively.

3.4.1.3 Heavy metals.

The concentrations of the heavy metals in core LL/S3B are shown in Table 3.3 along with the wet and dry weight, depth and reference number for each section. The average error for each of the metal concentrations, based on duplicate digestions, is less than ± 4 % ($\pm$ RSD of the mean). For each metal, a graph of concentration (mg kg^{-1} or %) against depth (cm) was plotted as shown in Figures 3.4-3.8.

As shown in Figure 3.4, Fe exhibits a fairly constant level of ~ 5.50 % from about 5.25 cm down to the base of the core. Above 4.50 cm, within the zone of colour changes in the sediment, the concentration begins a steady upward trend until 1.95 cm where there is a sharp increase to a peak of 9.81 % at 1.35 cm (orange/brown coloured zone), dropping again to 5.38 % by 1.05 cm. The general trends for Mn (Fig. 3.5) are very similar to those of Fe although the constant level of ~ 0.22 % at depth shows less deviation. At 3.75 cm the concentration begins to increase steadily until 2.70 cm whereupon there is a sharp increase to a peak of 2.57 % at 1.05 cm. The peak covers only 0.9 cm before declining sharply to 0.40 % at the surface.

In Figure 3.6, the Pb concentration is constant below 28.5 cm at 15 ± 4 mg kg^{-1}. Above 28.5 cm the Pb concentration increases, especially above 18 cm, to reach a maximum of 158 mg kg^{-1} at 6.45 cm before declining to 65-81 mg kg^{-1} in the

uppermost 2.4 cm. The trends for Zn (Fig. 3.7) are similar to those for Pb, but start closer to the surface in the sediment column. Zn has a constant concentration of 100 ± 7 mg kg^{-1} at depth from the base of the core until 18.75 cm. Above this depth it starts to increase steadily until a depth of 9 cm. From 3-9 cm there is a broad, irregular peak with a maximum of 634 mg kg^{-1} at 7.5-7.8 cm. Above 3 cm the concentration declines steadily but the trend is interrupted at 1.8-0.9 cm.

In Figure 3.8, the level of Cu is constant below 17.1 cm at 25 ± 1.6 mg kg^{-1}. Above 17.1 cm, there is a slight increase giving a broad, shallow, peak reaching a maximum of 41 mg kg^{-1} at 4.65 cm. The concentration then decreases to a minimum at 1.35 cm after which it very sharply increases towards the surface to a maximum of 83 mg kg^{-1} in the top section.

3.4.1.4 Carbon and nitrogen.

The results for the C (%) and N (%) content[♦] for core LL/S3B are given in Table 3.3 along with the heavy metal data. Figure 3.9 is a plot of C (%) against depth (cm). The profile is exponential in shape rising from a value of about 2% below 30 cm to 7.28 % at the surface. The N content for all of the sections is below 0.45 %. The average error for C and N is ± 0.3 %.

[♦] Results for C and N are total inorganic and organic components.

Table 3.2 ^{210}Pb results for Loch Lomond (south) core LL/S3A.

Sample Code	Depth /cm	Dry wt / g	Mid cum. depth / g cm^{-2}	^{210}Pb / Bq kg^{-1}	σ(o) / Bq kg^{-1}	$^{210}Pb_{unsup}$	σ $^{210}Pb_{unsup}$	ln $^{210}Pb_{unsup}$	σ +ve	σ -ve	σ Ave
S3001A	0.0-0.3	0.711	0.010	3161	177.9	3088	179.2	8.04	0.06	0.06	0.06
S3002A	0.3-0.6	0.570	0.027	644	26.0	572	33.7	6.35	0.06	0.06	0.06
S3003A	0.6-0.9	0.848	0.046	383	10.8	311	24.0	5.74	0.07	0.08	0.08
S3004A	0.9-1.2	0.979	0.070	368	12.0	296	24.6	5.69	0.08	0.08	0.08
S3005A	1.2-1.5	1.137	0.098	342	8.4	270	23.0	5.60	0.08	0.09	0.08
S3006A	1.5-1.8	1.432	0.133	213	6.1	140	22.3	4.96	0.14	0.17	0.15
S3007A	1.8-2.1	1.878	0.177	188	4.3	116	21.9	4.77	0.17	0.20	0.18
S3008A	2.1-2.4	1.926	0.228	218	6.6	146	22.5	4.99	0.14	0.16	0.15
S3009A	2.4-2.7	1.932	0.279	275	9.4	203	23.4	5.32	0.11	0.12	0.11
S3010A	2.7-3.0	2.553	0.339	260	7.4	188	22.7	5.24	0.11	0.12	0.12
S3011A	3.0-3.3	1.796	0.398	270	9.5	198	23.5	5.30	0.11	0.12	0.12
S3012A	3.3-3.6	1.686	0.444	413	17.0	342	27.0	5.84	0.08	0.08	0.08
S3013A	3.6-3.9	1.081	0.481	249	9.6	177	23.5	5.19	0.12	0.14	0.13
S3014A	3.9-4.2	1.648	0.518	238	7.9	165	22.9	5.12	0.13	0.14	0.13
S3015A	4.2-4.5	1.547	0.560	240	5.1	167	22.1	5.13	0.12	0.14	0.13
S3016A	4.5-4.8	1.838	0.606	366	11.5	293	24.4	5.69	0.08	0.08	0.08
S3017A	4.8-5.1	1.599	0.652	364	23.0	291	31.5	5.68	0.10	0.11	0.11
S3018A	5.1-5.4	1.907	0.698	329	14.7	256	26.0	5.55	0.09	0.10	0.10
S3019A	5.4-5.7	3.907	0.776	167	5.1	94	22.1	4.57	0.20	0.25	0.23
S3020A	5.7-6.0	2.188	0.858	234	7.6	162	22.8	5.10	0.13	0.15	0.14
S3021A	6.0-6.3	1.845	0.912	234	8.4	162	23.1	5.10	0.13	0.15	0.14
S3022A	6.3-6.6	2.707	0.972	211	8.0	138	22.9	4.94	0.15	0.17	0.16
S3023A	6.6-6.9	4.245	1.065	238	9.2	166	23.4	5.12	0.13	0.15	0.14
S3024A	6.9-7.2	3.211	1.165	198	7.4	126	22.7	4.85	0.16	0.19	0.18
S3025A	7.2-7.5	2.862	1.246	179	8.0	108	22.0	4.68	0.19	0.23	0.21

Table 3.2 ^{210}Pb results for Loch Lomond (south) core LL/S3A, continued.

Sample Code	Depth /cm	Dry wt / g	Mid cum. depth / g cm^{-2}	^{210}Pb / Bq kg^{-1}	σ(o) / Bq kg^{-1}	$^{210}Pb_{unsup}$	σ $^{210}Pb_{unsup}$	ln $^{210}Pb_{unsup}$	σ +ve	σ -ve	σ Ave
S3026A	7.5-7.8	3.002	1.325	176	5.3	103	22.1	4.65	0.19	0.23	0.21
S3027A	7.8-8.1	3.113	1.407	175	6.4	103	22.4	4.65	0.19	0.23	0.21
S3028A	8.1-8.4	2.980	1.488	175	5.0	102	22.1	4.65	0.19	0.23	0.21
S3029A	8.4-8.7	3.367	1.573	191	8.0	118	22.9	4.79	0.17	0.21	0.19
S3030A	8.7-9.0	2.268	1.648	173	8.3	101	23.0	4.63	0.20	0.25	0.22
S3031A	9.0-9.3	3.155	1.721	166	6.5	93	22.4	4.55	0.21	0.26	0.24
S3032A	9.3-9.6	2.513	1.797	143	5.3	70	22.1	4.28	0.26	0.36	0.31
S3033A	9.6-9.9	2.920	1.869	129	6.2	57	22.3	4.07	0.32	0.47	0.39
S3034A	9.9-10.2	3.369	1.953	108	4.5	36	21.9	3.63	0.45	0.84	0.64
S3035A	10.2-10.5	2.820	2.036	100	3.9	28	21.8	3.38	0.55	1.30	0.92
S3036A	10.5-10.8	1.675	2.096	107	4.1	35	21.9	3.60	0.46	0.88	0.67
S3037A	10.8-11.1	2.665	2.154	110	4.2	38	21.9	3.67	0.43	0.78	0.61
S3038A	11.1-11.4	2.365	2.222	102	4.6	30	21.9	3.44	0.52	1.15	0.84
S3039A	11.4-11.7	4.279	2.310	65	4.0						
S3040A	11.7-12.0	2.072	2.395	59	4.1						
S3041A	12.0-12.3	2.620	2.458	67	3.9						
S3042A	12.3-12.6	2.629	2.528	69	3.2						
S3043A	12.6-12.9	3.665	2.612	56	2.4						
S3044A	12.9-13.2	3.446	2.707	46	3.5						
S3045A	13.2-13.5	3.201	2.796	103	2.8						
S3046A	13.5-13.8	4.329	2.897	109	3.3						
S3047A	13.8-14.1	1.943	2.981	53	2.6						
S3048A	14.1-14.4	1.924	3.033	80	2.4						

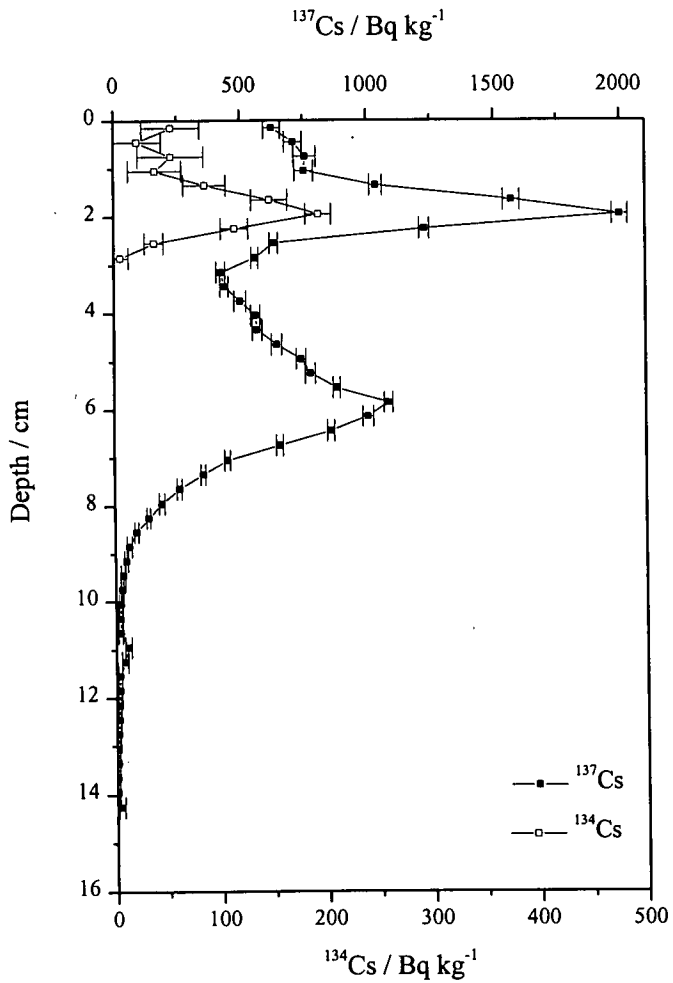

Figure 3.2 ^{134}Cs and ^{137}Cs (Bq kg^{-1}) vs depth (cm) in core LL/S3A.

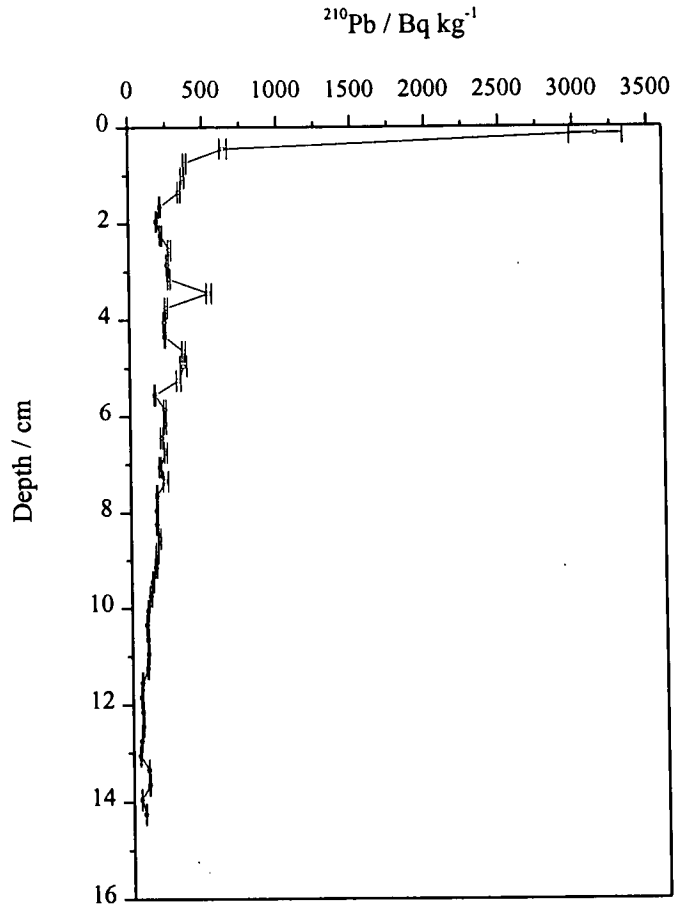

Figure 3.3 ^{210}Pb(Bq kg^{-1}) vs depth (cm) in core LL/S3A.

Table 3.3 Heavy metal, carbon, nitrogen and $^{206}Pb/^{207}Pb$ results for Loch Lomond (south) core LL/S3B.

Sample Code	Depth / cm	Wet wt / g	Dry wt / g	Mid cum. wt / g cm^{-2}	Fe / %	Mn / %	Pb / mg kg^{-1}	Zn / mg kg^{-1}	Cu / mg kg^{-1}	% C	% N	$^{206}Pb/^{207}Pb$	σ_{n-1}
S3001B	0.0-0.3	23.240	0.186	0.0028	5.25	0.40	75	463	83	7.28	< 0.10	1.135	0.006
S3002B	0.3-0.6	7.410	0.450	0.0124	4.72	0.52	76	471	55	6.90	0.30	1.136	0.007
S3003B	0.6-0.9	8.200	0.603	0.0215	4.78	1.67	66	471	41	6.23	< 0.10	1.141	0.003
S3004B	0.9-1.2	8.855	0.807	0.0336	5.38	2.57	65	413	33	5.62	< 0.10	1.141	0.002
S3005B	1.2-1.5	9.777	1.005	0.0488	9.81	1.17	71	375	29	6.23	< 0.10	1.139	0.002
S3006B	1.5-1.8	12.089	1.389	0.0697	8.32	0.80	75	337	32	5.49	0.34	1.141	0.002
S3007B	1.8-2.1	13.014	1.870	0.0979	6.50	1.19	73	426	33	5.15	0.42	1.135	0.001
S3008B	2.1-2.4	11.371	1.811	0.1252	6.50	0.70	81	499	34	5.38	0.38	1.140	0.004
S3009B	2.4-2.7	8.784	1.428	0.1467	6.36	0.45	112	469	34	5.17	0.35	1.135	0.001
S3010B	2.7-3.0	10.243	1.707	0.1724	6.06	0.36	107	529	35	5.36	0.45	1.137	0.002
S3011B	3.0-3.3	11.001	1.906	0.2011	5.80	0.35	124	625	38	5.17	0.45	1.135	0.005
S3012B	3.3-3.6	10.006	1.683	0.2265	5.63	0.34	136	567	37	5.13	0.40	1.129	0.004
S3013B	3.6-3.9	9.385	1.661	0.2515	5.33	0.28	148	560	40	4.93	0.33	1.127	0.004
S3014B	3.9-4.2	8.440	1.575	0.2753	5.04	0.27	150	531	38	4.91	0.35	1.131	0.005
S3015B	4.2-4.5	9.610	1.812	0.3026	5.10	0.28	135	568	39	4.72	0.23	1.133	0.006
S3016B	4.5-4.8	9.248	1.968	0.3322	5.24	0.28	136	621	41	4.90	0.24	1.138	0.005
S3017B	4.8-5.1	8.128	1.732	0.3583	5.17	0.28	132	597	41	5.06	0.28	1.141	0.005
S3018B	5.1-5.4	8.250	1.779	0.3851	5.36	0.32	139	585	40	4.65	0.29	1.139	0.005
S3019B	5.4-5.7	9.504	2.120	0.4171	5.30	0.32	131	614	40	4.68	< 0.10	1.139	0.005
S3020B	5.7-6.0	6.913	1.560	0.4406	5.61	0.31	149	548	40	5.06	< 0.10	1.141	0.005
S3021B	6.0-6.3	7.483	1.733	0.4667	5.54	0.31	150	539	39	4.38	< 0.10	1.140	0.003
S3022B	6.3-6.6	8.966	2.083	0.4981	5.51	0.31	158	530	39	4.23	< 0.10	1.144	0.005
S3023B	6.6-6.9	9.990	2.410	0.5344	5.58	0.31	149	558	39	4.28	< 0.10	1.147	0.005
S3024B	6.9-7.2	8.408	2.089	0.5659	5.47	0.28	149	582	38	4.35	< 0.10	1.147	0.005
S3025B	7.2-7.5	5.628	1.404	0.5871	5.31	0.28	147	584	39	4.39	< 0.10	1.149	0.004

Table 3.3 Heavy metal, carbon, nitrogen and $^{206}Pb/^{207}Pb$ results for Loch Lomond (south) core LL/S3B, continued.

Sample Code	Depth / cm	Wet wt / g	Dry wt / g	Mid cum. wt / g cm^{-2}	Fe / %	Mn / %	Pb / mg kg^{-1}	Zn / mg kg^{-1}	Cu / mg kg^{-1}	% C	% N	$^{206}Pb/^{207}Pb$	σ_{n-1}
S3026B	7.5-7.8	10.998	2.768	0.6288	5.43	0.30	147	634	37	4.42	< 0.10	1.150	0.005
S3027B	7.8-8.1	8.490	2.088	0.6602	5.39	0.29	151	614	37	4.45	< 0.10	1.151	0.005
S3028B	8.1-8.4	8.394	2.077	0.6915	5.40	0.29	151	628	38	4.58	< 0.10	1.153	0.005
S3029B	8.4-8.7	9.230	2.314	0.7264	5.49	0.30	155	621	37	4.52	< 0.10	1.152	0.005
S3030B	8.7-9.0	11.949	2.975	0.7712	5.59	0.30	154	544	37	4.44	< 0.10	1.158	0.002
S3031B	9.0-9.3	9.221	2.490	0.8088	5.32	0.28	156	485	34	not determined		1.160	0.005
S3032B	9.3-9.6	9.562	2.603	0.8480	5.41	0.25	145	461	34			1.159	0.005
S3033B	9.6-9.9	10.897	2.962	0.8926	5.36	0.31	144	456	35			1.162	0.005
S3034B	9.9-10.2	9.293	2.465	0.9298	5.65	0.33	141	437	33			1.161	0.005
S3035B	10.2-10.5	8.129	2.182	0.9626	6.05	0.36	145	401	33	3.82	0.19	1.162	0.005
S3036B	10.5-10.8	11.591	3.196	1.0108	5.85	0.36	137	382	34			1.170	0.005
S3037B	10.8-11.1	9.796	2.836	1.0535	5.93	0.33	146	351	32			1.168	0.005
S3038B	11.1-11.4	11.635	3.545	1.1070	5.65	0.29	144	330	33			1.167	0.005
S3039B	11.4-11.7	10.020	3.257	1.1560	5.20	0.24	130	309	33			1.166	0.005
S3040B	11.7-12.0	12.205	4.027	1.2167	4.96	0.22	123	303	32	3.71	0.33	1.170	0.003
S3041B	12.0-12.3	17.049	5.818	1.3044	4.87	0.22	108	268	31			1.171	0.005
S3042B	12.3-12.6	12.765	4.230	1.3681	4.88	0.24	107	259	31			1.172	0.005
S3043B	12.6-12.9	11.477	3.775	1.4250	5.17	0.24	115	250	31			1.167	0.005
S3044B	12.9-13.2	11.838	3.851	1.4831	5.59	0.26	123	254	32			1.170	0.005
S3045B	13.2-13.5	13.496	4.486	1.5507	5.56	0.26	125	239	33	2.95	0.24	1.168	0.005
S3046B	13.5-13.8	14.303	4.891	1.6244	5.51	0.25	127	242	32			1.174	0.005
S3047B	13.8-14.1	15.374	5.345	1.7049	5.33	0.23	123	218	31			1.170	0.005
S3048B	14.1-14.4	17.761	5.972	1.7949	5.34	0.25	133	212	30			1.175	0.005
S3049B	14.4-14.7	11.334	3.695	1.8506	5.44	0.25	126	202	31			1.169	0.005
S3050B	14.7-15.0	14.941	4.936	1.9250	5.30	0.25	102	192	30	3.51	0.31	1.171	0.007

Table 3.3 Heavy metal, carbon, nitrogen and $^{206}Pb/^{207}Pb$ results for Loch Lomond (south) core LL/S3B, continued.

Sample Code	Depth / cm	Wet wt / g	Dry wt / g	Mid cum. wt / g cm^{-2}	Fe / %	Mn / %	Pb / mg kg^{-1}	Zn / mg kg^{-1}	Cu / mg kg^{-1}	% C	% N	$^{206}Pb/^{207}Pb$	σ_{n-1}
S3051B	15.0-15.3	14.392	4.924	1.9992	5.02	0.24	105	172	27	not determined		1.171	0.006
S3052B	15.3-15.6	14.926	5.210	2.0777	5.39	0.25	122	166	29			1.169	0.002
S3053B	15.6-15.9	15.696	5.468	2.1601	5.19	0.23	135	150	27			1.170	0.005
S3054B	15.9-16.2	14.618	5.152	2.2377	5.26	0.23	111	148	28			1.170	0.005
S3055B	16.2-16.5	16.296	5.720	2.3239	5.23	0.23	95	135	28	2.46	0.17	1.172	0.004
S3056B	16.5-16.8	13.689	4.740	2.3953	5.37	0.24	85	124	28			1.170	0.005
S3057B	16.8-17.1	14.606	5.026	2.4711	5.32	0.26	75	121	26			1.170	0.003
S3058B	17.1-17.4	12.693	4.389	2.5372	5.52	0.25	59	125	26			1.170	0.005
S3059B	17.4-17.7	13.797	4.829	2.6100	5.27	0.26	53	126	27			1.172	0.004
S3060B	17.7-18.0	16.446	5.842	2.6980	5.18	0.22	45	124	27	2.77		1.170	0.006
S3061B	18.0-18.3	12.502	4.636	2.7679	5.20	0.21	40	113	26			1.176	0.005
S3062B	18.3-18.6	14.290	5.215	2.8465	5.45	0.21	41	122	28			1.174	0.003
S3063B	18.6-18.9	14.707	5.505	2.9294	5.22	0.24	41	106	24			1.175	0.005
S3064B	18.9-19.2	14.949	5.680	3.0150	4.83	0.22	42	109	23			1.177	0.005
S3065B	19.2-19.5	12.873	4.913	3.0891	5.50	0.23	40	100	26	2.33	0.14	1.180	0.003
S3066B	19.5-19.8	12.887	4.930	3.1634	5.39	0.21	42	107	25			1.177	0.001
S3067B	19.8-20.1	14.413	5.572	3.2473	5.40	0.22	40	108	26			1.179	0.001
S3068B	20.1-20.4	13.931	5.569	3.3312	5.73	0.21	43	114	27			1.178	0.004
S3069B	20.4-20.7	14.239	5.776	3.4183	5.49	0.21	32	110	28			1.175	0.004
S3070B	20.7-21.0	16.125	6.590	3.5176	5.09	0.21	31	117	28	2.23	0.12	1.175	0.001
S3071B	21.0-21.3	15.333	6.220	3.6113	4.98	0.20	31	108	28			1.179	0.004
S3072B	21.3-21.6	13.779	5.581	3.6954	4.82	0.21	29	108	27			1.177	0.003
S3073B	21.6-21.9	17.365	6.967	3.8004	5.11	0.22	28	104	26			1.175	0.004
S3074B	21.9-22.2	13.504	5.344	3.8809	5.04	0.22	31	115	27			1.168	0.004
S3075B	22.2-22.5	13.954	5.606	3.9654	5.00	0.22	30	113	27	2.65	0.18	1.171	0.003

Table 3.3 Heavy metal, carbon, nitrogen and $^{206}Pb/^{207}Pb$ results for Loch Lomond (south) core LL/S3B, continued.

Sample Code	Depth / cm	Wet wt / g	Dry wt / g	Mid cum. wt / g cm^{-2}	Fe / %	Mn / %	Pb / mg kg^{-1}	Zn / mg kg^{-1}	Cu / mg kg^{-1}	% C	% N	$^{206}Pb/^{207}Pb$	σ_{n-1}
S3076B	22.5-22.8	15.94	6.46	4.0627	4.37	0.23	28	110	24	not determined		1.177	0.002
S3077B	22.8-23.1	15.52	6.30	4.1576	4.80	0.21	29	108	27			1.178	0.001
S3078B	23.1-23.4	11.79	4.69	4.2282	4.95	0.22	31	100	26			1.178	0.004
S3079B	23.4-23.7	11.70	4.69	4.2989	5.28	0.23	27	99	24			1.170	0.002
S3080B	23.7-24.0	12.04	4.80	4.3712	5.20	0.22	25	103	24	2.96	0.18	1.176	0.004
S3081B	24.0-24.3	4.40	1.77	4.3980	5.13	0.22	23	104	24			1.173	0.005
S3082B	24.3-24.6	15.71	6.43	4.4949	5.36	0.22	20	108	24			1.176	0.005
S3083B	24.6-24.9	15.95	6.61	4.5945	5.38	0.22	23	100	25			1.177	0.003
S3084B	24.9-25.2	11.36	4.66	4.6647	5.28	0.21	23	98	24			1.174	0.004
S3085B	25.2-25.5	15.21	6.19	4.7579	5.53	0.22	25	105	26	2.69	<0.10	1.175	0.001
S3086B	25.5-25.8	10.97	4.42	4.8246	5.49	0.22	25	103	24			1.177	0.002
S3087B	25.8-26.1	9.34	3.75	4.8811	5.31	0.22	25	107	25			1.176	0.003
S3088B	26.1-26.4	12.47	5.03	4.9570	5.59	0.21	21	113	25			1.178	0.004
S3089B	26.4-26.7	9.93	4.04	5.0179	5.72	0.25	30	116	26			1.177	0.003
S3090B	26.7-27.0	16.00	6.59	5.1173	5.39	0.22	28	107	25	2.71	<0.10	1.178	0.003
S3091B	27.0-27.3	12.91	5.33	5.1976	5.35	0.23	24	104	24			1.178	0.003
S3092B	27.3-27.6	14.17	5.86	5.2859	5.77	0.24	23	115	26			1.178	0.003
S3093B	27.6-27.9	15.42	6.30	5.3809	5.46	0.23	16	109	24			1.172	0.002
S3094B	27.9-28.2	10.43	4.33	5.4462	5.55	0.22	28	112	25			1.170	0.002
S3095B	28.2-28.5	12.77	5.38	5.5273	5.37	0.21	30	103	24	2.50	<0.10	1.173	0.002
S3096B	28.5-28.8	12.01	5.14	5.6048	5.07	0.20	15	99	23			1.173	0.004
S3097B	28.8-29.1	11.77	5.03	5.6806	5.04	0.19	17	99	23			1.174	0.004
S3098B	29.1-29.4	12.42	5.21	5.7590	5.26	0.22	26	95	24			1.175	0.002
S3099B	29.4-29.7	11.83	4.94	5.8334	5.16	0.21	19	102	24			1.174	0.004
S3100B	29.7-30.0	13.41	5.58	5.9175	4.40	0.19	15	98	23	3.14	<0.10	1.174	0.004

Table 3.3 Heavy metal, carbon, nitrogen and $^{206}Pb/^{207}Pb$ results for Loch Lomond (south) core LL/S3B, continued.

Sample Code	Depth / cm	Wet wt / g	Dry wt / g	Mid cum. wt / g cm^{-2}	Fe / %	Mn / %	Pb / mg kg^{-1}	Zn / mg kg^{-1}	Cu / mg kg^{-1}	% C	% N	$^{206}Pb/^{207}Pb$	σ_{n-1}
S3101B	30.0-32.0	90.407	39.315	6.5100	5.47	0.21	19	94	24	not determined		1.174	0.003
S3102B	32.0-34.0	86.380	37.823	7.0799	5.52	0.19	19	94	24	2.03	<0.10	1.178	0.005
S3103B	34.0-36.0	85.080	36.258	7.6263	5.89	0.21	15	101	24	2.02	<0.10	1.175	0.002
S3104B	36.0-38.0	88.569	38.551	8.2073	5.55	0.20	20	97	22			1.173	0.003
S3105B	38.0-40.0	88.559	40.033	8.8105	5.28	0.19	16	90	22	1.89	<0.10	1.175	0.004
S3106B	40.0-42.0	88.187	38.476	9.3903	5.58	0.20	19	97	24	2.15	<0.10	1.168	0.005
S3107B	42.0-44.0	89.084	39.245	9.9817	6.52	0.24	19	116	26	2.12	<0.10	1.175	0.005
S3108B	44.0-46.0	87.610	38.368	10.5599	5.59	0.21	12	97	24			1.172	0.006
S3109B	46.0-48.0	85.761	37.642	11.1272	5.53	0.21	10	97	23	2.05	<0.10	1.178	0.005
S3110B	48.0-50.0	86.832	37.886	11.6981	5.37	0.22	10	90	22			1.174	0.006
S3111B	50.0-55.0	211.984	89.379	13.0450	5.68	0.22	13	100	23	2.16	0.16	1.175	0.004
S3112B	55.0-60.0	203.081	86.927	14.3549	5.18	0.21	15	99	22			1.174	0.010
S3113B	60.0-65.0	206.824	114.935	16.0869	5.39	0.22	18	102	23			1.172	0.007
S3114B	65.0-70.0	213.311	93.901	17.5019	5.38	0.20	13	98	23			1.176	0.004
S3115B	70.0-75.0	200.859	91.630	18.8827	6.14	0.22	11	102	24	2.31	0.17	1.173	0.006
S3116B	75.0-80.0	192.250	76.562	20.0364	6.39	0.25	15	114	25			1.168	0.006

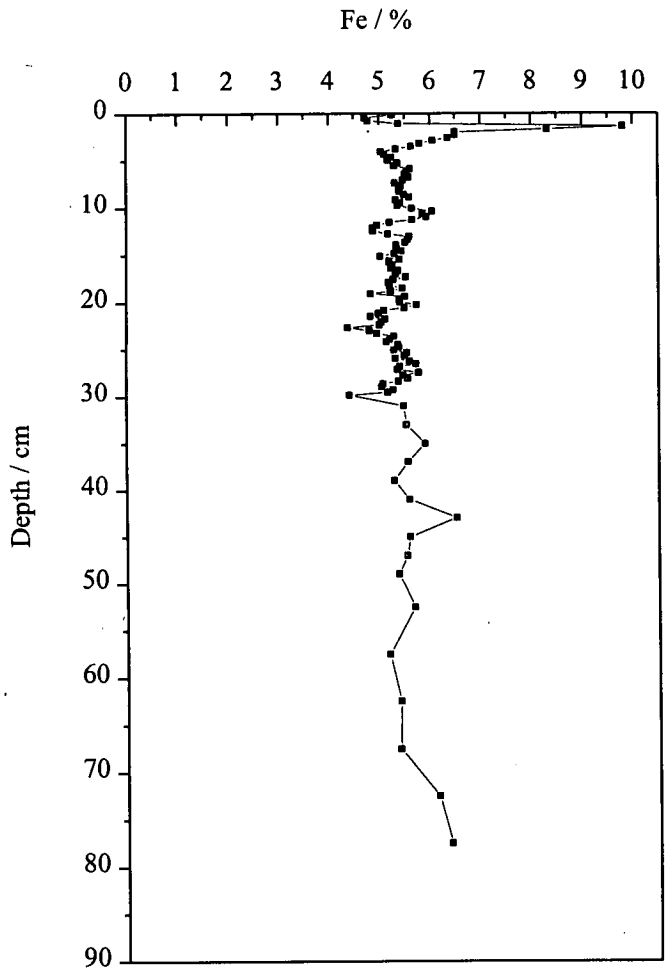

Figure 3.4 Fe (%) vs depth (cm) in core LL/S3B.

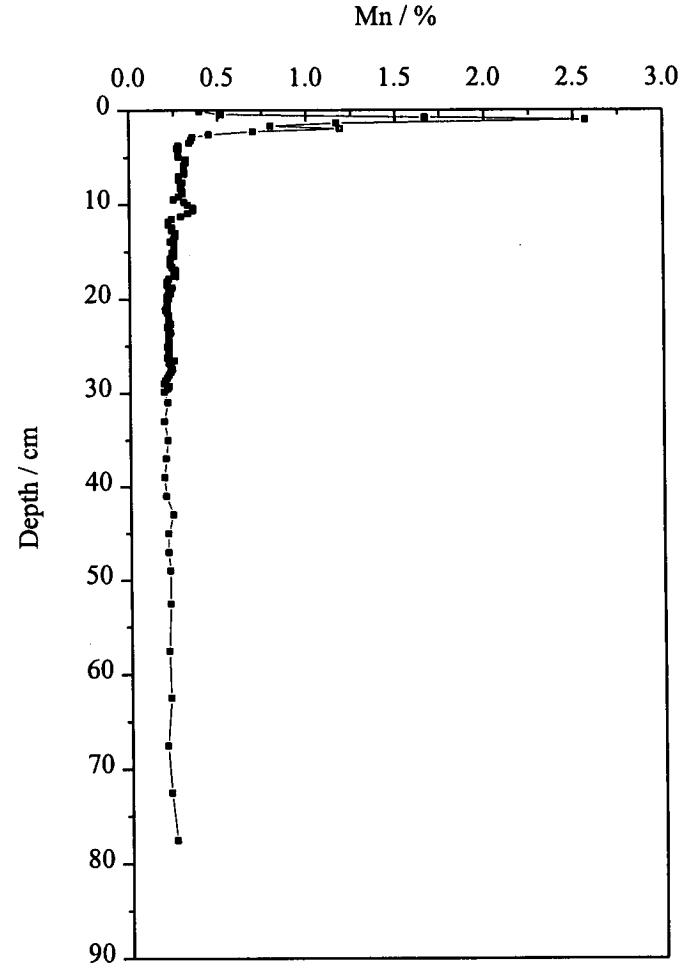

Figure 3.5 Mn (%) vs depth (cm) in core LL/S3B.

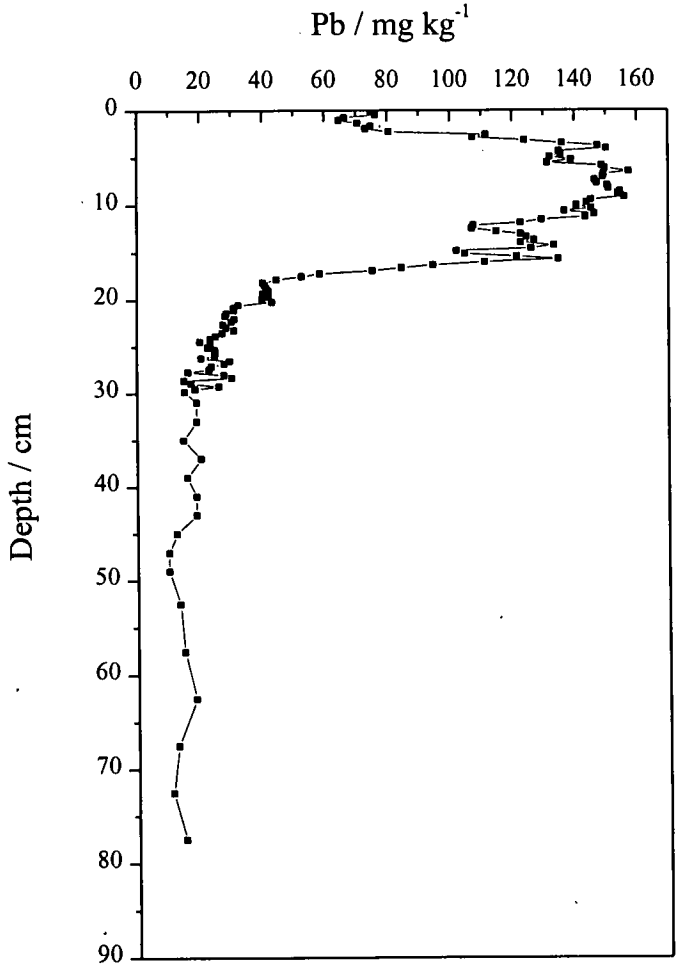

Figure 3.6 Pb (mg kg^{-1}) vs depth (cm) in core LL/S3B.

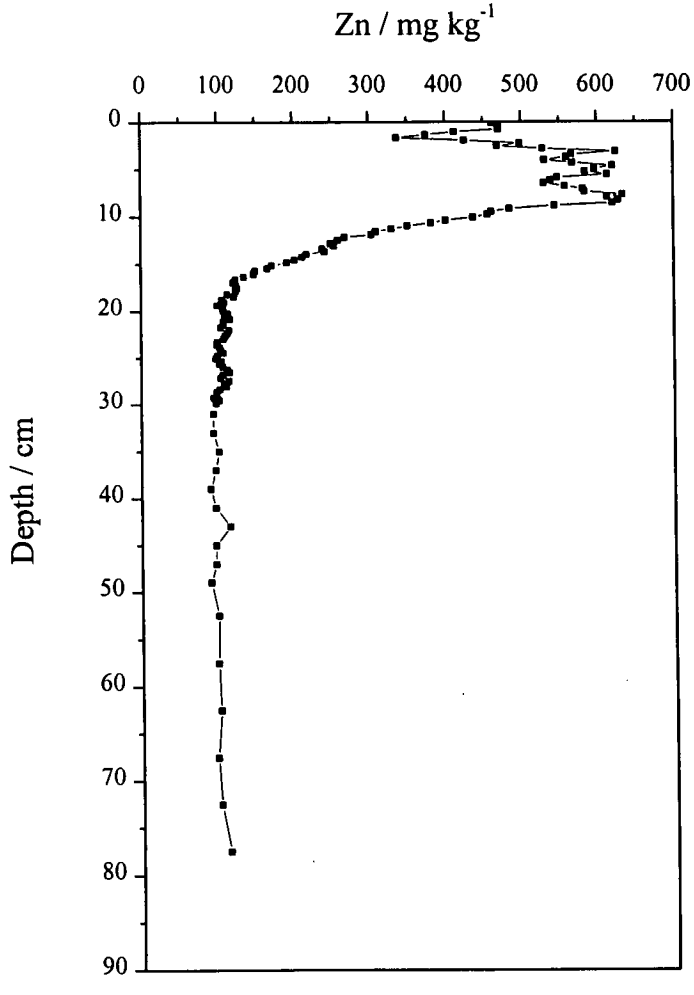

Figure 3.7 Zn (mg kg^{-1}) vs depth (cm) in core LL/S3B.

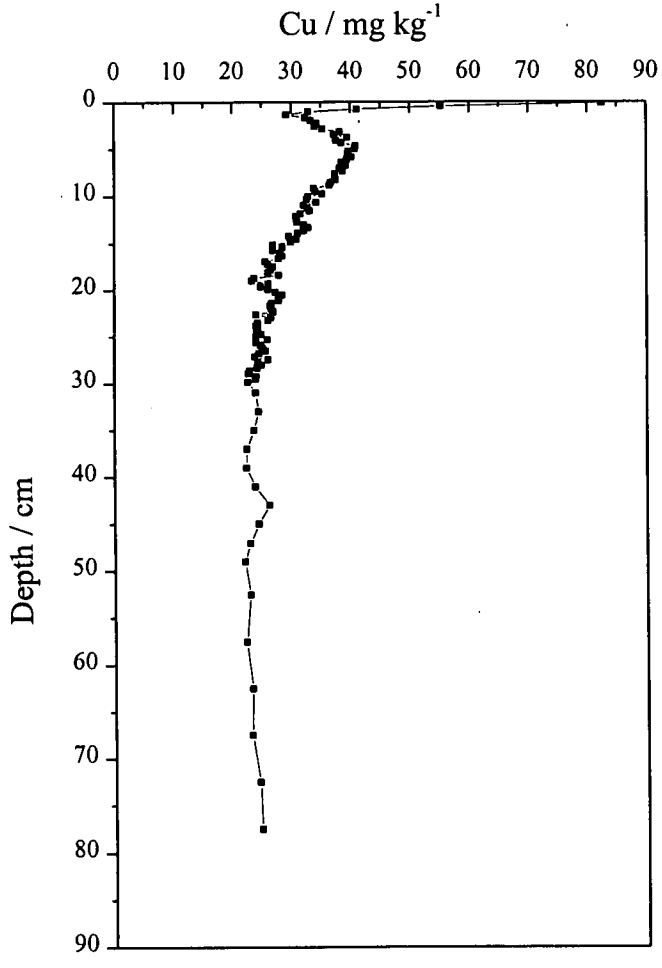

Figure 3.8 Cu (mg kg^{-1}) vs depth (cm) in core LL/S3B.

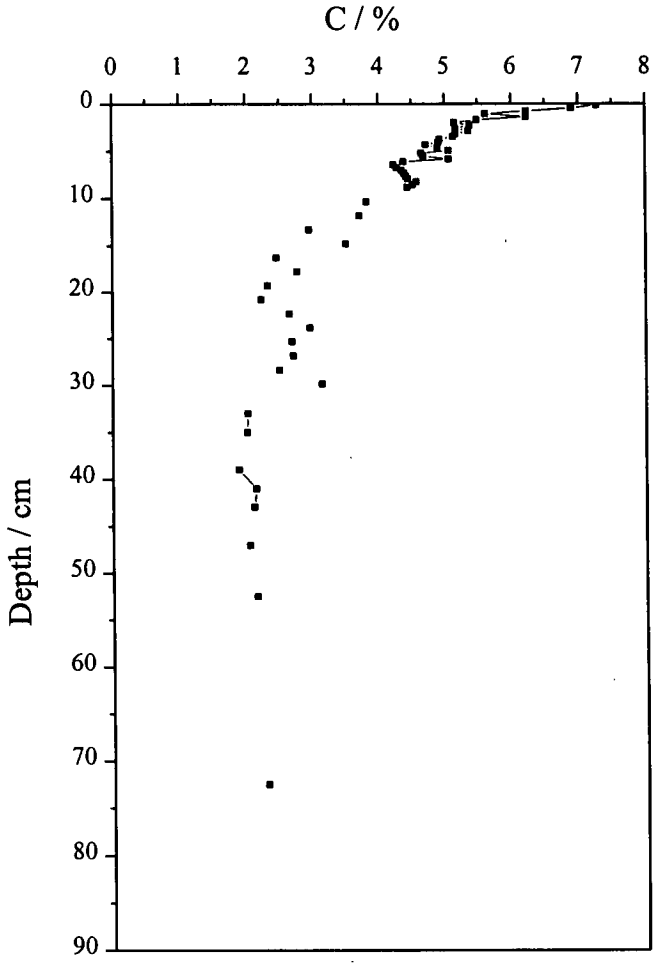

Figure 3.9 C (%) vs depth (cm) in core LL/S3B.

3.4.1.5 Stable lead isotopes.

Table 3.3 is a summary of the $^{206}Pb/^{207}Pb$ atom ratio and the Pb (mg kg^{-1}) concentration data for each section of the Mini-Mackereth core LL/S3B. There were no analytical data for the isotope ^{208}Pb for this core. Figure 3.10 is a plot of $^{206}Pb/^{207}Pb$ ratio and Pb concentration (mg kg^{-1}) against depth (cm). The Pb concentration and the $^{206}Pb/^{207}Pb$ ratio are constant below 28.5 cm, at 15 ± 4 mg kg^{-1} and 1.174 ± 0.002 respectively. Above 28.5 cm the Pb concentration increased, especially above 18 cm, reaching a maximum of 158 mg kg^{-1} at 6.45 cm. However, the $^{206}Pb/^{207}Pb$ ratio remained fairly constant until 10.5 cm, when it started to decline, reaching a minimum of 1.127 at 3.75 cm. This was followed by an upturn to 1.141 by the top of the core, accompanied by a decrease in the Pb concentration to ~70 mg kg^{-1} in the top 2.5 cm.

3.4.1.6 X-Ray diffraction.

Three samples were analysed by XRD (S3007A, S3019A and S3129A) and all were identical in the types of minerals identified and in the relative quantity of the minerals present. The following minerals were identified as being present in the samples in order of relative abundance: quartz, muscovite, albite, chamosite and hematite. A sixth mineral clinochlore gives a possible fit from the fingerprinting, but is often confused with chamosite.

The following is a summary of the formulae and some structural properties of the minerals identified.

Quartz: SiO_2 framework silicate

Muscovite: $K_2(Si_6Al_2)(Al_4)O_{20}(OH)_4$ and $K_2(Si_7Al_1)(Al,Fe^{3+})_3(Mg,Fe^{2+})O_{20}(OH)_4$
Mica, layer silicate, 2:1 dioctahedral, 10 Å.

Albite: $NaAlSi_3O_8$
Feldspar, framework silicate, 3.19 Å.

Figure 3.10 Pb (mg kg^{-1}) and ^{206}Pb / ^{207}Pb atom ratio vs depth (cm) in core LL/S3B.

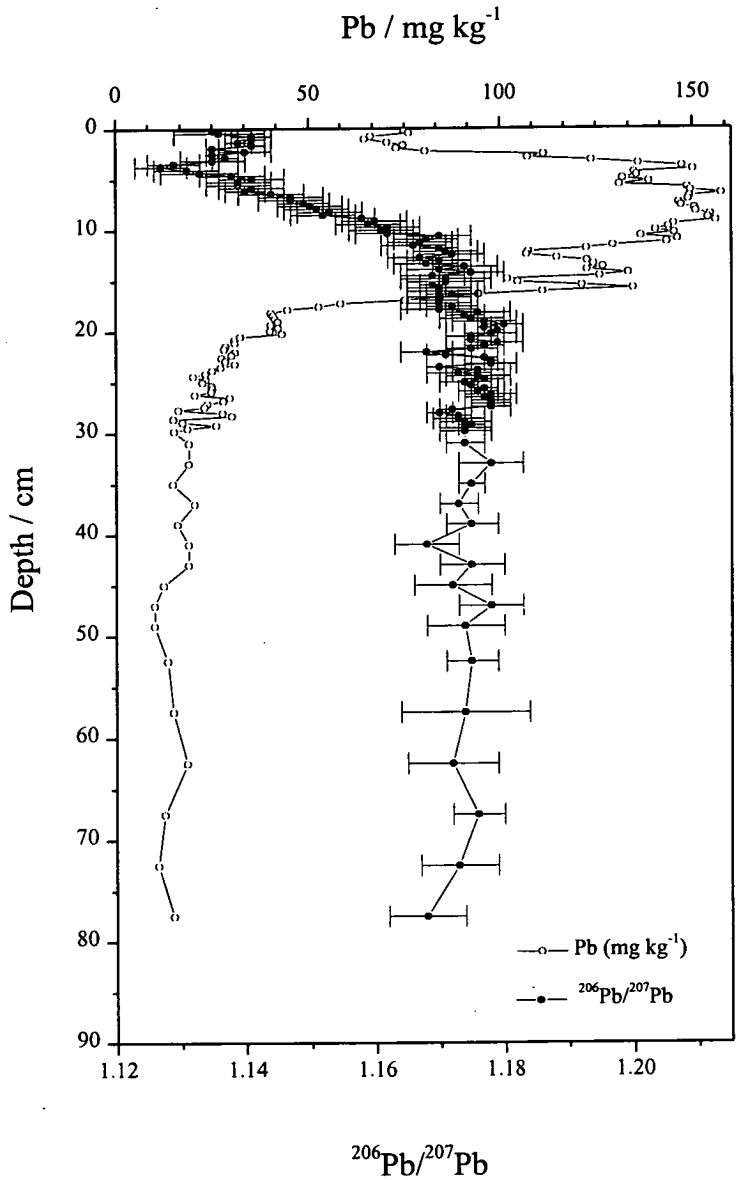

Hematite: Fe_2O_3

Chamosite: $(Fe,Al,Mg)_6(Si,Al)_4O_{10}(OH)_8$

Layer silicate, 2:1 dioctahedral, 10 Å.

3.4.2 Discussion.

3.4.2.1 Radiocaesium.

In Figure 3.2, the upper peak in ^{137}Cs, with its associated ^{134}Cs peak, is due to the releases from the Chernobyl accident which occurred on 26th April 1986. The broader, lower peak is due to weapons testing fallout. In order to characterise the upper ^{137}Cs peak and the ^{134}Cs peak, the ^{134}Cs:^{137}Cs activity ratio at the time of the accident can be calculated. Radiocaesium released from Chernobyl had a characteristic ^{134}Cs:^{137}Cs activity ratio of 0.55 (Horrill *et al.*, 1988). Table 3.4 shows the decay corrected ratios for the top 3 cm of the core. From these results, it can be seen that at the ^{137}Cs peak at 1.95 cm the ratio is in good agreement with that for Chernobyl. Below the peak, the ratio drops due to the continued influence of some residual weapons radiocaesium, which is devoid of any ^{134}Cs. Below 3 cm there is no longer any ^{134}Cs detectable. Above 1.2 cm the ratio varies somewhat, but it must be noted that the errors are much higher in this region.

This measured ratio can be used to separate the Chernobyl and weapons testing radiocaesium by correcting the activity of the ^{134}Cs back to 1st May 1986. Using the deposition ratio of 0.55, the amount of ^{137}Cs due to Chernobyl in 1986, and therefore, via correction for subsequent decay of ^{137}Cs, the amount which would still be present on the sampling date in November 1991 can be calculated. If this figure is subtracted from the total activity of ^{137}Cs, any excess is due to weapons testing fallout. Table 3.5 shows the excess ^{137}Cs due to weapons testing. Below 2.4 cm it can be seen that there is an increasing contribution to the sediment from weapons testing, but in the region of the Chernobyl peak, the input of ^{137}Cs from Chernobyl dominates as the

weapons testing input will be too small to be detected against the Chernobyl signal. Above 2.4 cm all the ^{134}Cs:^{137}Cs activity ratios are consistent, within error, with a Chernobyl origin. It is therefore impossible to identify any residual fallout component, so all of the radiocaesium in this region of the core is taken to be Chernobyl derived.

The calculated inventories for weapons testing and Chernobyl radiocaesium are shown in Table 3.6, along with reported atmospheric deposition values and the corresponding results for a core taken ~ 2 km to the NW of this site (Bryant *et al.*, 1993). The weapons radiocaesium inventories in the cores are similar, but both are higher than the reported deposition range. This could be due to a continued input of weathered material containing ^{137}Cs from the catchment in the period since 1963 but, as discussed above, it is not possible to separate the two sources in the region of the Chernobyl peak. The Chernobyl radiocaesium is within the range quoted for deposition (Clark and Smith, 1988), but is somewhat lower than the value derived by Bryant *et al.* (1993). This could be due to several factors relating to the location of the sample site. The channel between the two islands (Inchmurrin and Creinich) from where the core was taken, forms part of the main drainage system between the Strathcasheil Basin and the Fault Basin. It is possible that the movement of water through the channel restricts the amount of deposition occurring. It is further from any drainage from the land than sites in Bryant *et al.* (1993). Therefore, if radiocaesium is scavenged from the water column and transferred to the sediment at a fast rate, less radiocaesium may have been carried as far as the channel basin. Alternatively, or in addition, there may have been a slightly higher rainfall over one site compared with the other.

To calculate a sedimentation rate in mg cm^{-2} y^{-1} using the radiocaesium data, a new plot of the activity against the cumulative dry weight of sediment (g cm^{-2}) rather than the depth (cm) of sediment is required, as shown in Figure 3.11. By taking the two peaks to represent 1st May 1986 and 1963, respectively, the sedimentation rates for the increments 1991-1986, 1986-1963 and 1991-1963 are 32.2 ± 4.6, 29.6 ± 2.4 and

Table 3.4 ^{134}Cs : ^{137}Cs activity ratio results for core LL/S3A.

Depth / cm	Ratio / 1991	Error / 1991	Ratio / 1986	Error / 1986
0.0 - 0.3	0.085	0.043	0.495	0.248
0.3 - 0.6	0.031	0.032	0.178	0.185
0.6 - 0.9	0.072	0.041	0.417	0.241
0.9 - 1.2	0.051	0.034	0.298	0.196
1.2 - 1.5	0.083	0.019	0.481	0.110
1.5 - 1.8	0.093	0.011	0.541	0.063
1.8 - 2.1	0.097	0.007	0.561	0.036
2. 1- 2.4	0.093	0.011	0.539	0.063
2.4 - 2.7	0.060	0.015	0.351	0.086
2.7 - 3.0	0.012	0.014	0.086	0.082

Measured Value on 1/05/86 : 0.55

Table 3.5 Separation of weapons testing ^{137}Cs for core LL/S3A.

Depth / cm	Weapons specific activity / (1991) Bq kg^{-1}	σ_{n-1} Weapons specific activity / (1991) Bq kg^{-1}
0.0 - 0.3	60	288
0.3 - 0.6	480	243
0.6 - 0.9	180	327
0.9 - 1.2	344	263
1.2 - 1.5	132	212
1.5 - 1.8	26	183
1.8 - 2.1	-32	153
2. 1- 2.4	28	145
2.4 - 2.7	234	100
2.7 - 3.0	485	86

Table 3.6 Inventories of ^{137}Cs / kBq m^{-2} in Loch Lomond (south) sediments.

	Core date	Chernobyl *	Weapons testing #
Eades *et al.*, (1998)	1991	3.87 +/- 0.10	13.81 +/- 0.23
Bryant *et al.*, (1993)	1990	6.85 +/- 0.05	14.41 +/- 0.10
Reported Deposition Values		1-5**	6-8***

* 1986
# 1963
** Clark and Smith, 1988
*** Peirson *et al.*, 1982

Figure 3.11 Activity of ^{134}Cs and ^{137}Cs (Bq kg^{-1}) vs mid-cumulative weight depth (g cm^{-2}) in core LL/S3A.

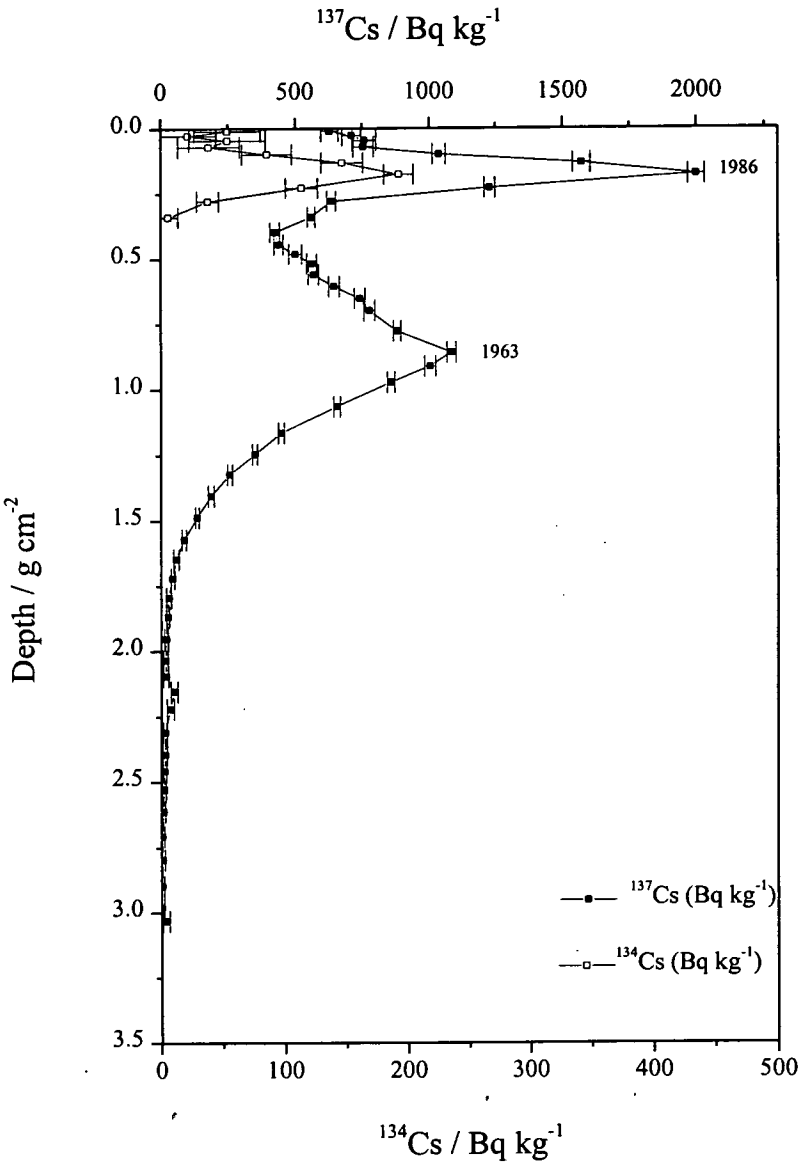

30.6 ± 1.1 mg cm^{-2} y^{-1} (based on cumulative weight to the centre of the peak). These derived values indicate no major change in the sedimentation rate over a 28 year period and are in reasonable agreement with the rate of 32-42 mg cm^{-2} y^{-1} recorded by Bryant *et al.* (1993) for a core from a nearby sampling site dated using ^{210}Pb.

Broadening of the radiocaesium peaks, which is often observed for sediment cores (Eades *et al.*, 1998), can be caused by a number of processes, including: (a) physical and/or biological mixing of the sediment, (b) diffusion of Cs in solution in the sediment interstitial water, and (c) input of weathered material containing radiocaesium from the catchment after the initial deposition event. On the basis of profiles obtained using 1 cm section intervals, it is difficult to distinguish between these processes (Bryant *et al.*, 1993). In contrast, the sharp peaks obtained for Chernobyl radiocaesium using 3-mm sections suggest that mixing and diffusion have had a relatively small effect in the 5.5 years since deposition. Both the ^{134}Cs and ^{137}Cs profiles, with relatively constant activities in the top four sections, would, however, be consistent with either continued input from the catchment in the period since 1986, or with highly efficient mixing of the surface 1 cm of the sediment. The upper portion of the weapons testing peak would also be consistent with continued input from the catchment, with a trend reflecting a gradual decrease in activity of material deposited since 1963. The distribution of ^{137}Cs below the weapons testing peak, with penetration to a depth of 10.4 cm (corresponding to a date of 1923 on the basis of a sedimentation rate of 30.6 mg cm^{-2} y^{-1}) provides evidence that diffusion or mixing over a longer timescale continues to affect the radiocaesium at this depth. Indeed the shape of the 'tail' of the profile gives an exponential fit, decreasing with depth, which is consistent with diffusive movement. However, in terms of the inventory, the amount of radiocaesium below the level corresponding to 1950 is less than 10 % of the total weapons ^{137}Cs inventory. It would therefore appear that the rate of diffusion is minimal and certainly not as significant as is often seen in sediments with a high organic fraction (Davies *et al.*, 1984), but is more in keeping with sediment with a high clay component.

Cs is taken up by clay minerals either by ion exchange into non-exchangeable sites, or by adsorption onto planar or edge sites. The Loch Lomond bedrocks contain the type of micas likely to yield clays with non-exchangeable sites (e.g. illite and vermiculite) and, as was shown from the three samples that were analysed using XRD, muscovite was one of the minerals identified. A degradation product of muscovite is illite, when the interlayer K^+ has been partly leached and replaced by weakly held water molecules or OH^- ions. Therefore it is suggested that whilst a significant proportion of the radiocaesium is taken up into these non-exchangeable sites, some has been adsorbed onto planar or edge sites. At some later date some of the radiocaesium has then desorbed into the pore-water and diffused downwards. Hence there are still distinguishable peaks in the sediment, but also some movement of the radiocaesium has occurred after burial.

3.4.2.2 ^{210}Pb.

As discussed in the introduction (Section 1.3.1) there are two main models that are commonly used in calculating the sediment accumulation rate using ^{210}Pb data. These are (1) the constant initial concentration model (CIC) and (2) the constant rate of supply model (CRS). For the Jenkin core, LL/S3A, both models were used to calculate the accumulation rate and the values obtained compared with that obtained from the radiocaesium data (Section 3.4.2.1).

From the data in Table 3.2 it can be seen that the specific activity of ^{210}Pb is relatively constant below 11.25 cm with an average value of 72.4 ± 21.5 Bq kg^{-1}. This was taken as the 'supported' ^{210}Pb, due to ^{226}Ra decay, and was subtracted from the total specific activity to derive the unsupported component. The natural logarithm of the unsupported activity was taken for each section (apart from the top section which was anomalously high) and then plotted on the y-axis against the mid-point of the cumulative weight (g cm^{-2}) in Figure 3.12. The errors pose an interesting problem, as taking natural logarithms of the unsupported specific activity $\pm 1\sigma$ creates asymmetric error bars in the logarithmic plot. This causes further problems

Figure 3.12 Weighted linear regression using average of +ve and - ve error for points 2-38 in core LL/S3A.

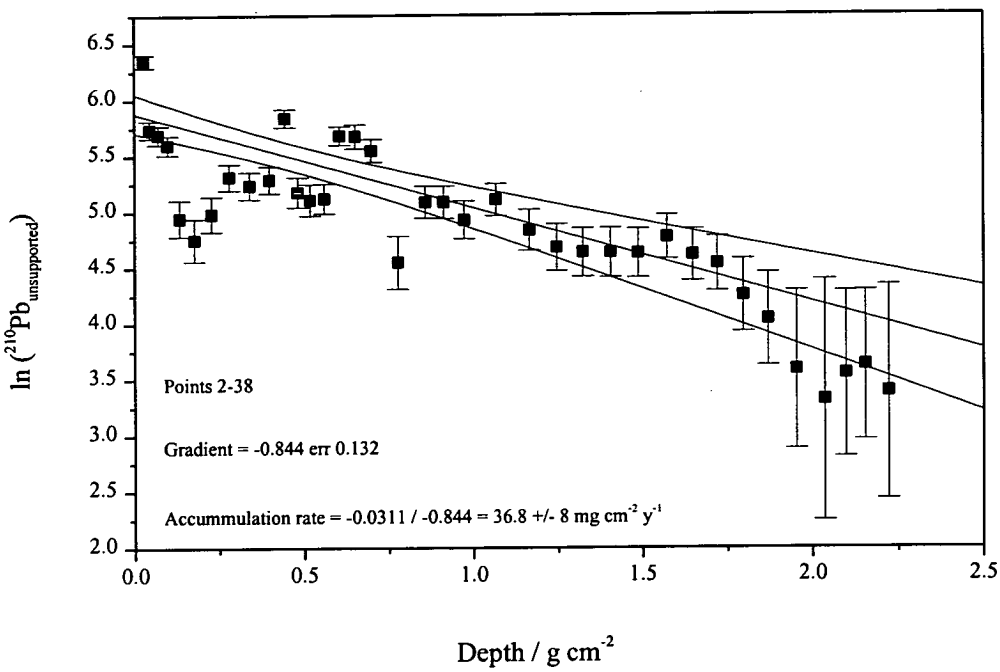

when carrying out the next step in the calculation, the linear regression of the ln ($^{210}Pb_{unsupp}$) against cumulative weight per unit area (g cm^{-2}) using a weighted fit. With a weighted linear regression fit, each point is given a 'weighting' according to its error such that the weighting is determined as the square root of the variance (Miller and Miller, 1988). However, as the software package employed (Microcal™ Origin) could not accommodate asymmetric errors, it was decided to take the average of the plus and minus error. Figure 3.12 shows the linear fit and its 95 % confidence intervals[♦]. The gradient of the line was found to be -0.844 ± 0.132, which gives an accumulation rate of 36.8 ± 8 mg cm^{-2} y^{-1}. This value gives a good correlation with the values of 32.2, 29.6 and 30.6 mg cm^{-2} y^{-1} calculated in Section 3.4.2.1 using radiocaesium, and is within the 32-42 mg cm^{-2} y^{-1} range of ^{210}Pb-derived values calculated by Bryant *et al.* (1993).

The CRS model assumes that there is a constant rate of supply of unsupported ^{210}Pb, no mixing and no post-depositional mobility of ^{210}Pb, but allows for the possibility of a change in sedimentation rate. The total inventory of unsupported ^{210}Pb (Bq m^{-2}) in the core and the inventories below the base of each section are calculated. The age of any individual section is then given by:

$$t_i = \frac{1}{\lambda} \ln \frac{I}{I_i}$$

Where: t_i is the age of the i^{th} layer, λ is the ^{210}Pb decay constant, I is the total unsupported ^{210}Pb inventory and I_i is the unsupported ^{210}Pb inventory below the i^{th} layer.

[♦] Figure shows the graph plotted with the average error bars.

The total inventory, I, was taken as 0.354 Bq cm^{-2}, corresponding to the cumulative inventory down to the base of section S3030A♦. The results for the CRS calculations are shown in Table 3.7 along with the dates derived by ^{210}Pb (CIC) and ^{137}Cs. From Table 3.7 it can be seen that the best agreement is between the ^{210}Pb (CIC) and ^{137}Cs models. The CRS model dates the lower sections of the core earlier than the CIC and ^{137}Cs derived dates. This arises from the likelihood that there is an under-estimation of the total ^{210}Pb inventory and of the total ^{210}Pb inventory below each section, thus giving an increasingly larger effect to the older ages down the core. If the analysis technique was more sensitive it is possible that the activity of ^{210}Pb could be determined closer to the detection limits with lower errors.

The average ^{210}Pb flux to the sediment can be calculated from the total inventory of unsupported ^{210}Pb by:

$$F = I \times \lambda$$

Where: I is the total inventory (Bq m^{-2}) and λ is the ^{210}Pb decay constant (y^{-1}).

For Loch Lomond (south) the flux is calculated as 112.3 Bq m^{-2} y^{-1}, which lies between the values found at two other sites in Loch Lomond of 152 and 72 Bq m^{-2} y^{-1} (Bryant, 1994).

3.4.2.3 Core chronology.

The sedimentation rates obtained via ^{137}Cs and the ^{210}Pb (CIC) model are comparable both to each other and to the findings of Bryant *et al.* (1993) for a core taken from nearby in the loch. For the remaining discussion the sedimentation rate 30.6 ± 1.1 mg cm^{-2} y^{-1}, calculated from the ^{137}Cs over the increment 1986-1963, will be applied to extrapolate a chronology for the core LL/S3A as it has the lowest error. Where appropriate, however, for key points, the date obtained for ^{210}Pb (CIC) will be quoted

♦ below this depth the errors for each section are greater than the calculated inventory for that section.

Table 3.7 Comparison of dates using ^{137}Cs and CIC and CRS ^{210}Pb models in core LL/S3A.

Sample Code	^{137}Cs Years of accumulation / y	^{137}Cs Date	CIC model Years of accumulation / y	CIC model Date	CRS model Years of accumulation / y	CRS model Date
S3001A	0.3	1990.6	0.3	1990.6	5.7	1985.2
S3002A	0.9	1990.0	0.7	1990.2	6.7	1984.2
S3003A	1.5	1989.4	1.2	1989.7	7.4	1983.5
S3004A	2.3	1988.6	1.9	1989.0	8.3	1982.6
S3005A	3.2	1987.7	2.6	1988.3	9.3	1981.6
S3006A	4.3	1986.6	3.5	1987.4	9.9	1981.0
S3007A	5.7	1985.2	4.7	1986.2	10.6	1980.3
S3008A	7.4	1983.5	6.1	1984.8	11.6	1979.3
S3009A	9.0	1981.9	7.5	1983.4	13.0	1977.9
S3010A	11.0	1979.9	9.1	1981.8	14.7	1976.2
S3011A	12.9	1978.0	10.6	1980.3	16.1	1974.8
S3012A	14.4	1976.5	11.8	1979.1	19.3	1971.6
S3013A	15.6	1975.3	12.8	1978.1	20.2	1970.7
S3014A	16.8	1974.1	13.8	1977.1	21.4	1969.5
S3015A	18.1	1972.8	14.9	1976.0	22.7	1968.2
S3016A	19.6	1971.3	16.1	1974.8	25.4	1965.5
S3017A	21.1	1969.8	17.4	1973.5	27.9	1963.0
S3018A	22.6	1968.3	18.6	1972.3	30.8	1960.1
S3019A	25.1	1965.8	20.7	1970.2	33.2	1957.7
S3020A	27.8	1963.1	22.9	1968.0	35.7	1955.2
S3021A	29.5	1961.4	24.3	1966.6	37.9	1953.0
S3022A	31.5	1959.4	25.9	1965.0	40.9	1950.0
S3023A	34.5	1956.4	28.4	1962.5	47.6	1943.3
S3024A	37.7	1953.2	31.1	1959.8	52.1	1938.8
S3025A	40.3	1950.6	33.2	1957.7	58.3	1932.6
S3026A	42.9	1948.0	35.3	1955.6	63.2	1927.7
S3027A	45.5	1945.4	37.5	1953.4	69.2	1921.7
S3028A	48.2	1942.7	39.7	1951.2	76.1	1914.8
S3029A	50.9	1940.0	41.9	1949.0	88.3	1902.6
S3030A	53.3	1937.6	44.0	1946.9	98.2	1892.7
S3031A	55.7	1935.2	45.9	1945.0	118.1	1872.8
S3032A	58.1	1932.8	47.9	1943.0	141.4	1849.5
S3033A	60.5	1930.4	49.8	1941.1		
S3034A	63.2	1927.7	52.1	1938.8		
S3035A	65.9	1925.0	54.3	1936.6		
S3036A	67.8	1923.1	55.9	1935.0		
S3037A	69.7	1921.2	57.4	1933.5		
S3038A	71.9	1919.0	59.2	1931.7		
S3039A	74.8	1916.1	61.6	1929.3		
S3040A	77.5	1913.4	63.9	1927.0		
S3041A	79.5	1911.4	65.5	1925.4		
S3042A	81.8	1909.1	67.4	1923.5		
S3043A	84.5	1906.4	69.7	1921.2		
S3044A	87.6	1903.3	72.2	1918.7		
S3045A	90.5	1900.4	74.6	1916.3		
S3046A	93.8	1897.1	77.3	1913.6		
S3047A	96.5	1894.4	79.5	1911.4		
S3048A	98.1	1892.8	80.9	1910.0		

alongside. The CRS model has not been used due to the likelihood that the ^{210}Pb inventory is under-estimated.

3.4.2.4 Stable lead isotopes and lead.

In order to look in more detail at changes in sources of Pb with time, the excess Pb concentration and its $^{206}Pb/^{207}Pb$ atom ratio were used to estimate the anthropogenic input of Pb. The constant value for Pb concentration and $^{206}Pb/^{207}Pb$ atom ratio at depth of 15 ± 4 mg kg^{-1} and 1.174 ± 0.002, respectively, were taken to represent the natural concentration and isotopic signature of Pb. Calculating the excess Pb concentration involved a straightforward subtraction of 15 ± 4 mg kg^{-1} from the Pb concentration for each section. The excess Pb concentration (mg kg^{-1}) was then multiplied by the sedimentation rate of ♦ 0.309 kg m^{-2} y^{-1} to give the excess Pb flux (mg m^{-2} y^{-1}). The $^{206}Pb/^{207}Pb$ ratio of the excess Pb was calculated using the following equation:

$$^{206}Pb/^{207}Pb\ ratio_{excess} = [(Pb_{meas} \times {}^{206}Pb/^{207}Pb_{meas}) - (15 \times 1.174)] / (Pb_{meas} - 15)$$

The results from these calculations are shown in Table 3.8 along with the original Pb isotope data.

♦ 0.309 kg m^{-2} y^{-1} is the figure published in Farmer *et al.* (1996) and was calculated taking the bottom, rather than the mid-point, of the 5.7-6.0 cm section in LL/S3A as 1963. This figure will be used here for consistency with the published data.

Table 3.8 Excess metal fluxes and excess $^{206}Pb/^{207}Pb$ atom ratios for Loch Lomond (south) core LL/S3B.

Sample Code	Depth /cm	Date	Excess Pb flux / mg m^{-2} y^{-1}	Excess Zn flux / mg m^{-2} y^{-1}	Excess Cu flux / mg m^{-2} y^{-1}	$^{206}Pb/^{207}Pb$	σ_{n-1}	Excess $^{206}Pb/^{207}Pb$	σ_{n-1}
S3001B	0.0-0.3	1990.8	18.5	112.2	18.4	1.135	0.006	1.125	0.008
S3002B	0.3-0.6	1990.5	18.8	114.6	9.9	1.136	0.007	1.127	0.009
S3003B	0.6-0.9	1990.0	15.8	114.6	5.6	1.141	0.003	1.131	0.004
S3004B	0.9-1.2	1989.3	15.4	96.7	3.1	1.141	0.002	1.131	0.003
S3005B	1.2-1.5	1988.4	17.3	85.0	1.9	1.139	0.002	1.130	0.003
S3006B	1.5-1.8	1987.2	18.5	73.2	2.9	1.141	0.002	1.133	0.003
S3007B	1.8-2.1	1985.7	17.9	100.7	3.2	1.135	0.001	1.125	0.001
S3008B	2.1-2.4	1983.9	20.4	123.3	3.5	1.140	0.004	1.132	0.005
S3009B	2.4-2.7	1982.3	30.0	114.0	3.4	1.135	0.001	1.129	0.001
S3010B	2.7-3.0	1980.8	28.4	132.6	3.8	1.137	0.002	1.131	0.002
S3011B	3.0-3.3	1979.0	33.7	162.2	4.7	1.135	0.005	1.130	0.006
S3012B	3.3-3.6	1977.2	37.4	144.3	4.4	1.129	0.004	1.123	0.005
S3013B	3.6-3.9	1975.6	41.1	142.1	5.1	1.127	0.004	1.122	0.005
S3014B	3.9-4.2	1974.0	41.7	133.2	4.5	1.131	0.005	1.126	0.006
S3015B	4.2-4.5	1972.4	37.1	144.6	4.8	1.133	0.006	1.128	0.007
S3016B	4.5-4.8	1970.5	37.4	161.0	5.5	1.138	0.005	1.134	0.006
S3017B	4.8-5.1	1968.7	36.2	153.6	5.5	1.141	0.005	1.137	0.006
S3018B	5.1-5.4	1967.0	38.3	149.9	5.2	1.139	0.005	1.135	0.006
S3019B	5.4-5.7	1965.1	35.8	158.8	5.1	1.139	0.005	1.134	0.006
S3020B	5.7-6.0	1963.3	41.4	138.4	5.3	1.141	0.005	1.137	0.006
S3021B	6.0-6.3	1961.7	41.7	135.7	5.1	1.140	0.003	1.136	0.003
S3022B	6.3-6.6	1959.9	44.2	132.9	4.8	1.144	0.005	1.141	0.006
S3023B	6.6-6.9	1957.7	41.4	141.5	5.0	1.147	0.005	1.144	0.006
S3024B	6.9-7.2	1955.5	41.4	148.9	4.7	1.147	0.005	1.144	0.006
S3025B	7.2-7.5	1953.8	40.8	149.6	4.9	1.149	0.004	1.146	0.005

Table 3.8 Excess metal fluxes and excess $^{206}Pb/^{207}Pb$ atom ratios for Loch Lomond (south) core LL/S3B, continued.

Sample Code	Depth /cm	Date	Excess Pb flux / mg m^{-2} y^{-1}	Excess Zn flux / mg m^{-2} y^{-1}	Excess Cu flux / mg m^{-2} y^{-1}	$^{206}Pb/^{207}Pb$	σ_{n-1}	Excess $^{206}Pb/^{207}Pb$	σ_{n-1}
S3026B	7.5-7.8	1951.7	40.8	165.0	4.4	1.150	0.005	1.147	0.006
S3027B	7.8-8.1	1949.4	42.0	158.8	4.4	1.151	0.005	1.148	0.006
S3028B	8.1-8.4	1947.3	42.0	163.2	4.5	1.153	0.005	1.151	0.006
S3029B	8.4-8.7	1945.2	43.3	161.0	4.2	1.152	0.005	1.150	0.006
S3030B	8.7-9.0	1942.6	43.0	137.2	4.2	1.158	0.002	1.156	0.002
S3031B	9.0-9.3	1939.9	43.6	119.0	3.3	1.160	0.005	1.159	0.006
S3032B	9.3-9.6	1937.5	40.2	111.5	3.4	1.159	0.005	1.157	0.006
S3033B	9.6-9.9	1934.8	39.9	110.0	3.8	1.162	0.005	1.161	0.006
S3034B	9.9-10.2	1932.1	38.9	104.1	3.1	1.161	0.005	1.159	0.006
S3035B	10.2-10.5	1929.8	40.2	93.0	3.0	1.162	0.005	1.161	0.006
S3036B	10.5-10.8	1927.2	37.7	87.1	3.5	1.170	0.005	1.170	0.006
S3037B	10.8-11.1	1924.3	40.5	77.6	2.8	1.168	0.005	1.167	0.006
S3038B	11.1-11.4	1921.2	39.9	71.1	3.0	1.167	0.005	1.166	0.006
S3039B	11.4-11.7	1917.8	35.5	64.6	3.1	1.166	0.005	1.165	0.006
S3040B	11.7-12.0	1914.3	33.4	62.7	2.7	1.170	0.003	1.169	0.003
S3041B	12.0-12.3	1909.5	28.7	51.9	2.4	1.171	0.005	1.171	0.006
S3042B	12.3-12.6	1904.6	28.4	49.1	2.4	1.172	0.005	1.172	0.006
S3043B	12.6-12.9	1900.7	30.9	46.4	2.5	1.167	0.005	1.166	0.006
S3044B	12.9-13.2	1897.0	33.4	47.6	2.8	1.170	0.005	1.169	0.006
S3045B	13.2-13.5	1892.9	34.0	43.0	3.1	1.168	0.005	1.167	0.006
S3046B	13.5-13.8	1888.3	34.6	43.9	2.8	1.174	0.005	1.174	0.006
S3047B	13.8-14.1	1883.3	33.4	36.5	2.5	1.170	0.005	1.169	0.006
S3048B	14.1-14.4	1877.8	36.5	34.6	2.0	1.175	0.005	1.175	0.006
S3049B	14.4-14.7	1873.1	34.3	31.5	2.4	1.169	0.005	1.168	0.006
S3050B	14.7-15.0	1868.9	26.9	28.4	2.1	1.171	0.007	1.170	0.008

Table 3.8 Excess metal fluxes and excess $^{206}Pb/^{207}Pb$ atom ratios for Loch Lomond (south) core LL/S3B, continued.

Sample Code	Depth /cm	Date	Excess Pb flux / mg m^{-2} y^{-1}	Excess Zn flux / mg m^{-2} y^{-1}	Excess Cu flux / mg m^{-2} y^{-1}	$^{206}Pb/^{207}Pb$	σ_{n-1}	Excess $^{206}Pb/^{207}Pb$	σ_{n-1}
S3051B	15.0-15.3	1864.1	27.8	22.2	1.2	1.171	0.006	1.170	0.007
S3052B	15.3-15.6	1859.1	33.1	20.4	1.7	1.169	0.002	1.168	0.002
S3053B	15.6-15.9	1853.9	37.1	15.5	1.2	1.170	0.005	1.169	0.006
S3054B	15.9-16.2	1848.8	29.7	14.8	1.6	1.170	0.005	1.169	0.006
S3055B	16.2-16.5	1843.5	24.7	10.8	1.7	1.172	0.004	1.172	0.005
S3056B	16.5-16.8	1838.4	21.6	7.4	1.5	1.170	0.005	1.169	0.006
S3057B	16.8-17.1	1833.6	18.5	6.5	0.8	1.170	0.003	1.169	0.004
S3058B	17.1-17.4	1829.0	13.6	7.7	0.9	1.170	0.005	1.169	0.007
S3059B	17.4-17.7	1824.5	11.7	8.0	1.2	1.172	0.004	1.171	0.006
S3060B	17.7-18.0	1819.3	9.3	7.4	1.1	1.170	0.006	1.168	0.009
S3061B	18.0-18.3	1814.2	7.7	4.0	1.0	1.176	0.005	1.177	0.008
S3062B	18.3-18.6	1809.4	8.0	6.8	1.5	1.174	0.003	1.174	0.005
S3063B	18.6-18.9	1804.2	8.0	1.9	0.2	1.175	0.005	1.176	0.008
S3064B	18.9-19.2	1798.7	8.3	2.8	0.1	1.177	0.005	1.179	0.008
S3065B	19.2-19.5	1793.5	7.7	0.0	1.0	1.180	0.003	1.184	0.005
S3066B	19.5-19.8	1788.7	8.3	2.2	0.6	1.177	0.001	1.179	0.002
S3067B	19.8-20.1	1783.6	7.7	2.5	0.9	1.179	0.001	1.182	0.002
S3068B	20.1-20.4	1778.2	8.7	4.3	1.3	1.178	0.004	1.180	0.006
S3069B	20.4-20.7	1772.7	5.3	3.1	1.7	1.175	0.004	1.176	0.008
S3070B	20.7-21.0	1766.6	4.9	5.3	1.5	1.175	0.001	1.176	0.003
S3071B	21.0-21.3	1760.4	4.9	2.5	1.5	1.179	0.004	1.184	0.008
S3072B	21.3-21.6	1754.6	4.3	2.5	1.1	1.177	0.003	1.180	0.007
S3073B	21.6-21.9	1748.5	4.0	1.2	1.1	1.175	0.004	1.176	0.009
S3074B	21.9-22.2	1742.5	4.9	4.6	1.1	1.168	0.004	1.162	0.008
S3075B	22.2-22.5	1737.2	4.6	4.0	1.2	1.171	0.003	1.168	0.006

Table 3.8 Excess metal fluxes and excess $^{206}Pb/^{207}Pb$ atom ratios for Loch Lomond (south) core LL/S3B, continued.

Sample Code	Depth /cm	Date	Excess Pb flux / mg m^{-2} y^{-1}	Excess Zn flux / mg m^{-2} y^{-1}	Excess Cu flux / mg m^{-2} y^{-1}	$^{206}Pb/^{207}Pb$	σ_{n-1}	Excess $^{206}Pb/^{207}Pb$	σ_{n-1}
S3076B	22.5-22.8	1731.3	4.0	3.1	0.3	1.177	0.002	1.180	0.005
S3077B	22.8-23.1	1725.1	4.3	2.5	1.1	1.178	0.001	1.182	0.003
S3078B	23.1-23.4	1719.7	4.9	0.0	0.9	1.178	0.004	1.182	0.008
S3079B	23.4-23.7	1715.1	3.7	0.0	0.4	1.170	0.002	1.165	0.005
S3080B	23.7-24.0	1710.5	3.1	0.9	0.3	1.176	0.004	1.179	0.010
S3081B	24.0-24.3	1707.3	2.5	1.2	0.4	1.173	0.005	1.171	0.015
S3082B	24.3-24.6	1703.3	1.5	2.5	0.3	1.176	0.005	1.182	0.021
S3083B	24.6-24.9	1696.9	2.5	0.0	0.6	1.177	0.003	1.183	0.009
S3084B	24.9-25.2	1691.4	2.5	0.0	0.3	1.174	0.004	1.174	0.012
S3085B	25.2-25.5	1686.1	3.1	1.5	0.9	1.175	0.001	1.176	0.004
S3086B	25.5-25.8	1681.0	3.1	0.9	0.3	1.177	0.002	1.181	0.006
S3087B	25.8-26.1	1677.0	3.1	2.2	0.6	1.176	0.003	1.179	0.008
S3088B	26.1-26.4	1672.7	1.9	4.0	0.6	1.178	0.004	1.188	0.015
S3089B	26.4-26.7	1668.3	4.6	4.9	0.8	1.177	0.003	1.180	0.006
S3090B	26.7-27.0	1663.1	4.0	2.2	0.5	1.178	0.003	1.183	0.007
S3091B	27.0-27.3	1657.3	2.8	1.2	0.2	1.178	0.003	1.185	0.009
S3092B	27.3-27.6	1651.8	2.5	4.6	0.9	1.178	0.003	1.185	0.009
S3093B	27.6-27.9	1645.9	0.3	2.8	0.4	1.172	0.002		
S3094B	27.9-28.2	1640.7	4.0	3.7	0.6	1.170	0.002	1.165	0.005
S3095B	28.2-28.5	1636.0	4.6	0.9	0.4	1.173	0.002	1.172	0.005
S3096B	28.5-28.8	1630.8							
S3097B	28.8-29.1	1625.9							
S3098B	29.1-29.4	1620.9							
S3099B	29.4-29.7	1615.9							
S3100B	29.7-30.0	1610.8							

The excess Pb concentration and $^{206}Pb/^{207}Pb$ atom ratio are plotted against calendar date in Figure 3.13 (using the sedimentation rate derived from the radiocaesium dating). From this figure, four key periods can be identified: (1) From the mid-17th to early 19th Century (1634-1817), the $^{206}Pb/^{207}Pb$ atom ratio was fairly constant at 1.178 $\pm$ 0.006, during which time the flux slowly increased but never exceeded 8.7 mg m^{-2} y^{-1}. The total excess Pb deposited for this period was 0.84 g m^{-2}, 13 % of the inventory for the core of 6.36 g m^{-2}. (2) At the beginning of the 19th Century the ratio dropped to 1.169 but then remained steady at 1.169 $\pm$ 0.002 from 1817-1929, during which time there was a dramatic increase in flux, which was always $\geq$ 25 mg m^{-2} y^{-1} post-1847 and peaked at 40.5 mg m^{-2} y^{-1} in 1925, as the Industrial Revolution flourished. Prior to the Industrial Revolution there was a variable input of Pb from several sources, resulting in a variable atom ratio. A major influx of a dominant source will therefore have the effect of stabilising the atom ratio, giving rise to the constant value observed. The drop in the atom ratio which occurred at the end of the 18th Century may have been caused by the transition between wood burning and coal burning or from lead smelting. The total excess Pb deposited during 1817 - 1929 was 3.23 g m^{-2}, 51 % of the core inventory. (3) From 1929, soon after the introduction of leaded petrol (Nriagu, 1989b), the isotopic ratio decreased steadily to 1.122 by the mid 1970s, although the flux of Pb remained at $\geq$ 35 mg m^{-2} y^{-1}, peaking at 44.2 mg m^{-2} y^{-1} in 1960, and was still as high as 41.7 mg m^{-2} y^{-1} in 1974. Overall, the excess Pb deposited from 1929 to 1991 was 2.29 g m^{-2}, 36 % of the core inventory. (4) Thereafter, at the same time as steps were taken to reduce the Pb content of petrol in the UK (Monna *et al.*, 1997), the ratio increased slightly to 1.125-1.133 as the flux fell steeply to 15.4-18.8 mg m^{-2} y^{-1} by 1985-1991.

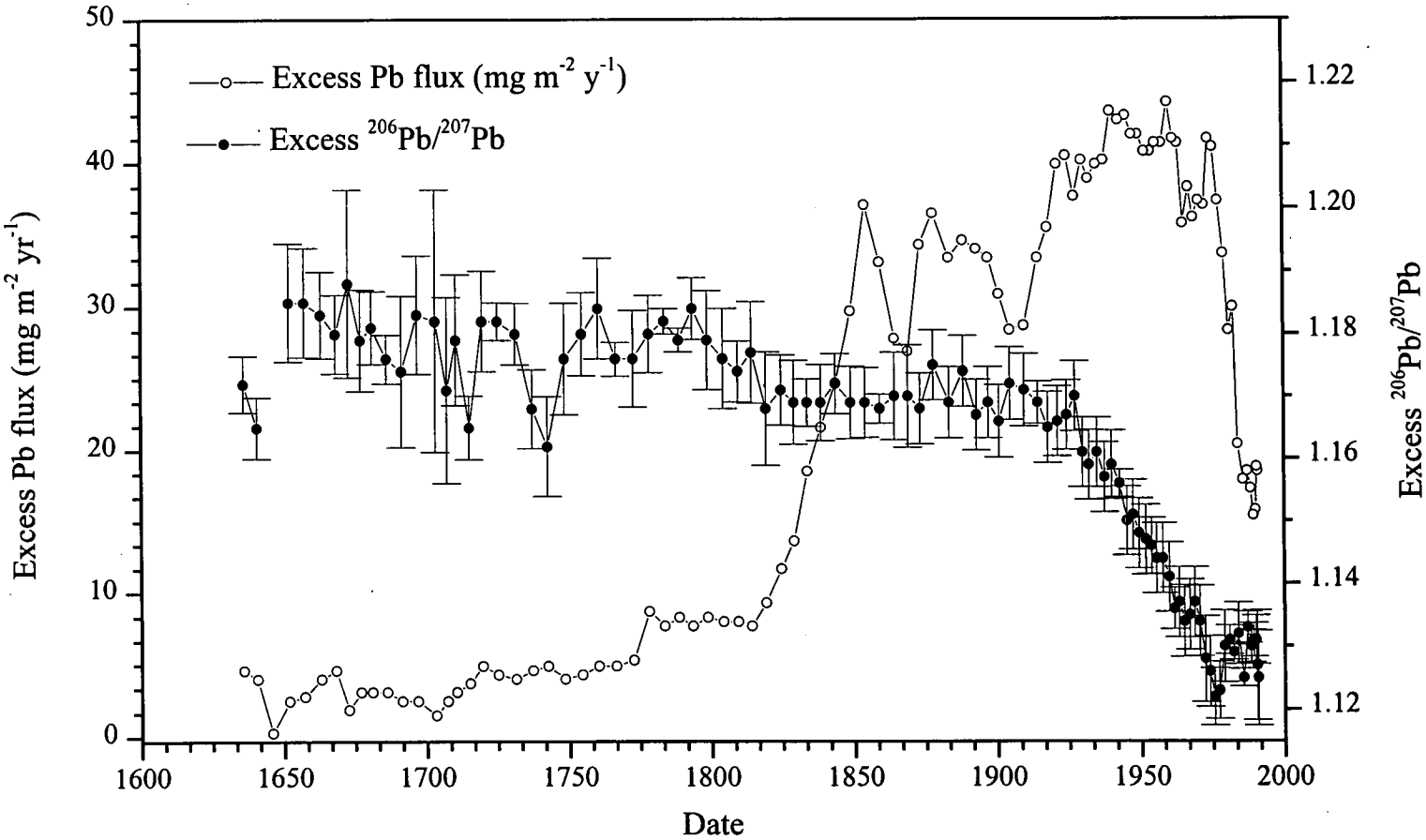

Figure 3.13 Excess Pb flux (mg m^{-2} y^{-1}) and excess ^{206}Pb / ^{207}Pb atom ratio vs date (based on ^{137}Cs) in core LL/S3B.

3.4.2.5 Lead, zinc and copper.

From the discussion in Section 3.4.2.4 it was demonstrated that variations in excess Pb flux were in good agreement with those for the $^{206}Pb/^{207}Pb$ atom ratio. In order to compare the metal fluxes, two graphs of excess metal flux against date were plotted for Pb, Zn and Cu (Figures 3.14 and 3.15). Comparison of the profiles shows that Pb was the first of the metals to increase from a constant background, starting from as early as 1634, whereas for Zn and Cu, the increase did not start until the beginning of the 19th Century. This is further highlighted in Table 3.9 where the distribution of excess inventories for three periods from 1634-1817, 1817-1929 and 1929-1991 show that most Zn and Cu was deposited after 1929. The rate of increase of the Zn deposition was also markedly different to that of Pb as it rose relatively continuously from baseline to its maximum in a period of 75 years. In contrast, the flux of Pb, which, until about the time of increased Zn flux, had been rising slowly, took a very sharp upturn over a period of about 30 years then remained at about this same level for 50 years before increasing again from the beginning of the 20th Century. If the differences in Pb and Zn are due to the differing nature of the input sources of Pb and Zn with time, it implies that there was a large contribution from a predominantly Pb-rich source in the 19th Century. More recently, despite the leaded petrol input post-1930, there has been a proportionally greater input of Zn from other sources. It could also be argued that Zn, which is elevated near the surface, could be subject to post-depostitional mobility, although it is not apparently related to Fe and Mn mobility. In a partitioning study on a site nearby in the loch (Bryant, 1993), it was concluded that Pb was immobile in the sediment and that Zn, although more labile than Pb (Zn was found in the pore-waters in the top 0-1 cm), still reflected historical input..

With Cu (Fig 3.8, 3.15) the situation is less clear, as the top 1 cm shows highly elevated levels of Cu. It is known that Cu is intimately associated with organic matter (e.g. Ridgway and Price, 1987), and it has been shown to be released during burial

Figure 3.14 Excess Pb and Zn flux (mg m^{-2} y^{-1}) vs date (based on ^{137}Cs) in core LL/S3B: (a) full scale and (b) expanded from 1500 A.D.

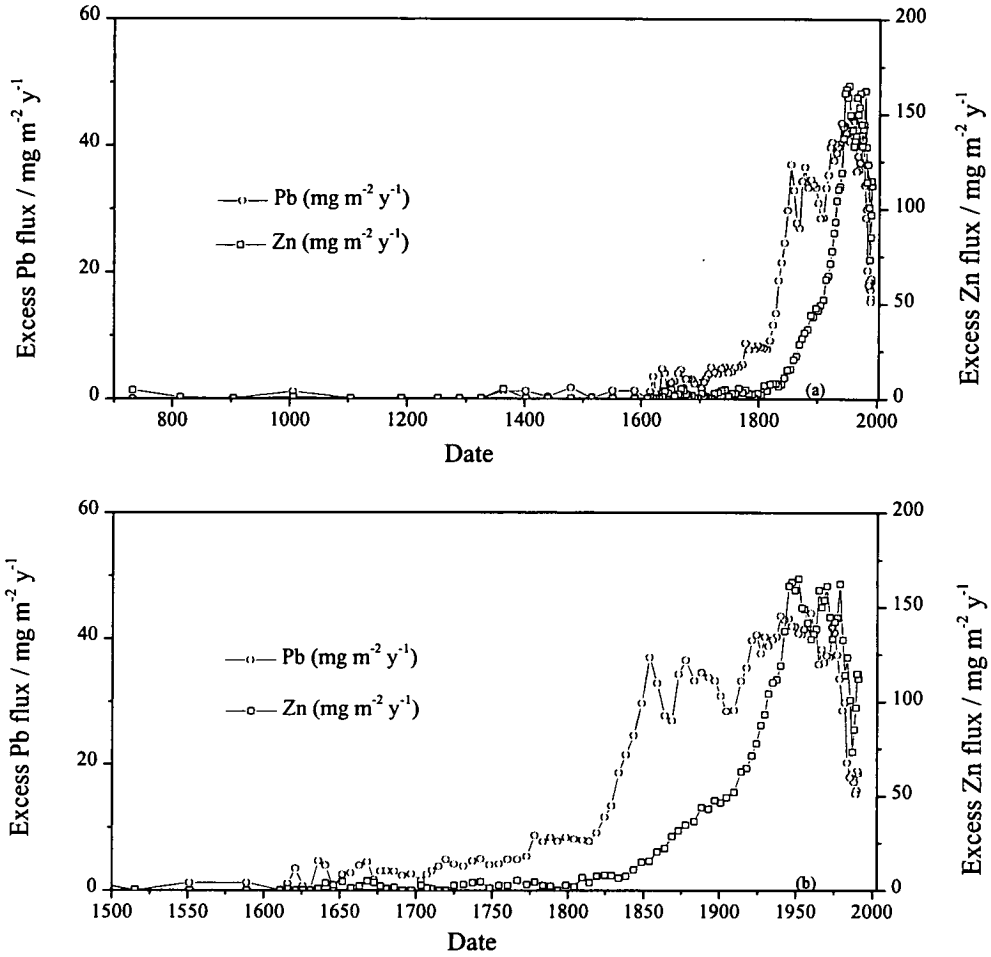

Figure 3.15 Excess Cu flux (mg m^{-2} y^{-1}) vs date (based on ^{137}Cs) in core LL/S3B, expanded from 1500 A.D.

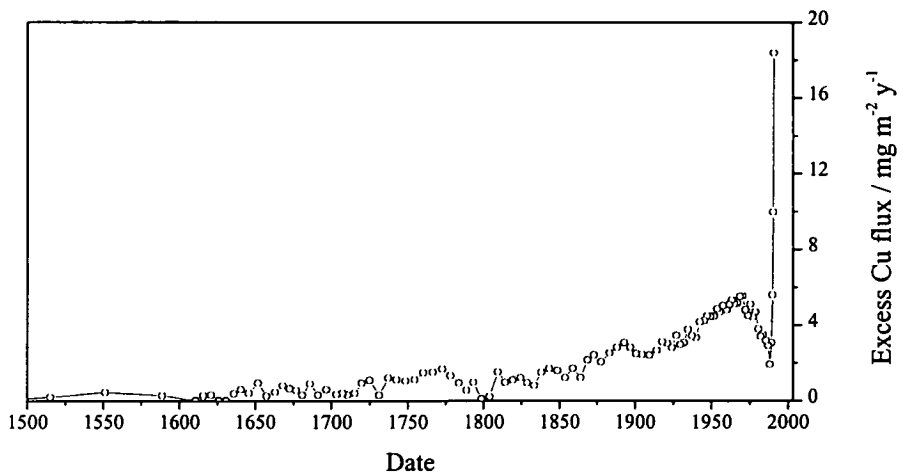

Table 3.9 Total excess inventories for Pb, Zn and Cu in core LL/S3B.

Metal	Background / mg kg^{-1}	Constant from depth / cm	Total excess inventory / g m^{-2}	Period 1634-1817 / g m^{-2}	1817-1929 / g m^{-2}	1929-1991 / g m^{-2}
Pb	15	28.50	6.36	0.84	3.23	2.29
Zn	100	18.75	12.1		2.90	9.15
Cu	23	18.45	0.50		0.20	0.30

in the sediment column (Klinkhammer, 1980). Cu is released from labile fulvic organics which are oxidised by nitrate and oxygen during early diagenesis. The Cu could therefore be released back into the water column or become associated with other sedimentary phases and be retained in the sediment column. The C concentration obtained for this core and for a core taken from an adjacent area (Bryant *et al.*, 1991), indicate a much higher C concentration in the top 1 cm in comparison to the rest of the core. Additionally, for this core the boundary between the oxic and sub-oxic sediment appeared to be at about 1 cm, which corresponds to the point where Cu is at a minimum. Zn is also slightly enhanced in the top 1 cm at the same point as elevated levels of Cu and C, suggesting that there may be an association with the organic material. The deposition of both metals declines after 1970 until the present.

The excess (i.e. anthropogenic) inventories of the metals in Table 3.9, show the values obtained for the metals Pb, Zn and Cu to be comparable with values obtained from two nearby sites from past studies with the exception of Zn, which was proportionally lower in the core studied by Farmer *et al.* (1980).

3.4.2.6 Iron and manganese.

Both profiles show a large sub-surface maximum, with concentrations in excess of the values observed for the rest of the core, over a very narrow zone of 1.20 cm (Fig. 3.16). The peaks in both cases are at their highest for only two 3-mm sections before dropping back to a level closer to that of the concentration at depth. The Mn peak is situated 3-mm closer to the sediment surface than that of Fe and there is an apparent sharp decrease in the concentration for two 3-mm sections from 1.2-1.8 cm before returning to a higher level by the next section. This sharp decrease corresponds to the point of maximum Fe concentration, suggesting that the Fe is having some effect on Mn due to its elevated concentrations.

Figure 3.16 Comparison of the positions of the Fe and Mn peaks in LL/S3B.

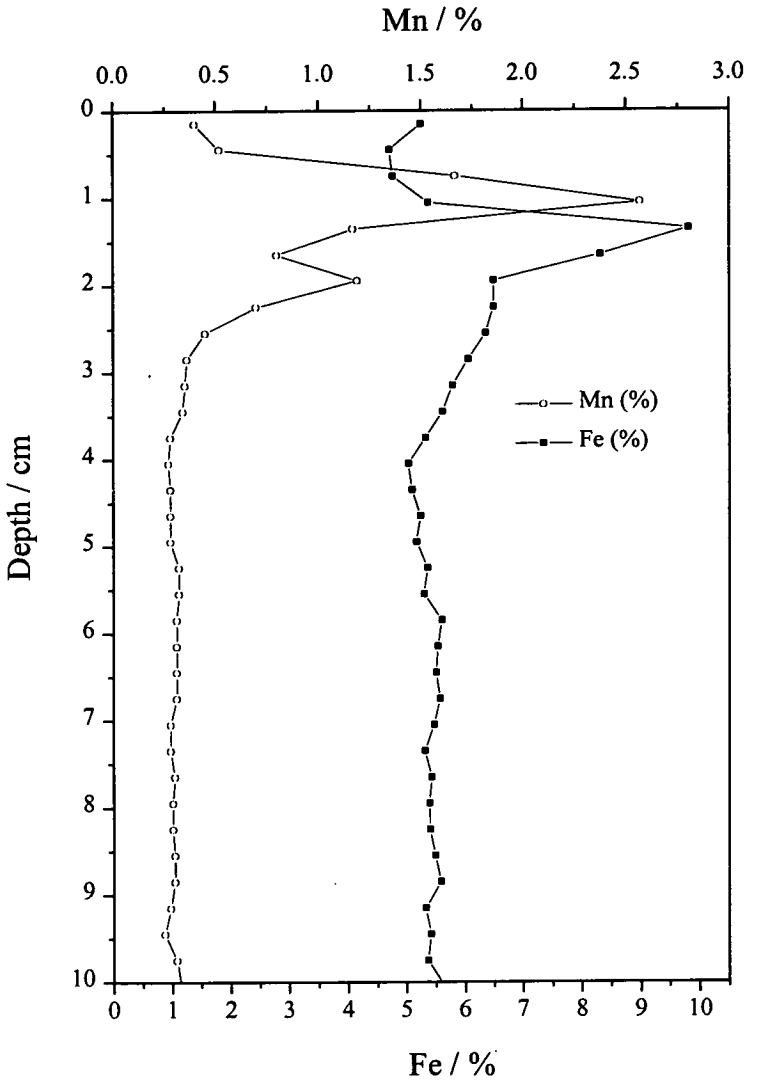

These depth profiles are typical of post-depositional diagenesis. Fe and Mn form insoluble oxide/hydroxide precipitates in the presence of oxygen. They are transferred to the loch bottom and subsequently buried over time. As the conditions in the sediment become anoxic (reducing) due to the degradation of organic matter, the Fe and Mn oxides/hydroxides are reduced to Fe(II) and Mn(II), respectively. In this soluble form they are released to the pore-water, diffusing upwards in the sediment interstitial water until encountering a region where the conditions are still aerobic (oxidising). At this point they are re-oxidised to their insoluble forms of Fe(III) and Mn (III,IV) and precipitate out, re-adsorbing onto the sediment. This usually occurs within a very narrow redoxcline (Stumm and Morgan, 1996). As the thermodynamic and kinetic conditions for these processes are slightly different for the two elements, the solid-phase concentration peaks are observed at different depths. This results from; (1) the reduction of Mn(III,IV) to dissolved Mn(II) occurring at higher redox potentials than that of Fe(III) reduction. (2) the rate of oxidation of Mn(II) to Mn(III,IV) oxides, even if catalysed by surfaces and/or micro-organisms, is usually slower than the oxidation of Fe(II). Therefore the position of the Mn peak in the sediment should occur closer to the surface than that of Fe. If Fe and Mn are plotted against depth (cm) as shown in Figure 3.16 the Mn peak is clearly above that of Fe. The separation is only 3 mm within the sediment, clearly highlighting the benefits of sectioning cores at sub-centimetre resolution. Had the core been sectioned at 1 cm intervals, this fine structure would have been lost.

3.5 Loch Lomond (North).

A Mini-Mackereth core was collected on 16/07/95 from site LL/North (Fig. 3.1) as described in section 2.1.2.1. The core was used for analysis of radionuclides (^{137}Cs, ^{241}Am, ^{210}Pb and ^{226}Ra), heavy metals (Pb, Zn, Cu, Cd, Fe and Mn), and stable Pb isotopes (^{206}Pb, ^{207}Pb and ^{208}Pb).

3.5.1 Results.

An initial inspection of the core (LL/NM) revealed an almost uniform grey colour over its entire length with the exception of the top 2 cm which was brown/orange in colour. Throughout the core, gas bubbles were present which caused some problems with the sectioning as previously mentioned in section 2.1.2.1.

3.5.1.1 Radiocaesium and americium.

The results for the specific activities of ^{137}Cs (Bq kg^{-1}) and ^{241}Am (Bq kg^{-1}) obtained by γ-spectrometry are shown in Table 3.10 and are plotted against depth (cm) in Figure 3.17. ^{134}Cs was not detected in this core as it was analysed 12 years after the Chernobyl deposition. As ^{134}Cs has a half-life of only 2.05 y, any ^{134}Cs deposited in the Chernobyl fallout would have decayed to non-detectable levels.

From Figure 3.17 it can be seen that there are two peaks for ^{137}Cs and that the ^{241}Am corresponds only to the peak situated lower in the sediment. The upper ^{137}Cs peak at 3.5 cm has a maximum specific activity of 2042 ± 223 Bq kg^{-1} and is fairly sharp, extending over less than 2 cm in the sediment. The lower ^{137}Cs peak with a maximum of 657 ± 14 Bq kg^{-1} at 11.5 cm is broader, extending over ~ 5 cm in the sediment. From the base of the lower peak the ^{137}Cs penetrates to a depth of 31 cm, tailing off exponentially. The ^{241}Am peak has a slight bimodal structure.

Table 3.10 ^{137}Cs and ^{241}Am results for Loch Lomond (north) core LL/NM.

Sample Code	Depth / cm	Wet wt / g	Dry wt / g	Mid cum. wt / g cm^{-2}	^{137}Cs / Bq kg^{-1}	σ_{n-1} ^{137}Cs / Bq kg^{-1}	^{241}Am / Bq kg^{-1}	σ_{n-1} ^{241}Am / Bq kg^{-1}
LL/NM001	0.0-0.2	14.444	3.006	0.045	387	22		n/d
LL/NM002	0.2-0.4	10.075	2.126	0.123	291	28		n/d
LL/NM003	0.4-0.6	10.983	2.466	0.192	273	25		n/d
LL/NM004	0.6-0.8	7.555	1.803	0.256	424	51		n/d
LL/NM005	0.8-1.0	8.330	2.160	0.316	429	44		n/d
LL/NM006	1.0-1.2	7.577	1.967	0.378	531	66		n/d
LL/NM007	1.2-1.4	11.768	2.933	0.452	357	28		n/d
LL/NM008	1.4-1.6	11.204	2.731	0.537	409	39		n/d
LL/NM009	1.6-1.8	8.316	2.266	0.613	539	67		n/d
LL/NM010	1.8-2.0	3.801	1.106	0.663	627	138		n/d
LL/NM011	2.0-2.2	9.500	2.309	0.715	482	60		n/d
LL/NM012	2.2-2.4	10.675	2.532	0.788	547	44		n/d
LL/NM013	2.4-2.6	9.567	2.210	0.859	708	66		n/d
LL/NM014	2.6-2.8	6.603	1.412	0.914	542	77		n/d
LL/NM015	2.8-3.0	9.186	1.909	0.964	927	110		n/d
LL/NM016	3.0-3.2	10.317	2.030	1.023	1269	121		n/d
LL/NM017	3.2-3.4	8.215	1.525	1.077	1338	98		n/d
LL/NM018	3.4-3.6	9.432	1.775	1.127	2042	223		n/d
LL/NM019	3.6-3.8	11.430	2.206	1.187	1351	54		n/d
LL/NM020	3.8-4.0	7.082	1.387	1.241	1478	140		n/d
LL/NM021	4.0-4.2	8.076	1.670	1.287	837	125		n/d
LL/NM022	4.2-4.4	6.530	1.442	1.334	286	58		n/d
LL/NM023	4.4-4.6	9.845	1.751	1.382	447	62		n/d
LL/NM024	4.6-4.8	9.373	1.583	1.432	377	32		n/d
LL/NM025	4.8-5.0	10.845	1.809	1.483	328	32		n/d

n/d not detected

Table 3.10 ^{137}Cs and ^{241}Am results for Loch Lomond (north) core LL/NM, continued.

Sample Code	Depth / cm	Wet wt / g	Dry wt / g	Mid cum. wt / g cm^{-2}	^{137}Cs / Bq kg^{-1}	σ_{n-1} ^{137}Cs / Bq kg^{-1}	^{241}Am / Bq kg^{-1}	σ_{n-1} ^{241}Am / Bq kg^{-1}
LL/NM026	5.0-6.0	33.262	5.594	1.595	366	16	8.0	3.6
LL/NM027	6.0-7.0	31.990	6.562	1.778	371	22	n/d	
LL/NM028	7.0-8.0	26.331	6.205	1.970	419	12	n/d	
LL/NM029	8.0-9.0	34.516	7.379	2.175	415	12	5.3	2.2
LL/NM030	9.0-10.0	35.638	6.887	2.390	457	18	6.3	2.9
LL/NM031	10.0-11.0	34.436	6.387	2.590	594	23	12.7	3.6
LL/NM032	11.0-12.0	30.994	5.734	2.773	657	14	13.8	4.4
LL/NM033	12.0-13.0	33.728	6.282	2.954	643	11	6.7	2.0
LL/NM034	13.0-14.0	34.170	6.374	3.144	562	21	13.0	3.5
LL/NM035	14.0-15.0	33.630	6.365	3.336	393	8	10.6	2.1
LL/NM036	15.0-16.0	33.342	6.873	3.536	228	14	6.3	2.1
LL/NM037	16.0-17.0	30.340	6.604	3.739	145	10	10.6	4.5
LL/NM038	17.0-18.0	23.719	6.766	3.940	136	17	n/d	
LL/NM039	18.0-19.0	29.701	7.334	4.153	66	5	n/d	
LL/NM040	19.0-20.0	31.662	6.874	4.367	77	16	n/d	
LL/NM041	20.0-22.0	65.401	13.486	4.674	42	5	n/d	
LL/NM042	22.0-24.0	67.251	14.614	5.097	27	2	n/d	
LL/NM043	24.0-26.0	66.226	14.531	5.536	34	3	n/d	
LL/NM044	26.0-28.0	62.184	13.707	5.962	22	5	n/d	
LL/NM045	28.0-30.0	68.343	15.904	6.408	18	4	n/d	
LL/NM046	30.0-32.0	68.118	16.112	6.891	22	4	n/d	
LL/NM047	32.0-34.0	64.162	15.008	7.360	n/a	n/a	n/d	
LL/NM048	34.0-36.0	66.829	15.560	7.820	n/a	n/a	n/d	
LL/NM049	36.0-38.0	65.925	15.780	8.293	n/a	n/a	n/d	
LL/NM050	38.0-40.0	66.307	16.138	8.774	n/a	n/a	n/d	

n/d not detected

Figure 3.17 ^{137}Cs (Bq kg^{-1}) and ^{241}Am (Bq kg^{-1}) vs depth (cm) in core LL/NM.

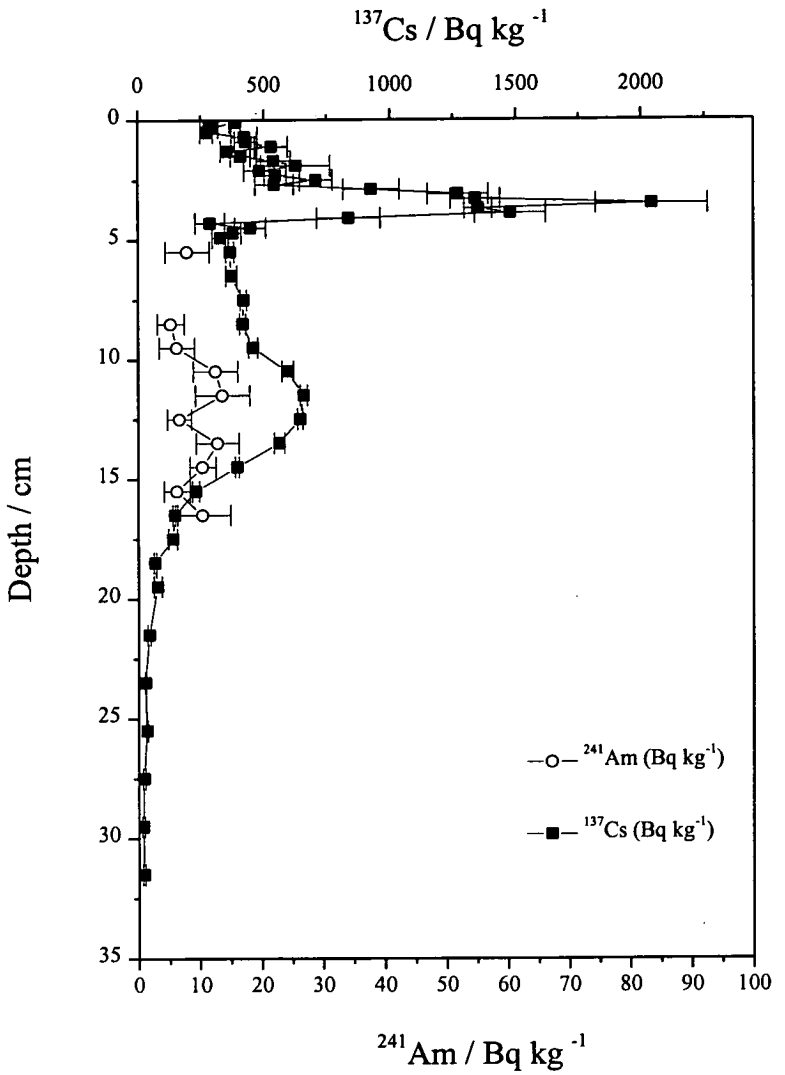

3.5.1.2 ^{210}Pb.

^{210}Pb in core LL/NM was detectable using both α- and γ-spectrometry although the errors using the latter were quite high (^{210}Pb was detectable only by α-spectrometry in core LL/S3A). The results for the specific activity of ^{210}Pb obtained by α- and γ-spectrometry are shown in Table 3.11 and are plotted against depth (cm) in Figure 3.18 (a) and (b), respectively.

Although the ^{210}Pb profiles obtained by the two different counting methods are similar, the errors in general are smaller with α-spectrometry. This is particularly the case in the upper sections where the section weights were much smaller than for the rest of the core. The results from only the α-spectrometry will be used for any subsequent treatment of the ^{210}Pb data.

In Figure 3.18 (a) the specific activity increases from ~ 65 Bq kg^{-1} at the base of the profile to 700 Bq kg^{-1} at the surface. There are two slight peaks with specific activities of 742 and 463 Bq kg^{-1} at 4.1 and 10.5 cm, respectively.

Table 3.11 ^{210}Pb results for Loch Lomond (north) core LL/NM.

Sample Code	Depth / cm	Wet wt / g	Dry wt / g	Mid cum. wt / g cm^{-2}	γ-Spectrometry ^{210}Pb / Bq kg^{-1}	σ_{n-1} ^{210}Pb / Bq kg^{-1}	α-Spectrometry ^{210}Pb / Bq kg^{-1}	σ_{n-1} ^{210}Pb / Bq kg^{-1}	$^{210}Pb_{unsup}$ / Bq kg^{-1}	ln $^{210}Pb_{unsup}$	σ +ve	σ -ve	σ Ave
LL/NM001	0.0-0.2	14.444	3.006	0.045	542	38	652	12	588.8	6.38	0.02	0.02	0.02
LL/NM002	0.2-0.4	10.075	2.126	0.123	807	109	659	11	596.6	6.39	0.02	0.02	0.02
LL/NM003	0.4-0.6	10.983	2.466	0.192	566	81	605	12	542.3	6.30	0.02	0.02	0.02
LL/NM004	0.6-0.8	7.555	1.803	0.256	588	132	573	18	510.2	6.23	0.03	0.04	0.04
LL/NM005	0.8-1.0	8.330	2.160	0.316	596	79	517	12	454.1	6.12	0.03	0.03	0.03
LL/NM006	1.0-1.2	7.577	1.967	0.378	738	157	523	11	460.7	6.13	0.02	0.02	0.02
LL/NM007	1.2-1.4	11.768	2.933	0.452	496	93	504	12	440.8	6.09	0.03	0.03	0.03
LL/NM008	1.4-1.6	11.204	2.731	0.537	568	140	518	13	455.2	6.12	0.03	0.03	0.03
LL/NM009	1.6-1.8	8.316	2.266	0.613	748	212	501	10	438.0	6.08	0.02	0.02	0.02
LL/NM010	1.8-2.0	3.801	1.106	0.663	871	279	632	13	569.1	6.34	0.02	0.02	0.02
LL/NM011	2.0-2.2	9.500	2.309	0.715	447	92	510	9	446.9	6.10	0.02	0.02	0.02
LL/NM012	2.2-2.4	10.675	2.532	0.788	570	103	509	9	445.8	6.10	0.02	0.02	0.02
LL/NM013	2.4-2.6	9.567	2.210	0.859	590	121	540	16	477.2	6.17	0.03	0.03	0.03
LL/NM014	2.6-2.8	6.603	1.412	0.914	752	242	582	13	519.4	6.25	0.03	0.03	0.03
LL/NM015	2.8-3.0	9.186	1.909	0.964	772	159	618	16	555.0	6.32	0.03	0.03	0.03
LL/NM016	3.0-3.2	10.317	2.030	1.023	587	151	581	11	518.3	6.25	0.02	0.02	0.02
LL/NM017	3.2-3.4	8.215	1.525	1.077	744	220	517	10	454.2	6.12	0.02	0.02	0.02
LL/NM018	3.4-3.6	9.432	1.775	1.127	567	245	486	10	423.1	6.05	0.02	0.02	0.02
LL/NM019	3.6-3.8	11.430	2.206	1.187	563	98	482	11	419.7	6.04	0.03	0.03	0.03
LL/NM020	3.8-4.0	7.082	1.387	1.241	1026	381	556	13	493.1	6.20	0.03	0.03	0.03
LL/NM021	4.0-4.2	8.076	1.670	1.287	581	180	742	23	679.6	6.52	0.03	0.04	0.03
LL/NM022	4.2-4.4	6.530	1.442	1.334	797	196	363	16	300.6	5.71	0.05	0.05	0.05
LL/NM023	4.4-4.6	9.845	1.751	1.382	621	179	503	21	440.0	6.09	0.05	0.05	0.05
LL/NM024	4.6-4.8	9.373	1.583	1.432	596	136	548	17	485.7	6.19	0.03	0.04	0.03
LL/NM025	4.8-5.0	10.845	1.809	1.483	825	212	562	16	499.5	6.21	0.03	0.03	0.03

Table 3.11 ^{210}Pb results for Loch Lomond (north) core LL/NM, continued.

Sample Code	Depth / cm	Wet wt / g	Dry wt / g	Mid cum. wt / g cm^{-2}	γ-Spectrometry ^{210}Pb / Bq kg^{-1}	σ_{n-1} ^{210}Pb / Bq kg^{-1}	α-Spectrometry ^{210}Pb / Bq kg^{-1}	σ_{n-1} ^{210}Pb / Bq kg^{-1}	$^{210}Pb_{unsup}$ / Bq kg^{-1}	ln $^{210}Pb_{unsup}$	σ +ve	σ -ve	σ Ave
LL/NM026	5.0-6.0	33.262	5.594	1.595	436	30	461	19	398.0	5.99	0.05	0.05	0.05
LL/NM027	6.0-7.0	31.990	6.562	1.778	450	29	405	17	342.2	5.84	0.05	0.05	0.05
LL/NM028	7.0-8.0	26.331	6.205	1.970	359	27	361	16	398.0	5.99	0.05	0.05	0.05
LL/NM029	8.0-9.0	34.516	7.379	2.175	306	27	354	16	342.2	5.84	0.05	0.05	0.05
LL/NM030	9.0-10.0	35.638	6.887	2.390	303	40	367	9	298.7	5.70	0.05	0.05	0.05
LL/NM031	10.0-11.0	34.436	6.387	2.590	507	27	463	16	304.5	5.72	0.03	0.03	0.03
LL/NM032	11.0-12.0	30.994	5.734	2.773	402	27	425	15	400.5	5.99	0.04	0.04	0.04
LL/NM033	12.0-13.0	33.728	6.282	2.954	393	20	391	16	362.6	5.89	0.04	0.04	0.04
LL/NM034	13.0-14.0	34.170	6.374	3.144	454	29	351	7	328.2	5.79	0.05	0.05	0.05
LL/NM035	14.0-15.0	33.630	6.365	3.336	356	16	360	12	288.0	5.66	0.02	0.02	0.02
LL/NM036	15.0-16.0	33.342	6.873	3.536	317	18	292	7	296.9	5.69	0.04	0.04	0.04
LL/NM037	16.0-17.0	30.340	6.604	3.739	305	26	263	7	228.8	5.43	0.03	0.03	0.03
LL/NM038	17.0-18.0	23.719	6.766	3.940	253	40	243	6	199.9	5.30	0.03	0.04	0.04
LL/NM039	18.0-19.0	29.701	7.334	4.153	244	17	225	9	179.8	5.19	0.03	0.03	0.03
LL/NM040	19.0-20.0	31.662	6.874	4.367	256	29	226	4	161.9	5.09	0.06	0.06	0.06
LL/NM041	20.0-22.0	65.401	13.486	4.674	179	9	206	6	163.0	5.09	0.03	0.03	0.03
LL/NM042	22.0-24.0	67.251	14.614	5.097	155	10	142	3	143.0	4.96	0.04	0.04	0.04
LL/NM043	24.0-26.0	66.226	14.531	5.536	184	9	133	6	79.3	4.37	0.05	0.05	0.05
LL/NM044	26.0-28.0	62.184	13.707	5.962	129	16	117	6	70.3	4.25	0.08	0.09	0.09
LL/NM045	28.0-30.0	68.343	15.904	6.408	108	9	120	16	54.7	4.00	0.10	0.12	0.11
LL/NM046	30.0-32.0	68.118	16.112	6.891	108	11	102	2	57.1	4.04	0.24	0.33	0.29
LL/NM047	32.0-34.0	64.162	15.008	7.360	88	8	93	2	39.1	3.67	0.08	0.08	0.08
LL/NM048	34.0-36.0	66.829	15.560	7.820	88	11	84	2	30.2	3.41	0.10	0.11	0.11
LL/NM049	36.0-38.0	65.925	15.780	8.293	89	16	69	2	21.2	3.06	0.14	0.16	0.15
LL/NM050	38.0-40.0	66.307	16.138	8.774	67	9	63	2	6.7	1.91	0.39	0.64	0.51

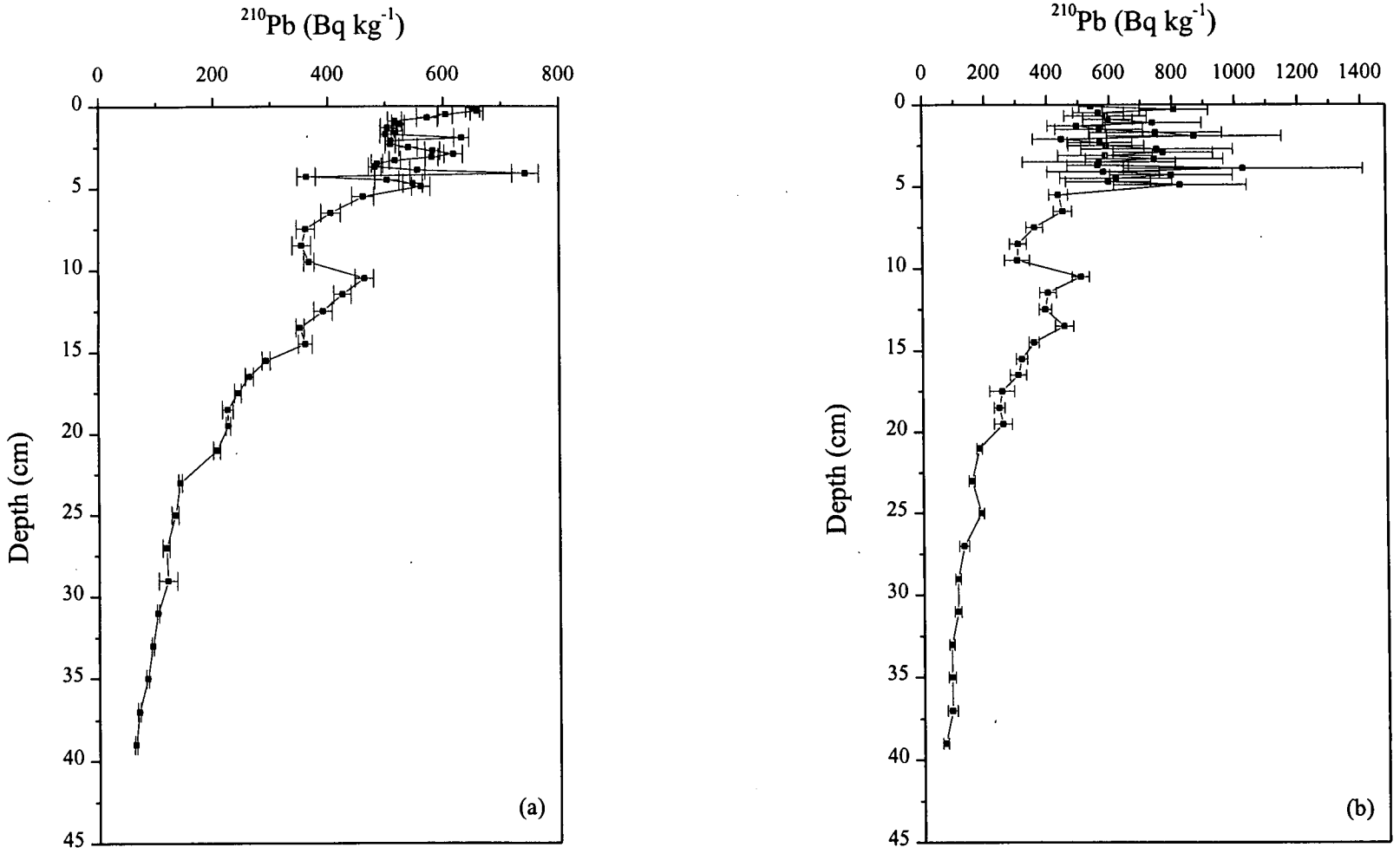

Figure 3.18 ^{210}Pb (Bq kg^{-1}) vs depth (cm) in core LL/NM: (a) α-spectrometry and (b) γ-spectrometry.

3.5.1.3 Heavy metals.

Table 3.12 is a summary of the dry and wet weights and heavy metal data for the Mini-Mackereth core LL/NM. For each metal, a graph of concentration (mg kg^{-1} or %) against depth (cm) was plotted as shown in Figures 3.19-3.24.

The Fe profile, in Figure 3.19, shows a general increase in concentration from 4.26 % at the base of the core to 7.68 % close to the surface with a sharp increase to 8.21 % at the surface. Other features include slight sub-surface peaks at 12.5 cm and 73 cm with a pronounced dip at 61 cm. In Figure 3.20, the Mn profile shows a very steady increase from the base of the core (0.07 %) to within 1.0 cm of the surface (0.21 %). Above this point there is a sharp rise to 0.71 % at the surface. Other minor features include slight dips at 61 and 8.0 cm.

The Pb profile (Fig. 3.21) rises gradually from 24 mg kg^{-1} at the base of the core until 47 cm, then at a faster rate to give a broad peak covering ~25 cm with a maximum of 170 mg kg^{-1} at 14.5 cm. As with both the Fe and Mn profiles, there is a decrease over 59-63 cm to a minimum of 39 mg kg^{-1} (a drop of ~29 mg kg^{-1}). Above 14.5 cm there is a steady decline to 60-70 mg kg^{-1} in the uppermost 2 cm.

As shown in Figure 3.22 the Zn concentration gradually increases from 89 mg kg^{-1} at the base to 132 mg kg^{-1} at 53 cm, except for a drop to 95 mg kg^{-1} at 59-63 cm. Above 53 cm, the rate of increase is greater until a maximum of 407 mg kg^{-1} is reached at 10.5 cm. Above that there is a decrease to 215 mg kg^{-1} at the surface. The Cd profile (Fig. 3.23) follows almost exactly the trends as those for Zn. The concentration rises slightly from 0.21 to 0.57 mg kg^{-1} between the base and 53 cm. The minimum at 59-63 cm is 0.22 mg kg^{-1}. From 53 cm the rise in concentration is steeper than in the bottom 30 cm and the profile rises to a maximum of 3.1 mg kg^{-1} at 13.5 cm. Thereafter there is a steady decrease to 1.0 mg kg^{-1} at the surface, interrupted briefly by a peak at 4.7 cm of 2.5 mg kg^{-1}.

The trends for Cu are quite different from those of the other metals (Fig. 3.24). There is an almost constant concentration throughout the core of ~45 mg kg^{-1}, the exception being a dip to 31 mg kg^{-1} at 61 cm. The dip is more pronounced than for the other metals and extends over a greater depth interval.

3.5.1.4 Carbon and Nitrogen.

The results for total C (%) and N (%) are shown in Table 3.12 along with the heavy metal data. Figure 3.25 is a plot of C (%) against depth (cm). The profile increases from 4.7 % at the base until reaching 11.5 % at 49 cm. Above 49 cm the concentration stays constant at 11.5 ± 0.4 % until 9.5 cm, then decreases to the surface, although there is a slight enhancement in the surface layer. Nitrogen remains at a relatively constant concentration of 0.45 ± 0.07 % throughout the core.

Table 3.12 Heavy metal, carbon and nitrogen results for Loch Lomond (north) core LL/NM.

Sample Code	Wet wt / g	Dry wt /g	Mid cum. wt / g cm^{-2}	Mid depth / cm	Fe / %	Mn / %	Pb / mg kg^{-1}	Zn / mg kg^{-1}	Cu / mg kg^{-1}	Cd / mg kg^{-1}	C / %	N / %
LL/NM001	14.444	3.006	0.045	0.1	8.21	0.71	70.2	215.2	49.6	1.04	8.76	0.55
LL/NM002	10.075	2.126	0.123	0.3	7.68	0.34	67.8	225.8	48.2	1.38	8.97	0.55
LL/NM003	10.983	2.466	0.192	0.5	7.47	0.28	64.3	220.2	46.3	1.38	8.00	0.47
LL/NM004	7.555	1.803	0.256	0.7	7.28	0.26	67.3	225.1	46.8	1.30	7.66	0.42
LL/NM005	8.330	2.160	0.316	0.9	7.16	0.25	67.0	230.9	47.4	1.40	7.56	0.48
LL/NM006	7.577	1.967	0.378	1.1	6.71	0.21	64.9	223.3	44.7	1.27	7.43	0.34
LL/NM007	11.768	2.933	0.452	1.3	6.68	0.21	63.5	217.2	44.5	1.30	7.57	0.41
LL/NM008	11.204	2.731	0.537	1.5	7.29	0.22	71.0	233.0	48.9	1.59	8.20	0.42
LL/NM009	8.316	2.266	0.613	1.7	7.21	0.20	68.4	224.0	50.0	1.47	8.39	0.40
LL/NM010	3.801	1.106	0.663	1.9	6.88	0.21	71.9	221.7	50.3	1.37	8.19	0.38
LL/NM011	9.500	2.309	0.715	2.1	6.85	0.20	85.8	226.5	50.0	1.39	not determined	
LL/NM012	10.675	2.532	0.788	2.3	6.90	0.21	77.7	226.6	50.5	1.46	8.57	0.43
LL/NM013	9.567	2.210	0.859	2.5	6.95	0.22	89.2	238.0	50.3	1.53		
LL/NM014	6.603	1.412	0.914	2.7	6.91	0.22	85.1	235.3	49.8	1.53		
LL/NM015	9.186	1.909	0.964	2.9	7.11	0.23	91.5	248.1	50.9	1.71	10.70	0.48
LL/NM016	10.317	2.030	1.023	3.1	7.38	0.24	95.9	255.4	53.3	1.85		
LL/NM017	8.215	1.525	1.077	3.3	7.02	0.22	93.6	252.2	52.0	1.75		
LL/NM018	9.432	1.775	1.127	3.5	6.88	0.22	97.7	262.9	53.8	1.73	9.74	0.48
LL/NM019	11.430	2.206	1.187	3.7	7.39	0.22	110.1	275.8	54.8	1.88		
LL/NM020	7.082	1.387	1.241	3.9	7.18	0.21	104.2	275.2	52.6	1.99	9.98	0.52
LL/NM021	8.076	1.670	1.287	4.1	7.18	0.21	111.6	291.9	51.2	2.27		
LL/NM022	6.530	1.442	1.334	4.3	7.15	0.20	116.7	290.9	51.2	2.18		
LL/NM023	9.845	1.751	1.382	4.5	7.15	0.21	121.7	308.4	51.5	2.29		
LL/NM024	9.373	1.583	1.432	4.7	6.86	0.22	128.1	364.3	54.3	2.53		
LL/NM025	10.845	1.809	1.483	4.9	6.85	0.21	129.1	357.0	53.5	2.23	10.76	0.55

Table 3.12 Heavy metal, carbon and nitrogen results for Loch Lomond (north) core LL/NM, continued.

Sample Code	Wet wt / g	Dry wt /g	Mid cum. wt / g cm^{-2}	Mid depth / cm	Fe / %	Mn / %	Pb / mg kg^{-1}	Zn / mg kg^{-1}	Cu / mg kg^{-1}	Cd / mg kg^{-1}	C / %	N / %
LL/NM026	33.262	5.594	1.595	5.5	6.52	0.20	122.3	355.3	51.8	2.20	not determined	
LL/NM027	31.990	6.562	1.778	6.5	6.37	0.17	122.4	347.6	50.3	2.03		
LL/NM028	26.331	6.205	1.970	7.5	5.98	0.16	123.5	348.0	49.9	2.03		
LL/NM029	34.516	7.379	2.175	8.5	6.20	0.16	128.0	316.9	45.9	2.18		
LL/NM030	35.638	6.887	2.390	9.5	6.04	0.17	147.1	378.6	51.4	2.38	10.19	0.48
LL/NM031	34.436	6.387	2.590	10.5	6.21	0.19	164.8	407.2	53.9	2.72		
LL/NM032	30.994	5.734	2.773	11.5	6.73	0.19	156.5	369.9	49.6	2.85	11.64	0.50
LL/NM033	33.728	6.282	2.954	12.5	6.77	0.18	157.1	368.0	51.0	2.98		
LL/NM034	34.170	6.374	3.144	13.5	6.36	0.19	166.3	392.3	52.0	3.14		
LL/NM035	33.630	6.365	3.336	14.5	6.55	0.18	170.2	382.5	49.4	2.85	11.51	0.48
LL/NM036	33.342	6.873	3.536	15.5	6.46	0.17	158.6	367.2	51.8	2.78		
LL/NM037	30.340	6.604	3.739	16.5	6.04	0.17	143.6	336.2	50.8	2.34		
LL/NM038	23.719	6.766	3.940	17.5	6.07	0.16	142.4	318.5	51.1	2.13		
LL/NM039	29.701	7.334	4.153	18.5	5.76	0.16	143.9	312.4	47.9	2.25		
LL/NM040	31.662	6.874	4.367	19.5	5.80	0.17	152.3	335.7	44.9	2.76	11.58	0.49
LL/NM041	65.401	13.486	4.674	21	5.40	0.16	152.4	346.9	44.8	2.64	11.36	0.51
LL/NM042	67.251	14.614	5.097	23	5.56	0.15	133.6	312.7	43.2	2.44	11.25	0.51
LL/NM043	66.226	14.531	5.536	25	5.75	0.16	134.5	298.2	44.1	2.41	11.63	0.48
LL/NM044	62.184	13.707	5.962	27	5.57	0.15	141.1	293.4	45.5	2.33	11.45	0.47
LL/NM045	68.343	15.904	6.408	29	5.34	0.15	138.0	286.5	44.4	2.20		
LL/NM046	68.118	16.112	6.891	31	5.27	0.14	136.7	274.1	46.2	1.83	11.06	0.43
LL/NM047	64.162	15.008	7.360	33	5.31	0.14	140.8	270.3	49.1	1.69		
LL/NM048	66.829	15.560	7.820	35	5.18	0.14	131.3	244.2	46.6	1.54	11.27	0.44
LL/NM049	65.925	15.780	8.293	37	5.23	0.14	119.3	217.4	45.8	1.16		
LL/NM050	66.307	16.138	8.774	39	5.10	0.13	111.9	208.0	44.7	1.18	12.10	0.57

Table 3.12 Heavy metal, carbon and nitrogen results for Loch Lomond (north) core LL/NM, continued.

Sample Code	Wet wt / g	Dry wt /g	Mid cum. wt / g cm^{-2}	Mid depth / cm	Fe / %	Mn / %	Pb / mg kg^{-1}	Zn / mg kg^{-1}	Cu / mg kg^{-1}	Cd / mg kg^{-1}	C / %	N / %
LL/NM051	66.453	16.354	9.263	41	5.33	0.13	111.5	205.5	45.7	1.19	11.42	0.53
LL/NM052	60.250	14.526	9.728	43	4.62	0.13	105.2	185.1	43.6	0.99	12.35	0.59
LL/NM053	62.176	14.878	10.172	45	4.92	0.13	93.8	170.9	41.1	0.99	not determined	
LL/NM054	62.016	15.620	10.631	47	5.01	0.12	81.2	159.8	41.3	0.85	11.41	0.45
LL/NM055	66.094	17.137	11.125	49	5.12	0.12	77.4	157.7	43.0	0.71	10.46	0.38
LL/NM056	66.993	17.326	11.644	51	5.15	0.12	71.9	144.8	44.2	0.62		
LL/NM057	60.109	15.941	12.145	53	5.02	0.11	71.4	131.6	42.5	0.57	9.47	0.50
LL/NM058	64.419	17.260	12.646	55	5.06	0.12	77.9	130.2	43.8	0.46	7.59	0.37
LL/NM059	65.998	17.168	13.165	57	4.82	0.11	68.7	122.2	40.6	0.44	9.31	0.40
LL/NM060	65.967	20.522	13.733	59	4.30	0.09	39.1	99.7	32.3	0.27	6.01	0.30
LL/NM061	63.763	20.201	14.346	61	4.16	0.09	40.1	95.2	30.6	0.22	7.31	0.35
LL/NM062	67.177	19.066	14.938	63	4.79	0.11	60.8	108.4	35.8	0.45	8.90	0.38
LL/NM063	61.753	16.865	15.479	65	5.02	0.12	67.8	111.7	39.8	0.35		
LL/NM064	66.232	18.469	16.012	67	5.15	0.12	63.0	109.1	42.1	0.34		
LL/NM065	60.125	17.136	16.548	69	5.09	0.11	61.8	108.4	42.7	0.29		
LL/NM066	58.742	17.573	17.071	71	5.28	0.11	51.5	110.4	44.8	0.26		
LL/NM067	66.817	21.407	17.659	73	5.40	0.11	47.4	110.2	48.5	0.29		
LL/NM068	67.708	21.096	18.299	75	5.09	0.10	41.3	106.2	47.0	0.19		
LL/NM069	69.891	21.859	18.947	77	4.81	0.10	38.5	102.0	46.0	0.23	7.45	0.28
LL/NM070	66.813	22.702	19.618	79	4.70	0.09	34.9	96.9	44.2	0.22		
LL/NM071	67.609	23.207	20.310	81	4.58	0.09	37.3	96.3	45.0	0.18		
LL/NM072	64.065	22.148	20.993	83	4.88	0.09	37.0	99.8	46.2	0.20		
LL/NM073	71.708	27.781	21.746	85	4.52	0.08	29.7	95.1	44.6	0.20	6.55	0.23
LL/NM074	69.093	28.430	22.593	87	4.72	0.08	28.5	94.6	46.5	0.17		
LL/NM075	54.083	24.384	23.389	89	4.26	0.07	23.8	89.3	43.5	0.12	4.71	0.14

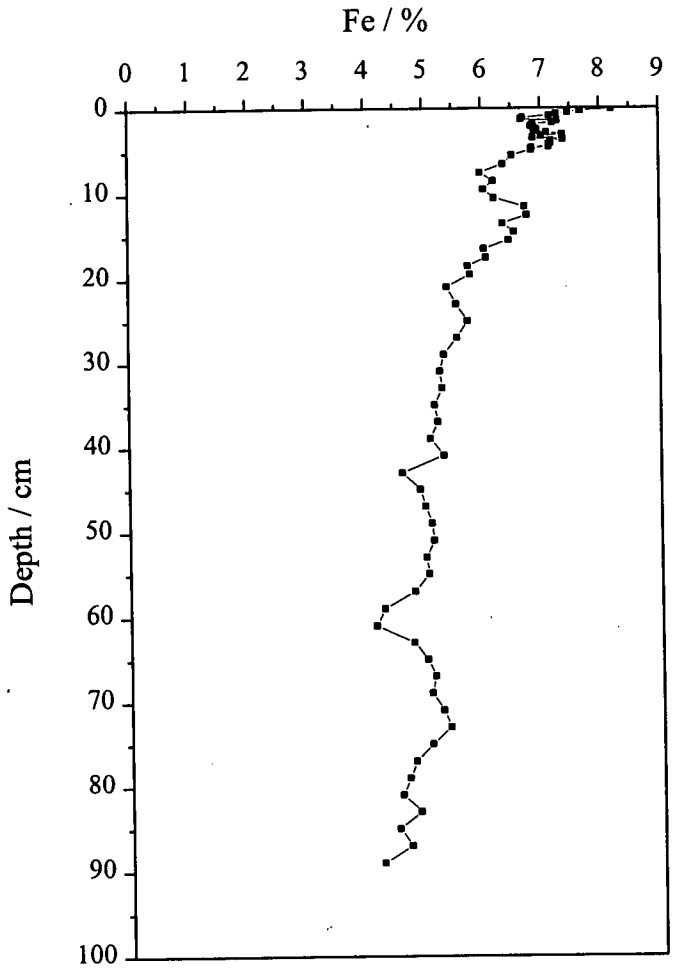

Figure 3.19 Fe (%) vs depth (cm) in core LL/NM.

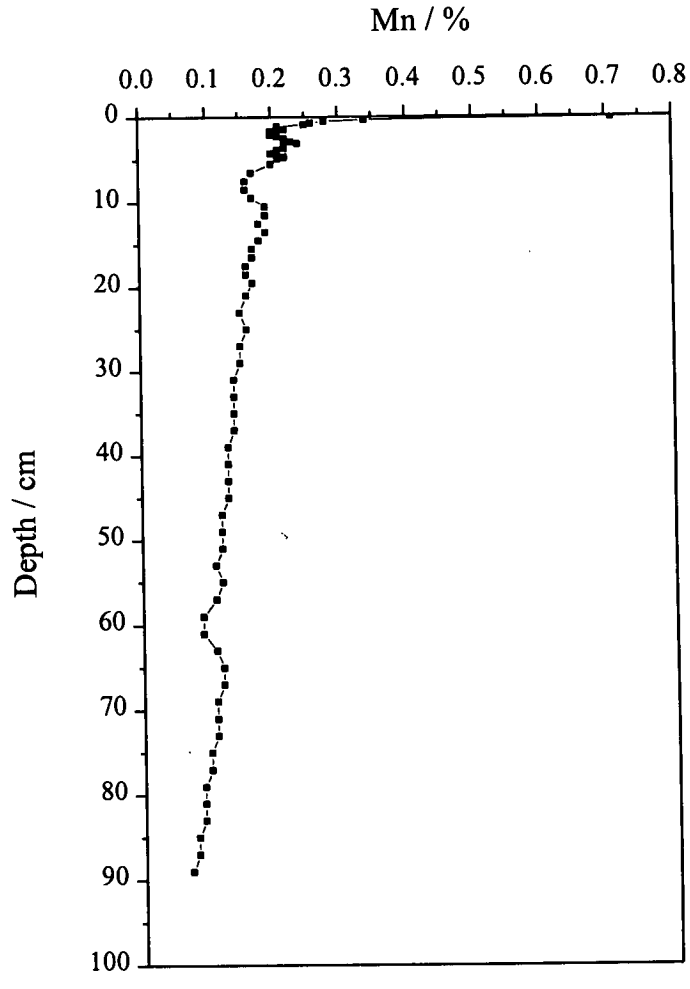

Figure 3.20 Mn (%) vs depth (cm) in core LL/NM.

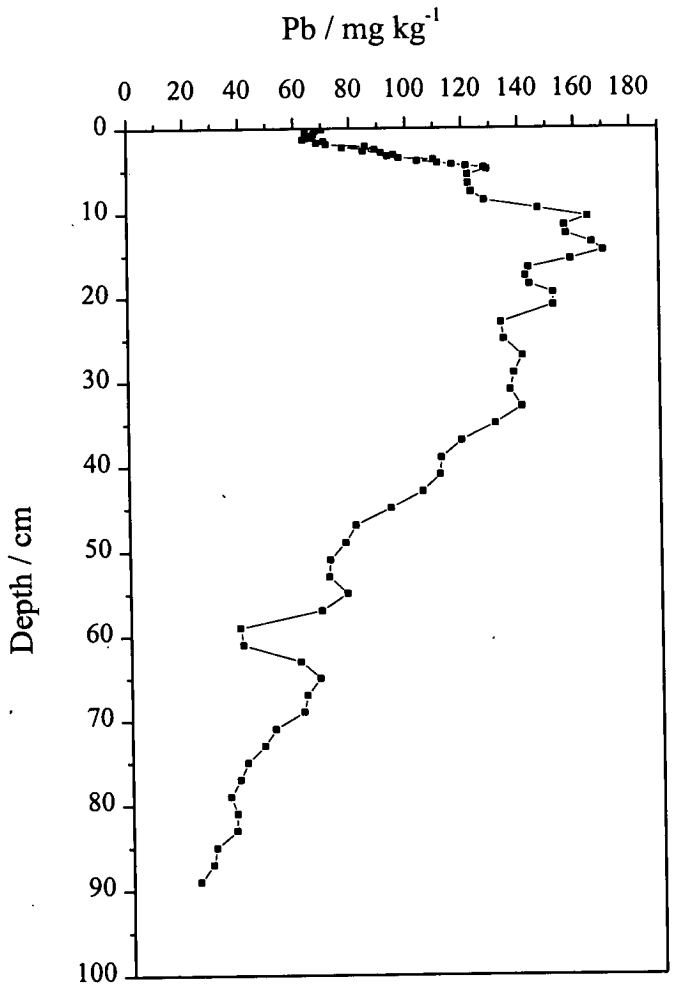

Figure 3.21 Pb (mg kg^{-1}) vs depth (cm) in core LL/NM.

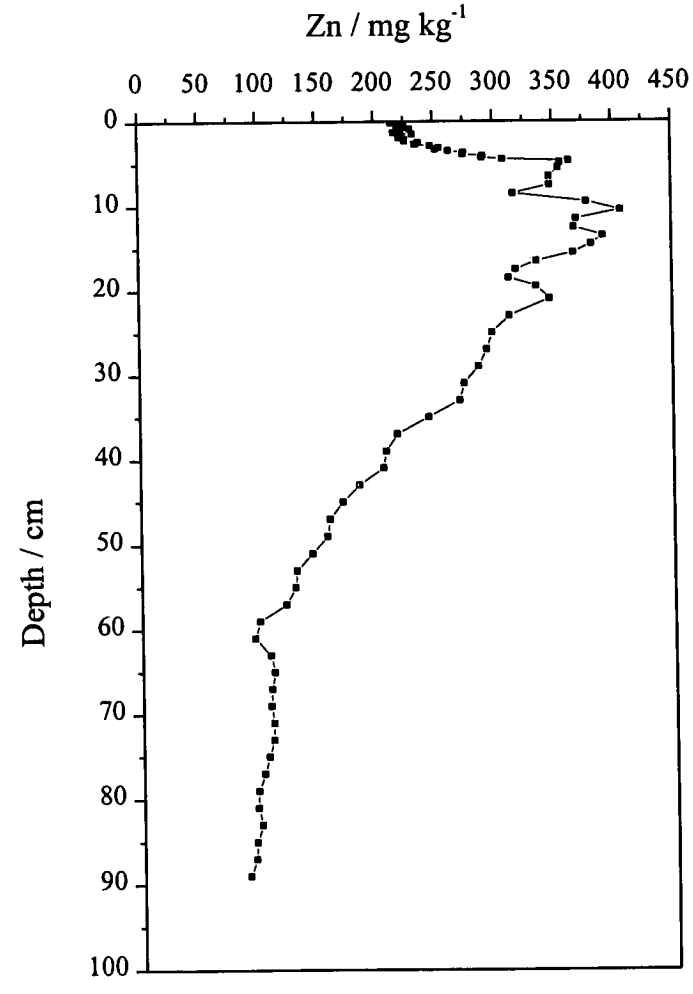

Figure 3.22 Zn (mg kg^{-1}) vs depth (cm) in core LL/NM.

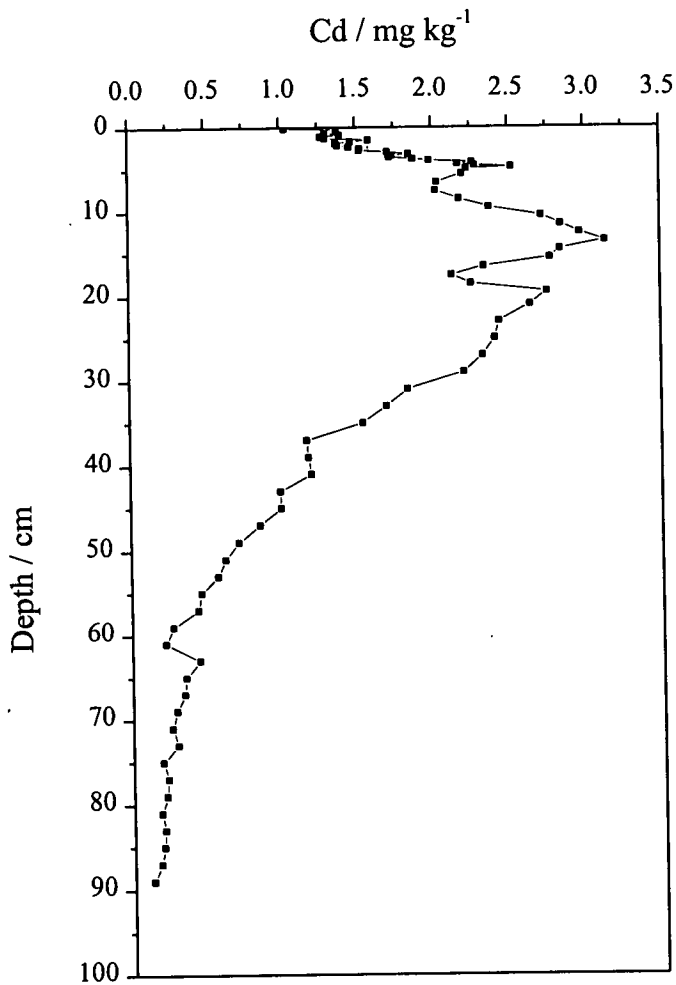

Figure 3.23 Cd (mg kg^{-1}) vs depth (cm) in core LL/NM.

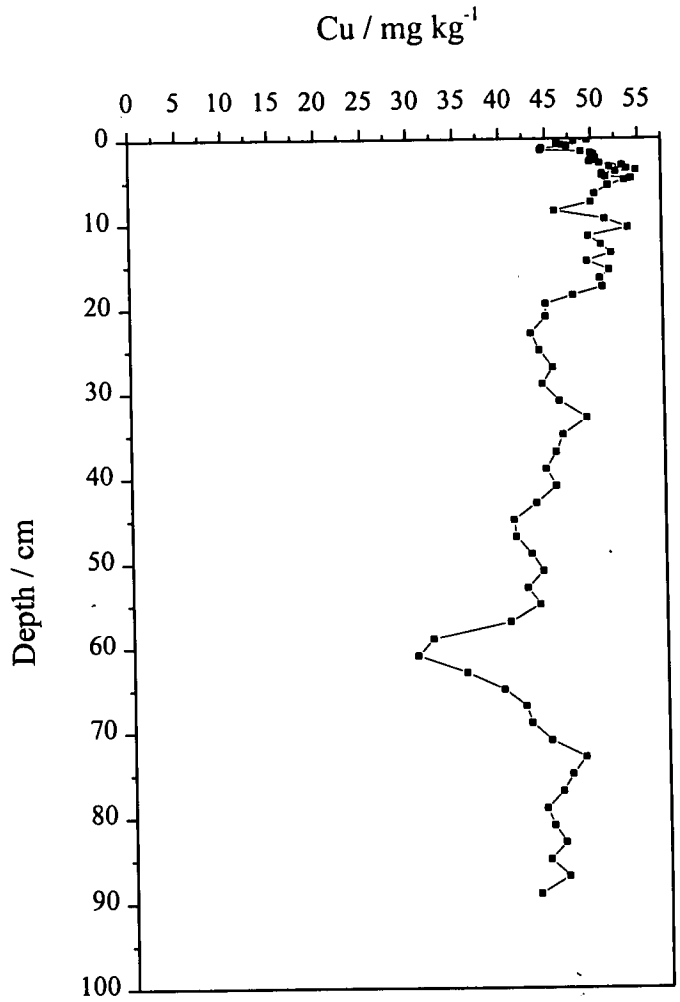

Figure 3.24 Cu (mg kg^{-1}) vs depth (cm) in core LL/NM.

Figure 3.25 C (%) vs depth (cm) in core LL/NM.

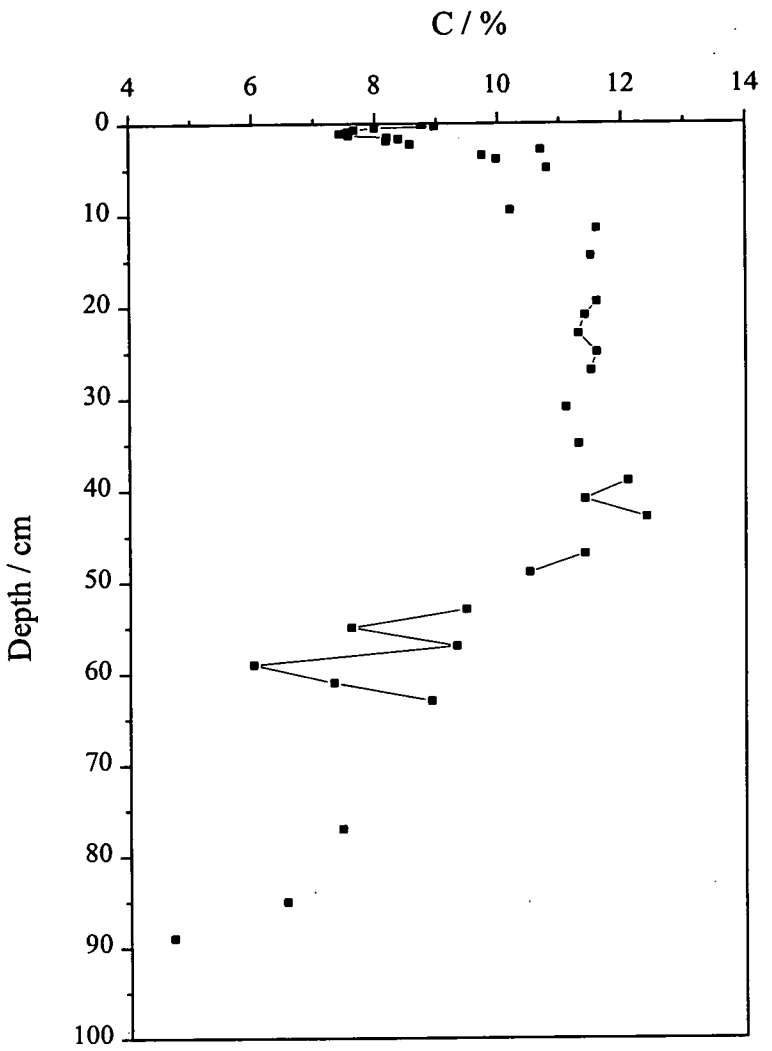

3.5.1.5 Stable lead isotopes.

The results for the stable Pb isotopes and Pb are shown in Table 3.13. Graphs of each of the three atom ratios, $^{206}Pb/^{207}Pb$, $^{208}Pb/^{206}Pb$ and $^{208}Pb/^{207}Pb$, together with Pb concentration (mg kg^{-1}) against depth (cm) are shown in Figures 3.26 (a)-(c) respectively.

As shown in Figure 3.26 (a) the $^{206}Pb/^{207}Pb$ ratio is 1.160 at the base of the core but within 10 cm it has risen to an average value of ~1.167. The ratio remains relatively constant, despite the rise in Pb concentration with a slight dip at 59-63 cm which corresponds to that seen in all of the heavy metal profiles. After the dip the ratio rises to an average value of ~1.169 until 35 cm when it begins a fairly rapid decline, reaching an intermediate minimum value of 1.138 at 11.5 cm. The ratio rises over an interval of 2 cm before continuing its decline to reach a minimum of 1.136 at 5.5 cm. The slight rise corresponds to a drop in the concentration of Pb. Above 5.5 cm the ratio increases to reach 1.150 by the surface.

The $^{208}Pb/^{206}Pb$ and $^{208}Pb/^{207}Pb$ atom ratio profiles in Figures 3.26 (b) and (c) are similar in shape but are very "noisy", with relatively large errors, throughout the core. Over the bottom 55 cm of the core there is an average of 2.114 ± 0.002 and 2.466 ± 0.002 for $^{208}Pb/^{206}Pb$ and $^{208}Pb/^{207}Pb$, respectively, apart from the dip centred on 63 cm. Above 35 cm the $^{208}Pb/^{206}Pb$ ratio rises slowly to reach a maximum of 2.160 at 2.1 cm and the $^{208}Pb/^{207}Pb$ a maximum of 2.467 at 2.7 cm before decreasing to 2.132 and 2.452, respectively, at the surface.

Stream sediment samples were taken from some of the major rivers flowing into the River Falloch, the main inflow to the Ardlui basin of Loch Lomond (Fig 3.1). The samples were analysed for Pb, Cu and stable Pb isotopes and the results are shown in Table 3.14. Eas Eonon, which spawns from the Ben Lui area, shows the highest concentrations of Pb and, with a $^{206}Pb/^{207}Pb$ atom ratio of 1.140, is quite distinct from the other streams. Allt Arnan shows an elevated concentration for Cu relative to the

other streams. The southern sampling site on the River Falloch lies down river from Eas Eonan and Allt Arnan causing the Pb and Cu values to be elevated relative to the northern sampling point.

Table 3.13 Stable Pb isotope and Pb concentration (mg kg^{-1}) results for core LL/NM.

Sample Code	Mid depth /cm	Mid cum. wt / g cm^{-2}	Pb / mg kg^{-1}	^{206}Pb / ^{207}Pb	σ_{n-1}	^{208}Pb / ^{206}Pb	σ_{n-1}	^{208}Pb / ^{207}Pb	σ_{n-1}
LL/NM001	0.1	0.045	70.2	1.150	0.0005	2.132	0.0029	2.452	0.0026
LL/NM002	0.3	0.123	67.8	1.150	0.0030	2.129	0.0100	2.447	0.0058
LL/NM003	0.5	0.192	64.3	1.151	0.0019	2.134	0.0026	2.456	0.0049
LL/NM004	0.7	0.256	67.3	1.151	0.0010	2.132	0.0053	2.454	0.0063
LL/NM005	0.9	0.316	67.0	1.149	0.0017	2.131	0.0034	2.448	0.0038
LL/NM006	1.1	0.378	64.9	1.149	0.0009	2.133	0.0037	2.451	0.0045
LL/NM007	1.3	0.452	63.5	1.148	0.0023	2.135	0.0048	2.452	0.0011
LL/NM008	1.5	0.537	71.0	1.147	0.0010	2.131	0.0016	2.444	0.0036
LL/NM009	1.7	0.613	68.4	1.149	0.0008	2.129	0.0041	2.445	0.0035
LL/NM010	1.9	0.663	71.9	1.150	0.0008	2.141	0.0045	2.461	0.0059
LL/NM011	2.1	0.715	85.8	1.144	0.0009	2.160	0.0036	2.452	0.0050
LL/NM012	2.3	0.788	77.7	1.150	0.0013	2.138	0.0059	2.459	0.0052
LL/NM013	2.5	0.859	89.2	1.146	0.0019	2.130	0.0078	2.441	0.0127
LL/NM014	2.7	0.914	85.1	1.147	0.0016	2.152	0.0019	2.467	0.0019
LL/NM015	2.9	0.964	91.5	1.145	0.0008	2.146	0.0012	2.458	0.0028
LL/NM016	3.1	1.023	95.9	1.145	0.0013	2.148	0.0050	2.460	0.0030
LL/NM017	3.3	1.077	93.6	1.145	0.0009	2.148	0.0019	2.458	0.0020
LL/NM018	3.5	1.127	97.7	1.143	0.0005	2.148	0.0013	2.456	0.0013
LL/NM019	3.7	1.187	110.1	1.140	0.0019	2.135	0.0035	2.435	0.0051
LL/NM020	3.9	1.241	104.2	1.139	0.0017	2.132	0.0021	2.429	0.0015
LL/NM021	4.1	1.287	111.6	1.137	0.0023	2.151	0.0035	2.446	0.0038
LL/NM022	4.3	1.334	116.7	1.137	0.0013	2.152	0.0032	2.446	0.0026
LL/NM023	4.5	1.382	121.7	1.137	0.0008	2.142	0.0035	2.435	0.0035
LL/NM024	4.7	1.432	128.1	1.137	0.0022	2.142	0.0052	2.436	0.0032
LL/NM025	4.9	1.483	129.1	1.139	0.0018	2.143	0.0038	2.434	0.0063

Table 3.13 Stable Pb isotope and Pb concentration (mg kg^{-1}) results for core LL/NM, continued.

Sample Code	Mid depth /cm	Mid cum. wt / g cm^{-2}	Pb / mg kg^{-1}	^{206}Pb / ^{207}Pb	σ_{n-1}	^{208}Pb / ^{206}Pb	σ_{n-1}	^{208}Pb / ^{207}Pb	σ_{n-1}
LL/NM026	5.5	1.595	122.3	1.136	0.0021	2.144	0.0028	2.436	0.0037
LL/NM027	6.5	1.778	122.4	1.139	0.0022	2.123	0.0029	2.418	0.0036
LL/NM028	7.5	1.970	123.5	1.137	0.0007	2.119	0.0054	2.410	0.0049
LL/NM029	8.5	2.175	128.0	1.141	0.0015	2.113	0.0093	2.410	0.0091
LL/NM030	9.5	2.390	147.1	1.140	0.0016	2.132	0.0046	2.430	0.0049
LL/NM031	10.5	2.590	164.8	1.140	0.0011	2.134	0.0045	2.432	0.0035
LL/NM032	11.5	2.773	156.5	1.138	0.0025	2.124	0.0072	2.417	0.0061
LL/NM033	12.5	2.954	157.1	1.140	0.0010	2.125	0.0063	2.422	0.0067
LL/NM034	13.5	3.144	166.3	1.142	0.0018	2.121	0.0030	2.423	0.0063
LL/NM035	14.5	3.336	170.2	1.142	0.0023	2.103	0.0124	2.402	0.0162
LL/NM036	15.5	3.536	158.6	1.143	0.0025	2.124	0.0063	2.427	0.0053
LL/NM037	16.5	3.739	143.6	1.146	0.0020	2.119	0.0153	2.429	0.0178
LL/NM038	17.5	3.940	142.4	1.148	0.0018	2.117	0.0048	2.431	0.0080
LL/NM039	18.5	4.153	143.9	1.149	0.0027	2.108	0.0086	2.423	0.0091
LL/NM040	19.5	4.367	152.3	1.152	0.0015	2.110	0.0084	2.430	0.0088
LL/NM041	21	4.674	152.4	1.154	0.0009	2.111	0.0073	2.436	0.0082
LL/NM042	23	5.097	133.6	1.158	0.0007	2.116	0.0098	2.449	0.0115
LL/NM043	25	5.536	134.5	1.159	0.0014	2.106	0.0129	2.440	0.0125
LL/NM044	27	5.962	141.1	1.164	0.0021	2.118	0.0039	2.464	0.0043
LL/NM045	29	6.408	138.0	1.165	0.0009	2.100	0.0123	2.448	0.0159
LL/NM046	31	6.891	136.7	1.164	0.0008	2.097	0.0033	2.441	0.0030
LL/NM047	33	7.360	140.8	1.171	0.0014	2.092	0.0104	2.431	0.0140
LL/NM048	35	7.820	131.3	1.167	0.0006	2.089	0.0025	2.438	0.0039
LL/NM049	37	8.293	119.3	1.169	0.0022	2.116	0.0033	2.473	0.0052
LL/NM050	39	8.774	111.9	1.169	0.0019	2.115	0.0054	2.472	0.0070

Table 3.13 Stable Pb isotope and Pb concentration (mg kg^{-1}) results for core LL/NM, continued.

Sample Code	Mid depth /cm	Mid cum. wt / g cm^{-2}	Pb / mg kg^{-1}	^{206}Pb / ^{207}Pb	σ_{n-1}	^{208}Pb / ^{206}Pb	σ_{n-1}	^{208}Pb / ^{207}Pb	σ_{n-1}
LL/NM051	41	9.263	111.5	1.169	0.0012	2.101	0.0026	2.455	0.0054
LL/NM052	43	9.728	105.2	1.170	0.0011	2.117	0.0034	2.477	0.0043
LL/NM053	45	10.172	93.8	1.168	0.0022	2.102	0.0038	2.455	0.0019
LL/NM054	47	10.631	81.2	1.171	0.0006	2.105	0.0008	2.464	0.0016
LL/NM055	49	11.125	77.4	1.169	0.0020	2.112	0.0023	2.470	0.0023
LL/NM056	51	11.644	71.9	1.171	0.0015	2.106	0.0033	2.446	0.0029
LL/NM057	53	12.145	71.4	1.167	0.0009	2.116	0.0041	2.469	0.0033
LL/NM058	55	12.646	77.9	1.166	0.0012	2.117	0.0042	2.468	0.0070
LL/NM059	57	13.165	68.7	1.165	0.0023	2.123	0.0043	2.474	0.0051
LL/NM060	59	13.733	39.1	1.164	0.0021	2.105	0.0032	2.450	0.0056
LL/NM061	61	14.346	40.1	1.165	0.0012	2.102	0.0016	2.449	0.0017
LL/NM062	63	14.938	60.8	1.168	0.0019	2.105	0.0044	2.459	0.0077
LL/NM063	65	15.479	67.8	1.167	0.0036	2.101	0.0027	2.452	0.0061
LL/NM064	67	16.012	63.0	1.167	0.0022	2.106	0.0072	2.457	0.0085
LL/NM065	69	16.548	61.8	1.166	0.0015	2.109	0.0063	2.461	0.0057
LL/NM066	71	17.071	51.5	1.167	0.0013	2.117	0.0017	2.471	0.0033
LL/NM067	73	17.659	47.4	1.168	0.0017	2.125	0.0062	2.481	0.0058
LL/NM068	75	18.299	41.3	1.168	0.0034	2.125	0.0032	2.482	0.0054
LL/NM069	77	18.947	38.5	1.168	0.0021	2.108	0.0036	2.463	0.0017
LL/NM070	79	19.618	34.9	1.165	0.0024	2.118	0.0024	2.466	0.0024
LL/NM071	81	20.310	37.3	1.165	0.0013	2.105	0.0027	2.452	0.0050
LL/NM072	83	20.993	37.0	1.166	0.0008	2.125	0.0057	2.477	0.0079
LL/NM073	85	21.746	29.7	1.163	0.0010	2.111	0.0028	2.455	0.0020
LL/NM074	87	22.593	28.5	1.160	0.0007	2.115	0.0027	2.454	0.0044
LL/NM075	89	23.389	23.8	1.160	0.0012	2.125	0.0016	2.466	0.0024

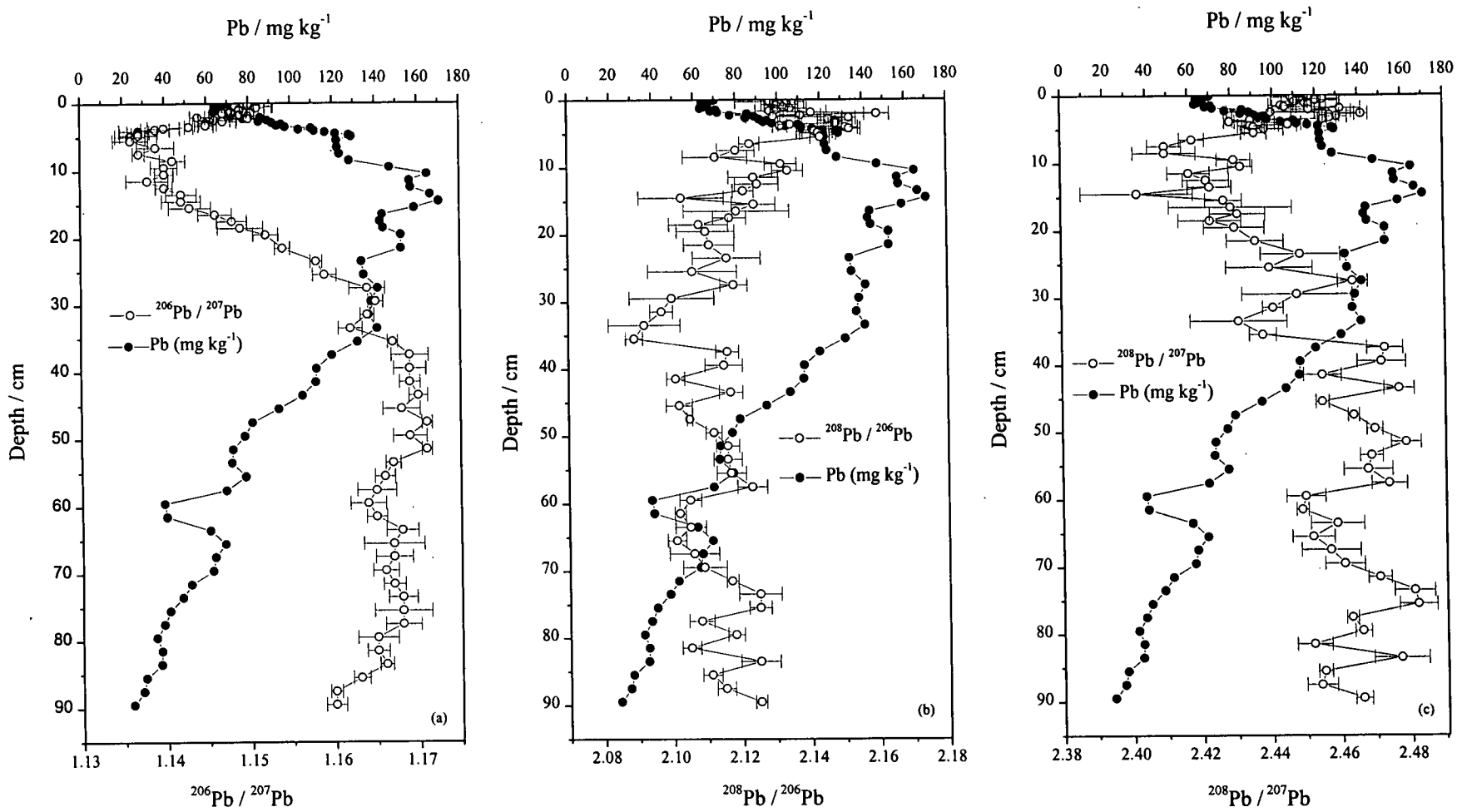

Figure 3.26 Stable Pb isotopes and Pb concentration (mg kg^{-1}) vs depth (cm) for core LL/NM.

(a) ^{206}Pb / ^{207}Pb, (b) ^{208}Pb / ^{206}Pb, and (c) ^{208}Pb / ^{207}Pb.

Table 3.14 Stream sediments samples from catchment water for northern basin in Loch Lomond.

Sample Site	Pb / mg kg^{-1}	Cu / mg kg^{-1}	$^{206}Pb / ^{207}Pb$	σ_{n-1}	$^{208}Pb / ^{206}Pb$	σ_{n-1}	$^{208}Pb / ^{207}Pb$	σ_{n-1}
River Falloch (N)	13.8	48.5	1.158	0.0010	2.124	0.0030	2.459	0.0020
Eas Eonan	110.7	42.8	1.140	0.0010	2.146	0.0022	2.466	0.0042
Allt Fionn Ghlinne	7.5	50.1	1.165	0.0018	2.125	0.0010	2.476	0.0047
Dubh Eas	15.2	36.8	1.149	0.0019	2.119	0.0026	2.436	0.0037
Ben Glas Burn	34.7	30.5	1.153	0.0014	2.130	0.0027	2.457	0.0051
River Falloch (S)	64.8	86.3	1.153	0.0016	2.124	0.0018	2.450	0.0044
Allt Arnan	34.0	90.4	1.147	0.0013	2.129	0.0036	2.442	0.0029

3.5.1.6 X-Ray diffraction.

Three samples were analysed by XRD (NM046, 061 and 074) and all were identical in the types of minerals identified and in the relative quantity of the minerals present. The following minerals were identified as being present in the samples in the order of relative abundance: quartz, muscovite, clinochlore, albite and augite. Sample NM061 was specifically chosen from the region of the core where all the heavy metal profiles show a sharp decline in concentration, but it showed no difference in either mineral type, or relative abundance in comparison with the rest of the core.

The following is a summary of the formulae and some structural properties of the minerals identified.

Quartz: SiO_2 framework silicate.

Muscovite: $K_2(Si_6Al_2)(Al_4)O_{20}(OH)_4$ and $K_2(Si_7Al_1)(Al,Fe^{3+})_3(MgFe^{2+})O_{20}(OH)_4$
Mica, layer silicate, 2:1 dioctahedral, 10 Å.

Albite: $NaAlSi_3O_8$.
Feldspar, framework silicate, 3.19 Å.

Clinochlore: $(Si_{8-x}Al_x)(Mg_{12-y},Al_y)O_{20}(OH)_{16}$.
Chlorite, layer silicate, trioctahedral.

Augite: $(Ca, Mg,Fe^{2+})_4(Al,Fe)_3 + Ti(Si,Al)_2O_6$
Clinopyroxene.

Augite was the only mineral not also identified in LL/South.

3.5.2 Discussion.

3.5.2.1 Radiocaesium and americium.

The two ^{137}Cs peaks present (Fig. 3.17) can be attributed to the Chernobyl accident in April 1986 and nuclear weapons testing in the 1950-1960s. ^{241}Am was not produced directly in nuclear weapons tests, but it does occur in the environment as a consequence of the decay of ^{241}Pu, which was produced as a significant component of weapons testing fallout. ^{241}Pu was not present in fallout from Chernobyl as the temperature in the reactor fire was not high enough to volatilize Pu. The ^{241}Am in core LL/NM is present in levels very close to the detection limit and with high errors. Despite this, however, the very fact that a trace is detected can be taken as evidence of its existence and hence evidence that the lower peak is due to weapons testing fallout. The amount of ^{241}Am is still increasing in the environment at present due to the decay of ^{241}Pu, which has a half-life of 14.4 y, and the ^{241}Am activities should reach a peak level in ~ 2010. The ^{241}Am also has a slight bimodal structure (Fig. 3.17), which is consistent with the two main periods of nuclear testing peaking in 1959 and 1963.

Without the ^{134}Cs data corresponding to the Chernobyl accident, it is not possible to separate the two radiocaesium inventories completely. However some assumptions can be made in order to obtain an approximate inventory. A constant continued input of weapons ^{137}Cs of 380 Bq kg^{-1} [†] from the catchment / atmosphere is assumed, and the excess above 4.5 cm is taken to be Chernobyl-derived. Hence, values of 27.1 kBq m^{-2} for weapons testing fallout (corrected to 1963) and 10.7 kBq m^{-2} for Chernobyl fallout (corrected to 1986) are obtained. These values will represent a minimum for Chernobyl and a maximum for weapons testing but are both significantly higher than those of the Loch Lomond south cores and may represent a

[†] This value taken as the approximately constant value over 2 cm just before the onset of the Chernobyl peak.

higher sediment input to this basin or focusing of sediment material to the sampling point.

In Figure 3.27 ^{137}Cs and ^{241}Am (Bq kg^{-1}) are plotted against depth as a function of cumulative weight of sediment per unit area. If the two ^{137}Cs peaks are taken to represent 1st May 1986 and 1963 respectively, the accumulation rate over the following age increments can be calculated: 1995-1986, 1986-1963 and 1995-1963. This procedure gives accumulation rates of 118.6 ± 2.8, 75.5 ± 9.2 and 89.5 ± 2.7 mg cm^{-2} y^{-1}, respectively. From these figures it can be seen that there has been a change from a higher to a lower sedimentation rate at some time between 1995 and 1963. Taking the two peaks in ^{241}Am to represent 1959 and 1963, a sedimentation rate of 92.7 ± 19 mg cm^{-2} y^{-1} is obtained.

Extrapolation of a two-component sedimentation rate using 118.6 mg cm^{-2} y^{-1} from the surface until 1.127 g cm^{-2}, then 75.5 mg cm^{-2} y^{-1} to the base, yields a date of 1909 for the penetration of the $^{137}Cs^{\blacklozenge}$ (and 1690 for the base of the core). If the sedimentation rate obtained using the weapons testing peak alone (89.5 mg cm^{-2} y^{-1}) is extrapolated to the base of the core, it gives a date for the base of the core of 1734 and a date of penetration of ^{137}Cs of 1918. Both of these dates are considerably earlier than the known start of weapons testing, providing evidence of movement of ^{137}Cs after deposition. Physical mixing can be ruled out for this core due to the sharpness of the Chernobyl peak. Therefore the movement is more likely to be due to chemical remobilisation.

$^{\blacklozenge}$ Values for ^{137}Cs below this depth are less than twice σ_{n-1}.

Figure 3.27 ^{137}Cs (Bq kg^{-1}) and ^{241}Am (Bq kg^{-1}) vs cumulative weight (g cm^{-2}) in core LL/NM.

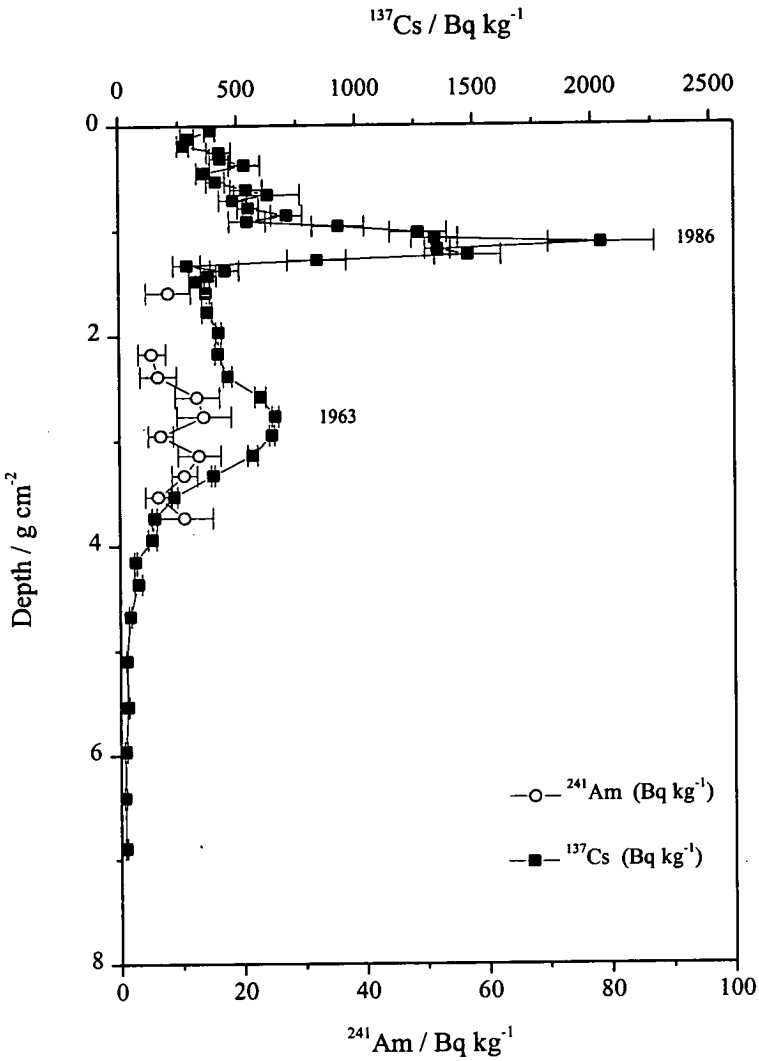

3.5.2.2 ^{210}Pb.

The two graphs in Figure 3.18 show that, while the ^{210}Pb specific activities are comparable for both methods of counting, the errors are much smaller for the α-spectrometry data which are therefore used in the calculations below.

As ^{226}Ra was not detectable by γ-spectrometry, the supported ^{210}Pb value from the α-spectrometry was taken as the value at the base of the profile, i.e. 63 Bq kg^{-1}. For the CIC model, a graph of ln ($^{210}Pb_{unsupp}$) was plotted against cumulative weight depth (g cm^{-2}) and a weighted linear regression fit of the data calculated (Fig. 3.28). From the graph it can be seen that there have been several changes in the sedimentation rate over the core. If a weighted fit is taken through all of the points (Fig. 3.28 (a)) a sedimentation rate of 103.7 ± 7.5 mg cm^{-2} y^{-1} is obtained. If the profile is broken down into sections where there are distinct breaks ((b) 1-30 (0-2.390 g cm^{-2}), (c) 31-41 (2.590-4.674 g cm^{-2}) and (d) 42-48 (5.097-7.820 g cm^{-2})), then sedimentation rates of 155.9 ± 38, 60.3 ± 3.6 and 71.5 ± 2.7 mg cm^{-2} y^{-1}, respectively, are obtained. Using the derived sedimentation rates yields a date at the base of the core of 1680 and a date for the penetration of ^{137}Cs of 1911.

The CRS model allows for changes in the sedimentation rate. In order to calculate the sedimentation rate the total inventory of ^{210}Pb in the core was taken as 1.78 ± 0.002 Bq m^{-2} (the inventory below this point was not significant due to high errors). The number of years of accumulation to the base of each section was calculated using the equation given in section 3.4.2.2. The results from the CRS calculations are shown in Table 3.15 together with the dates derived from the CIC model and ^{137}Cs. The total flux of ^{210}Pb is 554 Bq m^{-2} y^{-1} and is some five times that seen at the southern site.

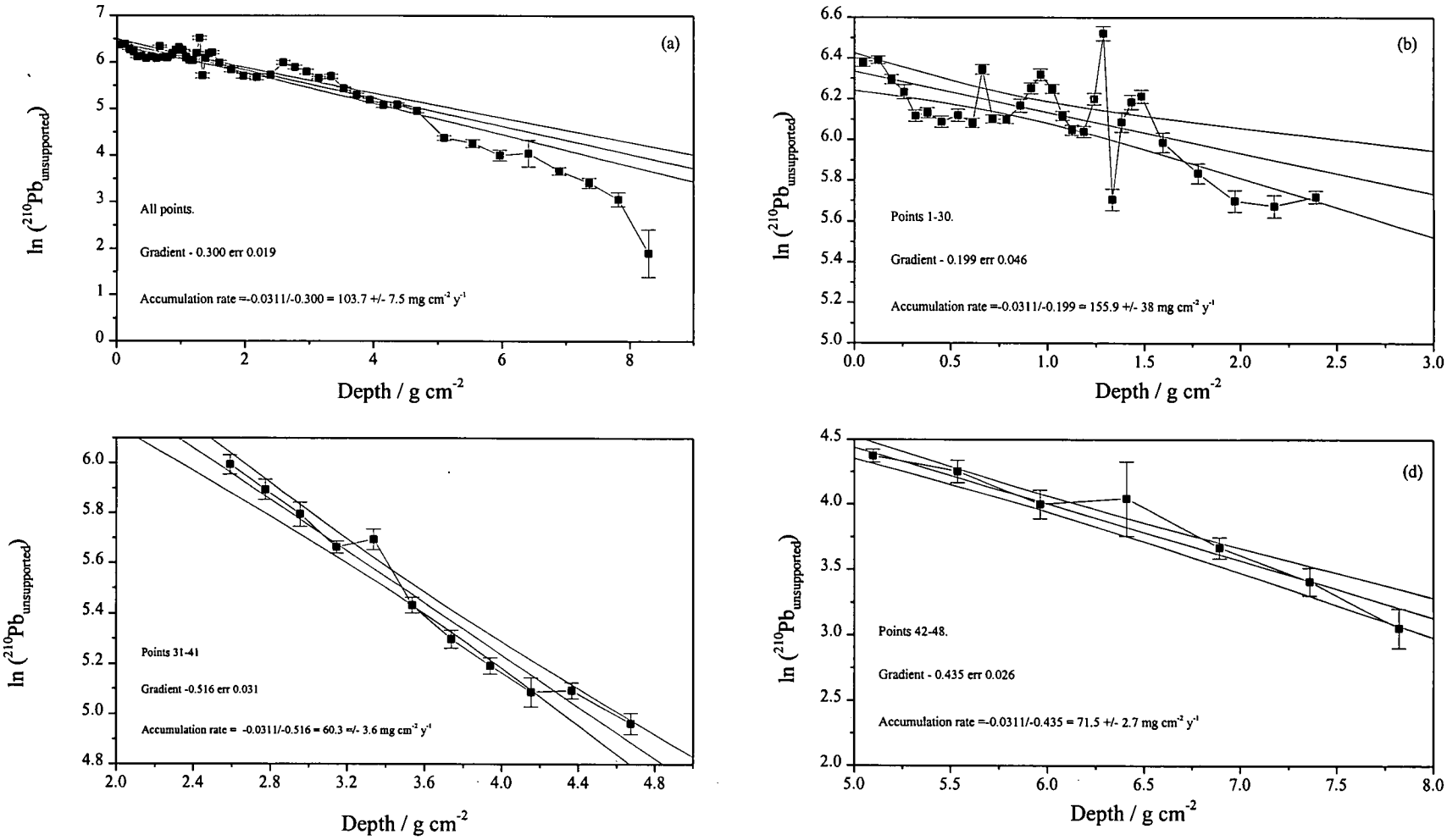

Figure 3. 28 ln $^{210}Pb_{unsupported}$ vs depth (g cm^{-2}) in core LL/NM. (a) allpoints, (b) points 1-30, (c) points 31-41 and (d) points 42-48.

Table 3.15 Comparison of dates for core LL/NM using the CIC, ^{137}Cs and CRS models.

Sample Code	Mid Cum. wt / g cm^{-2}	Cum. wt to base / kg m^{-2}	CIC 3 component / 155.9/60.3/71.5 mg cm^{-2} y^{-1}		CIC single component / 103.9 mg cm^{-2} y^{-1}		^{137}Cs 2 component / 118.6 / 75.5 mg cm^{-2} y^{-1}		^{137}Cs single component / 89.5 mg cm^{-2} y^{-1}		CRS	
			Yrs accum.	Date	Yrs accum.	Date	Yrs accum.	Date	Yrs accum.	Date	Yrs accum.	Date
LL/NM001	0.045	0.906	0.3	1994.6	0.4	1994.5	0.4	1994.5	0.5	1994.4	1.0	1993.9
LL/NM002	0.123	1.547	0.8	1994.1	1.2	1993.7	1.0	1993.9	1.4	1993.5	1.7	1993.2
LL/NM003	0.192	2.290	1.2	1993.7	1.8	1993.1	1.6	1993.3	2.1	1992.8	2.5	1992.4
LL/NM004	0.256	2.833	1.6	1993.3	2.5	1992.4	2.2	1992.7	2.9	1992.0	3.0	1991.9
LL/NM005	0.316	3.484	2.0	1992.9	3.0	1991.9	2.7	1992.2	3.5	1991.4	3.6	1991.3
LL/NM006	0.378	4.077	2.4	1992.5	3.6	1991.3	3.2	1991.7	4.2	1990.7	4.2	1990.7
LL/NM007	0.452	4.961	2.9	1992.0	4.4	1990.5	3.8	1991.1	5.0	1989.9	5.0	1989.9
LL/NM008	0.537	5.784	3.4	1991.5	5.2	1989.7	4.5	1990.4	6.0	1988.9	5.8	1989.1
LL/NM009	0.613	6.467	3.9	1991.0	5.9	1989.0	5.2	1989.7	6.8	1988.1	6.4	1988.5
LL/NM010	0.663	6.800	4.3	1990.6	6.4	1988.5	5.6	1989.3	7.4	1987.5	6.9	1988.0
LL/NM011	0.715	7.496	4.6	1990.3	6.9	1988.0	6.0	1988.9	8.0	1986.9	7.6	1987.3
LL/NM012	0.788	8.259	5.1	1989.8	7.6	1987.3	6.6	1988.3	8.8	1986.1	8.3	1986.6
LL/NM013	0.859	8.926	5.5	1989.4	8.3	1986.6	7.2	1987.7	9.6	1985.3	9.1	1985.8
LL/NM014	0.914	9.351	5.9	1989.0	8.8	1986.1	7.7	1987.2	10.2	1984.7	9.6	1985.3
LL/NM015	0.964	9.926	6.2	1988.7	9.3	1985.6	8.1	1986.8	10.8	1984.1	10.4	1984.5
LL/NM016	1.023	10.538	6.6	1988.3	9.9	1985.0	8.6	1986.3	11.4	1983.5	11.2	1983.7
LL/NM017	1.077	10.998	6.9	1988.0	10.4	1984.5	9.1	1985.8	12.0	1982.9	11.8	1983.1
LL/NM018	1.127	11.533	7.2	1987.7	10.9	1984.0	9.5	1985.4	12.6	1982.3	12.4	1982.5
LL/NM019	1.187	12.198	7.6	1987.3	11.4	1983.5	0.8	1984.6	13.3	1981.6	13.1	1981.8
LL/NM020	1.241	12.616	8.0	1986.9	12.0	1982.9	1.5	1983.9	13.9	1981.0	13.7	1981.2
LL/NM021	1.287	13.119	8.3	1986.6	12.4	1982.5	2.1	1983.3	14.4	1980.5	14.6	1980.3
LL/NM022	1.334	13.554	8.6	1986.3	12.9	1982.0	2.7	1982.7	14.9	1980.0	15.0	1979.9
LL/NM023	1.382	14.081	8.9	1986.0	13.3	1981.6	3.4	1982.0	15.4	1979.5	15.7	1979.2
LL/NM024	1.432	14.558	9.2	1985.7	13.8	1981.1	4.0	1981.4	16.0	1978.9	16.4	1978.5
LL/NM025	1.483	15.104	9.5	1985.4	14.3	1980.6	4.7	1980.7	16.6	1978.3	17.2	1977.7

Table 3.15 Comparison of dates for core LL/NM using the CIC, ^{137}Cs and CRS models, continued.

Sample Code	Mid Cum. wt / g cm^{-2}	Cum. wt to base / kg m^{-2}	CIC 3 component / 155.9/60.3/71.5 mg cm^{-2} y^{-1}		CIC single component / 103.9 mg cm^{-2} y^{-1}		^{137}Cs 2 component / 118.6 / 75.5 mg cm^{-2} y^{-1}		^{137}Cs single component / 89.5 mg cm^{-2} y^{-1}		CRS	
			Yrs accum.	Date	Yrs accum.	Date	Yrs accum.	Date	Yrs accum.	Date	Yrs accum.	Date
LL/NM026	1.595	16.790	10.2	1984.7	15.4	1979.5	6.2	1979.2	17.8	1977.1	19.3	1975.6
LL/NM027	1.778	18.767	11.4	1983.5	17.1	1977.8	8.6	1976.8	19.9	1975.0	21.6	1973.3
LL/NM028	1.970	20.637	12.6	1982.3	19.0	1975.9	11.2	1974.2	22.0	1972.9	23.7	1971.2
LL/NM029	2.175	22.861	14.0	1980.9	21.0	1973.9	13.9	1971.5	24.3	1970.6	26.2	1968.7
LL/NM030	2.390	24.937	15.3	1979.6	23.0	1971.9	16.7	1968.7	26.7	1968.2	28.9	1966.0
LL/NM031	2.590	26.862	3.3	1976.3	25.0	1969.9	19.4	1966.0	28.9	1966.0	32.5	1962.4
LL/NM032	2.773	28.590	6.3	1973.3	26.7	1968.2	21.8	1963.6	31.0	1963.9	35.8	1959.1
LL/NM033	2.954	30.483	9.3	1970.3	28.5	1966.4	24.2	1961.2	33.0	1961.9	39.4	1955.5
LL/NM034	3.144	32.404	12.5	1967.1	30.3	1964.6	26.7	1958.7	35.1	1959.8	43.0	1951.9
LL/NM035	3.336	34.323	15.7	1963.9	32.2	1962.7	29.3	1956.1	37.3	1957.6	47.2	1947.7
LL/NM036	3.536	36.394	19.0	1960.6	34.1	1960.8	31.9	1953.5	39.5	1955.4	51.2	1943.7
LL/NM037	3.739	38.385	22.4	1957.2	36.1	1958.8	34.6	1950.8	41.8	1953.1	54.9	1940.0
LL/NM038	3.940	40.424	25.7	1953.9	38.0	1956.9	37.3	1948.1	44.0	1950.9	58.8	1936.1
LL/NM039	4.153	42.634	29.2	1950.4	40.0	1954.9	40.1	1945.3	46.4	1948.5	63.1	1931.8
LL/NM040	4.367	44.706	32.8	1946.8	42.1	1952.8	42.9	1942.5	48.8	1946.1	67.8	1927.1
LL/NM041	4.674	48.770	37.9	1941.7	45.1	1949.8	47.0	1938.4	52.2	1942.7	77.8	1917.1
LL/NM042	5.097	53.175	5.9	1935.8	49.2	1945.7	52.6	1932.8	57.0	1937.9	85.8	1909.1
LL/NM043	5.536	57.554	12.1	1929.6	53.4	1941.5	58.4	1927.0	61.9	1933.0	95.1	1899.8
LL/NM044	5.962	61.685	18.0	1923.7	57.5	1937.4	64.0	1921.4	66.6	1928.3	104.1	1890.8
LL/NM045	6.408	66.479	24.3	1917.4	61.8	1933.1	70.0	1915.4	71.6	1923.3	120.0	1874.9
LL/NM046	6.891	71.335	31.0	1910.7	66.4	1928.5	76.3	1909.1	77.0	1917.9	139.0	1855.9
LL/NM047	7.360		37.6	1904.1	71.0	1923.9	82.6	1902.8	82.2	1912.7		
LL/NM048	7.820		44.0	1897.7	75.4	1919.5	88.7	1896.7	87.4	1907.5		
LL/NM049	8.293		50.6	1891.1	80.0	1914.9	94.9	1890.5	92.7	1902.2		
LL/NM050	8.774		57.3	1884.4	84.6	1910.3	101.3	1884.1	98.0	1896.9		

Table 3.15 Comparison of dates for core LL/NM using the CIC, ^{137}Cs and CRS models, continued.

Sample Code	Mid Cum. wt / g cm^{-2}	Cum. wt to base / kg m^{-2}	CIC 3 component / 155.9/60.3/71.5 mg cm^{-2} y^{-1}		CIC single component / 103.9 mg cm^{-2} y^{-1}		^{137}Cs 2 component / 118.6 / 75.5 mg cm^{-2} y^{-1}		^{137}Cs single component / 89.5 mg cm^{-2} y^{-1}		CRS	
			Yrs accum.	Date	Yrs accum.	Date	Yrs accum.	Date	Yrs accum.	Date	Yrs accum.	Date
LL/NM051	9.263		64.2	1877.5	89.3	1905.6	107.8	1877.6	103.5	1891.4		
LL/NM052	9.728		70.7	1871.0	93.8	1901.1	113.9	1871.5	108.7	1886.2		
LL/NM053	10.172		76.9	1864.8	98.1	1896.8	119.8	1865.6	113.6	1881.3		
LL/NM054	10.631		83.3	1858.4	102.5	1892.4	125.9	1859.5	118.8	1876.1		
LL/NM055	11.125		90.2	1851.5	107.3	1887.6	132.4	1853.0	124.3	1870.6		
LL/NM056	11.644		97.5	1844.2	112.3	1882.6	139.3	1846.1	130.1	1864.8		
LL/NM057	12.145		104.5	1837.2	117.1	1877.8	145.9	1839.5	135.7	1859.2		
LL/NM058	12.646		111.5	1830.2	121.9	1873.0	152.6	1832.8	141.3	1853.6		
LL/NM059	13.165		118.8	1822.9	126.9	1868.0	159.4	1826.0	147.1	1847.8		
LL/NM060	13.733		126.7	1815.0	132.4	1862.5	167.0	1818.4	153.4	1841.5		
LL/NM061	14.346		135.3	1806.4	138.3	1856.6	175.1	1810.3	160.3	1834.6		
LL/NM062	14.938		143.6	1798.1	144.0	1850.9	182.9	1802.5	166.9	1828.0		
LL/NM063	15.479		151.1	1790.6	149.3	1845.6	190.1	1795.3	173.0	1821.9		
LL/NM064	16.012		158.6	1783.1	154.4	1840.5	197.2	1788.2	178.9	1816.0		
LL/NM065	16.548		166.1	1775.6	159.6	1835.3	204.3	1781.1	184.9	1810.0		
LL/NM066	17.071		173.4	1768.3	164.6	1830.3	211.2	1774.2	190.7	1804.2		
LL/NM067	17.659		181.6	1760.1	170.3	1824.6	219.0	1766.4	197.3	1797.6		
LL/NM068	18.299		190.6	1751.1	176.5	1818.4	227.5	1757.9	204.5	1790.4		
LL/NM069	18.947		199.6	1742.1	182.7	1812.2	236.0	1749.4	211.7	1783.2		
LL/NM070	19.618		209.0	1732.7	189.2	1805.7	244.9	1740.5	219.2	1775.7		
LL/NM071	20.310		218.7	1723.0	195.9	1799.0	254.1	1731.3	226.9	1768.0		
LL/NM072	20.993		228.2	1713.5	202.4	1792.5	263.1	1722.3	234.6	1760.3		
LL/NM073	21.746		238.8	1702.9	209.7	1785.2	273.1	1712.3	243.0	1751.9		
LL/NM074	22.593		250.6	1691.1	217.9	1777.0	284.3	1701.1	252.4	1742.5		
LL/NM075	23.389		261.7	1680.0	225.5	1769.4	294.9	1690.5	261.3	1733.6		

3.5.2.3 Core chronology.

The dates for each section calculated using the sedimentation rates derived in section 3.5.2.1 and 3.5.2.2, are shown together in Table 3.15. From Table 3.15 it can be seen that all of the models give a good correlation for the position of the Chernobyl peak but only the ^{137}Cs models give dates commensurate with weapons testing. In comparison with the other methods, the CRS model gives progressively older dates down the core. The divergence in the CRS model is probably due to an underestimation of both the total ^{210}Pb inventory and the inventory below each section.

The ^{137}Cs chronology has smaller errors associated with it in comparison with the CIC model and does not have problems with the irregularities seen in the top of the ^{210}Pb profile. Therefore, for the remainder of the discussion the ^{137}Cs sedimentation rate will be used to fit a chronology to the heavy metal profiles. However, for key points a range of dates will be quoted, taking into account the ^{210}Pb models.

3.5.2.4 Stable lead isotopes and lead.

Calculation of an excess Pb concentration and associated $^{206}Pb/^{207}Pb$ atom ratio, representing the anthropogenic input of Pb, is complicated in this core because it is not clear whether the Pb concentration at the base of the core has reached a constant value. However, the bottom section has reached a minimum value with respect to the rest of the core, and this was taken to enable the calculation of excess Pb flux.

The assumed natural Pb concentration of 23.8 mg kg^{-1} was used to calculate the excess Pb concentration. The excess concentration was then multiplied by the sedimentation rate of 1.19 kg m^{-2} y^{-1} from the surface to 3.5 cm and 0.75 kg m^{-2} y^{-1} from 3.5 cm to the base (representing the change in sedimentation rate as discussed in section 3.5.2.1) to yield the excess Pb flux (mg m^{-2} y^{-1}). The value of 1.160 for the $^{206}Pb/^{207}Pb$ atom ratio from the bottom section of the core was used to calculate the

atom ratio of the excess Pb using the equation given in section 3.4.2.3. A summary of the results is given in Table 3.16, and the excess Pb flux and excess $^{206}Pb/^{207}Pb$ atom ratio are plotted against calendar date in Figure 3.29.

There are four main periods that can be identified for the excess $^{206}Pb/^{207}Pb$ atom ratio relating to pre-industrial and industrial input and the addition and removal of leaded petrol. At the beginning of the 18th Century the ratio rose quite rapidly over about a 10 year period to an average of 1.177 ± 0.002 until about 1770, after which it dropped to a relatively constant value of 1.172 ± 0.002 which lasted until the start of the 20th Century. During this period the total excess Pb deposited was 7.3 g m^{-2}, 52 % of the inventory of 14.1 g m^{-2} for the core. After 1902 the ratio dropped initially to 1.165 for about 25 years, then continued a downward trend due to the onset of use of leaded petrol, to reach a minimum of 1.130 by 1979. The excess Pb flux rose to above 100 mg m^{-2} y^{-1} over the period 1953-1966 during which time the $^{206}Pb/^{207}Pb$ atom ratio was still rapidly declining. The total inventory for the period from 1927 until the present was 6.1 g m^{-2}, 43 % of the core inventory, although only 0.94 g m^{-2} was deposited after 1980. The calculated fluxes of Pb are higher in the northern basin than in the south, a consequence of the higher sedimentation rate and sediment focusing. This could be taken as further evidence of sediment focusing as has already been observed in the radiocaesium.

The base of the core is given a date of 1690 using the ^{137}Cs chronology (Table 3.15, Fig 3.29) although the dates towards the bottom of the core are perhaps less reliable due to the chronology being extrapolated. Historically there was a Pb smelter situated at the foot of Glen Falloch where Pb from the Tyndrum mines was smelted between 1741 and 1745 (Wilson, 1921). Tyndrum Pb has a $^{206}Pb/^{207}Pb$ atom ratio of 1.144 and this could account for the slight dip in $^{206}Pb/^{207}Pb$ atom ratio coupled with a slight increase in Pb flux from 1720-1740 (subject to error on the dates at this depth). The excess Pb flux is higher than seen in the southern basin, the reverse of what might be expected on the basis of proximity to the central Scotland industrial belt,

apparently suggesting an independent source of Pb entering the northern basin. Table 3.14 shows the results for stream sediments from the main catchment of the Ardlui basin. The sample from Eas Eonan (1.140), which originates from close to the Ben Lui (an area of Pb mineralisation) has a $^{206}Pb/^{207}Pb$ atom ratio similar to that of Tyndrum ore (1.144) and the ratio at the surface of the core (1.145). It is also elevated in Pb relative to the other stream sediments. The stable Pb atom ratios of the stream sediments closest to the loch are similar to those of the top sections of the core. The stream sediment samples remote from the entry point of the loch do show some differences in $^{206}Pb/^{207}Pb$ atom ratio. Allt Fionn Ghlinne has the highest atom ratio of 1.165 but a low Pb content.

The other feature in the profile of interest is the depression at 1802-1818 observed for all of the metals determined. It is not reflected in any major change in the Pb isotope ratio profiles, thus ruling out the possibility of it being caused by a major change in the source of Pb being deposited.

Table 3.16 Excess metal fluxes and excess $^{206}Pb/^{207}Pb$ atom ratios for core LL/NM.

Sample Code	Mid depth /cm	Pb / mg kg^{-1}	$^{206}Pb/^{207}Pb$	σ_{n-1}	Date (based on 2 comp. ^{137}Cs)	Excess $^{206}Pb/^{207}Pb$	σ_{n-1xs}	Excess Pb flux / mg m^{-2} y^{-1}	Excess Zn flux / mg m^{-2} y^{-1}	Excess Cu flux / mg m^{-2} y^{-1}	Excess Cd flux / mg m^{-2} y^{-1}
LL/NM001	0.1	70.2	1.150	0.0005	1994.5	1.145	0.0021	55.0	150.2	23.3	1.09
LL/NM002	0.3	67.8	1.150	0.0030	1993.9	1.145	0.0036	52.1	162.8	21.6	1.50
LL/NM003	0.5	64.3	1.151	0.0019	1993.3	1.146	0.0028	48.0	156.1	19.4	1.50
LL/NM004	0.7	67.3	1.151	0.0010	1992.7	1.146	0.0022	51.5	162.0	20.0	1.41
LL/NM005	0.9	67.0	1.149	0.0017	1992.2	1.143	0.0026	51.1	168.9	20.7	1.52
LL/NM006	1.1	64.9	1.149	0.0009	1991.7	1.143	0.0022	48.7	159.8	17.5	1.37
LL/NM007	1.3	63.5	1.148	0.0023	1991.1	1.141	0.0030	47.0	152.6	17.3	1.41
LL/NM008	1.5	71.0	1.147	0.0010	1990.4	1.140	0.0022	55.9	171.4	22.5	1.75
LL/NM009	1.7	68.4	1.149	0.0008	1989.8	1.143	0.0022	52.9	160.7	23.8	1.61
LL/NM010	1.9	71.9	1.150	0.0008	1989.3	1.145	0.0022	57.0	157.9	24.1	1.49
LL/NM011	2.1	85.8	1.144	0.0009	1988.9	1.138	0.0022	73.6	163.6	23.8	1.51
LL/NM012	2.3	77.7	1.150	0.0013	1988.3	1.146	0.0024	63.9	163.7	24.4	1.59
LL/NM013	2.5	89.2	1.146	0.0019	1987.7	1.141	0.0028	77.6	177.3	24.1	1.68
LL/NM014	2.7	85.1	1.147	0.0016	1987.2	1.142	0.0026	72.6	174.1	23.6	1.67
LL/NM015	2.9	91.5	1.145	0.0008	1986.8	1.140	0.0022	80.3	189.3	24.9	1.90
LL/NM016	3.1	95.9	1.145	0.0013	1986.3	1.140	0.0024	85.5	198.0	27.8	2.06
LL/NM017	3.3	93.6	1.145	0.0009	1985.9	1.140	0.0022	82.9	194.2	26.1	1.93
LL/NM018	3.5	97.7	1.143	0.0005	1985.4	1.137	0.0021	87.8	206.9	28.3	1.91
LL/NM019	3.7	110.1	1.140	0.0019	1984.6	1.134	0.0028	65.0	141.0	18.7	1.33
LL/NM020	3.9	104.2	1.139	0.0017	1983.9	1.133	0.0026	60.6	140.6	17.1	1.41
LL/NM021	4.1	111.6	1.137	0.0023	1983.3	1.131	0.0030	66.1	153.2	16.0	1.62
LL/NM022	4.3	116.7	1.137	0.0013	1982.7	1.131	0.0024	70.0	152.4	16.0	1.55
LL/NM023	4.5	121.7	1.137	0.0008	1982.0	1.131	0.0022	73.8	165.6	16.3	1.63
LL/NM024	4.7	128.1	1.137	0.0022	1981.4	1.132	0.0030	78.6	207.9	18.3	1.82
LL/NM025	4.9	129.1	1.139	0.0018	1980.7	1.134	0.0027	79.4	202.3	17.8	1.59

Table 3.16 Excess metal fluxes and excess $^{206}Pb/^{207}Pb$ atom ratios for core LL/NM, continued.

Sample Code	Mid depth /cm	Pb / mg kg^{-1}	$^{206}Pb/^{207}Pb$	σ_{n-1}	Date (based on 2 comp. ^{137}Cs)	Excess $^{206}Pb/^{207}Pb$	σ_{n-1xs}	Excess Pb flux / mg m^{-2} y^{-1}	Excess Zn flux / mg m^{-2} y^{-1}	Excess Cu flux / mg m^{-2} y^{-1}	Excess Cd flux / mg m^{-2} y^{-1}
LL/NM026	5.5	122.3	1.136	0.0021	1979.2	1.130	0.003	74.2	201.1	16.5	1.57
LL/NM027	6.5	122.4	1.139	0.0022	1976.8	1.134	0.003	74.3	195.2	15.3	1.45
LL/NM028	7.5	123.5	1.137	0.0007	1974.2	1.131	0.002	75.1	195.5	15.0	1.44
LL/NM029	8.5	128.0	1.141	0.0015	1971.5	1.137	0.003	78.5	172.1	12.0	1.56
LL/NM030	9.5	147.1	1.140	0.0016	1968.7	1.136	0.003	92.9	218.6	16.1	1.70
LL/NM031	10.5	164.8	1.140	0.0011	1966.0	1.137	0.002	106.3	240.2	18.0	1.96
LL/NM032	11.5	156.5	1.138	0.0025	1963.6	1.134	0.003	100.0	212.1	14.8	2.06
LL/NM033	12.5	157.1	1.140	0.0010	1961.2	1.136	0.002	100.5	210.6	15.8	2.16
LL/NM034	13.5	166.3	1.142	0.0018	1958.7	1.139	0.003	107.4	229.0	16.6	2.28
LL/NM035	14.5	170.2	1.142	0.0023	1956.1	1.139	0.003	110.4	221.6	14.7	2.06
LL/NM036	15.5	158.6	1.143	0.0025	1953.5	1.140	0.003	101.6	210.0	16.5	2.01
LL/NM037	16.5	143.6	1.146	0.0020	1950.8	1.143	0.003	90.3	186.6	15.7	1.68
LL/NM038	17.5	142.4	1.148	0.0018	1948.1	1.146	0.003	89.4	173.3	15.9	1.52
LL/NM039	18.5	143.9	1.149	0.0027	1945.3	1.147	0.003	90.5	168.7	13.5	1.61
LL/NM040	19.5	152.3	1.152	0.0015	1942.5	1.151	0.003	96.9	186.3	11.2	1.99
LL/NM041	21.5	152.4	1.154	0.0009	1938.4	1.153	0.002	96.9	194.7	11.2	1.90
LL/NM042	23.5	133.6	1.158	0.0007	1932.8	1.158	0.002	82.7	168.9	10.0	1.75
LL/NM043	25.5	134.5	1.159	0.0014	1927.0	1.159	0.002	83.4	157.9	10.7	1.73
LL/NM044	27.5	141.1	1.164	0.0021	1921.4	1.165	0.003	88.4	154.3	11.7	1.67
LL/NM045	29.5	138.0	1.165	0.0009	1915.5	1.166	0.002	86.1	149.1	10.8	1.57
LL/NM046	31.5	136.7	1.164	0.0008	1909.1	1.165	0.002	85.1	139.8	12.2	1.29
LL/NM047	33.5	140.8	1.171	0.0014	1902.8	1.173	0.002	88.1	136.8	14.5	1.19
LL/NM048	35.5	131.3	1.167	0.0006	1896.7	1.169	0.002	81.0	117.2	12.5	1.07
LL/NM049	37.5	119.3	1.169	0.0022	1890.5	1.171	0.003	72.0	96.9	11.9	0.79
LL/NM050	39.5	111.9	1.169	0.0019	1884.1	1.171	0.003	66.4	89.8	11.1	0.80

Table 3.16 Excess metal fluxes and excess $^{206}Pb/^{207}Pb$ atom ratios for core LL/NM, continued.

Sample Code	Mid depth /cm	Pb / mg kg^{-1}	$^{206}Pb/^{207}Pb$	σ_{n-1}	Date (based on 2 comp. ^{137}Cs)	Excess $^{206}Pb/^{207}Pb$	σ_{n-1xs}	Excess Pb flux / mg m^{-2} y^{-1}	Excess Zn flux / mg m^{-2} y^{-1}	Excess Cu flux / mg m^{-2} y^{-1}	Excess Cd flux / mg m^{-2} y^{-1}
LL/NM051	41.5	111.5	1.169	0.0012	1877.6	1.171	0.002	66.1	88.0	11.9	0.81
LL/NM052	43.5	105.2	1.170	0.0011	1871.5	1.173	0.002	61.3	72.6	10.3	0.66
LL/NM053	45.5	93.8	1.168	0.0022	1865.6	1.171	0.003	52.7	61.8	8.4	0.66
LL/NM054	47.5	81.2	1.171	0.0006	1859.5	1.176	0.002	43.2	53.5	8.5	0.55
LL/NM055	49.5	77.4	1.169	0.0020	1853.0	1.173	0.003	40.3	51.9	9.8	0.44
LL/NM056	51.5	71.9	1.171	0.0015	1846.1	1.177	0.003	36.1	42.1	10.7	0.38
LL/NM057	53.5	71.4	1.167	0.0009	1839.5	1.171	0.002	35.8	32.2	9.4	0.34
LL/NM058	55.5	77.9	1.166	0.0012	1832.8	1.169	0.002	40.7	31.1	10.4	0.26
LL/NM059	57.5	68.7	1.165	0.0023	1826.0	1.168	0.003	33.7	25.1	8.0	0.24
LL/NM060	59.5	39.1	1.164	0.0021	1818.4	1.170	0.003	11.4	8.1	1.7	0.11
LL/NM061	61.5	40.1	1.165	0.0012	1810.3	1.172	0.002	12.2	4.7	0.4	0.08
LL/NM062	63.5	60.8	1.168	0.0019	1802.5	1.173	0.003	27.8	14.6	4.4	0.25
LL/NM063	65.5	67.8	1.167	0.0036	1795.3	1.171	0.004	33.0	17.1	7.4	0.17
LL/NM064	67.5	63.0	1.167	0.0022	1788.2	1.171	0.003	29.4	15.2	9.2	0.17
LL/NM065	69.5	61.8	1.166	0.0015	1781.1	1.170	0.003	28.6	14.6	9.6	0.13
LL/NM066	71.5	51.5	1.167	0.0013	1774.2	1.173	0.002	20.7	16.2	11.2	0.10
LL/NM067	73.5	47.4	1.168	0.0017	1766.4	1.176	0.003	17.7	16.0	14.0	0.13
LL/NM068	75.5	41.3	1.168	0.0034	1758.0	1.179	0.004	13.0	13.0	12.9	0.05
LL/NM069	77.5	38.5	1.168	0.0021	1749.4	1.181	0.003	11.0	9.8	12.1	0.08
LL/NM070	79.5	34.9	1.165	0.0024	1740.5	1.176	0.003	8.2	5.9	10.7	0.07
LL/NM071	81.5	37.3	1.165	0.0013	1731.3	1.174	0.002	10.0	5.5	11.3	0.05
LL/NM072	83.5	37.0	1.166	0.0008	1722.3	1.177	0.002	9.8	8.1	12.2	0.06
LL/NM073	85.5	29.7	1.163	0.0010	1712.3	1.176	0.002	4.3	4.6	11.0	0.06
LL/NM074	87.5	28.5	1.160	0.0007	1701.1	1.160	0.002	3.4	4.2	12.5	0.04
LL/NM075	89.5	23.8	1.160	0.0012	1690.5	1.160	0.002		0.2	10.2	0.00

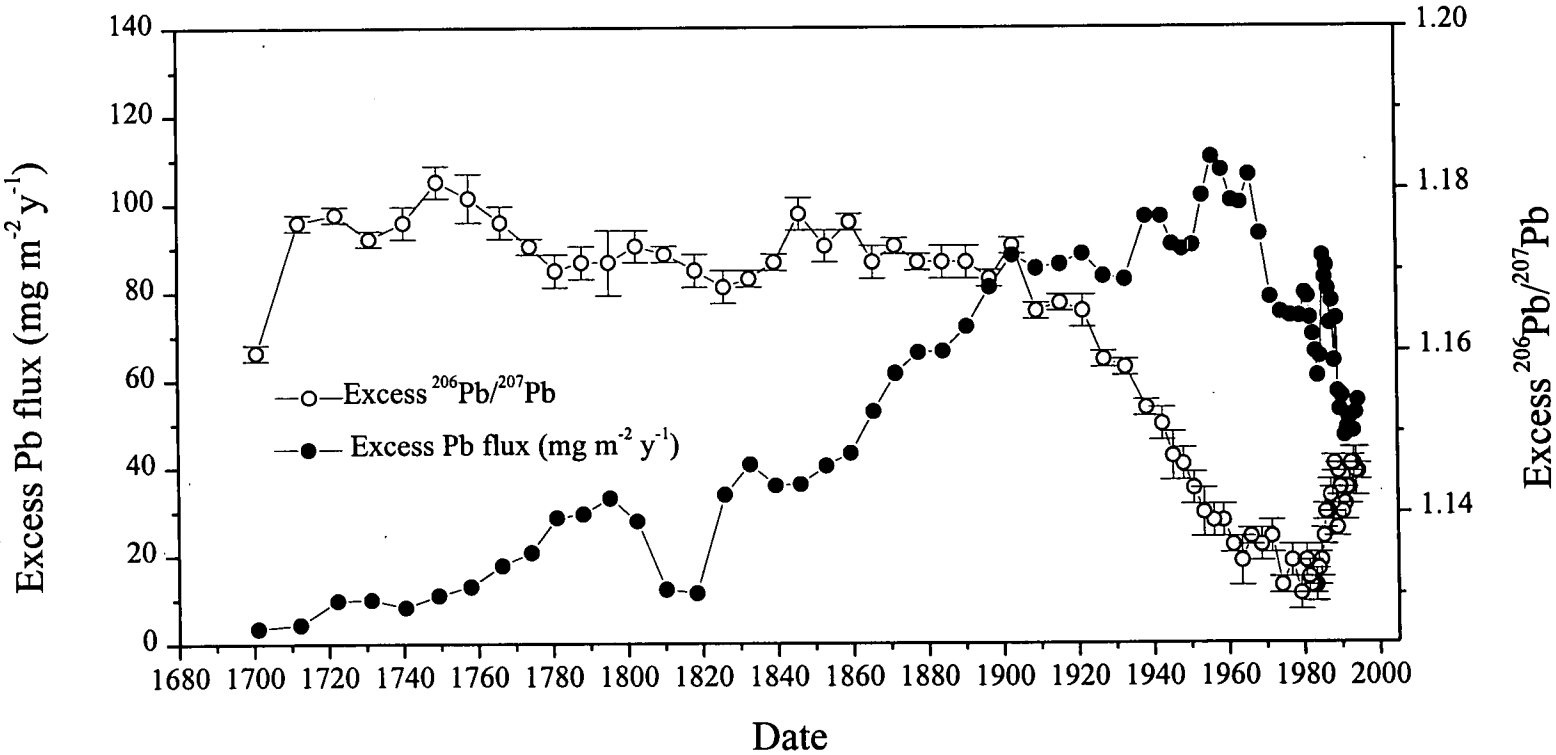

Figure 3.29 Excess Pb flux (mg m^{-2} y^{-1}) and excess ^{206}Pb/^{207}Pb atom ratio vs date (based on 2 component ^{137}Cs model) in core LL/NM.

3.5.2.5 Heavy metals.

In Figure 3.30 excess fluxes of Cd, Cu, Pb, and Zn (Table 3.16) are plotted against date (based on 2 component ^{137}Cs) in order to compare the historical trends in the metal inputs. Cd and Zn both show very similar profiles to that of Pb, although Cd and Zn did not begin to increase significantly until between 1840-1850, whereas Pb was increasing from the base of the core (1679, ^{137}Cs chronology, 2-component). All of the profiles have a significant depression at about 1820 and at 1970 (also observed in ^{210}Pb, Fe and Mn profiles). Cd, Pb and Zn have all been decreasing in input over the past 10-15 years.

The concentration profile of Cu contrasted with the other metals in that it was almost constant between 45-50 mg kg^{-1} throughout the core. The input did not begin to decrease until about 1980 and the rate of decrease was also significantly lower. This suggests that there is possibly a major natural input of Cu from the catchment runoff. From the concentration of Cu in the stream sediment samples (Table 3.14) it is observed that in some of the streams, these are higher than the concentrations observed in the core LL/NM. In particular, Allt Arnan has a concentration of 90.4 mg kg^{-1}. Cu increases in flux at the surface, as was observed for Loch Lomond (south), and is probably associated with organic matter.

The excess inventories for the heavy metals are summarised in Table 3.17. The background value used for each metal was that for the bottom section, with the exception of Cu where the total excess inventory was calculated using the minimum value at the depression situated at 60.5 cm. It is probable that these assumed natural values are an over estimation as it is not clear whether they have reached a baseline value. Hence the inventories should be taken as representing a minimum value.

If the total excess inventories in Loch Lomond north (1690-1766, 1766-1927 and 1927-1995) are taken over similar marker horizons as in Loch Lomond south (1634-1817, 1817-1929 and 1929-1991), it further highlights the fact that Cu (29, 40, and

Figure 3.30 Comparison of excess heavy metal flux (mg m^{-2} y^{-1}) vs date (based on 2 component ^{137}Cs) in core LL/NM.

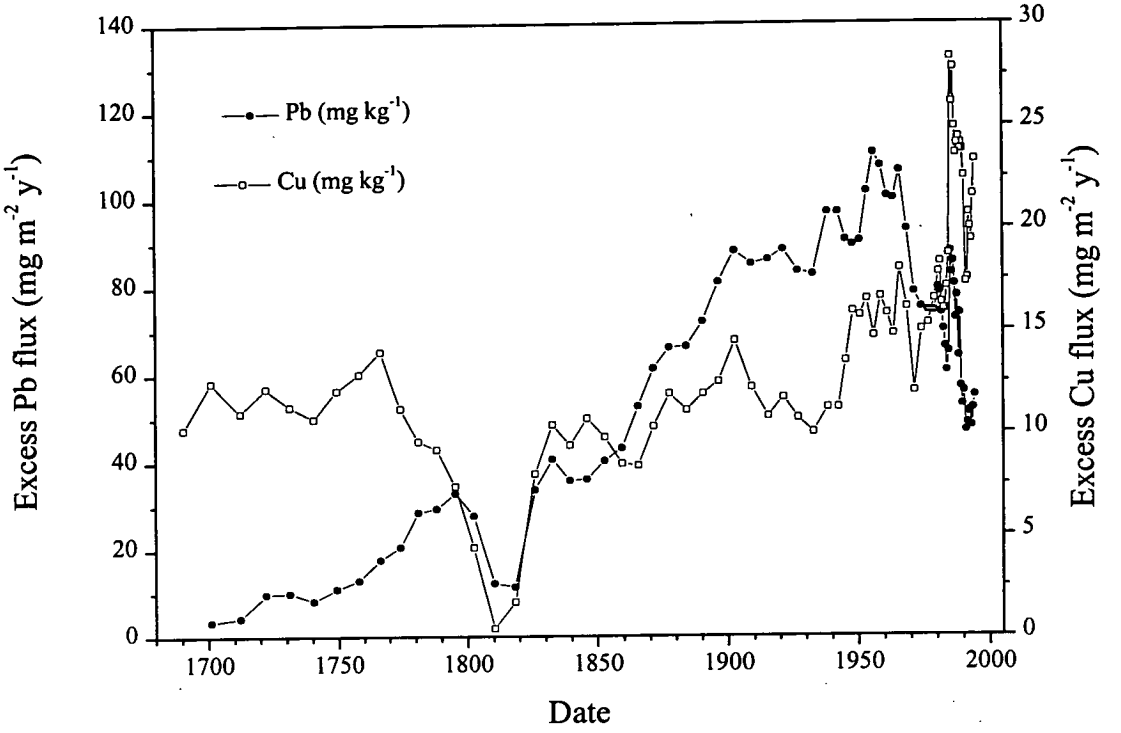

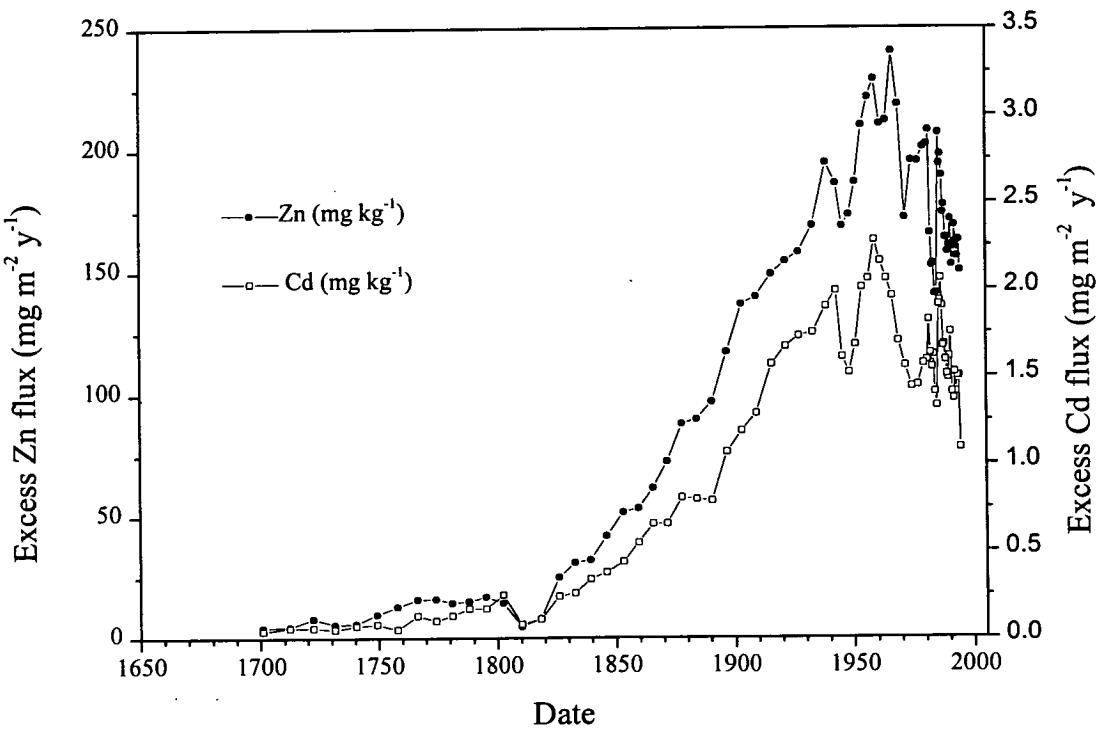

31 %) has had a relatively constant input since 1690. Zn and Cd are probably from the same source, with 3, 39 and 58 % of the total inventory for Zn, and 4, 41 and 54 % of the total inventory for Cd occurring over the above defined horizons.

The decrease in Cu from a flux of ~40 mg m^{-2} y^{-1} to near zero at about 1810 is the most pronounced of all the metals. There is no clear indication from the XRD, C, or ^{210}Pb data as to the cause of this depression. One possibility is a sudden increase in the sedimentation rate due to increased run off of material from the catchment, possibly as a result of forest clearances that are known to have occurred from late in the 17th Century until early 19th Century (Dickson *et al.*, 1978; Turner and Thompson, 1979). A future piece of work would be to examine possible changes in bulk sediment composition and, for example, to normalise concentrations of heavy metals to Al or Ti content.

3.5.2.6 Iron and manganese.

Fe and Mn (Figs. 3.19 and 3.20) both exhibit an enhancement at the surface of the sediment and a smaller peak situated at about 3-4 cm below the surface. The Mn enhancement at the surface is the most pronounced with a concentration 10 times that observed at the base of the core and ~ 2-4 times that of the rest of the core. The Mn and Fe concentrations are slightly lower than those in the south but the overall structures are similar. A core analysed by Farmer and Lovell (1984) from this basin also showed an enhancement in the surface layers for both of the metals.

Table 3.17 Total excess inventories for Pb, Zn, Cu and Cd in core LL/NM.

Metal	Background	Total excess inventory	Period		
			1690-1766	1766-1927	1927-1995
	/ mg kg^{-1}	/ g m^{-2}	/ g m^{-2}	/ g m^{-2}	/ g m^{-2}
Pb	24	14.1	0.7	7.3	6.1
Zn	89	22.9	0.6	9.0	13.2
Cu	30	3.48	1.01	1.40	1.07
Cd	0.12	0.22	0.01	0.09	0.12

Table 3.18 Comparison of excess Pb, Zn and Cu inventories for Loch Lomond.

Core	Core Date	Total excess inventory Pb / g m^{-2}	Total excess inventory Zn / g m^{-2}	Total excess inventory Cu / g m^{-2}	^{210}Pb flux / Bq m^{-2} y^{-1}
LL/South	1991	6.36	12.1	0.50	113
LL/North	1995	14.1	22.9	3.48	554
Bryant, 1994	1990	5.4	11.5	0.38	152
Farmer *et al*.,1980	1976	3.62	5.02	0.44	

3.6 Conclusions.

The inventories of all of the heavy metals studied (Pb, Zn, Cu (Cd)) are higher in the north than in the south, although the sectional concentrations are generally either similar or lower. The sedimentation rates calculated on the basis of ^{137}Cs are higher in the north (118.6 mg cm^{-2} y^{-1} for top sections, 75.5 mg cm^{-2} y^{-1} for lower sections) than in the south (30.9 mg cm^{-2} y^{-1}) reflecting a greater flux of settling particles and metals to the sediment in the north, probably as a result of sediment focusing. The heavy metal inventories are less likely to be influenced by industrial pollution in the north than in the south, although the northern basin is closer to a region of high mineralisation. The excess inventories of the two basins and from other published data for Loch Lomond (south) are summarised in Table 3.18 and it is evident that the northern basin receives a higher flux of the metals. The increase in Zn deposition occurred at around the same time at both sites. The core is not long enough in the north to ascertain whether Pb deposition started at similar times in the north and south.

The stable Pb isotopic ratios indicate that from about 1800 the sources of Pb to the sediment which have the most noticeable impact are the same at both sites. The decline of the British Pb mining industry and increasing imports of Australian/Canadian Pb ore at the start of the 20th Century brought about a drop in $^{206}Pb/^{207}Pb$ ratio and this was further enhanced with the introduction of leaded petrol from around the mid 1930s. Both cores show identical declines in the ratios in line with the aforementioned changes of Pb usage.

A more detailed comparison of these two study sites will be made in Chapter 7 along with all the other study sites.

4.1 Location.

The Lake of Menteith is situated 20 km to the west of Stirling and 20 km to the east of Loch Lomond (Figs. 1.13 and 4.1). It lies on the flat plain which separates the Menteith Hills to the north and the Gargunnock hills to the south and which also contains Flanders Moss, the largest remaining lowland raised peat bog in Britain. There are three islands situated in the west of the lake, the larger two, Inchmahome and Inch Talla, have a priory and a castle, respectively, while the smallest island, Dog Isle, is uninhabited. A further interesting feature is a submerged crannog (fortified island, partly natural and partly artificial), covered by about 1.3 m of water, in the north-east part of the lake close to Port of Menteith (Wewetzer, 1992).

4.2 Topography.

The lake lies between the Highland Boundary Fault to the north and the Ochil Fault to the south, in a broad plain of clays and peat mosses (Wewetzer, 1992; Wewetzer and Duck, 1995). It has a maximum length of 2.57 km, a mean width of 1.02 km and a surface area of 2.64 km^2. As a consequence of glaciation, the bottom of the lake is very irregular, and has been described as being a group of closely spaced kettle-holes (Fozzard and Marsden, 1990). There are four basins in the lake with a mean depth of 6 m but the basin to the north-west of Inchmahome island is significantly deeper than the others, with a depth of 23.5 m. During the summer, this deeper basin becomes thermally stratified whereas the rest of the lake remains isothermal all year. The lake displays many eutrophic characteristics, which are in keeping with its basin morphometry, and has a pH range of 6.5-7.5 (Fozzard and Marsden, 1990).

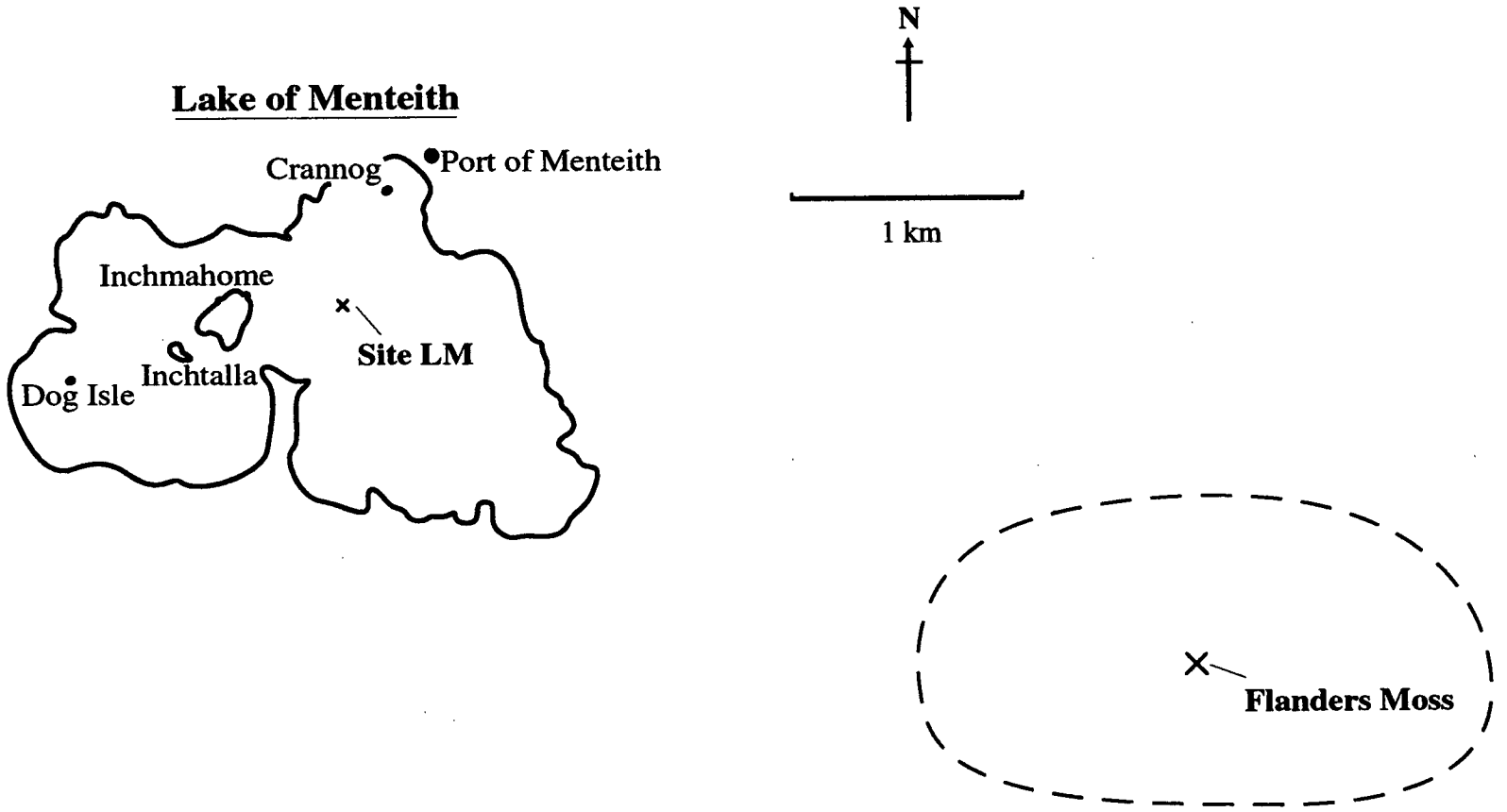

Figure 4.1 Location of sediment core site in Lake of Menteith and location of Flanders Moss.

4.3 Pollution sources.

There are no major sources of industrial pollution in close proximity to the lake. However, in Scotland because the winds generally prevail from the west, it may be affected by the main industrial and population belt situated ~30 km to the east. Grangemouth, the centre of the Scottish petrochemical industry and one of the main industrial sites in Scotland and a coal-fired power station at Kincardine, lie ~40 km to the east of the lake. However, due to the westerly prevailing winds they will not present a major pollution source. The A873, a major tourist road from Stirling to the Trossachs, runs along the northern shore of the lake. As the road lies between 10 and 500 m from the shore, the lake will be subject to input from local vehicle exhaust emissions. While there are a few small villages situated close to the lake, the nearest town of significance is Stirling, 30 km to the east.

4.4 Results.

A Mini-Mackereth core (LMM) and a Jenkin core (LMJ) were taken from site LM on 13/11/96 (Paterson, 1997) (Section 2.1.2.2). The Jenkin core was analysed for ^{137}Cs, ^{226}Ra and ^{210}Pb, and the Mini-Mackereth core for Fe, Mn, Pb, Zn, Cu, Cd, C, N and stable Pb isotopes.

4.4.1 ^{210}Pb and ^{226}Ra.

The results obtained for ^{210}Pb and ^{226}Ra specific activities in Lake of Menteith sediment core LMJ by γ-spectroscopy analysis are shown in Table 4.1. Figure 4.2 is a plot of the specific activity of ^{210}Pb (Bq kg^{-1}) against sediment depth (cm). The ^{210}Pb specific activity is fairly constant from 16 cm to the base of the core, with an average value of 101 ± 22 Bq kg^{-1}. Above 16 cm the specific activity increases to 167 Bq kg^{-1} at 9-10 cm, then rapidly to 574 Bq kg^{-1} at 4-5 cm, before remaining relatively constant until 2 cm from the surface, where there is a small increase to about 650 Bq kg^{-1} in the uppermost two sections.

Table 4.1 Radionuclide results for Lake of Menteith core LMJ.

				^{210}Pb		^{226}Ra		^{137}Cs	
Sample	Depth / cm	Wet Weight / g	Dry Weight / g	A(o) / Bq kg^{-1}	σ_{n-1} / Bq kg^{-1}	A(o) / Bq kg^{-1}	σ_{n-1} / Bq kg^{-1}	A(o) / Bq kg^{-1}	σ_{n-1} / Bq kg^{-1}
LMJ1	0.0-1.0	28.491	3.850	644	45	69.4	18	972.6	30
LMJ2	1.0-2.0	35.401	3.982	658	51	60.1	19	998.2	37
LMJ3	2.0-3.0	36.895	4.406	567	25	62.5	11	1066.0	27
LMJ4	3.0-4.0	36.178	4.477	562	34	62.5	16	1051.6	30
LMJ5	4.0-5.0	35.868	4.340	574	44	57.8	16	1011.6	35
LMJ6	5.0-6.0	35.789	4.449	488	47	62.7	18	918.5	32
LMJ7	6.0-7.0	36.352	4.917	453	20	50.2	8	589.0	16
LMJ8	7.0-8.0	36.049	5.654	389	63	57.9	17	423.8	17
LMJ9	8.0-9.0	38.885	5.474	255	38	57.8	14	303.4	17
LMJ10	9.0-10.0	38.583	5.544	167	15	50.6	10	173.5	10
LMJ11	10.0-11.0	37.120	5.168	166	36	61.2	12	166.5	12
LMJ12	11.0-12.0	37.626	5.046	157	44	54.7	12	106.9	16
LMJ13	12.0-13.0	39.051	5.274	127	25	20.3	8	77.1	13
LMJ14	13.0-14.0	36.185	4.867	129	33	54.1	10	85.6	8
LMJ15	14.0-15.0	39.157	5.251	149	21	49.0	7	69.8	7
LMJ16	15.0-16.0	36.997	5.375	132	35	60.7	12	29.3	13
LMJ17	16.0-17.0	37.428	5.456	103	26	54.8	10		
LMJ18	17.0-18.0	37.963	5.169	99	33	54.5	9		
LMJ19	18.0-19.0	39.008	6.218	107	42	60.1	12		
LMJ20	19.0-20.0	36.154	6.017	72	28	55.6	8		
LMJ21	20.0-21.0	35.879	5.128	144	45	39.2	13		
LMJ22	21.0-22.0	25.361	3.830	84	25	99.0	16		

The specific activity of ^{226}Ra (Bq kg^{-1}) is plotted against depth (cm) in Figure 4.3. The specific activity of ^{226}Ra, taken to represent the 'supported' ^{210}Pb, is fairly constant throughout the core, with an average of 57 ± 12 Bq kg^{-1}.

4.4.2 Radiocaesium.

The results obtained for ^{137}Cs specific activities in Lake of Menteith sediment core LMJ by γ-spectroscopy analysis are shown in Table 4.1. Figure 4.4 is a plot of the specific activity of ^{137}Cs (Bq kg^{-1}) against sediment depth (cm). The profile shows a large, broad peak with values in excess of 900 Bq kg^{-1} over the top 6 cm and a maximum of 1052-1066 Bq kg^{-1} at ~ 3 cm. Below 6 cm the specific activity decreases rapidly to 174 Bq kg^{-1} by 9-10 cm. Thereafter, the rate of decrease slows until, at 16 cm, there is no longer any detectable ^{137}Cs.

4.4.3 Heavy metals.

The results obtained for the heavy metals (Pb, Zn, Cu, Cd, Fe and Mn) in core LMM (Paterson, 1997) are shown in Table 4.2 and corresponding plots of concentration (mg kg^{-1} or %) against depth (cm) for each metal are shown in Figures 4.5-4.10.

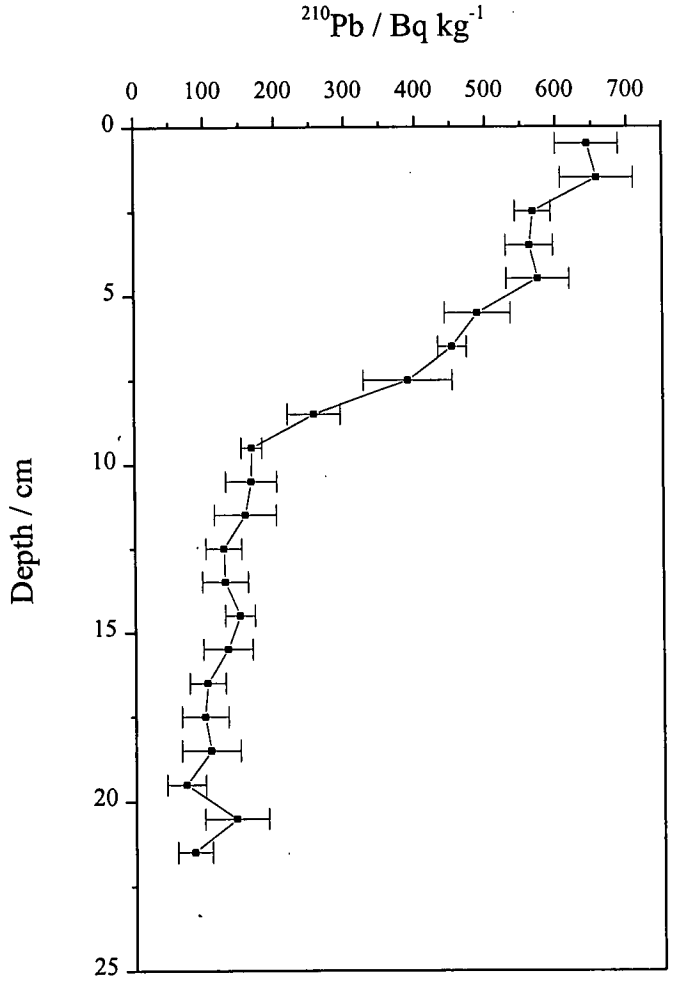

Figure 4.2 ^{210}Pb (Bq kg^{-1}) vs depth (cm) in core LMJ.

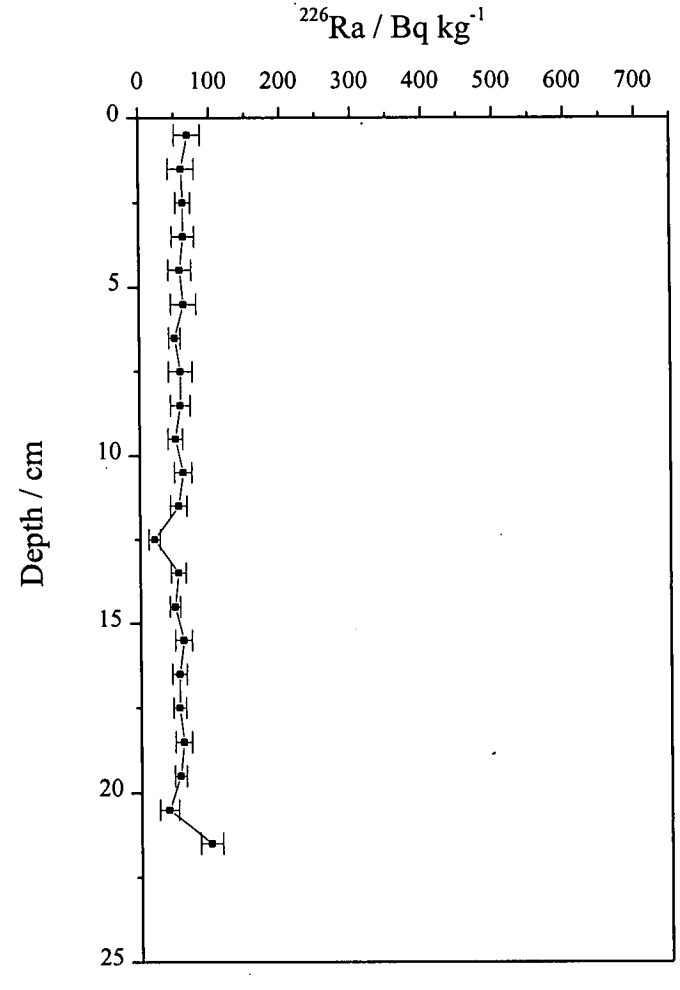

Figure 4.3 ^{226}Ra (Bq kg^{-1}) vs depth (cm) in core LMJ.

Figure 4.4 ^{137}Cs (Bq kg^{-1}) vs depth (cm) in core LMJ.

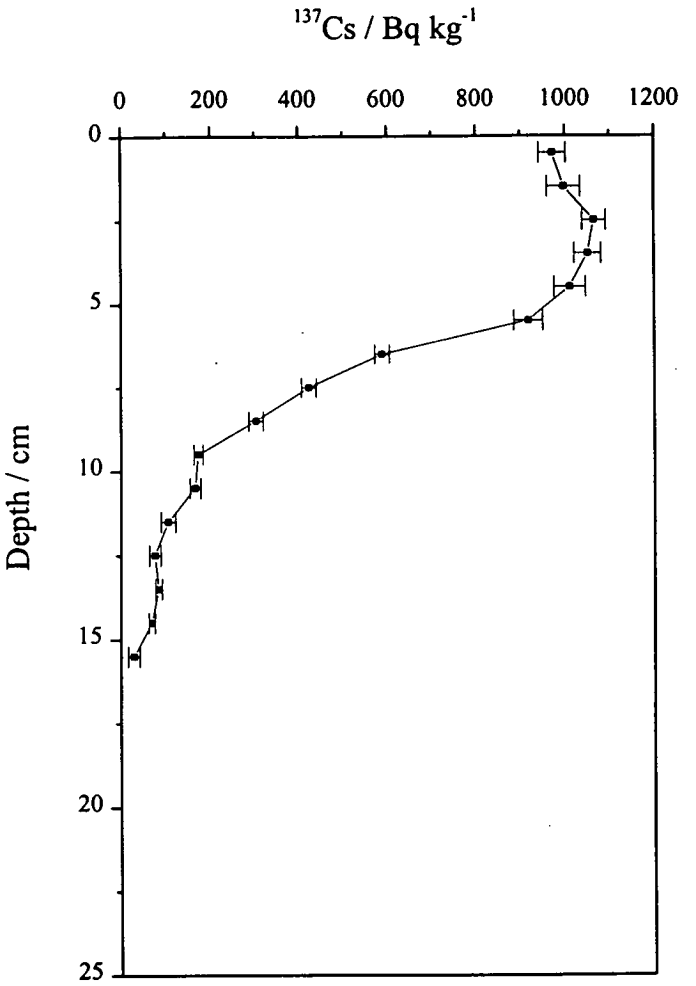

Table 4.2 Heavy metal, carbon and nitrogen results for Lake of Menteith core LMM.

Sample Code	Depth / cm (midpoint)	Wet wt / g	Dry wt / g	Pb / mg kg^{-1}	Zn / mg kg^{-1}	Cu / mg kg^{-1}	Cd / mg kg^{-1}	Fe / %	Mn / %	C / %	N / %
LMM1	0.10	22.922	0.275	198	400	60	2.5	6.19	0.609	not determined	
LMM2	0.30	10.151	0.580	186	412	59	2.2	5.66	0.679	12.61	1.16
LMM3	0.50	10.095	0.700	182	392	45	2.8	5.97	0.728	12.66	1.16
LMM4	0.70	9.522	0.665	175	363	40	2.2	6.18	0.565		
LMM5	0.90	14.107	1.100	176	381	42	2.1	6.54	0.496	12.48	1.21
LMM6	1.10	11.172	0.931	167	384	36	2.2	6.10	0.300		
LMM7	1.30	12.330	1.049	167	366	39	1.9	6.06	0.252	12.53	1.17
LMM8	1.50	12.790	1.153	157	368	47	2.2	5.58	0.215	12.45	1.15
LMM9	1.70	12.212	1.125	169	368	38	2.1	5.19	0.171		
LMM10	1.90	12.138	1.175	167	395	44	2.3	5.10	0.182	13.07	1.22
LMM11	2.10	11.613	1.115	168	378	41	2.2	4.61	0.163	12.82	1.15
LMM12	2.30	11.737	1.162	169	383	42	2.2	4.32	0.151		
LMM13	2.50	12.840	1.404	177	394	42	2.6	4.05	0.147	12.71	1.13
LMM14	2.70	12.679	1.294	174	377	41	2.3	3.84	0.132		
LMM15	2.90	13.355	1.434	186	419	43	2.9	4.21	0.137	12.45	1.13
LMM16	3.10	11.370	1.254	194	427	42	2.6	4.65	0.120		
LMM17	3.30	11.374	1.443	177	419	42	2.3	3.95	0.125	12.48	1.10
LMM18	3.50	12.769	1.345	181	403	43	2.4	3.73	0.120	12.27	1.11
LMM19	3.70	13.680	1.510	194	440	40	2.6	4.21	0.109		
LMM20	3.90	11.593	1.251	192	449	45	3.0	4.44	0.122	12.62	1.08
LMM21	4.10	14.482	1.572	192	452	42	2.7	4.65	0.116		
LMM22	4.30	10.373	1.104	200	451	43	3.0	4.53	0.117		
LMM23	4.50	12.307	1.354	206	462	44	2.5	4.49	0.100	12.42	1.14
LMM24	4.70	14.295	1.625	206	449	43	2.7	4.35	0.107		
LMM25	4.90	12.964	1.499	217	485	45	2.9	4.43	0.114		

Table 4.2 Heavy metal, carbon and nitrogen results for Lake of Menteith core LMM, continued.

Sample Code	Depth / cm (midpoint)	Wet wt / g	Dry wt / g	Pb / mg kg^{-1}	Zn / mg kg^{-1}	Cu / mg kg^{-1}	Cd / mg kg^{-1}	Fe / %	Mn / %	C / %	N / %
LMM26	5.25	20.418	2.412	210	444	40	3.0	4.26	0.106	12.59	1.22
LMM27	5.75	23.431	2.720	228	498	45	3.0	4.82	0.108	not determined	
LMM28	6.25	18.801	2.169	230	487	45	3.1	4.85	0.107	12.13	1.16
LMM29	6.75	19.412	2.264	236	500	46	3.5	4.91	0.107		
LMM30	7.25	21.826	2.549	219	461	49	2.8	4.31	0.099	12.02	1.16
LMM31	7.75	19.985	2.391	234	507	46	2.8	4.84	0.101	11.87	0.97
LMM32	8.25	17.733	2.224	228	469	45	2.8	4.25	0.098		
LMM33	8.75	21.647	2.722	224	475	44	2.8	4.10	0.099		
LMM34	9.25	20.001	2.499	220	499	44	2.9	4.87	0.101		
LMM35	9.75	20.359	2.604	230	486	49	3.0	4.75	0.107	12.24	1.11
LMM36	10.25	20.353	2.514	222	467	44	2.9	4.72	0.108		
LMM37	10.75	22.573	2.833	234	521	44	3.1	4.85	0.110		
LMM38	11.25	18.137	2.226	248	544	45	3.2	5.20	0.112	12.63	1.13
LMM39	11.75	18.624	2.294	245	553	48	2.9	5.12	0.109		
LMM40	12.25	20.387	2.563	250	579	47	3.0	5.29	0.113		
LMM41	12.75	22.875	3.103	231	497	48	2.8	4.72	0.103		
LMM42	13.25	23.992	3.381	245	509	45	2.7	4.60	0.104		
LMM43	13.75	24.412	3.422	222	457	42	2.5	4.50	0.102		
LMM44	14.25	19.705	2.668	240	479	45	2.8	4.84	0.105		
LMM45	14.75	20.314	2.735	240	457	44	3.5	4.84	0.112	11.56	0.95
LMM46	15.25	16.882	2.293	248	439	43	2.4	4.57	0.107		
LMM47	15.75	22.028	3.025	224	378	34	2.0	4.22	0.103		
LMM48	16.25	18.723	2.542	198	315	38	1.6	4.25	0.102		
LMM49	16.75	21.792	3.101	180	289	36	1.5	4.09	0.096		
LMM50	17.25	20.154	2.883	162	263	35	1.2	4.08	0.089		

Table 4.2 Heavy metal, carbon and nitrogen results for Lake of Menteith core LMM, continued.

Sample Code	Depth / cm (midpoint)	Wet wt / g	Dry wt / g	Pb / mg kg^{-1}	Zn / mg kg^{-1}	Cu / mg kg^{-1}	Cd / mg kg^{-1}	Fe / %	Mn / %	C / %	N / %
LMM51	17.75	20.652	3.021	156	251	37	1.5	3.61	0.091	10.90	0.89
LMM52	18.25	17.808	2.574	169	258	35	1.5	3.93	0.092	not determined	
LMM53	18.75	19.506	2.923	167	256	40	1.8	3.85	0.096	10.77	0.87
LMM54	19.25	17.870	2.714	162	229	31	1.3	3.66	0.091		
LMM55	19.75	18.058	2.710	182	258	38	1.5	4.42	0.104		
LMM56	20.25	18.636	2.788	186	253	37	1.4	4.50	0.104		
LMM57	20.75	16.965	2.481	178	238	38	0.8	4.01	0.094		
LMM58	21.25	17.810	2.644	198	268	39	1.3	4.33	0.093		
LMM59	21.75	15.396	2.290	176	233	31	1.4	4.43	0.099		
LMM60	22.25	17.343	2.611	172	229	35	1.4	4.78	0.116	10.23	0.84
LMM61	22.75	17.623	2.680	165	225	35	1.2	4.87	0.150		
LMM62	23.25	19.115	2.846	154	234	34	1.1	4.89	0.209		
LMM63	23.75	19.242	2.824	158	254	32	1.2	5.38	0.186		
LMM64	24.25	18.867	2.700	150	203	33	1.3	5.27	0.162		
LMM65	24.75	19.796	2.884	156	198	33	1.0	4.83	0.131	10.71	0.84
LMM66	25.25	20.686	3.025	151	200	31	1.1	4.85	0.108		
LMM67	25.75	19.934	2.970	149	198	32	1.1	4.09	0.108		
LMM68	26.25	22.386	3.391	139	181	31	1.0	3.95	0.099		
LMM69	26.75	20.056	3.139	139	162	32	0.8	3.96	0.100		
LMM70	27.25	20.957	3.333	135	164	30	0.9	4.08	0.101		
LMM71	27.75	18.859	2.744	136	161	33	0.9	4.33	0.102		
LMM72	28.25	20.989	3.429	117	155	28	0.7	4.52	0.095	11.11	0.61
LMM73	28.75	19.614	2.883	119	147	29	0.8	4.75	0.105		
LMM74	29.25	20.511	3.314	115	161	30	0.6	4.76	0.102		
LMM75	29.75	20.452	3.164	122	154	31	0.7	5.10	0.096		

Table 4.2 Heavy metal, carbon and nitrogen results for Lake of Menteith core LMM, continued.

Sample Code	Depth / cm (midpoint)	Wet wt / g	Dry wt / g	Pb / mg kg^{-1}	Zn / mg kg^{-1}	Cu / mg kg^{-1}	Cd / mg kg^{-1}	Fe / %	Mn / %	C / %	N / %
LMM76	30.25	20.410	4.049	107	138	28	0.7	4.25	0.100	not determined	
LMM77	30.75	20.302	3.184	107	112	27	0.5	4.55	0.104	11.62	0.76
LMM78	31.25	21.140	3.283	106	119	28	0.8	4.28	0.101		
LMM79	31.75	21.171	3.347	99	114	27	0.5	4.36	0.101		
LMM80	32.25	20.815	3.278	100	124	27	0.6	4.57	0.100		
LMM81	32.75	17.918	2.839	106	131	30	0.7	4.42	0.103		
LMM82	33.25	21.281	3.514	102	122	27	0.9	4.25	0.102		
LMM83	33.75	19.940	3.427	103	126	29	0.6	4.03	0.100		
LMM84	34.25	21.901	3.823	96	117	26	0.7	3.62	0.096	11.07	0.74
LMM85	34.75	19.668	3.449	97	110	28	0.5	3.70	0.095		
LMM86	35.25	21.597	3.894	92	108	28	0.5	3.70	0.099		
LMM87	35.75	22.704	4.047	87	95	28	0.4	3.55	0.096		
LMM88	36.25	21.310	3.942	73	84	26	0.3	3.61	0.090		
LMM89	36.75	18.506	3.343	56	81	23	0.3	3.30	0.084		
LMM90	37.25	20.410	3.833	49	65	25	0.3	3.38	0.091		
LMM91	37.75	19.472	3.557	49	80	25	0.3	3.94	0.091		
LMM92	38.25	18.526	3.354	47	64	24	0.3	3.43	0.090		
LMM93	38.75	18.137	3.181	40	70	23	0.2	3.19	0.081	10.55	0.45
LMM94	39.25	20.769	3.767	40	61	23	0.2	3.00	0.078		
LMM95	39.75	19.469	3.484	41	58	26	0.3	3.22	0.085		
LMM96	40.25	21.211	2.763	42	68	23	0.5	3.37	0.086		
LMM97	40.75	18.192	3.150	37	59	22	0.1	3.48	0.088		
LMM98	41.25	21.426	3.964	40	53	25	0.3	3.18	0.084		
LMM99	41.75	19.618	3.621	39	67	25	0.2	3.24	0.083	10.25	0.55
LMM100	42.25	16.561	3.068	39	57	24	0.8	3.42	0.086		

Table 4.2 Heavy metal, carbon and nitrogen results for Lake of Menteith core LMM, continued.

Sample Code	Depth / cm (midpoint)	Wet wt / g	Dry wt / g	Pb / mg kg^{-1}	Zn / mg kg^{-1}	Cu / mg kg^{-1}	Cd / mg kg^{-1}	Fe / %	Mn / %	C / %	N / %
LMM101	42.75	21.720	4.034	41	55	25	0.5	3.27	0.089	not determined	
LMM102	43.25	20.305	4.195	40	77	25	0.3	3.65	0.088		
LMM103	43.75	17.804	2.129	42	60	23	0.2	3.53	0.089		
LMM104	44.25	15.243	2.720	40	67	25	0.2	3.55	0.089	11.01	0.60
LMM105	44.75	16.645	2.995	42	75	26	0.4	3.81	0.092		
LMM106	45.25	21.002	3.784	39	57	26	0.3	3.49	0.090		
LMM107	45.75	19.744	3.527	38	54	24	0.4	3.12	0.088		
LMM108	46.25	17.119	3.109	42	62	25	0.3	3.59	0.094		
LMM109	46.75	19.261	2.485	35	62	23	0.2	3.53	0.088		
LMM110	47.25	20.857	2.801	35	59	24	0.2	3.34	0.092	12.43	0.75
LMM111	47.75	21.781	3.986	31	59	25	0.2	3.25	0.087		
LMM112	48.25	18.104	3.275	34	71	27	0.2	3.61	0.097		
LMM113	48.75	20.333	2.701	32	64	26	0.2	3.56	0.095		
LMM114	49.25	16.011	2.748	31	57	27	0.2	3.23	0.088		
LMM115	49.75	18.187	2.963	25	65	22	0.3	3.29	0.081		
LMM116	50.50	35.610	5.849	31	56	27	0.4	3.26	0.088	11.69	0.95
LMM117	51.50	32.007	5.020	27	66	26	0.3	3.63	0.091		
LMM118	52.50	35.576	5.860	27	74	26	0.2	3.45	0.088		
LMM119	53.50	33.910	5.533	28	56	26	0.2	3.39	0.088		
LMM120	54.50	33.162	5.235	25	60	24	0.4	3.44	0.092		
LMM121	55.50	28.787	2.092	23	73	25	0.2	3.62	0.089	10.92	0.91

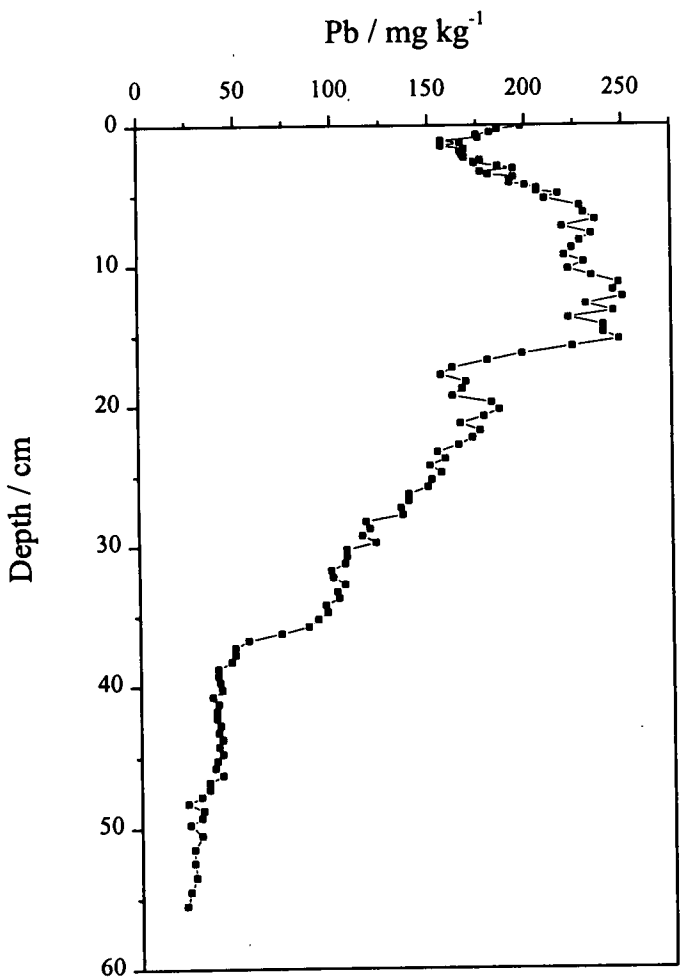

Figure 4.5 Pb (mg kg^{-1}) vs depth (cm) in core LMM.

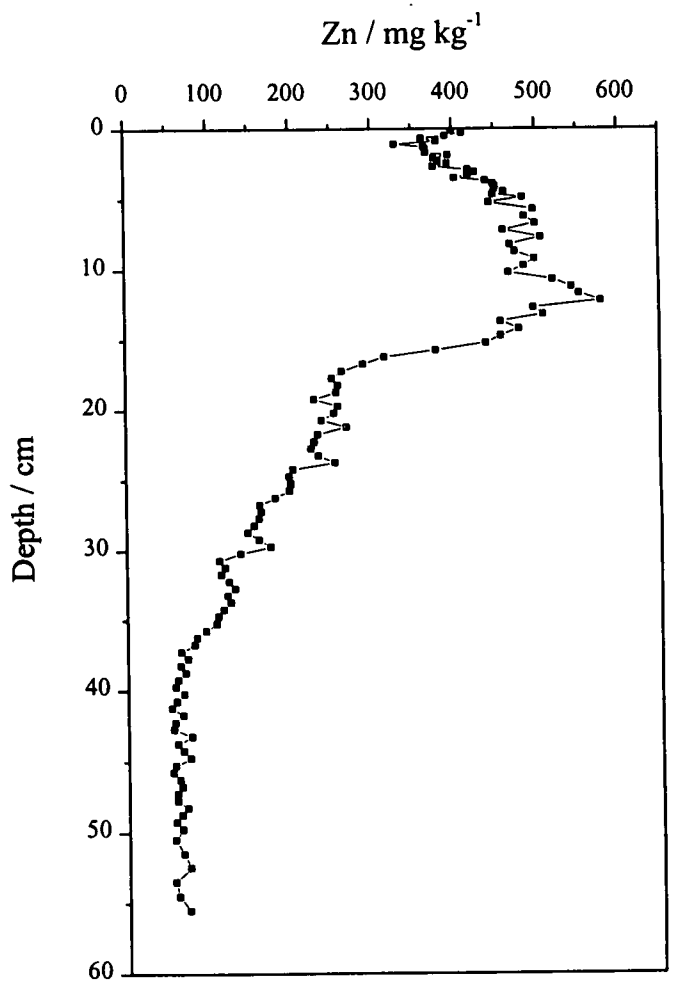

Figure 4.6 Zn (mg kg^{-1}) vs depth (cm) in core LMM.

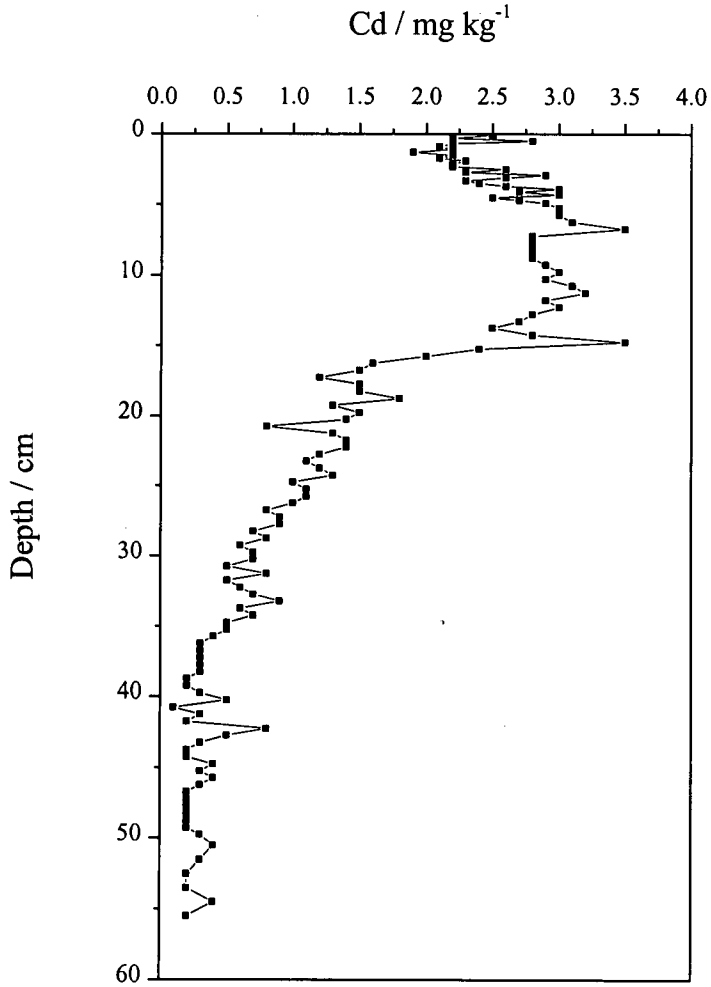

Figure 4.7 Cd (mg kg^{-1}) vs depth (cm) in core LMM.

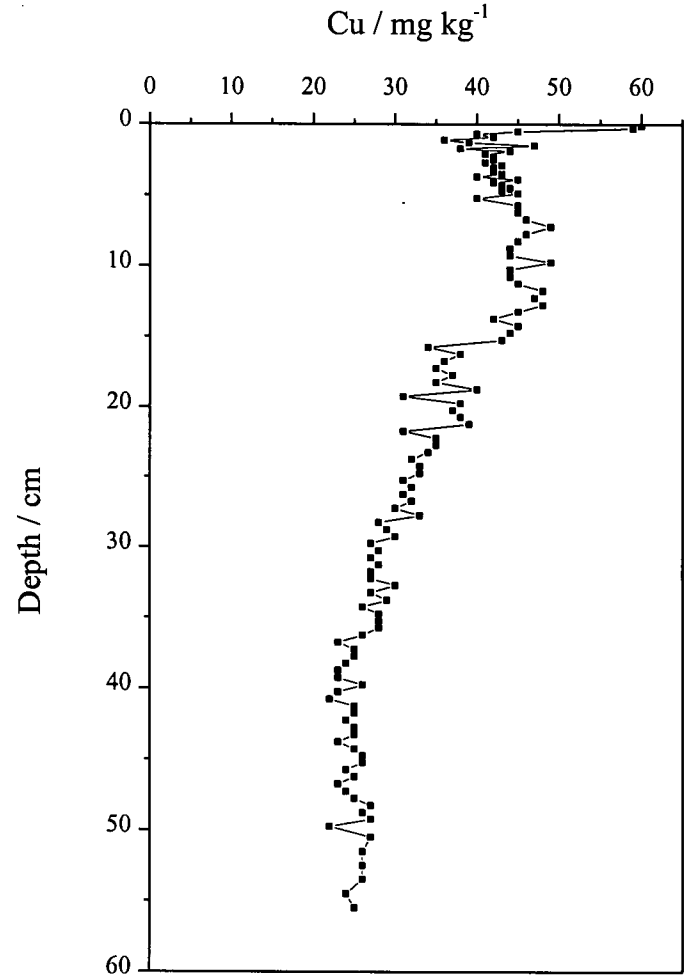

Figure 4.8 Cu (mg kg^{-1}) vs depth (cm) in core LMM.

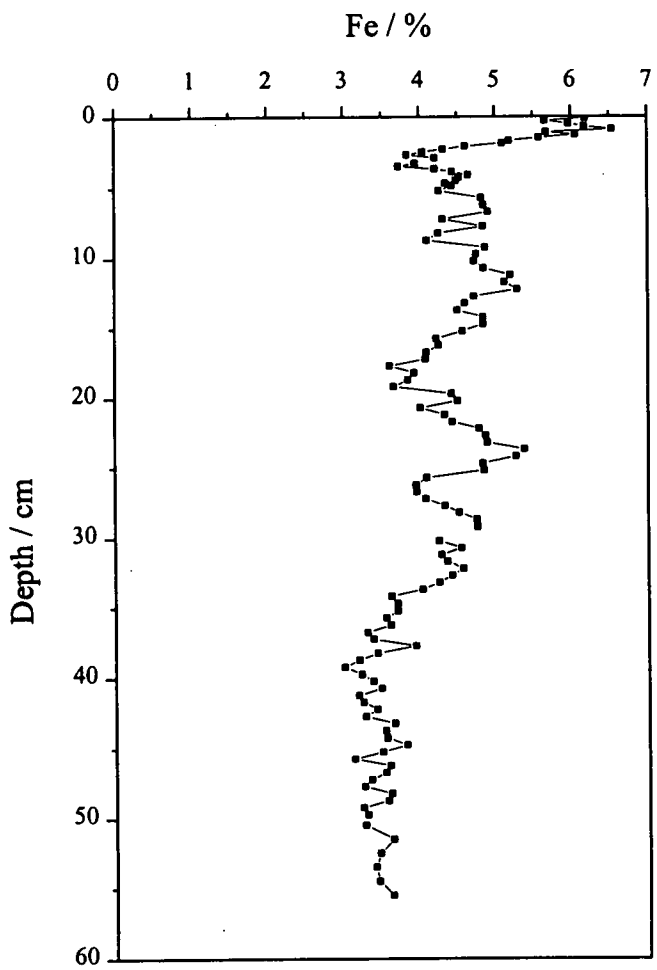

Figure 4.9 Fe (%) vs depth (cm) in core LMM.

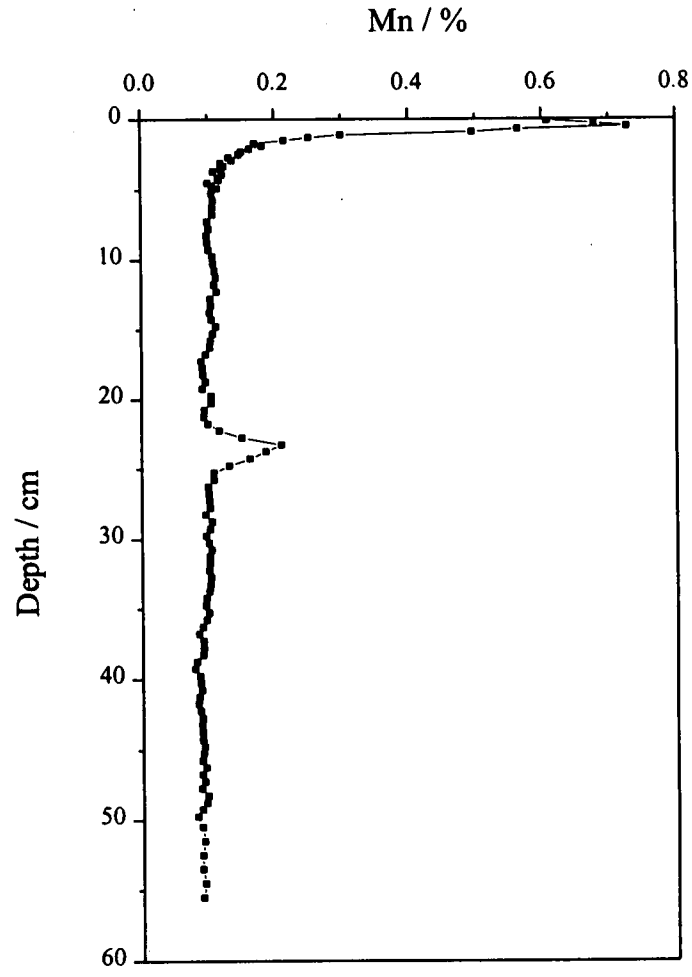

Figure 4.10 Mn (mg kg^{-1}) vs depth (cm) in core LMM.

The concentration of Pb (Fig. 4.5) is relatively constant in the lower regions of the core, averaging 28.2 ± 3.7 mg kg^{-1} from 55.5 cm to 47.75 cm then 39 ± 2.9 mg kg^{-1} until 38.75 cm. Above 38.75 cm, the concentration increases rapidly to 87 mg kg^{-1} over 3 cm, then more gradually, eventually reaching 186 mg kg^{-1} by 20.25 cm. Above this point the concentration decreases to 156 mg kg^{-1} by 17.75 cm before increasing sharply to a maximum of 222-250 mg kg^{-1} at 11.25-15.25 cm. Thereafter, the concentration declines fairly steadily to 157 mg kg^{-1} just below the sediment surface at 1.10 cm, but rises again to 188 mg kg^{-1} at the sediment surface.

In Figure 4.6 the concentration of Zn remains at a constant level of 63 ± 6.7 mg kg^{-1} from the base of the core until 37.25 cm. Above 37.25 cm the concentration begins a steady rise until reaching 251 mg kg^{-1} at 17.75 cm. Over the next 5 cm the concentration rises more rapidly to a maximum of 579 mg kg^{-1} at 12.25 cm before declining back to 363 mg kg^{-1} at 0.70 cm below the sediment surface. The concentration increases again to reach 400 mg kg^{-1} at the sediment surface.

Cadmium (Fig. 4.10) is relatively constant at 0.29 ± 0.13 mg kg^{-1} from the base of the core until 35.25 cm. Above 35.25 cm, the concentration begins to rise steadily until 16.25 cm then more rapidly to a sharp peak of 3.5 mg kg^{-1} at 14.75 cm. This then gives way to a broad peak for ~5 cm before rising for a second time to a sharp peak of 3.5 mg kg^{-1} at 6.75 cm. Above this the concentration declines to 2.5 mg kg^{-1} at the surface. Other sub-surface structure includes a small peak with a maximum of 0.8 mg kg^{-1} at 42.25 cm and a small sub-surface peak of 2.8 mg kg^{-1} at 0.50 cm.

Copper (Fig. 4.7) remains constant at 24.7 ± 1.4 mg kg^{-1} from the base of the core until 36.25 cm. Above 36.25 cm the concentration increases gradually to a broad peak between 12.75 and 7.25 cm with a maximum of 49 mg kg^{-1}. Above 7.25 cm the concentration decreases to 36 mg kg^{-1} at 1.10 cm before rising again to 60 mg kg^{-1}, the maximum for the core, at the sediment surface.

As shown in Figure 4.8, Fe is relatively constant at 3.4 ± 0.2 % from the base of the core until 36.75 cm. Above 36.75 cm the concentration rises to an average of 4.43 ± 0.45 % until 2 cm where it rises sharply to reach 6.54 % at 0.90 cm. The concentration tails off again towards the surface, although it is enhanced at the sediment surface. Other subsurface structure is a notable peak of 5.38 % at 23.75 cm and a smaller peak of 5.29 % at 12.25 cm.

In Figure 4.9, Mn is constant at 0.096 ± 0.008 % from the base of the core until 5 cm, except for a peak covering 3.5 cm with a maximum of 0.21 % at 23.25 cm. Above 5 cm the concentration increases slowly until 1.70 cm then rises rapidly to a maximum of 0.73 % at 0.50 cm before tailing off to 0.61 % at the sediment surface.

4.4.4 Carbon and nitrogen.

The results for C (%) and N (%) content of sections of the sediment core LMM, are shown in Table 4.2 and C (%) is plotted against sediment depth (cm) in Figure 4.11. The C profile starts to drop from ~12 % to ~10 % from 12 -22 cm depth. Below 22 cm the concentration varies between 10 and 12 % to the base of the core. The N concentration is relatively constant at 1.14 ± 0.06 % until 20 cm then drops to an average of 0.77 ± 0.16 % from 20 cm to the base of the core

4.4.5 Stable lead isotopes.

The results for stable Pb isotope atom ratios and Pb concentrations in sediment core LMM are shown in Table 4.3. Figures 4.12 (a)-(c) show the isotope ratios $^{206}Pb/^{207}Pb$, $^{208}Pb/^{206}Pb$ and $^{208}Pb/^{207}Pb$ together with Pb concentration (mg kg^{-1}) against depth (cm).

Figure 4.11 C (%) vs depth (cm) in core LMM.

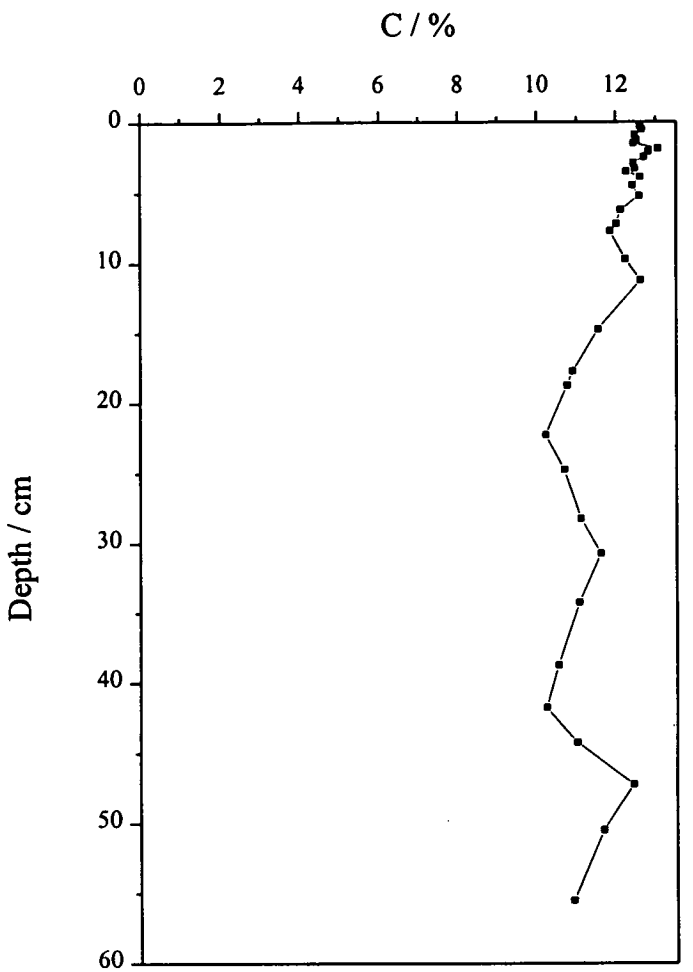

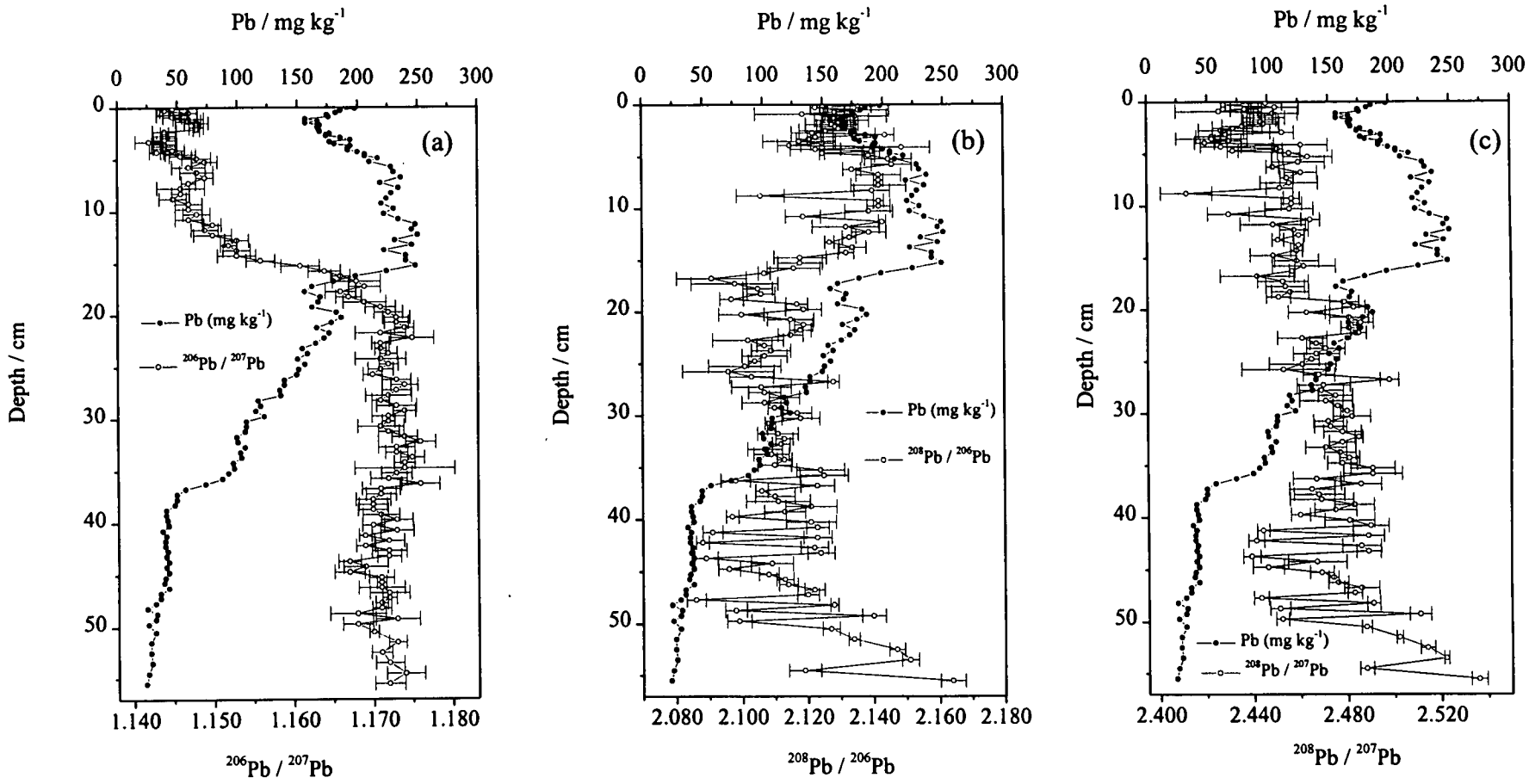

Figure 4.12 Stable lead isotopes and Pb(mg kg^{-1}) vs depth (cm) for core LMM:

(a) $^{206}Pb/^{207}Pb$, (b) $^{208}Pb/^{206}Pb$ and (c) $^{208}Pb/^{207}Pb$.

Table 4.3 Stable Pb isotope ratio and Pb concentration (mg kg^{-1}) results for Lake of Menteith core LMM.

Sample Code	Depth / cm (midpoint)	Pb / mg kg^{-1}	$^{206}Pb/^{207}Pb$	σ_{n-1}	$^{208}Pb/^{206}Pb$	σ_{n-1}	$^{208}Pb/^{207}Pb$	σ_{n-1}
LMM1	0.10	198	1.145	0.0019	2.136	0.0041	2.446	0.0071
LMM2	0.30	186	1.144	0.0006	2.123	0.0015	2.428	0.0009
LMM3	0.50	182	1.147	0.0011	2.136	0.0093	2.450	0.0101
LMM4	0.70	175	1.145	0.0020	2.129	0.0031	2.437	0.0059
LMM5	0.90	176	1.145	0.0012	2.119	0.0146	2.426	0.0185
LMM6	1.10	167	1.147	0.0019	2.135	0.0096	2.449	0.0108
LMM7	1.30	167	1.147	0.0016	2.131	0.0018	2.445	0.0041
LMM8	1.50	157	1.148	0.0015	2.131	0.0082	2.445	0.0092
LMM9	1.70	169	1.148	0.0002	2.130	0.0050	2.445	0.0056
LMM10	1.90	167	1.148	0.0009	2.128	0.0080	2.444	0.0075
LMM11	2.10	168	1.148	0.0004	2.129	0.0056	2.445	0.0069
LMM12	2.30	169	1.144	0.0015	2.130	0.0054	2.436	0.0086
LMM13	2.50	177	1.144	0.0005	2.126	0.0079	2.432	0.0086
LMM14	2.70	174	1.144	0.0015	2.122	0.0064	2.427	0.0096
LMM15	2.90	186	1.144	0.0015	2.144	0.0028	2.453	0.0051
LMM16	3.10	194	1.144	0.0014	2.123	0.0024	2.429	0.0022
LMM17	3.30	177	1.142	0.0017	2.121	0.0038	2.423	0.0066
LMM18	3.50	181	1.144	0.0016	2.118	0.0111	2.423	0.0152
LMM19	3.70	194	1.144	0.0016	2.125	0.0035	2.430	0.0055
LMM20	3.90	192	1.144	0.0014	2.115	0.0036	2.420	0.0042
LMM21	4.10	192	1.145	0.0015	2.149	0.0087	2.461	0.0115
LMM22	4.30	200	1.143	0.0009	2.123	0.0077	2.427	0.0087
LMM23	4.50	206	1.146	0.0019	2.140	0.0024	2.451	0.0022
LMM24	4.70	206	1.146	0.0014	2.125	0.0008	2.432	0.0023
LMM25	4.90	217	1.148	0.0018	2.139	0.0019	2.456	0.0049
LMM26	5.25	210	1.149	0.0016	2.145	0.0071	2.464	0.0105
LMM27	5.75	228	1.147	0.0021	2.146	0.0061	2.460	0.0113
LMM28	6.25	230	1.148	0.0021	2.134	0.0027	2.449	0.0027
LMM29	6.75	236	1.149	0.0011	2.142	0.0068	2.461	0.0070
LMM30	7.25	219	1.147	0.0009	2.142	0.0014	2.455	0.0028
LMM31	7.75	234	1.146	0.0030	2.142	0.0083	2.456	0.0123
LMM32	8.25	228	1.146	0.0011	2.140	0.0054	2.452	0.0057
LMM33	8.75	224	1.145	0.0017	2.106	0.0073	2.412	0.0110
LMM34	9.25	220	1.147	0.0017	2.142	0.0015	2.457	0.0035
LMM35	9.75	230	1.147	0.0017	2.142	0.0035	2.457	0.0044
LMM36	10.25	222	1.148	0.0017	2.139	0.0072	2.456	0.0103
LMM37	10.75	234	1.147	0.0017	2.119	0.0053	2.430	0.0089
LMM38	11.25	248	1.150	0.0011	2.143	0.0011	2.465	0.0040
LMM39	11.75	245	1.149	0.0017	2.132	0.0102	2.449	0.0141
LMM40	12.25	250	1.150	0.0024	2.139	0.0052	2.458	0.0061
LMM41	12.75	231	1.153	0.0015	2.133	0.0021	2.460	0.0024
LMM42	13.25	245	1.152	0.0010	2.127	0.0014	2.451	0.0025
LMM43	13.75	222	1.153	0.0017	2.134	0.0041	2.460	0.0020
LMM44	14.25	240	1.153	0.0024	2.132	0.0024	2.459	0.0025
LMM45	14.75	240	1.156	0.0018	2.118	0.0080	2.449	0.0099

Table 4.3 Stable Pb isotope ratio and Pb concentration (mg kg^{-1}) results for Lake of Menteith core LMM, continued.

Sample Code	Depth / cm (midpoint)	Pb / mg kg^{-1}	$^{206}Pb/^{207}Pb$	σ_{n-1}	$^{208}Pb/^{206}Pb$	σ_{n-1}	$^{208}Pb/^{207}Pb$	σ_{n-1}
LMM46	15.25	248	1.161	0.0024	2.118	0.0068	2.459	0.0095
LMM47	15.75	224	1.164	0.0020	2.116	0.0081	2.462	0.0135
LMM48	16.25	198	1.166	0.0012	2.107	0.0018	2.457	0.0012
LMM49	16.75	180	1.168	0.0030	2.091	0.0106	2.442	0.0158
LMM50	17.25	162	1.169	0.0020	2.098	0.0132	2.453	0.0109
LMM51	17.75	156	1.166	0.0019	2.105	0.0045	2.454	0.0083
LMM52	18.25	169	1.167	0.0016	2.106	0.0043	2.456	0.0080
LMM53	18.75	167	1.169	0.0027	2.097	0.0036	2.451	0.0052
LMM54	19.25	162	1.171	0.0019	2.117	0.0033	2.479	0.0062
LMM55	19.75	182	1.172	0.0018	2.119	0.0055	2.483	0.0049
LMM56	20.25	186	1.173	0.0017	2.100	0.0069	2.463	0.0079
LMM57	20.75	178	1.173	0.0015	2.115	0.0071	2.481	0.0083
LMM58	21.25	198	1.174	0.0012	2.119	0.0028	2.486	0.0053
LMM59	21.75	176	1.171	0.0032	2.118	0.0033	2.481	0.0035
LMM60	22.25	172	1.175	0.0027	2.115	0.0038	2.485	0.0034
LMM61	22.75	165	1.171	0.0011	2.102	0.0108	2.461	0.0106
LMM62	23.25	154	1.171	0.0007	2.107	0.0023	2.467	0.0027
LMM63	23.75	158	1.172	0.0011	2.109	0.0060	2.471	0.0082
LMM64	24.25	150	1.171	0.0032	2.107	0.0069	2.467	0.0099
LMM65	24.75	156	1.172	0.0012	2.104	0.0019	2.465	0.0032
LMM66	25.25	151	1.171	0.0016	2.101	0.0110	2.461	0.0143
LMM67	25.75	149	1.170	0.0012	2.096	0.0139	2.453	0.0179
LMM68	26.25	139	1.173	0.0018	2.103	0.0067	2.468	0.0067
LMM69	26.75	139	1.174	0.0017	2.128	0.0017	2.498	0.0039
LMM70	27.25	135	1.173	0.0018	2.106	0.0091	2.470	0.0113
LMM71	27.75	136	1.172	0.0029	2.107	0.0049	2.469	0.0094
LMM72	28.25	117	1.171	0.0011	2.113	0.0046	2.475	0.0073
LMM73	28.75	119	1.173	0.0025	2.107	0.0070	2.471	0.0112
LMM74	29.25	115	1.174	0.0014	2.110	0.0020	2.476	0.0021
LMM75	29.75	122	1.172	0.0021	2.117	0.0044	2.480	0.0028
LMM76	30.25	107	1.172	0.0008	2.118	0.0058	2.482	0.0079
LMM77	30.75	107	1.171	0.0029	2.108	0.0009	2.472	0.0063
LMM78	31.25	106	1.172	0.0013	2.109	0.0013	2.473	0.0068
LMM79	31.75	99	1.174	0.0016	2.111	0.0062	2.478	0.0080
LMM80	32.25	100	1.176	0.0019	2.113	0.0026	2.485	0.0017
LMM81	32.75	106	1.173	0.0023	2.112	0.0027	2.478	0.0056
LMM82	33.25	102	1.173	0.0014	2.107	0.0053	2.471	0.0088
LMM83	33.75	103	1.175	0.0015	2.109	0.0054	2.477	0.0067
LMM84	34.25	96	1.174	0.0013	2.113	0.0023	2.481	0.0042
LMM85	34.75	97	1.174	0.0063	2.110	0.0051	2.478	0.0063
LMM86	35.25	92	1.173	0.0019	2.124	0.0073	2.491	0.0094
LMM87	35.75	87	1.172	0.0023	2.125	0.0074	2.491	0.0125
LMM88	36.25	73	1.176	0.0024	2.098	0.0045	2.467	0.0101
LMM89	36.75	56	1.171	0.0024	2.123	0.0051	2.486	0.0085
LMM90	37.25	49	1.171	0.0019	2.106	0.0019	2.465	0.0097

Table 4.3 Stable Pb isotope ratio and Pb concentration (mg kg^{-1}) results for Lake of Menteith core LMM, continued.

Sample Code	Depth / cm (midpoint)	Pb / mg kg^{-1}	$^{206}Pb/^{207}Pb$	σ_{n-1}	$^{208}Pb/^{206}Pb$	σ_{n-1}	$^{208}Pb/^{207}Pb$	σ_{n-1}
LMM91	37.75	49	1.170	0.0022	2.110	0.0061	2.468	0.0108
LMM92	38.25	47	1.170	0.0018	2.111	0.0098	2.469	0.0136
LMM93	38.75	40	1.170	0.0019	2.121	0.0078	2.483	0.0085
LMM94	39.25	40	1.171	0.0023	2.113	0.0063	2.475	0.0089
LMM95	39.75	41	1.173	0.0020	2.097	0.0019	2.460	0.0041
LMM96	40.25	42	1.170	0.0014	2.121	0.0076	2.481	0.0106
LMM97	40.75	37	1.173	0.0021	2.123	0.0034	2.490	0.0077
LMM98	41.25	40	1.169	0.0008	2.091	0.0030	2.444	0.0026
LMM99	41.75	39	1.172	0.0019	2.123	0.0043	2.489	0.0066
LMM100	42.25	39	1.169	0.0012	2.088	0.0019	2.441	0.0034
LMM101	42.75	41	1.172	0.0022	2.122	0.0042	2.486	0.0083
LMM102	43.25	40	1.172	0.0015	2.124	0.0041	2.489	0.0052
LMM103	43.75	42	1.167	0.0014	2.089	0.0035	2.439	0.0037
LMM104	44.25	40	1.169	0.0028	2.109	0.0064	2.467	0.0125
LMM105	44.75	42	1.167	0.0019	2.096	0.0033	2.446	0.0067
LMM106	45.25	39	1.171	0.0016	2.108	0.0030	2.469	0.0051
LMM107	45.75	38	1.171	0.0006	2.113	0.0026	2.474	0.0021
LMM108	46.25	42	1.171	0.0029	2.114	0.0029	2.476	0.0042
LMM109	46.75	35	1.172	0.0025	2.122	0.0031	2.486	0.0075
LMM110	47.25	35	1.172	0.0009	2.120	0.0033	2.483	0.0031
LMM111	47.75	31	1.171	0.0008	2.086	0.0029	2.443	0.0032
LMM112	48.25	34	1.171	0.0012	2.128	0.0012	2.491	0.0028
LMM113	48.75	32	1.168	0.0035	2.098	0.0033	2.451	0.0043
LMM114	49.25	31	1.173	0.0028	2.140	0.0036	2.511	0.0046
LMM115	49.75	25	1.168	0.0019	2.099	0.0037	2.452	0.0027
LMM116	50.50	31	1.170	0.0006	2.127	0.0026	2.488	0.0022
LMM117	51.50	27	1.173	0.0011	2.134	0.0017	2.502	0.0014
LMM118	52.50	27	1.171	0.0013	2.147	0.0024	2.514	0.0031
LMM119	53.50	28	1.172	0.0018	2.151	0.0026	2.522	0.0011
LMM120	54.50	25	1.174	0.0024	2.119	0.0049	2.488	0.0030
LMM121	55.50	23	1.172	0.0019	2.164	0.0038	2.536	0.0034

Figure 4.12 (a) shows that the $^{206}Pb/^{207}Pb$ ratio remains constant at 1.172 ± 0.0019 from the base of the core to 20 cm[♦]. Above 20 cm there is a fairly rapid decline to 1.153 by 14.25 cm, and then a more gradual decline to 1.145 at 8.75 cm. From 8.75 cm the ratio essentially remains in the range of 1.142-1.149 to the surface, although there are two small peaks of 1.149 and 1.148 at 5.25-6.75 cm and 1.5-1.9 cm, respectively.

In Figures 4.12 (b) and (c), the structure of the two profiles $^{208}Pb/^{206}Pb$ and $^{208}Pb/^{207}Pb$ is much less clear than that of the $^{206}Pb/^{207}Pb$. At depth, average ratios of 2.112 ± 0.012 and 2.474 ± 0.016 respectively, hold until 28.25 cm. Above 28.25 cm there is a trough in the $^{208}Pb/^{206}Pb$ profile with a minimum at 25.75 cm of 2.096. The $^{208}Pb/^{207}Pb$ ratio starts to diverge from that of the $^{208}Pb/^{206}Pb$ ratio from 16.0 cm. The $^{208}Pb/^{207}Pb$ ratio from 16.0-5.0 cm remains at a constant value of 2.454 ± 0.011, whereas the $^{208}Pb/^{206}Pb$ ratio rises to give a more constant value of approximately 2.150. From 5 cm to the surface all three profiles show a decrease in ratio for ~ 2.5 cm before rising again to the surface.

4.4.5 X-Ray diffraction.

Three samples were analysed from core LMM (LMM40, 71 and 115) and were identical with respect to the types of minerals identified and the quantity of the minerals present. The following minerals were identified in order of relative abundance: quartz, muscovite, albite, and clinochlore. In all of the samples there was a broad, unresolved peak between the 2θ angles 20-30 °, suggesting that there is a significant proportion of non-crystalline material present in the lake sediment.

The following is a summary of the formulae and some structural properties of the minerals identified.

♦ The $^{206}Pb/^{207}Pb$ ratio is 1.171 ± 0.0018 from the base to the point (38.75 cm) where the Pb concentration begins to increase from a baseline value.

Quartz: SiO_2 framework silicate

Muscovite: $K_2(Si_6Al_2)(Al_4)O_{20}(OH)_4$ and $K_2(Si_7Al_1)(Al,Fe^{3+})_3(Mg,Fe^{2+})O_{20}(OH)_4$

Mica, 2:1 dioctahedral, layer silicate, 10 Å.

Albite: $NaAlSi_3O_8$

Feldspar, framework silicate, 3.19 Å.

Clinochlore: $(Si_{8-x}, Al_x)(Mg_{12-y}, Al_y)O_{20}(OH)_{16}$,

Chlorite, layer silicate, trioctahedral

4.5 Discussion.

4.5.1 Radiocaesium.

From the profile in Figure 4.4 it can be seen that there is one major peak with two slight shoulders at 10-11 cm and 13-14 cm. By comparison with results for the other cores studied, it can reasonably be assumed that the major peak probably relates to the Chernobyl input in May 1986. It is, however, very broad suggesting either that there is mixing in the top few centimetres, or that there has been diffusion of Cs in the sediment. The carbon content in the sediment is fairly high (10-12 % throughout the core) and it is known from other organic-rich systems (Bryant *et al.*, 1993) that radiocaesium may be mobile in the sediment. This would have the effect of broadening the Chernobyl peak and smearing the two contributions from weapons and Chernobyl together.

Due to the absence of ^{134}Cs and the lack of any obvious peak for weapons testing it is not possible to separate the Chernobyl and weapons inventories. The total inventory for ^{137}Cs, at the date of sampling (13/11/96), is 9.71 kBq m^{-2}. This is comparable to the total activity in Loch Lomond south, where the total inventory was 11.9 kBq m^{-2} at the date of sampling (26/11/91). The inventories for ^{137}Cs in Flanders Moss peat cores (Farmer *et al.*, 1997b) are lower than observed in Lake of Menteith or in Loch

Lomond south[♦]. Radiocaesium is not retained in peat and it can move both vertically and laterally (Schell *et al.*, 1989, Pulford *et al.*, 1995).

If the weight of sediment (g cm^{-2}) between the surface and the Chernobyl peak is assumed to have accumulated over a period of 10.4 years, a sedimentation rate of 31.4 ± 11 mg cm^{-2} y^{-1} is obtained. Taking the shoulder at 10-11 cm to represent the maximum deposition of weapons testing fallout (1963) gives a sedimentation rate between the Chernobyl and weapons testing peaks of 46.6 ± 5 mg cm^{-2} y^{-1}, and a rate from the surface to the weapons testing peak of 41.2 ± 3.1 mg cm^{-2} y^{-1}. However if the weapons peak is the lower peak at 13-14 cm the rates are 64 ± 2 and 53.2 ± 3.5 mg cm^{-2} y^{-1}, respectively.

4.5.2. ^{210}Pb.

The CIC and CRS ^{210}Pb models (cf. section 3.4.2.2) were used to estimate the sedimentation rate of the Lake of Menteith. In order to apply the CIC model, a plot of ln ($^{210}Pb_{unsup}$) against cumulative weight (g cm^{-2}) was constructed (Figure 4.13 (a)), where $^{210}Pb_{unsup}$ was calculated by subtracting the corresponding activity of ^{226}Ra from each section. The resultant graph is comprised of two components, with a sharp drop between them, suggesting a disruption in the sedimentation rate has occurred. The sedimentation rate, based on the gradient calculated from a weighted linear regression through all of the points (-1.032, err 0.166), is 30.1 ± 3.8 mg cm^{-2} y^{-1}. In Figures 4.13 (b)-(d), the graph has been broken down into the different components and a weighted linear regression performed for each one. The top nine points (Fig. 4.13 (b)) have a shallow gradient of -0.630 (err 0.123), giving a sedimentation rate of 49.3 ± 10 mg cm^{-2} y^{-1}. After the sharp break in the profile at section 9-10 cm, the gradient changes to -0.653 (err 0.233), giving a lower sedimentation rate of 47.6 ± 19 mg cm^{-2} y^{-1} (Fig. 4.13 (c) using 9-16); or if all the points from 9-19 are used, 42.4 ± 11 mg cm^{-2} y^{-1}, but errors are higher (Fig. 4.13 (d)).

[♦] A summary of the radiocaesium inventories is shown in Table 4.6 (p200).

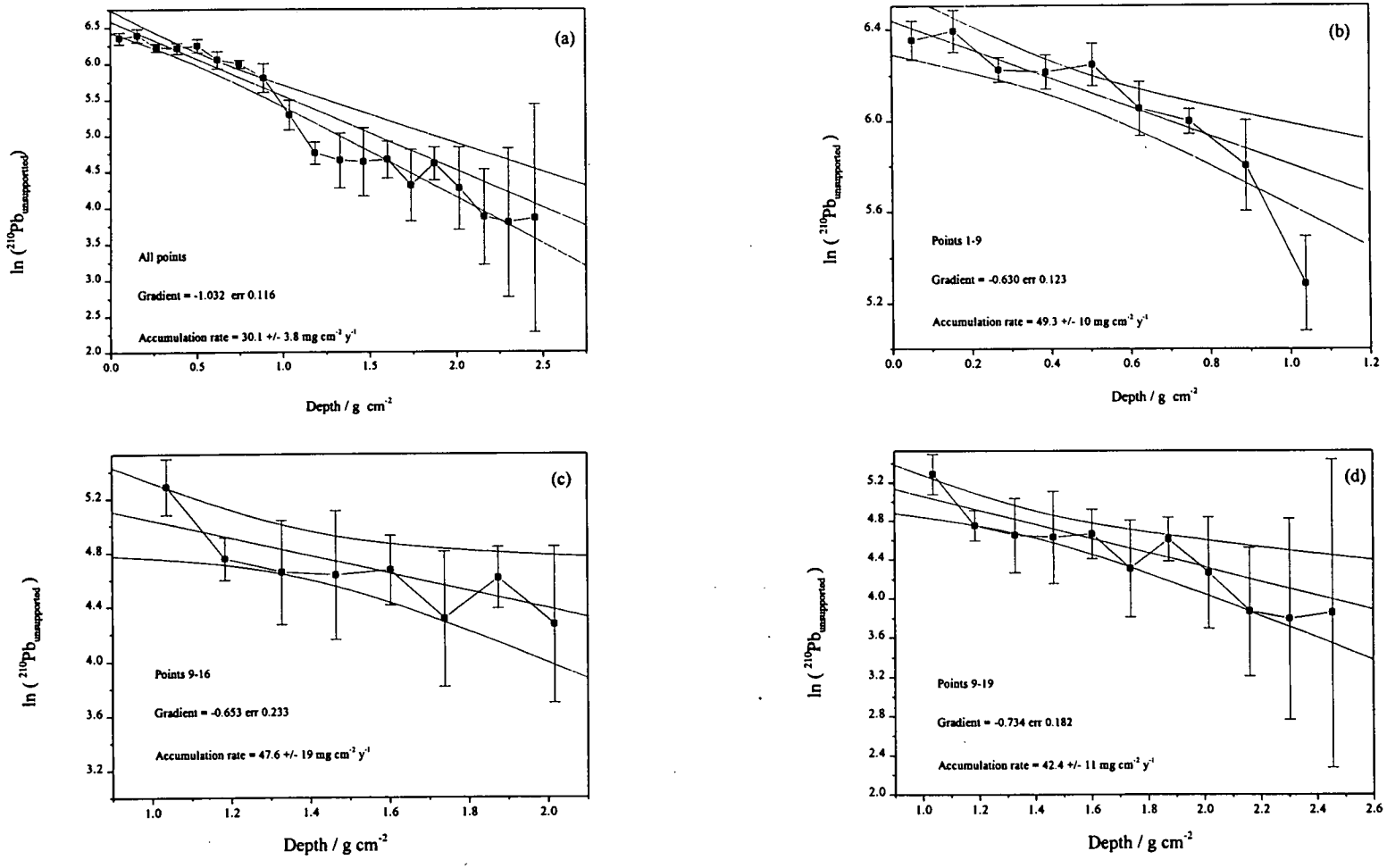

Figure 4.13 $\ln^{210}Pb_{unsupported}$ vs depth (g cm^{-2}) in core LMJ.

Weighted linear regression through: (a) all points, (b) points 1-9, (c) points 9-16 and (d) points 9-19.

It seems more likely that the changes in gradient are due to changes in sedimentation rate rather than to mixing. This could be attributable to a change in land use, possibly due to the planting of forest in the surrounding area covering the main catchment for the lake or by erosion of the sediment. Furthermore in Figures 4.5-4.8 there is a definite structure to the heavy metal and stable Pb isotope profiles which would have been lost if there had been mixing to a depth of 8 cm.

Using the CRS method, the total inventory of unsupported ^{210}Pb in the core was calculated at 6.03 kBq m^{-2} from 0-16 cm. Below 16 cm the errors are too high. The years of accumulation and date (cf. section 3.4.2.2) for each section are shown in Table 4.4 (a). At the top of the core the CRS dates are comparable with those from the CIC method but, lower down, begin to diverge.

The average flux of unsupported ^{210}Pb to the lake was calculated from the total inventory of unsupported ^{210}Pb (cf. section 3.4.2.2) and gave a value of 180 Bq m^{-2} y^{-1}, notably higher than the 110, 72 and 35 Bq m^{-2} y^{-1} for Flanders Moss peat cores (Farmer *et al.*, 1997b).

4.5.3 Core chronology.

Defining a sedimentation rate for this core is not as clear cut as for Loch Lomond (South). The post-depositional movement of radiocaesium has made defining the weapons testing peak difficult and therefore will not be used. The discontinuity in the ^{210}Pb profile suggests there has been a major change in the sedimentation rate or sediment type for a short time during the 1970s. For the purpose of the subsequent discussion a chronology based upon the two component ^{210}Pb CIC model (using 49.3 ± 10 mg cm^{-2} y^{-1} for 0 to 1.038 g cm^{-2} and 47.6 ± 19 mg cm^{-2} y^{-1} from 1.038 g cm^{-2} to the base of the core) will be used. The CRS dates will be quoted for key points in the discussion. It must be stressed that for this core none of the dating methods are without problems. Table 4.4 (b) is a summary of the chronology derived for the Mini-Mackereth core LMM using the above models.

Table 4.4 (a) Chronology for core LMJ derived using CRS and CIC ^{210}Pb models.

Sample code	Depth / cm	Cum. wt base / g cm^{-2}	CRS using LMJ16 for total inventory. Yrs acum.	Date	*CIC single component / 30.1 mg cm^{-2} y^{-1} Yrs acum.	Date	* CIC 2 component / 49.3 / 47.6 mg cm^{-2} y^{-1} Yrs acum.	Date
LMJ1	0-1	0.103	3.5	1992.4	3.4	1992.5	2.1	1993.8
LMJ2	1-2	0.209	7.8	1988.1	7.0	1988.9	4.2	1991.7
LMJ3	2-3	0.327	12.4	1983.5	10.9	1985.0	6.6	1989.3
LMJ4	3-4	0.447	17.8	1978.1	14.9	1981.0	9.1	1986.8
LMJ5	4-5	0.563	24.3	1971.6	18.7	1977.2	11.4	1984.5
LMJ6	5-6	0.682	31.1	1964.8	22.7	1973.2	13.8	1982.1
LMJ7	6-7	0.814	40.1	1955.8	27.0	1968.9	16.5	1979.4
LMJ8	7-8	0.965	51.9	1944.0	32.1	1963.8	19.6	1976.3
LMJ9	8-9	1.111	61.4	1934.5	36.9	1959.0	22.5	1973.4
LMJ10	9-10	1.260	68.7	1927.2	41.8	1954.1	3.1	1970.3
LMJ11	10-11	1.398	76.5	1919.4	46.4	1949.5	6.0	1967.4
LMJ12	11-12	1.533	86.3	1909.6	50.9	1945.0	8.9	1964.5
LMJ13	12-13	1.674	102.1	1893.8	55.6	1940.3	11.8	1961.6
LMJ14	13-14	1.804	118.9	1877.0	59.9	1936.0	14.6	1958.8
LMJ15	14-15	1.944			64.6	1931.3	17.5	1955.9
LMJ16	15-16	2.088			69.4	1926.5	20.5	1952.9
LMJ17	16-17	2.234			74.2	1921.7	23.6	1949.8
LMJ18	17-18	2.372			78.8	1917.1	26.5	1946.9
LMJ19	18-19	2.539			84.3	1911.6	30.0	1943.4
LMJ20	19-20	2.699			89.7	1906.2	33.4	1940.0
LMJ21	20-21	2.837			94.2	1901.7	36.3	1937.1
LMJ22	21-22	2.939			97.6	1898.3	38.4	1935.0

*Cumulative weight to base used to enable direct comparison with CRS model.

Table 4.4 (b) Chronology for core LMM derived using CIC and CRS ^{210}Pb models.

Sample Code	Depth / cm	Mid cum. wt / g cm^{-2}	CIC 2 component / 49.3 / 47.6 mg cm^{-2} y^{-1}		CIC 2 component / 49.3 / 42.4 mg cm^{-2} y^{-1}		CIC single component / 30.1 mg cm^{-2} y^{-1}		Approximate equivalent date from CRS model (Table 4.4 (a))
			Yrs acum.	Date	Yrs acum.	Date	Yrs acum.	Date	
LMM1	0.1	0.004	0.1	1995.8	0.1	1995.8	0.1	1995.8	
LMM2	0.3	0.017	0.3	1995.6	0.3	1995.6	0.6	1995.3	
LMM3	0.5	0.036	0.7	1995.2	0.7	1995.2	1.2	1994.7	
LMM4	0.7	0.057	1.2	1994.7	1.2	1994.7	1.9	1994.0	
LMM5	0.9	0.083	1.7	1994.2	1.7	1994.2	2.8	1993.1	
LMM6	1.1	0.114	2.3	1993.6	2.3	1993.6	3.8	1992.1	1992
LMM7	1.3	0.144	2.9	1993.0	2.9	1993.0	4.8	1991.1	
LMM8	1.5	0.177	3.6	1992.3	3.6	1992.3	5.9	1990.0	
LMM9	1.7	0.211	4.3	1991.6	4.3	1991.6	7.0	1988.9	1988
LMM10	1.9	0.246	5.0	1990.9	5.0	1990.9	8.2	1987.7	
LMM11	2.1	0.281	5.7	1990.2	5.7	1990.2	9.3	1986.6	
LMM12	2.3	0.315	6.4	1989.5	6.4	1989.5	10.5	1985.4	1983
LMM13	2.5	0.354	7.2	1988.7	7.2	1988.7	11.7	1984.2	
LMM14	2.7	0.394	8.0	1987.9	8.0	1987.9	13.1	1982.8	
LMM15	2.9	0.435	8.8	1987.1	8.8	1987.1	14.5	1981.4	1978
LMM16	3.1	0.476	9.7	1986.2	9.7	1986.2	15.8	1980.1	
LMM17	3.3	0.517	10.5	1985.4	10.5	1985.4	17.2	1978.7	
LMM18	3.5	0.559	11.3	1984.6	11.3	1984.6	18.6	1977.3	1971
LMM19	3.7	0.602	12.2	1983.7	12.2	1983.7	20.0	1975.9	
LMM20	3.9	0.643	13.0	1982.9	13.0	1982.9	21.4	1974.5	
LMM21	4.1	0.686	13.9	1982.0	13.9	1982.0	22.8	1973.1	1965
LMM22	4.3	0.726	14.7	1981.2	14.7	1981.2	24.1	1971.8	
LMM23	4.5	0.763	15.5	1980.4	15.5	1980.4	25.4	1970.5	
LMM24	4.7	0.808	16.4	1979.5	16.4	1979.5	26.8	1969.1	1956
LMM25	4.9	0.855	17.3	1978.6	17.3	1978.6	28.4	1967.5	

Table 4.4 (b) Chronology for core LMM derived using CIC and CRS ^{210}Pb models, continued.

Sample Code	Depth / cm	Mid cum. wt / g cm^{-2}	CIC 2 component / 49.3 / 47.6 mg cm^{-2} y^{-1}		CIC 2 component / 49.3 / 42.4 mg cm^{-2} y^{-1}		CIC single component / 30.1 mg cm^{-2} y^{-1}		Approximate equivalent date from CRS model (Table 4.4 (a))
			Yrs acum.	Date	Yrs acum.	Date	Yrs acum.	Date	
LMM26	5.25	0.914	18.5	1977.4	18.5	1977.4	30.4	1965.5	
LMM27	5.75	0.991	20.1	1975.8	20.1	1975.8	32.9	1963.0	1944
LMM28	6.25	1.065	1.5	1974.3	1.7	1974.1	35.4	1960.5	
LMM29	6.75	1.132	3.0	1972.8	3.3	1972.5	37.6	1958.3	1934
LMM30	7.25	1.204	4.5	1971.3	5.0	1970.8	40.0	1955.9	
LMM31	7.75	1.279	6.0	1969.8	6.8	1969.0	42.5	1953.4	1927
LMM32	8.25	1.348	7.5	1968.3	8.4	1967.4	44.8	1951.1	
LMM33	8.75	1.423	9.1	1966.7	10.2	1965.6	47.3	1948.6	1919
LMM34	9.25	1.501	10.7	1965.1	12.0	1963.8	49.9	1946.0	
LMM35	9.75	1.578	12.3	1963.5	13.8	1962.0	52.4	1943.5	1909
LMM36	10.25	1.656	14.0	1961.8	15.7	1960.1	55.0	1940.9	1893
LMM37	10.75	1.736	15.6	1960.2	17.6	1958.2	57.7	1938.2	
LMM38	11.25	1.812	17.2	1958.6	19.4	1956.4	60.2	1935.7	1877
LMM39	11.75	1.880	18.7	1957.1	21.0	1954.8	62.5	1933.4	
LMM40	12.25	1.954	20.2	1955.6	22.7	1953.1	64.9	1931.0	
LMM41	12.75	2.039	22.0	1953.8	24.7	1951.1	67.7	1928.2	
LMM42	13.25	2.137	24.1	1951.7	27.0	1948.8	71.0	1924.9	
LMM43	13.75	2.239	26.2	1949.6	29.4	1946.4	74.4	1921.5	
LMM44	14.25	2.331	28.1	1947.7	31.6	1944.2	77.4	1918.5	
LMM45	14.75	2.412	29.9	1945.9	33.5	1942.3	80.1	1915.8	
LMM46	15.25	2.488	31.4	1944.4	35.3	1940.5	82.7	1913.2	
LMM47	15.75	2.568	33.1	1942.7	37.2	1938.6	85.3	1910.6	
LMM48	16.25	2.652	34.9	1940.9	39.2	1936.6	88.1	1907.8	
LMM49	16.75	2.737	36.7	1939.1	41.2	1934.6	90.9	1905.0	
LMM50	17.25	2.827	38.6	1937.2	43.3	1932.5	93.9	1902.0	

Table 4.4 (b) Chronology for core LMM derived using CIC and CRS ^{210}Pb models, continued.

Sample Code	Depth / cm	Mid cum. wt / g cm^{-2}	CIC 2 component / 49.3 / 47.6 mg cm^{-2} y^{-1}		CIC 2 component / 49.3 / 42.4 mg cm^{-2} y^{-1}		CIC single component / 30.1 mg cm^{-2} y^{-1}		Approximate equivalent date from CRS model (Table 4.4 (a))
			Yrs acum.	Date	Yrs acum.	Date	Yrs acum.	Date	
LMM51	17.75	2.916	40.4	1935.4	45.4	1930.4	96.9	1899.0	
LMM52	18.25	3.001	42.2	1933.6	47.4	1928.4	99.7	1896.2	
LMM53	18.75	3.084	44.0	1931.8	49.3	1926.5	102.4	1893.5	
LMM54	19.25	3.169	45.7	1930.1	51.3	1924.5	105.3	1890.6	
LMM55	19.75	3.250	47.5	1928.3	53.3	1922.5	108.0	1887.9	
LMM56	20.25	3.333	49.2	1926.6	55.2	1920.6	110.7	1885.2	
LMM57	20.75	3.412	50.9	1924.9	57.1	1918.7	113.4	1882.5	
LMM58	21.25	3.490	52.5	1923.3	58.9	1916.9	115.9	1880.0	
LMM59	21.75	3.564	54.1	1921.7	60.7	1915.1	118.4	1877.5	
LMM60	22.25	3.638	55.6	1920.2	62.4	1913.4	120.9	1875.0	
LMM61	22.75	3.718	57.3	1918.5	64.3	1911.5	123.5	1872.4	
LMM62	23.25	3.801	59.0	1916.8	66.3	1909.5	126.3	1869.6	
LMM63	23.75	3.886	60.8	1915.0	68.3	1907.5	129.1	1866.8	
LMM64	24.25	3.970	62.6	1913.2	70.2	1905.6	131.9	1864.0	
LMM65	24.75	4.054	64.3	1911.5	72.2	1903.6	134.7	1861.2	
LMM66	25.25	4.143	66.2	1909.6	74.3	1901.5	137.6	1858.3	
LMM67	25.75	4.233	68.1	1907.7	76.5	1899.3	140.6	1855.3	
LMM68	26.25	4.329	70.1	1905.7	78.7	1897.1	143.8	1852.1	
LMM69	26.75	4.427	72.2	1903.6	81.0	1894.8	147.1	1848.8	
LMM70	27.25	4.525	74.2	1901.6	83.3	1892.5	150.3	1845.6	
LMM71	27.75	4.617	76.2	1899.6	85.5	1890.3	153.4	1842.5	
LMM72	28.25	4.710	78.1	1897.7	87.7	1888.1	156.5	1839.4	
LMM73	28.75	4.805	80.1	1895.7	89.9	1885.9	159.6	1836.3	
LMM74	29.25	4.898	82.1	1893.7	92.1	1883.7	162.7	1833.2	
LMM75	29.75	4.996	84.1	1891.7	94.4	1881.4	166.0	1829.9	

Table 4.4 (b) Chronology for core LMM derived using CIC and CRS ^{210}Pb models, continued.

Sample Code	Depth / cm	Mid cum. wt / g cm^{-2}	CIC 2 component / 49.3 / 47.6 mg cm^{-2} y^{-1}		CIC 2 component / 49.3 / 42.4 mg cm^{-2} y^{-1}		CIC single component / 30.1 mg cm^{-2} y^{-1}		Approximate equivalent date from CRS model (Table 4.4 (a))
			Yrs acum.	Date	Yrs acum.	Date	Yrs acum.	Date	
LMM76	30.25	5.104	86.4	1889.4	97.0	1878.8	169.6	1826.3	
LMM77	30.75	5.213	88.7	1887.1	99.6	1876.2	173.2	1822.7	
LMM78	31.25	5.311	90.7	1885.1	101.9	1873.9	176.4	1819.5	
LMM79	31.75	5.411	92.8	1883.0	104.2	1871.6	179.8	1816.1	
LMM80	32.25	5.511	94.9	1880.9	106.6	1869.2	183.1	1812.8	
LMM81	32.75	5.603	96.9	1878.9	108.8	1867.0	186.1	1809.8	
LMM82	33.25	5.698	98.9	1876.9	111.0	1864.8	189.3	1806.6	
LMM83	33.75	5.803	101.1	1874.7	113.5	1862.3	192.8	1803.1	
LMM84	34.25	5.912	103.4	1872.4	116.1	1859.7	196.4	1799.5	
LMM85	34.75	6.022	105.7	1870.1	118.6	1857.2	200.1	1795.8	
LMM86	35.25	6.133	108.0	1867.8	121.3	1854.5	203.7	1792.2	
LMM87	35.75	6.252	110.5	1865.3	124.1	1851.7	207.7	1788.2	
LMM88	36.25	6.373	113.1	1862.7	126.9	1848.9	211.7	1784.2	
LMM89	36.75	6.482	115.4	1860.4	129.5	1846.3	215.4	1780.5	
LMM90	37.25	6.591	117.6	1858.2	132.1	1843.7	219.0	1776.9	
LMM91	37.75	6.702	120.0	1855.8	134.7	1841.1	222.7	1773.2	
LMM92	38.25	6.806	122.2	1853.6	137.1	1838.7	226.1	1769.8	
LMM93	38.75	6.905	124.2	1851.6	139.5	1836.3	229.4	1766.5	
LMM94	39.25	7.009	126.4	1849.4	141.9	1833.9	232.9	1763.0	
LMM95	39.75	7.118	128.7	1847.1	144.5	1831.3	236.5	1759.4	
LMM96	40.25	7.213	130.7	1845.1	146.7	1829.1	239.6	1756.3	
LMM97	40.75	7.302	132.6	1843.2	148.8	1827.0	242.6	1753.3	
LMM98	41.25	7.409	134.8	1841.0	151.4	1824.4	246.1	1749.8	
LMM99	41.75	7.523	137.2	1838.6	154.1	1821.7	249.9	1746.0	
LMM100	42.25	7.624	139.3	1836.5	156.4	1819.4	253.3	1742.6	

Table 4.4 (b) Chronology for core LMM derived using CIC and CRS ^{210}Pb models, continued.

Sample Code	Depth / cm	Mid cum. wt / g cm^{-2}	CIC 2 component / 49.3 / 47.6 mg cm^{-2} y^{-1}		CIC 2 component / 49.3 / 42.4 mg cm^{-2} y^{-1}		CIC single component / 30.1 mg cm^{-2} y^{-1}		Approximate equivalent date from CRS model (Table 4.4 (a))
			Yrs acum.	Date	Yrs acum.	Date	Yrs acum.	Date	
LMM101	42.75	7.731	141.6	1834.2	159.0	1816.8	256.8	1739.1	
LMM102	43.25	7.855	144.2	1831.6	161.9	1813.9	261.0	1734.9	
LMM103	43.75	7.950	146.2	1829.6	164.1	1811.7	264.1	1731.8	
LMM104	44.25	8.023	147.7	1828.1	165.9	1809.9	266.6	1729.3	
LMM105	44.75	8.110	149.5	1826.3	167.9	1807.9	269.4	1726.5	
LMM106	45.25	8.212	151.7	1824.1	170.3	1805.5	272.8	1723.1	
LMM107	45.75	8.322	154.0	1821.8	172.9	1802.9	276.5	1719.4	
LMM108	46.25	8.422	156.1	1819.7	175.2	1800.6	279.8	1716.1	
LMM109	46.75	8.506	157.9	1817.9	177.2	1798.6	282.6	1713.3	
LMM110	47.25	8.586	159.5	1816.3	179.1	1796.7	285.2	1710.7	
LMM111	47.75	8.688	161.7	1814.1	181.5	1794.3	288.6	1707.3	
LMM112	48.25	8.798	164.0	1811.8	184.1	1791.7	292.3	1703.6	
LMM113	48.75	8.888	165.9	1809.9	186.2	1789.6	295.3	1700.6	
LMM114	49.25	8.970	167.6	1808.2	188.2	1787.6	298.0	1697.9	
LMM115	49.75	9.056	169.4	1806.4	190.2	1785.6	300.9	1695.0	
LMM116	50.5	9.189	172.2	1803.6	193.3	1782.5	305.3	1690.6	
LMM117	51.5	9.352	175.7	1800.1	197.2	1778.6	310.7	1685.2	
LMM118	52.5	9.516	179.1	1796.7	201.1	1774.7	316.2	1679.7	
LMM119	53.5	9.688	182.7	1793.1	205.1	1770.7	321.9	1674.0	
LMM120	54.5	9.850	186.1	1789.7	208.9	1766.9	327.3	1668.6	
LMM121	55.5	9.961	188.4	1787.4	211.5	1764.3	330.9	1665.0	

4.5.4 Stable lead isotopes and lead.

The baseline values for Pb concentration and ^{206}Pb / ^{207}Pb atom ratio were taken from the average value below 47.75 cm and were 28.2 ± 3.7 mg kg^{-1} and 1.171 ± 0.002 respectively. The excess Pb flux (mg m^{-2} y^{-1}) was calculated using a sedimentation rate of 49.3 ± 10 mg cm^{-2} y^{-1} from 0-1.038 g cm^{-2} and 47.6 ± 19 mg cm^{-2} y^{-1} from 1.038 g cm^{-2} to the base, and the excess ^{206}Pb / ^{207}Pb atom ratio calculated using the formulae in section 3.4.1.5. The values for the excess flux and atom ratios are summarised in Table 4.5. The excess Pb flux (mg m^{-2} y^{-1}) and excess $^{206}Pb/^{207}Pb$ atom ratio were plotted against date (based on the two component ^{210}Pb model) as shown in Figure 4.14.

The excess $^{206}Pb/^{207}Pb$ atom ratio remains fairly constant at 1.173 ± 0.002 despite the increase in excess Pb flux throughout the 19th Century. It gives a reasonable comparison with Flanders Moss peat cores, where the average for this period was 1.169 ± 0.004 (Farmer *et al.*, 1997b), and with Loch Lomond South 1.169 ± 0.002 (Farmer *et al.*, 1996) and Loch Lomond North 1.171 ± 0.003 (Farmer, 1994) over this period in history. The Pb flux at this time steadily increased from 13 to 80 mg m^{-2} y^{-1}, reaching a peak ~1923. From about 1930 the ratio begins to decline steadily to reach a minimum of 1.139 between 1982 and 1989. The decrease appears to start at the same time as was observed in Loch Lomond at around the time that Australian ^{206}Pb depleted ore started to be used in this country. The decline is also evident in the Flanders Moss peat cores (Farmer *et al.*, 1997b). The decline in isotope ratio corresponds to a rapid increase in the flux of excess Pb, which after 1925 had been starting to decline, from 63 mg m^{-2} y^{-1}, to a peak flux in 1956 of 105 mg m^{-2} y^{-1}. The isotope ratio increased slightly in ~1970 to 1.146 for a period of ~6 years over the period where there was a dramatic change in the sedimentation rate. Since the end of the 1980s, there has been a slight reversal of the decline due to the phasing out of alkyl Pb-additives in petrol. The reversal is not as pronounced as was observed in Loch Lomond.

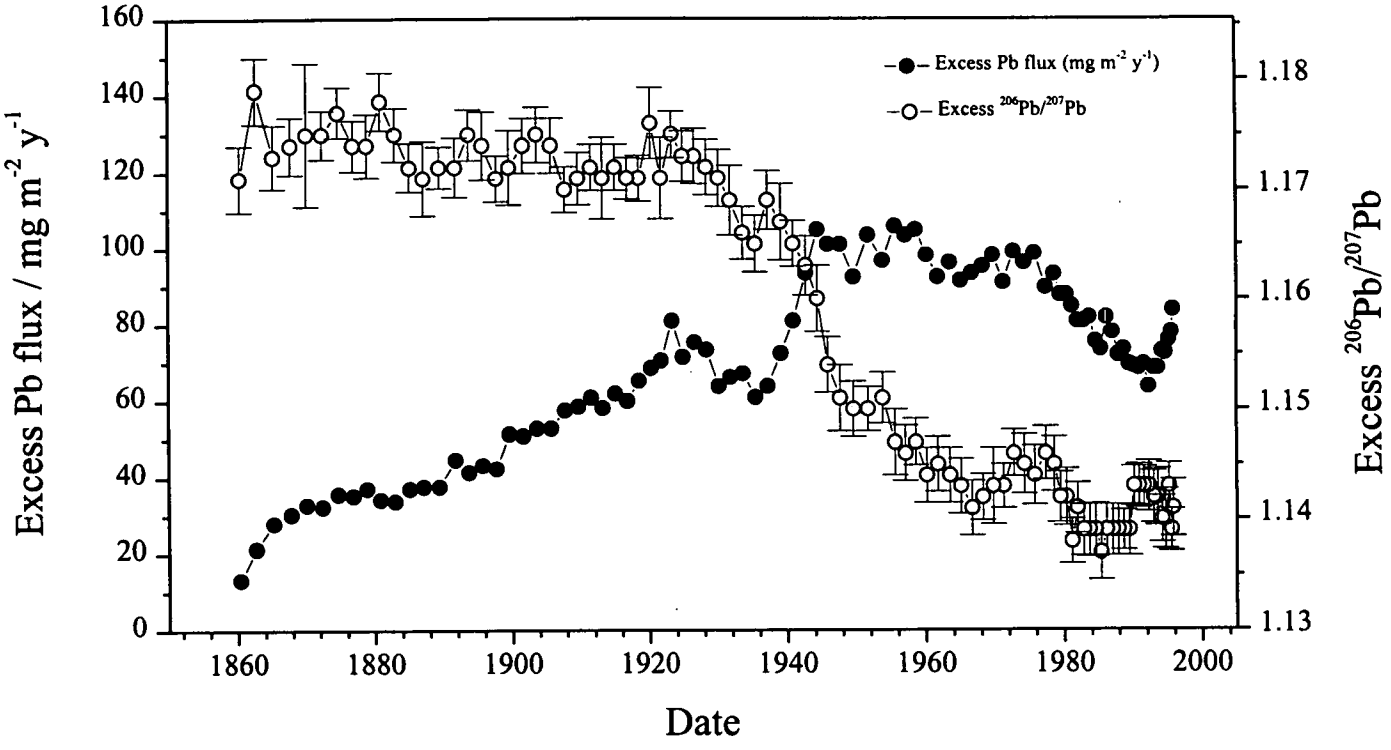

Figure 4.14 Excess Pb flux (mg m^{-2} y^{-1}) and excess $^{206}Pb/^{207}Pb$ atom ratio vs date in core LMM.

Table 4.5 Excess $^{206}Pb/^{207}Pb$ atom ratio and excess heavy metal fluxes (mg m^{-2} y^{-1}) in core LMM.

Sample Code	Depth / cm	Date (using 2 component CIC ^{210}Pb, 49.3/47.6 mg cm^{-2} y^{-1})	Excess $^{206}Pb/^{207}Pb$	σ_{n-1}	Excess Pb flux / mg m^{-2} y^{-1}	Excess Zn flux / mg m^{-2} y^{-1}	Excess Cu flux / mg m^{-2} y^{-1}	Excess Cd flux / mg m^{-2} y^{-1}
LMM1	0.1	1995.8	1.141	0.0026	83.69	165.9	17.4	1.08
LMM2	0.3	1995.6	1.139	0.0019	77.77	171.8	16.9	0.94
LMM3	0.5	1995.2	1.143	0.0021	75.80	162.0	10.0	1.23
LMM4	0.7	1994.7	1.140	0.0027	72.35	147.7	7.5	0.94
LMM5	0.9	1994.2	1.140	0.0021	72.84	156.5	8.5	0.89
LMM6	1.1	1993.6	1.142	0.0026	68.40	158.0	5.6	0.94
LMM7	1.3	1993.0	1.142	0.0024	68.40	149.1	7.0	0.79
LMM8	1.5	1992.3	1.143	0.0023	63.47	150.1	11.0	0.94
LMM9	1.7	1991.6	1.143	0.0018	69.39	150.1	6.5	0.89
LMM10	1.9	1990.9	1.143	0.0020	68.40	163.4	9.5	0.99
LMM11	2.1	1990.2	1.143	0.0018	68.90	155.1	8.0	0.94
LMM12	2.3	1989.5	1.139	0.0023	69.39	157.5	8.5	0.94
LMM13	2.5	1988.7	1.139	0.0018	73.33	163.0	8.5	1.13
LMM14	2.7	1987.9	1.139	0.0023	71.85	154.6	8.0	0.99
LMM15	2.9	1987.1	1.139	0.0023	77.77	175.3	9.0	1.28
LMM16	3.1	1986.2	1.139	0.0023	81.71	179.2	8.5	1.13
LMM17	3.3	1985.4	1.137	0.0025	73.33	175.3	8.5	0.99
LMM18	3.5	1984.6	1.139	0.0024	75.31	167.4	9.0	1.04
LMM19	3.7	1983.7	1.139	0.0024	81.71	185.6	7.5	1.13
LMM20	3.9	1982.9	1.139	0.0023	80.73	190.1	10.0	1.33
LMM21	4.1	1982.0	1.141	0.0023	80.73	191.5	8.5	1.18
LMM22	4.3	1981.2	1.138	0.0020	84.67	191.1	9.0	1.33
LMM23	4.5	1980.4	1.142	0.0026	87.63	196.5	9.5	1.08
LMM24	4.7	1979.5	1.142	0.0023	87.63	190.1	9.0	1.18
LMM25	4.9	1978.6	1.145	0.0025	93.05	207.8	10.0	1.28

Table 4.5 Excess $^{206}Pb/^{207}Pb$ atom ratio and excess heavy metal fluxes (mg m^{-2} y^{-1}) in core LMM, continued.

Sample Code	Depth / cm	Date (using 2 component CIC ^{210}Pb, 49.3/47.6 mg cm^{-2} y^{-1})	Excess $^{206}Pb/^{207}Pb$	σ_{n-1}	Excess Pb flux / mg m^{-2} y^{-1}	Excess Zn flux / mg m^{-2} y^{-1}	Excess Cu flux / mg m^{-2} y^{-1}	Excess Cd flux / mg m^{-2} y^{-1}
LMM26	5.25	1977.4	1.146	0.0024	89.60	187.6	7.5	1.33
LMM27	5.75	1975.8	1.144	0.0027	98.48	214.2	10.0	1.33
LMM28	6.25	1974.3	1.145	0.0027	96.03	201.6	9.6	1.33
LMM29	6.75	1972.8	1.146	0.0021	98.89	207.8	10.1	1.52
LMM30	7.25	1971.3	1.143	0.0020	90.80	189.2	11.6	1.19
LMM31	7.75	1969.8	1.143	0.0035	97.94	211.1	10.1	1.19
LMM32	8.25	1968.3	1.142	0.0021	95.08	193.0	9.6	1.19
LMM33	8.75	1966.7	1.141	0.0025	93.18	195.9	9.2	1.19
LMM34	9.25	1965.1	1.143	0.0025	91.27	207.3	9.2	1.24
LMM35	9.75	1963.5	1.144	0.0025	96.03	201.1	11.6	1.29
LMM36	10.25	1961.8	1.145	0.0025	92.23	192.1	9.2	1.24
LMM37	10.75	1960.2	1.144	0.0025	97.94	217.8	9.2	1.33
LMM38	11.25	1958.6	1.147	0.0021	104.60	228.7	9.6	1.38
LMM39	11.75	1957.1	1.146	0.0025	103.17	233.0	11.1	1.24
LMM40	12.25	1955.6	1.147	0.0030	105.55	245.4	10.6	1.29
LMM41	12.75	1953.8	1.151	0.0023	96.51	206.4	11.1	1.19
LMM42	13.25	1951.7	1.150	0.0020	103.17	212.1	9.6	1.14
LMM43	13.75	1949.6	1.150	0.0025	92.23	187.3	8.2	1.05
LMM44	14.25	1947.7	1.151	0.0030	100.79	197.8	9.6	1.19
LMM45	14.75	1945.9	1.154	0.0025	100.79	187.3	9.2	1.52
LMM46	15.25	1944.4	1.160	0.0030	104.60	178.8	8.7	1.00
LMM47	15.75	1942.7	1.163	0.0027	93.18	149.7	4.4	0.81
LMM48	16.25	1940.9	1.165	0.0021	80.80	119.7	6.3	0.62
LMM49	16.75	1939.1	1.167	0.0035	72.23	107.4	5.4	0.57
LMM50	17.25	1937.2	1.169	0.0027	63.67	95.0	4.9	0.43

Table 4.5 Excess heavy metal fluxes (mg m^{-2} y^{-1}) and excess $^{206}Pb/^{207}Pb$ atom ratio in core LMM, continued.

Sample Code	Depth / cm	Date (using 2 component CIC ^{210}Pb, 49.3/47.6 mg cm^{-2} y^{-1})	Excess $^{206}Pb/^{207}Pb$	σ_{n-1}	Excess Pb flux / mg m^{-2} y^{-1}	Excess Zn flux / mg m^{-2} y^{-1}	Excess Cu flux / mg m^{-2} y^{-1}	Excess Cd flux / mg m^{-2} y^{-1}
LMM51	17.75	1935.4	1.165	0.0026	60.81	89.3	5.8	0.57
LMM52	18.25	1933.6	1.166	0.0024	67.00	92.6	4.9	0.57
LMM53	18.75	1931.8	1.169	0.0032	66.05	91.6	7.3	0.71
LMM54	19.25	1930.1	1.171	0.0026	63.67	78.8	3.0	0.48
LMM55	19.75	1928.3	1.172	0.0025	73.19	92.6	6.3	0.57
LMM56	20.25	1926.6	1.173	0.0025	75.09	90.2	5.8	0.52
LMM57	20.75	1924.9	1.173	0.0023	71.28	83.1	6.3	0.24
LMM58	21.25	1923.3	1.175	0.0021	80.80	97.4	6.8	0.48
LMM59	21.75	1921.7	1.171	0.0037	70.33	80.7	3.0	0.52
LMM60	22.25	1920.2	1.176	0.0032	68.43	78.8	4.9	0.52
LMM61	22.75	1918.5	1.171	0.0021	65.09	76.9	4.9	0.43
LMM62	23.25	1916.8	1.171	0.0019	59.86	81.2	4.4	0.38
LMM63	23.75	1915.0	1.172	0.0021	61.76	90.7	3.5	0.43
LMM64	24.25	1913.2	1.171	0.0037	57.95	66.4	3.9	0.48
LMM65	24.75	1911.5	1.172	0.0021	60.81	64.0	3.9	0.33
LMM66	25.25	1909.6	1.171	0.0024	58.43	65.0	3.0	0.38
LMM67	25.75	1907.7	1.170	0.0021	57.48	64.0	3.5	0.38
LMM68	26.25	1905.7	1.174	0.0025	52.72	55.9	3.0	0.33
LMM69	26.75	1903.6	1.175	0.0025	52.72	46.9	3.5	0.24
LMM70	27.25	1901.6	1.174	0.0025	50.81	47.9	2.5	0.29
LMM71	27.75	1899.6	1.172	0.0034	51.29	46.4	3.9	0.29
LMM72	28.25	1897.7	1.171	0.0021	42.25	43.6	1.6	0.19
LMM73	28.75	1895.7	1.174	0.0031	43.20	39.8	2.0	0.24
LMM74	29.25	1893.7	1.175	0.0023	41.29	46.4	2.5	0.14
LMM75	29.75	1891.7	1.172	0.0027	44.63	43.1	3.0	0.19

Table 4.5 Excess $^{206}Pb/^{207}Pb$ atom ratio and excess heavy metal fluxes (mg m^{-2} y^{-1}) in core LMM, continued.

Sample Code	Depth / cm	Date (using 2 component CIC ^{210}Pb, 49.3/47.6 mg cm^{-2} y^{-1})	Excess $^{206}Pb/^{207}Pb$	σ_{n-1}	Excess Pb flux / mg m^{-2} y^{-1}	Excess Zn flux / mg m^{-2} y^{-1}	Excess Cu flux / mg m^{-2} y^{-1}	Excess Cd flux / mg m^{-2} y^{-1}
LMM76	30.25	1889.4	1.172	0.0019	37.49	35.5	1.6	0.19
LMM77	30.75	1887.1	1.171	0.0034	37.49	23.1	1.1	0.10
LMM78	31.25	1885.1	1.172	0.0022	37.01	26.4	1.6	0.24
LMM79	31.75	1883.0	1.175	0.0024	33.68	24.1	1.1	0.10
LMM80	32.25	1880.9	1.178	0.0026	34.15	28.8	1.1	0.14
LMM81	32.75	1878.9	1.174	0.0029	37.01	32.1	2.5	0.19
LMM82	33.25	1876.9	1.174	0.0023	35.11	27.9	1.1	0.29
LMM83	33.75	1874.7	1.177	0.0023	35.58	29.8	2.0	0.14
LMM84	34.25	1872.4	1.175	0.0022	32.25	25.5	0.6	0.19
LMM85	34.75	1870.1	1.175	0.0065	32.73	22.1	1.6	0.10
LMM86	35.25	1867.8	1.174	0.0026	30.35	21.2	1.6	0.10
LMM87	35.75	1865.3	1.173	0.0029	27.97	15.0	1.6	0.05
LMM88	36.25	1862.7	1.179	0.0030	21.30	9.8	0.6	
LMM89	36.75	1860.4	1.171	0.0030	13.21			
LMM90	37.25	1858.2						

4.5.5 Heavy metals.

The excess fluxes (mg m^{-2} y^{-1}) of the metals were calculated using the sedimentation rates 49.3 mg cm^{-2} y^{-1} from 0-1.038 g cm^{-2} and 47.6 mg cm^{-2} y^{-1} from 1.038 g cm^{-2} to the base. The results are summarised in Table 4.5 and a graph of the excess flux of each metal against date plotted in Figure 4.15. Of the four metals, the increase in Pb deposition occurred the earliest. The excess Pb flux gradually increased from the base of the core (dated 1860), whereas the increase in Zn and Cd does not start until 1890 and in Cu, later still, in 1900. The rate of increase in the deposition of all of the metals rises rapidly from 1940 and there is a maximum input of all of the metals over a period of 20 years before any decrease starts to occur, with 75, 72 and 75 % of the total inventory of Zn, Cu and Cd being deposited after 1940, respectively. Since ~1980 there has been a steady decline in the deposition of all of the metals. The Cu profile has its highest concentration and flux in the topmost section of the core, suggesting possible association with organic matter diagenesis. If this is the case then the flux profile will not represent a historical profile.

The total inventories for Pb, Zn, Cu and Cd are 8.95, 14.6, 0.73 and 0.06 g m^{-2} respectively (Table 4.6). The inventory for excess Pb is significantly higher than was observed in Flanders Moss peat cores (Farmer *et al.*, 1997b), but is in line with the figure of 6.36 g m^{-2} for Loch Lomond (south).

Fe and Mn (Figs. 4.8 and 4.9) show classic diagenetic profiles with the enhancement in Mn occurring 4 mm higher in the sediment than that of Fe. This phenomenon was also evident in the Loch Lomond (south) core. There is a second peak in both metals situated at 23.75 and 23.25 cm for Fe an Mn respectively. The peaks are dated at about 1915-1917 and are not particularly evident in any of the other metals.

Figure 4.15 Comparison of excess heavy metal fluxes (mg m^{-2} y^{-1}) vs date in core LMM.

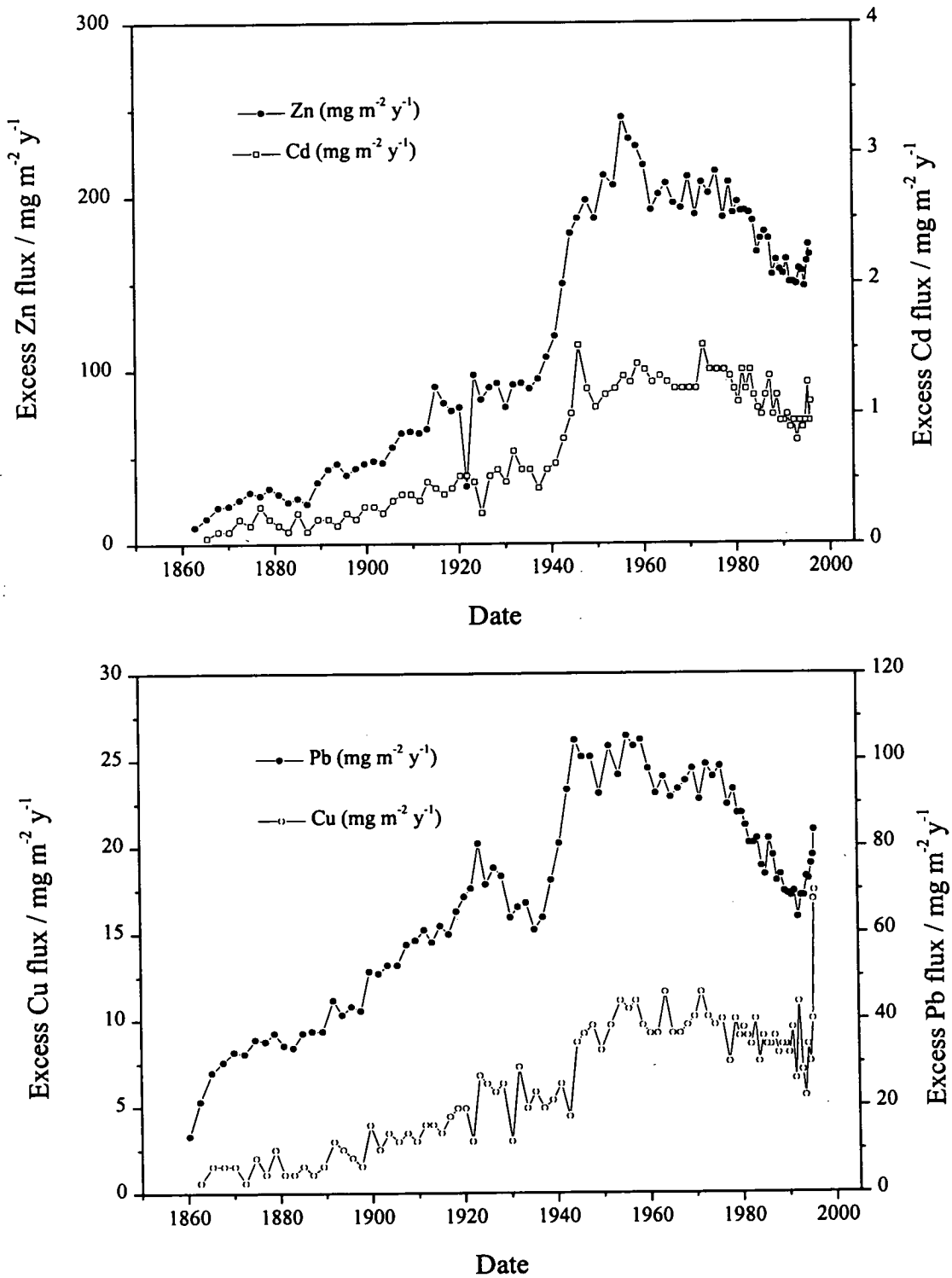

Table 4.6 Comparison of inventories and fluxes in Lake of Menteith sediments with Flanders Moss peat.

	^{210}Pb inventory / k Bq m^{-2}	^{210}Pb flux / Bq m^{-2} y^{-1}	Total ^{137}Cs inventory / k Bq m^{-2}		Pb inventory / g m^{-2}	Zn inventory / g m^{-2}	Cu inventory / g m^{-2}	Cd inventory / g m^{-2}
Lake of Menteith 1996	6.03	180	9.71		8.95	14.6	0.73	0.06
			^{137}Cs Chernobyl inventory / k Bq m^{-2}	^{137}Cs weapons inventory / k Bq m^{-2}				
Loch Lomond (south), 1992			3.41	7.27				
Flanders Moss (Farmer et al. 1997)								
A 15 Dec 1990	3.53	110	2.24	0.4	3.39			
C 16 Nov 1994	2.32	72	3.69	8.58	2.44			
D 16 Nov 1994	1.13	35	1.13	0.27	1.78			

4.6 Conclusions.

The overall trends in the stable Pb isotopes and Pb are fairly consistent with those seen in Loch Lomond. Comparison with Flanders Moss peat cores show similar profiles but the total excess inventories and fluxes are higher in Lake of Menteith. The sedimentation rate at this site underwent a brief major change in the middle of the 20th Century. The heavy metals Zn, Cd, and Pb show a pattern of historical input with major increases in inventory occurring from the mid 19th Century until about 1980. There is the possibility that the Cu profile is associated with organic matter diagenesis and may not represent a historical record. The stable Pb isotope ratio has an 'industrial' signature of 1.173 ± 0.002 which starts to be affected by the input of Australian Pb ore from 1930. The reduction in the use of leaded petrol in the mid 1980s has led to a slight upturn in the ratio.

A comparison with the other study sites will be made in Chapter 7.

Chapter 5 Loch Tay.

5.1 Location.

Loch Tay is situated 60 km west-north-west of Perth (Fig.1.13). The loch, which forms part of the River Tay's course, is slightly sinuous in shape and its long axis runs east-west. Figure 5.1 shows the sampling sites for the sediment cores and the stream sediment sites in Loch Tay.

5.2 Topography.

Loch Tay is 23.4 km in length and has an area of 26.4 km^2 (Murray and Pullar, 1910). The loch is glacial in origin and runs parallel to the Highland Boundary Fault which lies to the south of it. The centre of the loch is cut by the Loch Tay - Glen Tilt Fault. The loch varies in depth from 15 to 150 m and is a stratified, oligotrophic system. The underlying bedrock is metamorphic in nature, forming part of the Dalradian series, and consists of slates, phyllites, mica-schists and biotite-gneiss. There is a narrow outcrop of limestone at the western end of the loch (Whittow, 1979). The Loch Tay catchment area is rich in mineral deposits, for example of Au, Ag, Cu, Pb, and Fe. The main inflows to the loch are the River Dochart (from Tyndrum) and the River Lochay (from Glen Lochay), while the major outflow is eastwards via the River Tay.

5.3 Pollution sources.

Although Loch Tay is not close to any large sources of industrial activity, it has a long history of mining and smelting activity in the area due to the high degree of mineralisation at places in the catchment. Pb ore (galena) was mined at Tyndrum (25 km to the west of Loch Tay) from 1750-1790 and then for shorter periods from 1830 until 1925 (Sinclair, 1791-1799; Butt, 1967). Other ores (Cu, Zn and Au) have been mined on smaller scales in the area.

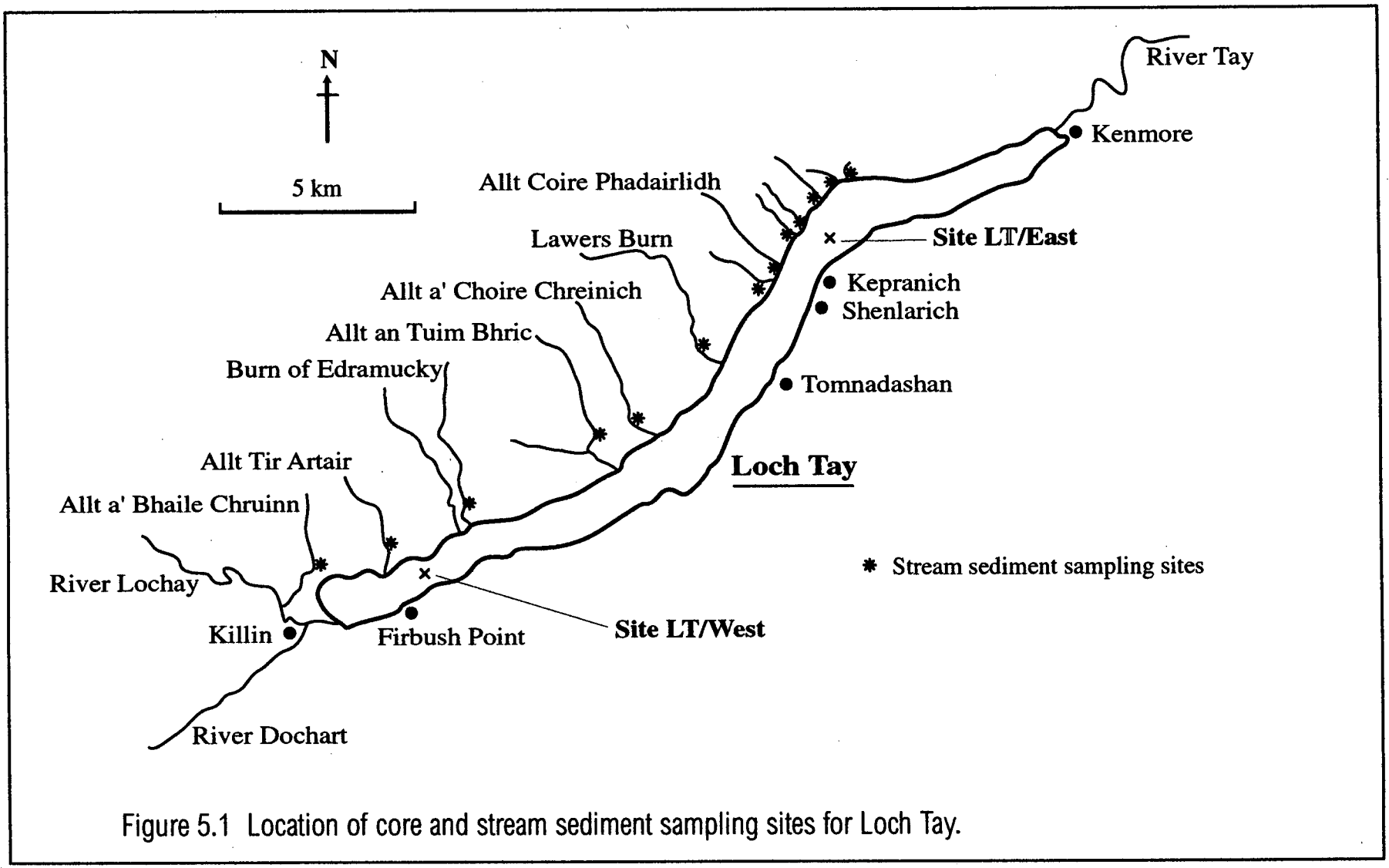

Figure 5.1 Location of core and stream sediment sampling sites for Loch Tay.

5.4 Loch Tay (East).

5.4.1 Results.

A Mini-Mackereth core (LT/EM) and a Jenkin core (LT/EJ) were taken from site LT/East on 18/9/96 (Section 2.1.2.3). The Jenkin core was analysed for ^{137}Cs and ^{210}Pb, and the Mini-Mackereth core for Fe, Mn, Pb, Zn, Cu, Cd, C, N and stable Pb isotopes.

5.4.1.1 Radiocaesium.

Table 5.1 presents a summary of the results for ^{137}Cs in core LT/EJ. Figure 5.2 is a plot of the specific activity of ^{137}Cs (Bq kg^{-1}) against depth (cm). ^{137}Cs penetrates to the base of the core and has two peaks in activity at 4.5 cm and 11.9 cm. The peak at 4.5 cm is sharp, covering 1.6 cm in the sediment, and has a maximum specific activity of 6485 Bq kg^{-1}. The lower peak is smaller and broader with a maximum of 641 Bq kg^{-1} at 11.9 cm, and covers a depth interval of 2.5 cm in the sediment. Above the narrow peak at 4.5 cm the activity tails off sharply, reaching 529 Bq kg^{-1} just below the surface. At the surface there is an enhancement to 851 Bq kg^{-1}.

5.4.1.2 ^{210}Pb.

Table 5.1 also contains a summary of the results for ^{210}Pb in core LT/EJ. Figure 5.3 is a plot of the specific activity of ^{210}Pb (Bq kg^{-1}) against depth (cm). The specific activity of ^{210}Pb generally increases from 83 Bq kg^{-1} at the base of the core to 1234 Bq kg^{-1} at the surface. The profile has a complex structure, having three small peaks at 14.9, 8.3 and 6.9 cm with activities of 414, 1081 and 869 Bq kg^{-1}, respectively. At 3.1 and 1.7 cm the activity drops briefly from the upward trend, to 406 and 567 Bq kg^{-1}, respectively.

Table 5.1 Radiocaesium and ^{210}Pb results for Loch Tay (east) core LT/EJ.

Sample code	Depth / cm	Wet wt / g	Dry wt / g	Mid cum. wt / g cm^{-2}	^{137}Cs / Bq kg^{-1}	σ_{n-1} / Bq kg^{-1}	^{210}Pb / Bq kg^{-1}	σ_{n-1} / Bq kg^{-1}	$^{210}Pb_{unsupp}$ / Bq kg^{-1}	σ(O)	ln $^{210}Pb_{unsupp}$	Ave err
LT/EJ001	0.0-0.2	12.002	0.198	0.003	851	141	1234	25	1151	25	7.05	0.02
LT/EJ002	0.2-0.4	11.576	0.380	0.010	529	66	929	26	846	26	6.74	0.03
LT/EJ003	0.4-0.6	10.503	0.405	0.021	546	55	873	24	790	24	6.67	0.03
LT/EJ004	0.6-0.8	10.354	0.425	0.032	581	39	867	19	784	19	6.66	0.02
LT/EJ005	0.8-1.0	9.709	0.448	0.044	674	50	913	30	830	30	6.72	0.04
LT/EJ006	1.0-1.2	9.674	0.636	0.058	591	52	721	15	638	15	6.46	0.02
LT/EJ007	1.2-1.4	9.459	0.661	0.075	637	52	669	18	586	18	6.37	0.03
LT/EJ008	1.4-1.6	9.912	0.811	0.095	730	56	601	16	518	16	6.25	0.03
LT/EJ009	1.6-1.8	9.133	0.976	0.119	736	46	567	16	484	16	6.18	0.03
LT/EJ010	1.8-2.0	9.184	0.735	0.142	817	54	930	27	848	28	6.74	0.03
LT/EJ011	2.0-2.2	9.895	0.699	0.161	940	66	909	42	826	42	6.72	0.05
LT/EJ012	2.2-2.4	6.557	0.400	0.176	906	53	707	36	624	36	6.44	0.06
LT/EJ013	2.4-2.6	9.837	0.792	0.192	1027	39	809	15	726	15	6.59	0.02
LT/EJ014	2.6-2.8	6.604	0.482	0.209	1097	36	767	21	684	21	6.53	0.03
LT/EJ015	2.8-3.0	7.449	0.735	0.225	1098	40	540	23	457	23	6.12	0.05
LT/EJ016	3.0-3.2	13.176	1.693	0.258	1075	40	406	10	323	10	5.78	0.03
LT/EJ017	3.2-3.4	6.464	0.542	0.287	1295	60	646	21	563	21	6.33	0.04
LT/EJ018	3.4-3.6	8.056	0.610	0.303	1741	79	913	48	830	48	6.72	0.06
LT/EJ019	3.6-3.8	8.632	0.710	0.320	1790	80	785	20	702	20	6.55	0.03
LT/EJ020	3.8-4.0	10.941	0.897	0.342	2130	66	853	25	770	26	6.65	0.03
LT/EJ021	4.0-4.2	6.520	0.442	0.360	2781	82	802	18	719	18	6.58	0.03
LT/EJ022	4.2-4.4	11.121	0.889	0.378	4578	98	835	23	752	23	6.62	0.03
LT/EJ023	4.4-4.6	7.540	0.565	0.397	6485	134	759	18	676	18	6.52	0.03
LT/EJ024	4.6-4.8	8.344	0.669	0.414	3182	98	730	15	647	15	6.47	0.02
LT/EJ025	4.8-5.0	8.554	0.651	0.431	980	67	837	15	754	15	6.63	0.02

Table 5.1 Radiocaesium and ^{210}Pb results for Loch Tay core LT/EJ, continued.

Sample code	Depth / cm	Wet wt / g	Dry wt / g	Mid cum. wt / g cm^{-2}	^{137}Cs / Bq kg^{-1}	σ_{n-1} / Bq kg^{-1}	^{210}Pb / Bq kg^{-1}	σ_{n-1} / Bq kg^{-1}	$^{210}Pb_{unsupp}$ / Bq kg^{-1}	σ(O)	ln $^{210}Pb_{unsupp}$	Ave err
LT/EJ026	5.0-5.2	9.263	0.704	0.449	602	43	773	34	690	34	6.54	0.05
LT/EJ027	5.2-5.4	9.762	0.795	0.469	505	14	789	27	706	27	6.56	0.04
LT/EJ028	5.4-5.6	6.407	0.552	0.487	634	49	740	23	657	24	6.49	0.04
LT/EJ029	5.6-5.8	9.098	0.762	0.505	519	27	731	20	649	20	6.47	0.03
LT/EJ030	5.8-6.0	6.663	0.536	0.522	458	36	655	22	572	22	6.35	0.04
LT/EJ031	6.0-6.2	6.590	0.589	0.537	446	38	673	27	590	27	6.38	0.05
LT/EJ032	6.2-6.4	7.856	0.643	0.554	488	38	628	24	545	25	6.30	0.05
LT/EJ033	6.4-6.6	8.519	0.817	0.573	446	30	642	15	559	15	6.33	0.03
LT/EJ034	6.6-6.8	6.845	0.556	0.592	448	40	732	21	649	21	6.48	0.03
LT/EJ035	6.8-7.0	6.799	0.525	0.606	420	32	869	38	786	38	6.67	0.05
LT/EJ036	7.0-7.2	6.822	0.578	0.621	462	35	692	27	609	27	6.41	0.04
LT/EJ037	7.2-7.4	7.668	0.738	0.639	549	51	618	25	535	25	6.28	0.05
LT/EJ038	7.4-7.6	9.084	0.992	0.662	447	11	680	20	597	20	6.39	0.03
LT/EJ039	7.6-7.8	6.474	0.615	0.683	416	33	615	38	532	38	6.28	0.07
LT/EJ040	7.8-8.0	8.713	0.694	0.701	381	28	834	40	751	40	6.62	0.05
LT/EJ041	8.0-8.2	7.276	0.568	0.718	401	69	839	52	756	52	6.63	0.07
LT/EJ042	8.2-8.4	9.388	0.716	0.735	361	44	1081	110	998	110	6.91	0.11
LT/EJ043	8.4-8.6	7.503	0.649	0.753	403	32	583	12	500	12	6.21	0.02
LT/EJ044	8.6-8.8	8.680	0.823	0.773	365	24	574	14	491	14	6.20	0.03
LT/EJ045	8.8-9.0	8.830	0.981	0.797	409	29	543	12	460	12	6.13	0.03
LT/EJ046	9.0-9.2	7.768	0.795	0.821	456	32	492	11	409	11	6.01	0.03
LT/EJ047	9.2-9.4	8.254	0.927	0.844	408	20	517	13	435	13	6.07	0.03
LT/EJ048	9.4-9.6	9.394	1.001	0.869	404	29	536	11	454	11	6.12	0.02
LT/EJ049	9.6-9.8	6.694	0.638	0.891	429	28	604	13	521	13	6.26	0.02
LT/EJ050	9.8-10.0	11.857	1.128	0.915	414	28	581	12	498	12	6.21	0.02

Table 5.1 Radiocaesium and ^{210}Pb results for Loch Tay core LT/EJ, continued.

Sample code	Depth / cm	Wet wt / g	Dry wt / g	Mid cum. wt / g cm^{-2}	^{137}Cs / Bq kg^{-1}	σ_{n-1} / Bq kg^{-1}	^{210}Pb / Bq kg^{-1}	σ_{n-1} / Bq kg^{-1}	$^{210}Pb_{unsupp}$ / Bq kg^{-1}	σ(O)	ln $^{210}Pb_{unsupp}$	Ave err
LT/EJ051	10.0-10.2	6.066	0.451	0.936	507	38	591	12	508	12	6.23	0.02
LT/EJ052	10.2-10.4	6.753	0.575	0.950	416	32	525	19	442	19	6.09	0.04
LT/EJ053	10.4-10.6	5.773	0.528	0.965	464	31	535	15	452	15	6.11	0.03
LT/EJ054	10.6-10.8	8.496	0.824	0.983	479	35	509	8	426	8	6.05	0.02
LT/EJ055	10.8-11.0	6.615	0.715	1.003	519	33	518	21	435	21	6.07	0.05
LT/EJ056	11.0-11.2	7.512	0.855	1.024	573	34	481	13	398	13	5.99	0.03
LT/EJ057	11.2-11.4	6.602	0.734	1.045	580	39	482	17	399	18	5.99	0.04
LT/EJ058	11.4-11.6	6.289	0.663	1.064	534	18	442	16	359	16	5.88	0.05
LT/EJ059	11.6-11.8	9.718	0.957	1.086	583	36	454	11	371	11	5.92	0.03
LT/EJ060	11.8-12.0	6.848	0.692	1.108	641	36	505	14	422	14	6.05	0.03
LT/EJ061	12.0-12.2	8.718	0.897	1.129	551	43	467	16	384	16	5.95	0.04
LT/EJ062	12.2-12.4	7.555	0.820	1.152	466	35	370	9	287	9	5.66	0.03
LT/EJ063	12.4-12.6	7.439	0.832	1.174	448	32	338	11	255	11	5.54	0.04
LT/EJ064	12.6-12.8	5.939	0.740	1.195	389	29	355	13	272	13	5.61	0.05
LT/EJ065	12.8-13.0	10.903	1.350	1.223	323	22	296	7	213	7	5.36	0.03
LT/EJ066	13.0-13.2	6.322	0.702	1.251	357	31	438	8	355	8	5.87	0.02
LT/EJ067	13.2-13.4	6.247	0.569	1.268	315	30	390	13	307	13	5.73	0.04
LT/EJ068	13.4-13.6	8.914	0.918	1.287	297	23	316	8	233	8	5.45	0.03
LT/EJ069	13.6-13.8	8.956	0.883	1.311	132	9	319	8	236	8	5.47	0.03
LT/EJ070	13.8-14.0	5.293	0.470	1.330	272	46	274	10	191	10	5.25	0.05
LT/EJ071	14.0-14.2	6.917	0.810	1.347	n/a	n/a			331	19	5.80	0.06
LT/EJ072	14.2-14.4	8.453	1.115	1.372	n/a	n/a	398	10	269	11	5.60	0.04
LT/EJ073	14.4-14.6	6.528	0.784	1.398	124	27			258	7	5.55	0.03
LT/EJ074	14.6-14.8	6.715	0.741	1.418	n/a	n/a			190	11	5.25	0.06
LT/EJ075	14.8-15.0	5.822	0.607	1.436	175	38	414	19	105	5	4.65	0.05

Table 5.1 Radiocaesium and ^{210}Pb results for Loch Tay core LT/EJ, continued.

Sample code	Depth / cm	Wet wt / g	Dry wt / g	Mid cum. wt / g cm^{-2}	^{137}Cs / Bq kg^{-1}	σ_{n-1} / Bq kg^{-1}	^{210}Pb / Bq kg^{-1}	σ_{n-1} / Bq kg^{-1}	$^{210}Pb_{unsupp}$ / Bq kg^{-1}	σ(O)	ln $^{210}Pb_{unsupp}$	Ave err
LT/EJ076	15.0-15.2	9.366	1.024	1.458	n/a	n/a			119	9	4.78	0.08
LT/EJ077	15.2-15.4	5.697	0.694	1.481	n/a	n/a	263	69	70	4	4.25	0.06
LT/EJ078	15.4-15.6	9.095	1.036	1.504	103	24			0	3		
LT/EJ079	15.6-15.8	7.508	0.922	1.530	n/a	n/a						
LT/EJ080	15.8-16.0	9.003	0.951	1.555	103	16	352	11				
LT/EJ081	16.0-16.2	6.468	0.697	1.577	n/a	n/a						
LT/EJ082	16.2-16.4	6.153	0.727	1.596	n/a	n/a						
LT/EJ083	16.4-16.6	8.969	1.018	1.620	n/a	n/a						
LT/EJ084	16.6-16.8	9.131	0.931	1.646	n/a	n/a						
LT/EJ085	16.8-17.0	7.447	0.760	1.668	76	22	341	7				
LT/EJ086	17.0-17.2	6.735	0.679	1.688	n/a	n/a						
LT/EJ087	17.2-17.4	7.566	0.749	1.707	n/a	n/a						
LT/EJ088	17.4-17.6	4.935	0.510	1.724	n/a	n/a						
LT/EJ089	17.6-17.8	6.687	0.741	1.740	n/a	n/a						
LT/EJ090	17.8-18.0	6.959	0.799	1.761	110	19	273	11				
LT/EJ091	18.0-18.2	9.451	1.022	1.785	n/a	n/a						
LT/EJ092	18.2-18.4	12.073	1.491	1.819	n/a	n/a						
LT/EJ093	18.4-18.6	11.830	1.455	1.858	n/a	n/a						
LT/EJ094	18.6-18.8	7.031	0.856	1.889	n/a	n/a						
LT/EJ095	18.8-19.0	7.888	0.872	1.912	86	24	188	4				
LT/EJ096	19.0-19.2	7.332	0.846	1.935	n/a	n/a						
LT/EJ097	19.2-19.4	8.788	1.073	1.961	n/a	n/a						
LT/EJ098	19.4-19.6	9.067	1.055	1.989	n/a	n/a						
LT/EJ099	19.6-19.8	7.411	0.854	2.015	n/a	n/a						
LT/EJ100	19.8-20.0	6.978	0.911	2.039	84	19	202	9				

Table 5.1 Radiocaesium and ^{210}Pb results for Loch Tay core LT/EJ, continued.

Sample code	Depth / cm	Wet wt / g	Dry wt / g	Mid cum. wt / g cm^{-2}	^{137}Cs / Bq kg^{-1}	σ_{n-1} / Bq kg^{-1}	^{210}Pb / Bq kg^{-1}	σ_{n-1} / Bq kg^{-1}	$^{210}Pb_{unsupp}$ / Bq kg^{-1}	σ(O)	ln $^{210}Pb_{unsupp}$	Ave err
LT/EJ101	20.0-21.0	31.625	4.116	2.106	n/a	n/a						
LT/EJ102	21.0-22.0	34.957	4.905	2.226	n/a	n/a	211	5				
LT/EJ103	22.0-23.0	34.307	4.719	2.355	n/a	n/a						
LT/EJ104	23.0-24.0	37.407	5.838	2.496	n/a	n/a						
LT/EJ105	24.0-25.0	33.807	4.567	2.635	41	9	153	3				
LT/EJ106	25.0-26.0	35.453	5.696	2.773	n/a	n/a						
LT/EJ107	26.0-27.0	37.320	5.939	2.928	n/a	n/a	117	55				
LT/EJ108	27.0-28.0	34.693	5.143	3.076	n/a	n/a						
LT/EJ109	28.0-29.0	51.214	9.257	3.269	n/a	n/a						
LT/EJ110	29.0-30.0	12.886	2.352	3.424	57	10	83	2				

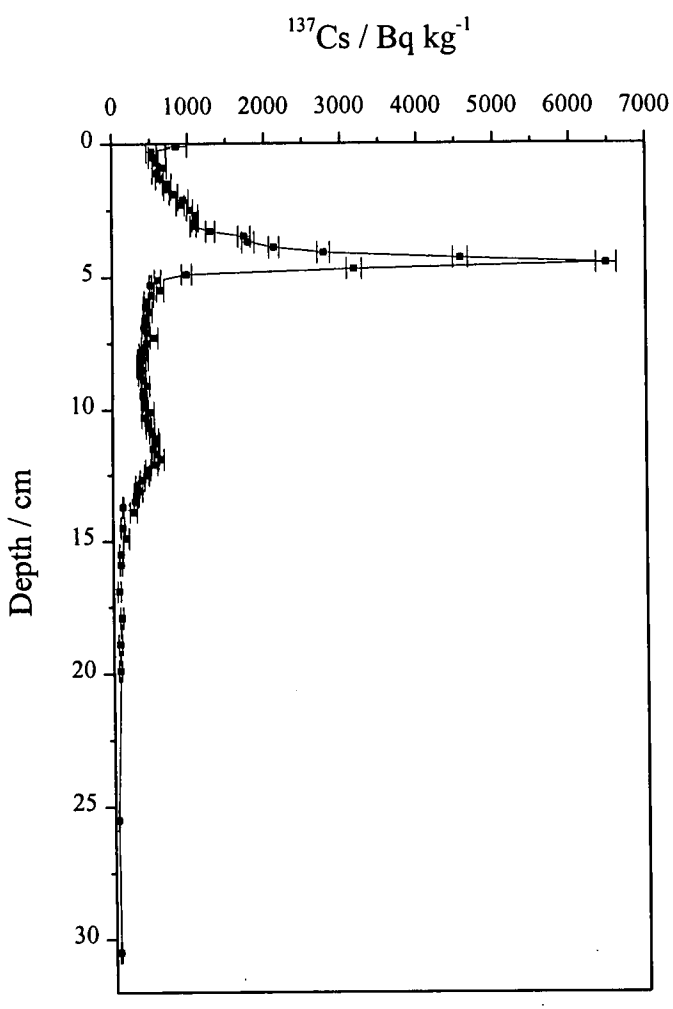

Figure 5.2 ^{137}Cs (Bq kg^{-1}) vs depth (cm) in core LT/EJ.

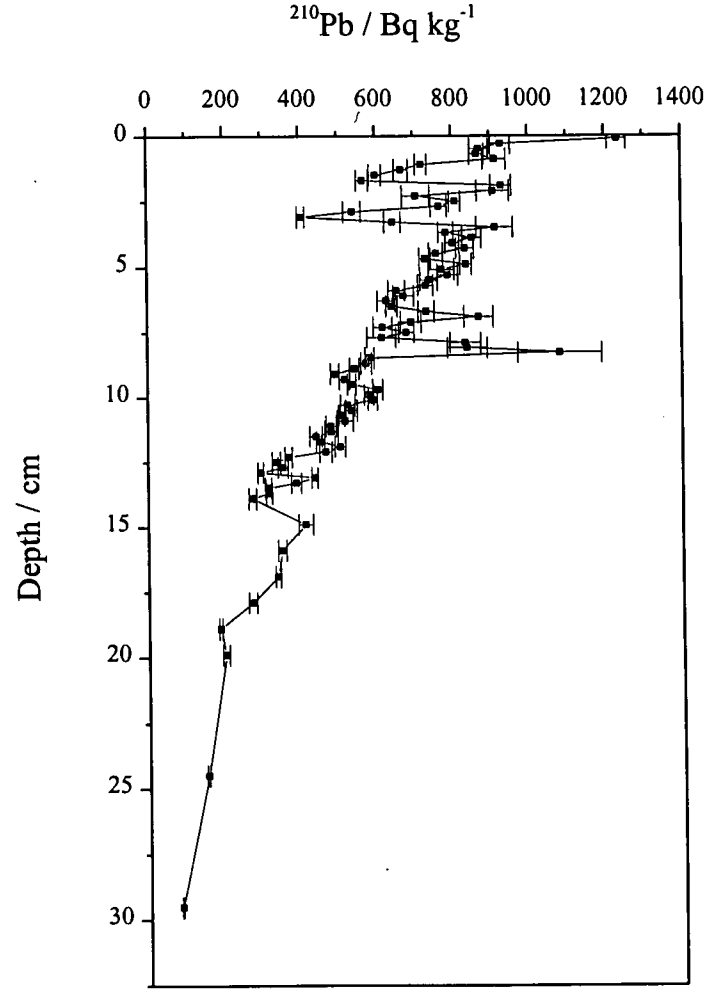

Figure 5.3 ^{210}Pb (Bq kg^{-1}) vs depth (cm) in core LT/EJ.

5.4.1.3 Heavy metals.

The concentrations of the heavy metals in core LT/EM are shown in Table 5.2 along with the wet and dry weights, depth and reference number for each section. For each metal a graph of concentration (mg kg^{-1} or %) against depth (cm) is shown in Figures 5.4-5.9.

As illustrated in Figure 5.4, the Pb concentration shows a completely different profile from that exhibited by any of the cores from the other lochs investigated. The Pb concentration generally increases with increasing depth and has a maximum value at the base of the core. From 393 mg kg^{-1} at the base of the core the concentration drops slowly to reach a constant value of 298 ± 10 mg kg^{-1} from 50-14 cm. Above 14 cm the concentration drops more steeply towards the surface, reaching a minimum value of 207 mg kg^{-1} at 1.1 cm. The top 0.4 cm of the core shows an elevated level of 258-271 mg kg^{-1}.

In Figure 5.5 the Zn concentration is relatively constant from the base of the core until 20 cm, with an average value of 684 ± 24 mg kg^{-1}. From 20 cm the concentration tails off to a minimum of 501 mg kg^{-1} at 2.7 cm. The concentration increases to reach a maximum at the surface of 712 mg kg^{-1}. Cadmium (Fig. 5.6), as with Pb, exhibits a very high concentration of 6.0 mg kg^{-1} at the base of the core, above which it drops until 71 cm. Above this it remains constant at 4.89 ± 0.09 mg kg^{-1} until 21.5 cm where it drops to reach a new constant level of 4.60 ± 0.21 mg kg^{-1} which holds until 4.5 cm. The concentration drops to 3.8 mg kg^{-1} from 4.5 cm to the surface, although there is a slight enhancement in the top 0.4 cm to 4.4 mg kg^{-1}.

For Cu (Fig. 5.7) the concentration is constant from the base to 51 cm at 81.5 ± 2.2 mg kg^{-1}. It drops to a new constant value of 72.7 ± 2.5 mg kg^{-1} from 51-19.7 cm. From this depth to just below the surface there is a broad, but shallow, depression with a minimum of 63 mg kg^{-1} at 6.5 cm. The concentration in the surface 0.8 cm is elevated, reaching 129 mg kg^{-1} at the surface.

In Figure 5.8 the Fe is constant from the base of the core at 8.57 ± 0.39 % until 8 cm. There is a slight peak at 6.1 cm with a maximum of 9.41 %. The surface section is enhanced, reaching a maximum of 9.52 %. Manganese (Fig. 5.9) exhibits the most variable structure of the metal profiles, with a series of small broad peaks and two large broad peaks. The largest of the peaks, at 45 cm, covers 12 cm in the sediment and has a maximum concentration of 1.3 %. The other large peak is situated at 8.3 cm, covers 9.2 cm and has a maximum concentration of 1.14 %. There is a small enhancement from a minimum of 0.76 % at 2.7 cm to 1.06 % in the surface layer.

5.4.1.4 Carbon and nitrogen.

The results for C and N for core LT/EM are shown in Table 5.2 along with the heavy metal data. Figure 5.10 is a plot of C (%) against depth (cm). From the base of the core, the C drops from 10.96 to 10.13 % at 69 cm, above which, it settles to a constant value of 10.07 ± 0.37 % until 14.9 cm. From 14.9 cm to 0.4 cm there is a slight broad peak with a maximum of 11.60 % at 5.5 cm. Above 0.4 cm, the concentration rises sharply to 12.2 % at the surface. Nitrogen is constant at 0.66 ± 0.09 % from the surface of the core down to 36.5 cm. Below 36.5 cm it drops to 0.49 ± 0.03 % to the base of the core.

Table 5.2 Heavy metal, carbon and nitrogen results for Loch Tay (east) core LT/EM.

Sample Code	Depth / cm	Wet Wt / g	Dry Wt / g	Fe / %	Mn / %	Pb / mg kg^{-1}	Cu / mg kg^{-1}	Zn / mg kg^{-1}	Cd / mg kg^{-1}	C / %	N / %
LT/EM001	0.0-0.2	20.784	0.399	9.52	1.06	271	129	712	4.4	12.21	0.76
LT/EM002	0.2-0.4	6.974	0.488	8.92	0.92	258	116	671	4.2	11.24	0.65
LT/EM003	0.4-0.6	5.954	0.511	8.74	0.84	229	112	623	3.9	10.06	0.53
LT/EM004	0.6-0.8	6.589	0.613	8.17	0.80	220	131	560	3.8	10.26	0.55
LT/EM005	0.8-1.0	8.261	0.813	8.52	0.81	211	85	550	3.6	10.32	0.51
LT/EM006	1.0-1.2	7.244	0.684	8.22	0.80	207	75	523	3.9	10.87	0.52
LT/EM007	1.2-1.4	8.036	0.754	8.39	0.83	217	77	535	3.9	10.55	0.51
LT/EM008	1.4-1.6	10.325	0.971	8.03	0.77	210	73	505	3.9	10.33	0.45
LT/EM009	1.6-1.8	6.469	0.619	8.21	0.81	212	74	516	3.8	10.59	0.48
LT/EM010	1.8-2.0	7.577	0.711	8.05	0.80	210	73	521	3.9	10.08	0.41
LT/EM011	2.0-2.2	6.447	0.606	8.45	0.83	216	76	538	4.0	11.36	0.49
LT/EM012	2.2-2.4	5.054	0.487	8.43	0.82	213	76	530	4.0	10.56	0.49
LT/EM013	2.4-2.6	8.525	0.825	8.48	0.81	228	78	502	4.0	10.69	0.65
LT/EM014	2.6-2.8	8.580	0.833	8.10	0.76	213	77	501	3.9	10.79	0.69
LT/EM015	2.8-3.0	4.596	0.410	8.16	0.79	222	74	509	4.0	10.32	0.64
LT/EM016	3.0-3.2	6.788	0.665	8.35	0.79	222	77	526	3.9	10.28	0.63
LT/EM017	3.2-3.4	6.378	0.604	8.62	0.81	223	76	535	3.9	10.34	0.63
LT/EM018	3.4-3.6	8.282	0.817	8.71	0.83	218	76	509	3.8	10.31	0.63
LT/EM019	3.6-3.8	5.306	0.501	8.77	0.84	225	74	533	3.9	10.45	0.65
LT/EM020	3.8-4.0	10.632	1.014	8.53	0.82	218	73	543	3.7	10.34	0.64
LT/EM021	4.0-4.2	5.596	0.550	8.67	0.85	219	69	574	4.0	10.61	0.68
LT/EM022	4.2-4.4	7.466	0.703	8.65	0.87	224	68	598	3.9	10.52	0.68
LT/EM023	4.4-4.6	7.094	0.677	8.90	0.93	231	70	616	4.1	10.96	0.75
LT/EM024	4.6-4.8	8.382	0.789	8.98	0.97	241	72	639	4.4	11.45	0.71
LT/EM025	4.8-5.0	5.250	0.474	9.01	1.03	243	69	632	4.4	11.36	0.84

Table 5.2 Heavy metal, carbon and nitrogen results for Loch Tay (east) core LT/EM, continued.

Sample Code	Depth / cm	Wet Wt / g	Dry Wt / g	Fe / %	Mn / %	Pb / mg kg^{-1}	Cu / mg kg^{-1}	Zn / mg kg^{-1}	Cd / mg kg^{-1}	C / %	N / %
LT/EM026	5.0-5.2	7.395	0.677	9.00	1.02	250	68	633	4.3	11.45	0.77
LT/EM027	5.2-5.4	5.220	0.480	9.00	1.05	231	65	600	4.3	11.40	0.70
LT/EM028	5.4-5.6	6.934	0.648	9.29	1.02	260	70	651	4.5	11.60	0.71
LT/EM029	5.6-5.8	6.430	0.570	9.38	1.01	243	69	579	4.6	11.36	0.71
LT/EM030	5.8-6.0	6.978	0.636	9.21	1.05	241	67	572	4.3	11.21	0.68
LT/EM031	6.0-6.2	7.379	0.677	9.41	1.05	249	68	583	4.9	11.19	0.64
LT/EM032	6.2-6.4	4.784	0.440	9.30	1.04	249	68	569	4.6	10.97	0.65
LT/EM033	6.4-6.6	4.910	0.434	9.26	1.02	235	63	562	4.4	11.27	0.69
LT/EM034	6.6-6.8	5.936	0.553	9.26	1.05	250	66	593	4.4	11.09	0.64
LT/EM035	6.8-7.0	6.034	0.558	9.30	1.04	258	67	598	4.7	11.32	0.67
LT/EM036	7.0-7.2	7.216	0.658	8.98	1.05	249	69	601	5.0	11.39	0.67
LT/EM037	7.2-7.4	5.974	0.559	7.56	1.05	257	69	621	4.4	11.21	0.68
LT/EM038	7.4-7.6	7.701	0.702	7.68	1.06	243	69	613	4.4	11.11	0.67
LT/EM039	7.6-7.8	5.592	0.496	7.83	1.07	255	69	620	4.4	10.82	0.66
LT/EM040	7.8-8.0	5.733	0.520	7.93	1.06	261	71	615	4.6	11.12	0.66
LT/EM041	8.0-8.2	5.545	0.525	7.98	1.09	257	65	597	4.3	11.09	0.93
LT/EM042	8.2-8.4	9.724	0.907	8.14	1.14	261	68	612	4.4	11.13	0.88
LT/EM043	8.4-8.6	5.408	0.497	8.64	1.11	256	68	636	4.6	11.20	0.78
LT/EM044	8.6-8.8	5.005	0.450	8.34	1.05	254	66	628	4.6	10.98	0.76
LT/EM045	8.8-9.0	3.263	0.294	8.65	1.09	243	68	622	4.5	10.89	0.71
LT/EM046	9.0-9.2	5.616	0.510	7.98	1.05	249	67	510	4.4	11.17	0.72
LT/EM047	9.2-9.4	10.181	0.953	8.48	1.07	259	68	646	4.4	10.93	0.70
LT/EM048	9.4-9.6	3.344	0.298	8.60	1.03	256	68	624	4.4	10.57	0.67
LT/EM049	9.6-9.8	6.956	0.639	8.33	0.98	259	74	624	4.4	11.09	0.72
LT/EM050	9.8-10.0	6.782	0.657	8.66	1.00	264	71	691	4.7	10.94	0.68

Table 5.2 Heavy metal, carbon and nitrogen results for Loch Tay (east) core LT/EM, continued.

Sample Code	Depth / cm	Wet Wt / g	Dry Wt / g	Fe / %	Mn / %	Pb / mg kg^{-1}	Cu / mg kg^{-1}	Zn / mg kg^{-1}	Cd / mg kg^{-1}	C / %	N / %
LT/EM051	10.0-10.2	7.036	0.669	7.97	0.96	258	68	677	4.6	11.03	0.71
LT/EM052	10.2-10.4	7.310	0.693	8.01	0.95	267	70	664	4.6	10.76	0.68
LT/EM053	10.4-10.6	5.805	0.553	7.74	0.91	269	67	678	4.7	10.90	0.68
LT/EM054	10.6-10.8	7.993	0.747	8.36	0.95	269	68	680	4.5	10.83	0.69
LT/EM055	10.8-11.0	3.973	0.385	7.98	0.93	269	68	677	4.6	10.76	0.68
LT/EM056	11.0-11.2	6.366	0.595	8.15	0.93	265	69	668	4.6	10.96	0.71
LT/EM057	11.2-11.4	7.716	0.773	8.44	0.96	264	68	669	4.6	10.38	0.58
LT/EM058	11.4-11.6	8.343	0.849	8.79	0.96	270	68	675	4.7	10.30	0.59
LT/EM059	11.6-11.8	7.055	0.686	8.79	0.98	275	71	659	4.5	10.26	0.58
LT/EM060	11.8-12.0	9.663	0.976	8.45	0.98	260	70	645	4.6	10.60	0.57
LT/EM061	12.0-12.2	5.590	0.546	8.79	0.96	278	70	659	4.6	10.26	0.57
LT/EM062	12.2-12.4	6.747	0.730	8.47	0.94	274	67	634	4.5	10.42	0.58
LT/EM063	12.4-12.6	12.228	1.281	8.57	0.93	280	71	647	4.7	10.30	0.57
LT/EM064	12.6-12.8	6.282	0.652	8.78	0.92	275	68	639	4.6	10.14	0.55
LT/EM065	12.8-13.0	3.448	0.342	8.66	0.88	281	70	652	4.7	10.53	0.56
LT/EM066	13.0-13.2	5.788	0.586	8.79	0.89	273	72	666	4.6	10.53	0.57
LT/EM067	13.2-13.4	9.880	0.996	8.08	0.90	283	73	659	4.6	10.36	0.57
LT/EM068	13.4-13.6	9.221	0.952	7.71	0.86	289	70	663	4.7	10.63	0.57
LT/EM069	13.6-13.8	6.140	0.600	8.18	0.83	286	70	641	4.6	10.67	1.08
LT/EM070	13.8-14.0	7.572	0.764	8.84	0.85	291	72	666	4.7	10.57	0.85
LT/EM071	14.0-14.2	5.398	0.536	8.74	0.84	294	73	644	4.7	10.55	0.78
LT/EM072	14.2-14.4	5.403	0.545	8.92	0.84	285	72	643	4.9	10.67	0.76
LT/EM073	14.4-14.6	5.484	0.558	8.84	0.84	294	73	651	4.8	10.66	0.72
LT/EM074	14.6-14.8	4.641	0.461	8.68	0.84	294	73	668	4.9	10.63	0.69
LT/EM075	14.8-15.0	3.474	0.351	8.36	0.83	292	72	650	4.7	10.50	0.67

Table 5.2 Heavy metal, carbon and nitrogen results for Loch Tay (east) core LT/EM, continued.

Sample Code	Depth / cm	Wet Wt / g	Dry Wt / g	Fe / %	Mn / %	Pb / mg kg^{-1}	Cu / mg kg^{-1}	Zn / mg kg^{-1}	Cd / mg kg^{-1}	C / %	N / %
LT/EM076	15.0-15.2	6.374	0.679	8.59	0.83	299	69	624	4.6	10.40	0.68
LT/EM077	15.2-15.4	6.050	0.647	8.53	0.84	289	70	642	4.8	10.34	0.65
LT/EM078	15.4-15.6	8.266	0.898	9.06	0.88	300	74	638	4.8	10.29	0.66
LT/EM079	15.6-15.8	4.548	0.486	8.78	0.88	288	73	631	4.7	10.25	0.63
LT/EM080	15.8-16.0	8.602	0.913	8.75	0.89	304	73	672	4.7	10.33	0.64
LT/EM081	16.0-16.2	9.276	0.990	8.53	0.88	296	71	645	4.6	10.45	0.62
LT/EM082	16.2-16.4	6.779	0.739	8.38	0.88	296	74	639	4.7	10.31	0.62
LT/EM083	16.4-16.6	7.697	0.819	8.11	0.83	294	72	615	4.4	10.26	0.62
LT/EM084	16.6-16.8	4.675	0.507	8.13	0.82	297	73	610	4.4	10.10	0.64
LT/EM085	16.8-17.0	6.713	0.698	8.00	0.82	287	73	624	4.1	10.16	0.61
LT/EM086	17.0-17.2	6.969	0.737	8.31	0.85	301	73	640	4.4	10.25	0.67
LT/EM087	17.2-17.4	7.851	0.853	8.30	0.87	315	75	643	4.5	10.20	0.64
LT/EM088	17.4-17.6	6.094	0.620	8.56	0.90	313	78	629	4.5	10.28	0.68
LT/EM089	17.6-17.8	5.122	0.536	8.43	0.94	305	78	634	4.6	10.21	0.64
LT/EM090	17.8-18.0	6.201	0.649	8.17	0.88	304	76	646	4.6	10.16	0.65
LT/EM091	18.0-18.2	11.708	1.305	8.29	0.84	310	74	635	4.4	10.14	0.64
LT/EM092	18.2-18.4	5.520	0.586	8.62	0.93	309	73	665	4.7	10.29	0.66
LT/EM093	18.4-18.6	10.329	1.153	8.58	0.91	309	77	660	4.7	10.35	0.76
LT/EM094	18.6-18.8	10.240	1.141	8.55	0.90	304	75	660	4.7	10.21	0.69
LT/EM095	18.8-19.0	4.331	0.442	8.17	0.90	281	70	706	5.8	12.09	0.80
LT/EM096	19.0-19.2	9.524	1.064	8.64	0.95	308	74	646	4.6	10.07	0.66
LT/EM097	19.2-19.4	5.303	0.578	8.64	0.94	315	75	675	4.7	10.57	0.68
LT/EM098	19.4-19.6	6.640	0.717	8.23	0.90	300	72	612	4.6	10.39	0.66
LT/EM099	19.6-19.8	5.928	0.620	8.53	0.92	301	75	653	4.8	10.20	0.65
LT/EM100	19.8-20.0	6.607	0.716	8.79	0.91	326	77	684	4.8	10.37	0.64

Table 5.2 Heavy metal, carbon and nitrogen results for Loch Tay (east) core LT/EM, continued.

Sample Code	Depth / cm	Wet Wt / g	Dry Wt / g	Fe / %	Mn / %	Pb / mg kg^{-1}	Cu / mg kg^{-1}	Zn / mg kg^{-1}	Cd / mg kg^{-1}	C / %	N / %
LT/EM101	20.0-21.0	30.068	3.480	8.81	0.85	305	76	694	4.6	9.94	0.64
LT/EM102	21.0-22.0	30.430	3.607	8.60	0.82	307	76	680	4.9	10.00	0.66
LT/EM103	22.0-23.0	30.043	3.505	8.45	0.81	311	75	683	4.9	10.39	0.69
LT/EM104	23.0-24.0	30.335	3.521	8.74	0.81	308	74	678	5.0	10.27	0.68
LT/EM105	24.0-25.0	30.031	3.405	8.69	0.81	306	74	687	4.9	10.23	0.65
LT/EM106	25.0-26.0	30.167	3.396	8.62	0.81	310	74	673	4.9	9.87	0.65
LT/EM107	26.0-27.0	28.689	3.415	8.58	0.79	302	73	663	4.9	9.90	0.65
LT/EM108	27.0-28.0	31.375	3.405	8.75	0.84	301	72	681	4.9	10.12	0.66
LT/EM109	28.0-29.0	32.305	3.538	9.09	0.92	298	73	658	5.0	9.88	0.64
LT/EM110	29.0-30.0	31.876	3.551	8.90	0.93	298	74	661	4.8	9.95	0.63
LT/EM111	30.0-31.0	32.528	3.608	8.95	0.91	287	73	641	4.7	9.72	0.65
LT/EM112	31.0-32.0	29.061	3.199	9.03	0.94	299	73	674	4.8	9.79	0.66
LT/EM113	32.0-33.0	33.537	3.746	8.84	0.93	294	71	681	4.9	9.98	0.64
LT/EM114	33.0-34.0	30.829	3.468	8.42	0.92	294	71	663	4.9	9.91	0.65
LT/EM115	34.0-35.0	32.084	3.559	8.78	0.91	301	72	671	4.9	10.04	0.67
LT/EM116	35.0-36.0	33.744	3.789	8.53	0.89	303	72	671	4.9	9.88	0.64
LT/EM117	36.0-37.0	33.543	3.677	8.92	0.91	302	74	673	4.9	9.82	0.53
LT/EM118	37.0-38.0	31.765	3.480	8.76	0.96	297	74	703	4.8	10.01	0.54
LT/EM119	38.0-39.0	31.234	3.461	8.92	1.14	292	65	701	4.7	9.58	0.50
LT/EM120	39.0-40.0	29.773	3.423	9.23	1.25	296	68	705	4.9	9.77	0.47
LT/EM121	40.0-42.0	68.881	7.651	9.12	1.33	293	69	694	4.9	9.55	0.51
LT/EM122	42.0-44.0	70.076	7.931	9.19	1.31	296	72	702	4.7	9.47	0.49
LT/EM123	44.0-46.0	66.007	7.436	9.13	1.32	295	71	676	4.8	9.75	0.45
LT/EM124	46.0-48.0	64.830	7.267	9.11	1.21	303	72	705	4.9	9.87	0.51
LT/EM125	48.0-50.0	68.506	7.590	9.10	1.17	307	72	696	4.8	9.77	0.50

Table 5.2 Heavy metal, carbon and nitrogen results for Loch Tay (east) core LT/EM, continued.

Sample Code	Depth / cm	Wet Wt / g	Dry Wt / g	Fe / %	Mn / %	Pb / mg kg^{-1}	Cu / mg kg^{-1}	Zn / mg kg^{-1}	Cd / mg kg^{-1}	C / %	N / %
LT/EM126	50.0-52.0	68.349	7.624	9.27	0.96	323	81	703	4.9	10.08	0.46
LT/EM127	52.0-54.0	65.740	7.386	9.21	0.95	321	79	690	4.8	10.04	0.44
LT/EM128	54.0-56.0	68.837	7.724	9.27	0.94	319	81	686	4.8	9.61	0.45
LT/EM129	56.0-58.0	65.619	7.444	8.90	0.92	326	81	685	4.9	9.74	0.53
LT/EM130	58.0-60.0	68.350	7.797	8.78	0.99	327	79	690	5.0	9.56	0.45
LT/EM131	60.0-62.0	66.550	7.638	9.13	1.07	325	80	688	5.0	9.61	0.47
LT/EM132	62.0-64.0	69.683	7.983	9.03	1.08	334	80	690	5.0	10.03	0.51
LT/EM133	64.0-66.0	61.479	6.903	9.12	1.06	338	80	694	5.0	9.72	0.43
LT/EM134	66.0-68.0	66.255	7.458	8.87	1.00	335	84	741	4.9	9.75	0.46
LT/EM135	68.0-70.0	68.365	7.559	8.96	0.98	343	85	734	5.1	10.13	0.48
LT/EM136	70.0-72.0	65.831	7.256	8.95	0.95	349	83	724	5.0	10.31	0.52
LT/EM137	72.0-74.0	65.875	7.314	8.83	0.93	352	85	720	5.3	10.61	0.54
LT/EM138	74.0-76.0	68.861	7.644	9.23	0.97	358	78	717	5.4	10.63	0.52
LT/EM139	76.0-78.0	67.345	7.476	8.90	1.03	367	84	697	5.6	10.36	0.50
LT/EM140	78.0-80.0	65.357	6.913	9.41	1.02	369	83	700	5.7	10.60	0.49
LT/EM141	80.0-93.0	382.92	40.350	9.09	1.01	393	82	686	6.0	10.96	0.57

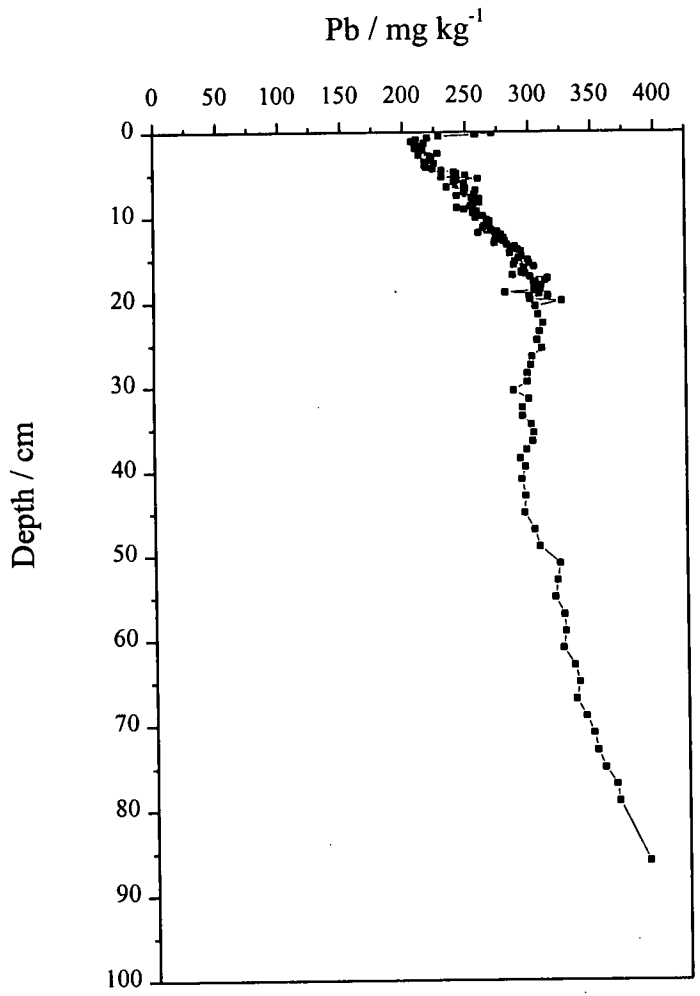

Figure 5.4 Pb (mg kg^{-1}) vs depth (cm) in core LT/EM.

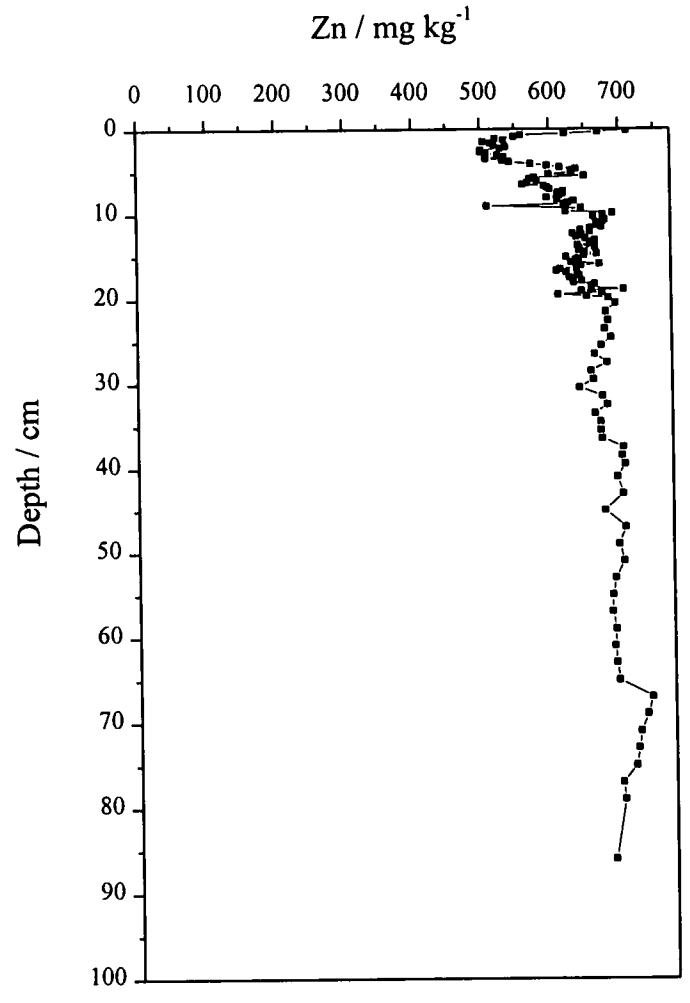

Figure 5.5 Zn (mg kg^{-1}) vs depth (cm) in core LT/EM.

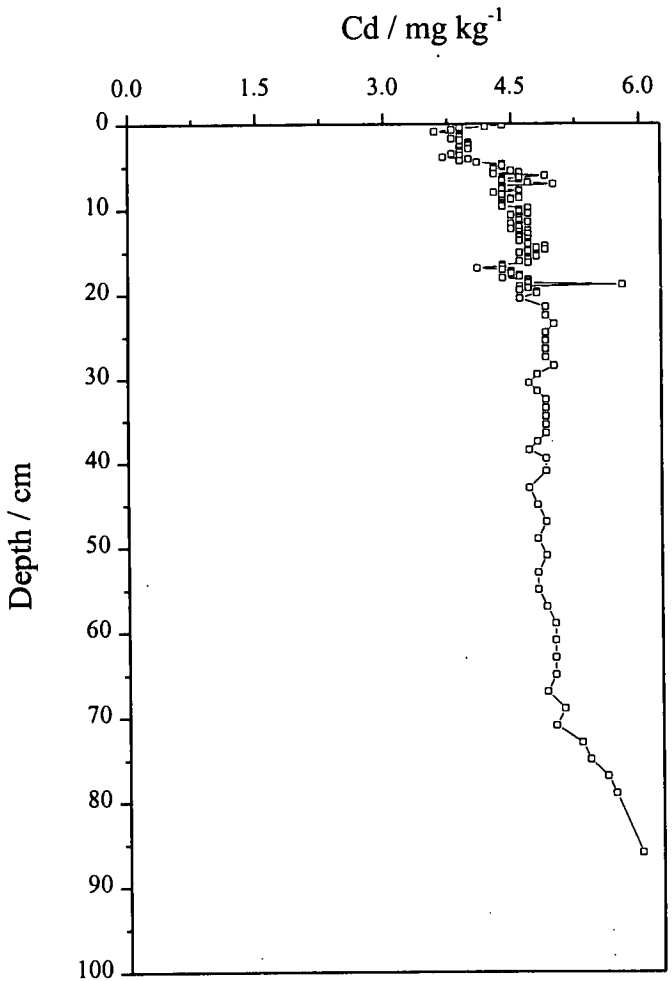

Figure 5.6 Cd (mg kg^{-1}) vs depth (cm) in core LT/EM.

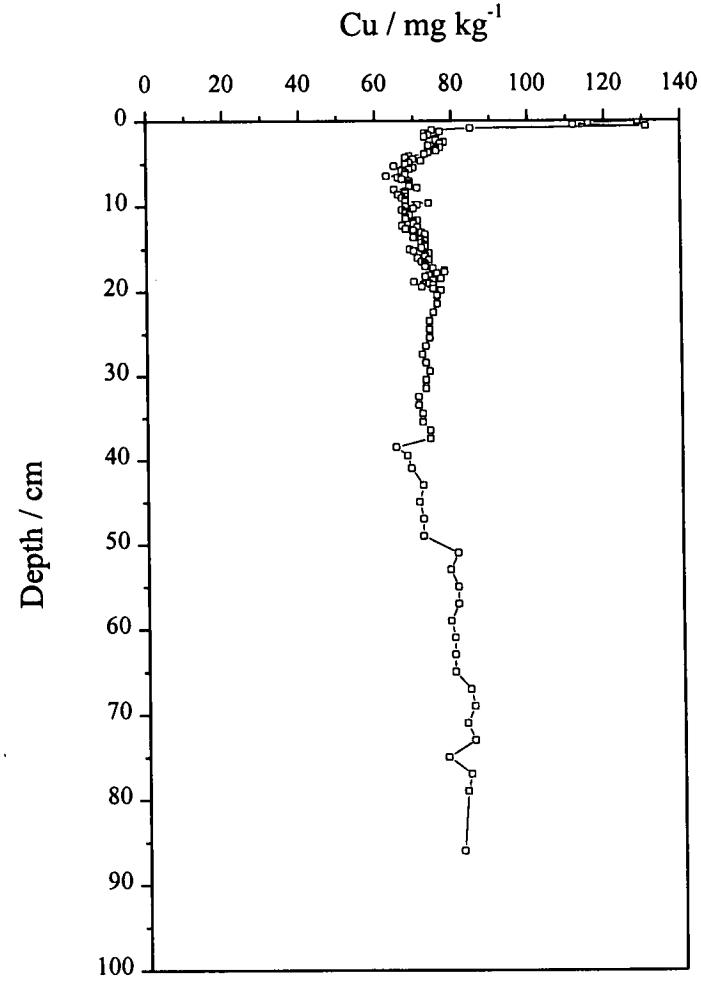

Figure 5.7 Cu (mg kg^{-1}) vs depth (cm) in core LT/EM.

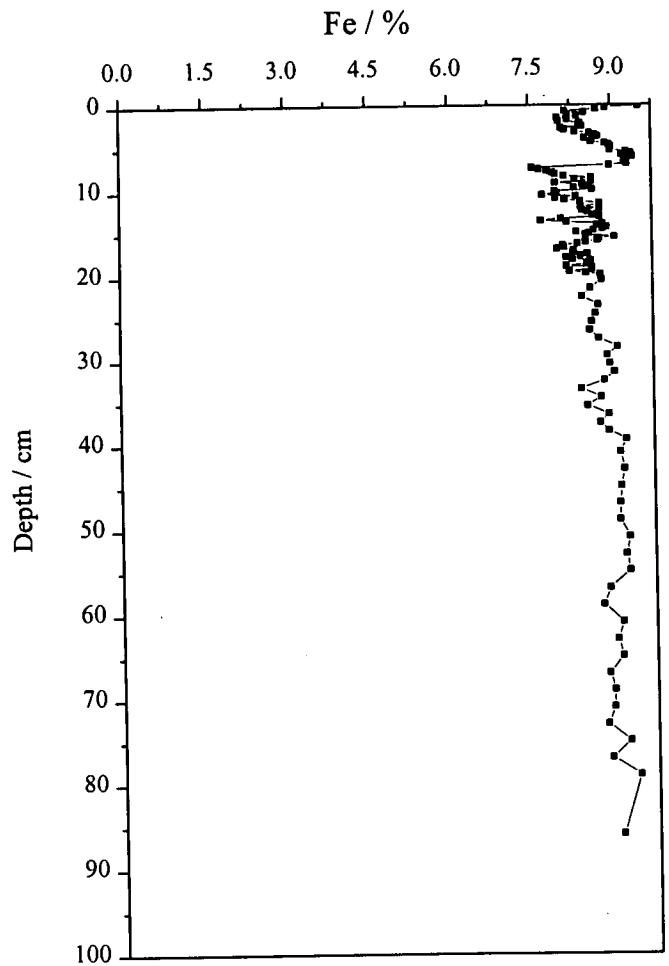

Figure 5.8 Fe (%) vs depth (cm) in core LT/EM.

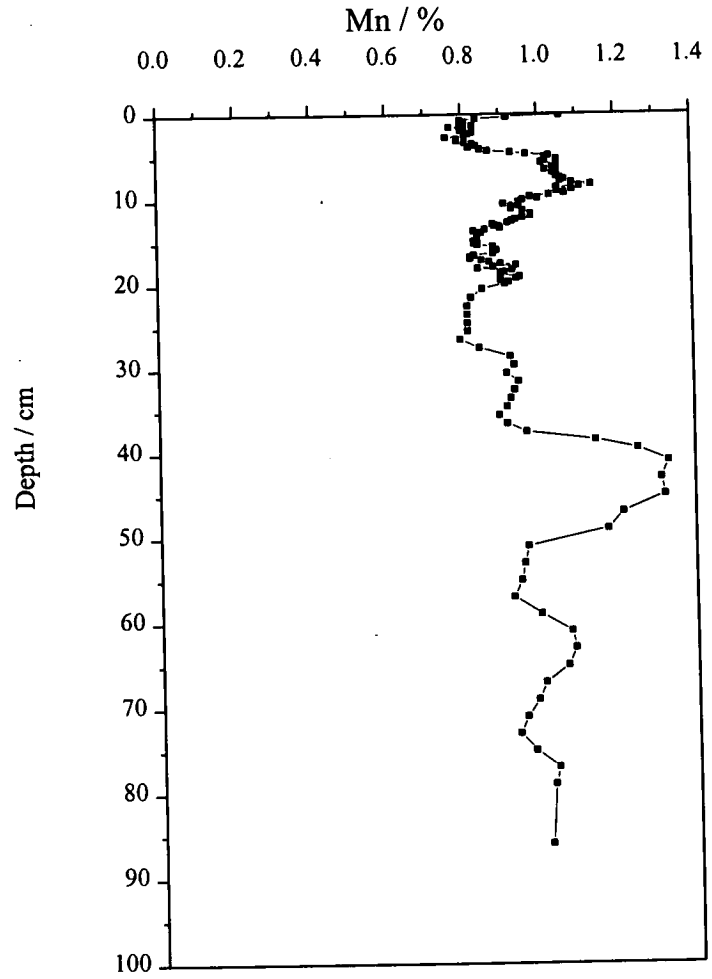

Figure 5.9 Mn (%) vs depth (cm) in core LT/EM.

Figure 5.10 C (%) vs depth (cm) in core LT/EM.

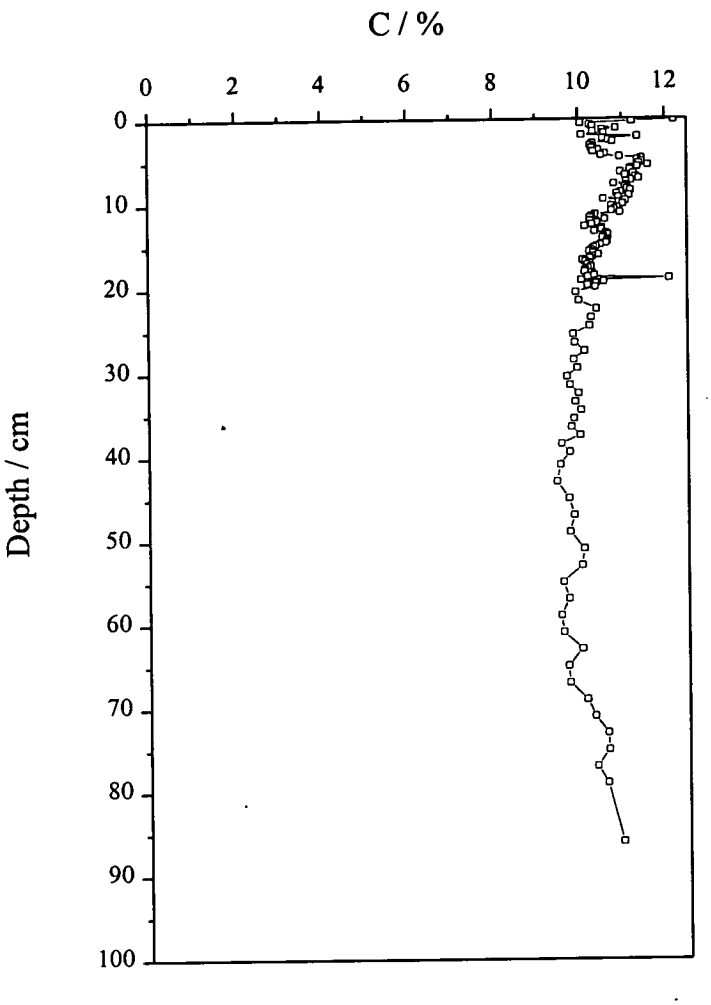

5.4.1.5 Stable lead isotopes.

Table 5.3 is a summary of the $^{206}Pb/^{207}Pb$ atom ratio and the Pb concentration (mg kg^{-1}) data for each section of the Mini-Mackereth core LT/EM. A plot of each of the three atom ratios, $^{206}Pb/^{207}Pb$, $^{208}Pb/^{206}Pb$ and $^{208}Pb/^{207}Pb$, against depth (cm) and Pb (mg kg^{-1}) is shown in Figures 5.11 (a)-(c), respectively. From Figure 5.11 (a) it can be seen that the $^{206}Pb/^{207}Pb$ atom ratio is effectively constant throughout the core at 1.145 ± 0.002 with the exception of a peak at 28 cm, covering 4 cm, where it rises to 1.150.

The profiles of $^{208}Pb/^{206}Pb$ and $^{208}Pb/^{207}Pb$ follow similar trends (Figs. 5.11 (b) and (c), respectively). At the base of the core, the $^{208}Pb/^{206}Pb$ and $^{208}Pb/^{207}Pb$ atom ratios increase from 2.095 and 2.402 to reach 2.117 and 2.438, respectively, by 75 cm. Above this, the ratios remain constant at 2.124 ± 0.005 and 2.434 ± 0.005, respectively, until, at 31.5 cm, they start to rise, reaching 2.157 and 2.473 at 19.1 cm. Above 19.1 cm the ratios drop again to approximately 2.134 and 2.444, although the decrease is quite irregular with peaks of 2.146 and 2.468 and 2.155 and 2.469 for $^{208}Pb/^{206}Pb$ and $^{208}Pb/^{207}Pb$, respectively, at approximately 15 and 10 cm. Above 5 cm, the ratios rise to reach 2.142 and 2.447 at the surface.

Stream sediment samples were taken from some of the major rivers flowing into Loch Tay from the northern shore and the southern shore (Lancaster, 1996). The samples were analysed for Pb and stable Pb isotopes, the results of which are shown in Tables 5.4 (a) and (b).

Table 5.3 Stable lead isotope ratio and Pb concentration (mg kg^{-1}) results for core LT/EM.

Sample Code	Mid Depth / cm	Pb / mg kg^{-1}	$^{206}Pb/^{207}Pb$	σ_{n-1}	$^{208}Pb/^{207}Pb$	σ_{n-1}	$^{208}Pb/^{206}Pb$	σ_{n-1}
LT/EM001	0.1	271	1.143	0.0018	2.447	0.0040	2.142	0.0035
LT/EM002	0.3	258	1.142	0.0020	2.461	0.0049	2.155	0.0029
LT/EM003	0.5	229	1.143	0.0026	2.466	0.0047	2.157	0.0038
LT/EM004	0.7	220	1.144	0.0024	2.477	0.0039	2.164	0.0050
LT/EM005	0.9	211	1.144	0.0016	2.470	0.0045	2.160	0.0022
LT/EM006	1.1	207	1.144	0.0012	2.468	0.0043	2.158	0.0021
LT/EM007	1.3	217	1.143	0.0015	2.464	0.0073	2.155	0.0042
LT/EM008	1.5	210	1.143	0.0017	2.464	0.0054	2.157	0.0047
LT/EM009	1.7	212	1.144	0.0017	2.466	0.0069	2.156	0.0066
LT/EM010	1.9	210	1.144	0.0023	2.452	0.0048	2.143	0.0051
LT/EM011	2.1	216	1.145	0.0010	2.455	0.0058	2.144	0.0061
LT/EM012	2.3	213	1.144	0.0017	2.452	0.0020	2.143	0.0033
LT/EM013	2.5	228	1.144	0.0013	2.459	0.0051	2.149	0.0027
LT/EM014	2.7	213	1.144	0.0016	2.455	0.0070	2.146	0.0033
LT/EM015	2.9	222	1.144	0.0006	2.453	0.0040	2.144	0.0041
LT/EM016	3.1	222	1.143	0.0023	2.455	0.0069	2.147	0.0027
LT/EM017	3.3	223	1.144	0.0017	2.456	0.0037	2.147	0.0037
LT/EM018	3.5	218	1.143	0.0015	2.456	0.0043	2.148	0.0053
LT/EM019	3.7	225	1.143	0.0023	2.447	0.0021	2.140	0.0059
LT/EM020	3.9	218	1.145	0.0021	2.447	0.0055	2.137	0.0046
LT/EM021	4.1	219	1.147	0.0013	2.445	0.0082	2.133	0.0071
LT/EM022	4.3	224	1.145	0.0016	2.446	0.0054	2.137	0.0046
LT/EM023	4.5	231	1.145	0.0019	2.449	0.0037	2.138	0.0053
LT/EM024	4.7	241	1.147	0.0020	2.450	0.0076	2.137	0.0062
LT/EM025	4.9	243	1.146	0.0017	2.445	0.0072	2.134	0.0064

Table 5.3 Stable lead isotope ratio and Pb concentration (mg kg^{-1}) results for core LT/EM, continued.

Sample Code	Depth / cm	Pb / mg kg^{-1}	$^{206}Pb/^{207}Pb$	σ_{n-1}	$^{208}Pb/^{207}Pb$	σ_{n-1}	$^{208}Pb/^{206}Pb$	σ_{n-1}
LT/EM026	5.1	250	1.144	0.0036	2.446	0.0072	2.137	0.0042
LT/EM027	5.3	231	1.145	0.0013	2.443	0.0043	2.134	0.0049
LT/EM028	5.5	260	1.143	0.0020	2.435	0.0189	2.129	0.0137
LT/EM029	5.7	243	1.143	0.0006	2.441	0.0083	2.135	0.0068
LT/EM030	5.9	241	1.143	0.0023	2.441	0.0099	2.135	0.0055
LT/EM031	6.1	249	1.142	0.0030	2.432	0.0247	2.129	0.0190
LT/EM032	6.3	249	1.144	0.0019	2.439	0.0116	2.133	0.0081
LT/EM033	6.5	235	1.142	0.0010	2.438	0.0081	2.135	0.0064
LT/EM034	6.7	250	1.143	0.0023	2.448	0.0074	2.141	0.0046
LT/EM035	6.9	258	1.144	0.0015	2.440	0.0041	2.134	0.0053
LT/EM036	7.1	249	1.142	0.0019	2.438	0.0075	2.135	0.0063
LT/EM037	7.3	257	1.141	0.0022	2.439	0.0079	2.137	0.0051
LT/EM038	7.5	243	1.143	0.0013	2.445	0.0079	2.140	0.0057
LT/EM039	7.7	255	1.143	0.0013	2.438	0.0100	2.133	0.0078
LT/EM040	7.9	261	1.142	0.0012	2.440	0.0074	2.137	0.0043
LT/EM041	8.1	257	1.142	0.0020	2.434	0.0064	2.131	0.0043
LT/EM042	8.3	261	1.139	0.0019	2.427	0.0134	2.130	0.0123
LT/EM043	8.5	256	1.141	0.0018	2.426	0.0168	2.126	0.0117
LT/EM044	8.7	254	1.143	0.0018	2.434	0.0169	2.130	0.0148
LT/EM045	8.9	243	1.145	0.0012	2.463	0.0027	2.151	0.0018
LT/EM046	9.1	249	1.146	0.0009	2.471	0.0015	2.156	0.0020
LT/EM047	9.3	259	1.145	0.0027	2.469	0.0023	2.157	0.0026
LT/EM048	9.5	256	1.148	0.0024	2.505	0.0025	2.182	0.0039
LT/EM049	9.7	259	1.138	0.0007	2.367	0.0018	2.079	0.0016
LT/EM050	9.9	264	1.146	0.0003	2.468	0.0016	2.154	0.0014

Table 5.3 Stable lead isotope ratio and Pb concentration (mg kg^{-1}) results for core LT/EM, continued.

Sample Code	Depth / cm	Pb / mg kg^{-1}	$^{206}Pb/^{207}Pb$	σ_{n-1}	$^{208}Pb/^{207}Pb$	σ_{n-1}	$^{208}Pb/^{206}Pb$	σ_{n-1}
LT/EM051	10.1	258	1.144	0.0004	2.455	0.0005	2.145	0.0007
LT/EM052	10.3	267	1.146	0.0010	2.469	0.0039	2.155	0.0025
LT/EM053	10.5	269	1.146	0.0007	2.465	0.0023	2.152	0.0022
LT/EM054	10.7	269	1.144	0.0014	2.436	0.0064	2.130	0.0030
LT/EM055	10.9	269	1.143	0.0012	2.436	0.0062	2.132	0.0056
LT/EM056	11.1	265	1.144	0.0010	2.433	0.0056	2.127	0.0031
LT/EM057	11.3	264	1.144	0.0020	2.438	0.0044	2.130	0.0048
LT/EM058	11.5	270	1.145	0.0009	2.438	0.0041	2.130	0.0042
LT/EM059	11.7	275	1.143	0.0024	2.433	0.0052	2.128	0.0034
LT/EM060	11.9	260	1.144	0.0027	2.439	0.0068	2.131	0.0064
LT/EM061	12.1	278	1.144	0.0013	2.435	0.0059	2.129	0.0037
LT/EM062	12.3	274	1.144	0.0026	2.436	0.0096	2.130	0.0047
LT/EM063	12.5	280	1.142	0.0015	2.436	0.0044	2.133	0.0039
LT/EM064	12.7	275	1.142	0.0020	2.436	0.0051	2.133	0.0032
LT/EM065	12.9	281	1.144	0.0018	2.443	0.0031	2.135	0.0035
LT/EM066	13.1	273	1.143	0.0016	2.438	0.004	2.133	0.0026
LT/EM067	13.3	283	1.143	0.0007	2.439	0.0037	2.133	0.0029
LT/EM068	13.5	289	1.143	0.0030	2.438	0.0028	2.134	0.0055
LT/EM069	13.7	286	1.142	0.0012	2.433	0.0042	2.129	0.0026
LT/EM070	13.9	291	1.143	0.0013	2.434	0.0024	2.131	0.0021
LT/EM071	14.1	294	1.145	0.0017	2.436	0.0042	2.129	0.0023
LT/EM072	14.3	285	1.148	0.0028	2.451	0.0212	2.135	0.0136
LT/EM073	14.5	294	1.149	0.0025	2.450	0.0129	2.132	0.0072
LT/EM074	14.7	294	1.150	0.0015	2.452	0.0079	2.132	0.0055
LT/EM075	14.9	292	1.151	0.0034	2.468	0.0071	2.144	0.0040

Table 5.3 Stable lead isotope ratio and Pb concentration (mg kg^{-1}) results for core LT/EM, continued.

Sample Code	Depth / cm	Pb / mg kg^{-1}	$^{206}Pb/^{207}Pb$	σ_{n-1}	$^{208}Pb/^{207}Pb$	σ_{n-1}	$^{208}Pb/^{206}Pb$	σ_{n-1}
LT/EM076	15.1	299	1.144	0.0022	2.450	0.0055	2.141	0.0009
LT/EM077	15.3	289	1.143	0.0024	2.452	0.0063	2.146	0.0028
LT/EM078	15.5	300	1.141	0.0013	2.435	0.0154	2.134	0.0136
LT/EM079	15.7	288	1.141	0.0018	2.426	0.0122	2.126	0.0099
LT/EM080	15.9	304	1.140	0.0009	2.426	0.0073	2.128	0.0074
LT/EM081	16.1	296	1.145	0.0011	2.440	0.0029	2.131	0.0016
LT/EM082	16.3	296	1.146	0.0014	2.439	0.0023	2.128	0.0033
LT/EM083	16.5	294	1.146	0.0019	2.443	0.0052	2.131	0.0073
LT/EM084	16.7	297	1.147	0.0025	2.444	0.0038	2.130	0.0038
LT/EM085	16.9	287	1.146	0.0018	2.441	0.0028	2.130	0.0032
LT/EM086	17.1	301	1.147	0.0012	2.440	0.0016	2.127	0.0030
LT/EM087	17.3	315	1.146	0.0013	2.437	0.0027	2.126	0.0020
LT/EM088	17.5	313	1.146	0.0008	2.439	0.0029	2.128	0.0035
LT/EM089	17.7	305	1.146	0.0017	2.463	0.0134	2.150	0.0093
LT/EM090	17.9	304	1.145	0.0010	2.461	0.0045	2.149	0.0027
LT/EM091	18.1	310	1.145	0.0007	2.452	0.0103	2.141	0.0079
LT/EM092	18.3	309	1.146	0.0007	2.449	0.0055	2.137	0.0042
LT/EM093	18.5	309	1.145	0.0010	2.447	0.0071	2.137	0.0010
LT/EM094	18.7	304	1.145	0.0016	2.450	0.0087	2.139	0.0060
LT/EM095	18.9	281	1.146	0.0006	2.462	0.0110	2.148	0.0101
LT/EM096	19.1	308	1.147	0.0003	2.473	0.0033	2.157	0.0027
LT/EM097	19.3	315	1.147	0.0014	2.468	0.0125	2.152	0.0100
LT/EM098	19.5	300	1.143	0.0023	2.447	0.0078	2.140	0.0071
LT/EM099	19.7	301	1.144	0.0013	2.445	0.0114	2.137	0.0013
LT/EM100	19.9	326	1.145	0.0017	2.458	0.0078	2.147	0.0044

Table 5.3 Stable lead isotope ratio and Pb concentration (mg kg^{-1}) results for core LT/EM, continued.

Sample Code	Depth / cm	Pb / mg kg^{-1}	$^{206}Pb/^{207}Pb$	σ_{n-1}	$^{208}Pb/^{207}Pb$	σ_{n-1}	$^{208}Pb/^{206}Pb$	σ_{n-1}
LT/EM101	20.5	305	1.144	0.0012	2.462	0.0145	2.151	0.0119
LT/EM102	21.5	307	1.145	0.0015	2.450	0.0111	2.140	0.0075
LT/EM103	22.5	311	1.146	0.0028	2.456	0.0198	2.144	0.0143
LT/EM104	23.5	308	1.146	0.0010	2.456	0.0131	2.155	0.0098
LT/EM105	24.5	306	1.145	0.0009	2.468	0.0089	2.167	0.0067
LT/EM106	25.5	310	1.150	0.0018	2.453	0.0038	2.133	0.0032
LT/EM107	26.5	302	1.150	0.0018	2.454	0.0019	2.133	0.0027
LT/EM108	27.5	301	1.150	0.0017	2.449	0.0020	2.129	0.0028
LT/EM109	28.5	298	1.150	0.0003	2.454	0.0051	2.134	0.0042
LT/EM110	29.5	298	1.149	0.0019	2.453	0.0106	2.134	0.0072
LT/EM111	30.5	287	1.148	0.0038	2.451	0.0038	2.134	0.0025
LT/EM112	31.5	299	1.147	0.0018	2.416	0.0113	2.106	0.0084
LT/EM113	32.5	294	1.146	0.0009	2.439	0.0020	2.128	0.0024
LT/EM114	33.5	294	1.147	0.0011	2.442	0.0046	2.130	0.0037
LT/EM115	34.5	301	1.143	0.0024	2.429	0.0034	2.124	0.0027
LT/EM116	35.5	303	1.144	0.0010	2.432	0.0062	2.126	0.0061
LT/EM117	36.5	302	1.144	0.0028	2.430	0.0060	2.125	0.0027
LT/EM118	37.5	297	1.145	0.0011	2.430	0.0046	2.122	0.0046
LT/EM119	38.5	292	1.145	0.0011	2.433	0.0062	2.126	0.0051
LT/EM120	39.5	296	1.143	0.0021	2.429	0.0023	2.125	0.0029
LT/EM121	41	293	1.145	0.0012	2.429	0.0114	2.121	0.0101
LT/EM122	43	296	1.145	0.0013	2.434	0.0055	2.126	0.0031
LT/EM123	45	295	1.144	0.0019	2.433	0.0059	2.126	0.0057
LT/EM124	47	303	1.145	0.0013	2.442	0.0079	2.132	0.0058
LT/EM125	49	307	1.146	0.0017	2.437	0.0048	2.127	0.0021

Table 5.3 Stable lead isotope ratio and Pb concentration (mg kg^{-1}) results for core LT/EM, continued.

Sample Code	Depth / cm	Pb / mg kg^{-1}	$^{206}Pb/^{207}Pb$	σ_{n-1}	$^{208}Pb/^{207}Pb$	σ_{n-1}	$^{208}Pb/^{206}Pb$	σ_{n-1}
LT/EM126	51	323	1.144	0.0024	2.429	0.0046	2.123	0.0035
LT/EM127	53	321	1.147	0.0011	2.437	0.0028	2.125	0.0024
LT/EM128	55	319	1.147	0.0018	2.436	0.0025	2.124	0.0035
LT/EM129	57	326	1.147	0.0012	2.434	0.0083	2.122	0.0055
LT/EM130	59	327	1.147	0.0016	2.435	0.0026	2.124	0.0019
LT/EM131	61	325	1.145	0.0015	2.434	0.0024	2.125	0.0028
LT/EM132	63	334	1.148	0.0020	2.434	0.0099	2.120	0.0060
LT/EM133	65	338	1.148	0.0008	2.438	0.0024	2.124	0.0024
LT/EM134	67	335	1.148	0.0012	2.438	0.0033	2.124	0.0033
LT/EM135	69	343	1.147	0.0009	2.441	0.0024	2.129	0.0021
LT/EM136	71	349	1.148	0.0016	2.437	0.0058	2.123	0.0034
LT/EM137	73	352	1.148	0.0011	2.437	0.0038	2.122	0.0021
LT/EM138	75	358	1.147	0.0006	2.438	0.0022	2.127	0.0025
LT/EM139	77	367	1.145	0.0014	2.422	0.0016	2.115	0.0030
LT/EM140	79	369	1.148	0.0016	2.423	0.0028	2.111	0.0033
LT/EM141	86	393	1.146	0.0007	2.402	0.0043	2.095	0.0033

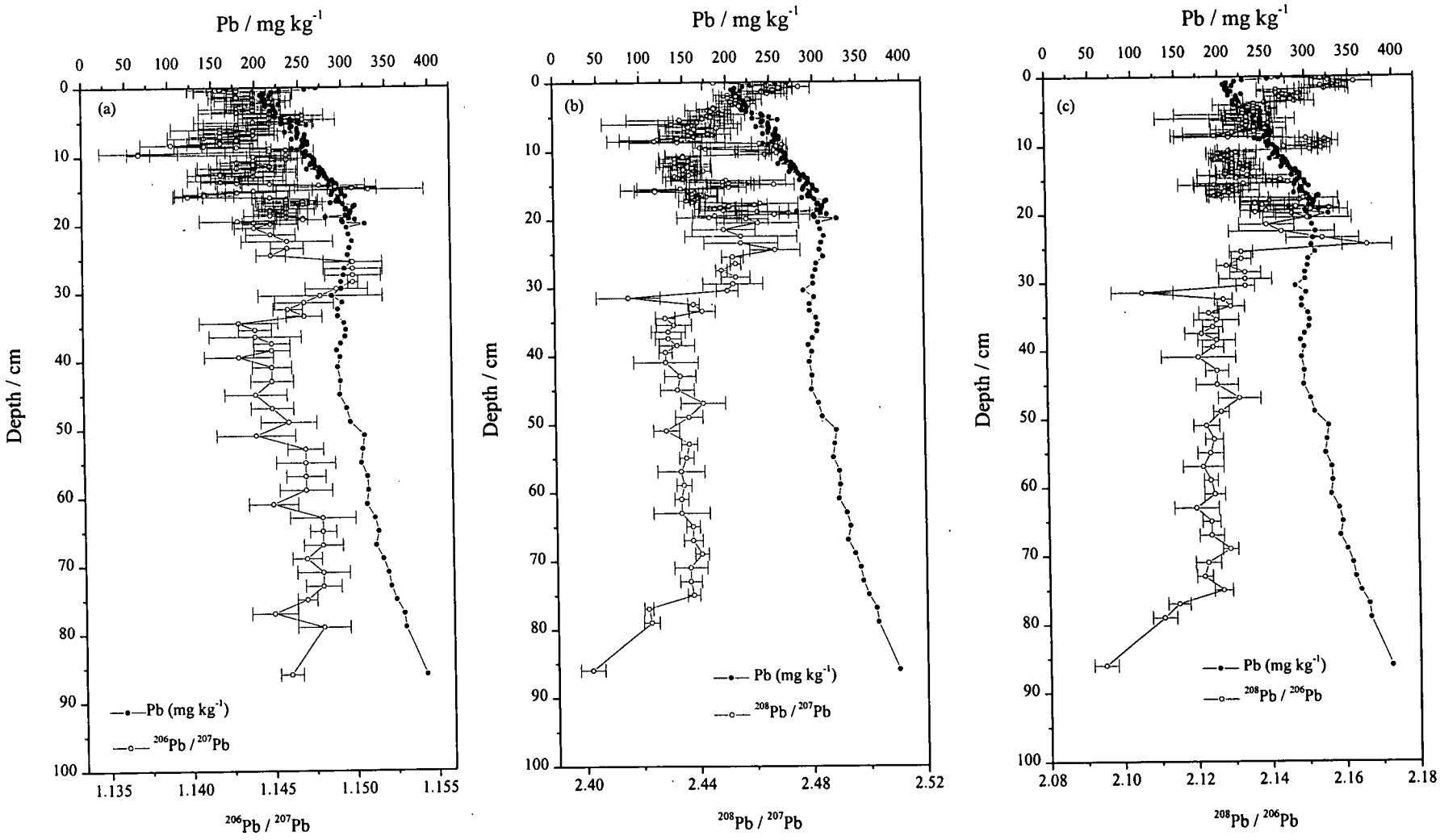

Figure 5.11 Stable Pb isotope ratios and Pb concentration (mg kg^{-1}) in core LT/EM: (a) ^{206}Pb / ^{207}Pb, (b)^{208}Pb / ^{207}Pb and (c)^{208}Pb / ^{206}Pb

Table 5.4 (a) Stream sediment samples from Loch Tay catchment, northern shore.

Sample	Pb / mg kg^{-1}	$^{206}Pb/^{207}Pb$	σ_{n-1}	$^{208}Pb/^{207}Pb$	σ_{n-1}	$^{208}Pb/^{206}Pb$	σ_{n-1}
Fearnan	30	1.158	0.0015	2.460	0.0013	2.124	0.0026
Outdoor centre	10	1.172	0.0015	2.479	0.0038	2.115	0.0019
Forestry 1	4.8	1.175	0.0023	2.471	0.0053	2.103	0.0014
Forestry 2	2.5	1.205	0.0022	2.534	0.0016	2.102	0.0031
Forestry 3	3.9	1.193	0.0023	2.509	0.0051	2.103	0.0029
Allt Coire Phadairlidh	3.7	1.190	0.0013	2.488	0.0034	2.091	0.0029
Cloan Lawers Farm	0.89	1.178	0.0019	2.469	0.0042	2.096	0.0012
Lawers Burn	10.2	1.178	0.0019	2.469	0.0042	2.096	0.0012
Allt an Tuim Bhric	7.1	1.181	0.0013	2.475	0.0035	2.095	0.0015
Burn of Edramucky	6.5	1.170	0.0010	2.446	0.0025	2.090	0.0015
Allt Tir Artair	18.8	1.168	0.0009	2.456	0.0010	2.102	0.0008
Allt a' Bhaile Chruinn	6	1.169	0.0013	2.468	0.0021	2.111	0.0032
Loch Tay (c)	4.5	1.181	0.0015	2.503	0.0029	2.120	0.0025

Table 5.4 (b) Stream sediment samples from Loch Tay catchment, southern shore (Lancaster, 1996).

Sample	Pb / mg kg^{-1}	$^{206}Pb/^{207}Pb$	σ_{n-1}
Allt Ruadh	46	1.156	0.003
Lurglomand Burn	23	1.144	0.004
Achianich Burn	19	1.157	0.006
Allt an Duin	20	1.143	0.005
Allt nan Cno	19	1.161	0.007
Ardradnaig	47	1.155	0.004
Kepranich	120	1.140	0.003
Shenlarich	98	1.139	0.003
Skaig	17	1.151	0.007

5.4.1.6 X-Ray diffraction.

The two samples analysed from core LT/EM (LT/EM38 and 132) were identical with respect to the types of minerals identified and the quantity of the minerals present. The following minerals were identified: quartz, muscovite, albite, and clinochlore. The following is a summary of the formulae and some structural properties of the minerals identified.

Quartz: SiO_2 framework silicate

Muscovite: $K_2(Si_6Al_2)(Al_4)O_{20}(OH)_4$ and $K_2(Si_7Al_1)(Al,Fe^{3+})_3(Mg,Fe^{2+})O_{20}(OH)_4$
Mica, 2:1 dioctahedral, layer silicate, 10 Å.

Albite: $NaAlSi_3O_8$
Feldspar, framework silicate, 3.19 Å.

Clinochlore: $(Si_{8-x}, Al_x)(Mg_{12-y}, Al_y)O_{20}(OH)_{16}$
Chlorite, layer silicate, trioctahedral

5.5 Discussion.

5.5.1 Radiocaesium.

Following the procedure previously established, the two peaks in ^{137}Cs activity (Figure 5.2) can be assigned to the Chernobyl accident in May 1986 and nuclear weapons testing in the 1950-1960s. In order to estimate the accumulation rate, a graph of ^{137}Cs against depth as a function of cumulative weight per unit area is plotted in Figure 5.12. If the two peaks are taken to represent 1986 and 1963 respectively, the accumulation rate over the following age increments can be calculated: 1996-1986, 1986-1963 and 1996-1963. This procedure gives accumulation rates of 38.9 ± 0.7, 30.9 ± 1.9 and 33.6 ± 1.1 mg cm^{-2} y^{-1}, respectively. The values are all quite close but suggest that there has been a relatively recent increase in sedimentation rate. Extrapolation of the rate 33.6 mg cm^{-2} y^{-1} to 30 cm (the base of the core LT/EJ), where there is still a detectable amount of ^{137}Cs, gives a

Figure 5.12 ^{137}Cs vs cumulative depth (g cm^{-2}) in core LT/EJ.

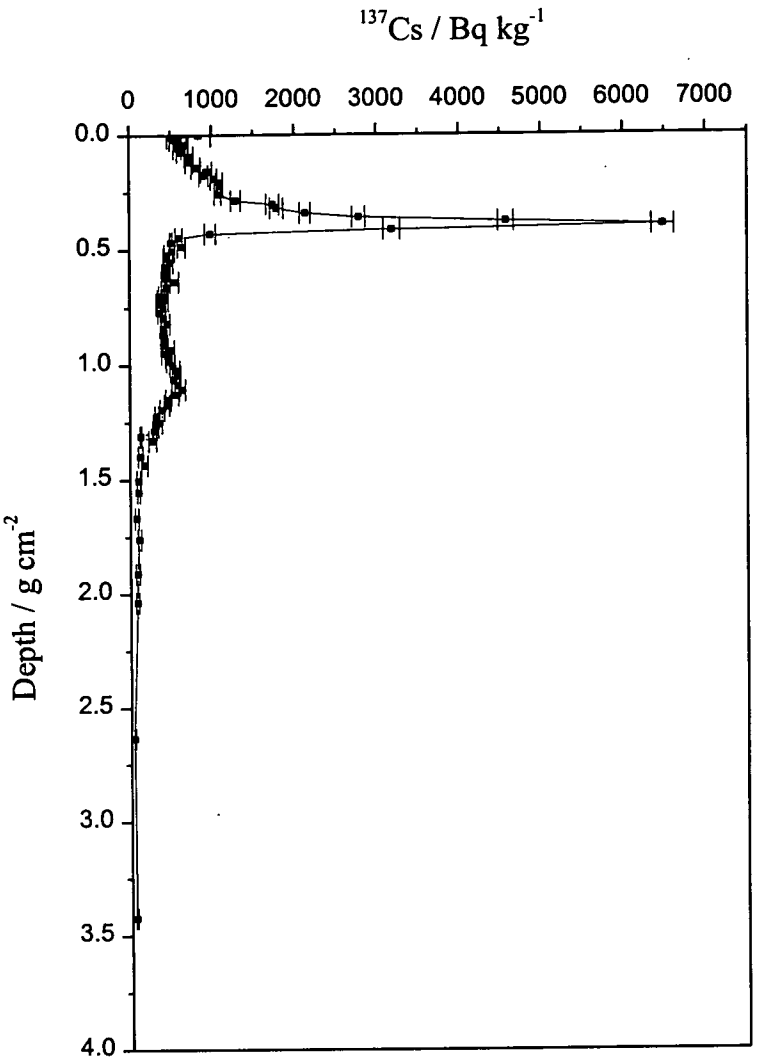

date of ~1886. As this date is considerably earlier than the known influx of the radionuclide into the environment, there has therefore been some post-depositional movement of radiocaesium.

Any ^{134}Cs that may originally have been present from the Chernobyl accident has decayed to non-detectable levels due to its short half life of 2.05 years. Therefore it is not possible to separate fully the inventories from the two sources of ^{137}Cs. However, if it is assumed that the constant value of 404 ± 26 Bq kg^{-1}, which is maintained between the two peaks, is a contribution from the continued input of weapons testing ^{137}Cs from the catchment, and continues to the surface, an approximate indication of the inventories can be calculated. Using the above assumptions, values of 6.58 kBq m^{-2} for Chernobyl (corrected to 1986) and 12.53 kBq m^{-2} for weapons testing (corrected to 1963) are obtained. If, however, it is taken that there is no weapons contribution above the Chernobyl peak then values of 7.67 and 10.66 kBq m^{-2} are obtained for Chernobyl and weapons, respectively. These values are similar to those reported for Loch Tay west where the inventory for Chernobyl was 7.13 kBq m^{-2}, and for weapons testing was 9.41 kBq m^{-2}[♦] (Kesterton, 1993).

5.5.2 ^{210}Pb.

In order to calculate an accumulation rate for the core LT/EJ a graph of ln ($^{210}Pb_{unsupp}$) against depth (g cm^{-2}) was plotted (Figure 5.13 (a)) where the $^{210}Pb_{unsupp}$ was calculated by subtracting a value of 83 Bq kg^{-1} (base section) from each section (with the assumption that this represents the supported level). The results from the calculations are shown in Table 5.5. A weighted linear regression was carried out in order to obtain the gradient (-0.776 err 0.053), and hence the sedimentation rate, 40.1 ± 2.9 mg cm^{-2} y^{-1}. As the top portion of the graph is highly irregular to just above the position of the Chernobyl peak, a further two graphs were prepared by

[♦] Using an assumption that weapons testing fallout extends into region of Chernobyl peak.

Figure 5.13 ln $^{210}Pb_{unsupported}$ vs depth (g cm^{-2}) in core LT/EJ:
(a) all points, (b) points 1-23 and (c) points 23-base.

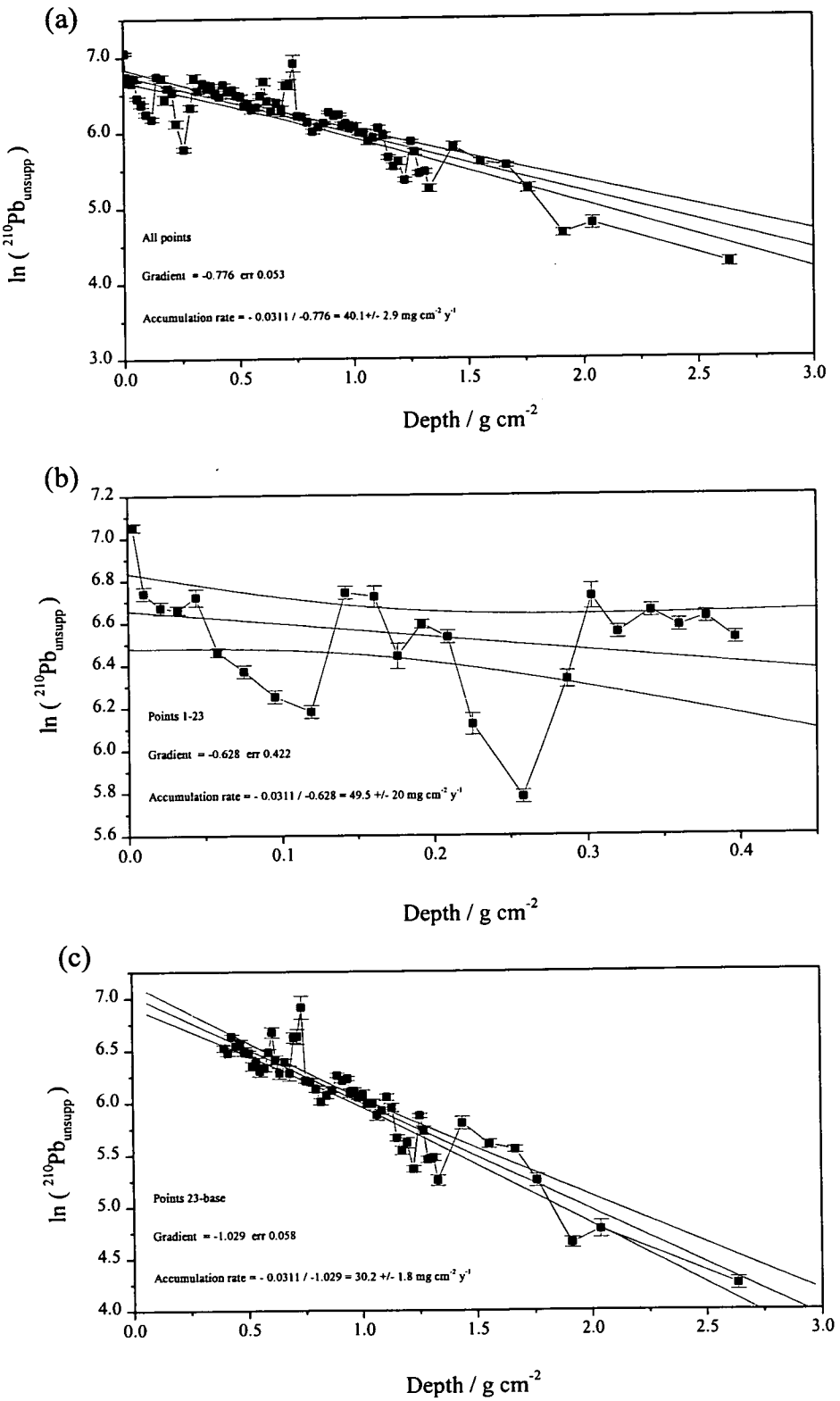

Table 5.5 Calculations for the ^{210}Pb CIC and CRS models applied to core LT/EJ.

Sample Code	Mid cum wt / g cm^{-2}	^{210}Pb / Bq kg^{-1}	σ(O)	$^{210}Pb_{unsupp}$ / Bq kg^{-1}	σ(O)	ln $^{210}Pb_{unsupp}$	σ-pos	σ-neg	σ-ave	Section wt. to base / kg m^{-2}	Cum. inventory $^{210}Pb_{unsupp}$ / Bq m^{-2}	Yrs accum to base of section	Date (CRS) to base of section
EJ001	0.003	1234	25	1151	25	7.05	0.02	0.02	0.02	0.053	61	0.2	1995.4
EJ002	0.010	929	26	846	26	6.74	0.03	0.03	0.03	0.102	147	0.5	1995.1
EJ003	0.021	873	24	790	24	6.67	0.03	0.03	0.03	0.108	233	0.8	1994.8
EJ004	0.032	867	19	784	19	6.66	0.02	0.02	0.02	0.114	322	1.1	1994.5
EJ005	0.044	913	30	830	30	6.72	0.04	0.04	0.04	0.120	421	1.5	1994.1
EJ006	0.058	721	15	638	15	6.46	0.02	0.02	0.02	0.170	530	1.9	1993.7
EJ007	0.075	669	18	586	18	6.37	0.03	0.03	0.03	0.177	633	2.2	1993.4
EJ008	0.095	601	16	518	16	6.25	0.03	0.03	0.03	0.217	746	2.7	1992.9
EJ009	0.119	567	16	484	16	6.18	0.03	0.03	0.03	0.261	872	3.1	1992.5
EJ010	0.142	930	27	848	28	6.74	0.03	0.03	0.03	0.197	1038	3.8	1991.8
EJ011	0.161	909	42	826	42	6.72	0.05	0.05	0.05	0.187	1193	4.4	1991.2
EJ012	0.176	707	36	624	36	6.44	0.06	0.06	0.06	0.107	1260	4.6	1991.0
EJ013	0.192	809	15	726	15	6.59	0.02	0.02	0.02	0.212	1414	5.2	1990.4
EJ014	0.209	767	21	684	21	6.53	0.03	0.03	0.03	0.129	1502	5.6	1990.0
EJ015	0.225	540	23	457	23	6.12	0.05	0.05	0.05	0.197	1591	6.0	1989.6
EJ016	0.258	406	10	323	10	5.78	0.03	0.03	0.03	0.453	1738	6.6	1989.0
EJ017	0.287	646	21	563	21	6.33	0.04	0.04	0.04	0.145	1819	6.9	1988.7
EJ018	0.303	913	48	830	48	6.72	0.06	0.06	0.06	0.163	1955	7.5	1988.1
EJ019	0.320	785	20	702	20	6.55	0.03	0.03	0.03	0.190	2088	8.1	1987.5
EJ020	0.342	853	25	770	26	6.65	0.03	0.03	0.03	0.240	2273	8.9	1986.7
EJ021	0.360	802	18	719	18	6.58	0.02	0.03	0.03	0.118	2358	9.3	1986.3
EJ022	0.378	835	23	752	23	6.62	0.03	0.03	0.03	0.238	2536	10.1	1985.5
EJ023	0.397	759	18	676	18	6.52	0.03	0.03	0.03	0.151	2638	10.6	1985.0
EJ024	0.414	730	15	647	15	6.47	0.02	0.02	0.02	0.179	2754	11.1	1984.5
EJ025	0.431	837	15	754	15	6.63	0.02	0.02	0.02	0.174	2885	11.8	1983.8

Table 5.5 Calculations for the ^{210}Pb CIC and CRS models applied to core LT/EJ, continued.

Sample Code	Mid cum wt / g cm^{-2}	^{210}Pb / Bq kg^{-1}	σ(O)	$^{210}Pb_{unsupp}$ / Bq kg^{-1}	σ(O)	ln $^{210}Pb_{unsupp}$	σ-pos	σ-neg	σ-ave	Section wt. to base / kg m^{-2}	Cum. inventory $^{210}Pb_{unsupp}$ / Bq m^{-2}	Yrs accum to base of section	Date (CRS) to base of section
EJ026	0.449	773	34	690	34	6.54	0.05	0.05	0.05	0.188	3015	12.4	1983.2
EJ027	0.469	789	27	706	27	6.56	0.04	0.04	0.04	0.213	3166	13.2	1982.4
EJ028	0.487	740	23	657	24	6.49	0.04	0.04	0.04	0.148	3263	13.7	1981.9
EJ029	0.505	731	20	649	20	6.47	0.03	0.03	0.03	0.204	3395	14.4	1981.2
EJ030	0.522	655	22	572	22	6.35	0.04	0.04	0.04	0.143	3477	14.8	1980.8
EJ031	0.537	673	27	590	27	6.38	0.04	0.05	0.05	0.158	3570	15.3	1980.3
EJ032	0.554	628	24	545	25	6.30	0.04	0.05	0.05	0.172	3664	15.8	1979.8
EJ033	0.573	642	15	559	15	6.33	0.03	0.03	0.03	0.219	3786	16.5	1979.1
EJ034	0.592	732	21	649	21	6.48	0.03	0.03	0.03	0.149	3882	17.1	1978.5
EJ035	0.606	869	38	786	38	6.67	0.05	0.05	0.05	0.140	3993	17.7	1977.9
EJ036	0.621	692	27	609	27	6.41	0.04	0.04	0.04	0.155	4087	18.3	1977.3
EJ037	0.639	618	25	535	25	6.28	0.05	0.05	0.05	0.197	4192	18.9	1976.7
EJ038	0.662	680	20	597	20	6.39	0.03	0.03	0.03	0.265	4351	19.9	1975.7
EJ039	0.683	615	38	532	38	6.28	0.07	0.07	0.07	0.164	4438	20.5	1975.1
EJ040	0.701	834	40	751	40	6.62	0.05	0.05	0.05	0.186	4577	21.4	1974.2
EJ041	0.718	839	52	756	52	6.63	0.07	0.07	0.07	0.152	4692	22.2	1973.4
EJ042	0.735	1081	110	998	110	6.91	0.10	0.12	0.11	0.191	4883	23.5	1972.1
EJ043	0.753	583	12	500	12	6.21	0.02	0.02	0.02	0.174	4970	24.1	1971.5
EJ044	0.773	574	14	491	14	6.20	0.03	0.03	0.03	0.220	5078	24.9	1970.7
EJ045	0.797	543	12	460	12	6.13	0.03	0.03	0.03	0.262	5199	25.8	1969.8
EJ046	0.821	492	11	409	11	6.01	0.03	0.03	0.03	0.213	5286	26.5	1969.1
EJ047	0.844	517	13	435	13	6.07	0.03	0.03	0.03	0.248	5394	27.4	1968.2
EJ048	0.869	536	11	454	11	6.12	0.02	0.02	0.02	0.268	5515	28.3	1967.3
EJ049	0.891	604	13	521	13	6.26	0.02	0.02	0.02	0.171	5604	29.1	1966.5
EJ050	0.915	581	12	498	12	6.21	0.02	0.02	0.02	0.302	5754	30.4	1965.2

Table 5.5 Calculations for the ^{210}Pb CIC and CRS models applied to core LT/EJ, continued.

Sample Code	Mid cum wt / g cm^{-2}	^{210}Pb / Bq kg^{-1}	σ(O)	$^{210}Pb_{unsupp}$ / Bq kg^{-1}	σ(O)	ln $^{210}Pb_{unsupp}$	σ-pos	σ-neg	σ-ave	Section wt. to base / kg m^{-2}	Cum. inventory $^{210}Pb_{unsupp}$ / Bq m^{-2}	Yrs accum to base of section	Date (CRS) to base of section
EJ051	0.936	591	12	508	12	6.23	0.02	0.02	0.02	0.121	5816	30.9	1964.7
EJ052	0.950	525	19	442	19	6.09	0.04	0.04	0.04	0.154	5884	31.5	1964.1
EJ053	0.965	535	15	452	15	6.11	0.03	0.03	0.03	0.141	5947	32.1	1963.5
EJ054	0.983	509	8	426	8	6.05	0.02	0.02	0.02	0.220	6041	33.0	1962.6
EJ055	1.003	518	21	435	21	6.07	0.05	0.05	0.05	0.191	6124	33.8	1961.8
EJ056	1.024	481	13	398	13	5.99	0.03	0.03	0.03	0.229	6215	34.7	1960.9
EJ057	1.045	482	17	399	18	5.99	0.04	0.04	0.04	0.196	6294	35.5	1960.1
EJ058	1.064	442	16	359	16	5.88	0.04	0.05	0.05	0.177	6357	36.2	1959.4
EJ059	1.086	454	11	371	11	5.92	0.03	0.03	0.03	0.256	6452	37.2	1958.4
EJ060	1.108	505	14	422	14	6.05	0.03	0.03	0.03	0.185	6530	38.0	1957.6
EJ061	1.129	467	16	384	16	5.95	0.04	0.04	0.04	0.240	6623	39.1	1956.5
EJ062	1.152	370	9	287	9	5.66	0.03	0.03	0.03	0.219	6686	39.8	1955.8
EJ063	1.174	338	11	255	11	5.54	0.04	0.04	0.04	0.223	6742	40.5	1955.1
EJ064	1.195	355	13	272	13	5.61	0.05	0.05	0.05	0.198	6796	41.1	1954.5
EJ065	1.223	296	7	213	7	5.36	0.03	0.03	0.03	0.361	6873	42.1	1953.5
EJ066	1.251	438	8	355	8	5.87	0.02	0.02	0.02	0.188	6940	43.0	1952.6
EJ067	1.268	390	13	307	13	5.73	0.04	0.04	0.04	0.152	6987	43.6	1952.0
EJ068	1.287	316	8	233	8	5.45	0.03	0.03	0.03	0.246	7044	44.3	1951.3
EJ069	1.311	319	8	236	8	5.47	0.03	0.03	0.03	0.236	7100	45.1	1950.5
EJ070	1.330	274	10	191	10	5.25	0.05	0.05	0.05	0.126	7124	45.4	1950.2
EJ071	not analysed									0.217	7167	46.0	1949.6
EJ072										0.298	7227	46.9	1948.7
EJ073										0.210	7269	47.5	1948.1
EJ074										0.198	7308	48.1	1947.5
EJ075	1.436	414	19	331	19	5.80	0.05	0.06	0.06	0.162	7362	49.0	1946.6

Table 5.5 Calculations for the ^{210}Pb CIC and CRS models applied to core LT/EJ, continued.

Sample Code	Mid cum wt / g cm^{-2}	^{210}Pb / Bq kg^{-1}	σ(O)	$^{210}Pb_{unsupp}$ / Bq kg^{-1}	σ(O)	ln $^{210}Pb_{unsupp}$	σ-pos	σ-neg	σ-ave	Section wt. to base / kg m^{-2}	Cum. inventory $^{210}Pb_{unsupp}$ / Bq m^{-2}	Yrs accum to base of section	Date (CRS) to base of section
EJ076	not analysed									0.274	7417	49.8	1945.8
EJ077										0.186	7454	50.4	1945.2
EJ078										0.277	7509	51.4	1944.2
EJ079										0.247	7559	52.2	1943.4
EJ080	1.555	352	11	269	11	5.60	0.04	0.04	0.04	0.254	7627	53.4	1942.2
EJ081										0.186	7664	54.1	1941.5
EJ082										0.194	7703	54.8	1940.8
EJ083										0.272	7758	55.8	1939.8
EJ084										0.249	7808	56.8	1938.8
EJ085	1.668	341	7	258	7	5.55	0.03	0.03	0.03	0.203	7860	57.9	1937.7
EJ086										0.182	7896	58.7	1936.9
EJ087										0.200	7936	59.5	1936.1
EJ088										0.136	7964	60.1	1935.5
EJ089										0.198	8003	61.0	1934.6
EJ090	1.761	273	11	190	11	5.25	0.06	0.06	0.06	0.214	8044	61.9	1933.7
EJ091										0.273	8098	63.2	1932.4
EJ092										0.399	8178	65.3	1930.3
EJ093										0.389	8256	67.3	1928.3
EJ094										0.229	8302	68.6	1927.0
EJ095	1.912	188	4	105	5	4.65	0.05	0.05	0.05	0.233	8326	69.4	1926.2
EJ096										0.226	8349	70.0	1925.6
EJ097										0.287	8378	70.9	1924.7
EJ098										0.282	8406	71.8	1923.8
EJ099										0.228	8429	72.5	1923.1
EJ100	2.039	202	9	119	9	4.78	0.07	0.08	0.08	0.244	8458	73.5	1922.1

Table 5.5 Calculations for the ^{210}Pb CIC and CRS models applied to core LT/EJ, continued.

Sample Code	Mid cum wt / g cm^{-2}	^{210}Pb / Bq kg^{-1}	σ(O)	$^{210}Pb_{unsupp}$ / Bq kg^{-1}	σ(O)	ln $^{210}Pb_{unsupp}$	σ-pos	σ-neg	σ-ave	Section wt. to base / kg m^{-2}	Cum. inventory $^{210}Pb_{unsupp}$ / Bq m^{-2}	Yrs accum to base of section	Date (CRS) to base of section
EJ101	not analysed									1.101	8568	77.4	1918.2
EJ102										1.312	8699	82.8	1912.8
EJ103										1.262	8825	89.1	1906.5
EJ104										1.561	8981	98.9	1896.7
EJ105	2.635	153	3	70	4	4.25	0.05	0.06	0.06	1.221	9067	106.0	1889.6
EJ106										1.523	9143	113.9	1881.7
EJ107										1.588	9222	125.0	1870.6
EJ108										1.376	9291	139.2	1856.4
EJ109										2.476	9415	406.8	1588.8
EJ110	3.424	83	2	0	3					0.629			

plotting from points 1-23 (Fig. 5.13 (b)) and from point 23 to the base of the core (Fig. 5.12 (c)). The two graphs gave gradients of -0.628 (err 0.422) and -1.029, (err 0.058), respectively, and sedimentation rates of 49.5 ± 20 and 30.2 ± 1.8 mg cm^{-2} y^{-1}, respectively.

The CRS model is difficult to apply to this core since not all of the sections were analysed. However, in order to give an approximate set of values and to allow an assessment of the ^{210}Pb inventory and average flux it was assumed that the inventories of unanalysed sections were between those of overlying and underlying sections that were analysed. The calculated results for each section are summarised in Table 5.5 and the dates derived shown together with the ^{137}Cs and the ^{210}Pb CIC derived chronology in Table 5.6 (a).

The approximate flux of ^{210}Pb to the sediment is 293 Bq m^{-2} y^{-1} and the total $^{210}Pb_{unsupp}$ inventory is 9.42 kBq m^{-2} at this site in Loch Tay. These probably represent minimum values due to (a) the approximations made for the unanalysed sections and (b) the fact that a constant ^{210}Pb value had not been reached by the base of the core. The flux is high in comparison to that for Loch Lomond south (113 Bq m^{-2} y^{-1}) but lower than that seen for Loch Lomond north (554 Bq m^{-2} y^{-1}).

Table 5.6 (a) Comparison of chronologies for core LT/EJ using ^{210}Pb and ^{137}Cs.

Sample Code	Depth Midpoint / cm	Mid cum wt / g cm^{-2}	^{210}Pb / 49.5 mg cm^{-2} y^{-1} to section 23 then 30.2 mg cm^{-2} y^{-1} to base		^{137}Cs / 38.9 mg cm^{-2} y^{-1} to section 23 then 30.9 mg cm^{-2} y^{-1} to base		CRS ^{210}Pb model		
			Yrs Accum.	Date	Yrs Accum.	Date	Cum. wt to base.	Yrs Accum.	Date
EJ001	0.1	0.003	0.1	1995.5	0.1	1995.5	0.005	0.2	1995.4
EJ002	0.3	0.010	0.2	1995.4	0.3	1995.3	0.011	0.5	1995.1
EJ003	0.5	0.021	0.4	1995.2	0.5	1995.1	0.012	0.8	1994.8
EJ004	0.7	0.032	0.6	1995.0	0.8	1994.8	0.013	1.1	1994.5
EJ005	0.9	0.044	0.9	1994.7	1.1	1994.5	0.013	1.5	1994.1
EJ006	1.1	0.058	1.2	1994.4	1.5	1994.1	0.018	1.9	1993.7
EJ007	1.3	0.075	1.5	1994.1	1.9	1993.7	0.020	2.2	1993.4
EJ008	1.5	0.095	1.9	1993.7	2.4	1993.2	0.024	2.7	1992.9
EJ009	1.7	0.119	2.4	1993.2	3.1	1992.5	0.028	3.1	1992.5
EJ010	1.9	0.142	2.9	1992.7	3.6	1992.0	0.023	3.8	1991.8
EJ011	2.1	0.161	3.3	1992.3	4.1	1991.5	0.021	4.4	1991.2
EJ012	2.3	0.176	3.6	1992.0	4.5	1991.1	0.013	4.6	1991.0
EJ013	2.5	0.192	3.9	1991.7	4.9	1990.7	0.022	5.2	1990.4
EJ014	2.7	0.209	4.2	1991.4	5.4	1990.2	0.015	5.6	1990.0
EJ015	2.9	0.225	4.5	1991.1	5.8	1989.8	0.021	6.0	1989.6
EJ016	3.1	0.258	5.2	1990.4	6.6	1989.0	0.047	6.6	1989.0
EJ017	3.3	0.287	5.8	1989.8	7.4	1988.2	0.019	6.9	1988.7
EJ018	3.5	0.303	6.1	1989.5	7.8	1987.8	0.018	7.5	1988.1
EJ019	3.7	0.320	6.5	1989.1	8.2	1987.4	0.021	8.1	1987.5
EJ020	3.9	0.342	6.9	1988.7	8.8	1986.8	0.026	8.9	1986.7
EJ021	4.1	0.360	7.3	1988.3	9.3	1986.3	0.014	9.3	1986.3
EJ022	4.3	0.378	7.6	1988.0	9.7	1985.9	0.025	10.1	1985.5
EJ023	4.5	0.397	8.0	1987.6	10.2	1985.4	0.018	10.6	1985.0
EJ024	4.7	0.414	0.5	1987.0	0.5	1984.9	0.020	11.1	1984.5
EJ025	4.9	0.431	1.1	1986.4	1.1	1984.3	0.019	11.8	1983.8

Table 5.6 (a) Comparison of chronologies for core LT/EJ using ^{210}Pb and ^{137}Cs, continued.

Sample Code	Depth Midpoint / cm	Mid cum wt / g cm^{-2}	^{210}Pb / 49.5 mg cm^{-2} y^{-1} to section 23 then 30.2 mg cm^{-2} y^{-1} to base		^{137}Cs / 38.9 mg cm^{-2} y^{-1} to section 23 then 30.9 mg cm^{-2} y^{-1} to base		Cum. wt to base.	CRS ^{210}Pb model	
			Yrs Accum.	Date	Yrs Accum.	Date		Yrs Accum.	Date
EJ026	5.1	0.449	1.7	1985.8	1.7	1983.7	0.021	12.4	1983.2
EJ027	5.3	0.469	2.4	1985.2	2.3	1983.1	0.023	13.2	1982.4
EJ028	5.5	0.487	3.0	1984.6	2.9	1982.5	0.017	13.7	1981.9
EJ029	5.7	0.505	3.6	1984.0	3.5	1981.9	0.022	14.4	1981.2
EJ030	5.9	0.522	4.1	1983.4	4.1	1981.3	0.017	14.8	1980.8
EJ031	6.1	0.537	4.6	1982.9	4.5	1980.9	0.017	15.3	1980.3
EJ032	6.3	0.554	5.2	1982.4	5.1	1980.3	0.019	15.8	1979.8
EJ033	6.5	0.573	5.8	1981.7	5.7	1979.7	0.024	16.5	1979.1
EJ034	6.7	0.592	6.4	1981.1	6.3	1979.1	0.017	17.1	1978.5
EJ035	6.9	0.606	6.9	1980.7	6.8	1978.6	0.016	17.7	1977.9
EJ036	7.1	0.621	7.4	1980.2	7.2	1978.1	0.017	18.3	1977.3
EJ037	7.3	0.639	8.0	1979.6	7.8	1977.6	0.021	18.9	1976.7
EJ038	7.5	0.662	8.8	1978.8	8.6	1976.8	0.029	19.9	1975.7
EJ039	7.7	0.683	9.5	1978.1	9.3	1976.1	0.019	20.5	1975.1
EJ040	7.9	0.701	10.1	1977.5	9.8	1975.6	0.020	21.4	1974.2
EJ041	8.1	0.718	10.6	1977.0	10.4	1975.0	0.017	22.2	1973.4
EJ042	8.3	0.735	11.2	1976.4	10.9	1974.5	0.021	23.5	1972.1
EJ043	8.5	0.753	11.8	1975.8	11.5	1973.9	0.019	24.1	1971.5
EJ044	8.7	0.773	12.4	1975.1	12.2	1973.2	0.024	24.9	1970.7
EJ045	8.9	0.797	13.2	1974.3	12.9	1972.5	0.029	25.8	1969.8
EJ046	9.1	0.821	14.0	1973.6	13.7	1971.7	0.024	26.5	1969.1
EJ047	9.3	0.844	14.8	1972.8	14.4	1970.9	0.027	27.4	1968.2
EJ048	9.5	0.869	15.6	1971.9	15.3	1970.1	0.029	28.3	1967.3
EJ049	9.7	0.891	16.4	1971.2	16.0	1969.4	0.020	29.1	1966.5
EJ050	9.9	0.915	17.1	1970.4	16.8	1968.6	0.032	30.4	1965.2

Table 5.6 (a) Comparison of core chronology for core LT/EJ using ^{210}Pb and ^{137}Cs, continued.

Sample Code	Depth Midpoint / cm	Mid cum wt / g cm^{-2}	^{210}Pb / 49.5 mg cm^{-2} y^{-1} to section 23 then 30.2 mg cm^{-2} y^{-1} to base		^{137}Cs / 38.9 mg cm^{-2} y^{-1} to section 23 then 30.9 mg cm^{-2} y^{-1} to base		Cum. wt to base.	CRS ^{210}Pb model	
			Yrs Accum.	Date	Yrs Accum.	Date		Yrs Accum.	Date
EJ051	10.1	0.936	17.8	1969.7	17.4	1968.0	0.015	30.9	1964.7
EJ052	10.3	0.950	18.3	1969.3	17.9	1967.5	0.017	31.5	1964.1
EJ053	10.5	0.965	18.8	1968.8	18.4	1967.0	0.016	32.1	1963.5
EJ054	10.7	0.983	19.4	1968.2	18.9	1966.4	0.024	33.0	1962.6
EJ055	10.9	1.003	20.1	1967.5	19.6	1965.8	0.021	33.8	1961.8
EJ056	11.1	1.024	20.8	1966.8	20.3	1965.1	0.025	34.7	1960.9
EJ057	11.3	1.045	21.5	1966.1	21.0	1964.4	0.022	35.5	1960.1
EJ058	11.5	1.064	22.1	1965.5	21.6	1963.8	0.020	36.2	1959.4
EJ059	11.7	1.086	22.8	1964.8	22.3	1963.1	0.028	37.2	1958.4
EJ060	11.9	1.108	23.5	1964.0	23.0	1962.4	0.021	38.0	1957.6
EJ061	12.1	1.129	24.2	1963.3	23.7	1961.7	0.026	39.1	1956.5
EJ062	12.3	1.152	25.0	1962.6	24.4	1961.0	0.025	39.8	1955.8
EJ063	12.5	1.174	25.7	1961.8	25.1	1960.2	0.025	40.5	1955.1
EJ064	12.7	1.195	26.4	1961.2	25.8	1959.6	0.022	41.1	1954.5
EJ065	12.9	1.223	27.3	1960.2	26.7	1958.7	0.038	42.1	1953.5
EJ066	13.1	1.251	28.3	1959.3	27.6	1957.8	0.023	43.0	1952.6
EJ067	13.3	1.268	28.8	1958.8	28.2	1957.2	0.017	43.6	1952.0
EJ068	13.5	1.287	29.5	1958.1	28.8	1956.6	0.026	44.3	1951.3
EJ069	13.7	1.311	30.3	1957.3	29.6	1955.8	0.026	45.1	1950.5
EJ070	13.9	1.330	30.9	1956.7	30.2	1955.2	0.015	45.4	1950.2

Table 5.6 (a) Comparison of core chronology for core LT/EJ using ^{210}Pb and ^{137}Cs, continued.

Sample Code	Depth Midpoint / cm	Mid cum wt / g cm^{-2}	^{210}Pb / 49.5 mg cm^{-2} y^{-1} to section 23 then 30.2 mg cm^{-2} y^{-1} to base		^{137}Cs / 38.9 mg cm^{-2} y^{-1} to section 23 then 30.9 mg cm^{-2} y^{-1} to base		CRS ^{210}Pb model		
			Yrs Accum.	Date	Yrs Accum.	Date	Cum. wt to base.	Yrs Accum.	Date
EJ075	14.9	1.436	34.4	1953.2	33.6	1951.8	0.018	49.0	1946.6
EJ080	15.9	1.555	38.4	1949.2	37.5	1947.9	0.028	53.4	1942.2
EJ085	16.9	1.668	42.1	1945.5	41.1	1944.2	0.023	57.9	1937.7
EJ090	17.9	1.761	45.2	1942.4	44.1	1941.3	0.024	61.9	1933.7
EJ095	18.9	1.912	50.2	1937.4	49.0	1936.4	0.026	69.4	1926.2
EJ100	19.9	2.039	54.4	1933.2	53.1	1932.3	0.027	73.5	1922.1
EJ105	24.5	2.635	74.1	1913.5	72.4	1913.0	0.139	106	1889.6
EJ110	29.5	3.424	100.2	1887.3	98.0	1887.4			

5.5.3 Core chronology.

Although the ln ($^{210}Pb_{unsupp}$) profile for the top 0.4 g cm^{-2} of the core is highly irregular, the sedimentation rates calculated from all of the points (Fig. 5.13 (a)) and from those below section 23 (4.4-4.6 cm) (Fig. 5.13 (c)) give good correlation with the rates obtained using ^{137}Cs. Table 5.6 (a) is a summary of the dates obtained for core LT/EJ using: (1) the ^{210}Pb CIC model using a sedimentation rate of 49.5 mg cm^{-2} y^{-1} for the top 0.397 g cm^{-2} and 30.2 mg cm^{-2} y^{-1} extrapolated to the base of the core, (2) the CRS model, and (3) a 2-component ^{137}Cs model using a sedimentation rate of 38.9 mg cm^{-2} y^{-1} for the top 0.397 g cm^{-2} and 30.9 mg cm^{-2} y^{-1} to extrapolate from the Chernobyl peak to the base of the core.

The three chronologies give very similar dates throughout the core. The error on the ^{210}Pb upper section is very high due to the irregularities in the activities in this part of the core. Therefore a rate of 38.9 ± 0.7 mg cm^{-2} y^{-1} (from the ^{137}Cs model) for the top 0.4 g cm^{-2} and 30.2 ± 1.8 mg cm^{-2} y^{-1} (from the ^{210}Pb CIC model) for the remainder of the core will be used to fit a chronology to the Mini-Mackereth core LT/EM (Table 5.6 (b)). The CRS model will not be used due to the approximations that had to be made in order to calculate the total inventory.

Table 5.6 (b) Chronology for Loch Tay (east) core LT/EM.

Sample Code	Wet Wt / g	Dry wt / g	Mid cum. wt / g cm^{-2}	Yrs accum. based on 2 component ^{137}Cs and ^{210}Pb (CIC) model.	Date based on 2 component ^{137}Cs and ^{210}Pb (CIC) model (38.9/ 30.2 mg cm^{-2} y^{-1}).
LT/EM001	20.784	0.399	0.006	0.2	1995.3
LT/EM002	6.974	0.488	0.019	0.5	1995.0
LT/EM003	5.954	0.511	0.034	0.9	1994.6
LT/EM004	6.589	0.613	0.051	1.3	1994.2
LT/EM005	8.261	0.813	0.073	1.9	1993.6
LT/EM006	7.244	0.684	0.095	2.5	1993.0
LT/EM007	8.036	0.754	0.117	3.0	1992.5
LT/EM008	10.325	0.971	0.143	3.7	1991.8
LT/EM009	6.469	0.619	0.167	4.3	1991.2
LT/EM010	7.577	0.711	0.187	4.8	1990.7
LT/EM011	6.447	0.606	0.207	5.3	1990.2
LT/EM012	5.054	0.487	0.223	5.7	1989.8
LT/EM013	8.525	0.825	0.243	6.3	1989.2
LT/EM014	8.580	0.833	0.268	6.9	1988.6
LT/EM015	4.596	0.410	0.287	7.4	1988.1
LT/EM016	6.788	0.665	0.303	7.8	1987.7
LT/EM017	6.378	0.604	0.322	8.3	1987.2
LT/EM018	8.282	0.817	0.344	8.8	1986.7
LT/EM019	5.306	0.501	0.363	9.3	1986.2
LT/EM020	10.632	1.014	0.386	9.9	1985.6
LT/EM021	5.596	0.550	0.410	0.8	1984.8
LT/EM022	7.466	0.703	0.429	1.4	1984.2
LT/EM023	7.094	0.677	0.450	2.1	1983.5
LT/EM024	8.382	0.789	0.472	2.8	1982.7
LT/EM025	5.250	0.474	0.491	3.5	1982.1
LT/EM026	7.395	0.677	0.508	4.0	1981.5
LT/EM027	5.220	0.480	0.525	4.6	1981.0
LT/EM028	6.934	0.648	0.542	5.2	1980.4
LT/EM029	6.430	0.570	0.561	5.8	1979.8
LT/EM030	6.978	0.636	0.579	6.4	1979.2
LT/EM031	7.379	0.677	0.599	7.0	1978.5
LT/EM032	4.784	0.440	0.616	7.6	1978.0
LT/EM033	4.910	0.434	0.629	8.0	1977.5
LT/EM034	5.936	0.553	0.644	8.5	1977.0
LT/EM035	6.034	0.558	0.660	9.1	1976.5
LT/EM036	7.216	0.658	0.679	9.7	1975.9
LT/EM037	5.974	0.559	0.697	10.3	1975.3
LT/EM038	7.701	0.702	0.716	10.9	1974.7
LT/EM039	5.592	0.496	0.734	11.5	1974.1
LT/EM040	5.733	0.520	0.749	12.0	1973.5
LT/EM041	5.545	0.525	0.765	12.5	1973.0
LT/EM042	9.724	0.907	0.787	13.3	1972.3
LT/EM043	5.408	0.497	0.808	14.0	1971.6
LT/EM044	5.005	0.450	0.822	14.4	1971.1
LT/EM045	3.263	0.294	0.833	14.8	1970.8

Table 5.6 (b) Chronology for Loch Tay (east) core LT/EM, continued.

Sample Code	Wet Wt / g	Dry wt / g	Mid cum. wt / g cm^{-2}	Yrs accum. based on 2 component ^{137}Cs and ^{210}Pb (CIC) model.	Date based on 2 component ^{137}Cs and ^{210}Pb (CIC) model (38.9/ 30.2 mg cm^{-2} y^{-1}).
LT/EM046	5.616	0.510	0.846	15.2	1970.4
LT/EM047	10.181	0.953	0.868	15.9	1969.6
LT/EM048	3.344	0.298	0.886	16.6	1969.0
LT/EM049	6.956	0.639	0.901	17.0	1968.5
LT/EM050	6.782	0.657	0.920	17.7	1967.9
LT/EM051	7.036	0.669	0.940	18.3	1967.2
LT/EM052	7.310	0.693	0.961	19.0	1966.6
LT/EM053	5.805	0.553	0.979	19.6	1965.9
LT/EM054	7.993	0.747	0.999	20.3	1965.3
LT/EM055	3.973	0.385	1.016	20.9	1964.7
LT/EM056	6.366	0.595	1.031	21.3	1964.2
LT/EM057	7.716	0.773	1.051	22.0	1963.5
LT/EM058	8.343	0.849	1.076	22.8	1962.7
LT/EM059	7.055	0.686	1.099	23.6	1962.0
LT/EM060	9.663	0.976	1.124	24.4	1961.1
LT/EM061	5.590	0.546	1.147	25.2	1960.4
LT/EM062	6.747	0.730	1.166	25.8	1959.7
LT/EM063	12.228	1.281	1.196	26.8	1958.7
LT/EM064	6.282	0.652	1.226	27.8	1957.8
LT/EM065	3.448	0.342	1.241	28.3	1957.3
LT/EM066	5.788	0.586	1.255	28.7	1956.8
LT/EM067	9.880	0.996	1.278	29.5	1956.0
LT/EM068	9.221	0.952	1.308	30.5	1955.1
LT/EM069	6.140	0.600	1.331	31.3	1954.3
LT/EM070	7.572	0.764	1.352	32.0	1953.6
LT/EM071	5.398	0.536	1.371	32.6	1953.0
LT/EM072	5.403	0.545	1.388	33.2	1952.4
LT/EM073	5.484	0.558	1.404	33.7	1951.9
LT/EM074	4.641	0.461	1.420	34.2	1951.4
LT/EM075	3.474	0.351	1.432	34.6	1951.0
LT/EM076	6.374	0.679	1.447	35.1	1950.4
LT/EM077	6.050	0.647	1.467	35.8	1949.8
LT/EM078	8.266	0.898	1.491	36.6	1949.0
LT/EM079	4.548	0.486	1.511	37.3	1948.3
LT/EM080	8.602	0.913	1.533	38.0	1947.6
LT/EM081	9.276	0.990	1.561	38.9	1946.7
LT/EM082	6.779	0.739	1.587	39.8	1945.8
LT/EM083	7.697	0.819	1.611	40.5	1945.0
LT/EM084	4.675	0.507	1.631	41.2	1944.4
LT/EM085	6.713	0.698	1.649	41.8	1943.8
LT/EM086	6.969	0.737	1.670	42.5	1943.0
LT/EM087	7.851	0.853	1.694	43.3	1942.3
LT/EM088	6.094	0.620	1.717	44.1	1941.5
LT/EM089	5.122	0.536	1.734	44.6	1940.9
LT/EM090	6.201	0.649	1.752	45.2	1940.4

Table 5.6 (b) Chronology for Loch Tay (east) core LT/EM, continued.

Sample Code	Wet Wt / g	Dry wt / g	Mid cum. wt / g cm^{-2}	Yrs accum. based on 2 component ^{137}Cs and ^{210}Pb (CIC) model.	Date based on 2 component ^{137}Cs and ^{210}Pb (CIC) model (38.9/ 30.2 mg cm^{-2} y^{-1}).
LT/EM091	11.708	1.305	1.781	46.2	1939.4
LT/EM092	5.520	0.586	1.810	47.1	1938.4
LT/EM093	10.329	1.153	1.836	48.0	1937.6
LT/EM094	10.240	1.141	1.871	49.1	1936.4
LT/EM095	4.331	0.442	1.894	49.9	1935.6
LT/EM096	9.524	1.064	1.917	50.7	1934.9
LT/EM097	5.303	0.578	1.942	51.5	1934.1
LT/EM098	6.640	0.717	1.961	52.2	1933.4
LT/EM099	5.928	0.620	1.982	52.8	1932.7
LT/EM100	6.607	0.716	2.002	53.5	1932.1
LT/EM101	30.068	3.480	2.065	55.6	1930.0
LT/EM102	30.430	3.607	2.172	59.1	1926.4
LT/EM103	30.043	3.505	2.279	62.7	1922.9
LT/EM104	30.335	3.521	2.385	66.2	1919.4
LT/EM105	30.031	3.405	2.489	69.6	1915.9
LT/EM106	30.167	3.396	2.592	73.0	1912.5
LT/EM107	28.689	3.415	2.694	76.4	1909.1
LT/EM108	31.375	3.405	2.797	79.8	1905.7
LT/EM109	32.305	3.538	2.902	83.3	1902.3
LT/EM110	31.876	3.551	3.009	86.8	1898.7
LT/EM111	32.528	3.608	3.116	90.4	1895.2
LT/EM112	29.061	3.199	3.219	93.8	1891.8
LT/EM113	33.537	3.746	3.324	97.3	1888.3
LT/EM114	30.829	3.468	3.432	100.9	1884.7
LT/EM115	32.084	3.559	3.538	104.4	1881.2
LT/EM116	33.744	3.789	3.649	108.0	1877.5
LT/EM117	33.543	3.677	3.761	111.8	1873.8
LT/EM118	31.765	3.480	3.869	115.3	1870.2
LT/EM119	31.234	3.461	3.974	118.8	1866.8
LT/EM120	29.773	3.423	4.078	122.2	1863.3
LT/EM121	68.881	7.651	4.245	127.8	1857.8
LT/EM122	70.076	7.931	4.479	135.5	1850.0
LT/EM123	66.007	7.436	4.711	143.2	1842.4
LT/EM124	64.830	7.267	4.932	150.5	1835.0
LT/EM125	68.506	7.590	5.156	157.9	1827.6
LT/EM126	68.349	7.624	5.386	165.5	1820.0
LT/EM127	65.740	7.386	5.612	173.0	1812.5
LT/EM128	68.837	7.724	5.840	180.6	1805.0
LT/EM129	65.619	7.444	6.068	188.1	1797.4
LT/EM130	68.350	7.797	6.298	195.7	1789.8
LT/EM131	66.550	7.638	6.530	203.4	1782.1
LT/EM132	69.683	7.983	6.766	211.2	1774.3
LT/EM133	61.479	6.903	6.990	218.7	1766.9
LT/EM134	66.255	7.458	7.206	225.8	1759.7
LT/EM135	68.365	7.559	7.433	233.3	1752.2
LT/EM136	65.831	7.256	7.656	240.7	1744.9
LT/EM137	65.875	7.314	7.876	248.0	1737.6
LT/EM138	68.861	7.644	8.101	255.5	1730.1
LT/EM139	67.345	7.476	8.329	263.0	1722.6
LT/EM140	65.357	6.913	8.546	270.2	1715.4
LT/EM141	382.92	40.350	9.258	293.8	1691.8

5.4.5.4 Stable lead isotopes and lead.

The core (LT/EM) was not long enough for any background level of Pb or pre-industrial $^{206}Pb/^{207}Pb$ ratio to be assessed. As an approximation, however, the values obtained for the core taken from the western basin in the Loch (Kesterton, 1993; Farmer *et al.*, 1997a) were used. Hence, the measured Pb and $^{206}Pb/^{207}Pb$ profiles were corrected for a baseline contribution of 16 ± 3 mg kg^{-1}, a ratio of 1.192 ± 0.002 and a sedimentation rate of 38.9 ± 0.7 mg cm^{-2} y^{-1} (from the ^{137}Cs) for the top 0.4 g cm^{-2} and 30.2 ± 1.8 mg cm^{-2} y for 0.4 g cm^{-2} to the base, using the method defined in Appendix A. The results for the excess $^{206}Pb/^{207}Pb$ ratio, and the excess Pb flux (mg m^{-2} y^{-1}) are summarised in Table 5.7 and a graph of excess Pb flux (mg m^{-2} y^{-1}) and excess $^{206}Pb/^{207}Pb$ ratio against date plotted in Figure 5.14.

The influence of the indigenous Pb-ores at Tyndrum and on the southern shores of Loch Tay at Kepranich is clearly evident from the graph in Figure 5.14. From the base of the core (~1700 onwards) the excess $^{206}Pb/^{207}Pb$ ratio, which averages 1.145 ± 0.002 for the core, is in excellent agreement with the value of 1.144 ± 0.004 quoted for Tyndrum Pb ore deposits (Moorbath, 1962) and the value obtained for stream sediments at Kepranich (1.140, Lancaster, 1996). Tyndrum Pb ore was mined from 1739 intermittently until as recently as 1925 (Wilson, 1921: Craig, 1965). At no stage during the 19th Century does the ratio approach the value of 1.171 characteristic of the Pb being deposited throughout Scotland during the Industrial Revolution (Sugden *et al.*, 1991a,b: Farmer *et al.*, 1993). It is not until the last 20 years of the 19th Century that the ratio starts to be influenced by sources other than the Tyndrum ore. The slight increase from 1888 until 1912 could be due to the input of Pb with a higher $^{206}Pb/^{207}Pb$ ratio, e.g. from coal burning.

Tyndrum is situated 25 km from the head of the loch and a further 16 km from the sample site. From the stream sediment data in Table 5.4 (a) and (b), it is apparent that the $^{206}Pb/^{207}Pb$ atom ratios for the northern-shore streams are all higher than 1.158 and correspond to relatively low Pb concentrations. The $^{206}Pb/^{207}Pb$ atom ratios

are generally lower for the southern-shore streams and are closer to the values seen in the loch sediments. Of particular interest are the $^{206}Pb/^{207}Pb$ ratios for the two streams entering the loch at Kepranich and Shenlarich which are 1.140 ± 0.003 and 1.139 ± 0.003, with relatively high Pb concentrations of 120 and 98 mg kg^{-1}, respectively. If Tyndrum is the main source of the Pb and if aqueous input rather than atmospheric deposition of Pb is responsible, then relatively long transport distances for Pb-bearing suspended particulates or of Pb in association with dissolved organic matter must be involved.

The excess Pb fluxes are greater than 60 mg m^{-2} y^{-1} throughout the entire core but they had been steadily declining until ~1900. From 1900 until about 1950 there is a very slight increase in the flux during which time the $^{206}Pb/^{207}Pb$ ratio at first remains constant at 1.148 until 1912, before falling steeply to 1.143 by ~1920. These phenomena may be related to the re-working of the Tyndrum mines and old mine heaps from 1916-1925 (Wilson, 1921).

From 1985 the apparent increase in the flux of Pb is coincident with the change to both a slightly higher sedimentation rate and, very recently, to increased sedimentary concentrations of Pb.

Table 5.7 Excess heavy metal fluxes and excess $^{206}Pb/^{207}Pb$ ratios in core LT/EM.

Sample Code	Date	Excess $^{206}Pb/^{207}Pb$	σ_{n-1xs}	Excess Pb flux / mg m^{-2} y^{-1}	Excess Zn flux / mg m^{-2} y^{-1}	Excess Cd flux / mg m^{-2} y^{-1}	Excess Cu flux / mg m^{-2} y^{-1}
LT/EM001	1995.3	1.140	0.0027	99.0	222.4	1.65	28.4
LT/EM002	1995.0	1.139	0.0028	94.1	206.5	1.57	23.5
LT/EM003	1994.6	1.139	0.0033	82.7	187.7	1.44	21.7
LT/EM004	1994.2	1.140	0.0031	79.5	163.5	1.39	29.2
LT/EM005	1993.6	1.140	0.0026	75.8	159.5	1.33	11.5
LT/EM006	1993.0	1.140	0.0023	74.1	148.8	1.41	7.5
LT/EM007	1992.5	1.139	0.0025	78.1	153.8	1.45	8.0
LT/EM008	1991.8	1.139	0.0026	75.3	142.1	1.43	6.5
LT/EM009	1991.2	1.140	0.0026	76.1	146.3	1.40	7.0
LT/EM010	1990.7	1.140	0.0030	75.6	148.4	1.44	6.5
LT/EM011	1990.2	1.141	0.0022	77.7	154.6	1.48	7.8
LT/EM012	1989.8	1.140	0.0026	76.8	151.9	1.47	7.8
LT/EM013	1989.2	1.140	0.0024	82.3	140.6	1.49	8.7
LT/EM014	1988.6	1.140	0.0026	76.4	140.3	1.42	8.3
LT/EM015	1988.1	1.140	0.0021	80.0	143.7	1.46	6.9
LT/EM016	1987.7	1.139	0.0030	80.1	150.0	1.44	8.3
LT/EM017	1987.2	1.140	0.0026	80.6	153.5	1.42	7.9
LT/EM018	1986.7	1.139	0.0025	78.7	143.4	1.39	7.7
LT/EM019	1986.2	1.139	0.0030	81.4	152.9	1.43	7.1
LT/EM020	1985.6	1.141	0.0029	60.9	156.8	1.34	6.7
LT/EM021	1984.8	1.143	0.0024	61.4	131.2	1.10	3.8
LT/EM022	1984.2	1.141	0.0026	62.8	138.4	1.09	3.6
LT/EM023	1983.5	1.142	0.0028	65.0	143.6	1.14	4.1
LT/EM024	1982.7	1.144	0.0028	68.0	150.6	1.23	4.7
LT/EM025	1982.1	1.143	0.0026	68.4	148.6	1.23	4.0
LT/EM026	1981.5	1.141	0.0041	70.6	148.9	1.21	3.7
LT/EM027	1981.0	1.142	0.0024	64.9	139.0	1.19	2.9
LT/EM028	1980.4	1.140	0.0028	73.7	154.4	1.25	4.3
LT/EM029	1979.8	1.140	0.0021	68.6	132.5	1.31	3.8
LT/EM030	1979.2	1.140	0.0030	67.8	130.6	1.22	3.3
LT/EM031	1978.5	1.139	0.0036	70.3	133.8	1.39	3.6
LT/EM032	1978.0	1.141	0.0028	70.4	129.4	1.29	3.7
LT/EM033	1977.5	1.138	0.0022	66.2	127.3	1.24	2.2
LT/EM034	1977.0	1.140	0.0030	70.8	136.9	1.25	3.1
LT/EM035	1976.5	1.141	0.0025	72.9	138.4	1.31	3.4
LT/EM036	1975.9	1.139	0.0028	70.4	139.2	1.40	3.8
LT/EM037	1975.3	1.138	0.0030	72.6	145.4	1.23	4.0
LT/EM038	1974.7	1.140	0.0024	68.6	142.8	1.24	3.9
LT/EM039	1974.1	1.140	0.0024	72.1	144.9	1.25	3.8
LT/EM040	1973.5	1.139	0.0023	73.9	143.6	1.28	4.4

Table 5.7 Excess heavy metal fluxes and excess $^{206}Pb/^{207}Pb$ ratios in core LT/EM, continued.

Sample Code	Date	Excess $^{206}Pb/^{207}Pb$	σ_{n-1xs}	Excess Pb flux / mg m^{-2} y^{-1}	Excess Zn flux / mg m^{-2} y^{-1}	Excess Cd flux / mg m^{-2} y^{-1}	Excess Cu flux / mg m^{-2} y^{-1}
LT/EM041	1973.0	1.139	0.0027	72.6	137.9	1.20	2.7
LT/EM042	1972.3	1.136	0.0028	73.9	142.5	1.24	3.5
LT/EM043	1971.6	1.138	0.0033	72.4	149.8	1.30	3.6
LT/EM044	1971.1	1.140	0.0031	72.0	147.3	1.31	3.1
LT/EM045	1970.8	1.142	0.0026	68.4	145.6	1.27	3.6
LT/EM046	1970.4	1.143	0.0023	70.2	111.9	1.23	3.4
LT/EM047	1969.6	1.142	0.0025	73.4	152.7	1.23	3.6
LT/EM048	1969.0	1.145	0.0026	72.4	146.2	1.24	3.6
LT/EM049	1968.5	1.134	0.0026	73.5	146.1	1.25	5.3
LT/EM050	1967.9	1.143	0.0030	75.0	166.3	1.33	4.6
LT/EM051	1967.2	1.141	0.0022	73.1	162.1	1.29	3.6
LT/EM052	1966.6	1.143	0.0026	75.8	158.3	1.30	4.1
LT/EM053	1965.9	1.143	0.0024	76.4	162.5	1.34	3.2
LT/EM054	1965.3	1.141	0.0026	76.3	163.0	1.26	3.6
LT/EM055	1964.7	1.140	0.0021	76.3	162.1	1.28	3.6
LT/EM056	1964.2	1.141	0.0030	75.0	159.5	1.31	4.1
LT/EM057	1963.5	1.141	0.0026	75.0	159.7	1.29	3.7
LT/EM058	1962.7	1.142	0.0025	76.8	161.6	1.32	3.6
LT/EM059	1962.0	1.140	0.0030	78.1	156.7	1.27	4.5
LT/EM060	1961.1	1.141	0.0029	73.7	152.6	1.29	4.2
LT/EM061	1960.4	1.141	0.0024	79.0	156.7	1.29	4.1
LT/EM062	1959.7	1.141	0.0026	77.8	149.2	1.27	3.2
LT/EM063	1958.7	1.139	0.0028	79.8	153.1	1.32	4.6
LT/EM064	1957.8	1.139	0.0028	78.2	150.8	1.30	3.7
LT/EM065	1957.3	1.141	0.0026	79.9	154.5	1.34	4.2
LT/EM066	1956.8	1.140	0.0041	77.7	158.8	1.29	4.8
LT/EM067	1956.0	1.140	0.0024	80.5	156.6	1.31	5.1
LT/EM068	1955.1	1.140	0.0028	82.3	158.0	1.32	4.3
LT/EM069	1954.3	1.139	0.0021	81.5	151.2	1.30	4.1
LT/EM070	1953.6	1.140	0.0030	83.0	158.8	1.32	4.8
LT/EM071	1953.0	1.142	0.0036	83.9	152.1	1.32	5.0
LT/EM072	1952.4	1.145	0.0028	81.3	151.8	1.38	4.7
LT/EM073	1951.9	1.147	0.0022	83.8	154.4	1.35	5.1
LT/EM074	1951.4	1.148	0.0030	84.0	159.3	1.38	5.1
LT/EM075	1951.0	1.149	0.0025	83.3	154.1	1.34	4.8
LT/EM076	1950.4	1.141	0.0028	85.4	146.3	1.29	3.8
LT/EM077	1949.8	1.140	0.0030	82.5	151.7	1.36	4.3
LT/EM078	1949.0	1.138	0.0024	85.9	150.5	1.37	5.3
LT/EM079	1948.3	1.138	0.0024	82.0	148.3	1.32	5.0
LT/EM080	1947.6	1.137	0.0023	87.1	160.6	1.34	5.2

Table 5.7 Excess heavy metal fluxes and excess $^{206}Pb/^{207}Pb$ ratios in core LT/EM, continued.

Sample Code	Date	Excess $^{206}Pb/^{207}Pb$	σ_{n-1xs}	Excess Pb flux / mg m^{-2} y^{-1}	Excess Zn flux / mg m^{-2} y^{-1}	Excess Cd flux / mg m^{-2} y^{-1}	Excess Cu flux / mg m^{-2} y^{-1}
LT/EM081	1946.7	1.142	0.0023	84.7	152.4	1.29	4.7
LT/EM082	1945.8	1.143	0.0024	84.7	150.8	1.32	5.5
LT/EM083	1945.0	1.143	0.0028	83.9	143.3	1.25	4.9
LT/EM084	1944.4	1.144	0.0032	85.0	141.8	1.23	5.1
LT/EM085	1943.8	1.143	0.0027	81.7	146.0	1.16	5.0
LT/EM086	1943.0	1.144	0.0023	86.1	151.1	1.23	5.1
LT/EM087	1942.3	1.144	0.0024	90.4	151.8	1.27	8.0
LT/EM088	1941.5	1.144	0.0022	89.8	147.6	1.28	6.5
LT/EM089	1940.9	1.143	0.0026	87.2	149.2	1.29	6.5
LT/EM090	1940.4	1.142	0.0022	86.8	152.9	1.29	6.0
LT/EM091	1939.4	1.142	0.0021	88.7	149.3	1.24	5.4
LT/EM092	1938.4	1.143	0.0021	88.4	158.5	1.31	5.2
LT/EM093	1937.6	1.142	0.0022	88.6	156.9	1.32	6.3
LT/EM094	1936.4	1.142	0.0026	86.9	157.2	1.32	5.8
LT/EM095	1935.6	1.143	0.0021	80.1	170.9	1.67	4.1
LT/EM096	1934.9	1.145	0.0020	88.2	152.7	1.30	5.5
LT/EM097	1934.1	1.145	0.0024	90.1	161.4	1.34	5.7
LT/EM098	1933.4	1.140	0.0030	85.9	142.5	1.29	4.7
LT/EM099	1932.7	1.141	0.0024	86.1	155.0	1.35	5.8
LT/EM100	1932.1	1.143	0.0026	93.7	164.2	1.36	6.2
LT/EM101	1930.0	1.141	0.0023	87.3	167.4	1.28	6.0
LT/EM102	1926.4	1.142	0.0025	87.8	163.0	1.39	6.0
LT/EM103	1922.9	1.144	0.0034	89.0	164.1	1.39	5.6
LT/EM104	1919.4	1.143	0.0022	88.1	162.4	1.40	5.5
LT/EM105	1915.9	1.142	0.0022	87.4	165.1	1.39	5.5
LT/EM106	1912.5	1.148	0.0027	88.8	161.1	1.40	5.3
LT/EM107	1909.1	1.148	0.0027	86.5	157.8	1.38	5.0
LT/EM108	1905.7	1.148	0.0026	86.1	163.4	1.38	4.9
LT/EM109	1902.3	1.148	0.0020	85.0	156.6	1.41	5.1
LT/EM110	1898.7	1.147	0.0028	85.1	157.4	1.36	5.6
LT/EM111	1895.2	1.145	0.0043	81.8	151.3	1.31	5.2
LT/EM112	1891.8	1.144	0.0027	85.6	161.4	1.37	5.3
LT/EM113	1888.3	1.143	0.0022	84.0	163.3	1.38	4.6
LT/EM114	1884.7	1.144	0.0023	84.0	158.0	1.38	4.5
LT/EM115	1881.2	1.140	0.0031	85.9	160.3	1.39	4.7
LT/EM116	1877.5	1.141	0.0022	86.6	160.2	1.39	4.8
LT/EM117	1873.8	1.141	0.0034	86.3	161.1	1.40	5.5
LT/EM118	1870.2	1.142	0.0023	84.8	170.1	1.35	5.4
LT/EM119	1866.8	1.142	0.0023	83.4	169.4	1.34	2.8
LT/EM120	1863.3	1.140	0.0029	84.5	170.7	1.38	3.6

Table 5.7 Excess heavy metal fluxes and excess $^{206}Pb/^{207}Pb$ ratios in core LT/EM, continued.

Sample Code	Date	Excess $^{206}Pb/^{207}Pb$	σ_{n-1xs}	Excess Pb flux / mg m^{-2} y^{-1}	Excess Zn flux / mg m^{-2} y^{-1}	Excess Cd flux / mg m^{-2} y^{-1}	Excess Cu flux / mg m^{-2} y^{-1}
LT/EM121	1857.8	1.142		83.7	167.4	1.39	3.8
LT/EM122	1850.0	1.142		84.4	169.8	1.33	4.7
LT/EM123	1842.4	1.141		84.2	162.0	1.35	4.7
LT/EM124	1835.0	1.142		86.7	170.7	1.39	4.9
LT/EM125	1827.6	1.143		87.8	167.9	1.37	4.9
LT/EM126	1820.0	1.141		92.6	170.0	1.40	7.4
LT/EM127	1812.5	1.145		92.2	166.0	1.37	7.0
LT/EM128	1805.0	1.145		91.4	164.7	1.36	7.4
LT/EM129	1797.4	1.145		93.7	164.7	1.39	7.6
LT/EM130	1789.8	1.145		93.9	166.0	1.42	7.0
LT/EM131	1782.1	1.143		93.4	165.6	1.41	7.2
LT/EM132	1774.3	1.146		95.9	165.9	1.43	7.3
LT/EM133	1766.9	1.146		97.1	167.2	1.43	7.2
LT/EM134	1759.7	1.146		96.3	181.6	1.39	8.5
LT/EM135	1752.2	1.145		98.8	179.4	1.44	8.8
LT/EM136	1744.9	1.146		100.4	176.5	1.43	8.2
LT/EM137	1737.6	1.146		101.4	175.2	1.51	8.6
LT/EM138	1730.1	1.145		103.2	174.3	1.53	6.6
LT/EM139	1722.6	1.143		105.9	168.1	1.59	8.3
LT/EM140	1715.4	1.146		106.7	169.2	1.62	8.2
LT/EM141	1691.8	1.144		114.0	165.0	1.72	7.8

Figure 5.14 Excess Pb flux (mg m^{-2} y^{-1}) and excess $^{206}Pb/^{207}Pb$ atom ratio vs date in core LT/EM: (a) full scale and (b) expanded from 1900-2000 AD.

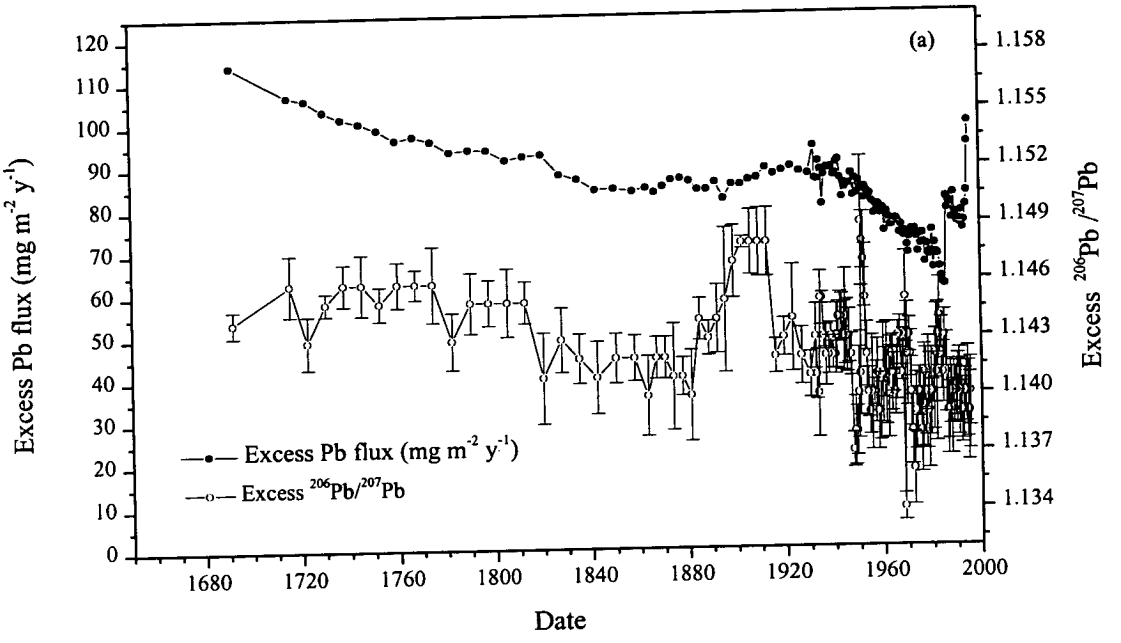

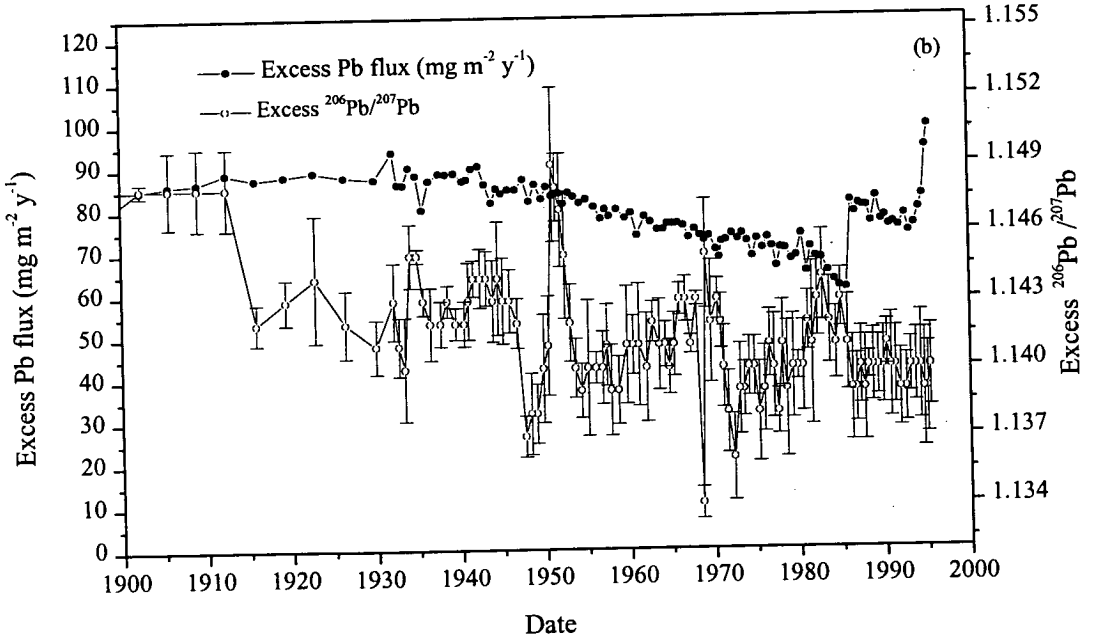

5.5.5 Heavy metals.

The other heavy metal pollutants, Zn, Cd and Cu, all show elevated levels throughout the core. Figure 5.15 is a plot of the excess flux of each metal against date. At Tyndrum there are also major deposits of Zn (Oliver, 1973). In addition there are several deposits of Cu situated within the direct catchment of Loch Tay, with several of these having been mined on small scales at various points in history. The deposits at Tomnadashan are often cited in the literature and are thought to have been mined intermittently during the time of the second Marquis of Breadalbane from 1838-1862 (Bainbridge, 1976), although the quantities mined were reputedly small. A continued input from the surrounding catchment would explain the near constant value for Cu seen throughout the core. The top 1 cm of the core shows elevated concentrations of Cu, and a similar pattern is also evident, to some extent, for all of the other elements analysed.

Table 5.8 is a summary of the excess inventories of the heavy metals Pb, Cu, Zn and Cd. The excess inventories for all of the metals are much greater than those seen in Loch Lomond south.

The Mn profile (Fig. 5.9) is very different from the classic diagenetic profile observed in Loch Lomond (Fig. 3.5) where a single massive peak is situated in the top few cm of the core. In Loch Tay (east) the Mn profile has a series of peaks throughout the core with the largest of these dated at 1831-1869. The peak at this point was not observed at the west end of the loch by Kesterton (1993) while a core further to the east analysed by Brechin (1994) was not long enough. The Cu workings at Tomnadashan coincide with the apparent date of this peak (1838-1862), suggesting that mining activity may have influenced the nature of sedimentation in the loch and led to the preservation of a diagenetic Mn peak in the sediment column. The other peaks may also have been caused at other periods of mining activity. Both Kesterton (1993) (see section 5.6.2.3) and Brechin (1994) reported a small enhancement in Mn and Fe at ~ 1940, the time of the closing of the Tyndrum mines,

and there is a slight peak at about this time in the core LT/EM. The Fe profile is relatively lacking in any features other than a slight peak at 1940, in line with the Mn peak and the closing of the Tyndrum mines.

Figure 5.15 Excess flux of heavy metals Zn, Cd and Cu (mg m^{-2} y^{-1}) vs date (based on 2 component ^{137}Cs and ^{210}Pb model) in core LT/EM.

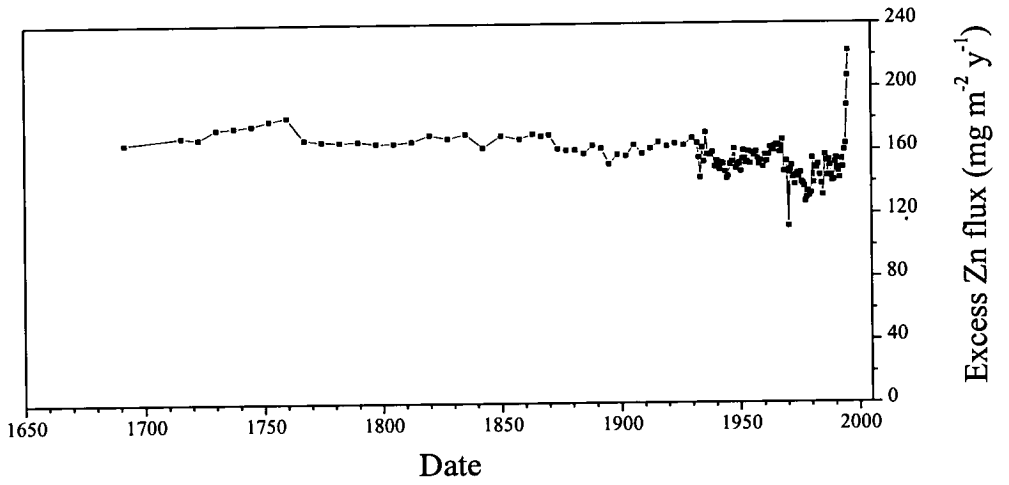

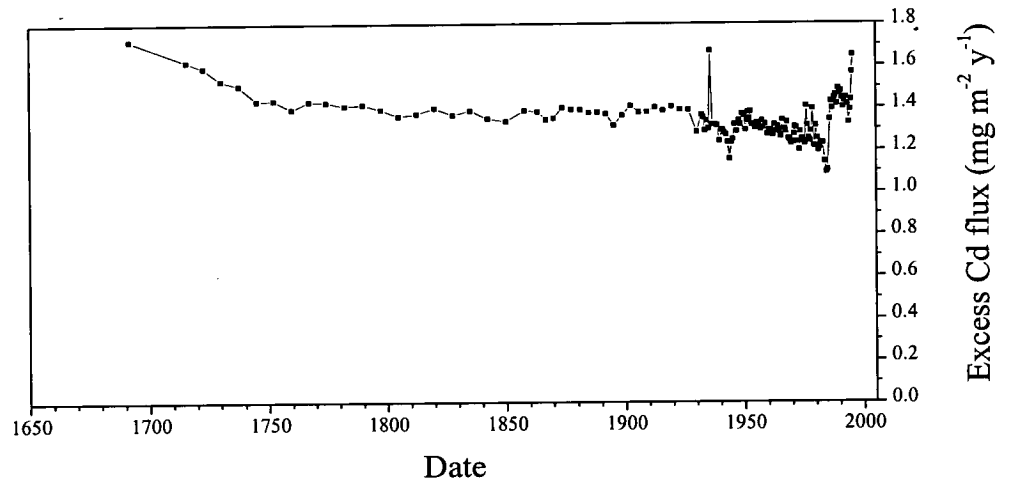

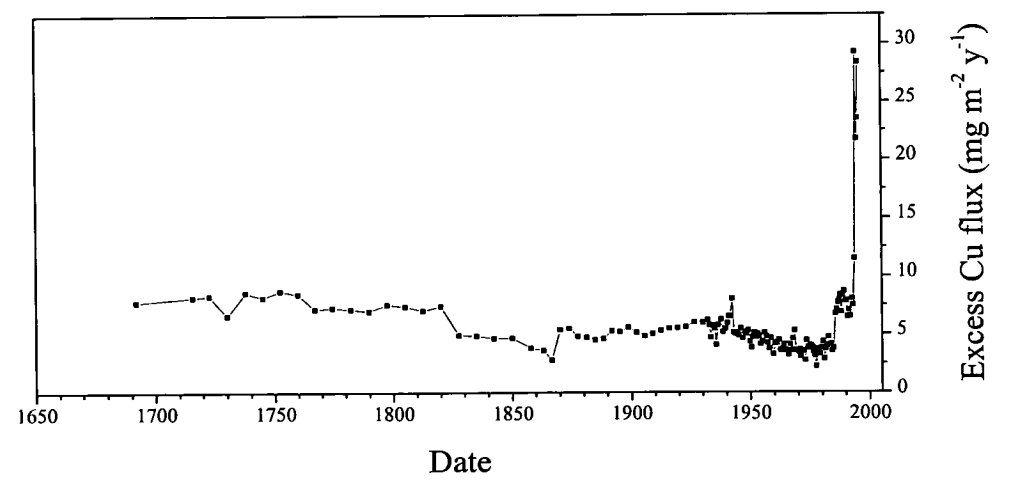

Table 5.8 Heavy metal inventories for Loch Tay core LT/EM.

	Core LT/EM	
	Background /	Excess inventory
Metal	mg kg^{-1}	/ g m^{-2}
Pb	16*	29.4
Cu	56	2.03
Zn	140	52.5
Cd	0.3	0.46

* value taken from core LT/WM.

5.6 Loch Tay (West).

Two cores were collected on 17/11/92 and analysed for ^{134}Cs, ^{137}Cs, ^{210}Pb, ^{226}Ra (LT/WJ), Pb, Zn, Cu, Fe and Mn (LT/WM) (Kesterton, 1993). The stable Pb isotopes were determined later and the results published (Farmer *et al.*, 1997a). The results for the stable Pb isotopes and the heavy metals are included in this chapter to help form a more complete picture of Loch Tay's recent history.

5.6.1 Results.

5.6.1.1 Radiocaesium

Table 5.9 is a summary of the results for the analysis of ^{134}Cs and ^{137}Cs by γ-spectrometry (LT/WJ). Figure 5.16 is a plot of the specific activities of ^{134}Cs and ^{137}Cs (Bq kg^{-1}) against depth (cm). ^{134}Cs penetrates only to a depth of 4-5 cm with a single peak of 173 Bq kg^{-1} at 2-3 cm. ^{137}Cs penetrates to a depth of 15-16 cm and has two peaks situated at 2-3 and 7-8 cm. The upper peak is sharp, covering only 2 cm and having a maximum specific activity of 2241 Bq kg^{-1}, whereas the lower peak is broader, covering ~5 cm in the core and having a maximum specific activity of 544 Bq kg^{-1}. Analytical precision was typically ± 5-20 % for ^{134}Cs and ± 1-5 % for ^{137}Cs.

5.6.1.2 ^{210}Pb.

A summary of the results for ^{210}Pb (LT/WJ) is shown in Table 5.9 and a graph of $^{210}Pb_{unsupp}$ against depth (cm) plotted in Figure 5.17. The $^{210}Pb_{unsupp}$ was calculated by subtraction of the ^{226}Ra (Bq kg^{-1}) value from the total ^{210}Pb (Bq kg^{-1}) for each section. Analytical precision was typically ± 5-10 % for ^{210}Pb.

Table 5.9 Radiocaesium and ^{210}Pb results for Loch Tay (west) core LT/WJ (Kesterton, 1993; Farmer *et al*., 1997a).

Sample Code	Section depth / cm	Wet wt / g	Dry wt / g	Mid cum. wt / g	Mid cum. wt / g cm^{-2}	$^{210}Pb_{unsupp}$ / Bq kg^{-1}	ln $^{210}Pb_{unsupp}$	^{134}Cs / Bq kg^{-1}	^{137}Cs / Bq kg^{-1}
LT/LTJ01	0-1	38.390	2.391	1.195	0.032	395	5.98	78	1062
LT/LTJ02	1-2	39.656	3.617	4.199	0.112	344	5.84	85	1313
LT/LTJ03	2-3	36.160	4.514	8.265	0.221	344	5.84	173	2241
LT/LTJ04	3-4	39.542	5.433	13.239	0.354	342	5.83	44	844
LT/LTJ05	4-5	38.514	5.412	18.661	0.499	334	5.81	16	539
LT/LTJ06	5-6	41.113	5.845	24.290	0.650	293	5.68	n/d	457
LT/LTJ07	6-7	39.661	5.634	30.029	0.803	279	5.63	n/d	535
LT/LTJ08	7-8	39.433	5.727	35.710	0.955	228	5.43	n/d	544
LT/LTJ09	8-9	45.175	6.772	41.959	1.122	152	5.02	n/d	425
LT/LTJ10	9-10	41.014	7.543	49.116	1.314	123	4.81	n/d	186
LT/LTJ11	10-11	47.232	8.149	56.962	1.523	100	4.61	n/d	85
LT/LTJ12	11-12	40.071	7.519	64.796	1.733	66	4.19	n/d	55
LT/LTJ13	12-13	40.487	7.135	72.123	1.929	102	4.62	n/d	44
LT/LTJ14	13-14	41.465	7.808	79.595	2.129	62	4.13	n/d	37
LT/LTJ15	14-15	44.200	8.660	87.829	2.349	37	3.61	n/d	32
LT/LTJ16	15-16	42.391	9.010	96.664	2.585	38	3.64	n/d	21
LT/LTJ17	16-17	44.768	9.711	106.024	2.836				
LT/LTJ18	17-18	41.072	8.734	115.247	3.082				
LT/LTJ19	18-19	43.606	9.865	124.546	3.331				

n/d not detected.

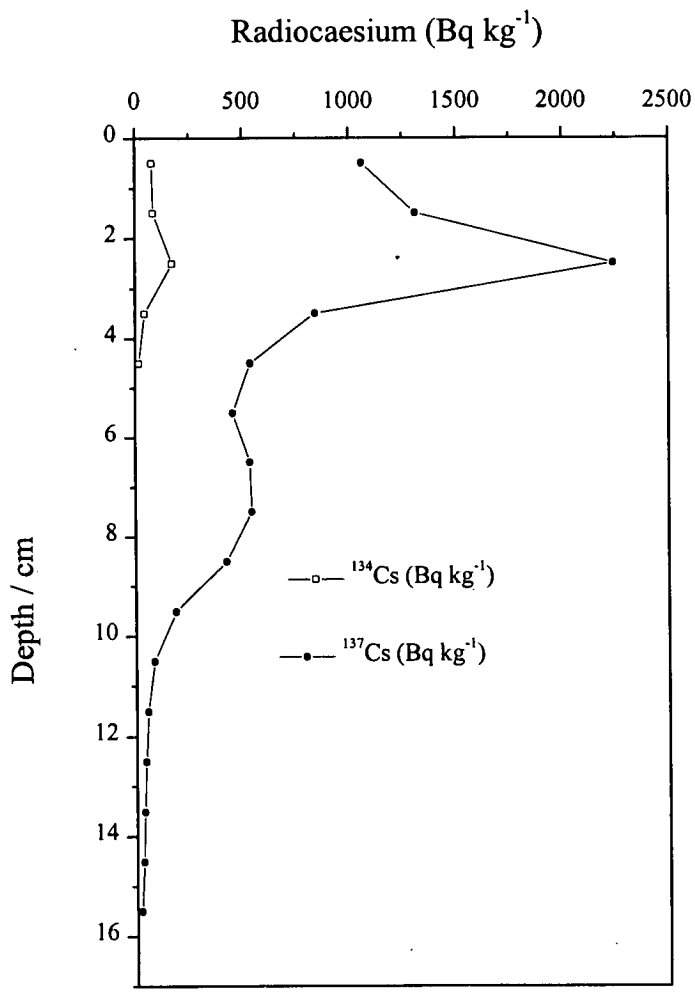

Figure 5.16 Radiocaesium (Bq kg^{-1}) vs depth (cm) in core LT/WJ.

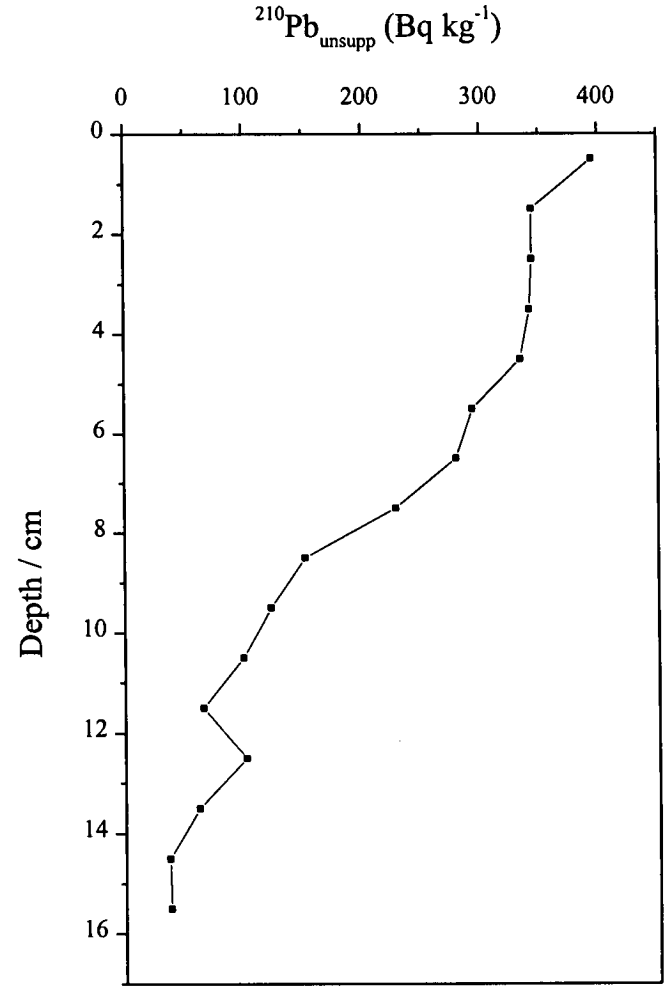

Figure 5.17 $^{210}Pb_{unsupp}$ (Bq kg^{-1}) vs depth (cm) in core LT/WJ.

5.6.1.3 Heavy metals.

The results for the heavy metals Pb, Zn, Cd, Cu, Fe and Mn (LT/WM) are summarised in Table 5.10 and the concentration of each metal plotted against depth (cm) in Figures 5.18-23.

The Pb concentration (Fig. 5.18) at the base of the core has a constant value of 16 ± 2.6 mg kg^{-1} below 60 cm. The concentration rises to give a broad peak of 230-253 mg kg^{-1} at 38-50 cm and then remains at an elevated level of 151-220 mg kg^{-1} until 15 cm. Above 15 cm the concentration rises steeply from 193 to 500 mg kg^{-1} for 3 cm before dropping off sharply again to 269 mg kg^{-1} followed by a steady decrease to 132 mg kg^{-1} at the sediment surface In Figure 5.19 the concentration of Zn is constant at 140 ± 4.3 mg kg^{-1} from the base of the core until 57.5 cm, above which it begins to increase steadily to reach a peak of 535 mg kg^{-1} at 12.5 cm. The concentration then drops to 450 mg kg^{-1} at 8.5 cm before rising again to a peak with a maximum of 591 mg kg^{-1} at 5.5 cm. Above 4 cm the concentration drops again reaching 374 mg kg^{-1} by the surface. The overall trends in Cd (Fig. 5.20) are the same as for Zn with a constant value from the base of <0.3 mg kg^{-1} until 52.5 cm. The concentration then begins to rise towards the surface with two peaks of 3.1 and 3.3 mg kg^{-1} at 13.5 and 5.5 cm, respectively. Above the second peak, the concentration declines to 1.6 mg kg^{-1} at the surface.

Copper (Fig. 5.21) exhibits a near constant value of 62 ± 5 mg kg^{-1} throughout the core with two small sub-surface peaks, of 73 and 70 mg kg^{-1} at 25 and 37 cm respectively. Above 5 cm the concentration rises to 87 mg kg^{-1}, the core maximum, at the surface.

As shown in Figure 5.22, Fe remains at a constant value of 4.68 ± 0.10 % from the base of the core until 27 cm, then rises slowly to reach 7.30 % at 3 cm before dropping back to 6.68 % at the surface. The profile is interrupted by a sharp peak at 11-12 cm of 7.45 %. Similarly with Mn (Fig. 5.23) the concentration remains

constant at 0.22 ± 0.01 % from the base of the core until 25 cm. Above 25 cm the concentration begins to rise slowly until 4 cm, but is interrupted by a sharp peak of 0.73 % from 9-10 cm. Above 4 cm, the concentration rises sharply to reach 2.36 %, the core maximum, at the surface.

5.6.1.4 Stable lead isotopes and lead.

Table 5.11 is a summary of the results for Pb and stable Pb isotope atom ratio $^{206}Pb/^{207}Pb$ along with the wet and dry weights for the core LT/WM. Figure 5.24 is a plot of Pb concentration and $^{206}Pb/^{207}Pb$ against depth (cm). The $^{206}Pb/^{207}Pb$ ratios for the core averaged 1.192 ± 0.003 below 60 cm before declining from 60-50 cm until a steady ratio of 1.153 ± 0.002 was achieved from 50-20 cm. The ratio then increased to 1.166 by 15-16 cm but above this, followed a more erratic path to a value of 1.156 at the sediment surface with a minimum of 1.145 at 3-4 cm.

Table 5.10 Heavy metal results in Loch Tay (west) core LT/WM (Kesterton, 1993; Farmer *et al*., 1997a).

Sample Code	Depth / cm	Wet wt / g	Dry wt / g	Pb / mg kg^{-1}	Zn / mg kg^{-1}	Cd / mg kg^{-1}	Cu / mg kg^{-1}	Fe / %	Mn / %
LTM001	0-1	29.423	1.881	132	374	1.6	87	6.68	2.36
LTM002	1-2	34.453	3.585	145	364	1.8	76	7.30	0.80
LTM003	2-3	34.587	4.109	158	444	1.8	76	7.30	0.51
LTM004	3-4	35.740	4.903	166	506	2.5	67	6.75	0.41
LTM005	4-5	37.839	5.023	180	591	3.0	65	6.32	0.42
LTM006	5-6	35.131	4.666	185	589	3.3	65	6.48	0.42
LTM007	6-7	36.482	5.149	186	485	2.3	66	6.69	0.39
LTM008	7-8	37.005	6.008	179	457	2.1	68	6.19	0.43
LTM009	8-9	37.572	6.728	166	450	2.5	68	5.70	0.35
LTM010	9-10	35.551	5.505	201	483	2.8	61	6.67	0.73
LTM011	10-11	37.988	6.725	192	471	2.5	63	5.96	0.43
LTM012	11-12	37.829	6.321	203	491	2.7	59	7.45	0.40
LTM013	12-13	35.927	6.236	269	535	3.0	61	5.72	0.33
LTM014	13-14	36.392	6.563	500	499	3.1	60	5.38	0.31
LTM015	14-15	37.153	7.387	497	495	2.7	63	5.52	0.30
LTM016	15-16	38.815	8.119	193	411	2.1	63	5.55	0.28
LTM017	16-17	35.802	7.384	193	410	2.2	62	5.26	0.29
LTM018	17-18	39.678	8.579	187	374	2.4	59	5.42	0.30
LTM019	18-19	37.378	8.382	182	369	2.0	61	5.25	0.28
LTM020	19-20	41.294	9.040	186	366	2.1	61	5.12	0.27

Table 5.10 Heavy metal results in Loch Tay (west) core LT/WM (Kesterton, 1993; Farmer *et al*., 1997a), continued.

Sample Code	Depth / cm	Wet wt / g	Dry wt / g	Pb / mg kg^{-1}	Zn / mg kg^{-1}	Cd / mg kg^{-1}	Cu / mg kg^{-1}	Fe / %	Mn / %
LTM022	20-22	74.670	16.003	199	362	2.0	67	5.34	0.30
LTM024	22-24	74.545	16.650	209	308	1.6	65	5.09	0.27
LTM026	24-26	79.999	23.069	172	254	1.1	73	5.11	0.22
LTM028	26-28	76.892	20.909	183	267	1.2	68	4.71	0.23
LTM030	28-30	74.923	18.797	191	274	1.4	61	5.00	0.24
LTM032	30-32	72.986	18.445	172	261	1.2	64	4.84	0.24
LTM034	32-34	73.405	18.889	220	266	1.4	64	4.97	0.23
LTM036	34-36	74.728	19.083	217	249	1.2	60	4.85	0.22
LTM038	36-38	75.146	19.905	151	233	0.9	70	4.95	0.21
LTM040	38-40	70.819	16.978	253	224	0.9	61	4.96	0.23
LTM045	40-45	167.584	39.898	233	205	0.7	59	4.80	0.21
LTM050	45-50	169.425	40.407	230	182	0.4	58	4.78	0.22
LTM055	50-55	167.441	43.125	88	150	<0.3	58	4.82	0.20
LTM060	55-60	167.269	41.924	24	140	<0.3	57	4.92	0.20
LTM065	60-65	165.290	40.834	18	139	<0.3	55	4.61	0.22
LTM070	65-70	172.600	42.310	18	140	<0.3	56	4.84	0.24
LTM075	70-75	174.527	45.819	17	143	<0.3	56	4.82	0.22
LTM080	75-80	171.253	46.797	11	133	<0.3	53	4.93	0.23
LTM085	80-85	173.535	49.313	16	138	<0.3	56	4.87	0.23
LTM090	85-90	178.716	46.546	17	147	<0.3	57	4.90	0.22

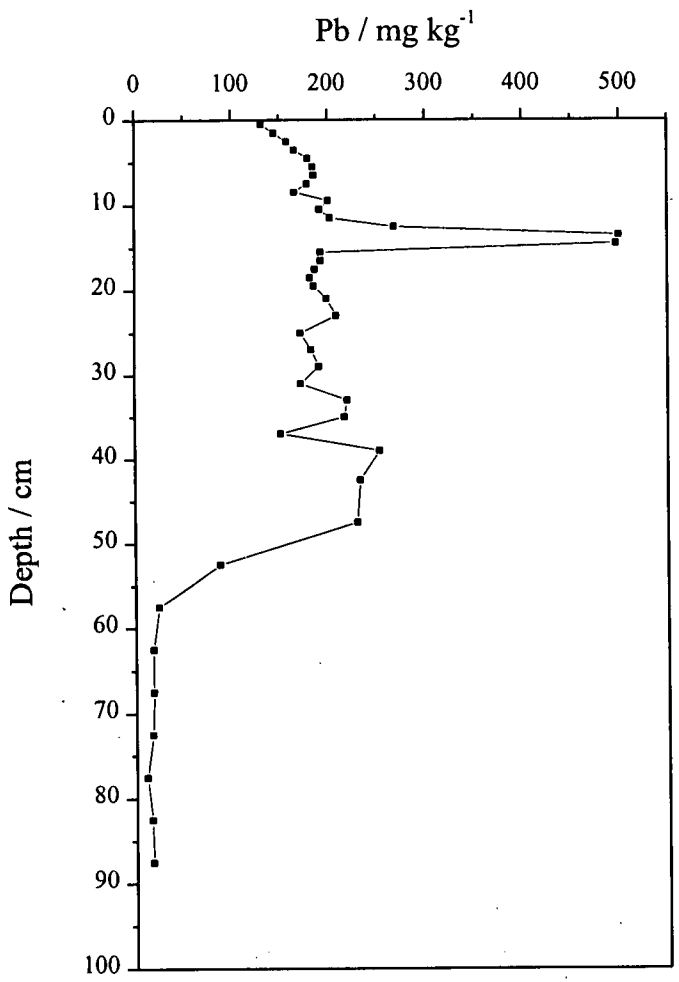

Figure 5.18 Pb (mg kg^{-1}) vs depth (cm) in core LT/WM.

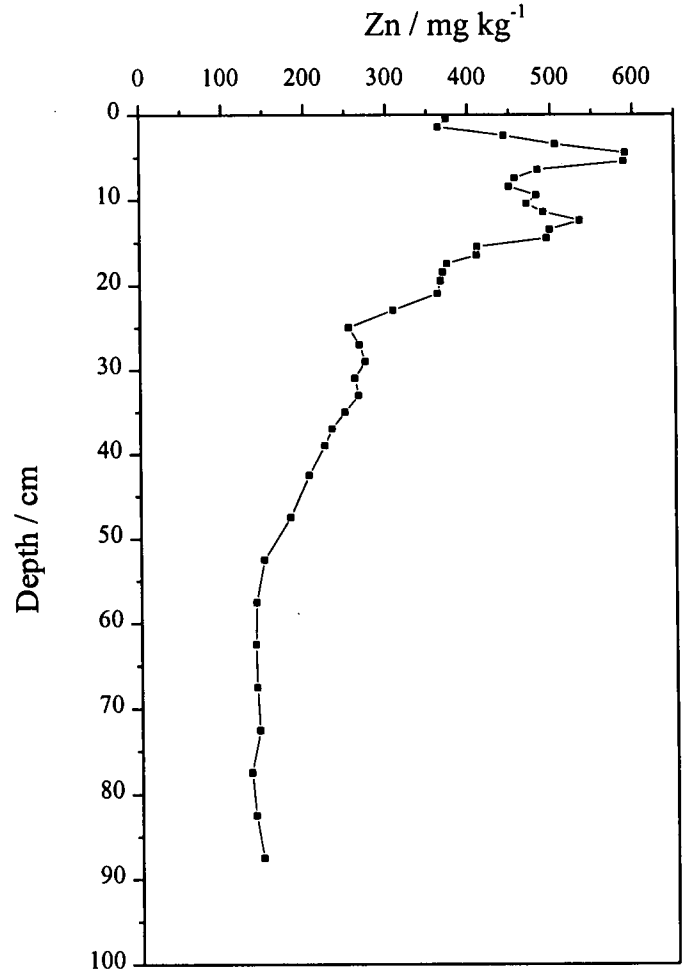

Figure 5.19 Zn (mg kg^{-1}) vs depth (cm) in core LT/WM.

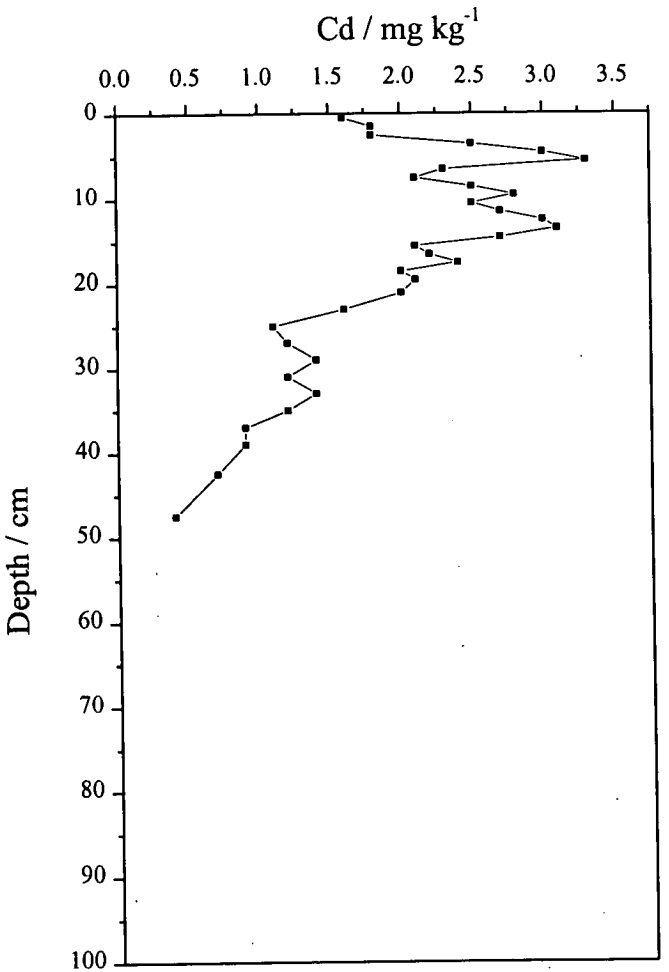

Figure 5.20 Cd (mg kg^{-1}) vs depth (cm) in core LT/WM.

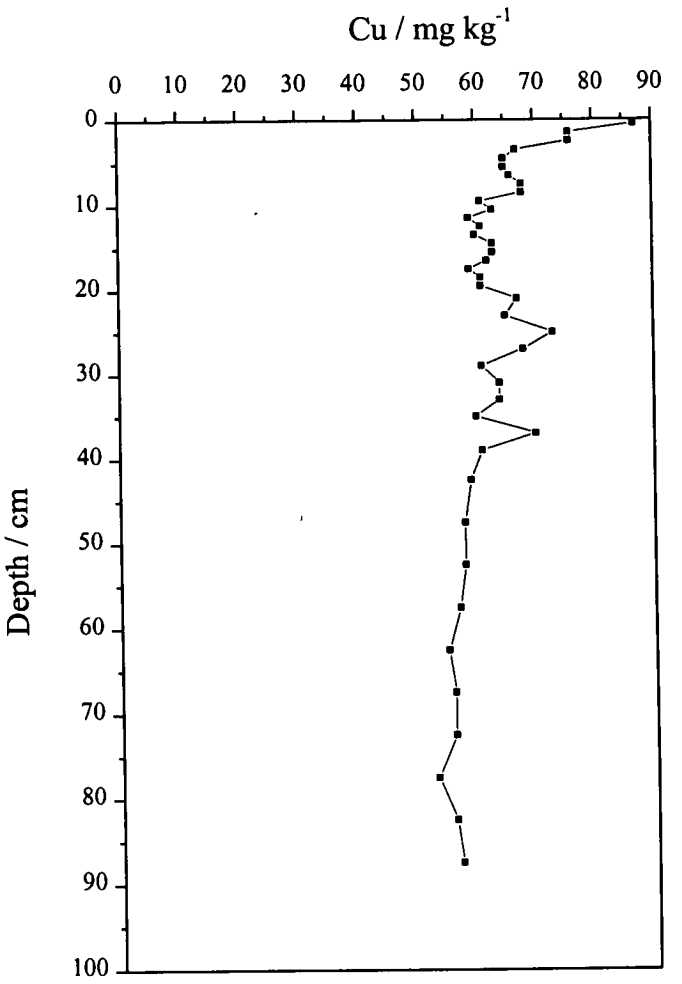

Figure 5.21 Cu (mg kg^{-1}) vs depth (cm) in core LT/WM.

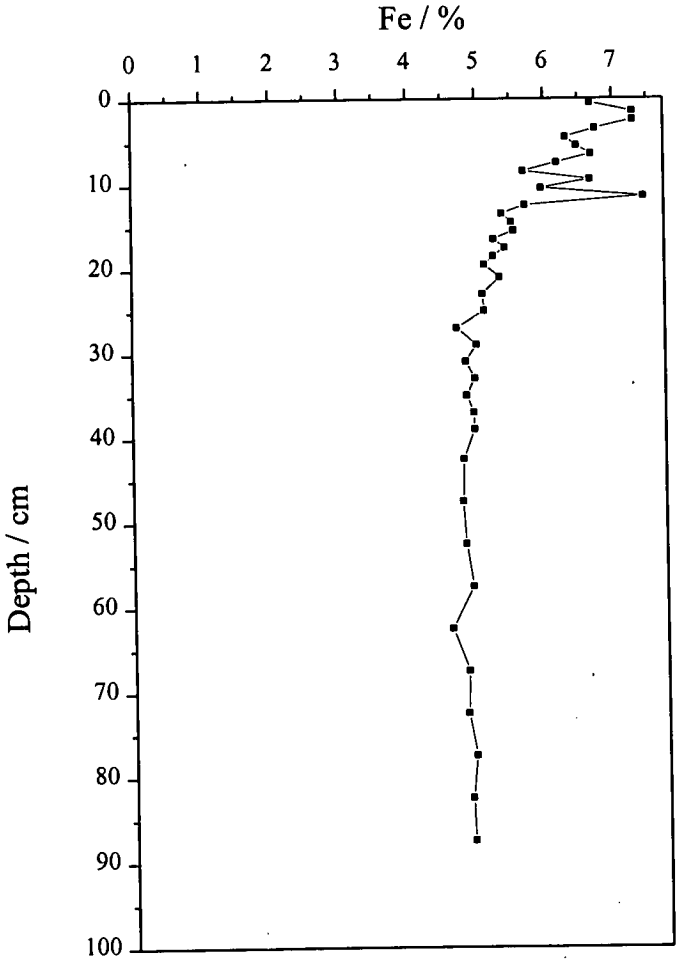

Figure 5.22 Fe (%) vs depth (cm) in core LT/WM.

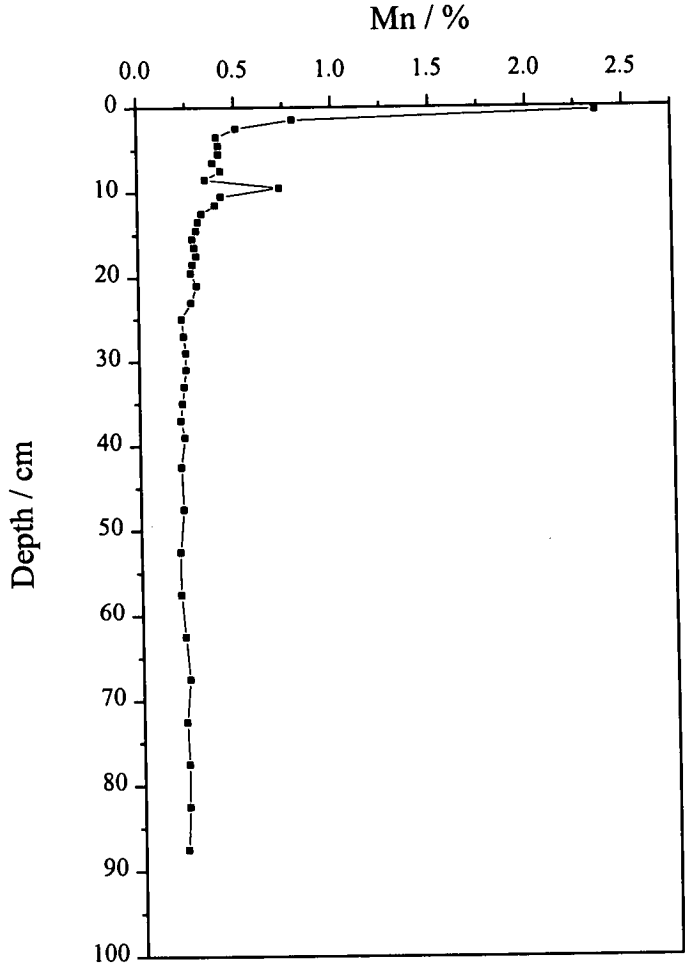

Figure 5.23 Mn (%) vs depth (cm) in core LT/WM.

Table 5.11 Pb concentration, stable Pb isotope ratio, excess stable Pb isotope and excess heavy metal flux results for core LT/WM.

Sample Code	Depth / cm	Pb / mg kg^{-1}	$^{206}Pb/^{207}Pb$	σ_{n-1}	Mid cum wt / g cm^{-2}	Date	Excess $^{206}Pb/^{207}Pb$	σ_{n-1xs}	Excess Pb flux / mg m^{-2} y^{-1}	Excess Zn flux / mg m^{-2} y^{-1}	Excess Cd flux / mg m^{-2} y^{-1}	Excess Cu flux / mg m^{-2} y^{-1}
LTM001	0-1	132	1.156	0.003	0.028	1990.9	1.151	0.0036	33	64.2	0.37	7.6
LTM002	1-2	145	1.157	0.003	0.111	1988.0	1.153	0.0036	37	61.4	0.42	4.5
LTM003	2-3	158	1.152	0.005	0.227	1983.9	1.147	0.0054	40	84.1	0.42	4.5
LTM004	3-4	166	1.145	0.002	0.362	1979.1	1.140	0.0028	42	101.6	0.62	2.0
LTM005	4-5	180	1.159	0.002	0.512	1973.8	1.156	0.0028	46	125.7	0.76	1.4
LTM006	5-6	185	1.160	0.004	0.658	1968.6	1.157	0.0045	48	125.1	0.85	1.4
LTM007	6-7	186	1.161	0.003	0.806	1963.4	1.158	0.0036	48	95.7	0.57	1.7
LTM008	7-8	179	1.150	0.002	0.974	1957.5	1.146	0.0028	46	87.7	0.51	2.3
LTM009	8-9	166	1.152	0.003	1.166	1950.7	1.148	0.0036	42	85.7	0.62	2.3
LTM010	9-10	201	1.148	0.002	1.350	1944.2	1.144	0.0028	52	95.1	0.71	0.3
LTM011	10-11	192	1.164	0.002	1.535	1937.7	1.161	0.0028	50	91.7	0.62	0.8
LTM012	11-12	203	1.158	0.004	1.731	1930.7	1.155	0.0045	53	97.4	0.68	0.0
LTM013	12-13	269	1.158	0.003	1.920	1924.0	1.156	0.0036	72	109.8	0.76	0.3
LTM014	13-14	500	1.154	0.003	2.113	1917.2	1.153	0.0036	137	99.6	0.79	0.0
LTM015	14-15	497	1.152	0.001	2.324	1909.8	1.151	0.0022	136	98.5	0.68	0.8
LTM016	15-16	193	1.166	0.004	2.557	1901.5	1.164	0.0045	50	74.7	0.51	0.8
LTM017	16-17	193	1.155	0.003	2.791	1893.3	1.152	0.0036	50	74.4	0.54	0.6
LTM018	17-18	187	1.159	0.005	3.031	1884.8	1.156	0.0054	48	64.2	0.59	0.0
LTM019	18-19	182	1.166	0.002	3.287	1875.8	1.163	0.0028	47	62.8	0.48	0.3
LTM020	19-20	186	1.163	0.004	3.550	1866.5	1.160	0.0045	48	62.0	0.51	0.3

Farmer *et al*., 1997a.

Table 5.11 Pb concentration, stable Pb isotope ratio, excess stable Pb isotope and excess heavy metal flux results for core LT/WM, continued.

Sample Code	Depth / cm	Pb / mg kg^{-1}	$^{206}Pb/^{207}Pb$	σ_{n-1}	Mid cum wt / g cm^{-2}	Date	Excess $^{206}Pb/^{207}Pb$	σ_{n-1xs}	Excess Pb flux / mg m^{-2} y^{-1}	Excess Zn flux / mg m^{-2} y^{-1}	Excess Cd flux / mg m^{-2} y^{-1}	Excess Cu flux / mg m^{-2} y^{-1}
LTM022	20-22	199	1.156	0.004	3.927	1853.1	1.153	0.0045	52	60.8	0.48	2.0
LTM024	22-24	209	1.152	0.002	4.419	1835.8	1.149	0.0028	55	45.6	0.37	1.4
LTM026	24-26	172	1.152	0.002	5.017	1814.6	1.148	0.0028	44	30.3	0.23	3.7
LTM028	26-28	183	1.150	0.004	5.680	1791.2	1.146	0.0045	47	34.0	0.25	2.3
LTM030	28-30	191	1.153	0.003	6.279	1770.0	1.149	0.0036	50	35.9	0.31	0.3
LTM032	30-32	172	1.153	0.002	6.840	1750.2	1.149	0.0028	44	32.3	0.25	1.1
LTM034	32-34	220	1.153	0.003	7.402	1730.3	1.150	0.0036	58	33.7	0.31	1.1
LTM036	34-36	217	1.152	0.002	7.975	1710.1	1.149	0.0028	57	28.9	0.25	
LTM038	36-38	151	1.154	0.003	8.562	1689.4	1.149	0.0036	38	24.3	0.17	
LTM040	38-40	253	1.155	0.003	9.118	1669.7	1.153	0.0036	67	21.8	0.17	
LTM045	40-45	233	1.155	0.002	9.975	1639.4	1.152	0.0028	61	16.4	0.11	
LTM050	45-50	230	1.153	0.001	11.185	1596.7	1.150	0.0022	61	9.9	0.03	
LTM055	50-55	88	1.162	0.003	12.444	1552.2	1.155	0.0036	20			
LTM060	55-60	24	1.184	0.003	13.726	1506.9	1.168	0.0036	2			
LTM065	60-65	18	1.190	0.004	14.973	1462.8		0.0045				
LTM070	65-70	18	1.189	0.006	16.226	1418.6		0.0063				
LTM075	70-75	17	1.194	0.004	17.554	1371.6		0.0045				
LTM080	75-80	11	1.198	0.004	18.949	1322.3		0.0045				
LTM085	80-85	16	1.194	0.006	20.398	1271.1		0.0063				
LTM090	85-90	17	1.191	0.003	21.842	1220.1		0.0036				

Farmer *et al*., 1997.

Figure 5.24 $^{206}Pb/^{207}Pb$ and Pb (mg kg^{-1}) vs depth (cm) in core LT/WM.

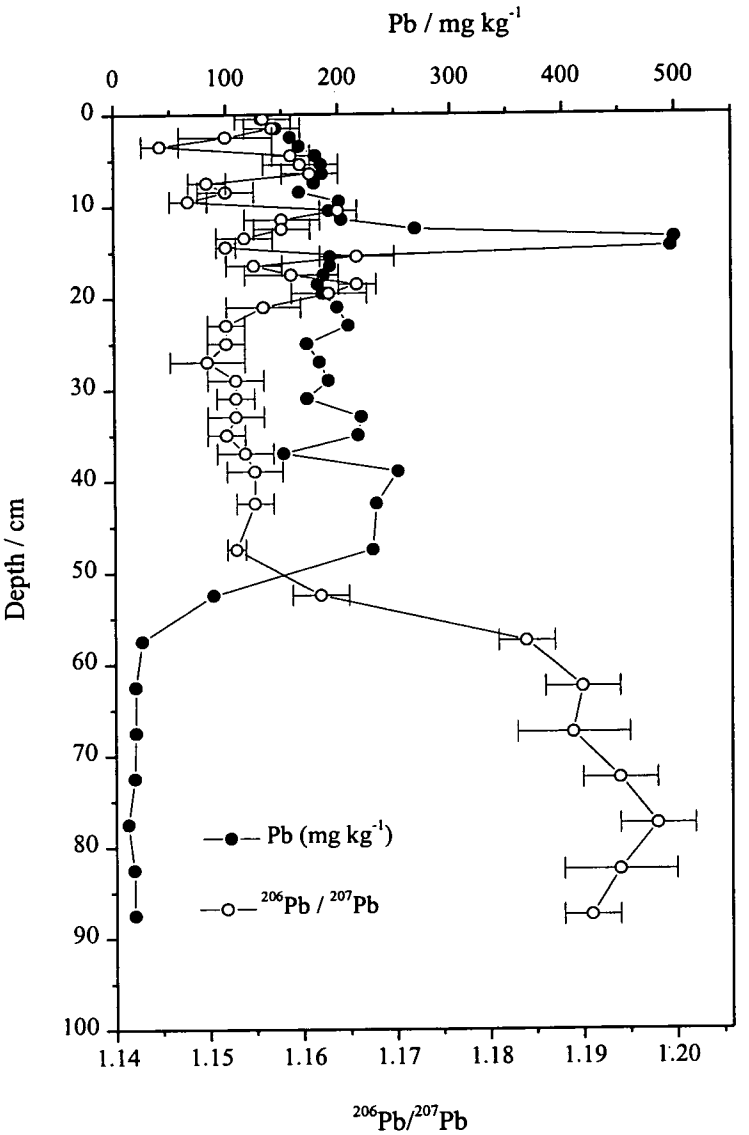

5.6.2 Discussion.

5.6.2.1 Core chronology.

The sedimentation rates obtained for the core were calculated using ^{210}Pb (CIC model) (28.3 mg cm^{-2} y^{-1}) and radiocaesium (28.6 mg cm^{-2} y^{-1}) and are in excellent agreement (Kesterton, 1993; Farmer *et al.*, 1997a). The sedimentation rate of 28.3 mg cm^{-2} y^{-1} (based on a non-weighted, linear regression of ln $^{210}Pb_{unsup}$ vs. depth (g cm^{-2}) shown in Figure 5.25) was used to derive dates for the core LT/WM and these are shown in Table 5.11.

5.6.2.2 Stable lead isotopes and lead.

The measured Pb and $^{206}Pb/^{207}Pb$ profiles were corrected for a baseline contribution of 16 mg kg^{-1}, with a ratio of 1.192 (Appendice A), in order to assess the pre-industrial $^{206}Pb/^{207}Pb$ ratio. The excess Pb flux (mg m^{-2} y^{-1}), due to industrial input, was calculated on the basis of a sedimentation rate of 28.3 mg cm^{-2} y^{-1}. The results are summarised in Table 5.11 and a graph of excess Pb flux (mg m^{-2} y^{-1}) and excess $^{206}Pb/^{207}Pb$ ratio against date is plotted in Figure 5.26.

The input of excess Pb appears to have started at the beginning of the 16th Century, although the extrapolation of the ^{210}Pb sedimentation rate may be invalid for earlier dates as there is a possibility that during mining periods, the sedimentation rates may have been higher. From 1600 onwards the flux was always in excess of 40 mg m^{-2} y^{-1}, other than at present. Throughout the 17-19th Centuries the excess Pb was in the region of 40-70 mg m^{-2} y^{-1}. The $^{206}Pb/^{207}Pb$ atom ratio remained relatively constant at 1.150 ± 0.002 throughout the 17th and 18th Century, despite the varying Pb fluxes. This value is markedly closer to the Tyndrum ore $^{206}Pb/^{207}Pb$ atom ratio of 1.144 ± 0.004, than that for atmospherically deposited Pb during that period of ~1.17 (Sugden *et al.*, 1991a,b; Farmer *et al.*, 1996). It was not until 1850 that an apparent change in the source of Pb started to have an effect on the isotopic signature, possibly

Figure 5.25 ln $^{210}Pb_{unsupp}$ vs depth (g cm^{-2})
in core LT/WJ: linear regression.

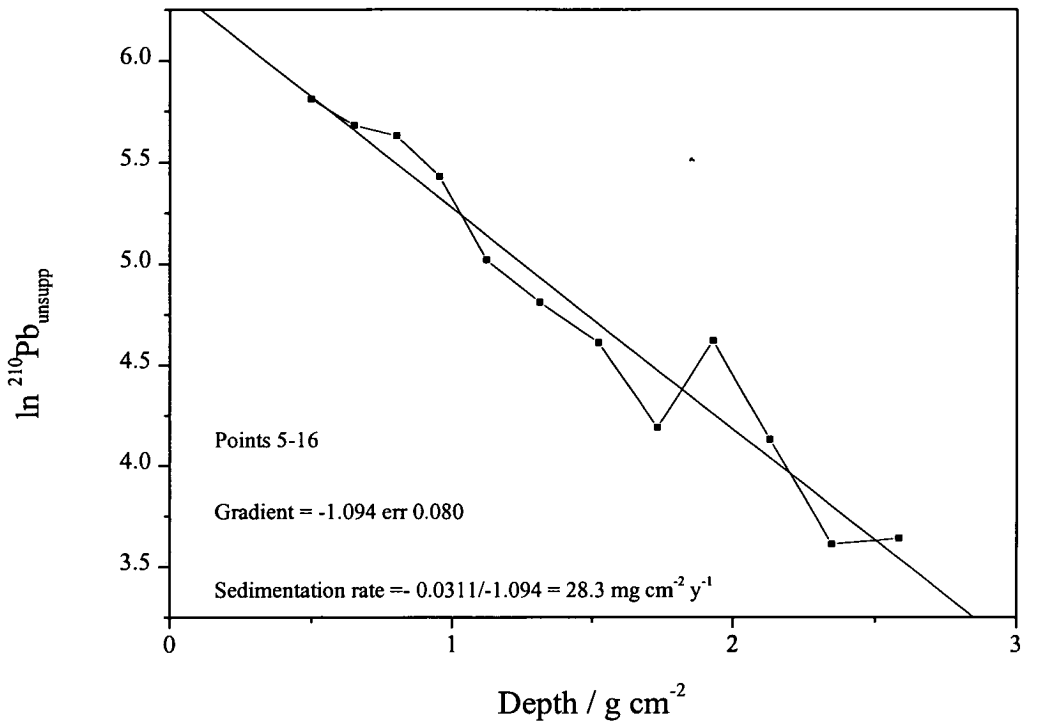

Figure 5.26 Excess Pb flux (mg m^{-2} y^{-1}) and excess $^{206}Pb/^{207}Pb$
vs date in core LT/WM.

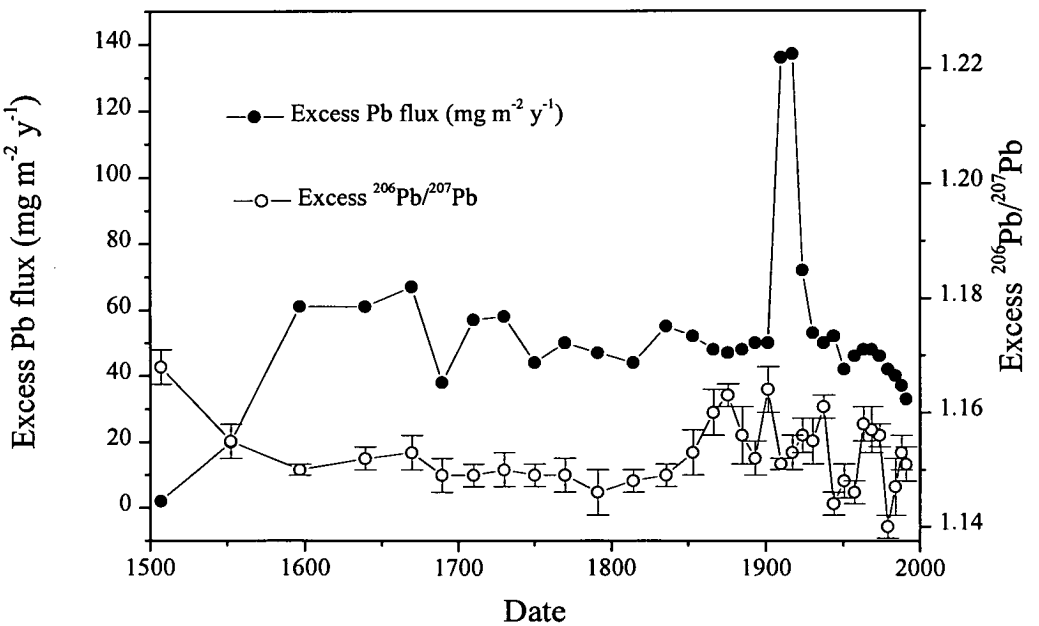

as a result of changing land use, deforestation and the move from wood burning to coal burning. Pb mining at Tyndrum also ceased in 1862 and the atom ratio increased towards 1.166. In 1916 a company was granted a lease to re-work dumps from previous mining operations at Tyndrum and to re-develop the mines. This resumption of activity corresponds to a massive peak in the Pb flux from 1906-1928 and a drop in the $^{206}Pb/^{207}Pb$ atom ratio back to 1.152 ± 0.003. From 1928 until the present, the ratio continued to average 1.152 ± 0.006 but is probably affected by a mixture of sources from a variety of atmospheric inputs, the most notable being ^{206}Pb-depleted alkyl Pb-additives in petrol, in addition to continuing industrial activity. Tyndrum will also probably continue to have an effect from water run off from the disused mines and slag heaps.

5.6.2.3 Heavy metals.

The major peak in Pb is accompanied by similar peaks in Zn and Cd (Fig. 5.27), although the concentrations are lower. There are major deposits of Zn at Tyndrum and it is likely that there is some Cd associated with the Zn deposits. The excess inventories of Pb, Zn, Cd and Cu are shown in Table 5.12 along with the inventories for LT/East and results from a short core collected in 1993 from a site further to the east of the LT/East site (Brechin, 1994).

The position and magnitude of the Fe and Mn peaks (Figs. 5.22 and 5.23) in the top 3 cm are indicative of natural enrichment due to post-depositional diagenesis (Farmer and Lovell, 1986; Farmer *et al.*, 1997a). There is a second peak in the sediment situated at 9-10 cm for Mn and at 11-12 cm for Fe which dates to the beginning of the 20th Century, similar to the re-working of the mine spoils. This may have led to an alteration of redox conditions in the water column and in the nature of sedimentary materials, in turn, causing an enrichment of the Fe and Mn.

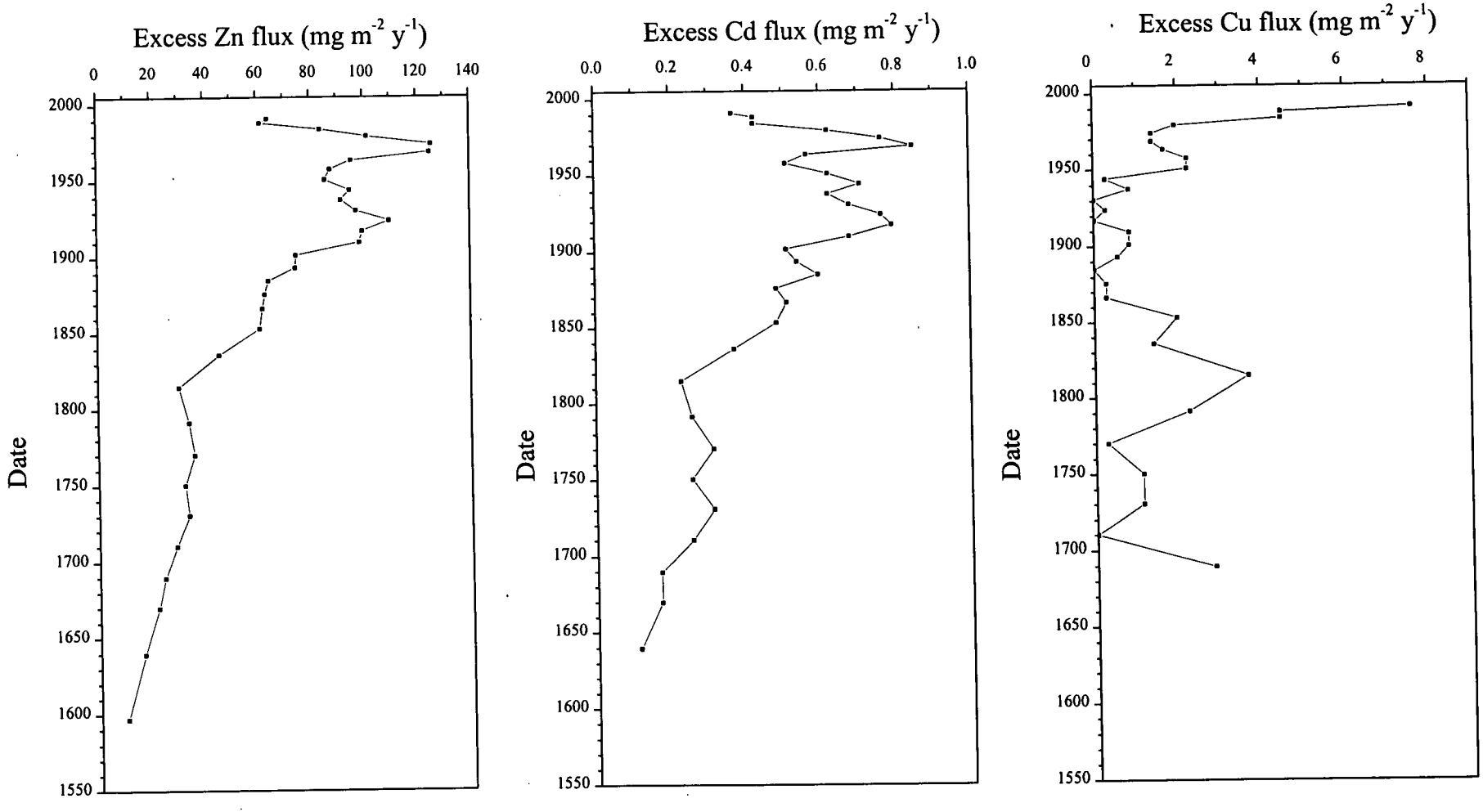

Figure 5.27 Excess heavy metal flux (mg m^{-2} y^{-1}) vs date in core LT/WM.

Table 5.12 A comparison of the heavy metal inventories for Loch Tay.

	Core LT/EM		Core LT/WM		Core LT/EB**	
	Background /	Inventory /	Background /	Inventory /	Background /	Inventory /
Metal	mg kg^{-1}	g m^{-2}	mg kg^{-1}	g m^{-2}	mg kg^{-1}	g m^{-2}
Pb	16*	29.4	16	24.14	16*	9.79#
Cu	56	2.03	60	0.93		
Zn	140	52.5	147	20.36		
Cd	0.3	0.46	0.3	0.14		

* value taken from core LT/WM.

core only 25 cm.

**Brechin, 1994.

5.7 Conclusions.

The heavy metal concentrations at both Loch Tay sites are considerably enhanced due to the high mineralisation of the area. However, in the eastern end of the loch, the excess inventories and fluxes are generally higher than in the west, as highlighted in Table 5.12 and in Figure 5.28. For Pb, Cu and Cd the inventories are 2-3 times greater, but for Zn the inventory is almost 6 times greater. This suggests that for all metals there may be a significant catchment input from deposits other than at Tyndrum, such as those situated at Tomnadashan. As with the other lochs there is an enhancement of Cu in the top sections of the cores for both Loch Tay sites. This is again perhaps attributable to remobilisation from organic matter diagenesis.

The $^{206}Pb/^{207}Pb$ atom ratios are consistent for both sites. Throughout the 18th Century the ratio was 1.145 ± 0.002 for the east and 1.150 ± 0.002 in the west. Both these ratios are consistent with a major influence of Pb from Tyndrum with a ratio of 1.144 ± 0.004 rather than the industrial ratio in Scotland at that time of ~1.17 (Sugden *et al.*, 1991a,b). From the end of the 19th Century until the present the ratios are affected by a variety of sources.

A comparison of Loch Tay with respect to the other study sites will be addressed in Chapter 7.

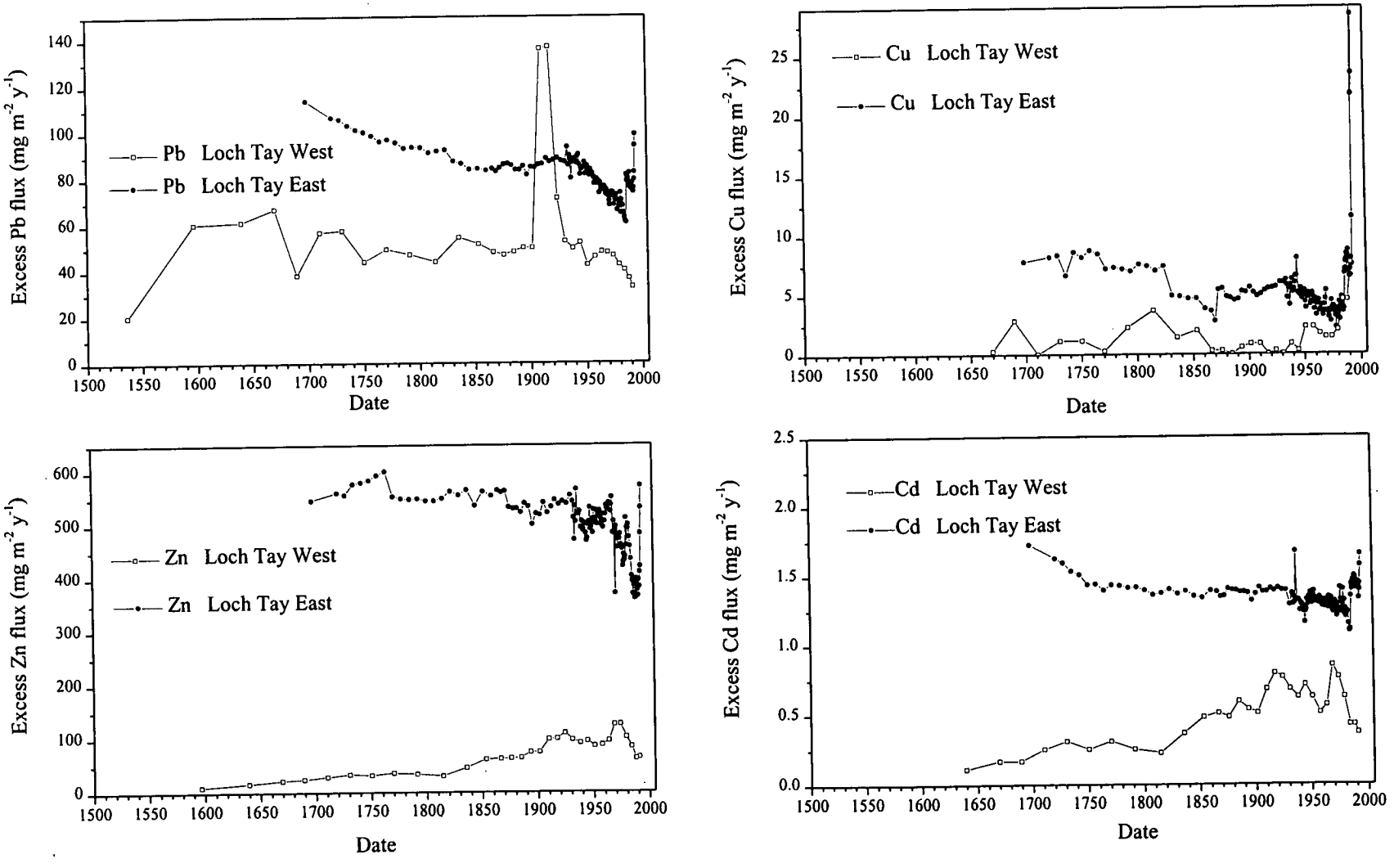

Figure 5.28 Comparison of heavy metal deposition between Loch Tay cores LT/EM and LT/WM.

6.1 Location.

Loch Ness is situated in the north of Scotland 12 km to the south-west of Inverness (Figs. 1.13, 2.3) and, although not the largest loch by area, contains the largest volume of freshwater in the United Kingdom, holding more water than all of the lakes of England and Wales combined (Murray and Pullar, 1910).

6.2 Topography.

Loch Ness (Fig. 6.1), a good example of a 'valley rock basin,' is one of a series of interlinked lochs which run parallel to the line of a fault following the Great Glen. The bedrock is Middle Old Red Sandstone resting on an undulating basement of Moine Gneiss and post orogenic granulites (Craig, 1983). The loch is ponded, partly by glacial deposits and fluvial-glacial gravels, and partly by raised beaches. It is also deeper than any part of the bed of the North Sea between the Norwegian Deep and Scotland (Craig, 1983). Loch Ness, with its head at Fort Augustus, runs in a north-east direction until the narrows at Bona Ferry (close to Inverness). The loch is 39 km in length, with a mean width of 1.45 km which is almost uniform throughout. It has a maximum depth of 230 m and a mean depth of 132 m (Murray and Pullar, 1910). It covers an area of 56.4 km^2 and contains a volume of 7.45 x 10^9 m^3 of freshwater. The floor of the loch is poor in flora due to the steep nature of the loch sides and a very strong wave action. Urquhart Bay, from where the core was taken, is one of the few places in Loch Ness where aquatic plants are abundant as the water is comparatively shallow.

The main inflows to Loch Ness are the River Oich, the River Moriston and the River Urquhart. The main outflow is by the River Ness.

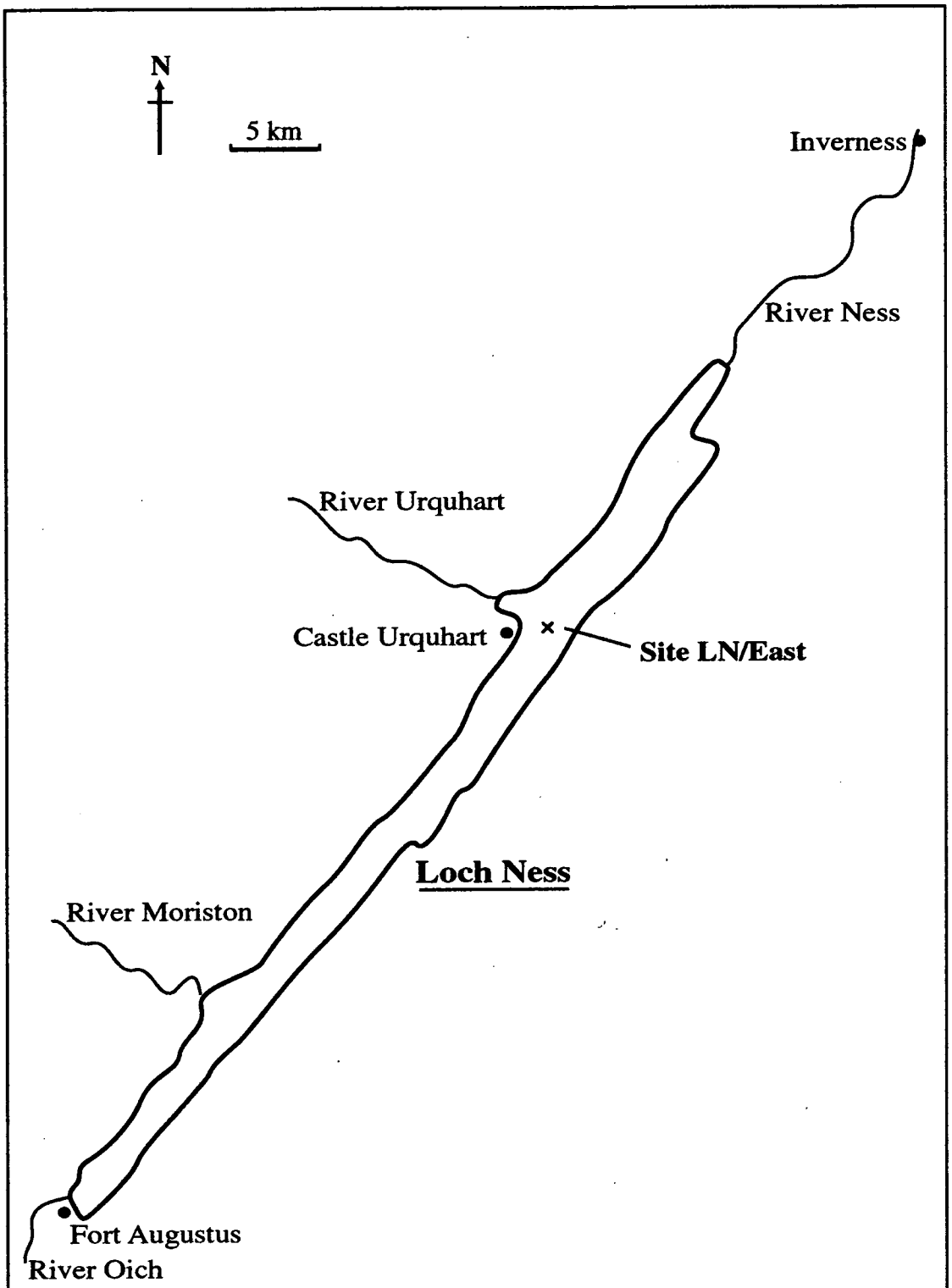

Figure 6.1 Location of sampling site for core LN/EM in Loch Ness.

6.3 Pollution sources.

Loch Ness is relatively remote from any major pollution sources. The largest population nearby is at Inverness, situated 12 km to the north-east. A major road, the A82, which is the principal tourist route and main link road from Fort William to Inverness, runs the full length of the loch alongside its north-western shore.

The loch is interlinked by a series of canals, collectively called the Caledonian Canal, which allows the passage of vessels from Fort William to the Moray Firth beyond Inverness.

6.4 Results.

A Mini-Mackereth core (LN/EM) was taken from site LN/East on 19/11/90 and sectioned as detailed in 2.1.2.4. The core was analysed for the radionuclides ^{210}Pb, ^{226}Ra and ^{137}Cs, heavy metals Pb, Zn, Cd, Cu, Fe and Mn (Whiteford, 1996), and stable Pb isotopes.

6.4.1 Radiocaesium.

Table 6.1 is a summary of the results obtained by γ-spectrometry analysis for ^{137}Cs (Whiteford, 1996). Figure 6.2 is a graph of the specific activity of ^{137}Cs (Bq kg^{-1}) against depth (cm). ^{137}Cs was detectable in only nine of the sections, with peak activities of 2424 Bq kg^{-1} and 3945 Bq kg^{-1} at 3 cm and 7 cm, respectively, below which it was detected intermittently to a maximum depth of 29 cm. The top sample, section 0-2 cm, was too small for analysis. ^{134}Cs was not detected in this core as it has a short half-life of 2.05 years and therefore any ^{134}Cs that may have been present will have decayed to below detectable levels by the date of analysis (November 1995-April 1996).

6.4.2 ^{210}Pb and ^{226}Ra.

Table 6.2 is a summary of the results for the γ-spectrometry analysis for ^{210}Pb and ^{226}Ra (Whiteford, 1996). Figure 6.3 is a graph of the specific activities of ^{210}Pb and ^{226}Ra (Bq kg^{-1}) against depth (cm). The specific activity of ^{210}Pb rises from 157 Bq kg^{-1} at 23 cm to a maximum of 754 Bq kg^{-1} at 3 cm. The specific activity of ^{226}Ra profile is relatively constant, from 12 cm to 23 cm, at 116-149 Bq kg^{-1}. Above 12 cm there is a depleted zone from 8-12 cm of 56-94 Bq kg^{-1}, then a zone of enhancement from 4-8 cm of 181-197 Bq kg^{-1}. The top sample, section 0-2 cm, was too small for analysis.

Table 6.1 Radiocaesium results for Loch Ness core LN/EM.

Sample Code	Depth / cm	Dry wt / g	Mid cum. wt / g cm^{-2}	^{137}Cs / Bq kg^{-1}	σ_{n-1} / Bq kg^{-1}
NTOP	0-2	0.7801	0.012	n/d	n/d
N1	2-4	4.1600	0.086	2424	43
N2	4-6	6.0175	0.240	1245	40
N3	6-8	5.8439	0.418	3945	232
N4	8-10	4.6318	0.576	1566	206
N5	10-12	5.3115	0.726	74	9
N6	12-14	5.5712	0.890	68	21
N7	14-16	5.3568	1.055	n/d	n/d
N8	16-18	5.7583	1.222	n/d	n/d
N9	18-20	6.7483	1.411	n/d	n/d
N10	20-22	6.0698	1.604	n/d	n/d
N11	22-24	7.6985	1.811	33	14
N12	24-26	7.5498	2.041	n/d	n/d
N13	26-28	7.2014	2.263	16	6
N14	28-30	10.4291	2.529	27	6

n/d = not detected

Table 6.2 ^{210}Pb and ^{226}Ra results for Loch Ness core LN/EM.

Sample Code	Depth / cm	Dry Weight / g	Mid cum. wt / g cm^{-2}	$^{210}Pb_{A(t)}$ / Bq kg^{-1}	$^{226}Ra_{A(t)}$ / Bq kg^{-1}	$^{210}Pb_{A(t)unsupp}$ / Bq kg^{-1}	$^{210}Pb_{unsupp}$ / Bq kg^{-1}	σ_{n-1} / Bq kg^{-1}	ln ($^{210}Pb_{unsupp}$)	σ +ve	σ -ve	σ ave
NTop	0-2	0.7801	0.012	n/d	n/d	n/d	n/d	n/d	n/d	n/d	n/d	n/d
N1	2-4	4.1600	0.086	754	128	626	733	46	6.60	0.06	0.06	0.06
N2	4-6	6.0175	0.240	472	197	275	322	35	5.77	0.10	0.12	0.11
N3	6-8	5.8439	0.418	401	181	220	257	38	5.55	0.14	0.16	0.15
N4	8-10	4.6318	0.576	265	94	171	199	26	5.29	0.12	0.14	0.13
N5	10-12	5.3115	0.726	225	56	169	199	15	5.29	0.07	0.08	0.08
N6	12-14	5.5712	0.890	275	129	146	171	22	5.14	0.12	0.14	0.13
N7	14-16	5.3568	1.055	232	147	85	100	15	4.61	0.14	0.16	0.15
N8	16-18	5.7583	1.222	165	149	16	19	7	2.94	0.31	0.46	0.39
N9	18-20	6.7483	1.411	194	137	57	67	13	4.20	0.18	0.22	0.20
N10	20-22	6.0698	1.604	128	116	12	14	4	2.64	0.25	0.34	0.29
N11	22-24	7.6985	1.811	157	148	9	11	4	2.40	0.31	0.45	0.38

Where A(t) is the specific activity of the radionuclide at time of counting.

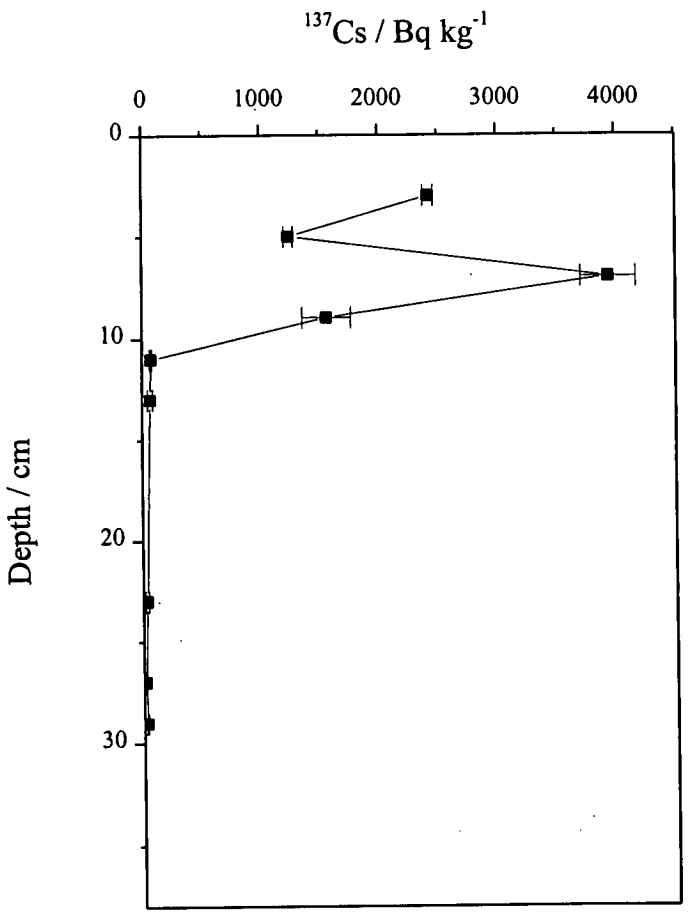

Figure 6.2 ^{137}Cs (Bq kg^{-1}) vs depth (cm) in core LN/EM.

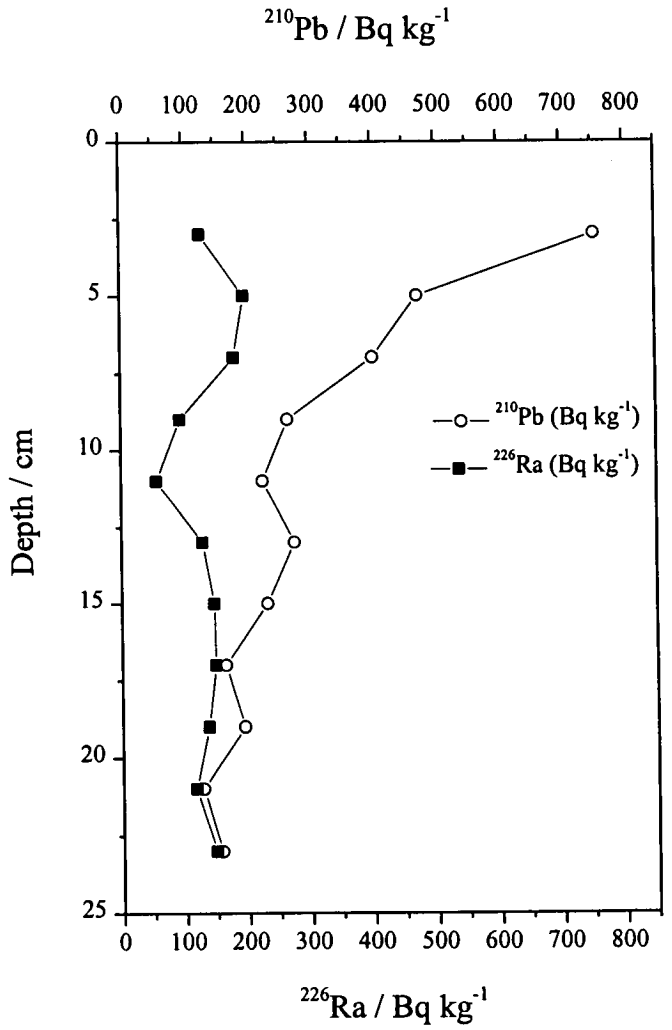

Figure 6.3 ^{210}Pb and ^{226}Ra (Bq kg^{-1}) vs depth (cm) in core LN/EM.

6.4.3 Heavy metals.

The concentrations of the heavy metals in core LN/EM are shown in Table 6.3 along with the wet and dry weight, depth and reference number for each section (Whiteford, 1996). The average error for each metal concentration, based on the relative standard deviation of the mean concentration for duplicate digestions, is less than 4 %. For each metal, a graph of concentration (mg kg^{-1} or %) against depth (cm) was plotted as shown in Figures 6.4-6.9.

In Figure 6.4, the concentration of Pb is relatively constant at 11.8 ± 3.3 mg kg^{-1} from the base of the core until 47 cm. Above 47 cm the concentration rises to give a small sharp peak at 40-46 cm with a value of 30 mg kg^{-1}. From 11 mg kg^{-1} at 39 cm, the Pb concentration rises to 37 mg kg^{-1} at 25 cm and then more steeply to 83 mg kg^{-1} at 9 cm, before declining to 58 mg kg^{-1} at the surface.

In the Zn profile (Fig 6.5) the concentration remains at a constant value of 81 ± 7 mg kg^{-1} from the base of the core until 23 cm. Above 23 cm it rises to a peak of 140 mg kg^{-1} at 9 cm, declining slightly to 120 mg kg^{-1} at 5 cm, thereafter increasing again to a core maximum of 164 mg kg^{-1} at the surface. In Figure 6.6, Cd shows similar trends to Zn with the concentration remaining constant at 0.22 ± 0.05 mg kg^{-1} from the base of the core until 23 cm. Above 23 cm the concentration rises to a peak of 1.02 mg kg^{-1} at 9 cm, thereafter declining (in contrast to Zn) to 0.54 mg kg^{-1} at the surface. Copper (Fig. 6.7) is effectively constant at 16.1 ± 1.8 mg kg^{-1} throughout the core with the exception of a slight increase above 8 cm to 26 mg kg^{-1} at the surface.

Iron (Fig. 6.8) exhibits a fairly constant value of 7.46 ± 0.45 % from 127 cm until 61 cm before dropping to a new constant value of 5.90 ± 0.44 % from 61 cm to 17 cm. The concentration then rises to 7.16 % at the surface. The concentration of Mn (Fig. 6.9) is constant at 0.53 ± 0.05 % from the base of the core until 23 cm. Above 23 cm it rises to a peak of 1.26 % at 3 cm before decreasing to 1.00 % at the surface.

Table 6.3 Heavy metal results for Loch Ness core LN/EM.

Sample Code	Depth / cm	Wet wt / g	Dry Wt / g	Wt / g cm^{-2}	Mid cum. wt / g cm^{-2}	Fe / %	Mn / %	Pb / mg kg^{-1}	Zn / mg kg^{-1}	Cd / mg kg^{-1}	Cu / mg kg^{-1}
NTop	0-2	5.8075	0.7801	0.0235	0.012	7.16	0.996	58	164	0.54	26
N1	2-4	32.7184	4.1600	0.1254	0.086	6.93	1.257	59	124	0.67	19
N2	4-6	44.0136	6.0175	0.1814	0.240	6.44	0.801	65	120	0.92	22
N3	6-8	46.6401	5.8439	0.1761	0.418	6.63	0.801	66	134	0.81	20
N4	8-10	43.2619	4.6318	0.1396	0.576	6.31	0.896	83	140	1.02	18
N5	10-12	42.1831	5.3115	0.1601	0.726	6.45	0.771	71	132	0.65	18
N6	12-14	43.7869	5.5712	0.1679	0.890	6.03	0.753	70	124	0.66	18
N7	14-16	40.9535	5.3568	0.1614	1.055	5.73	0.602	47	93	0.41	16
N8	16-18	41.2061	5.7583	0.1735	1.222	5.78	0.634	65	108	0.42	18
N9	18-20	43.9176	6.7483	0.2034	1.411	6.27	0.565	58	84	0.34	17
N10	20-22	42.5656	6.0698	0.1829	1.604	5.89	0.643	42	100	0.34	18
N11	22-24	43.7614	7.6985	0.2320	1.811	5.34	0.511	26	80	0.28	15
N12	24-26	41.5478	7.5498	0.2275	2.041	5.87	0.562	37	83	0.24	16
N13	26-28	41.2014	7.2014	0.2170	2.263	5.73	0.537	32	78	0.24	17
N14	28-30	45.9259	10.4291	0.3143	2.529	5.63	0.461	25	100	0.21	19
N15	30-32	42.5114	7.7747	0.2343	2.803	6.03	0.531	25	80	0.20	19
N16	32-34	42.5162	7.5603	0.2279	3.034	5.25	0.537	20	73	0.27	15
N17	34-36	41.8912	7.2467	0.2184	3.258	5.43	0.546	22	86	0.28	15
N18	36-38	45.5747	8.6049	0.2593	3.496	5.84	0.550	20	78	0.26	15
N19	38-40	44.9077	9.1117	0.2746	3.763	5.12	0.491	11	71	0.18	15
N20	40-42	42.8190	8.5808	0.2586	4.030	5.74	0.512	27	79	0.24	18
N21	42-44	45.9898	8.1149	0.2446	4.282	5.88	0.541	30	78	0.28	16

Table 6.3 Heavy metal results for Loch Ness core LN/EM, continued.

Sample Code	Depth / cm	Wet wt / g	Dry Wt / g	Wt / g cm^{-2}	Mid cum. wt / g cm^{-2}	Fe / %	Mn / %	Pb / mg kg^{-1}	Zn / mg kg^{-1}	Cd / mg kg^{-1}	Cu / mg kg^{-1}
N22	44-46	45.0592	8.5639	0.2581	4.5330	5.86	0.526	24	80	0.24	18
N23	46-48	40.9551	8.2669	0.2492	4.787	5.77	0.499	15	82	0.38	18
N24	48-50	44.7154	8.5255	0.2569	5.040	6.40	0.509	15	83	0.24	18
N25	50-52	40.7353	8.8416	0.2665	5.301	6.03	0.455	14	83	0.14	19
N26	52-54	38.2945	8.3357	0.2512	5.560	5.89	0.467	9	89	0.19	18
N27	54-56	43.1215	9.1362	0.2754	5.823	6.7	0.470	12	78	0.20	16
N28	56-58	44.8619	11.5656	0.3486	6.135	5.34	0.398	10	87	0.20	17
N29	58-60	42.4733	8.1417	0.2454	6.432	6.65	0.506	10	75	0.14	15
N30	60-62	40.1310	8.0097	0.2414	6.676	6.14	0.481	11	78	0.17	15
N31	62-64	41.1500	8.5807	0.2586	6.926	6.69	0.479	11	82	0.17	13
N32	64-66	44.5583	9.1960	0.2772	7.194	6.41	0.455	17	80	0.18	16
N33	66-68	42.4026	7.0845	0.2135	7.439	7.39	0.540	16	74	0.16	13
N34	68-70	44.5864	7.8157	0.2356	7.664	7.1	0.569	18	86	0.23	14
N35	70-72	40.1781	6.1592	0.1856	7.874	7.67	0.624	14	73	0.28	12
N36	72-74	44.7724	7.1504	0.2155	8.075	7.86	0.538	14	73	0.23	14
N37	74-76	43.6658	7.1193	0.2146	8.290	7.86	0.531	15	74	0.25	14
N38	76-78	40.7386	7.2716	0.2192	8.507	7.36	0.554	17	79	0.23	15
N39	78-80	45.5701	7.6643	0.2310	8.732	6.69	0.547	14	76	0.26	14
N40	80-82	41.0962	6.7717	0.2041	8.949	7.41	0.536	14	71	0.26	14
N41	82-84	42.3100	7.0731	0.2132	9.158	8.25	0.545	16	78	0.22	15
N42	84-86	40.3590	6.4633	0.1948	9.362	7.79	0.526	14	77	0.19	12
N43	86-88	42.4731	8.1710	0.2463	9.582	6.81	0.511	17	76	0.28	14

Table 6.3 Heavy metal results for Loch Ness core LN/EM, continued.

Sample Code	Depth / cm	Wet wt / g	Dry Wt / g	Wt / g cm^{-2}	Mid cum. wt / g cm^{-2}	Fe / %	Mn / %	Pb / mg kg^{-1}	Zn / mg kg^{-1}	Cd / mg kg^{-1}	Cu / mg kg^{-1}
N44	88-90	46.3589	8.1302	0.2450	9.828	7.33	0.534	9	78	0.17	16
N45	90-92	40.1822	7.3971	0.2229	10.062	6.8	0.517	9	79	0.21	16
N46	92-94	38.7050	7.4888	0.2257	10.296	6.97	0.509	9	84	0.18	16
N47	94-96	39.8281	7.5381	0.2272	10.513	7.34	0.499	10	93	0.14	17
N48	96-98	42.4046	7.7286	0.2329	10.743	7.03	0.537	10	83	0.23	17
N49	98-100	40.7669	6.6936	0.2017	10.960	8.05	0.569	9	81	0.24	15
N50	100-102	42.9207	7.9877	0.2407	11.181	7.22	0.635	16	91	0.33	17
N51	102-104	40.9985	7.4327	0.2240	11.414	7.8	0.538	14	82	0.20	14
N52	104-106	39.6130	6.8395	0.2061	11.629	7.39	0.553	9	78	0.24	17
N53	106-108	40.8881	8.0897	0.2438	11.854	7.21	0.494	10	82	0.17	18
N54	108-110	44.9281	10.1293	0.3053	12.128	7.49	0.454	11	85	0.17	19
N55	110-112	47.0235	9.6319	0.2903	12.426	6.46	0.504	11	93	0.21	17
N56	112-114	42.7967	8.3755	0.2524	12.698	6.99	0.507	8	83	0.17	16
N57	114-116	41.0904	8.1723	0.2463	12.947	7.71	0.522	8	76	0.24	18
N58	116-118	41.0010	7.2451	0.2184	13.179	8.15	0.594	9	77	0.24	19
N59	118-120	40.5996	6.9996	0.2110	13.394	8.08	0.543	8	77	0.17	17
N60	120-122	46.4378	7.8613	0.2369	13.618	7.74	0.553	8	76	0.23	17
N61	122-124	43.5518	7.0223	0.2116	13.842	7.95	0.579	6	83	0.20	15
N62	124-126	40.5807	7.3890	0.2227	14.059	7.28	0.590	8	78	0.27	15
N63	126-128	45.3595	7.5039	0.2262	14.284	7.52	0.597	7	74	0.28	15

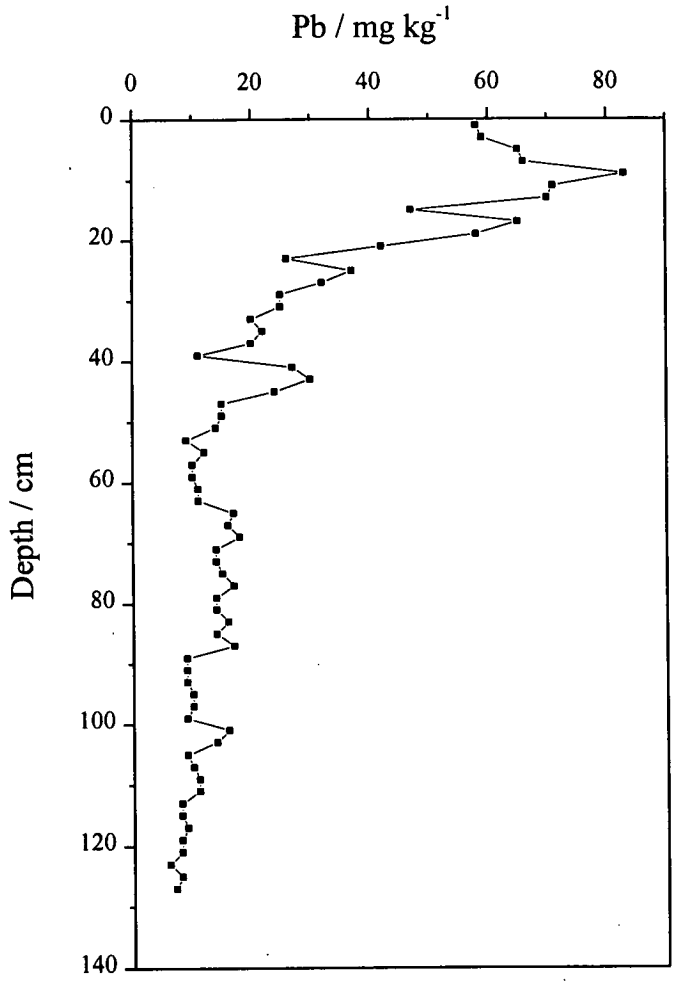

Figure 6.4 Pb (mg kg^{-1}) vs depth (cm) in core LN/EM.

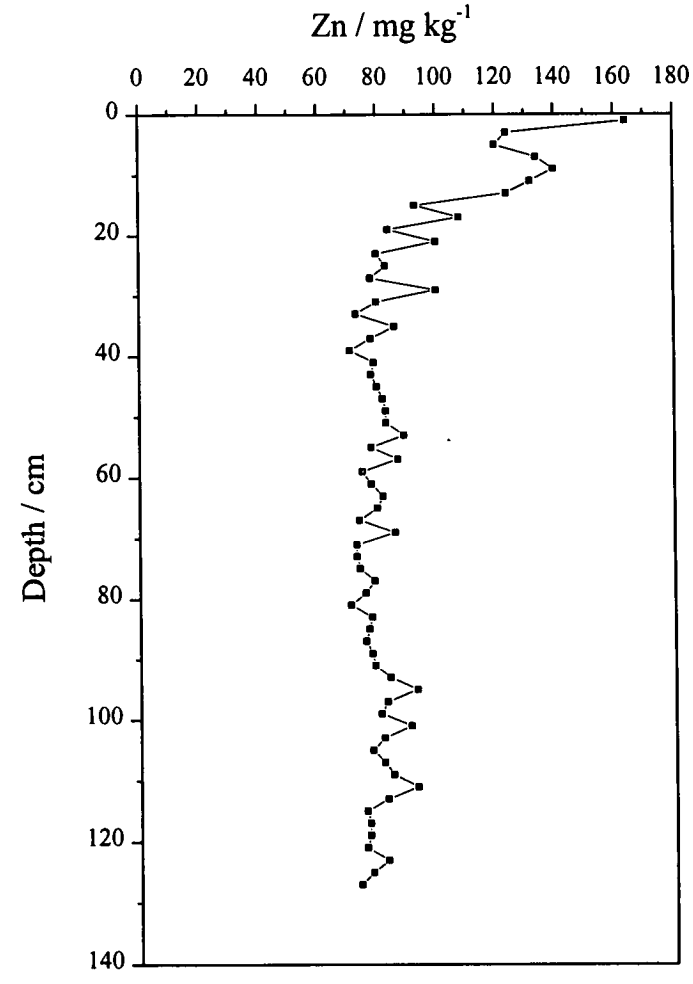

Figure 6.5 Zn (mg kg^{-1}) vs depth (cm) in core LN/EM.

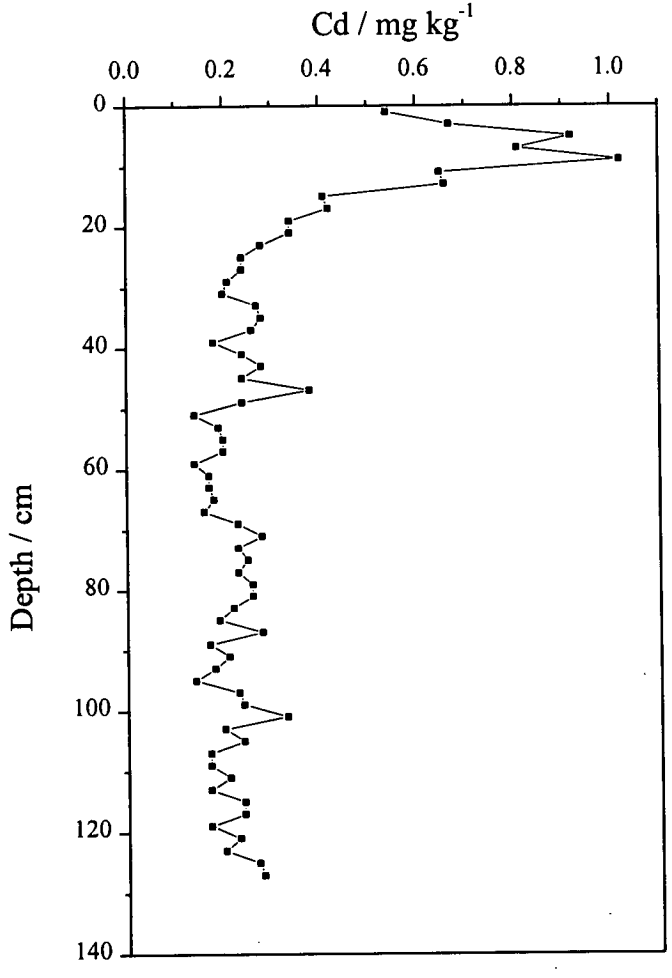

Figure 6.6 Cd (mg kg^{-1}) vs depth (cm) in core LN/EM.

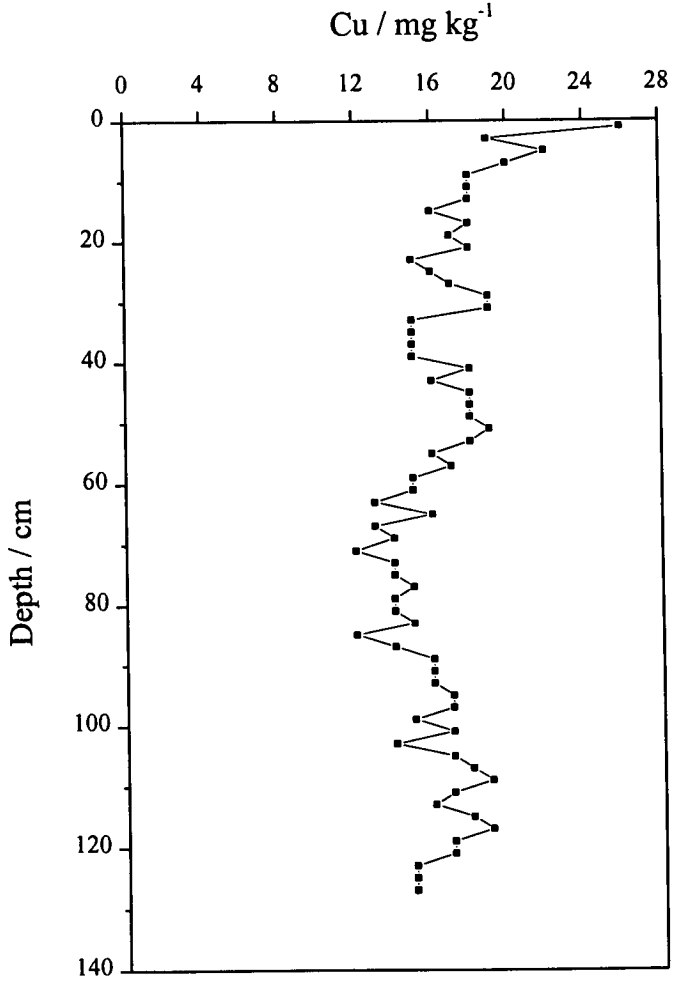

Figure 6.7 Cu (mg kg^{-1}) vs depth (cm) in core LN/EM.

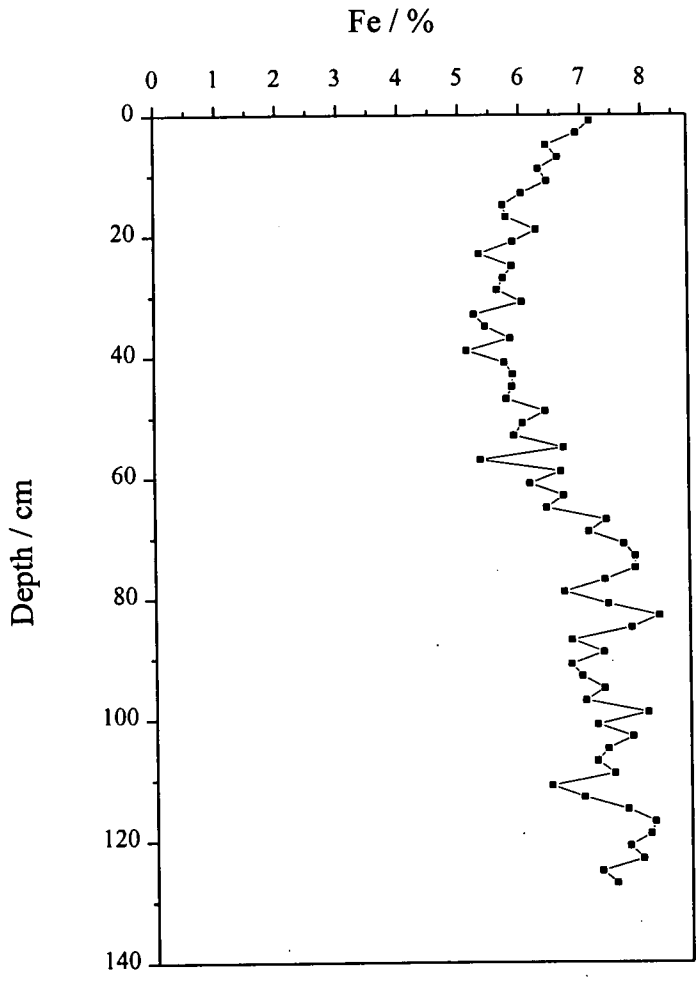

Figure 6.8 Fe (%) vs depth (cm) in core LN/EM.

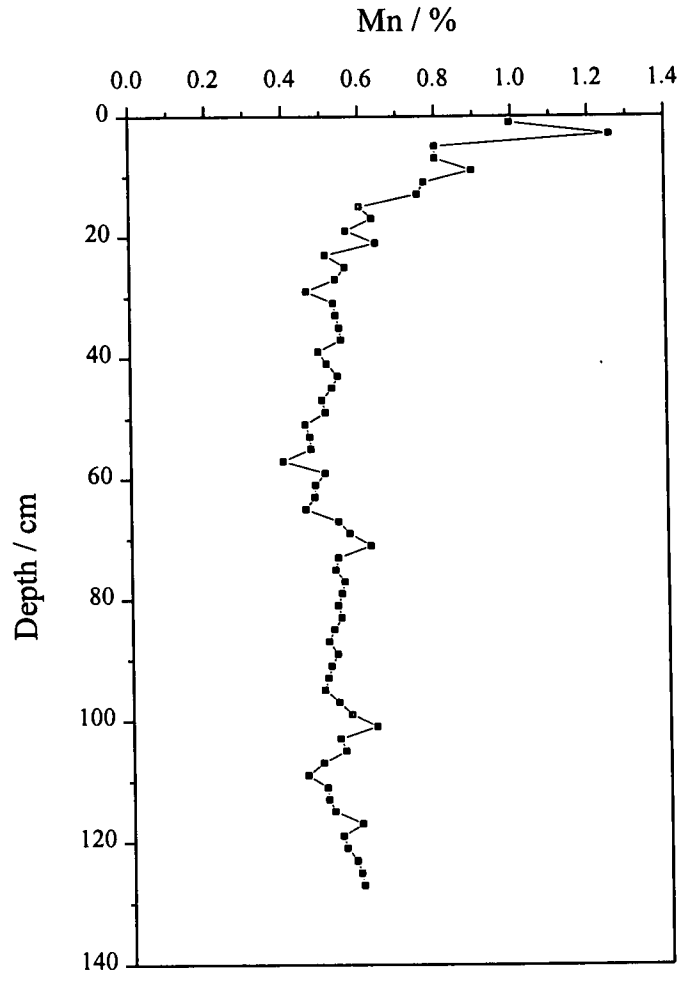

Figure 6.9 Mn (%) vs depth (cm) in core LN/EM.

6.4.4 Stable lead isotopes.

Table 6.4 is a summary of the results for stable Pb isotopes and Pb concentrations (mg kg^{-1}). A graph of each of the three atom ratios $^{206}Pb/^{207}Pb$, $^{208}Pb/^{206}Pb$ and $^{208}Pb/^{207}Pb$ against depth (cm) together with Pb (mg kg^{-1}), is shown in Figures 6.10 (a)-(c), respectively. As shown in Figure 6.10 (a) the $^{206}Pb/^{207}Pb$ atom ratio is 1.230 at the base of the core but drops almost immediately to a minimum of 1.193 by 113 cm. Above 113 cm the ratio rises to 1.214 and remains in this region until 29 cm, with an average of 1.218 ± 0.006 and a maximum of 1.229 at 93 cm. Above 29 cm, and at about the same point where the concentration of Pb begins to rise, the ratio drops sharply from 1.219 to 1.191 then continues to drop more gradually to 1.148 at the surface. Figure 6.10 (b) shows the $^{208}Pb/^{206}Pb$ ratio rising very slowly from 2.050 at the base of the core to 2.101 at 13 cm. Above 13 cm the ratio rises sharply to give a peak with a maximum of 2.151 at 9 cm before tailing off again to reach 2.135 at the surface. The $^{208}Pb/^{207}Pb$ atom ratio (Fig. 6.10 (c)) drops from 2.522 at the base to 2.483 by 113 cm. It rises to a broad peak with a maximum of 2.571 at 81 cm but then drops back to 2.515 until 61 cm. Above 61 cm it rises to a peak of 2.565 at 57 cm then declines to 2.450 at the surface.

6.4.5 Carbon and nitrogen.

Samples LN/N1, N38 and N56 were determined for C (%) and N (%). The C contents were 13.39 %, 10.11 % and 9.27 %, respectively. The N contents were 2.46 %, 1.36 % and 0.45 %, respectively. The precision of the analysis was ± 0.3 %.

6.4.6 X-ray diffraction.

Two samples from core LN/EM were analysed by XRD (N10 and N55) and both were found to be identical in the types of minerals identified, and in the relative quantity of the minerals present. The following minerals were identified as being

present in the samples in order of relative abundance: quartz, muscovite, albite, and hematite.

The following is a summary of the formula and some structural properties of the minerals identified.

Quartz: SiO_2 framework silicate

Muscovite: $K_2(Si_6Al_2)(Al_4)O_{20}(OH)_4$ and $K_2(Si_7Al_1)(Al,Fe^{3+})_3(Mg,Fe^{2+})O_{20}(OH)_4$
layer silicate, 2:1 dioctahedral, 10 Å.

Albite: $NaAlSi_3O_8$
Feldspar, framework silicate, 3.19 Å.

Hematite: Fe_2O_3

Table 6.4 Stable lead isotope and Pb concentration results for Loch Ness core LN/EM.

Sample Code	Depth mid point/ cm	Dry wt / g	Mid cum. wt / g cm^{-2}	Pb / mg kg^{-1}	$^{206}Pb/^{207}Pb$	σ_{n-1}	$^{208}Pb/^{207}Pb$	σ_{n-1}	$^{208}Pb/^{206}Pb$	σ_{n-1}
NTOP	1	0.7801	0.012	58	1.148	0.0015	2.450	0.0060	2.135	0.0030
N1	3	4.1600	0.086	59	1.146	0.0008	2.433	0.0041	2.122	0.0030
N2	5	6.0175	0.240	65	1.154	0.0011	2.464	0.0034	2.136	0.0036
N3	7	5.8439	0.418	66	1.155	0.0010	2.457	0.0120	2.128	0.0091
N4	9	4.6318	0.576	83	1.164	0.0031	2.505	0.0160	2.151	0.0116
N5	11	5.3115	0.726	71	1.177	0.0022	2.524	0.0085	2.145	0.0073
N6	13	5.5712	0.890	70	1.168	0.0014	2.455	0.0056	2.101	0.0027
N7	15	5.3568	1.055	47	1.174	0.0015	2.490	0.0017	2.121	0.0028
N8	17	5.7583	1.222	65	1.176	0.0019	2.465	0.0088	2.097	0.0044
N9	19	6.7483	1.411	58	1.184	0.0023	2.480	0.0122	2.095	0.0069
N10	21	6.0698	1.604	42	1.187	0.0005	2.481	0.0035	2.090	0.0023
N11	23	7.6985	1.811	26	1.192	0.0013	2.492	0.0072	2.091	0.0052
N12	25	7.5498	2.041	37	1.194	0.0014	2.491	0.0023	2.086	0.0035
N13	27	7.2014	2.263	32	1.191	0.0020	2.470	0.0054	2.073	0.0035
N14	29	10.4291	2.529	25	1.219	0.0037	2.534	0.0084	2.080	0.0042
N15	31	7.7747	2.803	25	1.223	0.0073	2.539	0.0085	2.076	0.0093
N16	33	7.5603	3.034	20	1.215	0.0068	2.533	0.0050	2.085	0.0130
N17	35	7.2467	3.258	22	1.207	0.0032	2.519	0.0094	2.087	0.0060
N18	37	8.6049	3.496	20	1.210	0.0056	2.527	0.0060	2.088	0.0100
N19	39	9.1117	3.763	11	1.214	0.0031	2.527	0.0113	2.081	0.0083
N20	41	8.5808	4.030	27	1.203	0.0009	2.501	0.0041	2.079	0.0034
N21	43	8.1149	4.282	30	1.197	0.0014	2.495	0.0111	2.085	0.0084
N22	45	8.5639	4.533	24	1.205	0.0012	2.507	0.0053	2.081	0.0029
N23	47	8.2669	4.787	15	1.210	0.0017	2.521	0.0097	2.084	0.0054
N24	49	8.5455	5.040	15	1.211	0.0022	2.524	0.0101	2.085	0.0061
N25	51	8.8416	5.302	14	1.216	0.0008	2.530	0.0022	2.081	0.0023

Table 6.4 Stable lead isotope results for Loch Ness core LN/EM, continued.

Sample Code	Depth mid point/ cm	Dry wt / g	Mid cum. wt / g cm^{-2}	Pb / mg kg^{-1}	$^{206}Pb/^{207}Pb$	sd +/-	$^{208}Pb/^{207}Pb$	sd +/-	$^{208}Pb/^{206}Pb$	sd +/-
N26	53	8.3357	5.561	9	1.219	0.0016	2.533	0.0014	2.079	0.0020
N27	55	9.1362	5.824	12	1.214	0.0016	2.510	0.0023	2.068	0.0022
N28	57	11.5656	6.136	10	1.217	0.0017	2.520	0.0020	2.070	0.0021
N29	59	8.1417	6.433	10	1.214	0.0021	2.524	0.0091	2.079	0.0063
N30	61	8.0097	6.676	11	1.212	0.0037	2.512	0.0077	2.072	0.0021
N31	63	8.5807	6.926	11	1.214	0.0032	2.518	0.0060	2.074	0.0031
N32	65	9.196	7.194	17	1.213	0.0011	2.514	0.0014	2.073	0.0023
N33	67	7.0845	7.440	16	1.210	0.0027	2.508	0.0071	2.073	0.0058
N34	69	7.8157	7.664	18	1.212	0.0014	2.516	0.0051	2.076	0.0039
N35	71	6.1592	7.875	14	1.215	0.0026	2.521	0.0060	2.075	0.0030
N36	73	7.1504	8.075	14	1.212	0.0050	2.529	0.0114	2.086	0.0049
N37	75	7.1193	8.290	15	1.216	0.0056	2.530	0.0094	2.081	0.0074
N38	77	7.2716	8.507	17	1.223	0.0023	2.541	0.0081	2.079	0.0034
N39	79	7.6643	8.732	14	1.223	0.0042	2.521	0.0057	2.062	0.0050
N40	81	6.7717	8.950	14	1.222	0.0015	2.571	0.0030	2.060	0.0027
N41	83	7.0731	9.158	16	1.224	0.0015	2.544	0.0031	2.069	0.0024
N42	85	6.4633	9.362	14	1.214	0.0021	2.564	0.0047	2.063	0.0018
N43	87	8.171	9.583	17	1.216	0.0021	2.553	0.0024	2.065	0.0020
N44	89	8.1302	9.829	9	1.223	0.0021	2.560	0.0041	2.057	0.0021
N45	91	7.3971	10.063	9	1.227	0.0009	2.547	0.0018	2.067	0.0020
N46	93	7.4888	10.287	9	1.229	0.0014	2.554	0.0052	2.057	0.0026
N47	95	7.5381	10.513	10	1.228	0.0032	2.555	0.0059	2.057	0.0047
N48	97	7.7286	10.743	10	1.224	0.0029	2.556	0.0019	2.053	0.0043
N49	99	6.6936	10.961	9	1.225	0.0015	2.514	0.0011	2.053	0.0030
N50	101	7.9877	11.182	16	1.214	0.0019	2.504	0.0038	2.063	0.0019
N51	103	7.4327	11.414	14	1.214	0.0031	2.505	0.0060	2.064	0.0034

Table 6.4 Stable lead isotope results for Loch Ness core LN/EM, continued.

Sample Code	Depth mid point/ cm	Dry wt / g	Mid cum. wt / g cm^{-2}	Pb / mg kg^{-1}	$^{206}Pb/^{207}Pb$	sd +/-	$^{208}Pb/^{207}Pb$	sd +/-	$^{208}Pb/^{206}Pb$	sd +/-
N52	105	6.8395	11.629	9	1.208	0.0033	2.500	0.0069	2.070	0.0041
N53	107	8.0897	11.854	10	1.203	0.0021	2.494	0.0041	2.073	0.0052
N54	109	10.1293	12.129	11	1.197	0.0014	2.483	0.0072	2.074	0.0049
N55	111	9.6319	12.427	11	1.213	0.0032	2.505	0.0030	2.066	0.0038
N56	113	8.3755	12.698	8	1.193	0.0028	2.483	0.0065	2.081	0.0059
N57	115	8.1723	12.948	8	1.211	0.0030	2.505	0.0056	2.069	0.0015
N58	117	7.2451	13.180	9	1.212	0.0023	2.505	0.0039	2.066	0.0026
N59	119	6.9996	13.394	8	1.218	0.0019	2.510	0.0074	2.061	0.0041
N60	121	7.8613	13.618	8	1.220	0.0035	2.515	0.0056	2.059	0.0061
N61	123	7.0223	13.843	6	1.227	0.0050	2.520	0.0089	2.054	0.0055
N62	125	7.389	14.060	8	1.224	0.0034	2.517	0.0048	2.056	0.0039
N63	127	7.5039	14.284	7	1.230	0.0023	2.522	0.0048	2.050	0.0039

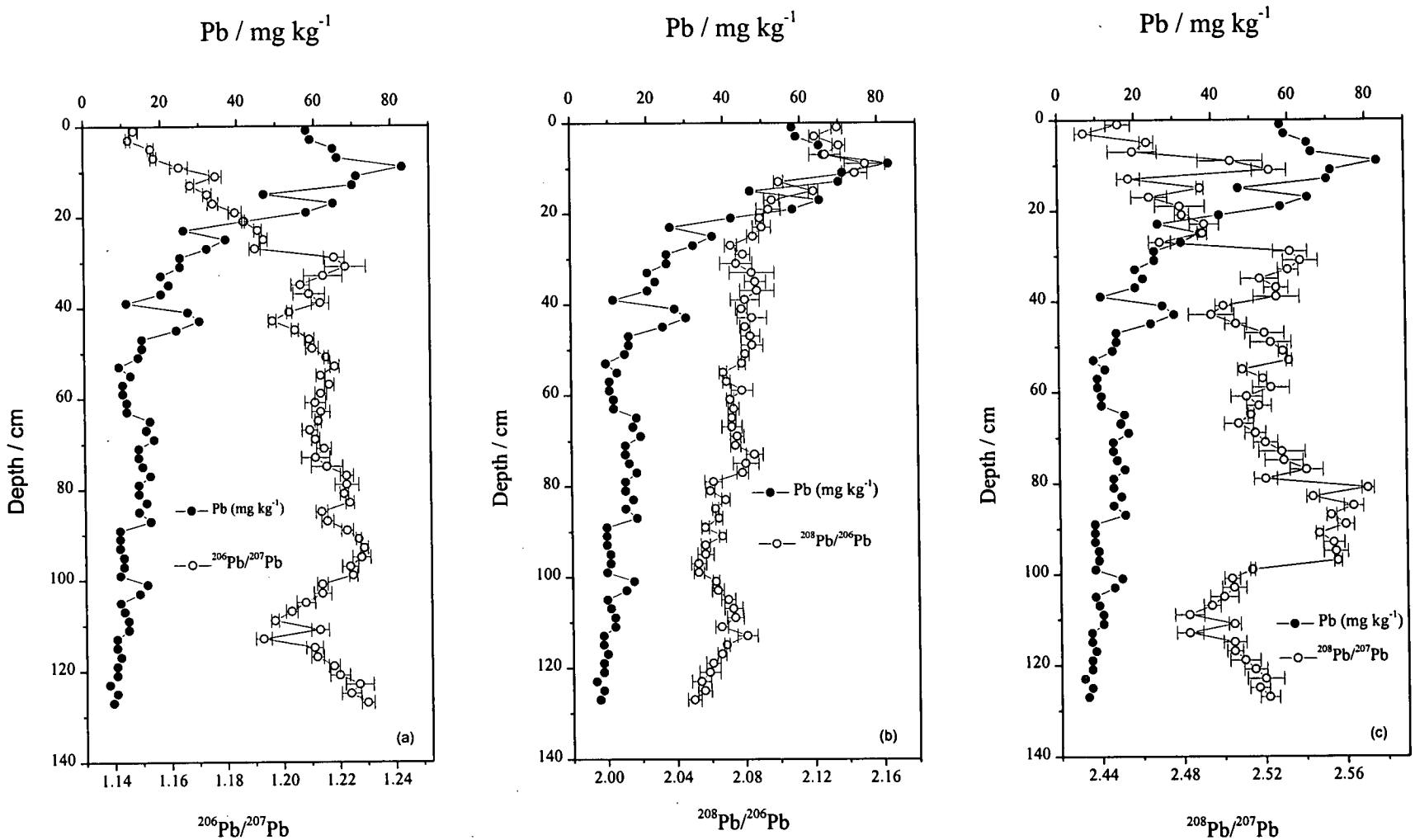

Figure 6.10 Stable lead isotope ratios and Pb concentration (mg kg^{-1}) vs depth (cm) in core LN/EM: (a) $^{206}Pb/^{207}Pb$, (b) $^{208}Pb/^{206}Pb$ and (c) $^{208}Pb/^{207}Pb$.

6.5 Discussion.

6.5.1 Radiocaesium.

Despite the limited data available for ^{137}Cs, it can be seen from Figure 6.2 that there are two peaks in the upper 10 cm of the core. Assuming that these are due to the Chernobyl accident (1st May 1986) and weapons testing fallout (1963), sedimentation rates can be calculated using the cumulative weight of sediment per unit area for the top 10 cm of the core. On this basis, the sedimentation rates for the intervals 1990-1986, 1986-1963 and 1990-1963 are 19.1 ± 14, 14.4 ± 1.1 and 15.5 ± 2.3 mg cm^{-2} y^{-1}, respectively. There is, however, some doubt over the certainty of the upper (Chernobyl) peak being at 3 cm, due to the lack of data available for section 0-2 cm and the possibility of some of the top of the core being lost at the time of sampling. Therefore the peak at 7 cm, representing 27 years of accumulation, is probably the more reliable of the two markers, although 15.5 ± 2.3 mg cm^{-2} y^{-1} should be taken to represent a minimum sedimentation rate for the core.

Using this rate gives a date of penetration for the radiocaesium of approximately 1827, which is too early for the onset of weapons testing, indicating that downward movement of radiocaesium has occurred.

The ^{137}Cs inventory was not able to be separated into Chernobyl and weapons testing components due to the lack of ^{134}Cs data. However the total inventory of ^{137}Cs is 14.7 kBq m^{-2} at the date of sampling (Nov 1990). This inventory is similar to the total inventories for the other three lochs, when the latter are expressed as 1990 values.

6.5.2 ^{210}Pb.

As the ^{210}Pb plot (Fig. 6.3) shows no evidence of mixing, all the available data were employed in the CIC model to give an estimate of the accumulation rate for the core.

The specific activities of $^{210}Pb_{unsupp}$ were calculated by subtracting the specific activities of ^{226}Ra from the specific activities of ^{210}Pb in each section (Table 6.2). The specific activities of the $^{210}Pb_{unsupp}$ were also corrected back to the date of sampling as some decay will have occurred in the 5 year gap between sampling and counting. The natural logarithm of the specific activities of $^{210}Pb_{unsupp}$ were plotted against the mid-point of the cumulative depth (g cm^{-2}) in Figure 6.11 and the gradient of the line was obtained using a weighted linear regression. From the gradient (-2.059 err 0.208), a sedimentation rate of 15.1 ± 1.7 mg cm^{-2} y^{-1} was calculated for the core. Two further gradients were calculated using points 1-7 (gradient -1.919 err 0.265), and 2-7 (gradient -1.178 err 0.199), giving sedimentation rates of 16.2 ± 2.6 and 26.4 ± 5.4 mg cm^{-2} y^{-1}, respectively (Figures 6.11 (b) and (c)). The sedimentation rates obtained using all of the points and the top 7 points were in good agreement. Removing the top point gives a slightly lower gradient leading to a higher sedimentation rate.

Due to the difficulty in assessing the total ^{210}Pb inventory, the CRS model could not be applied to this core. Approximate values for the total ^{210}Pb specific activity and ^{210}Pb flux to the site are 3.21 kBq m^{-2} and 100 Bq m^{-2} y^{-1}, respectively. These values, however, should be taken as a guide only and will be an underestimate of the true value.

Figure 6.11 ln ($^{210}Pb_{unsupp}$) vs depth (g cm^{-2}) in core LN/EM:
(a) all points, (b) points 1-7 and (c) points 2-7.

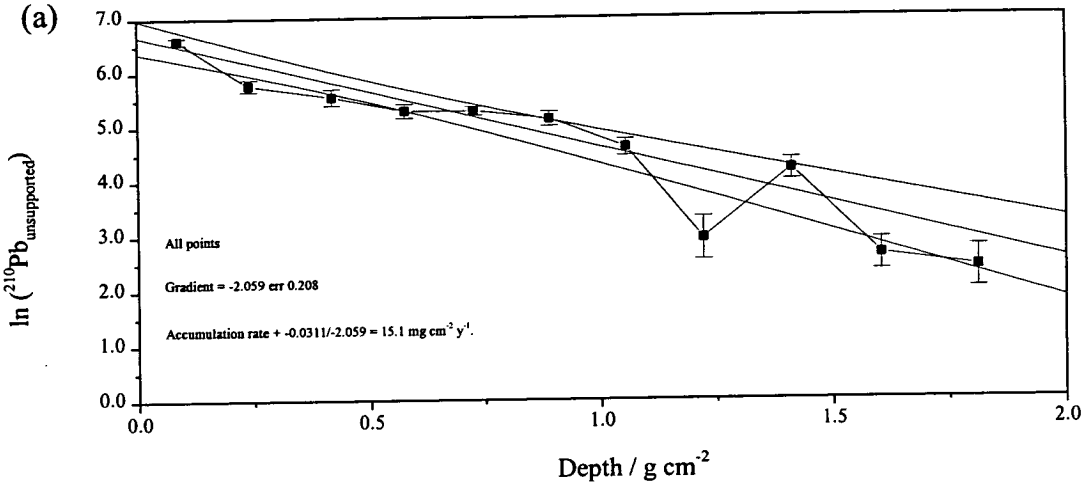

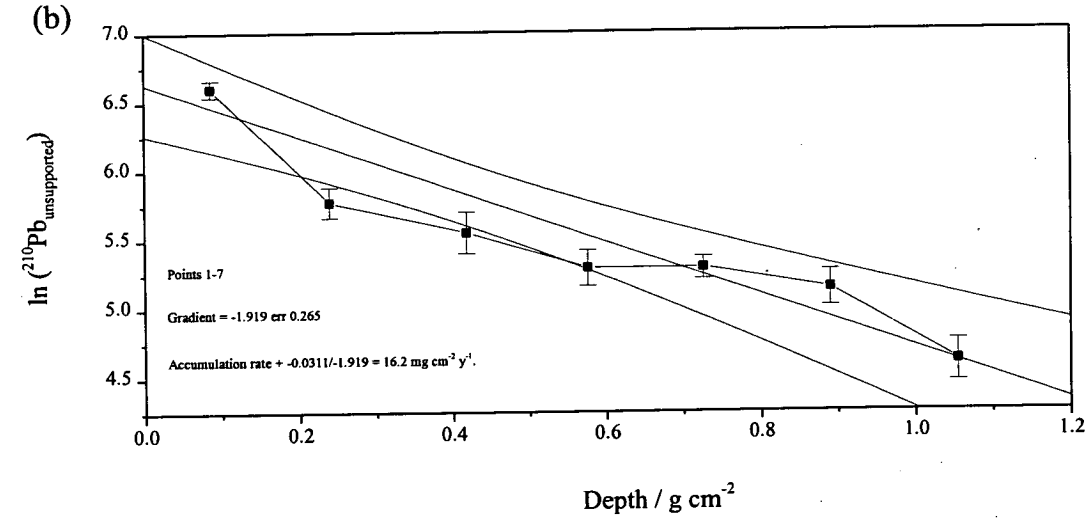

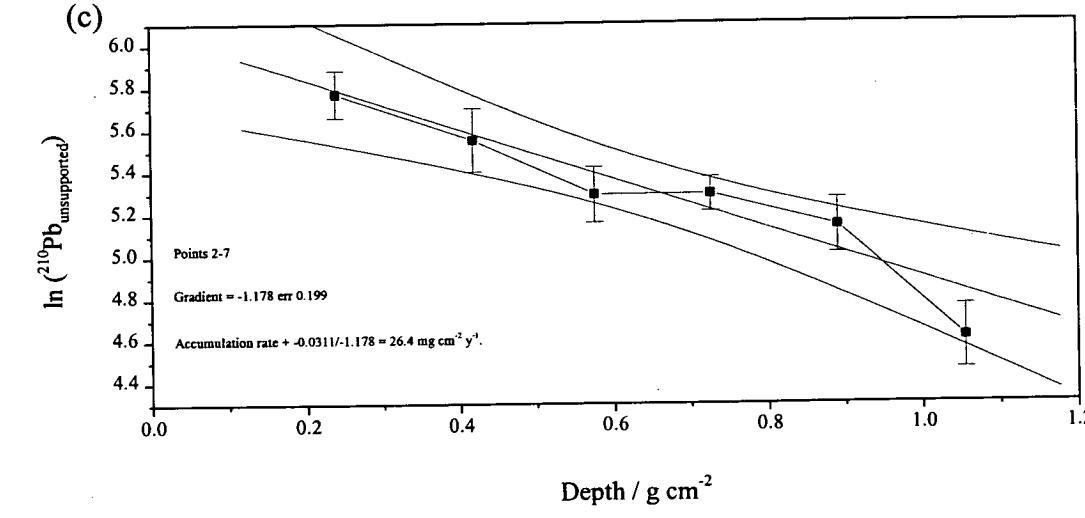

6.5.3 Core chronology.

The values of 15.1 ± 1.7 mg cm^{-2} y^{-1}, obtained for the ^{210}Pb (CIC) model (using all points), and 16.2 ± 2.4 mg cm^{-2} y^{-1} (where only the top 7 points were used) are in excellent agreement with the value of 15.5 ± 2.3 mg cm^{-2} y^{-1} obtained using the position of the weapons testing peak in the ^{137}Cs profile alone. This suggests that at most only a small section of the core was lost at the time of sampling. Table 6.5 shows a comparison of the dates for each section calculated using the two accumulation rates obtained from the CIC ^{210}Pb model. From the Table, there is very little difference between the dates derived using the CIC models (where all points are used) and the ^{137}Cs model (using position of the weapons testing peak). However, as there is some doubt over the position of the Chernobyl ^{137}Cs peaks due to loss of the top section of the core, the core chronology obtained using the ^{210}Pb dating will be used for all subsequent treatment of the data. The lower ^{210}Pb sedimentation rate gives the better fit for the position of the weapons testing peak.

Table 6.5 Comparison of calendar dates for core LN/EM using ^{210}Pb and ^{137}Cs dating.

Sample Code	Depth / cm	Dry wt / g	Mid cum. wt / g cm^{-2}	Years of accumulation ^{210}Pb (15.1 mg cm^{-2} y^{-1})	Date	Years of accumulation ^{210}Pb (16.2 mg cm^{-2} y^{-1})	Date	Years of accumulation ^{137}Cs (15.5 mg cm^{-2} y^{-1})	Date
NTOP	1	0.7801	0.012	0.8	1989.1	0.7	1989.2	0.8	1989.1
N1	3	4.1600	0.086	5.7	1984.2	5.3	1984.6	5.6	1984.3
N2	5	6.0175	0.240	15.9	1974.0	14.8	1975.1	15.5	1974.4
N3	7	5.8439	0.418	27.7	1962.2	25.8	1964.1	27.0	1962.9
N4	9	4.6318	0.576	38.2	1951.7	35.6	1954.3	37.2	1952.7
N5	11	5.3115	0.726	48.1	1941.8	44.8	1945.1	46.8	1943.1
N6	13	5.5712	0.890	58.9	1931.0	54.9	1935.0	57.4	1932.5
N7	15	5.3568	1.055	69.8	1920.1	65.1	1924.8	68.0	1921.9
N8	17	5.7583	1.222	80.9	1909.0	75.4	1914.5	78.9	1911.0
N9	19	6.7483	1.411	93.4	1896.5	87.1	1902.8	91.0	1898.9
N10	21	6.0698	1.604	106.2	1883.7	99.0	1890.9	103.5	1886.4
N11	23	7.6985	1.811	120.0	1869.9	111.8	1878.1	116.9	1873.0
N12	25	7.5498	2.041	135.2	1854.7	126.0	1863.9	131.7	1858.2
N13	27	7.2014	2.263	149.9	1840.0	139.7	1850.2	146.0	1843.9
N14	29	10.4291	2.529	167.5	1822.4	156.1	1833.8	163.2	1826.7
N15	31	7.7747	2.803	185.7	1804.2	173.0	1816.9	180.9	1809.0
N16	33	7.5603	3.034	201.0	1788.9	187.3	1802.6	195.8	1794.1
N17	35	7.2467	3.258	215.7	1774.2	201.1	1788.8	210.2	1779.7
N18	37	8.6049	3.496	231.6	1758.3	215.8	1774.1	225.6	1764.3
N19	39	9.1117	3.763	249.2	1740.7	232.3	1757.6	242.8	1747.1
N20	41	8.5808	4.030	266.9	1723.0	248.8	1741.1	260.0	1729.9
N21	43	8.1149	4.282	283.6	1706.3	264.3	1725.6	276.2	1713.7
N22	45	8.5639	4.533	300.2	1689.7	279.8	1710.1	292.4	1697.5
N23	47	8.2669	4.787	317.0	1672.9	295.5	1694.4	308.8	1681.1
N24	49	8.5455	5.040	333.8	1656.1	311.1	1678.8	325.2	1664.7
N25	51	8.8416	5.302	351.1	1638.8	327.3	1662.6	342.1	1647.8
N26	53	8.3357	5.561	368.3	1621.6	343.3	1646.6	358.8	1631.1
N27	55	9.1362	5.824	385.7	1604.2	359.5	1630.4	375.7	1614.2
N28	57	11.5656	6.136	406.4	1583.5	378.8	1611.1	395.9	1594.0
N29	59	8.1417	6.433	426.0	1563.9	397.1	1592.8	415.0	1574.9
N30	61	8.0097	6.676	442.1	1547.8	412.1	1577.8	430.7	1559.2
N31	63	8.5807	6.926	458.7	1531.2	427.6	1562.3	446.9	1543.0
N32	65	9.196	7.194	476.4	1513.5	444.1	1545.8	464.1	1525.8
N33	67	7.0845	7.440	492.7	1497.2	459.2	1530.7	480.0	1509.9
N34	69	7.8157	7.664	507.6	1482.3	473.1	1516.8	494.5	1495.4
N35	71	6.1592	7.875	521.5	1468.4	486.1	1503.8	508.1	1481.8
N36	73	7.1504	8.075	534.8	1455.1	498.5	1491.4	521.0	1468.9

Table 6.5 Comparison of calendar dates for core LN/EM using ^{210}Pb and ^{137}Cs dating, continued.

Sample Code	Depth / cm	Dry wt / g	Mid cum. wt / g cm^{-2}	Years of accumulation ^{210}Pb (15.1 mg cm^{-2} y^{-1})	Date	Years of accumulation ^{210}Pb (16.2 mg cm^{-2} y^{-1})	Date	Years of accumulation ^{137}Cs (15.5 mg cm^{-2} y^{-1})	Date
N37	75	7.1193	8.290	549.0	1440.9	511.8	1478.1	534.9	1455.0
N38	77	7.2716	8.507	563.4	1426.5	525.1	1464.8	548.9	1441.0
N39	79	7.6643	8.732	578.3	1411.6	539.0	1450.9	563.4	1426.5
N40	81	6.7717	8.950	592.7	1397.2	552.5	1437.4	577.4	1412.5
N41	83	7.0731	9.158	606.5	1383.4	565.3	1424.6	590.9	1399.0
N42	85	6.4633	9.362	620.0	1369.9	577.9	1412.0	604.0	1385.9
N43	87	8.171	9.583	634.6	1355.3	591.5	1398.4	618.3	1371.6
N44	89	8.1302	9.829	650.9	1339.0	606.7	1383.2	634.1	1355.8
N45	91	7.3971	10.063	666.4	1323.5	621.2	1368.7	649.2	1340.7
N46	93	7.4888	10.287	681.3	1308.6	635.0	1354.9	663.7	1326.2
N47	95	7.5381	10.513	696.3	1293.6	649.0	1340.9	678.3	1311.6
N48	97	7.7286	10.743	711.5	1278.4	663.2	1326.7	693.1	1296.8
N49	99	6.6936	10.961	725.9	1264.0	676.6	1313.3	707.1	1282.8
N50	101	7.9877	11.182	740.5	1249.4	690.2	1299.7	721.4	1268.5
N51	103	7.4327	11.414	755.9	1234.0	704.6	1285.3	736.4	1253.5
N52	105	6.8395	11.629	770.2	1219.7	717.9	1272.0	750.3	1239.6
N53	107	8.0897	11.854	785.1	1204.8	731.8	1258.1	764.8	1225.1
N54	109	10.1293	12.129	803.2	1186.7	748.7	1241.2	782.5	1207.4
N55	111	9.6319	12.427	823.0	1166.9	767.1	1222.8	801.7	1188.2
N56	113	8.3755	12.698	840.9	1149.0	783.8	1206.1	819.2	1170.7
N57	115	8.1723	12.948	857.5	1132.4	799.2	1190.7	835.3	1154.6
N58	117	7.2451	13.180	872.8	1117.1	813.6	1176.3	850.3	1139.6
N59	119	6.9996	13.394	887.1	1102.8	826.8	1163.1	864.2	1125.7
N60	121	7.8613	13.618	901.9	1088.0	840.6	1149.3	878.6	1111.3
N61	123	7.0223	13.843	916.7	1073.2	854.5	1135.4	893.1	1096.8
N62	125	7.3890	14.060	931.1	1058.8	867.9	1122.0	907.1	1082.8
N63	127	7.5039	14.284	946.0	1043.9	881.7	1108.2	921.6	1068.3

6.5.4 Stable lead isotopes and lead.

The excess Pb flux was calculated using a baseline value for non-anthropogenic Pb of 11.8 mg kg^{-1}, the average value from 48 cm to the base of the core, and a sedimentation rate of 0.151 kg m^{-2} y^{-1} (from the ^{210}Pb CIC model). The $^{206}Pb/^{207}Pb$ atom ratio of the excess Pb due to anthropogenic input was calculated using the equation shown in section 3.4.2.3. The background $^{206}Pb/^{207}Pb$ atom ratio used was 1.216, corresponding to the same sediment interval as used in calculating the baseline Pb value. The results are summarised in Table 6.6 and a plot of the excess Pb flux and excess $^{206}Pb/^{207}Pb$ atom ratio against date (^{210}Pb chronology) shown in Figure 6.12.

From the graph in Figure 6.12 it can be seen that the fluxes are very low in comparison to those observed much further south in Scotland. However, there are four distinct periods in the flux of excess Pb that can be identified. (1) From 1690-1774, the excess Pb flux rises above 2 mg m^{-2} y^{-1}, but the $^{206}Pb/^{207}Pb$ atom ratio remains relatively constant at 1.194 ± 0.006. (2) From 1774-1822 the excess Pb flux begins to rise steadily although it stays below the maximum value recorded in 1706 and the ratio rises to an average of 1.222 ± 0.008. (3) From 1822-1897 the excess Pb flux begins to increase more rapidly, and the ratio drops to 1.177 ± 0.004. This is slightly higher than the ~1.17 observed for the 'industrial' $^{206}Pb/^{207}Pb$ atom ratio found for 19th Century in Scotland by Sugden *et al.*, (1991a,b) and Farmer *et al.* (1996), but is still within error. (4) From 1897-1991 the excess Pb flux continues to rise, reaching a maximum of 10.8 mg m^{-2} y^{-1} in 1952 but declines again to 7 mg m^{-2} y^{-1} by 1991. During this period the ratio declines from 1.176 to a minimum of 1.129 in 1984, probably as a result of the same influences (e.g. use of ^{206}Pb-depleted ores from Australia in the manufacture of alkyl Pb additives for petrol) as at Loch Lomond and Lake of Menteith sites. The decline in ratio during the 20th Century has already been seen in all the other study sites. The excess Pb flux in the period 1897-1991 accounts for 55 % of the excess inventory of 1.29 g m^{-2}.

Table 6.6 Excess heavy metal fluxes and excess $^{207}Pb/^{207}Pb$ atom ratio in core LN/EM.

Sample Code	Mid depth / cm	Dry wt / g	Mid cum. wt / g cm^{-2}	Yrs. of accum. ^{210}Pb	Date	Excess $^{207}Pb/^{207}Pb$	σ_{n-1}	Excess Pb flux based on ^{210}Pb / mg m^{-2} y^{-1}	Excess Zn flux based on ^{210}Pb / mg m^{-2} y^{-1}	Excess Cd flux based on ^{210}Pb/ mg m^{-2} y^{-1}	Excess Cu flux based on ^{210}Pb / mg m^{-2} y^{-1}
NTOP	1	0.7801	0.012	0.8	1989.1	1.131	0.0025	7.0	12.5	0.048	1.5
N1	3	4.1600	0.086	5.7	1984.2	1.129	0.0022	7.1	6.5	0.068	0.4
N2	5	6.0175	0.240	15.9	1974.0	1.140	0.0023	8.0	5.9	0.105	0.9
N3	7	5.8439	0.418	27.7	1962.2	1.142	0.0022	8.2	8.0	0.089	0.6
N4	9	4.6318	0.576	38.2	1951.7	1.155	0.0037	10.8	8.9	0.120	0.3
N5	11	5.3115	0.726	48.1	1941.8	1.169	0.0030	8.9	7.7	0.065	0.3
N6	13	5.5712	0.890	58.9	1931.0	1.158	0.0024	8.8	6.5	0.066	0.3
N7	15	5.3568	1.055	69.8	1920.1	1.160	0.0025	5.3	1.8	0.029	< 0.1
N8	17	5.7583	1.222	80.9	1909.0	1.167	0.0028	8.0	4.1	0.030	0.3
N9	19	6.7483	1.411	93.4	1896.5	1.176	0.0030	7.0	0.5	0.018	0.1
N10	21	6.0698	1.604	106.2	1883.7	1.176	0.0021	4.6	2.9	0.018	0.3
N11	23	7.6985	1.811	120.0	1869.9	1.172	0.0024	2.1		0.009	< 0.1
N12	25	7.5498	2.041	135.2	1854.7	1.184	0.0024	3.8		0.003	< 0.1
N13	27	7.2014	2.263	149.9	1840.0	1.176	0.0028	3.1		0.003	0.1
N14	29	10.4291	2.529	167.5	1822.4	1.222	0.0042	2.0			0.4
N15	31	7.7747	2.803	185.7	1804.2	1.229	0.0076	2.0			0.4
N16	33	7.5603	3.034	201.0	1788.9	1.214	0.0071	1.2			< 0.1
N17	35	7.2467	3.258	215.7	1774.2	1.197	0.0038	1.5			< 0.1
N18	37	8.6049	3.496	231.6	1758.3	1.201	0.0059	1.2			< 0.1
N19	39	9.1117	3.763	249.2	1740.7	1.194	0.0037	0.0			< 0.1
N20	41	8.5808	4.030	266.9	1723.0	1.193	0.0022	2.3			0.3
N21	43	8.1149	4.282	283.6	1706.3	1.185	0.0024	2.7			< 0.1
N22	45	8.5639	4.533	300.2	1689.7	1.194	0.0023	1.8			0.3
N23	47	8.2669	4.787	317.0	1672.9	1.188	0.0026	0.5			0.3
N24	49	8.5455	5.040	333.8	1656.1	1.193	0.0030	0.5			0.3
N25	51	8.8416	5.302	351.1	1638.8	1.216	0.0022	0.3			0.4

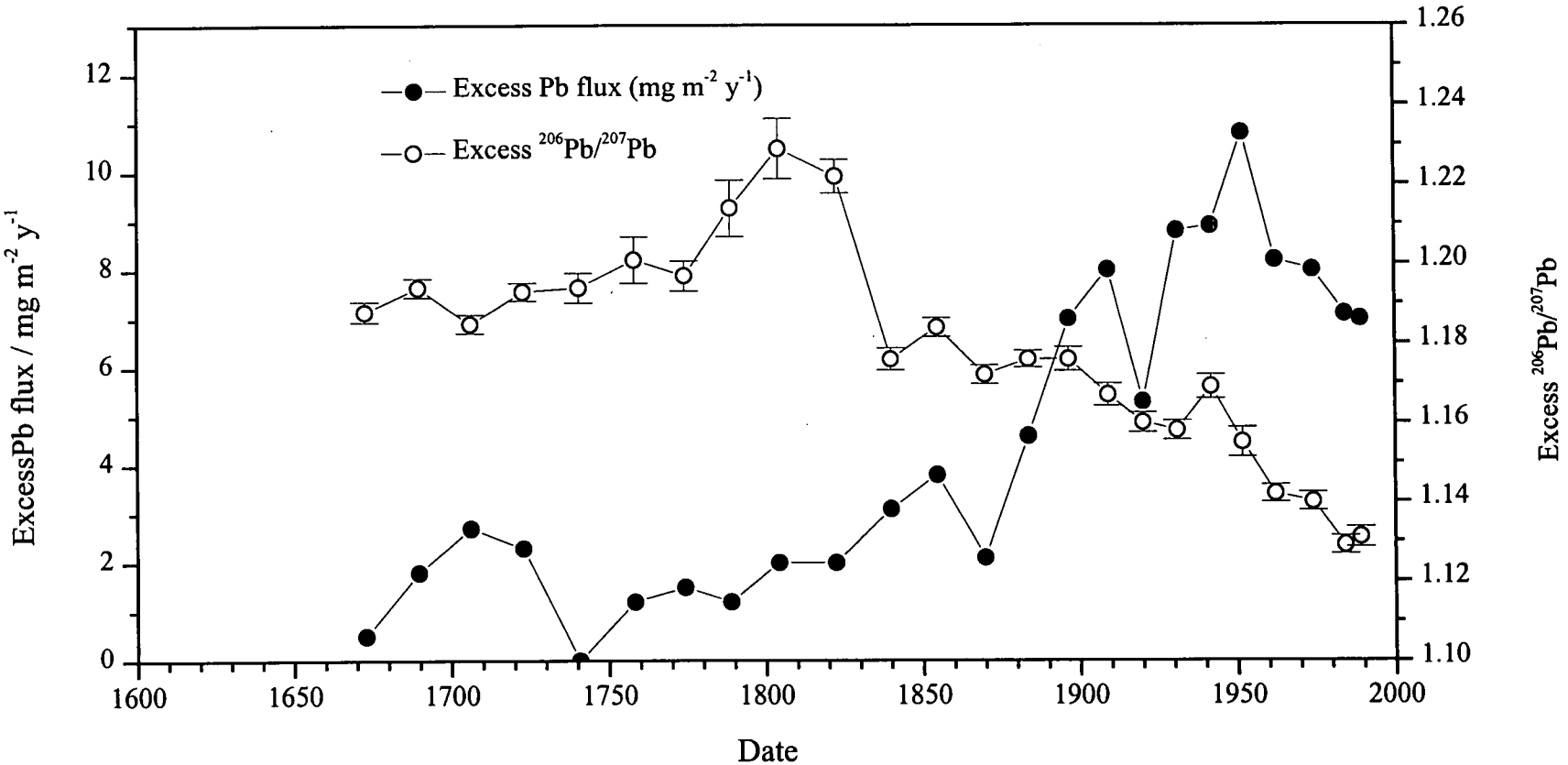

Figure 6.12 Excess Pb flux (mg m^{-2} y^{-1}) and excess $^{206}Pb/^{207}Pb$ vs date in core LN/EM.

6.5.5 Heavy metals.

The excess heavy metal fluxes (mg m^{-2} y^{-1}) are summarised in Table 6.6 and are plotted against date (^{210}Pb chronology) in Figure 6.13. With the exception of Pb, there are no significant increases in the fluxes of the heavy metals until the 20th Century. All the metals show peak levels of deposition at about 1950. Pb increases slowly from 1758 (although there is a small peak at 1706, cf. Table 6.6) until late 19th Century, after which the increase is more pronounced.

The heavy metal profiles all show a much lower level of deposition than has been seen in the other lochs studied. The total excess inventories for the metals Pb, Zn, Cu and Cd are shown in Table 6.7. The lower inventories reflect the remoteness of the location of the loch compared with the other three study sites. There is very little history of any major industry in the region.

Zinc and Cu both show sharp enhancements in concentration in the surface layer of the sediment. The C (%) is 13.39 % in this section (c.f. 9.27 % at 112 cm) suggesting that they are associated with organic matter diagenesis.

The Mn profile is a fairly classical example of diagenetic enhancement in the top few centimetres of the sediment. There is no corresponding peak in the Fe profile.

Figure 6.13 Comparison of excess heavy metal fluxes (mg m^{-2} y^{-1}) vs date in core LN/EM.

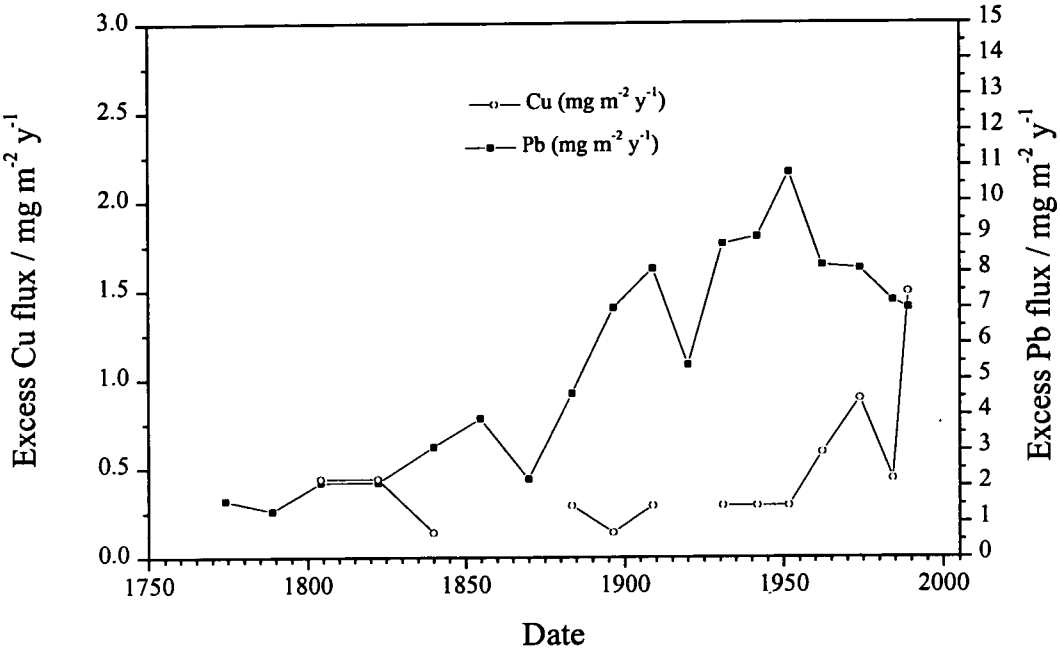

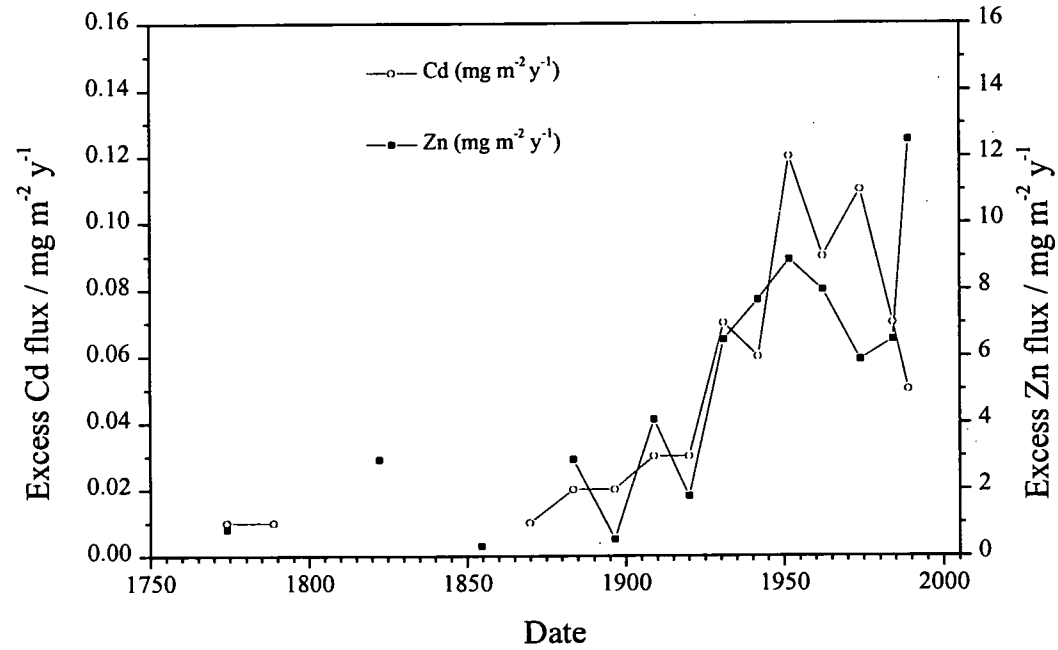

Table 6.7 Excess heavy metal inventories for Loch Ness core LN/EM.

Metal	Background / mg kg^{-1}	Total excess inventory / g m^{-2}	Inventory pre-1900 / %	Inventory post-1900 / %
Pb	11.8	1.29	45	55
Zn	81	0.6	7	93
Cd	0.22	0.03	90	90
Cu	16.1	0.07	0	100

6.6 Conclusions.

The remoteness of the site at Loch Ness is evident from the very low inventories of the heavy metals Pb, Zn, Cd, and Cu in comparison with those observed in the other lochs studied. The industrial signature of the $^{206}Pb/^{207}Pb$ atom ratio over the period 1820-1900 is slightly higher (at 1.177 ± 0.004) than that observed in other sediments in Scotland (1.169-1.171) over this time period, possibly due to the lower impact of industrial pollution, although the value is within the reported errors. As with all the other sites the introduction of Australian/Canadian ore has caused the $^{206}Pb/^{207}Pb$ atom ratio to decrease from the start of the 20th Century until the mid 1980s.

A comparison of the Loch Ness results with the other study sites will be addressed in Chapter 7.

Chapter 7 Comparison and overview of the radionuclide and heavy metal data for the four Scottish freshwater lochs.

The following chapter compares the four study lochs in terms of input fluxes, inventories and sources of radionuclides, Pb and other heavy metals, and their variations with time. In the wider context, comparison is made with findings for other sites in the UK and Europe.

7.1 ^{210}Pb.

Loch Lomond north (Fig. 3.18), Loch Tay east and west (Figs. 5.3 and 5.17) and Loch Ness (Fig. 6.3) all have similar depth profiles of ^{210}Pb with an approximate near-linear decrease in specific activity from the surface (there are some sub-surface peaks but the overall trend is decreasing) followed by steeper decreases from 22.5, 14.0, 11.5, and 9.0 cm, respectively. Lake of Menteith (Fig. 4.2) is also similar but the change (9.5 cm) is more marked. Loch Lomond south (Fig. 3.3) has a pronounced enhancement in the top section of the core followed by a uniform decrease to the base of the core. The only other core to show a slight enhancement at the surface is Loch Tay east.

In all of the cores, ln $^{210}Pb_{unsupp}$ was plotted against cumulative depth (g cm^{-2}) and a weighted linear regression performed to obtain the gradient and, hence, the sedimentation rate. Loch Lomond south, Loch Tay west and Loch Ness showed no major changes in slope, enabling a single sedimentation rate to be determined for the whole core using the majority of the points. The other lochs, however, showed that changes in sedimentation rate had occurred and required the plots to be split into separate components: three for Loch Lomond north and two for each of Lake of Menteith and Loch Tay east. For each component a separate weighted linear regression was performed. A summary of the sedimentation rates thus obtained is given in Table 7.1.

Table 7.1 Comparison of sedimentation rates using ^{137}Cs and ^{210}Pb CIC models for all of the cores.

Core	Surface date	^{137}Cs model Basis	^{137}Cs model Sedimentation rate mg cm^{-2} y^{-1}	^{137}Cs model Application	^{210}Pb CIC model Basis	^{210}Pb CIC model Sedimentation rate mg cm^{-2} y^{-1}	^{210}Pb CIC model Application
Loch Lomond south	1990.6	Surface to weapons peak.	**30.9 +/- 1.3**	applied to whole core.	Wt. linear regr. of all points.	36.8 +/- 8	applied to whole core
Loch Lomond north	1994.6	Surface to Chernobyl peak.	**118.6 +/- 2.6**	surface to 1.127 g cm^{-2}.	Wt. linear regr. using points from surface- first change in gradient.	155.9 +/- 38	0-2.390 g cm^{-2}
		Chernobyl to weapons peak.	**75.5 +/- 9.2**	1.127 g cm^{-2} to base.	Wt. linear regr. using points between first and second change of gradient.	60.3 +/- 3.6	2.590-4.674 g cm^{-2}
					Wt. linear regr. using points from second change in gradient to base.	71.5 +/- 2.7	5.094 g cm^{-2}-base
Lake of Menteith	1995.9	Not used due to movement of ^{137}Cs.			Wt. linear regr. using points from surface-change at 1.038 g cm^{-2}.	**49.3**	0-1.038 g cm^{-2}
					Wt. linear regr. using points from 1.038 g cm^{-2} to base.	**47.6**	1.038 g cm^{-2} to base
Loch Tay east	1995.5	Surface to Chernobyl peak.	**38.9 +/- 0.7**	0-0.397 g cm^{-2}.	Wt. linear regr. using points from surface- change in gradient.	49.5 +/- 20	0-0.397 g cm^{-2}
		Chernobyl to weapons peak.	30.9 +/-1.9	0.397 g cm^{-2} to base.	Wt. linear regr. using points from change in gradient to base.	**30.2 +/- 1.8**	0.397 g cm^{-2} to base
Loch Tay west	1991.9	Surface to weapons peak.	28.6	applied to whole core.	Wt. linear regr. using points 5-16.	**28.3**	applied to whole core
Loch Ness	1989.9	Surface to weapons peak.	15.5 +/- 2.3	applied to whole core.	Wt. linear regr. using all points.	**15.1 +/-1.7**	applied to whole core

Rates highlighted in **Bold** were used to derive the chronology.

Differences in inventories and fluxes of ^{210}Pb measured in lake sediments can be due to geographical rainfall variations or can reflect differences in the catchment runoff, the nature of the settling sedimentary particles or sediment focusing processes within the lake (Kada and Heit, 1992). Results from four different sites in Loch Lomond (Table 7.2) highlight the extent of the variation in ^{210}Pb fluxes that can occur, even in relatively adjacent sites. In the Ardlui basin in the north of Loch Lomond, fluxes and total ^{210}Pb inventories are 8 times higher than at site 1 in the upper reaches of the southern basin (Bryant, 1994) and 4 to 5 times higher than in the lower end of the southern basin. Similarly in Loch Tay there is a two-fold variation between the western and eastern ends of the loch.

Ombrotrophic peat bogs, which receive all of their water and nutrients from the air by wet and dry deposition, have a high capacity to retain a number of trace elements, especially Pb (Rosman *et al.*, 1998; Shotyk *et al.*, 1998). An ombrotrophic peat bog situated south-west of Glasgow (South Drumboy) and a minerotrophic peat bog[♦] to the north of Glasgow (Mugdock) show similar fluxes of ^{210}Pb (106 Bq m^{-2} y^{-1} and 109 Bq m^{-2} y^{-1}, respectively) to that of the southern core (LL/South) in Loch Lomond (MacKenzie *et al.*, 1998a). Fluxes to the ombrotrophic Flanders Moss peat bog are similar to those of the Glasgow peat and Loch Lomond south although there is some variation within the bog (Farmer *et al.*, 1997b).

7.2 Radiocaesium.

Loch Lomond south (Fig. 3.2), Loch Lomond north (Fig. 3.17), Loch Tay east and west (Fig. 5.2 and Fig. 5.16) and Loch Ness (Fig. 6.2) all show two clear peaks relating to the deposition of ^{137}Cs from Chernobyl and weapons testing fallout. Lake of Menteith, in contrast, has only one distinguishable peak. In acidic lochs and lochs with a low clay and high organic content, ^{137}Cs is taken up by organic matter which later decomposes, releasing the ^{137}Cs into the water column or, if buried, into the

[♦] Receives nutrients from ground-water in addition to air deposition.

Table 7.2 Comparison of ^{210}Pb inventories and fluxes and ^{137}Cs inventories for Scottish freshwater loch sediments.

Loch	Total ^{210}Pb / kBq m^{-2}	^{210}Pb flux / Bq m^{-2} y^{-1}	Chernobyl / kBq m^{-2}	Weapons / kBq m^{-2}	Ratio C:W	Total ^{137}Cs / kBq m^{-2} at date of sampling	at 1990
Loch Lomond south (LL/S3A*), 1991	3.66	113	3.87	13.8	0.28	11.9	12.2
Loch Lomond north (LL/NM), 1995	17.8	554	10.7	27.1	0.39	21.3	23.9
Lake of Menteith (LMJ), 1996	6.03	188	unable to be resolved			9.71	11.1
Loch Tay east (LT/EJ), 1996	9.41	293	7.67	10.7	0.72	11.1	12.7
Loch Tay west (LT/WJ), 1992	4.38	136	7.13	9.41	0.76	8.46	8.86
Loch Ness (LN/EM), 1990	**3.21	100	unable to be resolved			**14.7	14.7
* Jenkin core							
**minimum values due to loss of top section of core							
Sediment							
Loch Lomond (Bryant, 1994) site 1 south basin	2.32	72	2.64	10.2	0.26		
site 2 south basin	4.89	152	6.85	14.4	0.48		
Loch Coire nan Arr (Bryant, 1994)	5.40	168					
Clark and Smith (1988)			1-5				
Peirson *et al.* (1982)				6-8			
Peat cores							
Farmer *et al.* (1997) Flanders A	3.54	110	2.24	0.40			
C	2.32	72	3.69	8.58			
D	1.13	35	1.13	0.27			
MacKenzie *et al.* (1998) Mugdock	3.41	106					
S Drumboy	3.50	109					

porewaters (Bryant *et al.*, 1993). By contrast, in lake sediments with a high clay content, ^{137}Cs is taken up into the clay by ion exchange, or adsorption, and is retained in the solid phase during and after burial. Lake of Menteith falls into the first category, the other lochs into the latter.

One of the major aims of this work was to investigate the effect of sectioning cores at higher resolution than the 1-2 cm commonly adopted in the investigation of pollution histories via sediment core analysis. Cores LL/S3A and LT/EJ were sectioned at 3-mm and 2-mm increments, respectively, over the top 20 cm; LL/NM at 2-mm increments over the top 5 cm; LT/WJ and LMJ at 1-cm increments; and LN/EM at 2-cm increments. From Figure 7.1, it is clear that the higher resolution highlights the sharpness of the Chernobyl peak, showing that the majority of the atmospheric deposition occurred as a single, short event lasting a few days, as opposed to the weapons testing fallout, which occurred over a time scale spanning several years.

The sectioning interval also has the direct effect of improving the accuracy with which the sedimentation rates can be evaluated (Eades *et al.*, 1998). For Loch Lomond south, the Chernobyl peak, corresponding to 1986, occurs within the depth range 1.80-2.10 cm, and the weapons testing fallout, corresponding to 1963, in the depth range 5.70-6.00 cm. Therefore, the depth of sediment accumulated in the 23-year period between the weapons testing fallout and Chernobyl events was in the range 3.6-4.2 cm, giving a sedimentation rate in the range 0.16-0.18 cm y^{-1} (i.e. a range of $\pm$ 6% about the mean value of 0.17 cm y^{-1}). By contrast, on the basis of the data presented by Bryant *et al.* (1993), the Chernobyl and weapons testing peaks can be identified to occur in the depth increments 2-3 cm and 5-6 cm, respectively. This gives a range of 2-4 cm of sediment accumulated in the 23 years between the two events, corresponding to a range of sedimentation rates of 0.09-0.17 cm y^{-1} (i.e. a range of $\pm$ 31 % about the mean value of 0.13 cm y^{-1}). Thus, while there is overlap between the estimated ranges of sedimentation rates for the two cores, the uncertainty in the value derived using 1-cm increments is five times greater than that obtained using 3-mm increments.

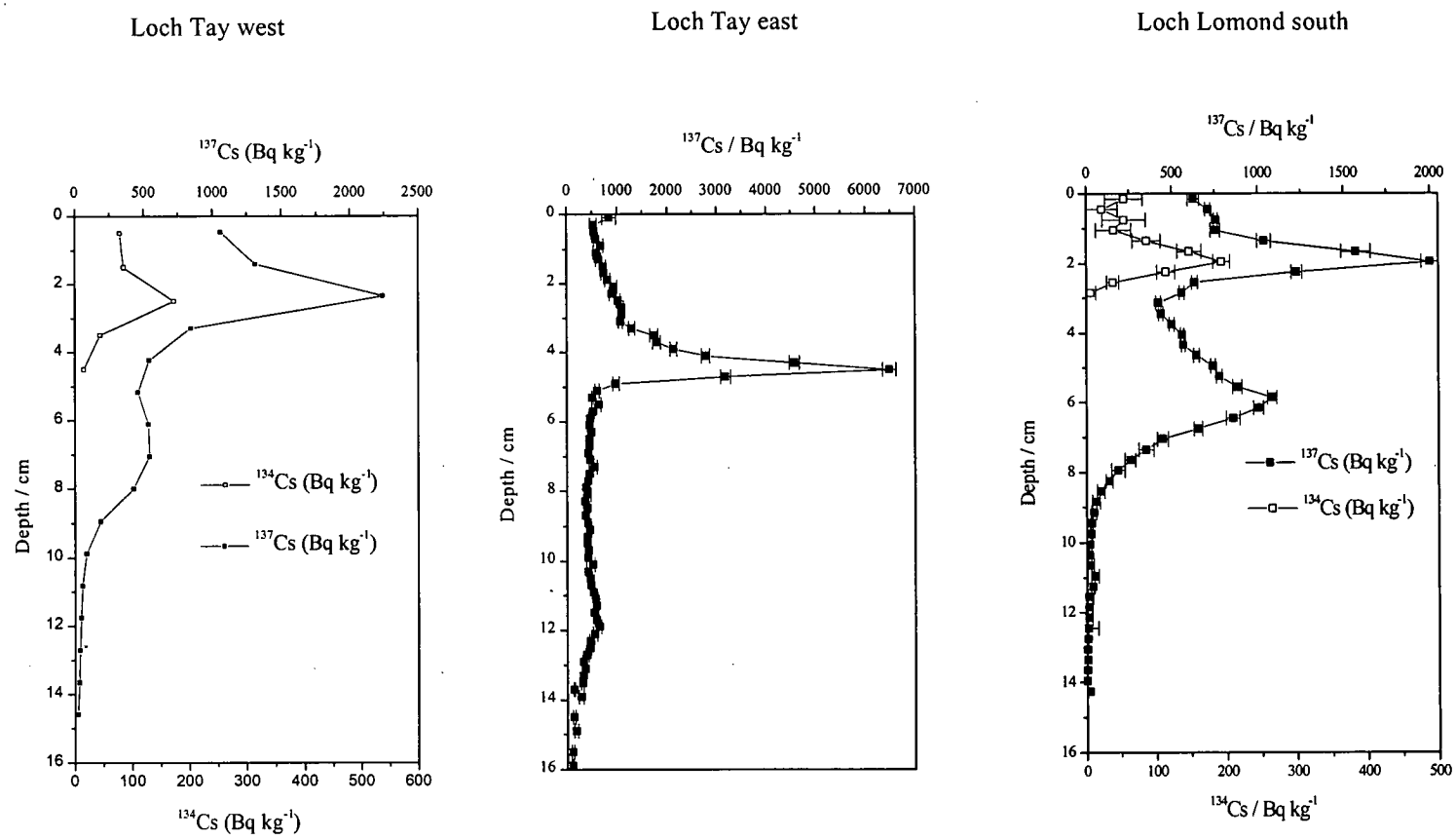

Figure 7.1 Comparison of different sectioning increments on radiocaesium profiles for Loch Tay and Loch Lomond south.

The higher resolution also enables a more accurate separation of the Chernobyl and weapons testing inventories (Eades *et al.*, 1998). Table 7.2 is a summary of the total ^{137}Cs inventories for the Chernobyl and weapons testing fallout for each of the lochs and surrounding peat bog cores. In the case of Lake of Menteith and Loch Ness, where the inventories were not separated, the total inventory at the time of sampling is shown.

The ^{137}Cs inventories for Loch Lomond and Loch Tay were able to be resolved into the two contributions from Chernobyl and weapons testing fallout. At first glance the Chernobyl input is apparently significantly lower in Loch Lomond south and the weapons testing fallout in Loch Lomond north significantly higher than observed in the other sites. However, if the ^{137}Cs inventories are normalised to ^{210}Pb inventories, Loch Lomond north and south, Loch Tay east and west give, for Chernobyl: 0.6, 1.1, 0.8 and 1.6, respectively, and for weapons testing: 3.8, 1.5, 1.1 and 2.1, respectively. The normalised data of Bryant (1994) give 1.1 and 1.4, respectively, for Chernobyl and 4.4 and 2.9, respectively, for weapons testing at Loch Lomond sites 1 and 2. These values illustrate that the higher ^{137}Cs inventories (and ^{210}Pb fluxes) in LL/North and, to a smaller extent, in LT/East are due to catchment input and/or focusing, rather than a higher atmospheric deposition at the site.

The ratio of Chernobyl:weapons testing fallout for ^{137}Cs is different when comparing Loch Lomond (0.28, 0.39) with Loch Tay (0.72, 0.76), so it would appear that Loch Tay has received a relatively greater input of Chernobyl fallout. This may be due to either greater deposition of Chernobyl fallout over Loch Tay, relative to Loch Lomond, or to differing magnitudes of catchment input for Chernobyl, relative to that of weapons, for Lomond and Tay.

For Loch Ness and Lake of Menteith only the total ^{137}Cs inventory was calculated but they both compare well with the other lochs if the inventories are corrected back to

1990[♦] and if the ^{137}Cs inventory for Loch Lomond north is normalised using the ^{210}Pb inventory.

7.3 Sedimentation rates.

The sedimentation rates derived for each loch on the basis of ^{137}Cs and ^{210}Pb models and the specific model used in each case, are summarised together in Table 7.1. In general the ^{137}Cs and the ^{210}Pb CIC models agreed with each other. ^{137}Cs could not be used to establish a chronology for Lake of Menteith due to post-depositional movement of the ^{137}Cs causing a smearing of the peaks. It is suggested that a lower clay content and higher organic fraction is responsible for the movement. In lochs with sediments of high organic content, input peaks of ^{137}Cs may not be retained in the sediment column (Torgensen and Longmore, 1984; Bryant *et al.*, 1993). The sedimentation rate for Loch Tay east is similar to the value of 25.2 ± 2 mg cm^{-2} y^{-1} measured in a core taken at the far eastern end of Loch Tay (Brechin, 1994). Loch Lomond north possessed the highest sedimentation rates (60-120 mg cm^{-2} y^{-1}) in comparison with the other lochs, which had rates in the range of 15-50 mg cm^{-2} y^{-1}.

[♦] Date of collection of the Loch Ness sediment core.

7.4 Stable lead isotopes and lead.

7.4.1 Comparison of lead fluxes with time for Loch Lomond, Lake of Menteith, Loch Tay and Loch Ness.

Figure 7.2 is a comparison of the fluxes of excess Pb against date in all of the cores from Loch Lomond, Lake of Menteith, Loch Tay and Loch Ness.

The longer cores from Loch Lomond and Loch Ness show an increase in Pb fluxes from the middle of the 18th Century and an even sharper increase from the middle of the 19th Century (Fig. 7.2). The fluxes increase more dramatically in the 19th Century through the period of major expansion of heavy industry, fueled by coal burning as the prime energy source. The fluxes continued to increase well into the 20th Century, although there was a temporary lull in the increase between about 1920 and 1930, which is most noticeable in Lake of Menteith. In Loch Tay, both of the cores show a near constant flux of Pb throughout the 18th-19th Century, consistent with the high input from local Pb-ore deposits in the catchment, and subsequent mining activity. Loch Lomond north has fluxes double those seen in Loch Lomond south, the opposite of what might be expected in terms of distance from the central industrial belt. However, the flux of ^{210}Pb is apparently five times higher in the north than in the south but the Pb fluxes are only two times higher (Table 3.17 and 3.18). Lead and ^{210}Pb deposition correlate spatially in water and sediment columns (Boyle *et al.*, 1994). Atmospheric ^{210}Pb is expected to be reasonably constant, as the emission of ^{222}Rn is constant, and changes in the emission of ^{222}Rn and formation of ^{210}Pb subject to less variability than Pb emissions. Thus the enhanced ^{210}Pb flux (and inventory) in Loch Lomond north can be attributed to enhanced catchment input/sediment focusing (Section 3.5.2.2) and Pb fluxes (and inventory) in Loch Lomond north, after normalisation to ^{210}Pb, are actually lower than in Loch Lomond south. Loch Ness, lying well to the north from Scotland's main industrial belt, exhibits a much lower flux of excess Pb.

Figure 7.2 A comparison of fluxes of excess Pb (mg cm^{-2} y^{-1}) against date in all cores.

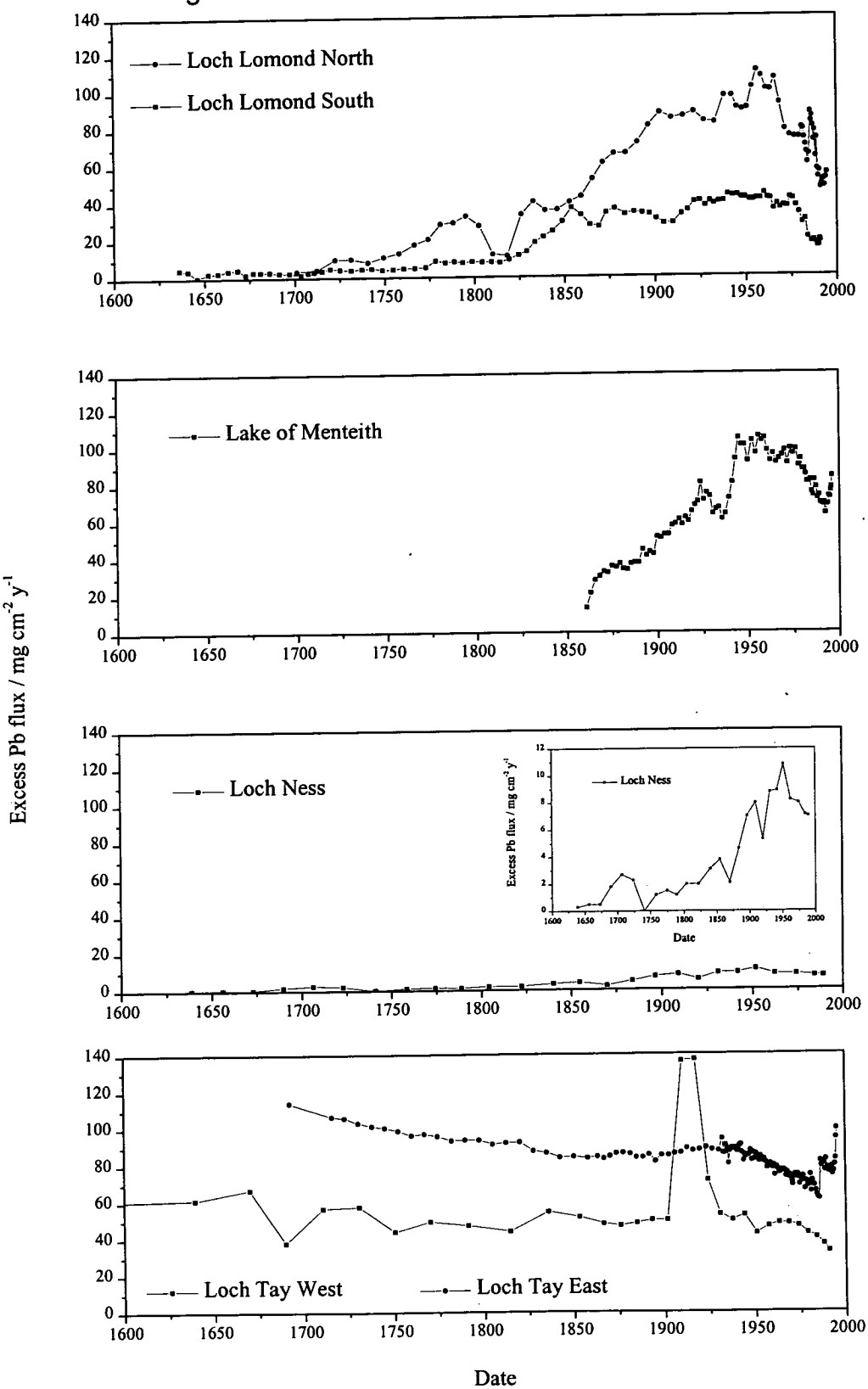

In all of the cores the Pb fluxes begin to decrease from about 1960-1970, similar to that observed elsewhere, e.g. in archived herbage samples from Rothamsted, southern England (Jones *et al.*, 1991). Atmospheric deposition of Pb has greatly reduced since 1986 due to the introduction of unleaded petrol. In Wales results showed a 52-61 % fall in air Pb which is in accord with this and the 63 % reduction in permissible Pb concentrations in petrol from 0.40 to 0.15 g l^{-1}. (Page *et al.*, 1988). AEA Technology (1998) reported a drop in the contribution of emissions of Pb from petrol engine vehicles to the atmosphere from 86 % in 1990 to 74 % in 1994.

7.4.2 Comparison of temporal trends in stable lead isotopic ratios of anthropogenic lead in the sediments of Loch Lomond, Lake of Menteith, Loch Ness and Loch Tay.

Figure 7.3 (a) and (b) is a plot of the $^{206}Pb/^{207}Pb$ atom ratio of excess Pb against date for all of the study sites. It is readily apparent that, whilst Loch Lomond, Lake of Menteith and Loch Ness display very similar profiles, Loch Tay is different and clearly affected by the high degree of mineralisation of the area.

Figure 7.3 (a) Comparison of ^{206}Pb / ^{207}Pb atom ratio of excess Pb vs date in Loch Lomond, Lake of Menteith and Loch Ness.

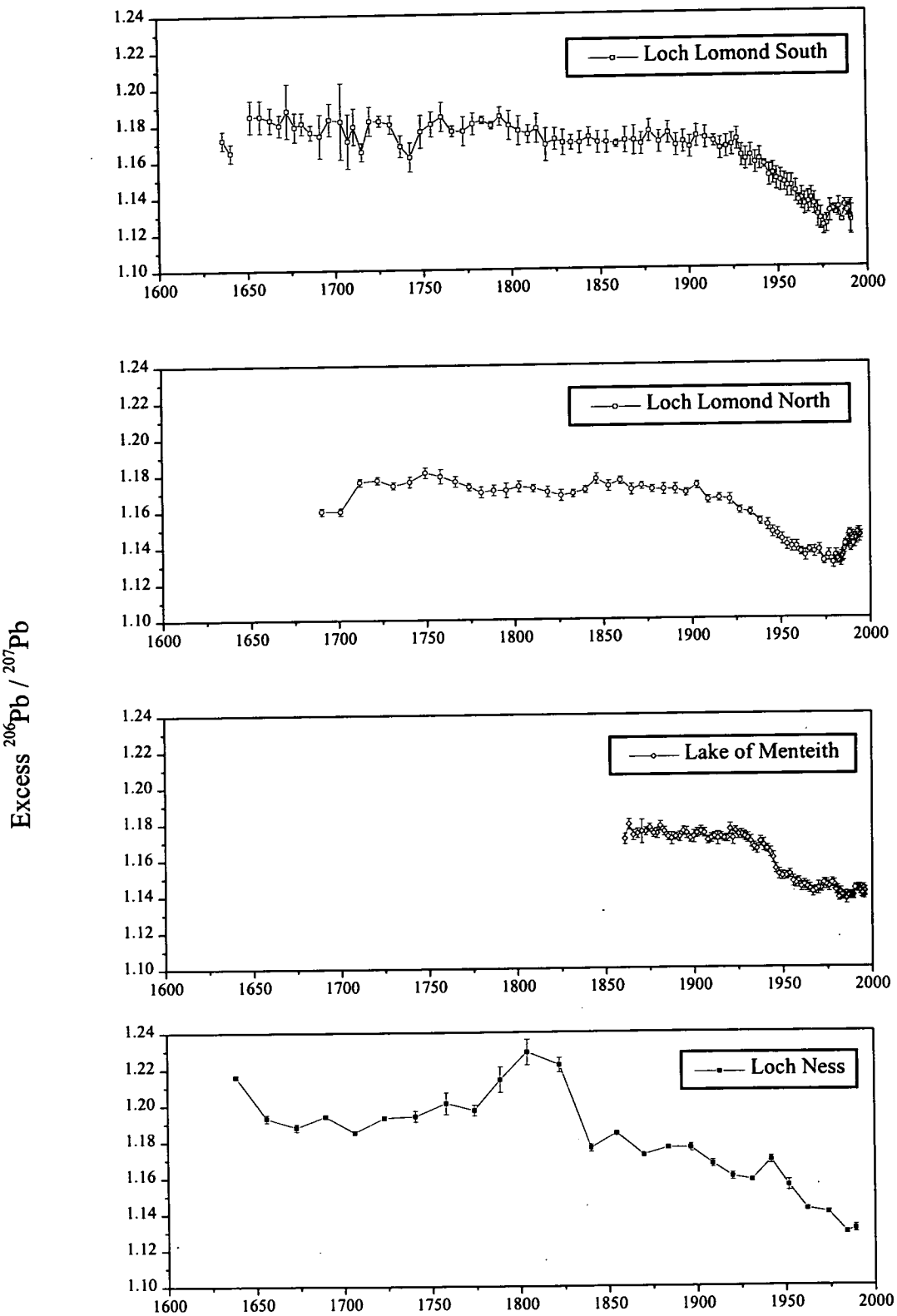

Figure 7.3 (b) Comparison of ^{206}Pb / ^{207}Pb for excess Pb in Loch Tay.

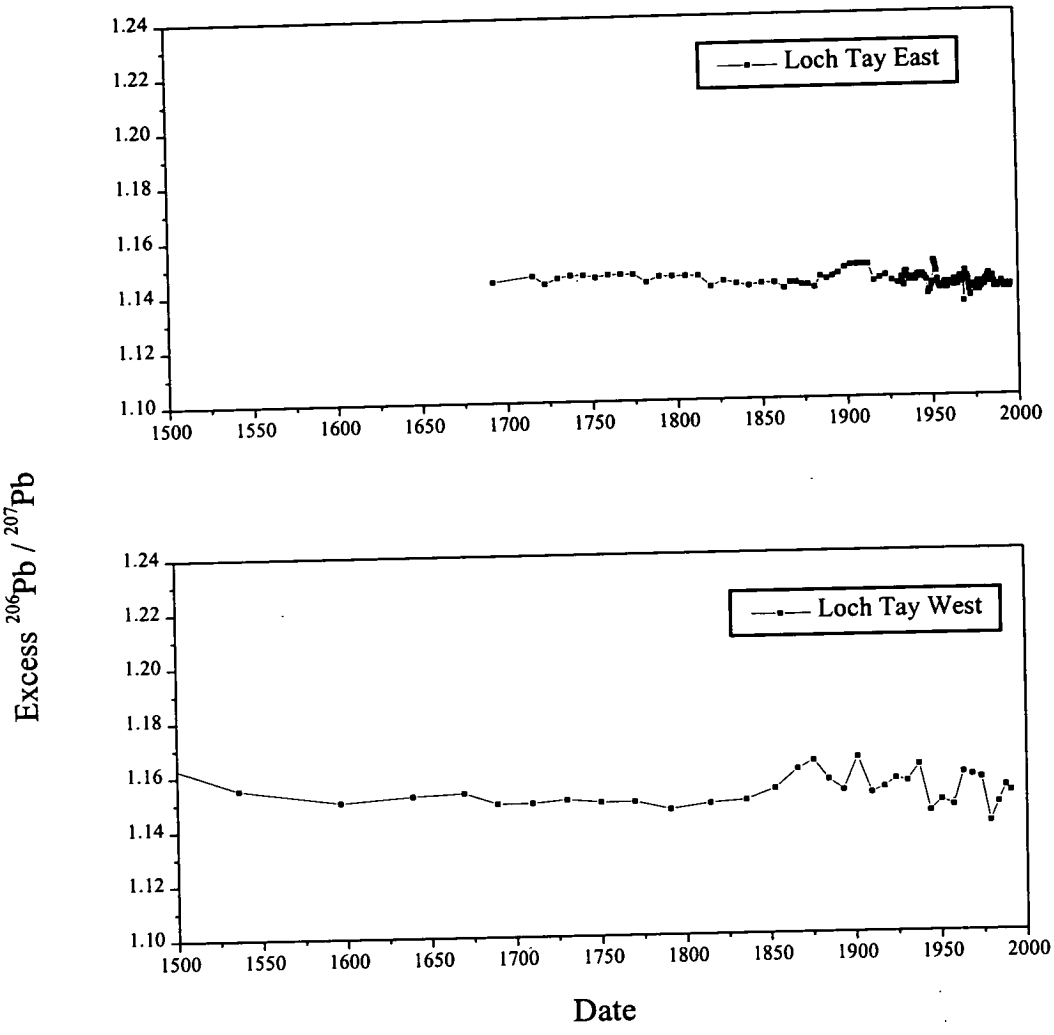

7.4.2.1 Loch Lomond, Lake of Menteith and Loch Ness.

A similar trend is exhibited in all four cores from Loch Lomond, Lake of Menteith and Loch Ness, with five, identifiable, periods for the changes in $^{206}Pb/^{207}Pb$ atom ratio of excess Pb (Fig 7.3 (a)): (1) Pre-1820, (2) 1820-1900, (3) 1900-1930, (4) 1930-1975/1985 and (5) 1975/85-present. Table 7.3 is a summary of the average values of $^{206}Pb/^{207}Pb$ atom ratio of excess Pb for these key periods.

(1) Pre-1820. The excess $^{206}Pb/^{207}Pb$ atom ratio profiles show more variability prior to the main onset of the Industrial Revolution. The ratios are generally higher, particularly for Loch Ness, and probably reflect a more indigenous geochemical origin. The Pb fluxes are much lower at this time and therefore changes in source will have a greater impact. Coal was beginning to be used as an energy and heating source in the central belt of Scotland and could account for the lower ratio in Loch Lomond in comparison with that of Loch Ness[♦]. Changes in source at this time were probably more climate driven with long-range aerosols having an effect. General goegenic $^{206}Pb/^{207}Pb$ atom ratios tend to be more radiogenic than Pb-ores, with $^{206}Pb/^{207}Pb$ atom ratios > 1.2 (Sturges and Barrie, 1987). This could explain the sudden rise in $^{206}Pb/^{207}Pb$ ratio observed to that of Loch Ness at the end of the 18th Century, which may have been caused by an increase in dust in the atmosphere due to volcanic eruptions in Iceland at around that time (e.g. $^{206}Pb/^{207}Pb$ ratios for volcanic ash from Mount Etna range from 1.211-1.280, Monna *et al.*, 1999).

(2) 1820-1900 At the beginning of the 19th Century the anthropogenic $^{206}Pb/^{207}Pb$ ratio fell to a constant value over the entire period in each of the cores. The values of 1.171 ± 0.002, 1.170 ± 0.002, 1.174 ± 0.002 and 1.177 ± 0.004 for Loch Lomond north and south, Lake of Menteith and Loch Ness, respectively, are all consistent with the value of 1.17 quoted by Sugden *et al.* (1991a,b) for 'industrial Pb' in the 19th Century. It is also very close to the values found for southern Scottish lead ores

[♦] Peat is likely to have been the major domestic fuel source around Loch Ness.

Table 7.3 Average values of $^{206}Pb/^{207}Pb$ atom ratios for excess Pb for the main historical periods of change.

				Range	Slope	1975-present	
	pre- 1820	1820-1900	1900-1930	1930-1975		minimum	surface
Loch Lomond south	1.176 +/- 0.003	1.170 +/- 0.002	1.169 +/- 0.002	1.170-1.122	-8.21E-04	1.123	1.131
Loch Lomond north	1.175 +/- 0.003	1.171 +/- 0.003	1.166 +/- 0.002	1.158-1.132	-5.46E-04	1.130	1.145
Lake of Menteith	not applicable	1.174 +/- 0.002	1.173 +/- 0.003	1.171-1.144	-6.96E-04	1.138	1.141
Loch Ness	1.202 +/- 0.014	1.177 +/- 0.004	1.162 +/- 0.005	1.167-1.140	-8.81E-04	1.129	1.131
Loch Tay east	1.147 +/- 0.003	1.145 +/- 0.002	1.147 +/- 0.002	1.143-1.138	-6.93E-04	1.139	1.140
Loch Tay west	*1.152 +/- 0.005	1.154 +/- 0.006	1.152 +/- 0.006	1.156-1.140	none	1.140	1.151

*1.192 pre 1500

of 1.171-1.175 (Sugden *et al.*, 1993). This value is also observed in peat bog cores from Flanders Moss (1.169 ± 0.004, Farmer *et al.*, 1997b) and South Drumboy, south-west of Glasgow (~1.18, MacKenzie *et al.*, 1998a). In Southern England the $^{206}Pb/^{207}Pb$ atom ratio was also found to be 1.170 from 1864-1880 in archived herbage samples (Bacon *et al.*, 1996). Bacon *et al.* suggested that the constancy of the ratio was maintained by either one dominant source or that the mix of sources remained very constant over a prolonged time period.

It was during this period that the onset of deep coal mining, following the introduction of steam powered engines, led to an increase in heavy industry (MacGregor and MacGregor, 1972). Coal, with an average $^{206}Pb/^{207}Pb$ atom ratio of 1.181 ± 0.011 for Scottish coals and 1.184 ± 0.006 for English coals, became an increasingly significant contributor of atmospheric Pb deposition in the UK (Farmer *et al.*, 1999). However, to maintain the ratio at 1.17, there must have been a contribution from some other source(s), most probably Pb smelting, both of indigenous and imported Australian ores.

(3) 1900-1930 The excess $^{206}Pb/^{207}Pb$ atom ratio dropped slightly during this period in Loch Lomond north and in Loch Ness from about 1910. The decline in the ratio did not occur as early as was observed in England where it started in ~1890 (Bacon *et al.*, 1996), nor did it drop by as much (to 1.1575 in Rothamsted in 1911-1915 compared with 1.165 in Loch Lomond north in 1909-1915). In England the decline has been attributed to the increasing import of ^{206}Pb-depleted ores following the decline in British Pb mining (Bacon *et al.*, 1996; Shotyk *et al.*, 1998). By 1930 the ratio in the south of England had fallen to 1.145 but in the four sediment cores the ratio was 1.158 for Loch Lomond north, 1.170 for Loch Ness, 1.161 for Loch Lomond south and 1.171 for Lake of Menteith. Farmer *et al.* (1999) have shown that a combination of Pb emissions from coal burning ($^{206}Pb/^{207}Pb$ 1.181) and smelting of indigenous Scottish Pb ores ($^{206}Pb/^{207}Pb$ 1.170 ± 0.003), with atmospheric transport of Pb from England, where ^{206}Pb-depleted Australian Pb ($^{206}Pb/^{207}Pb$ 1.04) was in greater use, has helped maintain the ratio closer to 1.17. The slight post-1860

decrease in $^{206}Pb/^{207}Pb$ to 1.160 in the late 1920s is also seen in ombrotrophic peat bog cores from south-west of Glasgow (MacKenzie *et al.*, 1998a) and Flanders Moss (Farmer *et al.*, 1997b).

(4) 1930-1975/1985 In all of the cores, the decline in $^{206}Pb/^{207}Pb$ atom ratio, which initially commenced from about 1910 in Scotland, started to decrease more rapidly after the introduction of alkyl Pb-additives in petrol ca. 1928. The isotopic ratio of leaded petrol in the UK is currently 1.06-1.09 (Sugden *et al.*, 1993; Monna *et al.*, 1997), reflecting the mix of Australian ore ($^{206}Pb/^{207}Pb$ atom ratio 1.04) with British Columbian ore ($^{206}Pb/^{207}Pb$ atom ratio 1.16).

In order to establish the nature and the extent of the decline, the change (Δ) in the ratio from the industrial baseline[♦] for each core is plotted against date and with a fourth order polynomial fit in Figures 7.4 (a) and (b). From Figure 7.4 (a) it can be seen that, with the possible exception of Loch Ness, the profiles are very similar. The Δ plot for Loch Lomond north starts to exhibit the decline slightly earlier than those of Loch Lomond south and Lake of Menteith but the gradients are similar (Table 7.3). Changes in values of Δ are highest between 1930 and 1975, with a decrease in Δ values of -0.041, -0.039, -0.035, and -0.035 for Loch Lomond south, Loch Lomond north, Lake of Menteith and Loch Ness, respectively. In Flanders Moss the decline over the same period also showed a change of -0.04 (Farmer *et al.*, 1997b) and for archived herbage in southern England -0.03 (Bacon *et al.*, 1996).

On a European scale, the drop in pre-industrial ratios apparently began in ~1880 at a time of advances in Pb smelting techniques fueled by coal burning. The $^{206}Pb/^{207}Pb$ atom ratios measured in an ombrotrophic peat bog core from the Jura Mountains in Switzerland decreased from 1.1819 ± 0.0003 to 1.1684 ± 0.0004 by 1905 (Shotyk *et al.*, 1998). The introduction of leaded petrol occurred later in Switzerland and therefore the steepening of the decline in $^{206}Pb/^{207}Pb$ occurred after 1945 in Swiss

♦ $\Delta = {}^{206}Pb/^{207}Pb_{ind} - {}^{206}Pb/^{206}Pb_{xs}$ where $^{206}Pb/^{207}Pb_{ind}$ is the constant $^{206}Pb/^{207}Pb$ ratio in each loch during the period 1820-1900.

Figure 7.4 (a) The change in the $^{206}Pb/^{207}Pb$ ratios of excess Pb in Loch Lomond, Lake of Menteith and Loch Ness.

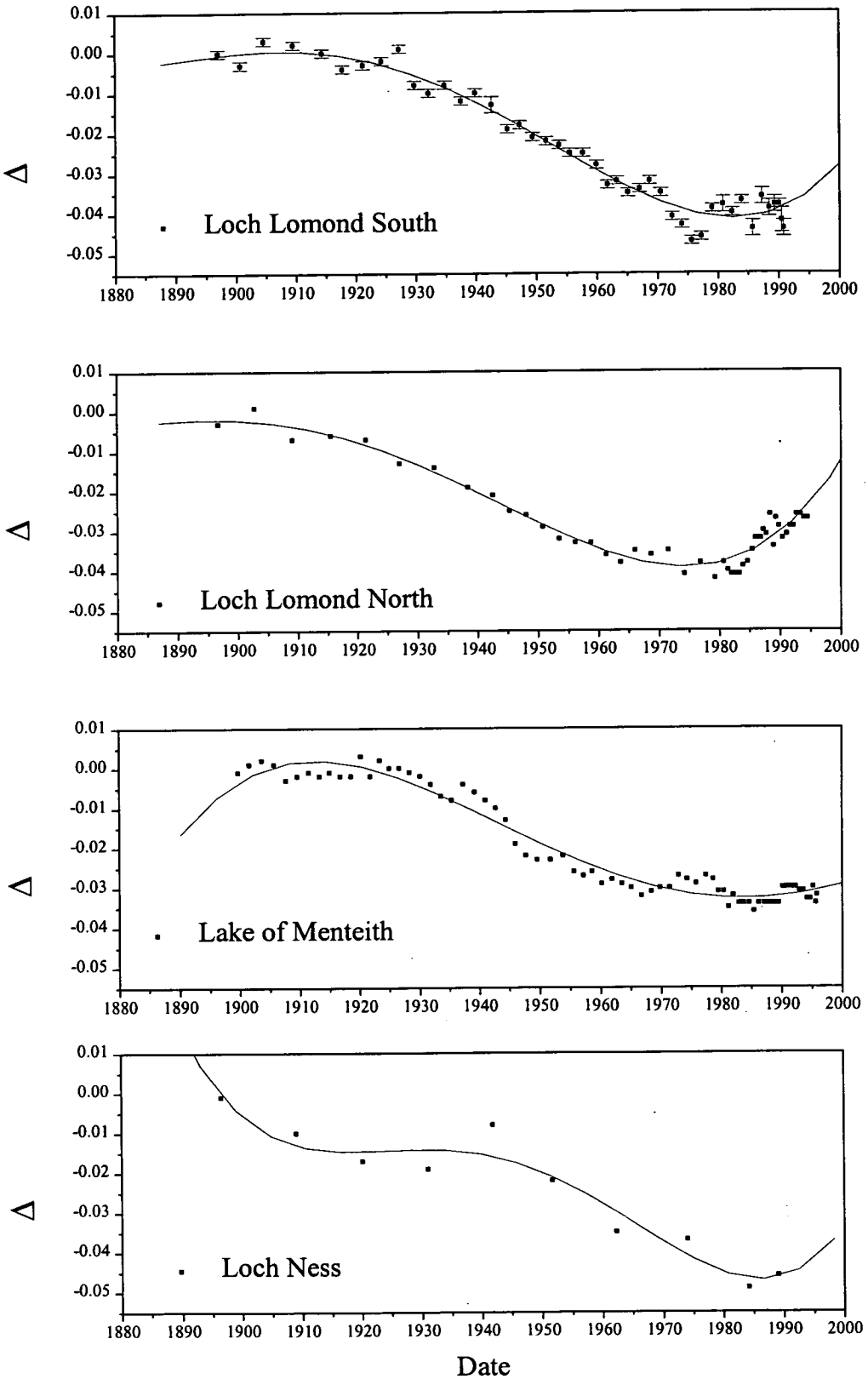

peat bog cores (Weiss *et al.*, 1999). In lake sediments in Switzerland the $^{206}Pb/^{207}Pb$ atom ratio decreased from 1.185 in 1900 to a minimum of 1.130 ~1980 then increased to 1.16 by ~1990 (Moor *et al.*, 1996). A similar downward decline in the ratio from 1.200 to 1.175 was also observed in sediments from Southern Belgium over the period 1880-1979 (Petit *et al.*, 1984). $^{206}Pb/^{207}Pb$ atom ratios in ombrotrophic peat bogs in southern Norway have fallen from ~1.17 ca 1921 to 1.123 ca 1991 (Dunlap *et al.*, 1999).

(5) 1975/85-present

The introduction of legislation in 1985 to phase out the use of leaded petrol has brought about an upturn in the $^{206}Pb/^{207}Pb$ atom ratios. The increase in ratio is most noticeable in the Loch Lomond cores with a rise of ~0.01. In Southern England the $^{206}Pb/^{207}Pb$ atom ratio rose from 1.0974 in 1981-1985 to 1.1286 in 1986-1988 (Bacon *et al.*, 1996). In a study on tree rings from England, the $^{206}Pb/^{207}Pb$ atom ratios for wood formed between 1965 and 1987 were relatively constant, at around 1.16, but increased sharply after 1987 to over 1.17 in 1993 (Watmough *et al.*, 1999).

The increase in $^{206}Pb/^{207}Pb$ atom ratio was not observed in the Flanders Moss peat cores or in southern Norway, probably due to inferior time resolution (Farmer *et al.*, 1997b; Dunlap *et al.*, 1999), but in peat from Switzerland, it was observed (Shotyk *et al.*, 1998). It has been estimated that emissions of Pb from petrol in the UK have fallen from 2900 tonnes in 1986 to 1000 tonnes in 1996 (DETR, 1997). With petrol Pb emissions falling significantly, other sources of Pb, such as incinerator emissions and the recycling of battery Pb, will play a more dominant role in determining the Pb isotope signature.

7.4.2.2 Loch Tay.

In Loch Tay the $^{206}Pb/^{207}Pb$ atom ratio profiles (Fig. 7.3 (b)) are markedly different from those of the other three lochs. The ratio is almost constant throughout the eastern core at 1.145 ± 0.002 and the western core at 1.153 ± 0.002 from 1600-1850, then rising to above 1.16 and remaining between 1.14-1.165 throughout the 20th Century. At depth in the western core and at dates preceding 1500, the ratio is significantly higher than seen from 1600 onwards, lying between 1.19 and 1.20. As the onset of mining at Tyndrum apparently did not occur until much later in 1739, it is possible that the extrapolated chronology is in error. This is perhaps a consequence of an alteration to the sedimentation rate due to mining activities.

Towards the end of the 19th Century, in both cores (but most noticably in the west) the ratio begins to rise, the opposite to what is observed in the other cores and in southern England. This could be due to a combination of a reduction in the amount of Pb-mining, coupled with increasing use of coal and heavy industry bringing the ratio up towards the value of 1.17 observed in the rest of the country. After the introduction of ^{206}Pb-depleted ores and their use in the production of alkyl Pb additives for petrol, the eastern core shows a drop in ratio from 1.147 to ~1.143 where it remains until about 1945. After 1945 there is a small, but noticeable drop (also observed in the western core), perhaps due to the reopening of the Tyndrum mines for a short period at this time.

The Δ plots (Fig 7.4(b)) for Loch Tay are very different from the other three lochs due to the dominant influence of the local Pb-deposits. The eastern core shows a slight downward decline from the start of the 20th Century but shows no upturn in ratio from 1986. The change in Δ for the decline is only -0.008, significantly different to the values of 0.03 and 0.04 obtained for the other three lochs. The values for the western core are scattered, but within ± 0.01, since the start of the 20th Century.

Figure 7.4 (b) The change in the $^{206}Pb/^{207}Pb$ ratios of excess Pb in Loch Tay.

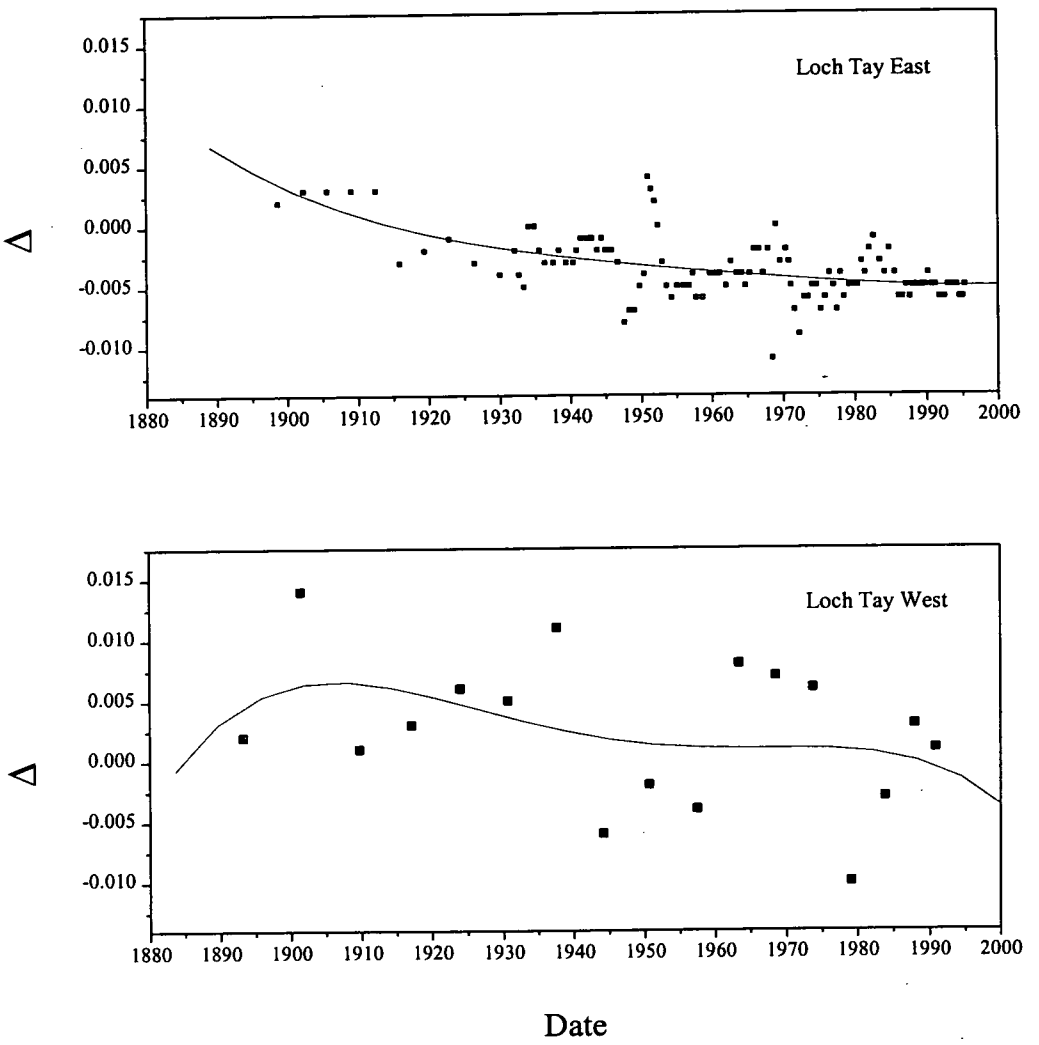

7.4.3 Source apportionment.

Source apportionment calculations can be used to estimate the influence of dominant sources on the atmospheric Pb load to the environment. It is generally assumed that leaded petrol has been the predominant source of Pb emissions since its introduction in the late 1920s. The following equation can be used to calculate the fractional contribution of leaded petrol to the anthropogenic Pb recorded in the lake sediments, assuming: (1) car-exhaust emissions were the sole source of the ^{206}Pb-depleted Pb used to manufacture alkyl Pb additives; and (2) the "industrial" $^{206}Pb/^{207}Pb$ atom ratio of ~1.17 to the atmosphere observed for the 19th Century persisted during the 20th Century,

$$Pb_{petrol}\,(\%) = \frac{^{206}Pb/^{207}Pb_{ind} - {}^{206}Pb/^{207}Pb_{excess}}{^{206}Pb/^{207}Pb_{ind} - {}^{206}Pb/^{207}Pb_{petrol}} \times 100$$

The ratio for $^{206}Pb/^{207}Pb_{ind}$ for each core was taken from the period 1820-1900. The ratio of the petrol lead has varied with time and information on the exact ratios is not known. However, measurements since 1989 have shown a range of 1.06-1.09 (Farmer *et al.*, 1996) and together with an upper limit of 1.12 (Hopper *et al.*, 1991) to reflect input from imported alkyl Pb additives from the United States, these values have been used to calculate the percentage of petrol Pb contribution to the anthropogenic Pb content of each section in all the cores. The results for the source apportionment calculations for each core are summarised in Table 7.4. In Figure 7.5, the contribution of petrol Pb to the excess inventory for that period (taking the average value for the petrol $^{206}Pb/^{207}Pb$ ratio of 1.09) is shown as a bar chart.

In the time period 1930 to the present, petrol Pb has contributed between 22 and 63 % (based on the $^{206}Pb/^{207}Pb$ ratios for leaded petrol of 1.06-1.12) of the anthropogenic Pb deposited in each of the lochs, but it represents only between 8 and 30 % of the total excess inventory in the sediments. The lochs all show a similar Pb contribution

Table 7.4 Source apportionment calculations to estimate the contribution from petrol Pb to the sediment inventory of anthropogenic Pb.

	1929-1995			1929-1975			1975-1995		
Loch Lomond north	1.06	1.09	1.12	1.06	1.09	1.12	1.06	1.09	1.12
Petrol Pb / g m^{-2}	1.78	2.43	3.87	1.50	20.60	3.27	0.27	0.37	0.59
Total Pb / g m^{-2}	6.45			5.54			0.91		
%	27.5	37.7	59.9	27.6	37.2	59.0	30.0	41.1	65.3
% of core	12.6	17.3	45.8						

	1929-1991			1929-1975			1975-1991		
Loch Lomond south	1.06	1.09	1.12	1.06	1.09	1.12	1.06	1.09	1.12
Petrol Pb / g m^{-2}	0.53	0.74	1.19	0.38	0.53	0.85	0.16	0.22	0.36
Total Pb / g m^{-2}	2.29			1.87			0.42		
%	23.3	32.2	51.9	20.4	28.1	45.3	37.9	52.3	84.4
% of core	8.4	11.6	18.7						

	1928-1996			1928-1975			1975-1996		
Lake of Menteith	1.06	1.09	1.12	1.06	1.09	1.12	1.06	1.09	1.12
Petrol Pb / g m^{-2}	1.26	1.71	2.67	0.86	1.17	1.82	0.40	0.54	0.84
Total Pb / g m^{-2}	5.75			4.38			1.37		
%	22.0	29.8	46.4	19.7	26.7	41.6	29.3	39.7	61.8
% of core	14.1	19.1	29.8						

	1930-1992			1930-1974			1974-1992		
Loch Ness	1.06	1.09	1.12	1.06	1.09	1.12	1.06	1.09	1.12
Petrol Pb / g m^{-2}	0.18	0.17	0.27	0.14	0.14	0.21	0.03	0.04	0.06
Total Pb / g m^{-2}	0.56			0.49			0.07		
%	31.9	31.2	47.5	29.6	27.6	42.2	47.9	55.4	84.5
% of core	13.8	13.5	20.6						

Figure 7.5 Source apportionment for Pb in petrol based on $^{206}Pb/^{207}Pb$ ratio of 1.09.

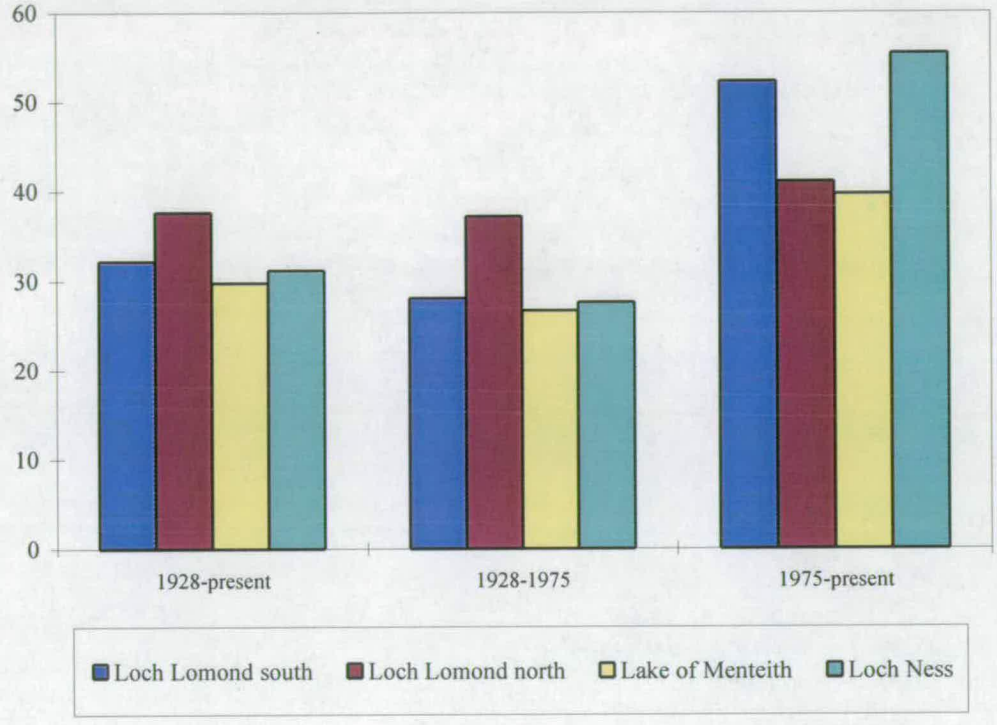

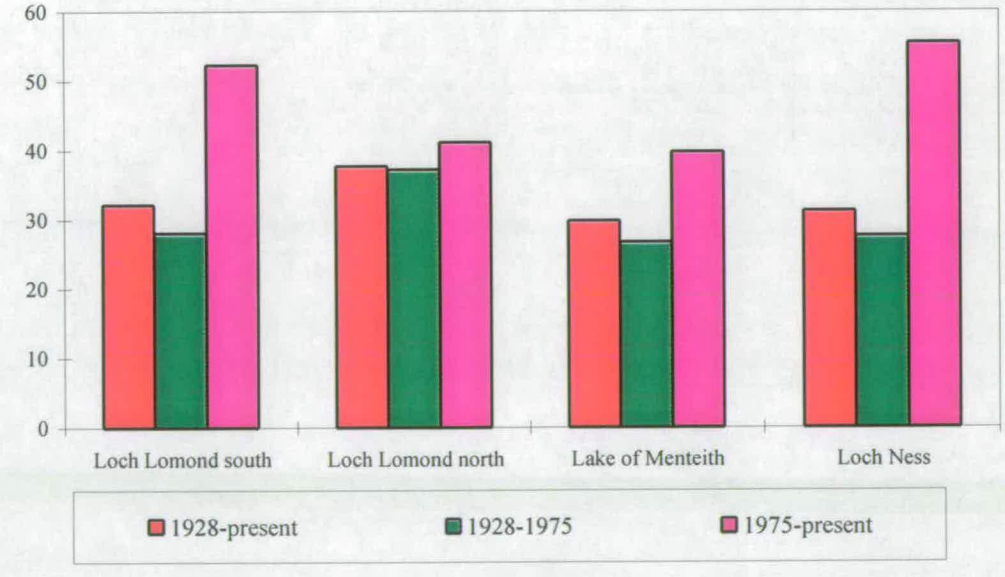

from petrol. The range in petrol Pb inventory (using the $^{206}Pb/^{207}Pb$ ratios 1.06-1.12) for Loch Ness is the highest out of the lochs (32-48 %).

This perhaps reflects a smaller influence from other industrial inputs. When split into two sections 1930-1975 and 1975-present, to reflect the decline in heavy industry, most of the lochs, with the exception of Loch Lomond north, show a slightly higher contribution due to petrol Pb since 1975. The contribution from petrol for Loch Lomond south (38-84 %) and Lake of Menteith (29-62 %) from 1975, for leaded petrol $^{206}Pb/^{207}Pb$ ratios of 1.06-1.12, is consistent with corresponding data (20-82%) from Flanders Moss peat bog cores (Farmer *et al.*, 1997b).

A second useful method for distinguishing between possible Pb sources is the use of the other isotopic ratios $^{208}Pb/^{207}Pb$ and $^{208}Pb/^{206}Pb$ (Shotyk *et al.*, 1998; Dunlap *et al.*, 1999). In Figure 7.6, the $^{208}Pb/^{206}Pb$ vs. $^{206}Pb/^{207}Pb$ profiles have been plotted for Loch Lomond north and Loch Tay east. Loch Lomond north shows a 2 component profile with a major shift at 1915. This indicates a major change in the predominant source of Pb brought about by the imports of foreign Pb-ore and the introduction of leaded petrol. Loch Tay by contrast shows a much smaller shift to higher $^{208}Pb/^{206}Pb$ atom ratios after 1900. The spread of data is very narrow, highlighting the dominant effect of the local Pb-ore deposits.

Figure 7.6 $^{208}Pb/^{206}Pb$ vs $^{206}Pb/^{207}Pb$ of anthropogenic Pb in Loch Lomond and Loch Tay.

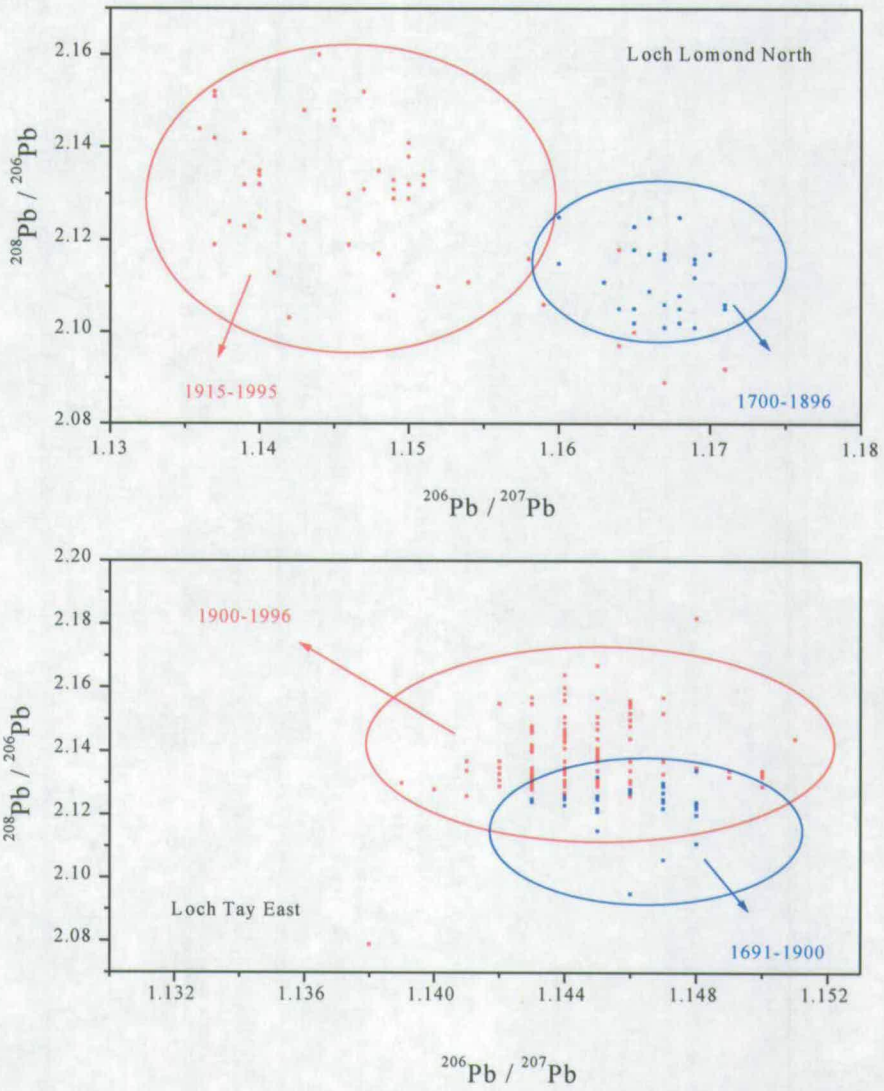

7.4.4 Inventories of excess lead.

Table 7.5 is a summary of the inventories of excess Pb split into the time periods pre-1820, 1820-1900, 1900-1930, 1930-present[♦]. The inventories for each period in each loch are shown graphically in Figure 7.7. The Pb inventories in Loch Lomond north and south and Lake of Menteith are similar, and are skewed towards the later part of the 20th Century. Loch Ness inventories are negligible in comparison with those of the other lochs, but does have a slightly higher inventory for 1930-present than in the periods pre-1930. Loch Tay, by comparison, has a bimodal profile, reflecting the input from Pb mining in the 18th-19th Centuries. The inventory decreased in the latter part of the 19th Century due to closure of the Pb mines but then, as with the other sites, increased as a result of the addition of alkyl-petrol Pb additives in the latter part of the 20th Century.

[♦] Date of collection of core.

Table 7.5 Inventories of excess (anthropogenic) Pb in the sediments of Scottish freshwater lochs.

	Loch Lomond south		Loch Lomond north		Lake of Menteith		Loch Ness		Loch Tay east	
Period	Inventory / g m^{-2}	% of total core	Inventory / g m^{-2}	% of total core	Inventory / g m^{-2}	% of total core	Inventory / g m^{-2}	% of total core	Inventory / g m^{-2}	% of total core
pre-1820	0.81	12.7	1.79	12.7	0.04	0.4	0.29	22.6	15.1	51.5
1820-1900	2.17	34.1	3.61	25.7	1.56	18	0.29	22.5	6.5	22.2
1900-1930	1.09	17.1	3.09	22	1.65	19.5	0.25	19.3	2.7	9.3
1930-present	2.29	36.0	5.57	39.6	5.7	62.1	0.46	35.7	5.0	17.1
Total	6.36		14.1		8.95		1.29		29.4	

Figure 7.7 Inventories of excess (anthropogenic) Pb in the sediments of Scottish freshwater lochs.

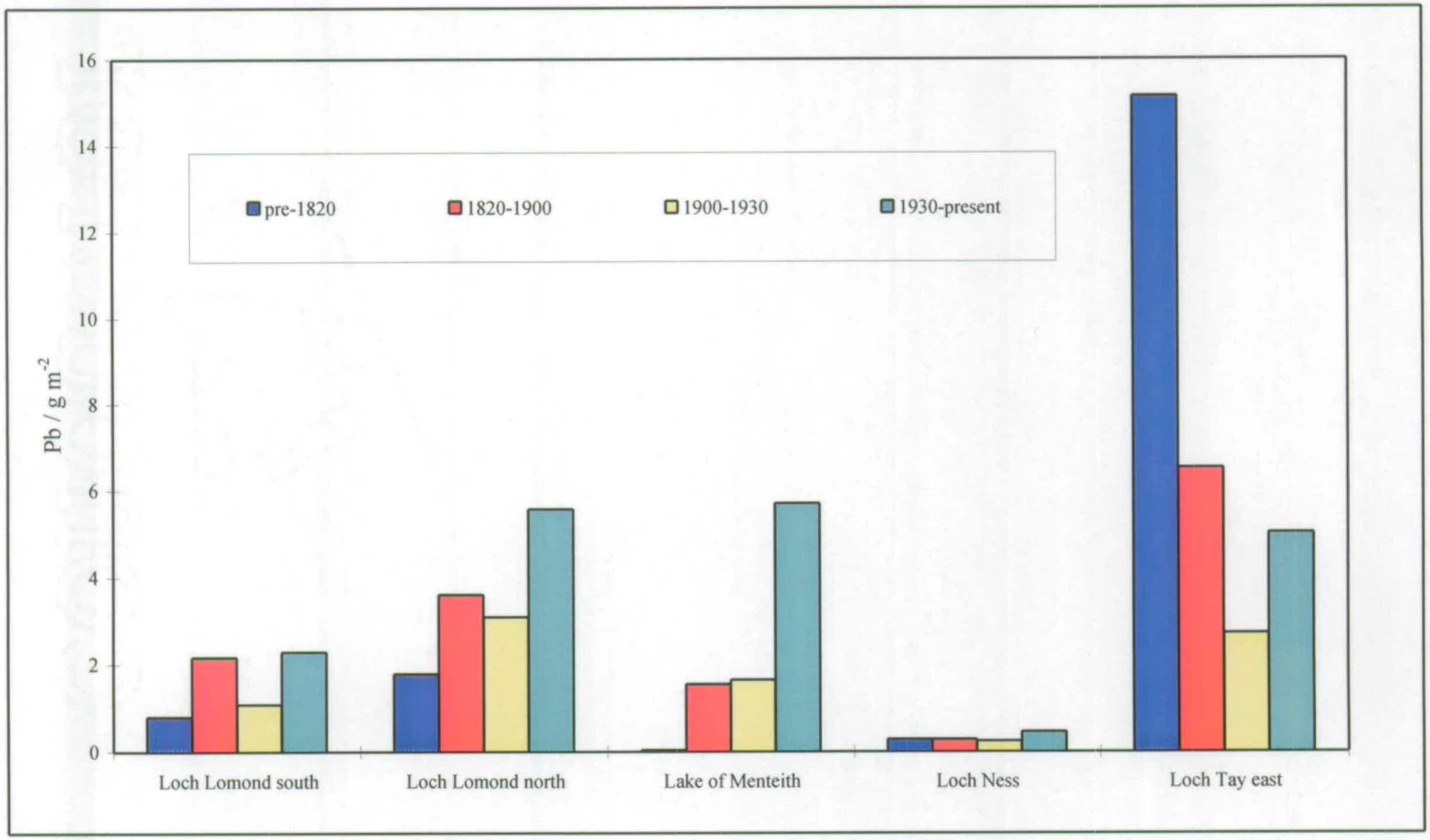

7.5 Heavy metals.

7.5.1 Comparison of heavy metal fluxes with time for Loch Lomond, Lake of Menteith, Loch Tay and Loch Ness.

Figures 7.8-7.10 are graphs of excess heavy metal flux (mg cm^{-2} y^{-1}) for Zn, Cd and Cu, respectively, against date for each of the cores.

7.5.1.1 Zinc.

Fluxes of Zn (Fig. 7.8) increased slightly above a natural background in the middle of the 18th Century in Loch Lomond. However, it was not until the beginning of the 19th Century that the fluxes of Zn began to increase more rapidly, although not at a rate similar to that for Pb until ~1850. Zinc fluxes in cores from lochs closest to the central industrial belt in Scotland reached a peak after 1950. A decline has been observed in all lochs since ~1975. In Loch Ness detectable increases in Zn flux did not occur until the 1870s, with a rapid rise taking place after ~1925. The Zn flux pattern in Loch Tay west is similar to that of Loch Lomond south but in the Loch Tay east site has been heavily influenced by the catchment input.

Loch Tay east and Loch Ness show a slight enhancement in Zn flux in the recent sediments, but not to the extent observed in the Cu profiles.

Figure 7.8 A comparison of fluxes of excess Zn (mg cm^{-2} y^{-1}) against date in all cores.

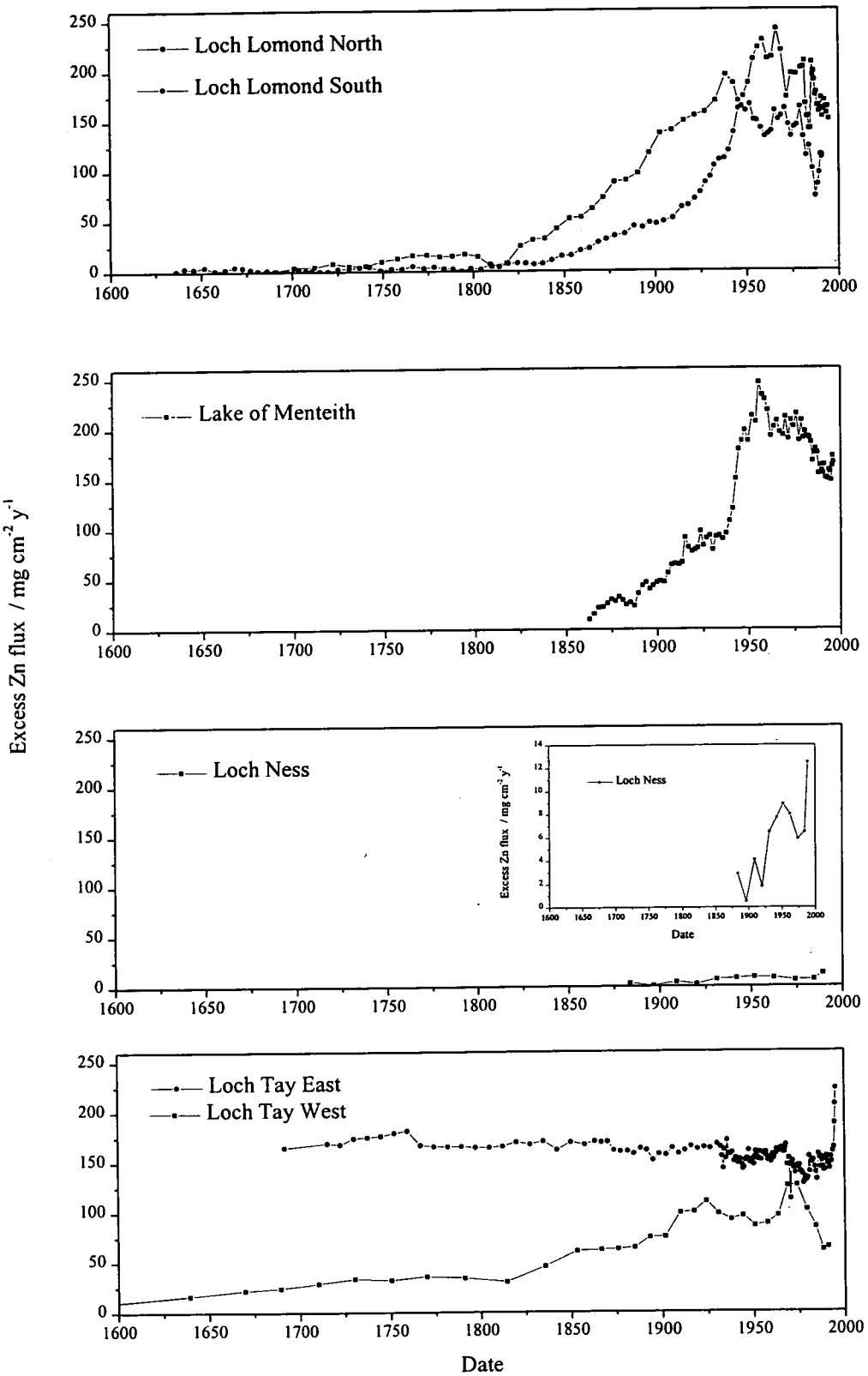

Figure 7.9 Comparison of excess Cd fluxes (mg cm^{-2} y^{-1}) vs date in all cores.

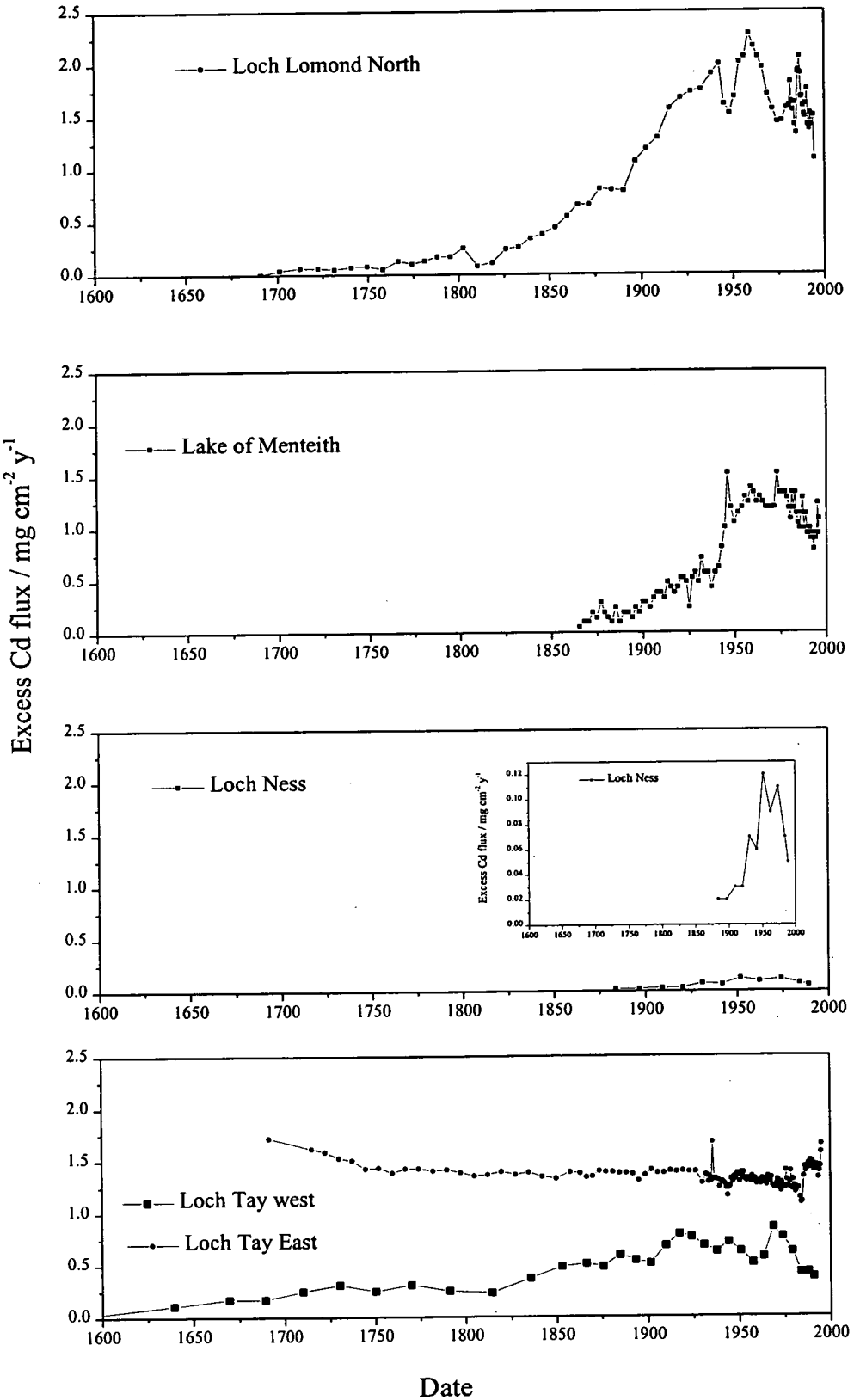

Figure 7.10 Comparison of excess Cu fluxes (mg cm^{-2} y^{-1}) vs date in all cores.

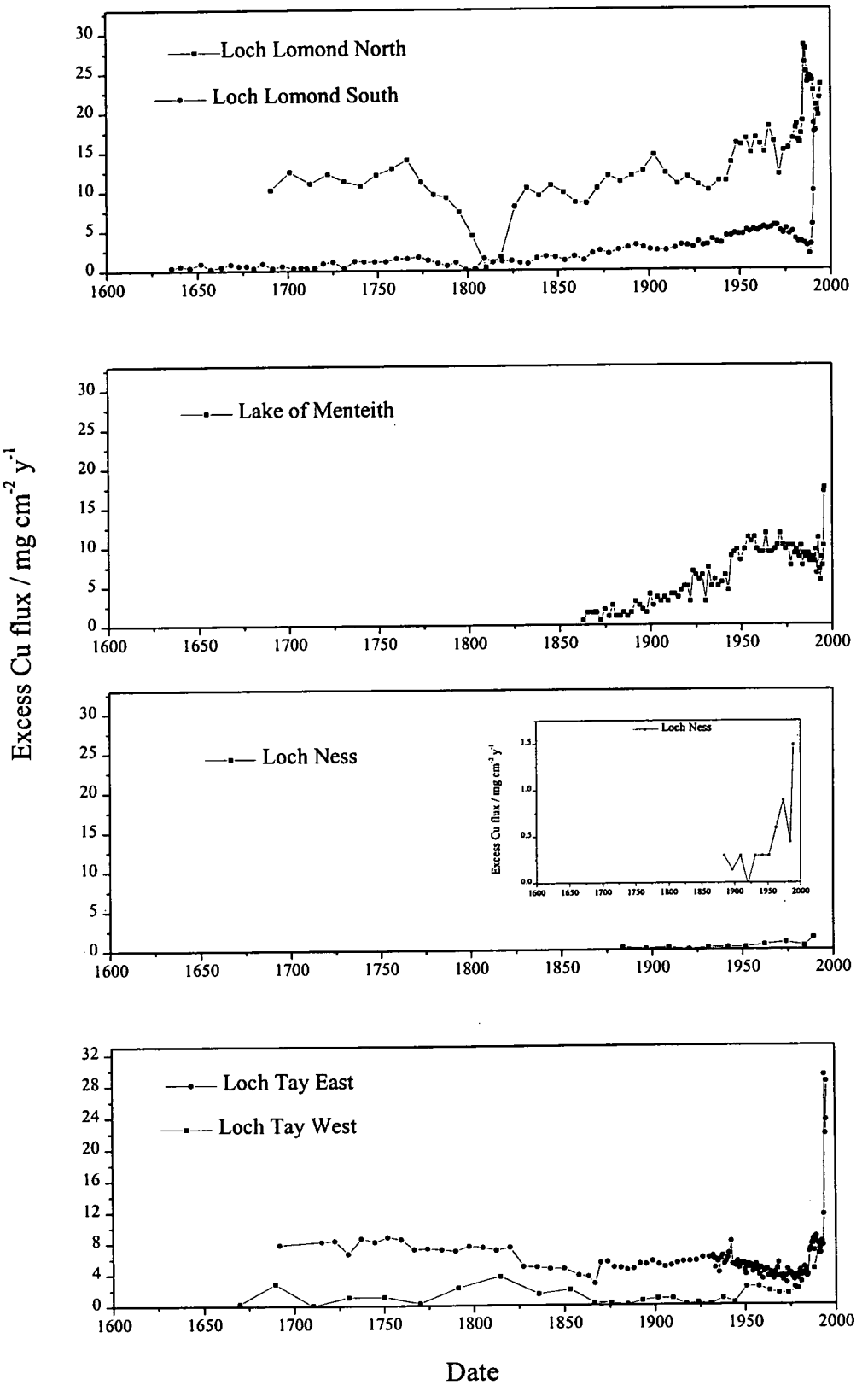

7.5.1.2 Cadmium.

Fluxes of Cd (Fig. 7.9) do not noticeably start to increase in Loch Lomond north until the start of the 19th Century. In Loch Ness, the most remote of the lochs, there is no noticeable increase until 1900. The increase in Cd flux is very similar in Loch Lomond north, Lake of Menteith and Loch Tay west with a small peak around 1925, rising to a maximum in about 1950-1960, followed by a decline since 1975. Loch Tay east has a near constant Cd flux throughout the core, suggesting that input from the mineral catchment dominates the flux of Cd to the site.

There is a small enhancement in Cd flux in the recent sediments in Loch Tay east similar to that observed for Zn.

7.5.1.3 Copper.

The apparent fluxes of Cu (Fig. 7.10) in Loch Lomond north and Loch Tay east are high throughout the core and are significantly higher than observed at any of the other sites. It is suggested that it is a result of mineral input from the catchment. Loch Lomond south, Lake of Menteith and Loch Ness appear to have anthropogenic profiles, although Cu is present in highest concentration in the very top section. This pronounced enhancement in the top section of the core is observed in all of the cores and throws doubt on the preservation of historical records for Cu in the cores. In particular, Loch Tay west (and to some extent Loch Lomond south) has a profile reminiscent of that observed for Mn, with a relatively low, constant concentration for most of the core, but rising to a sharp peak at the surface.

In work on ocean sediments, Cu was found to be recycled several times from the thin, carbon-rich layer covering pelagic sediments before eventual burial. The remobilisation occurred at a rate fast enough rate to prevent 90 % of the Cu from being buried (Klinkhammer *et al.,* 1982). In a study on the dynamics of Cu release during early aerobic degradation in estuarine sediments (Kerner and Geisler, 1995),

3.1-10.5 % of the total Cu bound to the seston material at the start of the experiment was released into the water overlying the seston layer. However, the Cu(II) was released only after the degradation of organic matter was nearly complete (100 hrs). Cd and Pb were not found to be recycled back to the open water. Similarly, Hamilton-Taylor *et al.* (1996) found the highest concentrations of Cu and Zn in Esthwaite water were maximal at, and immediately above, the sediment-water interface during the winter period when the lake was covered with ice. In this case, however, the enhanced remobilisation of Cu was found to coincide with enhanced Fe and Mn remobilisation rather than dissolved organic mater remobilisation.

The behavior and association of Cu with organic matter, Fe and Mn in surface lacustrine sediments is worthy of further investigation.

7.5.1.4 Inter-element comparison.

Flux profiles of Zn and Cd are similar within each core and, in terms of trend, for Loch Lomond north, Loch Ness and Lake of Menteith, with maximum deposition occurring in 1950 and a subsequent decrease after 1960. Cd is usually present as an impurity in Zn ores (plus to a lesser extent in Pb and Cu ores) (Habashi, 1997) and will therefore tend to be from the same source (pure deposits of Cd are very rare). Cd is also usually refined from one of the steps in the Zn smelting process. While the profiles of Pb, Zn and Cd are broadly similar, an earlier date of onset of increased Pb flux is observed in the longer cores.

Fluxes of Cu in Loch Lomond south and Lake of Menteith are the only ones that remotely resemble the profiles of the other metals. Loch Lomond north and Loch Tay east appear to be dominated by the catchment sources of Cu. Loch Lomond south and Loch Ness do not show any significant increase in flux until the 20th Century. The fluxes peak in 1965-1970, then decline towards the end of the 20th Century. All of the cores show a significant enhancement in Cu in the surface

sections of sediment relative to underlying sections, where there may be lack of retention of Cu resulting from the early diagenesis of organic matter.

Several of the lochs show sharp increases in fluxes of metals in the late 1940s to mid 1950s coinciding with the start of the post World War II era. There has been a marked decrease in the metal fluxes in all of the lochs since ~1960-1970, consistent with a decline in heavy industry in most areas of Scotland and the introduction of air quality legislation (Clean Air Acts of 1956 and 1968). Coal burning has been greatly reduced over this time with the shift to alternative forms of fuel for heating. In peat bog cores from the south-west of Glasgow, peak depositional fluxes occurred in the approximate period 1940-1950, with a pronounced decrease in the late 20th Century (MacKenzie *et al.*, 1998b).

7.5.2 Inventories of heavy metals zinc, cadmium and copper.

Table 7.6 is a summary of the total excess inventory for each of the metals in the cores. The total inventories of heavy metals over the time periods: pre-1820; 1820-1900; 1900-1930; and 1930-present[♦] are summarised in Tables 7.7-7.9 and shown graphically in Figures 7.11-7.13. The lochs fall into two categories again, with Loch Tay being distinct from the other lochs due to the high mineralisation of the area. The inventories for Pb, Zn, Cd and Cu in Loch Lomond south and Lake of Menteith are lower than Loch Tay (e.g. Pb 6.36 g m^{-2}; 8.95 g m^{-2} and Cu 0.51 g m^{-2}; 0.78 g m^{-2}), but compare well with inventories previously found near the Loch Lomond southern site (site 2: Pb, 5.4 g m^{-2}; Cu 0.38 g m^{-2}) (Bryant, 1994). The inventories of Cu in the northern basin of Loch Lomond and in Loch Tay east are higher than in the other lochs which is probably due to a higher input from local catchment run off. This is also highlighted in Figure 7.13 with the inventories over the periods pre-1820, 1820-1930 and 1930-present being almost identical. The inventories for Loch Ness are significantly lower due to the remoteness of the site. For all of the lochs, Zn and Cd are similarly apportioned suggesting that they originate from the same source.

♦ Date of core.

Table 7.6 Comparison of total excess metal inventories for all the lochs.

Loch	Excess inventory / g m^{-2}			
	Pb	Zn	Cd	Cu
Loch Lomond south	6.36	12.1	not determined	0.5
Loch Lomond north	14.1	22.9	0.22	3.48
Lake of Menteith	8.95	14.6	0.06	0.73
Loch Ness	1.29	2.26	0.03	0.15
Loch Tay east	29.4	52.5	0.46	2.03
Loch Tay west	24.1	20.4	0.14	0.93

Table 7.7 Inventories of excess (anthropogenic) Zn in the sediments of Scottish freshwater lochs.

	Loch Lomond south		Loch Lomond north		Lake of Menteith		Loch Ness		Loch Tay east	
Period	Inventory / g m^{-2}	% of total core	Inventory / g m^{-2}	% of total core	Inventory / g m^{-2}	% of total core	Inventory / g m^{-2}	% of total core	Inventory / g m^{-2}	% of total core
pre-1820	0.06	0.5	1.2	5.2	0	0	0	0	25.2	48.0
1820-1900	1.78	14.6	4.19	18.3	1.19	8.0	0.04	7.1	12.6	24.1
1900-1930	2.05	16.8	5.15	22.3	2.12	14.2	0.14	23.8	5.1	9.6
1930-present	8.31	68.1	12.3	53.9	11.6	77.9	0.4	69.1	9.6	18.3
Total	12.2		22.8		14.9		0.6		52.5	

Table 7.8 Inventories of excess (anthropogenic) Cd in the sediments of Scottish freshwater lochs.

	Loch Lomond north		Lake of Menteith		Loch Ness		Loch Tay east	
Period	Inventory / g m^{-2}	% of total core	Inventory / g m^{-2}	% of total core	Inventory / g m^{-2}	% of total core	Inventory / g m^{-2}	% of total core
pre-1820	0.01	5.4	0	0	0	0	0.23	49.4
1820-1900	0.04	18	0.01	11.1	0.001	14.3	0.10	22.9
1900-1930	0.05	23.8	0.01	11.1	0.001	14.3	0.04	9.4
1930-present	0.11	52.8	0.07	77.8	0.005	71.4	0.08	18.2
Total	0.21		0.09		0.007		0.46	

Table 7.9 Inventories of excess (anthropogenic) Cu in the sediments of Scottish freshwater lochs.

	Loch Lomond south		Loch Lomond north		Lake of Menteith		Loch Ness		Loch Tay east	
Period	Inventory / g m^{-2}	% of total core	Inventory / g m^{-2}	% of total core	Inventory / g m^{-2}	% of total core	Inventory / g m^{-2}	% of total core	Inventory / g m^{-2}	% of total core
pre-1820	0.01	2.4	1.3	37.4	0	0	0	0	1.15	56.7
1820-1900	0.14	27.5	0.73	20.9	0.06	8.2	0	0	0.36	17.7
1900-1930	0.09	17.4	0.44	12.6	0.12	16.3	0.002	6.5	0.17	8.4
1930-present	0.27	52.8	1.01	29.1	0.6	75.5	0.029	93.5	0.35	17.3
Total	0.51		3.48		0.78		0.031		2.03	

Figure 7.11 Inventories of excess (anthropogenic) Zn in the sediments of Scottish freshwater lochs.

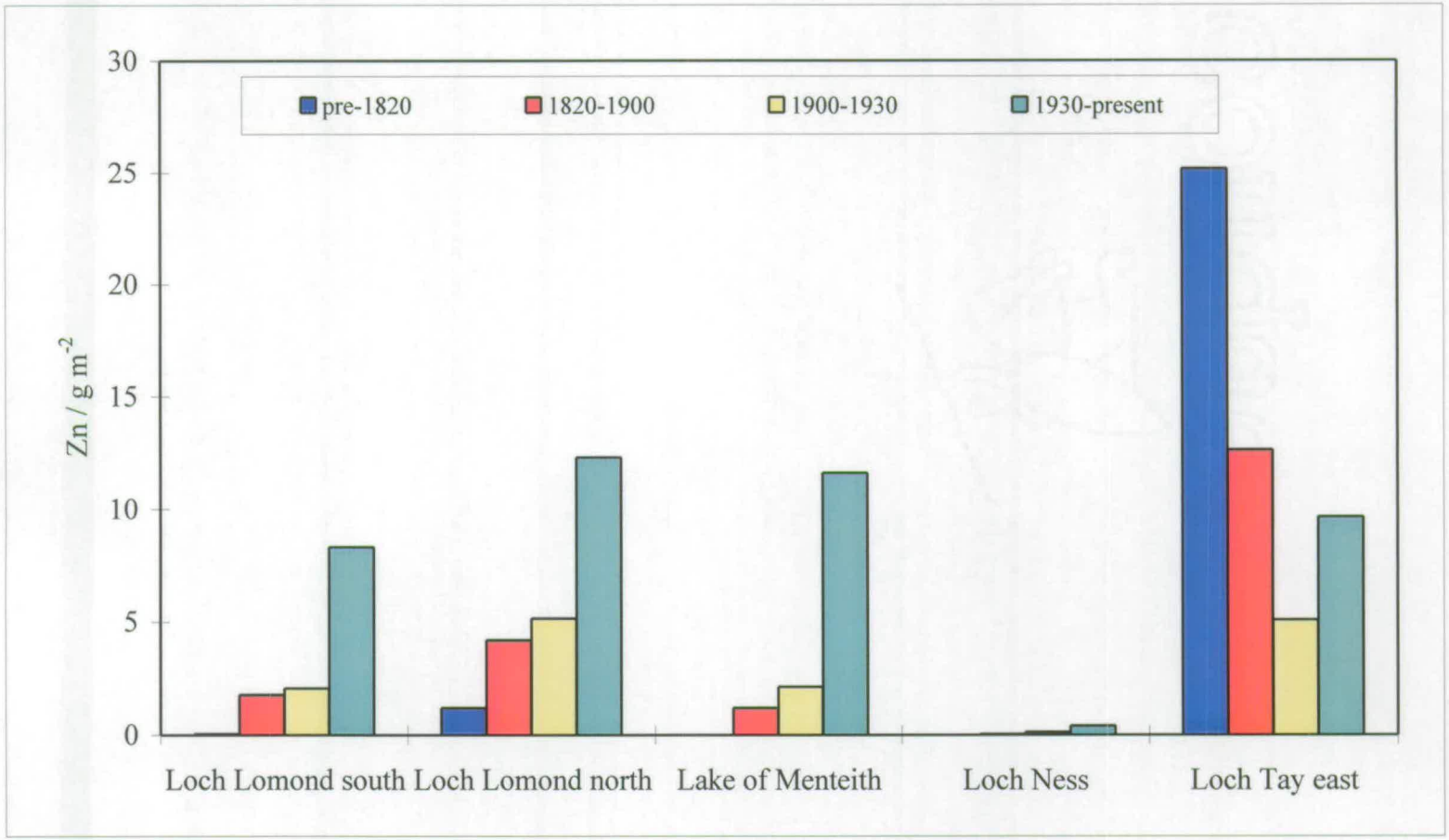

Figure 7.12 Inventories of excess (anthropogenic) Cd in the sediments of Scottish freshwater lochs.

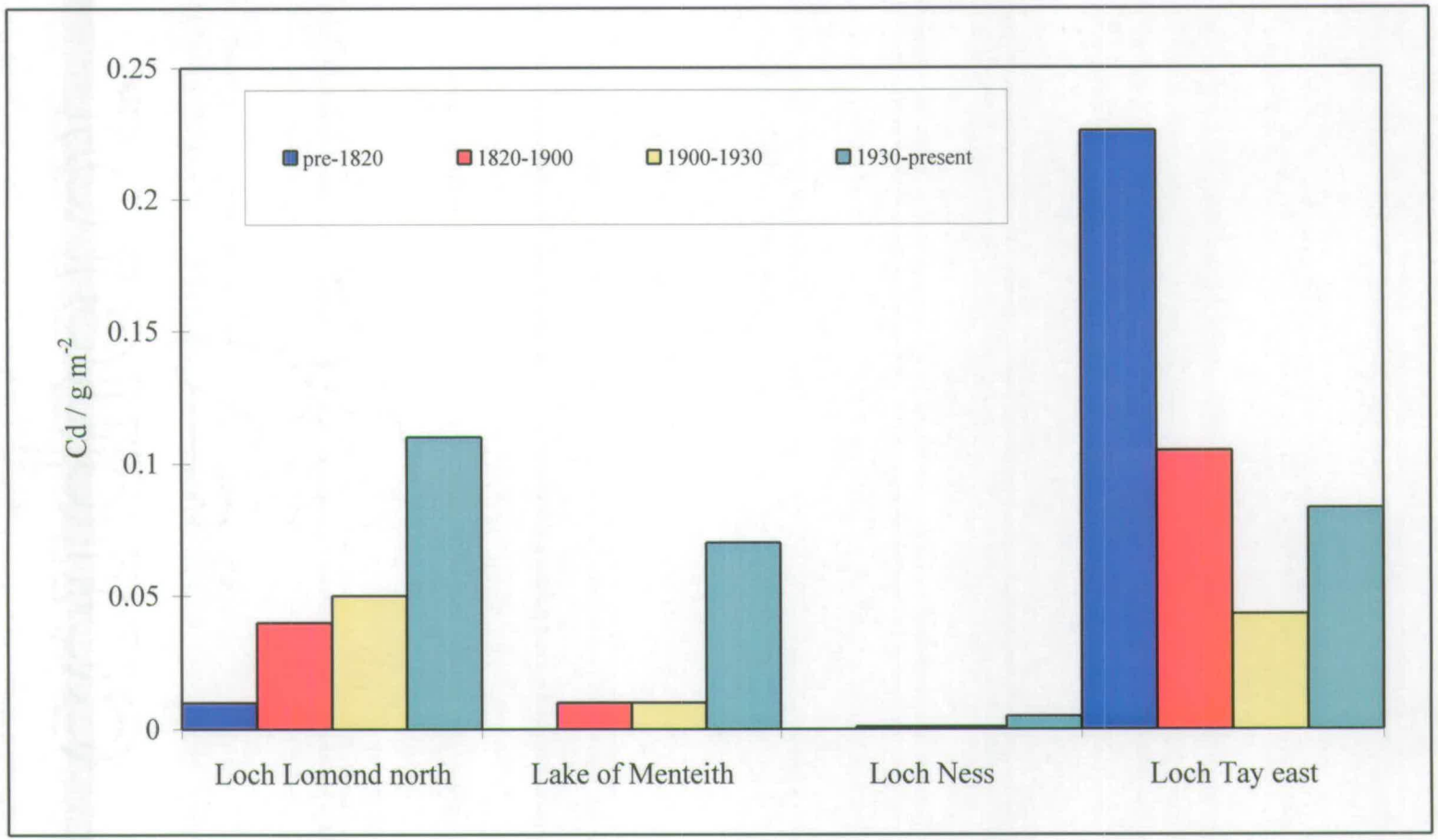

Figure 7.13 Inventories of excess (anthropogenic) Cu in the sediments of Scottish freshwater lochs.

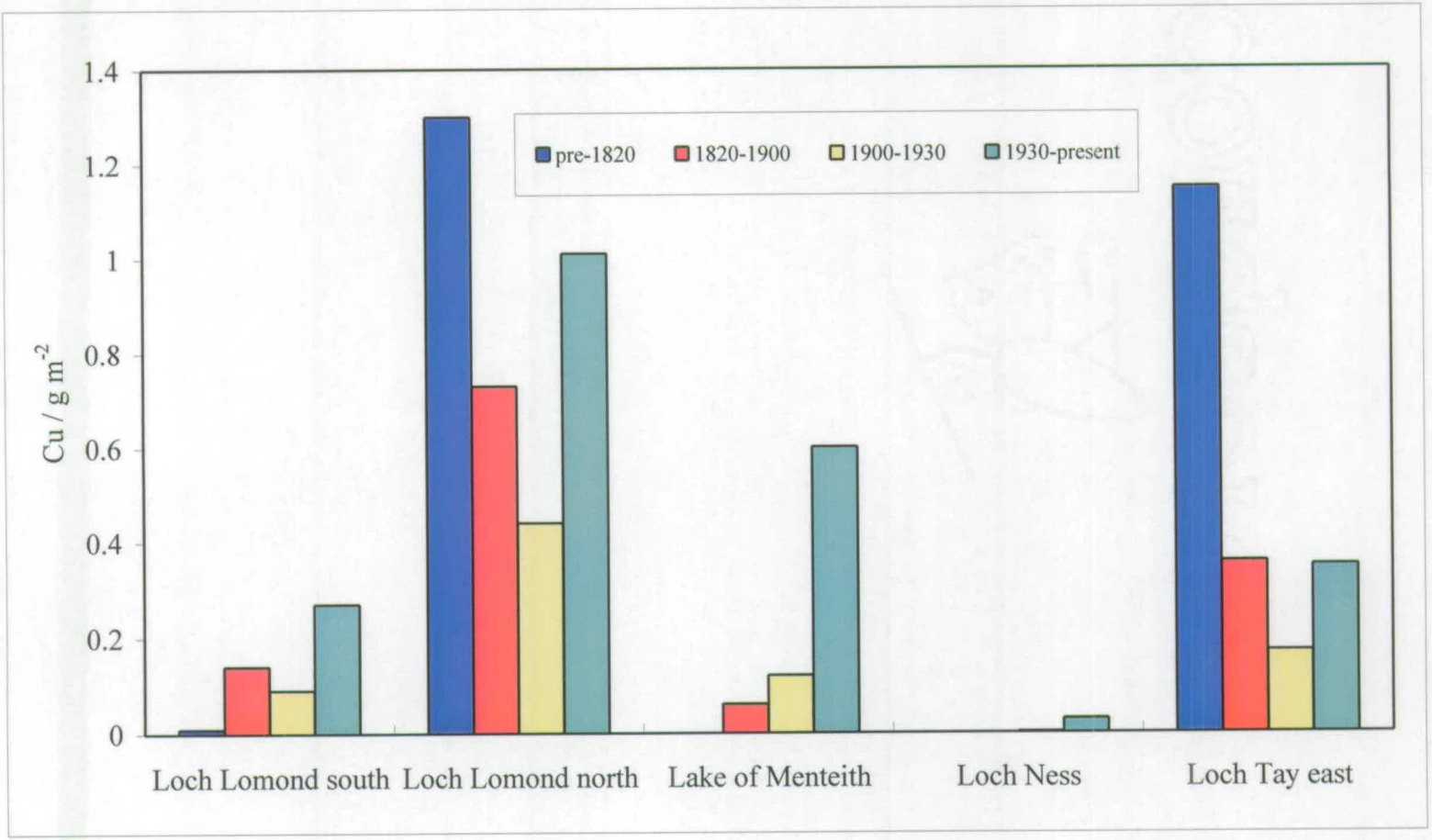

7.5.3 Sources of heavy metals.

The Industrial Revolution brought about a massive demand for metals, causing an exponential increase in emissions worldwide (Nriagu, 1996). Lead, however, has contaminated the northern hemisphere since long before the Industrial Revolution (Murozumi *et al.*, 1969). Figure 7.14 (a) is a graph of the recent historical changes in global mine production and anthropogenic emission of trace metals to the atmosphere (Nriagu, 1996) and Figure 7.14 (b) is the flux of Pb and Zn to sediments in Loch Lomond south.

Scotland was one of the countries heavily involved at the start of the Industrial Revolution and it is noticeable that the fluxes of Pb and Zn increased from an earlier date than is reported on a worldwide scale. In particular, Pb fluxes were increasing from as early as the beginning of the 19th Century in Scotland. Both of the fluxes have declined at a similar rate to that observed globally since about 1970-1980. (Nriagu, 1996).

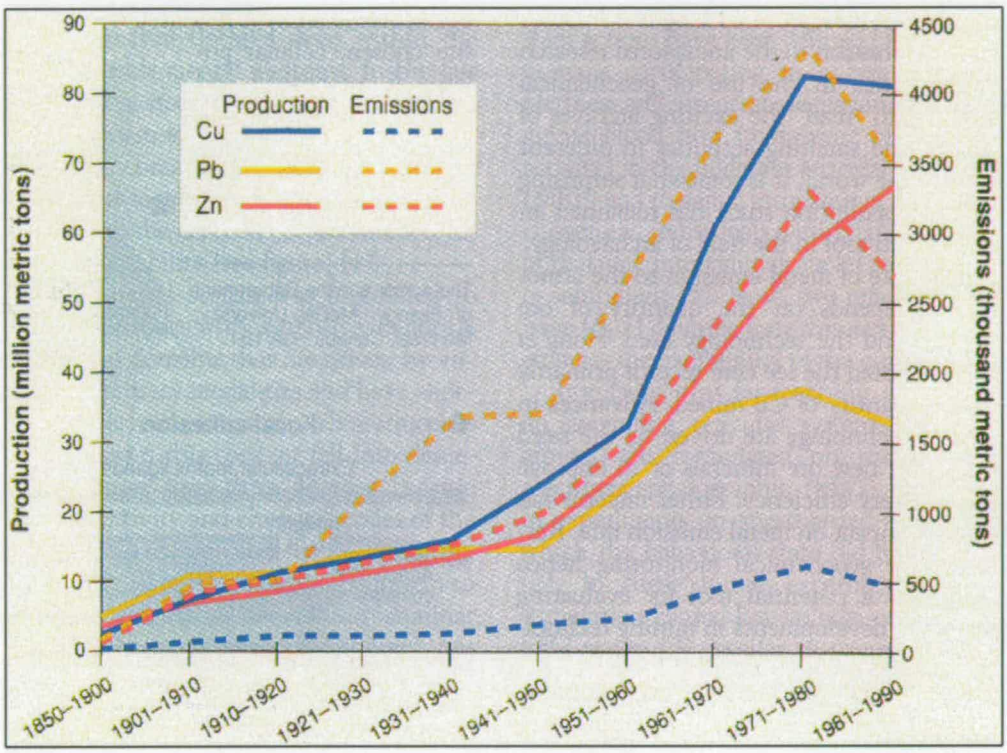

Figure 7.14 (a) Recent changes in mine production and anthropogenic emissions of trace metals to the atmosphere. (Nriagu, 1996).

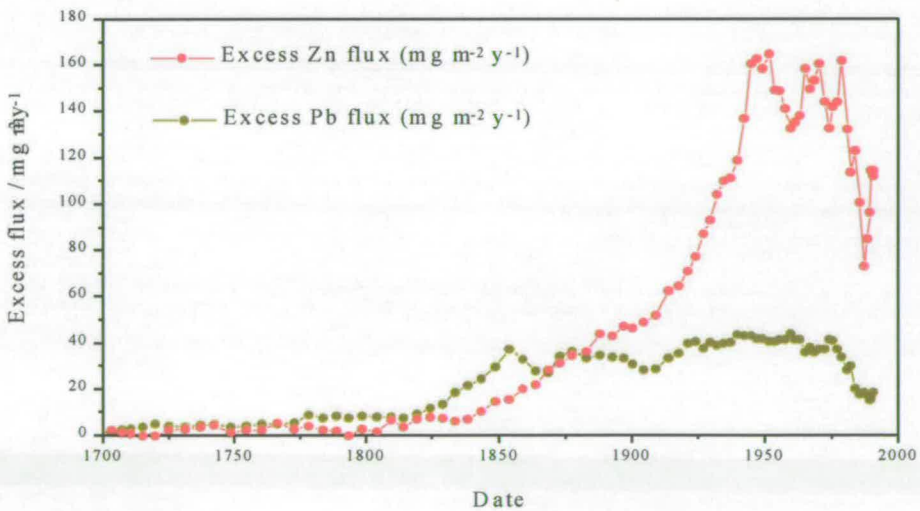

Figure 7.14 (b) Excess Pb and Zn fluxes due to anthropogenic sources for Loch Lomond south since 1700 A.D.

7.6 Iron and manganese.

The Fe (Fig 7.15) and Mn (Fig 7.16) profiles for all of the cores show diagenetically altered profiles. For Fe there is a sharp peak in the top 1-3 cm followed by smaller sub-surface peaks at a depth of about 10 to 12 cm. Apart from the diagenetic peaks, the concentrations of Fe in the majority of the cores are 4-6 % with the exception of Loch Tay east and Loch Ness where a higher concentration of about 8 % is observed.

The profiles for Mn in Loch Lomond north and south, Lake of Menteith , Loch Tay west and Loch Ness are similar, in as much as there is a diagenetic peak within the top 1.5 cm of the surface and a smaller peak situated at a depth of 8 to 10 cm. Loch Tay east is noticeably different with a small surface enhancement and a series of broader peaks down the core, the most pronounced of these being at about 40-45 cm. It is suggested that these peaks are due to changes in sediment deposition caused by either mine flooding or dumping of spoil waste during, or at the end, of periods of mining activity. This could have created conditions conducive to the development and preservation of peaks of redox-sensitive metals.

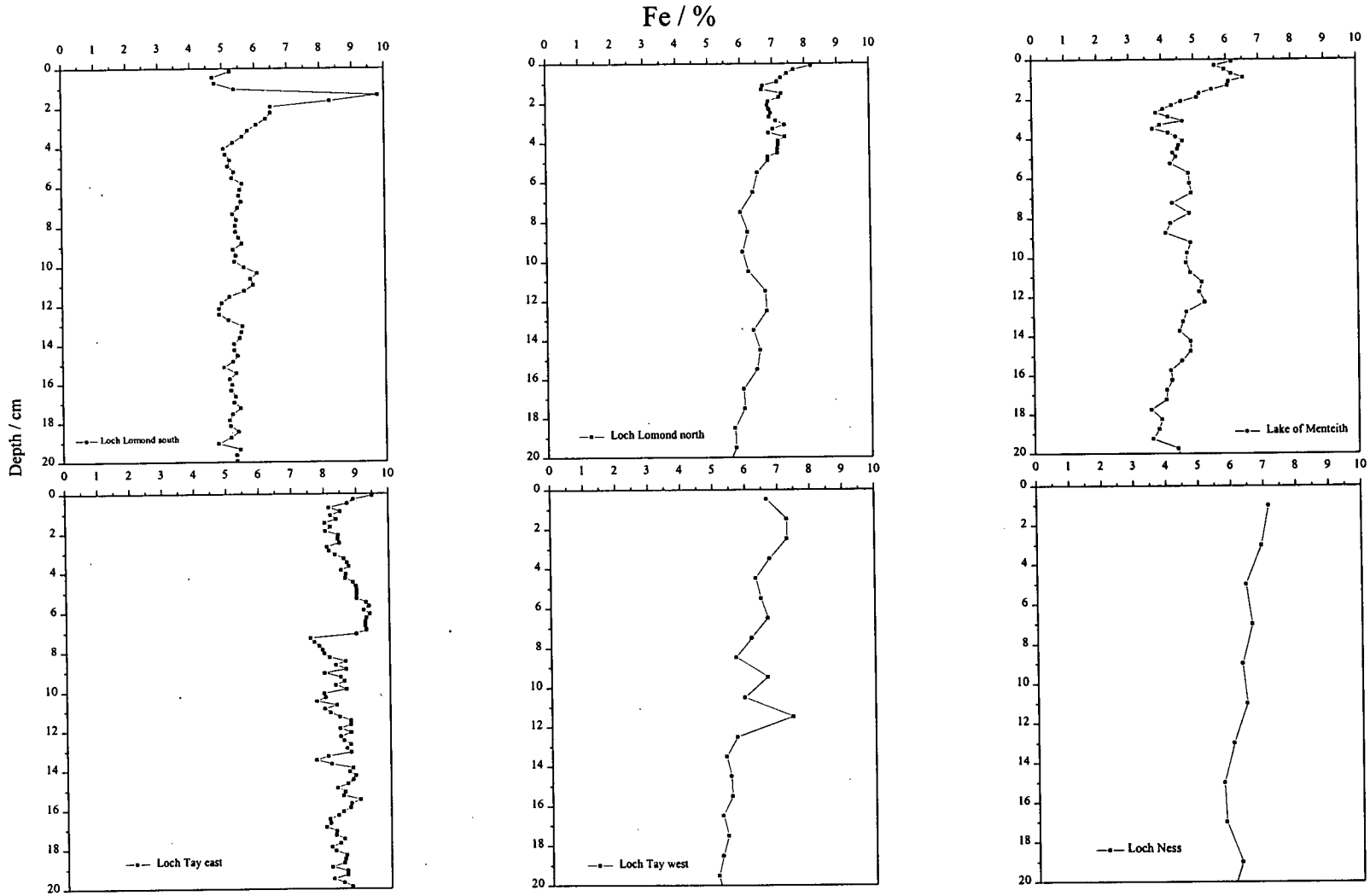

Figure 7.15 Comparison of Fe (%) against depth (cm) in all of the freshwater sediment cores.

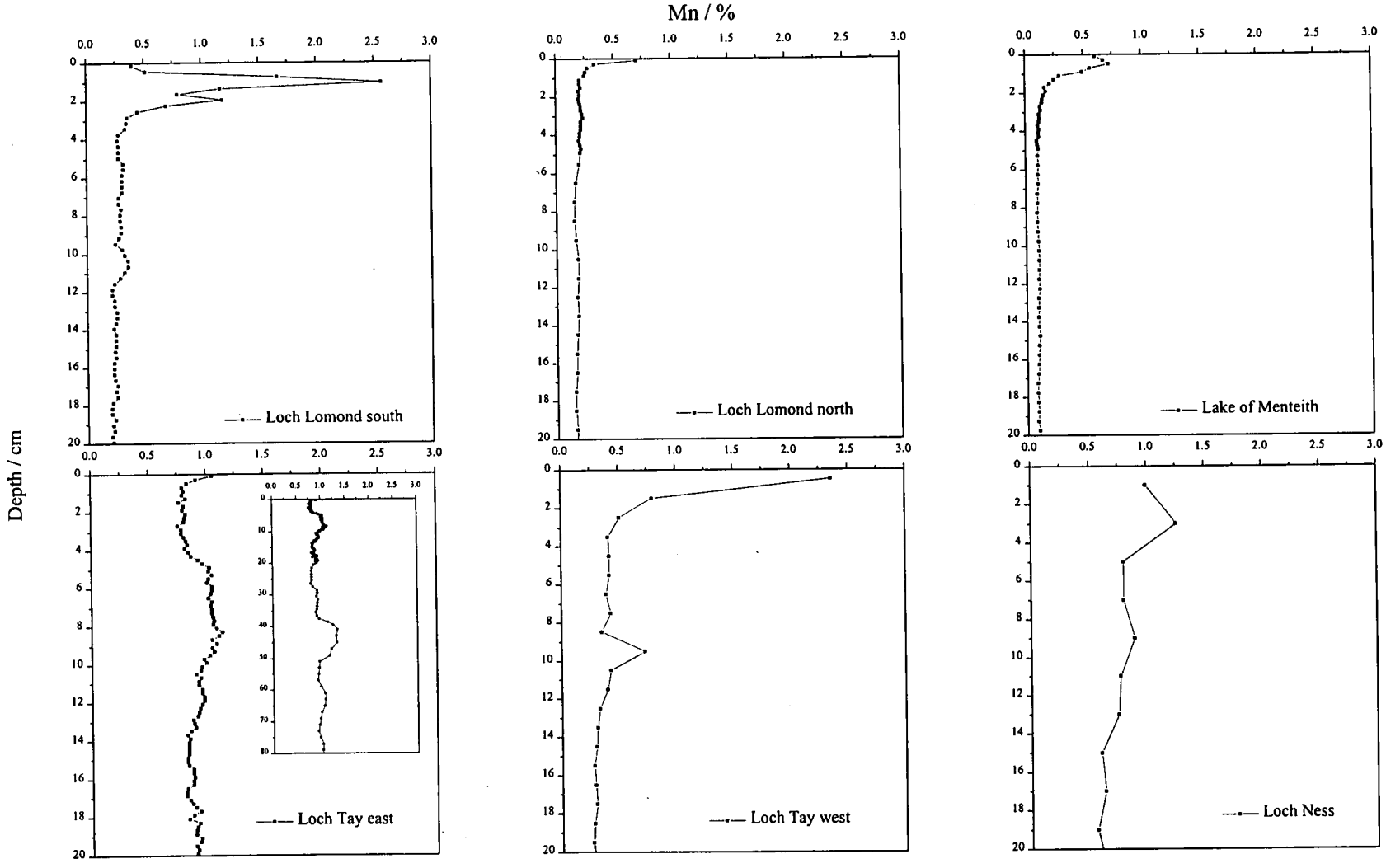

Figure 7.16 Mn (%) against depth (cm) in all of the freshwater sediment cores.

7.7 Conclusions.

Distinguishable ^{137}Cs peaks relating to deposition from the Chernobyl accident and nuclear weapons testing were observed in sediment cores from almost all of the lochs. The exception was Lake of Menteith, where mobility of the ^{137}Cs has caused a smearing of the two peaks. In the other lochs the relative positions of the two ^{137}Cs peaks enabled calculation of sedimentation rates that were generally in agreement with those derived from the ^{210}Pb CIC model. Sedimentation rates ranged from 15.1 mg cm^{-2} y^{-1} in Loch Ness to 118.6 mg cm^{-2} y^{-1} in Loch Lomond north.

The relative inventories of the two sources of radiocaesium were resolvable in Loch Lomond north and south, and in Loch Tay east and west. The ratio of Chernobyl:weapons inventories of ^{137}Cs was different for the two lochs. Loch Lomond (~0.3) has received a smaller input of ^{137}Cs from Chernobyl relative to weapons testing than has Loch Tay (~0.7). Total inventories of ^{137}Cs in all loch sediments were very similar[♦] (11.1 to 14.7 kBq m^{-2}), with the exception of Loch Lomond north (23.9 kBq m^{-2}). Fluxes of ^{210}Pb to the sediment varied from 113 Bq m^{-2} y^{-1} in Loch Lomond south to 554 Bq m^{-2} y^{-1} in Loch Lomond north, reflecting the variability of physical factors, such as sediment focusing, between sampling sites.

Lead was the first of the metals to show an increase in concentration above background in the longer cores, starting from ~1640. In Loch Lomond and Loch Ness, the fluxes increased more rapidly once the Industrial Revolution had started ~1750. The sediment core from Lake of Menteith was shorter, dating back only to 1850, but the fluxes were increasing at a similar rate to that observed in Loch Lomond and Loch Ness. Fluxes of Pb reached a peak between 1950-1960 in the three lochs but have been in decline since ~1970. The total inventories of Pb in Loch Lomond and Lake of Menteith are similar (6.36, 14.9, 8.95 g m^{-2}) but Loch Ness is significantly lower (1.29 g m^{-2}).

[♦] Based on activities corrected to 1990.

Fluxes of Pb to Loch Tay are distinctly different to the other three lochs due to significant influence of local Pb-ore mining and smelting activities. The fluxes are practically constant throughout the core, with the exception of a sharp increase at the western site in 1905-1925, due to the re-commencement of mining activity. There has been a slight decline since the closure of the Pb mines at Tyndrum ~1945. The inventories in Loch Tay (29.4; 24.1 g m^{-2}) are 2-4 times higher than observed in the other lochs.

In Loch Lomond north and south, Lake of Menteith and Loch Ness, the overall changes in $^{206}Pb/^{207}Pb$ atom ratio for the excess Pb deposited over the past 200 years were similar. The $^{206}Pb/^{207}Pb$ atom ratio for excess Pb 19th Century was ~1. 17. It remained at this value until about 1910 when a slight decline (~0.002) was observed, about 30 years later than a similar decline in England. The later date for this initial decline can be explained by the relatively higher input, in Scotland, of Pb from coal burning and the smelting of indigenous Scottish Pb ores.

The decline in the $^{206}Pb/^{207}Pb$ atom ratio increased after 1930 with the change in the ratio (Δ) reaching 0.03-0.04 in Loch Lomond north and south, Lake of Menteith and Loch Ness over the period 1930-1975. The decline in the $^{206}Pb/^{207}Pb$ atom ratio is attributed to the use of ^{206}Pb-depleted alkyl Pb as an 'antiknock' agent in petrol. In Loch Lomond north and south and Loch Ness a slight reversal of the decline has been observed since the middle of the 1980s, a direct result of the increasing use of unleaded petrol and a reduction in the maximum permitted concentration of Pb additives in petrol.

Loch Tay, in contrast, has been dominated by the high degree of mineralisation in the area. The $^{206}Pb/^{207}Pb$ atom ratio prior to the onset of mining at Tyndrum had a more geogenic value of 1.19. After mining commenced the $^{206}Pb/^{207}Pb$ atom ratio in the sediments dropped to 1.145 and it has remained close to this value until present, with only a slight discernible increase due to the input of "industrial" Pb ($^{206}Pb/^{207}Pb$ ~ 1.17) during the latter half of the 19th Century.

Temporal changes in fluxes of Zn and Cd were identical within each core and were similar for Loch Lomond north and south, Lake of Menteith, Loch Tay west and Loch Ness. The core from Loch Tay east has been dominated by input from the mineralised catchment. There is some doubt whether the profiles of Cu reflect a historical input due to possible diagenetic release of Cu from its predominant association with organic matter in surficial sediment.

Inventories of the heavy metals in bottom sediments are variable between the lochs due to localised catchment phenomena. Inventories for Loch Lomond south and Lake of Menteith are comparable but lower than for Loch Lomond north, which has been influenced by higher fluxes of sediment and focusing. Loch Tay east and west have the highest inventories due to the mineralisation of the area. Loch Ness has the lowest inventories for the metals as a result of its more remote location.

Diagenetic peaks in Mn and Fe were observed in the bottom sediments of all of the lochs. In Loch Tay sub-surface peaks of Mn (and, to a lesser extent, of Fe), were observed, in addition to the principal 'redox-cline' peak. These were attributed to the effects of sediment inputs from past mining activity, the change in conditions leading to preservation of relict peaks in the sediment.

Chapter 8. Conclusions.

8.1 The advantages/disadvantages of high resolution sectioning of freshwater lake sediment cores.

The sectioning of freshwater lake sediment cores at sub-centimetre increments has improved the resolution in the metal profiles and allowed a more accurate assessment of sedimentation rates. The following conclusions on the use of higher resolution sectioning can be drawn:

- Resolution of the radiocaesium profiles was enhanced. The Chernobyl peak was shown to be a discrete event, leading typically to a very sharp peak over only 1.2-1.6 cm in the core and a peak maximum over only 2-3 mm in the collected cores. The weapons testing peaks were broader, covering 3-6 cm in the sediment cores, but even here the maximum (corresponding to 1963) could be more readily identified.

- The sedimentation rates were able to be determined with a higher precision as a consequence of the ^{137}Cs peak maxima being isolated in thinner sections of sediment. Similarly, separation of the relative inventories of the Chernobyl and weapons testing fallout was improved.

- The dates of changes in the $^{206}Pb/^{207}Pb$ ratio of anthropogenic Pb profiles were better defined, enabling clearer identification of temporal trends in source input.

- Separation of the Mn and Fe diagenetic peaks present in the top few centimetres of sediment cores was more readily achievable using sub-centimetre increments, further highlighting the narrowness of the zones of Mn and Fe enrichment.

- Generation of more detailed ^{210}Pb profiles is perhaps the only area where higher resolution sectioning has not been proved to have benefited the subsequent

interpretation. This is partly due to the size of the sections, necessitating the use of α-spectrometry, a more laborious and time consuming technique. Furthermore, the analysis time on the detectors was long (typically 3-4 days) due to the small size of the samples. Longer counting times were also necessary for the γ-spectrometry used for $^{134,137}Cs$ and ^{241}Am, but here there were distinct advantages for the interpretation of data.

8.2 Historical records in Scottish freshwater loch sediments.

Radiocaesium and ^{210}Pb were used to establish a chronological scale for each of the sediment cores from the four Scottish freshwater lochs. While a historical record of Pb, Zn and Cd input was feasible for all of the cores, there is some doubt over Cu, for which significant surface enhancements were commonly observed. The Pb profiles were deconvoluted with the aid of stable Pb isotope ratios. From the radiochronological investigation of Pb and the other heavy metals, Zn, Cd and Cu, the following conclusions were drawn:

- Areas close to Scotland's industrial heartland have been subject to heavy metal pollution since the 17th Century. In particular, fluxes of Pb have been above a natural background since the mid-1600s in Loch Lomond. Fluxes of Zn and Cd did not start to increase until the beginning of the Industrial Revolution (ca 1750). Fluxes of Pb, Zn and Cd all rose dramatically after the beginning of the 19th Century, reaching a peak in the mid 1950-60s. After about 1970 the fluxes declined for these metals.

- The influence of changing sources of Pb to the environment is highlighted in the stable Pb isotope ratio profiles. Prior to anthropogenic influence, the $^{206}Pb/^{207}Pb$ ratio prevailing in the sediments was close to that of surrounding bedrock. With the onset of Pb mining and a change from wood burning to coal burning, the ratio dropped to an average 19th Century value for the lochs (excluding Loch Tay) of

1.173 ± 0.003. This is in excellent agreement with that obtained for atmospherically deposited Pb in Scottish ombrotrophic peat bogs.

- The $^{206}Pb/^{207}Pb$ ratio remained constant in Scotland until about 1910 when a slight decline in the $^{206}Pb/^{207}Pb$ ratio was observed in Loch Lomond north, Lake of Menteith and Loch Ness, somewhat earlier than in England and western Europe. The use of imported ^{206}Pb-depleted Australian Pb in England was counter-balanced to some extent in Scotland by the smelting of indigenous Pb ores and the relatively higher emissions of Pb from coal burning. Coal was the major energy source used by the iron and steel industry, of which Scotland was one of the world leaders.

- The advent in the use of ^{206}Pb-depleted alkyl Pb additives as antiknock agents in petrol had a pronounced effect on the $^{206}Pb/^{207}Pb$ ratio. In Loch Lomond, Lake of Menteith and Loch Ness the $^{206}Pb/^{207}Pb$ ratio fell by 0.03-0.04 from 1930-1975. The contribution of petrol-derived Pb to the sediment inventory of Pb since ~1930 was 22-52 % in central Scotland and 32-48 % in the north. With the increase in the use of unleaded petrol and a phasing out of leaded petrol since 1986, the $^{206}Pb/^{207}Pb$ ratio has begun to increase in recently deposited sediment.

- Loch Tay has been heavily dominated by the mining of Pb within its catchment. Prior to the onset of mining activity, Loch Tay west had a $^{206}Pb/^{207}Pb$ ratio of 1.192 but this fell to 1.150 ± 0.002 once mining of Tyndrum ore ($^{206}Pb/^{207}Pb$ ratio 1.144) had commenced. Similarly the $^{206}Pb/^{207}Pb$ ratio of Loch Tay east was effectively constant throughout the core at 1.145 ± 0.002.

- The influx of Cu appears to have been influenced by catchment material in Loch Lomond north and Loch Tay east. The presence of significantly higher concentrations of Cu in surface sections, compared with those below, suggests that the underlying vertical profile of Cu may be subsequently perturbed by

diagenetic influences. Hence, historical interpretation of Cu profiles is probably not valid at this stage.

8.3 Further research.

The following suggestion for further work could be considered:

1. Determination of a larger suite of metals, including some recently-introduced to the environment (e.g. Pt, Pd, Rh) through technological innovation (e.g. catalytic converters) in car-exhaust systems.

2. Determination of comparatively neglected organic pollutants (e.g. PAHs, PCBs) in Scottish freshwater loch sediments.

3. Investigation of processes affecting the potential mobility of Cu and of other metals and organic pollutants.

Abril J.M., Garcia-Leon M., Garcia-Tenorio R., Sanchez C.I. and El-Daoushy F. J. 1992. Dating of marine sediments by an incomplete mixing model. J. Environ. Radioactivity, 15, 135-151.

AEA Technology. http://www.aeat.co.uk/netcen/airqual/emissions/index/html1998.

Akhter S.M. and Madany I.M. 1993. Heavy metals in street and house dust in Bahrain. Water Air Soil Pollut., 66, 111-119.

Appleby P.G. and Oldfield. 1978. The calculation of ^{210}Pb dates assuming a constant rate of supply of unsupported ^{210}Pb to the sediment. Catena, 5, 1-8.

Appleby P.G. and Oldfield F. 1992. Application of ^{210}Pb to sedimentation studies. In: Uranium-series Disequilibrium: Application to Earth, Marine and Environmental Sciences, (Editors, Ivanovich M. and Harman R.S.), 2nd ed, Clarendon Press, Oxford, pp746.

Appleby P.G., Richardson N. and Smith J.T. 1993. The use of radionuclide records from Chernobyl and weapons test fallout for assessing the reliability of ^{210}Pb in dating very recent sediments. Verh. Internat. Verein. Limnol., 25, 226-269.

Bacon J.R., Jones K.C., McGrath S.P. and Johnston A.E. 1996. Isotopic character of lead deposited from the atmosphere at a grassland site in the United Kingdom since 1860. Environ. Sci. Technol., 30, 2511-2518.

Bainbridge J.N. 1970. A nineteenth century copper working: Tomnadashan, Loch Tayside. Indust. Archaeol., 7, 66-74.

Berger W.H. and Heath G.R. 1968. Vertical mixing in pelagic sediments. J. Mar. Res., 26, 134-143.

Berner R.A. 1980. Early Diagenesis: A theoretical approach. Princeton Univ. Press, Princeton, NJ, 241pp.

Best G. A. and Traill I. 1994. The physico-chemical limnology of Loch Lomond. Hydrobiol., 290, 29-37.

Blais J.M. and Kalff J. 1995. The influence of lake morphology on sediment focusing. Limnol. Oceanogr., 40, 582-588.

Boyle E.A., Sclater F.R. and Edmond J.M. 1977. Copper enrichment in deep sea clays. Earth Planet. Sci. Lett., 37, 38-54.

Boyle E.A., Sherrell R.M., and Bacon M.P. 1994. Lead variability in the western North Atlantic Ocean and central Greenland ice: implications for the search for decadal trends in anthropogenic emissions. Geochim. Cosmochim. Acta, 58, 3227-3238.

Brand T. and Shimmield G. 1990. The use of ^{210}Pb as an indicator of biological processes affecting the flux and sediments geochemistry of organic carbon in the NE Atlantic. In: The uses of radionuclides in the study of marine processes (Editors P.J. Kershaw and D.S. Woodhead). 222-233.

Brechin E.K. 1994. Heavy metals and radionuclides n the sediment column of Eastern Loch Tay. BSc. Thesis, The University of Edinburgh.

Bryant C.L. 1993. A study of heavy metals and radionuclides in Scottish freshwater loch sediments. PhD. Thesis, The University of Edinburgh.

Bryant C.L., Farmer J.G., MacKenzie A.B., Bailey-Watts A.E. and Kirika A. 1991. The biogeochemistry of heavy metals in an acidified Scottish fresh-water loch. Proc. 8th Intern. Conf. Heavy Metals Environ., 1, 347-350.

Bryant C.L., Farmer J.G., MacKenzie A.B., Bailey-Watts A.E. and Kirika A. 1993. Distribution and behavior of radiocaesium in Scottish freshwater loch sediments. Environ. Geochem. Health, 15, 153-161.

Bryant C.L., Farmer J.G., MacKenzie A.B., Bailey-Watts A.E. and Kirika A. 1997. Manganese behavior in the sediments of diverse Scottish freshwater lochs. Limnol and Oceanog., 42, 918-929.

Burdige D. and Gieskes J. 1983. A pore-water / solid phases diagenetic model for Mn in marine sediments. Amer. Journ. Sci., 283, 29-47.

Butt J. 1967. The Industrial Archaeology of Scotland, Newton Abbot David and Charles, Edinburgh.

Cambray R.S., Playford K. and Lewis G.N.J. 1982. Radioactive fallout in air and rain: Results to the middle of 1981. United Kingdom Atomic Energy Authority, Harwell report AERE-R 10485. HMSO, London.

Chow T.J., Snyder C.D. and Earl J.L. 1975. Isotopic ratios of lead as pollutant source indicators. In: Proceedings of IAEA-SM-191/4, International Atomic Energy Commission, Vienna, Austria, 95-108.

Christiensen E. and Klein R.J. 1991. "Unmixing" of ^{137}Cs, Pb, Zn, and Cd records in lake sediments. Environ. Sci. Technol., 25, 1627-1637.

Christiensen E. and Bhunia P. 1986. Model for the activity of radionuclides in sediments. J. Geophys. Res., 91, C7, 1171-1187.

Clark M.J. and Smith F.B. 1988. Wet and dry deposition of Chernobyl releases. Nature, 332, 245-249.

Coleman N.T., Craig D. and Lewis R.J. 1963a. Ion-exchange reactions of caesium. Soil Sci. Soc. Am. Proc., 27, 287-289.

Coleman N.T., Lewis R.J. and Craig D. 1963b. Sorption of caesium by soils and its displacement by salt solutions. Soil Sci. Soc. Am. Proc., 27, 290-294.

Craig G.Y. 1965. The Geology of Scotland. 2nd Ed, Oliver and Boyd, Edinburgh.

Craig G.Y. 1983 The Geology of Scotland. 3rd Ed, Oliver and Boyd, Edinburgh.

Date A.R., and Cheung Y.Y. 1987. Studies in the determination of lead isotope ratios by inductively coupled plasma spectrometry. Analyst, 112, 1531-1540.

Davies R.B., Hess C.T., Norton S.A., Hanson D.W., Hoogland K.D., and Anderson D.S. 1984. ^{137}Cs and ^{210}Pb dating of sediments from soft-water lakes in New England (USA) and Scandinavia: a failure of ^{137}Cs dating. Chem. Geol., 44, 151-185.

Davis J.A. 1982. Adsorption of natural dissolved organic matter at the oxide/water interface. Geochim. Cosmochim. Acta, 46, 2381-2393.

Davis J.A. 1984. Complexation of trace metals by adsorbed natural organic matter. Geochim. Cosmochim. Acta, 48, 679-691.

Davison W. 1985. Conceptual models for transport at a redox boundary. In: Chemical processes in Lakes. (Editor Stumm W.) Wiley, New York, 31-53.

Davison W., Grime G.W., Morgan J.A. and Clarke K. 1991. Distribution of dissolved Fe in sediment pore-waters at sub-millimetre resolution, Nature, 352, 323-325.

DETR. 1997. Digest of Environmental Statistics. The Stationery Office, London, No. 19.

Dickson J.H., Stewart D.A., Thompson G.T., Baxter M.S., Drndarski N.D. and Rose J. 1978. Palynology, palaeomagnetism and radiometric dating of Flandarian marine and freshwater sediments of Loch Lomond. Nature, *274*, 548-553.

Doe B.R. 1970. Lead isotopes. Springer, New York, 137 pp.

Dunlap C.E., Steinnes E. and Flegal A.R. 1999. A synthesis of Pb isotopes in two millennia of European air. Earth Planet. Sci. Lett., 167, 81-88.

Dukat D.A. and Kuehl S.A. 1995. Non-steady state ^{210}Pb flux and the use of $^{228}Ra/^{226}Ra$ as a geochronometer on the Amazon continental shelf. Mar. Geol., 125, 329-350.

Dzombak D.A. and Morel F.M.M. 1990. Surface complexation modeling, hydrous ferric oxide, Wiley-Interscience, New York.

Eades L.J., Farmer J.G., MacKenzie, A.B., Kirika A. and Bailey-Watts A.E. 1998. High-resolution profile of radiocaesium deposition in Loch Lomond sediments. J. Environ. Radioactivity, 39, 107-115.

Edgington D.N., Val Klump J., Robbins J.A., Kusner Y.S., Pampura V.D. and Sandimirov I.V. 1991. Sedimentation rates, residence times and radionuclide inventories in Lake Baikal from ^{137}Cs and ^{210}Pb in sediment cores. Nature, 359, 601-604.

Erel Y., Veron A. and Helices L. 1997. Tracing the transport of anthropogenic lead in the atmosphere and in soils using isotopic ratios. Geochim. Cosmochim. Acta, 61, 4495-4505.

Evans D.W., Alberts J.J. and Clark R.A. 1983. Reversible ion-exchange fixation of caesium-137 leading to mobilisation from reservoir sediments. Geochim. Cosmochim. Acta, 47, 1041-1049.

Farmer J.G. 1991. The perturbation of historical pollution records in aquatic sediments. Environ. Geochem. Health., 13, 76-83.

Farmer J.G. 1994. Environmental change and the chemical record in Loch Lomond sediments. Hydrobiol., 290, 39-49.

Farmer J.G and Cross J.D. 1979. The determination of arsenic in Loch Lomond sediment by instrumental neutron activation analysis. Radiochem. Radioanal. Lett. 39, 429-440.

Farmer J.G. and Lovell M.A. 1984. Massive diagenetic enhancement of manganese in Loch Lomond sediments. Environ. Technol. Lett., 5, 257-262.

Farmer J.G. and Lovell M.A. 1986. Natural enrichment of arsenic in Loch Lomond sediments. Geochim. Cosmochim. Acta, 50, 2059-2067.

Farmer J.G., Swan D.S. and Baxter M.S. 1980. Records and resources of metal pollutants in a dated Loch Lomond sediment core. Sci. Total Environ., 16, 131-147.

Farmer J.G., Eades L.J., MacKenzie A.B., Kirika A. and Bailey-Watts A.E. 1996. Stable lead isotope record of lead pollution in Loch Lomond sediments since 1630 A.D. Environ. Sci. Technol., 30, 3080-3083.

Farmer J.G., Eades L.J. and Graham M.C. 1999. The lead content and isotopic composition of British coals and their implications for past and present releases of lead to the U.K. environment. Env. Geochem. Health (in press).

Farmer J.G., MacKenzie A.B., Eades L.J., Kirika A. and Bailey-Watts A.E. 1997a. Influences on the extent and record of heavy metal pollution in sediment cores from Loch Tay in a mineralised area of Scotland. J. Geochem. Explor., 58, 195-202.

Farmer J.G., MacKenzie A.B., Sugden C.L., Edgar P.J. and Eades L.J. 1997b. A comparison of the historical lead pollution records in peat and freshwater lake sediments from central Scotland. Water, Air, Soil Pollut., 100, 253-270.

Faure G. 1986. Principles of Isotope Geology, 2nd Ed., John Wiley and Sons, London, 375-380.

Förstner U. and Salomons W. 1983. Trace metal speciation in surface waters: Interactions with particulate matter. In: (Editor, Leppard G.G.). Trace element speciation in surface waters and its ecological implications, Plenium Press, New York, p245.

Förstner U. and Salomons W. 1991. Mobilisation of metals from sediments. In (Editor Merian E.). Metals and their compounds in the environment, VCH, Weinheim, p69.

Fozzard I. and Marsden M. 1990. The Lake of Menteith, some aspects of its ecology. The Scottish Naturalist, 102, 97-129.

Francis C.W. and Brinkley F.S. 1976. Preferential adsorption of ^{137}Cs to micaceous minerals in contaminated freshwater sediment. Nature, 260, 511-513.

Furuta N. 1991. Optimisation of the mass scanning rate for the determination of lead isotope ratios using an inductively coupled plasma mass spectrometer. J. Anal. Atom. Spectrom., 6, 199-203.

Gilbertson D.D., Grattan J.P., Cressey M. and Pyatt F.B. 1997. An air-pollution history of metallurgical innovation in iron- and steel-making: A Geochemical archive of Sheffield. Water, Air, Soil Pollut., 100, 327-341.

Goldberg E.D. 1963. Geochronology with ^{210}Pb. Symposium on radioactive dating. Published IAEA Vienna Austria. 122-130.

Goldberg E.D. and Koide M. 1962. Geochronological studies of deep-sea sediments by the thorium method. Geochim. Cosmochim. Acta, 26, 417-450.

Graybeal A.L. and Heath G.R. 1984. Remobilisation of transition metals in surficial pelagic sediments from the Eastern Pacific. Geochim. Cosmochim. Acta, 48, 965-975.

Habashi F. 1997. Handbook of Extractive Metallurgy Vol. II, Wiley- VCH Weinheim, Federal Republic of Germany.

Hamelin B., Ferrand J.L., Alleman L., Nicolas E. and Veron A. 1997. Isotopic evidence of pollutant lead transport from North America to the subtropical North Atlantic gyre. Geochim. Cosmochim. Acta, 61, 4423-4428.

Hamilton-Taylor J., Davison W. and Morfett K. 1996. The biogeochemical cycling of Zn, Cu, Fe, Mn and dissolved organic C in a seasonally anoxic lake. Limnol. Oceanogr. 41, 408-418.

Hilton J., Lishman J.P. and Allen P.V. 1986. The dominant processes of sediment distribution and focusing in a small eutrophic, monomictic lake. Limnol. Oceanogr., 31, 125-133.

Hong S., Candelone J-P. and Boutron C.F. 1994. Greenland ice evidence of hemispheric lead pollution two millennia ago by Greek and Roman civilizations. Science, 265, 1841-1843.

Hong S., Candelone J-P., Patterson C.C. and Boutron C.F. 1996. History of ancient copper smelting pollution during Roman and Medieval times recorded in Greenland ice. Science, 272, 246-249.

Hopper J.F., Ross H.B., Sturges W.T. and Barrie L.A. 1991. Regional source descrimination of atmospheric aerosols in Europe using the isotopic composition of lead. Tellus, 43B, 45-60.

Horne A.J. and Goldman C.R. 1994. Limnology, 2nd Edition. M^{c}Graw-Hill Intern.

Horrill A.D., Lowe V.P.W and Hawson G. 1988. Chernobyl fallout in Great Britain. DOE Report No. DOE/RW/88/101, UK Department of the Environment, London.

Hunter K.A. 1980. Microelectrophoretic properties of natural surface-active organic matter in coastal seawater. Limnol. Oceanogr. 25, 807-822.

Jones K.C., Symon C., Taylor P.J.L., Walsh J. and Johnston A.E. 1991. Evidence for a decline in rural herbage lead levels in the U.K. Atmospheric Environment, 25, 361-369.

Kada J. and Heit M. 1992. The inventories of anthropogenic Pb, Zn, As, Cd, and radionuclides Cs-137 and excess Pb-210 in lake sediments of the Adriondack region, USA. Hydrobiol., 246, 231-241

Kerner M. and Geisler C.D. 1995. Dynamics of Cu release during early aerobic degradation in aggregated seston from the Elbe estuary. Mar. Chem., 51, 133-144.

Kershaw P.J., Swift D.J., Pentreath R.J. and Lovett M.B. 1983. Pu redistribution by biological activity in the Irish Sea. Nature, 306, 774-775.

Kesterton D. 1993. Heavy metals and radionuclides in Loch Tay sediments. BSc. Thesis, The University of Edinburgh.

Killops S.D. and Killops V.J. 1993. An introduction to organic geochemistry. Longman Scientific and Technical, England.

Klinkhammer G. 1980. Early diagenesis in sediments from the Eastern Equatorial Pacific. Pore-water results. Earth Planet. Sci. Lett., 49, 81-101.

Klinkhammer G., Heggie D.T. and Graham D.W. 1982. Metal diagenesis in oxic marine sediments. Earth Planet. Sci. Lett., 61, 211-219.

Koide M., Bruland K. and Goldberg E.D. 1973. $^{228}Th/^{232}Th$ and ^{210}Pb geochronologies in marine and lake sediments. Geochim. Cosmochim. Acta, 37, 1171-1187.

Krishnaswami S., Lal D., Martin M.J. and Meybeck M. 1971. Geochronology of lake sediments. Earth Planet. Sci. Lett., 11, 407-414.

Lancaster A.K. 1996. The effect of lead mining activity at Tyndrum on the stream sediments in the Loch Tay catchment area. BSc. Thesis, The University of Edinburgh.

Landrigan P.J. 1990. Current issues in epidemiology and toxicology of occupational exposure to lead. Environ. Health Persp., 89, 61-69.

Likens G.E. and Davis. M.B. 1975. History of Mirror Lake. Verh. Internat. Verein. Limnol., 19, 982-935.

Lippmann M. 1990. Lead and human health: background and recent findings. Environ. Res., 51, 1-8.

Lomenick T.F. and Tamura T. 1965. Naturally occurring fixation of caesium-137 on sediments of lacustrine origin. Soil Sci. Soc. Am. Proc., 29, 383-387.

Luoma S.N. and Davies J.A. 1983. Requirements for modeling trace metal partitioning in oxidised estuarine sediments. Mar. Chem., 12, 159-181.

MacDonald J.G. 1994. Geology of the Loch Lomond catchment. Hydrobiol., 290, 13-20.

MacGregor M. and MacGregor A.G. 1972. The Midland Valley of Scotland, H.M.S.O. Edinburgh.

MacKenzie A.B. and Scott R.D. 1979. Separation of Bismuth-210 and Polonium-210 from aqueous solutions by spontaneous adsorption on copper foils. Analyst, 104, 1151-1158.

MacKenzie A.B. and Scott R.D. 1984. Some aspects of coastal marine disposal of low-level liquid radioactive waste. The Nuclear Engineer, 25, 110-122.

MacKenzie A.B., Logan E.M., Cook G.T. and Pulford I.D. 1998a. A historical record of atmospheric depositional fluxes of contaminants in west-central Scotland derived from an ombrotrophic peat core. Sci. Total Environ., 222, 157-166.

MacKenzie A.B., Logan E.M., Cook G.T. and Pulford I.D. 1998b. Distributions, inventories and isotopic composition of lead in ^{210}Pb-dated peat cores from contrasting biogeochemical environments: Implications for lead mobility. Sci. Total Environ., 223, 25-35.

Mackereth F.S.H. 1969. A short core sampler for subaqueous deposits. Limol. Oceanogr., 14, 145-151.

Manahan S.E. 1990. Environmental Chemistry, 4th Edition. Lewis Publishers, Inc., London.

Miller J.C. and Miller J.N. 1988. In: Statistics for analytical chemistry. 2nd Ed. Publisher, Ellis Harwood LTD, Chichester.

Monna F., Ben Othman D. and Luck J.M. 1995. Pb isotopes and Pb, Zn and Cd concentrations in the rivers feeding a coastal pond (Thau, Southern France): constraints on the origin(s) and flux(es) of metals. Sci. Total Environ., 166, 19-34.

Monna F., Lancelot J., Croudace I.W., Cundy A.B. and Lewis J.T. 1997. Pb isotopic composition of airborne particulate material from France and the Southern United Kingdom: Implications for Pb pollution sources in urban areas. Environ. Sci. Technol., 31, 2277-2286.

Monna F., Aiuppa A., Varrica D. and Dongarra G. 1999. Pb isotope composition in lichens and aerosols from Eastern Sicily: Insights into the regional impact of volcanoes on the environment. Environ. Sci. Technol., 33, 2517-2523.

Moor H.C., Schaller T. and Sturm M. 1996. Recent changes in stable lead isotope ratios in sediments of Lake Zug, Switzerland. Environ. Sci. Technol., 30, 2928-2933.

Moorbath S. 1962. Lead isotopic abundance studies on mineral occurrences in the British Isles and their geological significance. Phil. Trans. Roy. Soc. London , A254, 295-360.

Murozumi M., Chow T.J. and Patterson C. 1969. Chemical concentrations of pollutant Pb aerosols, terrestrial dusts and sea salts in Greenland and Antarctic snow strata. Geochim. Cosmochim. Acta, 33, 1247-1294.

Murray J. and Pullar L. 1910. Bathymetrical survey 1902. Lochs of the Tay basin. In: Freshwater lochs of Scotland, 1-6, 53-83.

Nriagu J.O. 1978. Lead in the atmosphere. In: The biogeochemistry of lead in the environment. (Ed. Nriagu) Elsevier, 137-184.

Nriagu J.O. and Pacyna J.M. 1988. Quantitative assessment of worldwide contamination of air, water and soils by trace metals. Nature, 333, 134-139.

Nriagu J.O. 1989a. A global assessment of natural sources of atmospheric trace metals. Nature, 338, 47-49.

Nriagu J.O. 1989b. The history of leaded gasoline. In: Proc. 7th Intern. Conf. Heavy Metals Environ., 2, 361-366.

Nriagu J.O. 1990. The rise and fall of leaded gasoline. Sci. Tot. Environ., 92, 13-28.

Nriagu J.O. and Pacyna J.M. 1988. Qualitative assessment of worldwide contamination of air, water and soils by trace metals. Nature, 333, 134-139.

Nriagu J.O. 1996. A history of global metal pollution. Science, 272, 223-225.

Oakley S.M., Nelson P.O. and Williamson. K.J. 1981. Model of trace metal partitioning in marine sediments. Environ. Sci. Technol., 15, 474-480.

Ohnstad F.R. and Jones J.G. 1982. The Jenkin surface-mud sampler users manual. Freshwater Biological Association Occasional Publication No. 5.

Oliver B.G. 1973. Heavy metal levels of Ottawa and Rideau River sediments. Environ. Sci. Technol., 7, 135-137.

Page R.A., Cawse P.A. and Baker S.J. 1988. The effect of reducing petrol lead on airborne lead in Wales, U.K.. Sci. Total Environ., 68, 71-77.

Patterson C.C. 1965. Contaminated and natural lead environment of Man. Arch. Environ. Health, 11, 344-360.

Paterson N. 1997. Historical records and behavior of metals and radionuclides in Lake of Menteith sediments. BSc. Thesis, The University of Edinburgh.

Peirson D.H., Cambray R.S. Cawse P.A., Eakins J.D.and Pattenden N. 1982. Environmental radioactivity in Cumbria. Nature, 300, 27-31.

Peterson M.L. and Carpenter R. 1986. Arsenic distributions in porewaters and sediments of Puget Sound, Lake Washington, the Washington coast and Saanich Inlet, B.C. Geochim. Cosmochim. Acta, 50, 353-369.

Petit D., Mennessier J.P. and Lamberts L. 1984. Stable lead isotopes in pond sediments as tracer of past and present atmospheric pollution in Belgium. Atmos. Environ. 18, 1189-1193.

Pulford I.D., Maguire C.S., Cook G.T. and MacKenzie A.B. 1995. Mobility of ^{137}Cs and ^{210}Pb in organic soils. Proc.10th Intern. Conf. Heavy Metals Environ., Hamburg, 2, 137-146.

Ridgway M. and Price N.B. 1987. Geochemical associations and post-depositional mobility of heavy metals in coastal sediments: Loch Etive, Scotland. Mar. Chem., 21, 229-248.

Robbins J.A and Herche L.R. 1993. Radiochemical Limnology: Models and uncertainty in ^{210}Pb dating of sediments. Verh. Internat. Verein. Limnol., 25, 217-222.

Robbins J.A., Krezoski J. and Mozley S. 1977. Radioactivity in sediments of the Great Lakes: Post-depostional redistribution by deposit-feeding organisms. Earth Planet. Sci. Lett., 36, 325-333.

Robbins J.A., Lindner G., Pfeiffer W., Kleiner J., Stabel H.H. and Frenzel P. 1992. Epilimnetic scavenging of Chernobyl radionuclides in Lake Constance. Geochim. Cosmochim. Acta, 56, 2339-2361.

Rosman K.J.R., Ly C. and Steinnes E. 1998. Spatial and temporal variation in isotopic composition of atmospheric lead in Norwegian moss. Environ Sci. Technol., 32, 2542-2546.

Ruttner F. 1969. Fundamentals of limnology. 3rd edition, University of Toronto Press, 83-87: 204.

Salomons W. 1985. Sediments and water quality. Environ. Technol. Lett., 6, 315-326.

Santschi P., Höhener P., Benoit G.and Buchholtz-Ten Brink M. 1990. Chemical processes at the sediment-water interface. Mar. Chem., 30, 269-315.

Sawhney B.L. 1972. Selective sorption and fixation of cations by clay minerals: A review. Clays and Clay Minerals, 20, 93-100.

Schell W.R., Tobin M.J. and Massey C.D. 1989.. Evaluation of trace metal deposition history and potential element mobility in selected cores from peat and wetland ecosystems. Sci. Total Environ., 87/88, 19-42.

SEPA 96. State of the Environment report 1996. ISBN 1-901322-00-9. Stirling.

Settle D.M. and Patterson C.C. 1980. Lead in Albacore: Guide to lead pollution. Science, 207, 1167-1176.

Settle D.M. and Patterson C.C. 1982. Magnitudes and sources of precipitationand dry deposition fluxes of industrial and natural leads to the North Pacific at Enewetak. J. Geophys. Res. 87, 8857-8869.

Shotyk W., Weiss D., Appleby P.G., Cheburkin A.K., Frei R., Gloor M., Kramers J.D., Reese S. and Van Der Knaap W.O. 1998. History of atmospheric lead deposition since 12,370 ^{14}C y BP from a peat bog, Jura Mountains, Switzerland. Science, 281, 1635-1640.

Sigg L. and Stumm W. 1994. Aquatische Chemie, Eine Einfhrüng in die Chemie Wässriger Lösungen und natürlicher Gewässer. 3rd Ed. Teubner, Stutgart.

Sinclair J. The Statistical Account of Scotland 1791-1799. North and west Perthshire. Wakefield publishing, 12.

Skoog D.A. 1985. In: Principles of instrumental analysis. 3rd Edition., Saunders College, USA.

Slack H.D. 1954. The bottom deposits of Loch Lomond. Proc. Roy. Soc. Edin., B65, 213-238.

Stevenson F.J. 1994. In: Humus Chemistry. Genesis, Composition, Reactions. 2nd Edition. Publisher, J Wiley and Sons Inc., New York.

Stumm W. and Morgan J.J. 1996. Aquatic Chemistry : An introduction emphasising chemical equilibria in natural waters. (3rd Ed) Pub. John Wiley and Sons, New York Chichester.

Sturges W.T. and Barrie L.A. 1987. Lead 206/207 isotope ratios in the atmosphere of North America as tracers of US and Canadian emissions. Nature, 329, 144-146.

Sugden C.L. 1993. Isotopic studies of the environmental chemistry of lead. PhD. Thesis, The University of Edinburgh.

Sugden C.L., Farmer J.G. and MacKenzie A.B, 1991a. Isotopic characterisation of lead inputs and behavior in recent Scottish freshwater loch sediments. In: Proc. 8th Intern. Conf. Heavy Metals Environ., Edinburgh: CEP Consultants, 1, 511-514

Sugden C.L., Farmer J.G. and MacKenzie A.B. 1991b. Lead and $^{206}Pb/^{207}Pb$ profiles in ^{210}Pb dated peat cores from Scotland. Proc. 8th Intern. Conf. Heavy Metals Environ., Edinburgh: CEP Consultants, 1, 90-93.

Sugden C.L., Farmer J.G. and MacKenzie A.B. 1993. Isotopic ratios of lead in contemporary environmental materials from Scotland. Environ. Geochem. Health, 15, 59-65.

Tessier A., Fortin D., Belzile N., DeVitre R.R. and Leppard G.G. 1996. Metal sorption to diagenetic iron and manganese oxyhydroxides and associated organic matter: narrowing the gap between field and laboratory measurements. Geochim. Cosmochim. Acta, 60, 387-404.

Torgensen T. and Longmore N.E. 1984. ^{137}Cs diffusion in the highly organic sediment of Hidden Lake, Fraser Island, Queensland. Aus. J. Freshwater Res., 35, 537-548.

Turner G.M. and Thompson R. 1979. Behavior of the Earth's magnetic field as recorded in sediment of Loch Lomond. Earth Planet. Sci. Lett., 42, 412-426.

Viczian M., Lasztity A. and Barnes R.M. 1990. Identification of potential environmental sources of childhood lead poisoning by inductively coupled plasma mass spectrometry. verification an case studies. J. Anal. Atom. Spectrom., 5, 293-300.

Watmough S.A., Hughes R.J. and Hutchinson T.C. 1999. $^{206}Pb/^{207}Pb$ ratios in tree rings as monitors of environmental change. Environ. Sci. Technol, 33, 670 - 673.

Weiss D., Shotyk W., Cheburkin A.K. Gloor M. and Reese S. 1997. Atmospheric lead deposition from 12,400 to CA. 2,00 yrs BP in a peat bog profile, Jura Mountains, Switzerland. Water, Air, Soil Pollut., 100, 311-324.

Weiss D., Shotyk W., Appleby P.G., Kramers I.D. and Cheburkin A.K 1999. Atmospheric Pb deposition since the industrial revolution recorded by five Swiss peat profiles: Enrichment factors, fluxes, isotopic composition and sources. Environ Sci. Technol., 33, 1340-1352.

Wewetzer S.F.K. 1992. A bathymetric resurvey of the Lake of Menteith. Forth Naturalist and Historian, 18, 13-20.

Wewetzer S.F.K and Duck R. W. 1995. Identification of lacustrine dissolved oxygen depletion by acoustic remote sensing. Phys. Chem. Earth, 20, 163-167.
White J.R. and Driscoll C.T., 1987a. Manganese cycling in an acidic Adirondack lake. Biogeochem., 3, 87-103.

White J.R. and Driscoll C.T., 1987b. Zinc cycling in an acidic Adirondack lake. Environ. Sci. Technol., 21, 211-216.

Whiteford J.M. 1996. The determination and interpretation of heavy metal and radionuclide profiles in Loch Ness sediment. BSc. Thesis, The University of Edinburgh.

Whittow J.B. 1979. The Grampian Highlands. In: Hall P. (ed.), Geology and scenery in Scotland, 170-193. Pelican.

Wilson F. 1921. In: The lead, zinc, copper and nickel ores of Scotland. Memoirs of the Geological Survey Special reports on the mineral resources of Great Britain, Scotland, Dilson and Flet, 7, 93-107.

Appendices.

A. Calculations for analytical techniques.

A.1 α-spectrometry (^{210}Pb)

For the analysis of samples from the Loch Lomond (south) core, a ^{210}Po spike containing no ^{208}Po was used. The calculations used were:

$$^{210}\text{Pb (Bq)} = \frac{\text{cps}^{210}\text{Po}}{\text{cps}^{209}\text{Po}} \times \text{Activity of spike at the time of analysis (Bq)}$$

For Loch Lomond (north) and Lake of Menteith, a new ^{208}Po spike was used, thus:

$$^{210}\text{Pb (Bq)} = \frac{\text{cps}^{210}\text{Po}}{\text{cps}^{208}\text{Po}} \times \text{Activity of spike at the time of analysis (Bq)}$$

$$\text{A(t) (Bq kg}^{-1}\text{)} = \frac{^{210}\text{Pb (Bq)}}{\text{Dry Weight (g)} / 1000}$$

where A(t) is the specific activity of ^{210}Pb at time of counting.

$$\text{A(o) (Bq kg}^{-1}\text{)} = \text{A(t) (Bq kg}^{-1}\text{)} \times e^{(\lambda t)}$$

where: A(o) is the specific activity at the time of sampling

$\lambda = \ln 2 / t_{1/2}$, and $t_{1/2} = 22.35$ y

t = time elapsed between date of sampling and date of counting (yr).

Errors:

$$\sigma = \sqrt{N}$$

$$S_N = \frac{\sigma_N}{N} \times 100\ \%$$

where N= count rate x time counted (s)

$$S = \sqrt{\left(S^{209}Po\right)^2 + \left(S^{210}Po\right)^2}\ \%$$

$$S_{(spike)} = 1\ \%$$

$$S_{A(o)} = \sqrt{\left(S_{(counting)}\right)^2 + (1)^2}\ \%$$

A.1.2 CIC model for estimating accumulation rate.

$$^{210}Pb_d = {}^{210}Pb_s \times e^{-\lambda t}$$

Where $^{210}Pb_d$ is the specific activity of $^{210}Pb_{unsup}$ at depth d, $^{210}Pb_s$ is the specific activity of $^{210}Pb_{unsup}$ at the surface, t is the age of the sediment and λ is the decay constant of ^{210}Pb.

$$^{210}Pb_{unsup} = {}^{210}Pb_{total} - {}^{226}Ra \quad \text{or} \quad {}^{210}Pb_{total} - {}^{210}Pb_{(at\ depth)}$$

Error:

$$S\,{}^{210}Pb_{unsup} = \sqrt{\left(S^{226}Ra\right)^2 + \left(S^{210}Pb_{total}\right)^2}\ \ Bq\ kg^{-1}$$

The ln $^{210}Pb_{unsup}$ (y-axis) is plotted against cumulative mass (g cm^{-2}) on the x-axis and a weighted linear regression performed to obtain the gradient. The accumulation rate is then given by:

$$\text{accumulation rate (g cm}^{-2}\text{ y}^{-1}\text{)} = -\lambda / \text{gradient}$$

Where: λ is the decay constant for ^{210}Pb.

Cumulative mass (g cm^{-2}) = dry weight to middle of section (g) / cross sectional area (cm^2)

Where cross sectional area = πr^2

Jenkin core, r = 3.45 cm. = 37.39 cm^2

Mini-Mackereth core r = 3.25 cm. = 33.18 cm^2

Date of each section can be calculated thus:

years of accumulation (y) = depth of section (g cm^{-2}) / accumulation rate (g cm^{-2} y^{-1}).

The calendar date is given by : date of core collection - years of accumulation.

A.1.2 CRS model for estimating accumulation rate.

The total inventory of unsupported ^{210}Pb (Bq m^{-2}) in the core is calculated plus the inventories below the base of each section. Where:

Inventory of each section (Bq m^{-2}) = $^{210}Pb_{unsup}$ (Bq kg^{-1}) / (Wt (kg) / c.s.a (m^2))
(where c.s.a is cross sectional area for the corer used).

The age of any individual section is then given by:

$$t_i = \frac{1}{\lambda} \ln \frac{I}{I_i}$$

Where: t_i is the age of the base of the i^{th} layer, λ is the ^{210}Pb decay constant, I is the total unsupported ^{210}Pb inventory and I_i is the unsupported ^{210}Pb inventory below the i^{th} layer.

The calendar date is given by : date of core collection - years of accumulation.

The average ^{210}Pb flux to the sediment can be calculated from the total inventory of unsupported ^{210}Pb by:

$$F = I \times \lambda$$

Where: I is the total inventory (Bq m^{-2}) and λ is the ^{210}Pb decay constant (y^{-1}).

A.2 γ-Spectrometry (^{137}Cs, ^{226}Ra, ^{210}Pb and ^{241}Am).

$$\text{Efficiency} = \frac{\text{Count rate (cps)}}{\text{A(t) (Bq)}} \times \frac{100}{1} \%$$

Where: Intensity is the number of counts of the spiked standard and A(t) is the total activity of spike added.

Errors:

$$S_{eff} = \sqrt{(S_{Spike})^2 + (S_{Counts})^2} \%$$

Where: S_{Spike} is taken as 1 %.

$$\text{Activity of sample at time of counting (Bq kg}^{-1}) = \frac{\text{Count rate (cps)} \times \text{Efficiency}}{\text{Weight (kg)}}$$

$$A(t)\ (Bq\ kg^{-1}) = A(o) \times e^{(\lambda t)}$$

Where: A(t) is the activity of sample at time of sampling, A(o) is the activity of the sample at time of counting, t is the time elapsed between sampling and counting and $\lambda = \frac{\ln 2}{t_{1/2}}$ and $t_{1/2}$ is the half-life of the radionuclide.

Errors:

$$S(o) = \sqrt{(S_{eff})^2 + (S_{cnts})^2}\ \%$$

A.2.1 Calculation of the $^{134}Cs/^{137}Cs$ activity ratio at time of deposition of Chernobyl fallout.

To calculate the activity ratio applicable at the time of deposition of Chernobyl fallout, the specific activity of ^{134}Cs is divided by the specific activity of ^{137}Cs and corrected back to the date of the Chernobyl accident (26th April 1986) using the following equation:

$$R(o) = R(t) \times e^{\lambda t}$$

Where: R(o) is the ratio at the time of the accident, R(t) is the ratio at the time of sampling, t is the time lapse between the sampling and the accident and λ is equal to $\lambda\ ^{134}Cs - \lambda\ ^{137}Cs$.

A.3. Stable lead isotope ratios.

The excess Pb flux and $^{206}Pb/^{207}Pb$ ratio due to anthropogenic input of Pb were calculated. The values for Pb concentration and $^{206}Pb/^{207}Pb$ ratio, where the background has reached a constant value, were taken to represent the pre-industrial values. For example, in LL/S3A the Pb concentration and $^{206}Pb/^{207}Pb$ ratio had a constant value below 28.5 cm of 15 ± 4 mg kg^{-1} and 1.174 ± 0.002 respectively. To

calculate the excess Pb flux the background, pre-industrial Pb concentration (15 mg kg^{-1}), is subtracted from each section then multiplied by the sedimentation rate of 0.309 kg m^{-2} yr^{-1} to give the excess Pb flux (mg m^{-2} yr^{-1}). The $^{206}Pb/^{207}Pb$ ratio of the excess Pb was calculated using the following equation:

$$\text{Excess } ^{206}Pb/^{207}Pb = [(Pb_{meas} \times ^{206}Pb/^{207}Pb_{meas}) - (15 \times 1.174)] / (Pb_{meas} - 15)$$

A.4. Heavy metals (Fe, Mn, Zn, Pb, Cu and Cd).

A.4.1 Concentration calculations.

Standard Concentration / mg l^{-1}	Standard Absorbance
0	0.00
1	0.01
5	0.05
10	0.10
Sample	0.06

Calibration graph

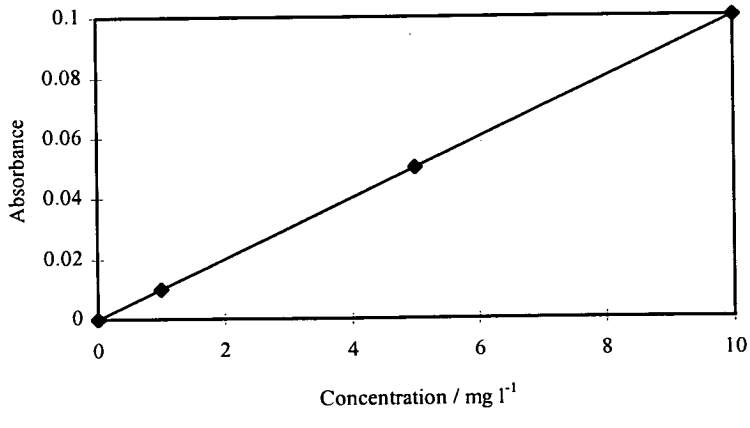

$$\text{Sample concentration (mg kg}^{-1}\text{)} = \frac{\text{Sample conc. (mg l}^{-1}\text{)} \times \text{volume (ml)}}{\text{Weight (g)}}$$

A.4.2 Inventory calculations.

The excess inventory I of each metal due to anthropogenic input is calculated by summing the excess inventory for each section.

$$[M]_{XS}\ (\text{mg kg}^{-1}) = [M]_{total} - [M]_{background}$$

$$[I]_{XS}\ (\text{g m}^{-2}) = ([M]_{XS}\ (\text{mg kg}^{-1}) / 1000) \times (\text{wt (kg)} / \text{cross sectional area (m}^2))$$

Sample ident.: CHEM 7-Jun-1999 16:38

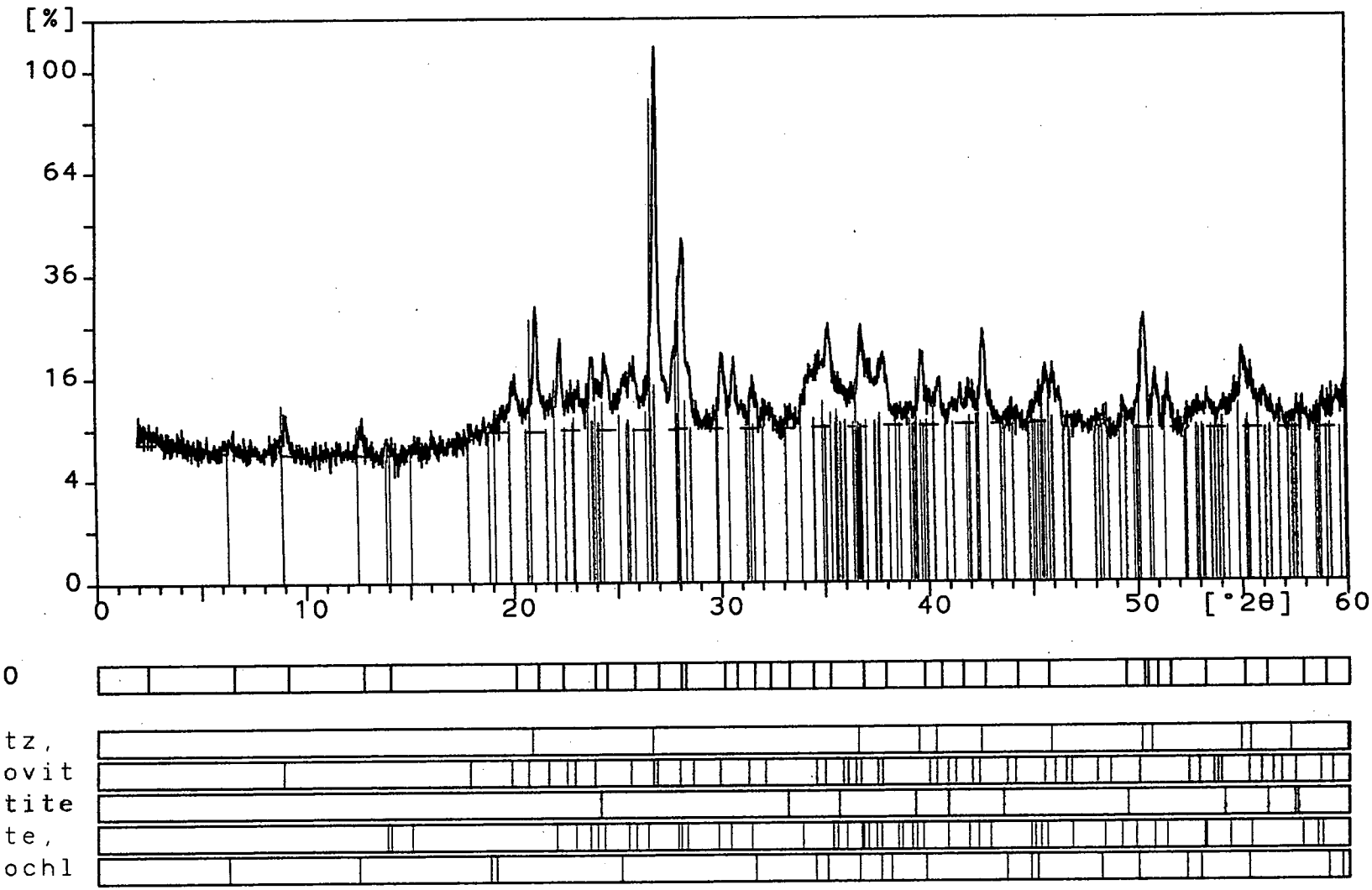

Sample identification: CHEM 8-Jun-1999 10:16

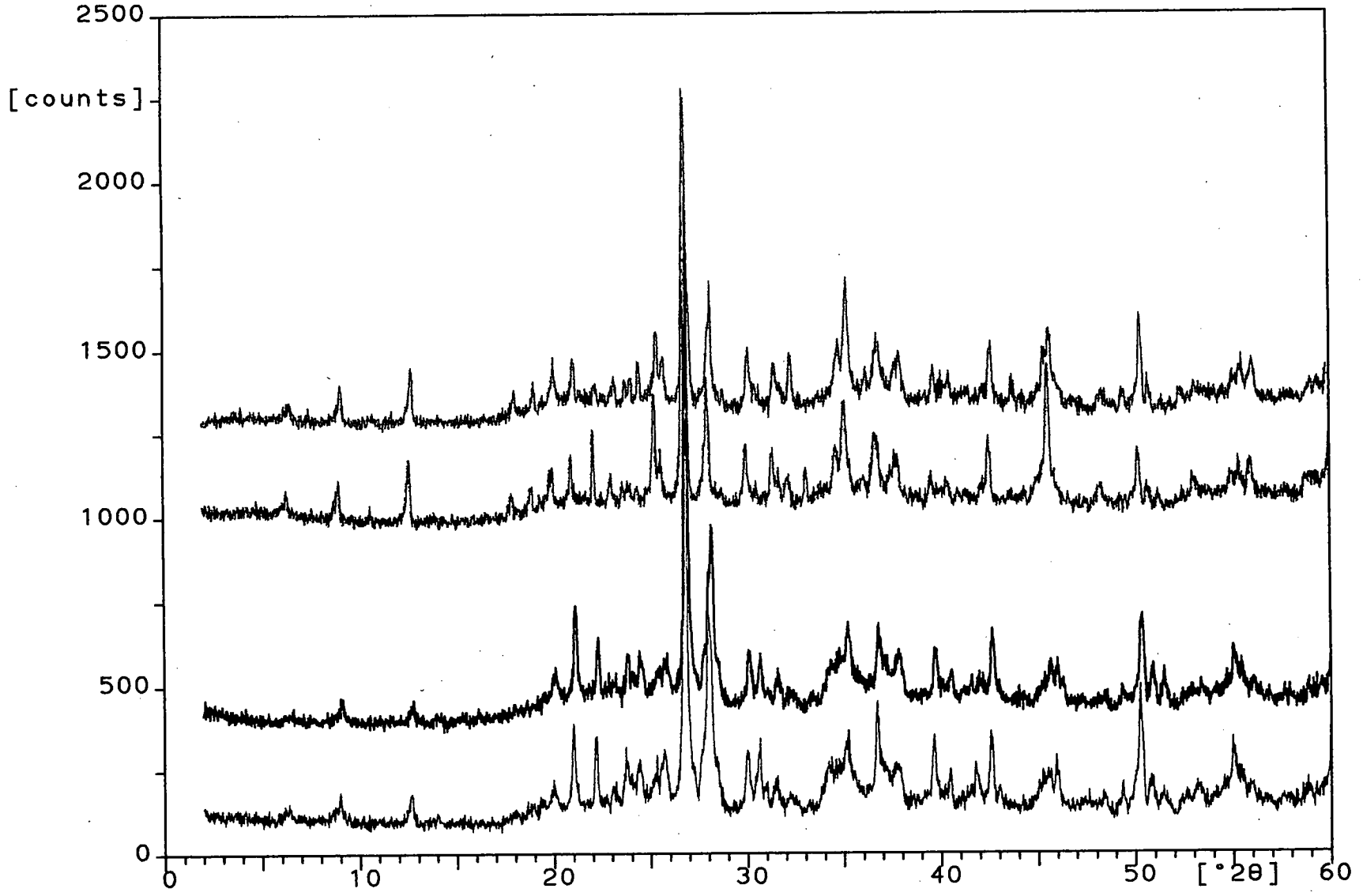

CHN10.RD CHN55.RD CHEM038.RD CHEM132.RD

ELSEVIER

J. Environ. Radioactivity, Vol. 39, No. 2, pp. 107–115, 1998

Printed in Great Britain
PII: S0265-931X(97)00054-4 0265-931X/98 $19.00 + 0.00

High-resolution Profile of Radiocaesium Deposition in Loch Lomond Sediments

L. J. Eades,[a] J. G. Farmer,[a] A. B. MacKenzie,[b] A. Kirika[c] & A. E. Bailey-Watts[c]

[a] Department of Chemistry, The University of Edinburgh, Edinburgh EH9 3JJ, UK
[b] Scottish Universities Research and Reactor Centre, East Kilbride, Glasgow G75 0QF, UK
[c] Natural Environment Research Council Institute of Freshwater Ecology, Bush Estate, Penicuik, Midlothian EH26 0QB, UK

(Received 20 July 1996; accepted 27 June 1997)

ABSTRACT

A sediment core from the southern basin of freshwater Loch Lomond, Scotland, was thinly sectioned at 3 mm intervals and analysed for radiocaesium, present as a result of fallout from the atmospheric nuclear weapons' testing programme of the 1950s and 1960s and from the Chernobyl reactor accident of April 1986. The high-resolution sampling enabled much improved resolution of peaks from weapons testing fallout and Chernobyl and led to the estimation of a sedimentation rate (30·9 mg cm^{-2} y^{-1}) for which the uncertainty was a factor of five times less than that of a previous study based on a 1 cm sampling frequency. Further potential advantages of high-resolution sampling in distinguishing possible influences upon the vertical distribution of radiocaesium in sediments are discussed. © *1998 Elsevier Science Ltd. All rights reserved.*

INTRODUCTION

Sediment cores from freshwater lakes are often used in the reconstruction of historical pollution records (Alderton, 1985). Freshwater lake sediment chronologies and mixing regimes have been successfully characterised in systems with a high clay-mineral content and low organic-matter concentration using ^{137}Cs ($t_{1/2}$ = 30·2 year) from weapons testing fallout, with maximum input in 1963, and ^{134}Cs ($t_{1/2}$ = 2·05 year) and ^{137}Cs from the Chernobyl accident in April 1986 (e.g. Pennington *et al.*, 1976; Bonnett and Cambray, 1991; Bryant *et al.*, 1993). Such studies have often been used to

support and/or assess the reliability of ^{210}Pb dating (e.g. Appleby *et al.*, 1993). In organic-rich sediments, radiocaesium dating is unreliable as a consequence of diffusive movement in the interstitial water (Torgerson and Longmore, 1984; Davis *et al.*, 1984), possibly promoted by the inhibition of caesium uptake on clay surfaces by humic molecules (Maguire *et al.*, 1992).

One limitation of the use of radiocaesium dating in suitable, clay-rich sediments is that the depth interval used in sampling the sediment cores is usually 1 or 2 cm and this may obscure detail of the radiocaesium distribution, resulting in increased uncertainty in assessing accumulation rates and in characterising the effects of mixing. In order to evaluate the significance of this effect, a study was performed of the distribution of radiocaesium in the sediments of Loch Lomond, in Scotland, using the thinnest vertical increments that could practicably be obtained using simple, conventional sectioning methods. The data obtained are here compared with a previous study of this system by radiocaesium and ^{210}Pb dating when larger sample increments were used (Bryant *et al.*, 1993).

SAMPLING AND ANALYSIS

A sediment core was collected on 26 November 1991 from a site in the southern basin of Loch Lomond (UK National Grid Reference NS391884), which is situated in west-central Scotland, some 30 km NW of Glasgow (Fig. 1). The core, of length 14·4 cm and diameter 69 mm, was collected using a Jenkin surface-mud sampler, which minimises disturbance of the surface layers of sediment (Ohnstad and Jones, 1982). The water depth was 18 m and well-oxygenated conditions prevail in this section of the loch. The sediments have low organic-matter concentrations and are clay rich (Bryant *et al.*, 1993).

The sediment was extruded from the plastic core tube using a piston, driven by a hydraulic water pump, which allowed very fine control of the upward movement of the core. A sectioning ring, comprising a 1 cm section of core tube with a piece of camera film positioned on the outside to mark a height of 3 mm above the base, was placed on the top of the sediment tube. The sediment was extruded into the sectioning ring until the surface reached the 3 mm mark and was then removed using a perspex sheet of thickness 0·3 mm.

Depending upon the weight of dried, ground material available for individual sections, samples of 0·5, 1·0, 1·5, 2·0 or 2·5 g were accurately weighed into polypropylene pots which were accurately positioned in a reproducible geometry in contact with the end window of a Canberra

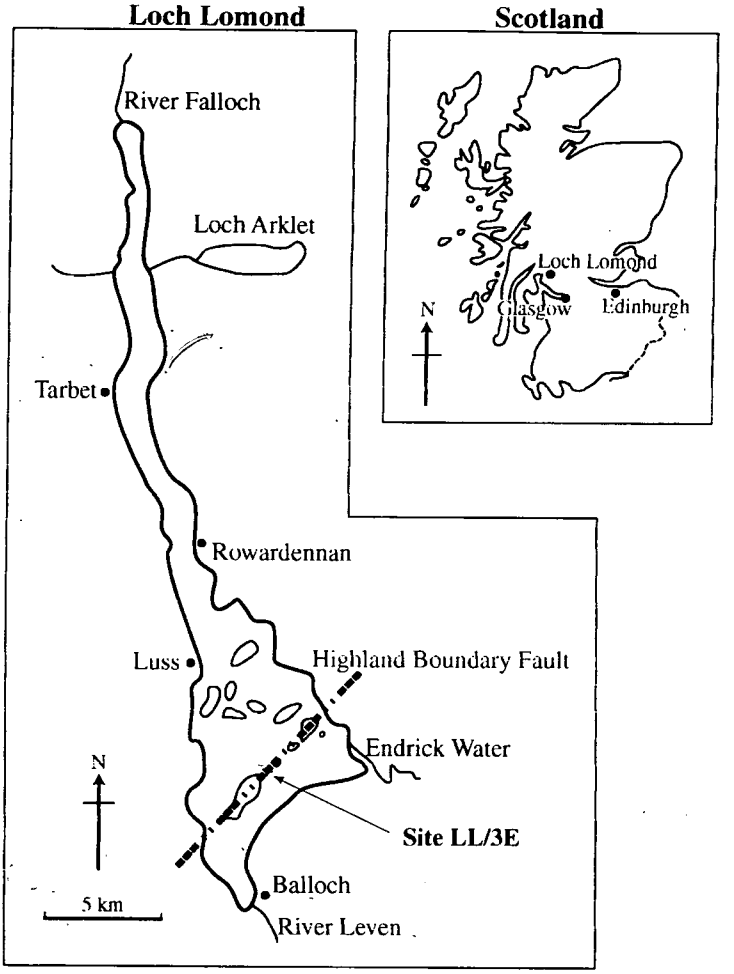

Fig. 1. Location of sampling site LL-3E in Loch Lomond, Scotland.

n-type high purity Ge gamma photon detector (25% relative efficiency). Gamma spectra of the samples were recorded, typically over 2 to 4 day counting periods, and ^{134}Cs and ^{137}Cs analysed using the gamma lines at 605 and 661 keV, respectively. Sediment from deeper sections of a core from this location, below the level to which radiocaesium could be detected, was 'spiked' with known activities of ^{134}Cs and ^{137}Cs and was used to determine the detection efficiencies for the selected sample weights.

An additional core, of length 80 cm, was collected from this location using a mini-Mackereth corer (Mackereth, 1969). This core was also sectioned in 3 mm increments to a depth of 30 cm and the sediment analysed

for metals and stable lead isotope ratios, the results of which are reported elsewhere (Farmer *et al.*, 1996). Subsamples of this core were also used for determination of the major mineral content by X-ray diffraction analysis and organic carbon content using a Philips PW 1800 Diffractometer and Perkin-Elmer 2400 CHN analyser, respectively.

RESULTS AND DISCUSSION

The radiocaesium analytical data are presented in Table 1 and the specific activity profiles plotted in Fig. 2. ^{137}Cs was detectable to a depth of 10·65 cm and the profile displayed peaks at 1·95 cm, with a maximum specific activity of 2000 Bq kg^{-1}, and at 5·85 cm, with a specific activity of 1084 Bq kg^{-1}. The upper peak can be identified as originating from Chernobyl fallout by the presence of ^{134}Cs, with a maximum specific activity of 193 Bq kg^{-1}, coincident with the maximum ^{137}Cs activity, whereas the lower peak, containing ^{137}Cs in the absence of ^{134}Cs, can be attributed to weapons testing fallout.

This distribution of radiocaesium compares well with data presented by Bryant *et al.* (1993) for a core collected from a nearby sampling site in Loch Lomond in 1990, which also showed clear peaks from Chernobyl and weapons testing fallout (Fig. 3). The sampling increment used by Bryant *et al.*, however, was 1 cm and it is immediately apparent that this resulted in broader peaks (in particular for Chernobyl fallout) and a poorer resolution of the peaks than was obtained in the present work. This has a direct effect on the accuracy with which the sediment accumulation rate can be evaluated. Thus, in the present work, the Chernobyl peak, corresponding to 1986, occurs within the depth range 1·80–2·10 cm, and the weapons testing fallout peak, corresponding to 1963, occurs in the depth range 5·70–6·00 cm. Therefore, the depth of sediment accumulated in the 23 year period between the weapons testing fallout maximum and Chernobyl events was in the range 3·6–4·2 cm, giving a sedimentation rate in the range 0·16–0·18 cm year^{-1} (i.e. a range of $\pm$ 6% about the mean value of 0·17 cm year^{-1}). In contrast, on the basis of the data presented by Bryant *et al.* (1993), the Chernobyl and weapons testing peaks can be identified to occur, respectively, in the depth increments 2–3 cm and 5–6 cm. This gives a range of 2–4 cm of sediment accumulated in the 23 years between the two events, corresponding to a range of sedimentation rates of 0·09–0·17 cm year^{-1} (i.e. a range of $\pm$ 31% about the mean value of 0·13 cm year^{-1}). Thus, while there is overlap between the estimated ranges of sedimentation rates for the two cores, the uncertainty in the value derived using 1 cm increments is five times greater than that obtained using 3 mm increments.

TABLE 1
Radiocaesium data for Loch Lomond core LL-3E, collected on 26 November 1991

Section depth (cm)	*Specific activity ($\pm 1\sigma$)*		
	^{134}Cs *(Bq kg^{-1})*	^{137}Cs *(Bq kg^{-1})*	$^{134}Cs/^{137}Cs$ *($\pm 1\sigma$) (decay-corrected to 1986)*
0·0–0·3	54 ± 27	628 ± 45	0·50 ± 0·25[a]
0·3–0·6	22 ± 23	712 ± 15	0·18 ± 0·19[a]
0·6–0·9	55 ± 31	759 ± 12	0·42 ± 0·24[a]
0·9–1·2	39 ± 25	755 ± 13	0·30 ± 0·19[a]
1·2–1·5	86 ± 20	1037 ± 27	0·48 ± 0·11
1·5–1·8	147 ± 17	1573 ± 40	0·54 ± 0·06
1·8–2·1	193 ± 12	2000 ± 86	0·56 ± 0·04
2·1–2·4	114 ± 13	1228 ± 49	0·54 ± 0·07
2·4–2·7	38 ± 9	634 ± 31	0·35 ± 0·08
2·7–3·0	7 ± 8	559 ± 18	0·07 ± 0·08
3·0–3·3		423 ± 15	
3·3–3·6		437 ± 14	
3·6–3·9		500 ± 13	
3·9–4·2		561 ± 14	
4·2–4·5		568 ± 9	
4·5–4·8		644 ± 10	
4·8–5·1		741 ± 16	
5·1–5·4		777 ± 13	
5·4–5·7		880 ± 17	
5·7–6·0		1084 ± 27	
6·0–6·3		1004 ± 26	
6·3–6·6		858 ± 29	
6·6–6·9		655 ± 39	
6·9–7·2		447 ± 25	
7·2–7·5		350 ± 31	
7·5–7·8		256 ± 44	
7·8–8·1		186 ± 31	
8·1–8·4		133 ± 40	
8·4–8·7		85 ± 21	
8·7–9·0		56 ± 22	
9·0–9·3		43 ± 21	
9·3–9·6		29 ± 15	
9·6–9·9		25 ± 7	
9·9–10·2		19 ± 7	
10·2–10·5		16 ± 7	
10·5–10·8		18 ± 10	

[a] Large error on ratio as a result of small sample size and associated large counting error on ^{134}Cs activity.

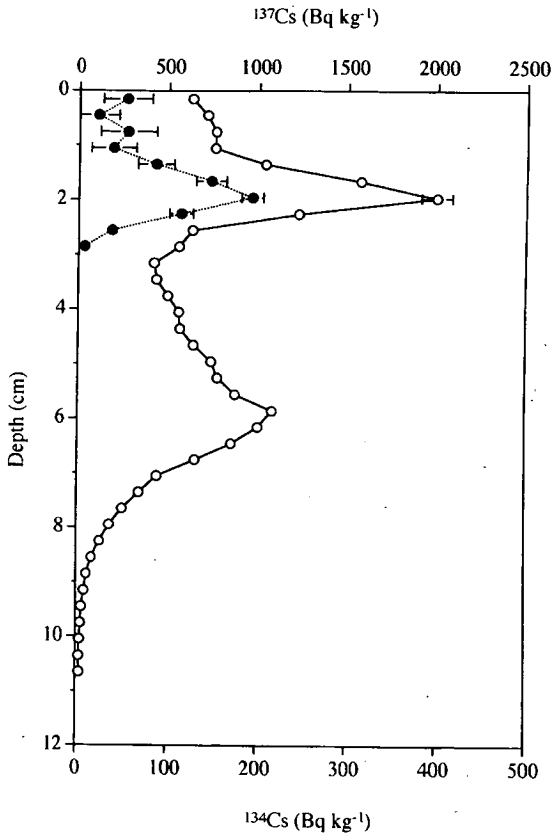

Fig. 2. Profiles of specific activity (Bq kg^{-1}) of ^{134}Cs (●) and ^{137}Cs (○) versus depth (cm) in Loch Lomond sediment core LL-3E, collected on 26 November 1991.

Estimation of the flux of sediment from the core in this study eliminates the influence of sediment compaction and the value of 30·9 mg cm^{-2} year^{-1} obtained in this way compares favourably with the range of 32–42 mg cm^{-2} year^{-1} obtained by Bryant *et al.* (1993) via ^{210}Pb dating of a core from a nearby sampling site.

Broadening of the radiocaesium peaks in the sediment can be caused by a number of processes, including: (a) physical and/or biological mixing of the sediment, (b) diffusion of Cs in solution in the sediment interstitial water, and (c) input of weathered material containing radiocaesium from the catchment after the initial deposition event. On the basis of the profiles obtained using a 1 cm sampling increment (Fig. 3), it is difficult to distinguish between these processes. In contrast, the sharp peaks obtained for Chernobyl radiocaesium using 3 mm increments suggests that mixing and

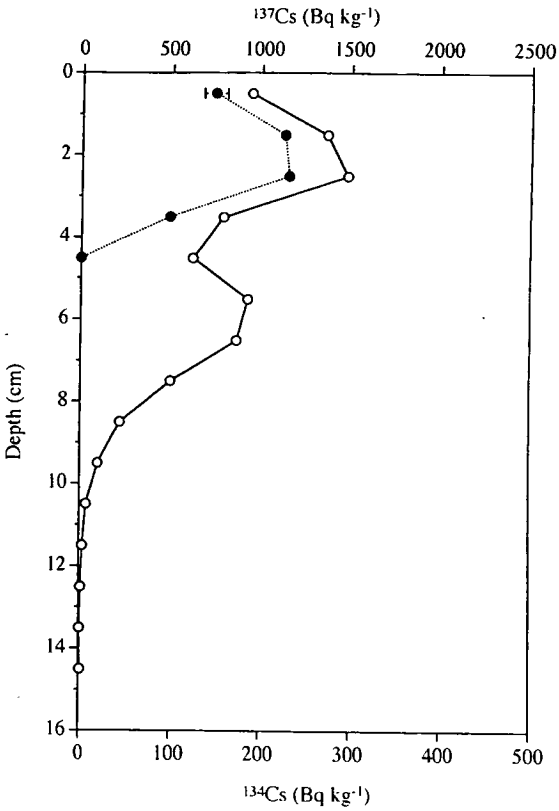

Fig. 3. Profiles of specific activity (Bq kg^{-1}) of ^{134}Cs (●) and ^{137}Cs (○) versus depth (cm) in a sediment core from the southern basin of Loch Lomond (UK National Grid Reference NS372881), collected on 26 April 1990 (Bryant *et al.*, 1993).

diffusion have had a relatively small effect in the 5·5 years since deposition. Both the ^{134}Cs and ^{137}Cs profiles, with relatively constant activities in the top four sections, would, however, be consistent with continued input of Chernobyl contaminated material from the catchment in the period since 1986 or highly efficient mixing of the surface 1 cm of sediment. The upper portion of the weapons testing peak would also be consistent with continued input from the catchment, with a trend reflecting a gradual decrease in activity of material deposited since 1963. The distribution of ^{137}Cs below the weapons testing peak, with penetration to a depth of 10·65 cm (corresponding to a date of 1923 on the basis of a sedimentation rate of 30·9 mg cm^{-2} year^{-1}) provides evidence that diffusion or mixing over a longer timescale continues to affect the sediment at this depth.

On the basis of the observed $^{134}Cs/^{137}Cs$ activity ratio of about 0·55 for Chernobyl fallout at the time of deposition (Horrill *et al.*, 1988) and the corresponding decay-corrected values for LL-3E (Table 1), the ^{137}Cs present in the core can be resolved into separate Chernobyl and weapons testing fallout components to give the corresponding inventories. The weapons testing inventory (decay corrected to 1963) of 13·8 ± 0·2 kBq m^{-2} derived in the present case compares favourably with the value of 14·4 ± 0·1 kBq m^{-2} calculated for the sediment from this area by Bryant *et al.* (1993), but both are higher than the estimated deposition range of 6–8 kBq m^{-2} (Peirson *et al.*, 1982), consistent with continued input of weathered material containing ^{137}Cs from the catchment in the period since 1963. The Chernobyl ^{137}Cs inventory of 3·9 ± 0·1 kBq m^{-2} obtained in the present work is within the estimated deposition range of 1–5 kBq m^{-2} (Clark and Smith, 1988), but is somewhat lower than the value of 6·9 ± 0·1 kBq m^{-2} derived by Bryant *et al.* (1993). On the basis of only these two observations, it is not possible to identify the cause of this difference.

CONCLUSIONS

Sampling of a Loch Lomond sediment core in 3 mm increments provided sedimentation rates and radiocaesium inventories that were generally compatible with previous studies of this system using 1 cm sampling frequency. The uncertainty in the estimated sedimentation rate, however, was a factor of five times lower using the high-resolution sampling. In addition, superior resolution of peaks from weapons testing fallout and Chernobyl was possible, providing greater sensitivity in attempts to distinguish between the influences of mixing, diffusion and continued input of contaminated material from the catchment after the primary deposition event.

ACKNOWLEDGEMENTS

We would like to thank R. Tippett, R. McMath (both Glasgow University Field Station, Rowardennan), C. L. Bryant and C. L. Sugden for their assistance with field sampling, C. Robertson (Scottish Universities Research and Reactor Centre) for help with the γ-spectroscopy analysis, and G. Angel (Geology Department, The University of Edinburgh) for his assistance with the XRD analysis.

REFERENCES

Alderton, D. H. M. (1985). Sediments. In *Historical Monitoring*, MARC Report No. 31. MARC, London, pp. 1–95.

Appleby, P. G., Richardson, N. and Smith, J. T. (1993) The use of radionuclide records from Chernobyl and weapons test fallout for assessing the reliability of ^{210}Pb in dating very recent sediments. *Verhandlungen der Internationalen Vereinigung für theoretische und angewandte Limnologie*, **25,** 226–269.

Bonnet, P. J. P. and Cambray, R. S. (1991) The record of deposition of radionuclides in the sediments of Ponsonby Tarn, Cumbria. *Hydrobiologia* **214,** 63–70.

Bryant, C. L., Farmer, J. G., MacKenzie, A. B., Bailey-Watts, A. E. and Kirika, A. (1993) Distribution and behaviour of radiocaesium in Scottish freshwater loch sediments. *Environmental Geochemistry and Health*, **15,** 153–161.

Clark, M. J. and Smith, F. B. (1988) Wet and dry deposition of Chernobyl releases. *Nature* **322,** 245–249.

Davis, R. B., Hess, C. T., Norton, S. A., Hanson, D. W., Hoagland, K. D. and Anderson, D. S. (1984) ^{137}Cs and ^{210}Pb dating of sediments from soft-water lakes in New England (USA) and Scandinavia: a failure of ^{137}Cs dating. *Chemical Geology* **44,** 151–185.

Farmer, J. G., Eades, L. J., MacKenzie, A. B., Kirika, A. and Bailey-Watts, A. E. (1996) Stable lead isotope record of lead pollution in Loch Lomond sediments since 1630 A.D. *Environmental Science and Technology* **30,** 3080–3083.

Horrill, A. D., Lowe, V. P. W. and Hawson, G. (1988) Chernobyl fallout in Great Britain. DOE Report No. DOE/RW/88/101, UK Department of the Environment, London.

Mackereth, F. J. H. (1969) A short core sampler for subaqueous deposits. *Limnology and Oceanography* **14,** 145–151.

Maguire, S., Pulford, I. D., Cook, G. T. and MacKenzie, A. B. (1992) Caesium sorption-desorption in clay-humic acid systems. *Journal of Soil Science* **43,** 689–696.

Ohnstad, F. R. and Jones, J. G. (1982) The Jenkin surface-mud sampler user manual. Freshwater Biological Association Occasional Publication No. 5.

Peirson, D. H., Cambray, R. S., Cawse, P. A., Eakins, J. D. and Pattenden, N. J. (1982) Environmental radioactivity in Cumbria. *Nature* **300,** 27–31.

Pennington, W., Cambray, R. S., Eakins, J. D. and Harkness, D. D. (1976) Radionuclide dating of the recent sediments of Blelham Tarn. *Freshwater Biology* **6,** 317–331.

Torgersen, T. and Longmore, M. E. (1984) ^{137}Cs diffusion in the highly organic sediment of Hidden Lake, Fraser Island, Queensland. *Australian Journal of Freshwater Research* **35,** 537–548.

Reprinted from

JOURNAL OF GEOCHEMICAL EXPLORATION

Journal of Geochemical Exploration 58 (1997) 195–202

Influences on the extent and record of heavy metal pollution in sediment cores from Loch Tay in a mineralised area of Scotland

J.G. Farmer [a], A.B. MacKenzie [b], L.J. Eades [a], A. Kirika [c], A.E. Bailey-Watts [c]

[a] *Department of Chemistry, University of Edinburgh, Edinburgh EH9 3JJ, Scotland, UK*
[b] *Scottish Universities Research and Reactor Centre, East Kilbride, Glasgow G75 0QF, Scotland, UK*
[c] *Natural Environment Research Council Institute of Freshwater Ecology, Bush Estate, Penicuik, Midlothian EH26 0QB, Scotland, UK*

Received 1 October 1996; accepted 1 November 1996

ELSEVIER

JOURNAL OF GEOCHEMICAL EXPLORATION

Journal of the Association of Exploration Geochemists
Editor-in-Chief: Eion M. Cameron

Scope of the journal

The *Journal of Geochemical Exploration* covers all aspects of the application of geochemistry to the exploration and study of mineral resources, and related fields, including the geochemistry of the environment. Topics include: the description and evaluation of new or improved methods of geochemical exploration: sampling and analytical techniques and methods of interpretation; geochemical distributions in and around mineralized environments; and processes of geochemical dispersion in rocks, soils, vegetation, water and the atmosphere.

(see further inside back cover)

THE ASSOCIATION OF EXPLORATION GEOCHEMISTS

President
William B. Coker
BHP Minerals Canada Ltd.
33 Yonge Street, Suite 610
Toronto, Ont. K1A 0E8, CANADA
Tel: +1-416-368-3884 / Fax: + 1-416-365-0763

Vice Presidents

David L. Garnett
Becquerel Laboratories Pty Ltd, PMB 1
Menai, NSW 2234, AUSTRALIA
Tel: +61-2-543-2644
Fax: +61-2-543-2655
E-mail: bq@atom.ansto.gov.au

Peter R. Simpson
Min. & Geochem. Surveys Division
British Geological Survey
Keyworth, Nottingham, NG12 5GG, UK
Tel: +44-1159-363532
Fax: +44-1159-363200
E-mail p.simpson@bgs.ac.uk

Secretary
Sherman P. Marsh
U.S. Geological Survey
MS 973, Denver Federal Center
PO Box 25046, Denver, CO 80225, USA
Tel: +1-303-236-5521
Fax: +1-303-236-3200
E-mail smarsh@helios.cr.usgs.gov

Treasurer
Gwendy E.M. Hall
Geological Survey of Canada
601 Booth St, Room 555
Ottawa, Ont. K1A 0E8, CANADA
Tel: +1 613 992-6425
Fax: +1 613 992-3726
E-mail hall@gsc.emr.ca

Councillors

1995–1997
Graham F. Taylor
Steve Cone
Mark A. Fedikow
R. Steve Friberg
Alastair J. Sinclair
Barry W. Smee

1996–1998
Stephen J. Cook
Richard K. Glanzman
Gwendy E.M. Hall
Beth M. McClenaghan
J. Thomas Nash
Erick F. Weiland

Regional Councillors

Australia 1996-1998
Mark Elliott
Leigh F. Bettenay
Nigel W. Radford

Brazil
Marcondes L. Da Costa

China
Guangsheng Yan

Europe
Vacant

Great Britain and Ireland
Peter R. Simpson

Northern Countries
Clemens Reimann

Southeast Asia
Tawsaporn Nuchanong

Southern Africa
Vacant

An international organization specializing in the field of exploration geochemistry whose purpose is to:
– advance the science of geochemistry as it relates to exploration
– further the common scientific interests of exploration geochemists
– facilitate the acquisition and distribution of professional knowledge
– promote interchange of information
– encourage research and development
– advance the status of the profession
– sponsor symposia, seminars and technical meetings

Annual membership (1997) is $70.00 which includes an annual subscription to the Journal of Geochemical Exploration and a quarterly newsletter with current happenings in exploration geochemistry. Members are also entitled to receive free or at reduced cost special publications. These include the proceedings of A.E.G.-sponsored symposia and meetings, bibliography volumes and geochemical handbooks.

Application forms for membership in the Association can be obtained from the permanent office at the address given below. Information about changes of address or enquiries about non-delivery of newsletter or journal issue (for members only) should also be directed to the permanent office:

Association of Exploration Geochemists,
Betty Arseneault, *Business Manager,*
P.O. Box 26099, 72 Robertson Road,
Nepean, Ont. K2H 9R0, Canada,
Tel: 613-828-0199; Fax 613-828-9288,
e-mail aeg@geology.isis.org.

ELSEVIER

Journal of Geochemical Exploration 58 (1997) 195–202

JOURNAL OF GEOCHEMICAL EXPLORATION

Influences on the extent and record of heavy metal pollution in sediment cores from Loch Tay in a mineralised area of Scotland

J.G. Farmer [a], A.B. MacKenzie [b], L.J. Eades [a], A. Kirika [c], A.E. Bailey-Watts [c]

[a] *Department of Chemistry, University of Edinburgh, Edinburgh EH9 3JJ, Scotland, UK*
[b] *Scottish Universities Research and Reactor Centre, East Kilbride, Glasgow G75 0QF, Scotland, UK*
[c] *Natural Environment Research Council Institute of Freshwater Ecology, Bush Estate, Penicuik, Midlothian EH26 0QB, Scotland, UK*

Received 1 October 1996; accepted 1 November 1996

Abstract

The distribution and inventories of Pb in the sediments of Loch Tay have been strongly influenced by inputs from past Pb mining activity, as demonstrated by correlation with the characteristic $^{206}Pb/^{207}Pb$ signature of the Tyndrum ore deposit. A major depositional event, perhaps associated with the cessation of Pb mining in the area, has been dated at 1906–1928 by the ^{210}Pb method. Zinc and Cu have been influenced to a lesser extent by mining, as shown by comparison with inventories in Loch Lomond. Profiles of As, Mn and Fe have been affected by post-depositional diagenetic remobilisation processes. The results serve as a benchmark, with Au mining set to commence at Cononish, near Tyndrum, in 1996.

Keywords: heavy metals; pollution; lake sediments; Loch Tay, Scotland

1. Introduction

In the Central Highlands of Scotland, Loch Tay, the fourth largest by volume of the Scottish freshwater lochs, lies within the Dalradian Belt, which is characterised by important occurrences of mineral deposits (Plant et al., 1990) (Fig. 1). Lead mining began at Tyndrum, near the headwaters of the Tay river system and some 25 km to the west of Loch Tay, in 1739, continuing intermittently until as recently as 1925 (Wilson, 1921; Craig, 1965). There have been other Pb and Zn mines, although of smaller scale, and Cu mining (e.g. at Tomnadashan) in the Loch Tay area, sometimes with associated smelting activity (Wilson, 1921; Bainbridge, 1970; British Geological Survey, 1990) (Fig. 2). Cononish, near Tyndrum, is now a site for commercial Au mine development, stream sediments in the area having shown elevated levels of As, a useful pathfinder element for Au (British Geological Survey, 1990). To investigate the current extent of metal contamination and the possible records of previous mining activity contained within the sediment column of Loch Tay, sediment cores were collected for the determination of metals, stable Pb isotopes and, for dating purposes, radionuclides. The uses and limitations of sediment cores for the purposes of historical reconstruction have been reviewed elsewhere (Farmer, 1991, 1994).

2. Area description

Loch Tay (56°30′ N, 4°10′ W), situated 20 km to the north of the Highland Boundary Fault and ap-

0375-6742/97/$17.00
PII S0375-6742(96)00060-X

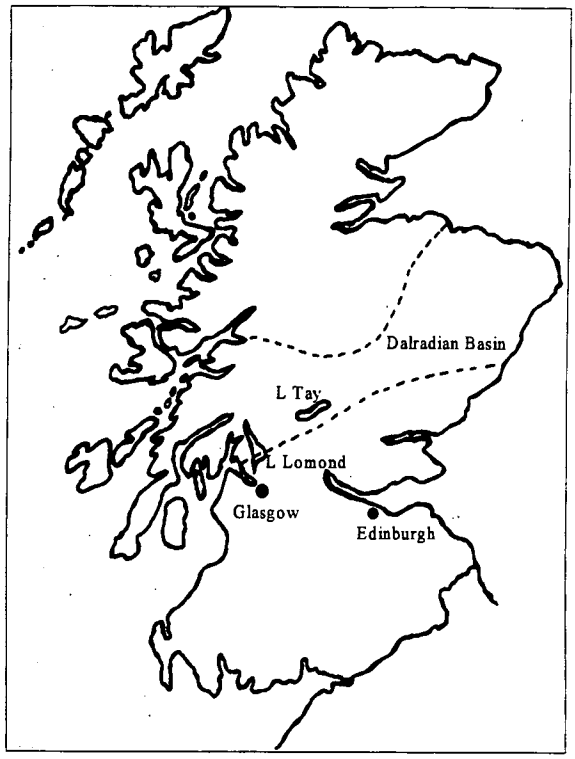

Fig. 1. Map of Scotland, showing the location of Loch Tay and Loch Lomond.

proximately 115 km northeast of Glasgow and 135 km northwest of Edinburgh (Fig. 1), is a typical

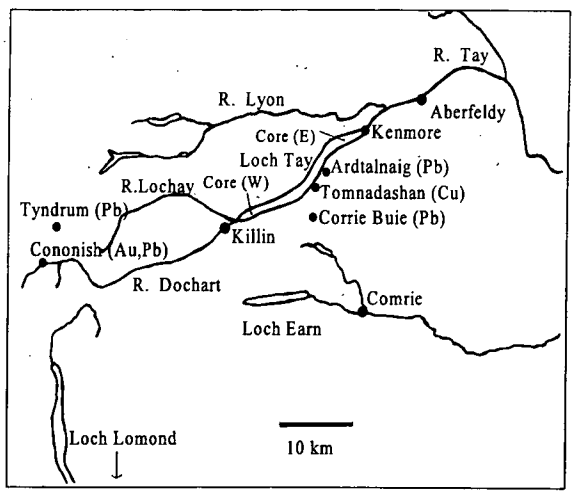

Fig. 2. Map of the Loch Tay area, showing the location of former mines and the sediment core sampling sites.

Scottish clear, deep-water loch, i.e. oligotrophic and with a pH of 6–7. Some 23.4 km long, Loch Tay is slightly sinuous in outline and trends in a south-west/northeast direction, with minimum and maximum breadths of 1.1 km and 1.7 km, an area of 26.4 km^2, and mean and maximum depths of 61 m and 155 m, the deepest basins occurring towards the eastern end (Fig. 2). The loch drains a catchment area of 576 km^2, with principal inflows from the Rivers Dochart and Lochay at its western end and outflow via the River Tay at the eastern end (Murray and Pullar, 1910; Maitland and Smith, 1987). Loch Tay's sediments, which are mainly fine-grained silts, are derived from an area composed primarily of metamorphic rocks consisting of slates, phyllites, mica-schist and biotite-gneiss, with some quartz and a narrow band of limestone on the western side (Whittow, 1979).

3. Sampling and analysis

The devices which were used to sample bottom sediments, a Jenkin gravity corer (Ohnstad and Jones, 1982) and a mini-Mackereth piston corer (Mackereth, 1969), are designed to minimise disturbance to the sediments. A 19-cm Jenkin core and a 90-cm mini-Mackereth core were collected at a water depth of 48 m in the centre of the loch ~ 3 km from the western end in November 1992 (Fig. 2). A further two Jenkin cores, of 23 and 24 cm in length, were collected at a depth of 68 m in the centre of the loch ~ 3.75 km from the eastern end in November 1993 (Fig. 2). (As it did not prove possible to collect a long mini-Mackereth core at the eastern end, discussion of the historical record of heavy metal pollution at that location will be restricted in this paper to a few appropriate comparisons with the western end). The Jenkin cores were sliced into 1-cm sections, and the mini-Mackereth core into 1-cm sections to 20 cm, then 2-cm sections to 40 cm, and 5-cm sections to 90 cm, before drying. The sediments at both locations were of high porosity, with organic carbon concentrations ranging from 7 to 10%.

Metal (Mn, Fe, Pb, Zn, Cu, Cd) concentrations were determined in the mini-Mackereth and 24-cm Jenkin core by flame AAS, As concentrations in the mini-Mackereth core by HGAAS, and stable Pb

isotope ratios ($^{206}Pb/^{207}Pb$) in both cores by ICP-MS following acid digestion of the dried sediment sections by nitric/hydrochloric (Bryant et al., 1991), hydrochloric (Johnson and Farmer, 1987), or nitric (Sugden et al., 1991a, 1993) acids as appropriate. For duplicate analysis, precision ($\pm 1\sigma$, RSD) was typically $\pm 3\%$ for Pb, Zn, Cu and Cd, $\pm 4\%$ for Mn and Fe, and $\pm 6\%$ for As, while the analytical precision ($\pm 1\sigma$) for $^{206}Pb/^{207}Pb$ ratios in the range 1.145–1.198 was ± 0.003. The mean $^{206}Pb/^{207}Pb$ ratio for the reference material IAEA SL-1, lake sediment, was 1.214 ± 0.006 (n = 34), in agreement with the 1.214 ± 0.012 value of Viczian et al. (1990). Analysis for ^{210}Pb and radiocaesium (^{134}Cs, ^{137}Cs), for estimation of sediment accumulation rates, was carried out on the 19-cm and 23-cm Jenkin cores by direct gamma-spectrometry, using a low background high purity Ge gamma photon detector (Bryant et al., 1993). Analytical precision ($\pm 1\sigma$) was typically ± 5–10% for ^{210}Pb, ± 5–20% for ^{134}Cs and ± 1–5% for ^{137}Cs.

4. Results

In the sediment core from the western end of Loch Tay, Mn concentrations increased from an average 0.22% below 24 cm to a maximum of 2.36% (0–1 cm) in the highly enriched surface layer (0–2 cm), with a sub-surface peak of 0.73% at 9–10 cm (Fig. 3a). Iron concentrations increased from an average 4.9% below 24 cm to 7.30% (1–3 cm), with a sub-surface peak of 7.45% at 11–12 cm (Fig. 3b). Arsenic concentrations increased from an average 20 mg kg^{-1} below 50 cm to 68 mg kg^{-1} (1–3 cm) near the surface, again with a sub-surface peak of 55 mg kg^{-1} at 11–12 cm (Fig. 3c). At the eastern end, Mn peaked at 3.70% (0–1 cm), Fe at 8.00% (2–3 cm) and As at 87 mg kg^{-1} (2–3 cm), again with evidence of more minor sub-surface peaks at greater depths.

Of the traditional heavy metal pollutants, Cu increased only slightly in concentration from an average 56 mg kg^{-1} below 55 cm to 87 mg kg^{-1} in the 0–1 cm section, exceeding 70 mg kg^{-1} only from 0–3 cm and at 24–26 cm (Fig. 3d). Zinc concentrations increased from an average 140 mg kg^{-1} below 55 cm to 590 mg kg^{-1} (4–6 cm), with a sub-surface peak of 535 mg kg^{-1} at 12–13 cm, before declining to 370 mg kg^{-1} at 0–2 cm (Fig. 3e). Cadmium concentrations increased from < 0.3 mg kg^{-1} below 50 cm to 3.0–3.3 mg kg^{-1} at 4–6 cm, with a sub-surface peak of 3.1 mg kg^{-1} at 12–14 cm, before declining to 1.6 mg kg^{-1} at 0–1 cm (Fig. 3f).

The most dramatic changes in concentration were observed for Pb, which increased from an average 16 mg kg^{-1} below 60 cm to a broad peak of 230–253 mg kg^{-1} at 38–50 cm and then remained elevated at 151–220 mg kg^{-1} up to 15 cm, where a remarkable and steep increase to 269–500 mg kg^{-1} was found over three sections at 12–15 cm. Above 12 cm, Pb concentrations declined fairly steadily to 132 mg kg^{-1} at 0–1 cm (Fig. 3g). Significantly, the Pb concentration profile over the 24 cm of the much shorter core, from a position some 17 km distant at the eastern end of the loch, was very similar, with a major sub-surface peak at 14–15 cm of 618 mg kg^{-1} (Fig. 3g). As at the western end, highly elevated Zn (553 mg kg^{-1}) and Cd (5.0 mg kg^{-1}) concentrations were also found in this section of the eastern core. In contrast, the highest Cu concentration (98 mg kg^{-1}) in the eastern core occurred at 21–22 cm (Fig. 3d). The $^{206}Pb/^{207}Pb$ ratios for the core from the western end averaged 1.192 ± 0.003 below 60 cm, before declining, over the 50–60 cm interval, until a steady 1.153 ± 0.002 was achieved from 20 to 50 cm. The ratio then increased to 1.166 by 15–16 cm but thereafter followed an apparently erratic path to a value of 1.156 at 0–1 cm, with a minimum of 1.145 at 3–4 cm. At the Pb peak (13–15 cm) of 500 mg kg^{-1}, the $^{206}Pb/^{207}Pb$ ratio was 1.152 ± 0.002 (Fig. 3h). In the eastern core, the ratio was 1.154 ± 0.004 for the Pb peak at 14–15 cm.

Sedimentation rates based on profiles of naturally occurring ^{210}Pb and of radiocaesium deposited from nuclear weapons testing and the Chernobyl accident were in good agreement at each site, yielding values of 28.3 mg cm^{-2} y^{-1} for the western end (Fig. 4) and 22.3 mg cm^{-2} y^{-1} for the eastern end of the loch. As the profiles suggested sediment mixing was only slight and was restricted to the top 5 cm (corresponding, at the top of the cores, to less than 20 years' accumulation), the derived dates of 1906–1928 for 12–15 cm in the western mini-Mackereth core and 1907–1915 for 14–15 cm in the 24-cm eastern Jenkin core, where the sediments are of higher poros-

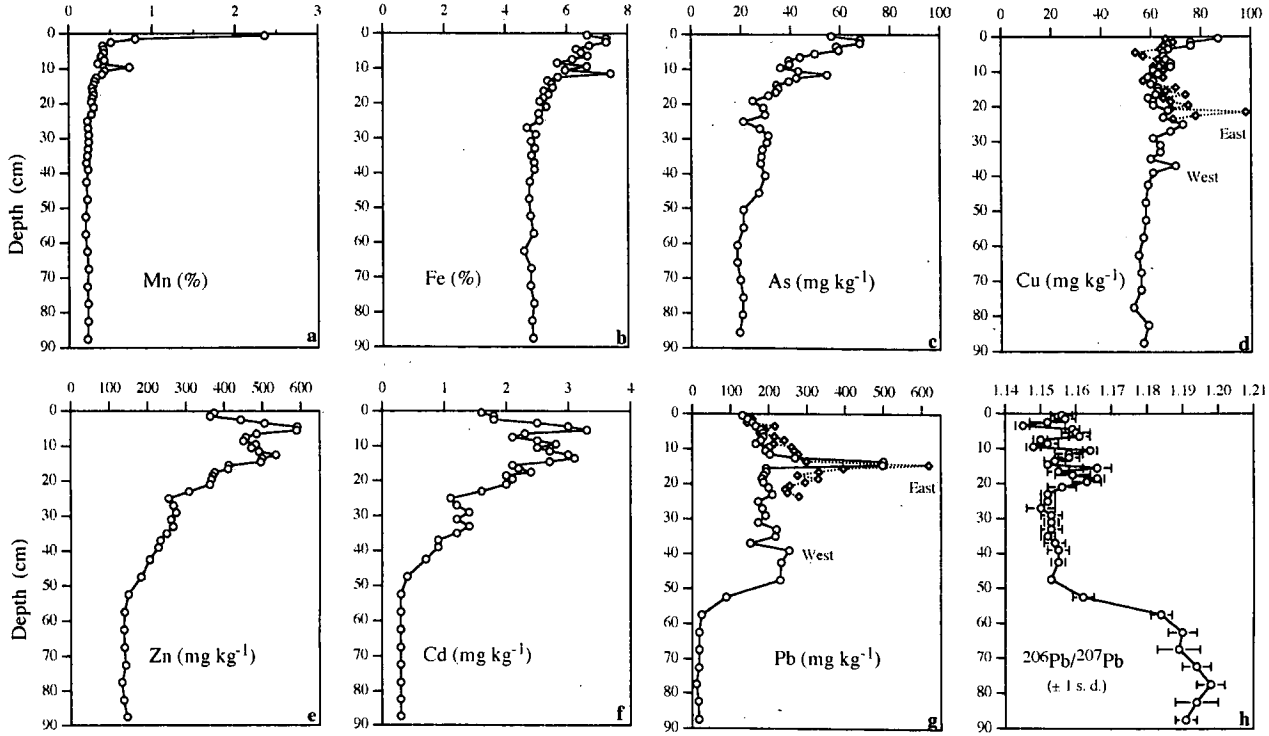

Fig. 3. Concentration versus depth profiles for Mn (a), Fe (b), As (c), Cu (d), Zn (e), Cd (f) and Pb (g) and the $^{206}Pb/^{207}Pb$ profile (h) in the 90-cm sediment core (17/11/92) from the western basin of Loch Tay. The Cu and Pb profiles for the 24-cm core (17/11/93) from the eastern basin are also shown (dotted lines in d and g).

ity, should be reasonably accurate. Extrapolated dates for the western core of 1844–1862 for 20–22 cm, 1574–1678 for 38–50 cm and 1483 for 60 cm, which are based on an assumption of a similar and constant sedimentation rate below 15 cm, are subject to large uncertainties and are much less credible, as discussed later.

5. Discussion

The magnitude and relative position of the Mn and Fe/As peaks in the top 3 cm of the western core are indicative of natural enrichment through post-depositional diagenetic redox-controlled mobilisation/diffusion/precipitation/adsorption processes (Farmer and Lovell, 1986). While it is possible that the peaks further down the core, at 9–10 cm for Mn and 11–12 cm for Fe/As, could be a similar recent phenomenon, perhaps resulting from a variable redox boundary, it seems much more likely that they are relics associated with a specific sediment deposition event earlier this century, as suggested below by the heavy metal and dating evidence.

The remarkable peaks in Pb, Zn and Cd concentrations at 12–15 cm in the western core and at 14–15 cm in the eastern core have been dated at 1906–1928 and 1907–1915 respectively. These dates are close to the known cessation of Pb mining activity at Tyndrum (Craig, 1965), suggesting that the heavy metal peaks are related to inputs of metal bearing material at that time, e.g. perhaps as a consequence of mine flooding or of dumping of spoil waste. This could have helped to create conditions conducive to the development and preservation of the sub-surface peaks of the redox-sensitive elements Mn, Fe and As in the adjacent sediment sections.

The influence of Pb mining is most clearly seen in the $^{206}Pb/^{207}Pb$ profile. It is known that the $^{206}Pb/^{207}Pb$ ratio for the mined 5.50×10^8-yr Pb ore deposit at Tyndrum is 1.144 ± 0.004 (Moorbath, 1962). When the measured Pb and $^{206}Pb/^{207}Pb$ profiles are corrected for a baseline contribution of 16 mg kg^{-1} at a ratio of 1.192, the average $^{206}Pb/^{207}Pb$ value for the "excess" Pb from 20 to 60 cm (i.e.

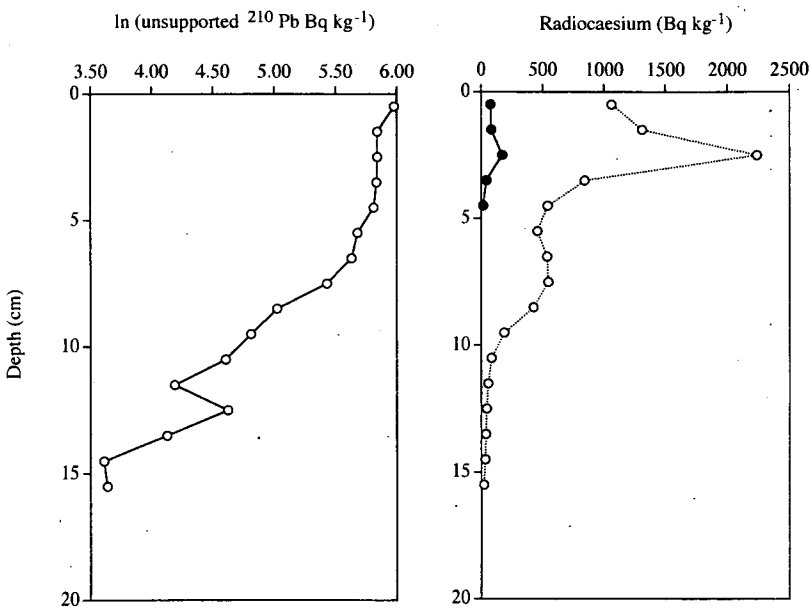

Fig. 4. Activity versus depth profiles for unsupported ^{210}Pb (ln), ^{134}Cs (closed circles) and ^{137}Cs (open circles) in the 19-cm sediment core (17/11/92) from the western basin of Loch Tay. Application of a constant initial concentration model to the ^{210}Pb data from 4–5 cm to 15–16 cm yields a sedimentation rate of 28.3 mg cm^{-2} y^{-1}, in good agreement with that derived from the mass of sediment accumulated between the Chernobyl (1986) and nuclear fallout (1963) radiocaesium peaks at 2.5 cm and 7 cm, respectively.

from the onset of Pb mining to ca. 1860) is 1.150 ± 0.002 (Fig. 5), very close to the Tyndrum value and rather distinct from the 1.171 previously reported as an average value for Pb deposited from the atmosphere in Scotland as a result of industrial activity during the 19th Century (Sugden et al., 1991a,b; Farmer et al., 1993) and the 1.169 ± 0.002 more recently obtained for 1817–1929 from a high-resolution study on a Loch Lomond sediment core (Farmer et al., 1996). The average "excess" $^{206}Pb/^{207}Pb$ value in the sediment increases to 1.159 ± 0.005 for 15–20 cm (i.e. to 1906) (Fig. 5), suggesting an increasing contribution from "industrial" Pb. Then, for 1906–1928 (Fig. 5), a decrease to 1.152 ± 0.003 for the major Pb peak at 12–15 cm confirms the substantial input and predominance of "mining" Pb at that time. Thereafter, from 1928 to the present (Fig. 5), although the "excess" $^{206}Pb/^{207}Pb$ in the core continues to average 1.152 ± 0.006 (range 1.140–1.161), it cannot be taken as evidence of "mining" Pb input alone. This is because of the atmospheric input resulting from the introduction in the late 1920s of leaded petrol additives considerably depleted in ^{206}Pb (e.g. ca. 1.08 for the $^{206}Pb/^{207}Pb$ ratio today), due to the use of Australian ores (Sugden et al., 1993), as well as from continuing industrial activity. Overall, the $^{206}Pb/^{207}Pb$ ratio for the total Pb in the core reflects contributions from "baseline" Pb (1.192), "industrial" Pb (1.170), "mining" Pb (1.144) and "petrol" Pb (1.08). The associated fluxes of "excess" Pb deposited in the sediments, peaking at 137 mg m^{-2} y^{-1} during the 1906–1928 period, are also shown in Fig. 5.

Table 1
A comparison of inventories of "excess" Pb in Loch Tay (western basin) and Loch Lomond (southern basin) sediments

Period	Loch Tay			Loch Lomond
	Total ($g m^{-2}$)	Mining [a] ($g m^{-2}$)	Industrial [b] ($g m^{-2}$)	Total ($g m^{-2}$)
1928–1992	2.99			2.29 [c]
1906–1928	2.50	1.73	0.77	0.77
1862–1906	2.15	0.91	1.24	1.44
pre-1862	16.50	12.69	3.81	1.85
Total	24.14			6.35

[a] Based on $^{206}Pb/^{207}Pb$ of Tyndrum mine Pb = 1.144 (Moorbath, 1962).
[b] Based on $^{206}Pb/^{207}Pb$ of "industrial" Pb = 1.170 (Sugden et al., 1991a,b; Farmer et al., 1993, 1996).
[c] to which "petrol" Pb has contributed 24–53%, based on $^{206}Pb/^{207}Pb$ of "petrol" Pb = 1.06–1.12 (Farmer et al., 1996).

The influence of past Pb mining activity can be seen not only in the calculated relative contributions

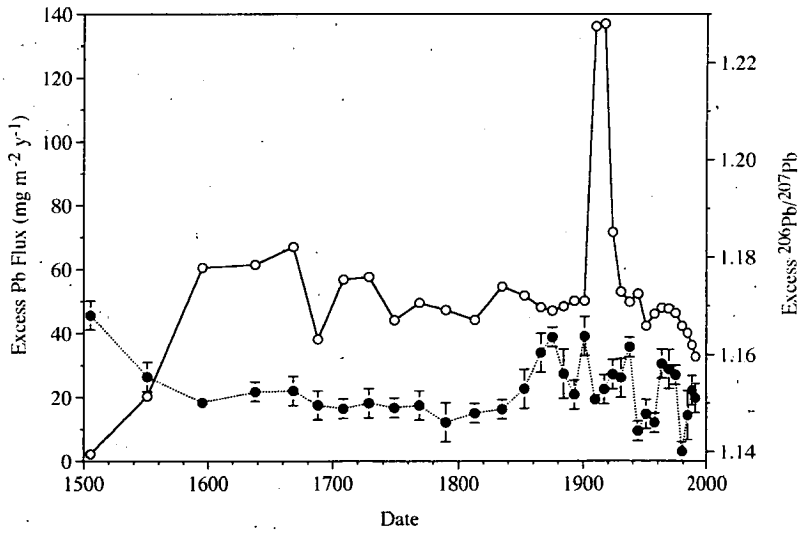

Fig. 5. Fluxes (open circles) and $^{206}Pb/^{207}Pb$ ratios (closed circles) of excess Pb deposited in the sediments of the western basin of Loch Tay versus calendar year based on an extrapolation of the ^{210}Pb-derived sedimentation rate of 28.3 mg cm^{-2} y^{-1}. As Pb mining in the area is believed to have commenced ca. 1739, dates prior to 1860 are considered unreliable (see text).

of different sources of "excess" Pb but also in the integrated "excess" Pb inventory for Loch Tay of 24.1 g m^{-2}, almost four times the 6.36 g m^{-2} for the southern basin of Loch Lomond (Farmer et al., 1993, 1996) (Table 1), which, at 50 km to the southwest, is much closer to the formerly industrialised and more heavily populated central belt of Scotland. Furthermore, for marker depths of 12 cm (1928), 15 cm (1906), 20 cm (1862?) and 38 cm (1678?), the cumulative percentages of "excess" Pb (24.1 g m^{-2}), viewed from the top of the core, are 12%, 23%, 32% and 69%, markedly different from the 31%, 42%, 57% and 91% for "excess" Zn (20.3 g m^{-2}; cf. 12.4 g m^{-2} for Loch Lomond), the 28%, 40%, 56% and 94% for "excess" Cd (0.14 g m^{-2}), and the 21%, 25%, 32% and 88% for "excess" Cu (0.93 g m^{-2}; cf. 0.52 g m^{-2} for Loch Lomond). As Pb mining at Tyndrum began only in 1739, however, the apparent finding that 44% of the "excess" Pb in the core was deposited before then (i.e. below 32 cm) strongly suggests that the sedimentation rate during periods of mining activity in the 18th and 19th Centuries (when changes in land use, such as deforestation, may also have been influential) was much higher ($\times 2.5$, on average) than that derived for the 20th Century. Alternatively, perhaps there were other significant episodes of mining, pre-dating Tyndrum, in the Loch Tay area.

Certainly, there were other mines, although smaller and not known to be operational before 1739, to the south of Loch Tay (Fig. 2). Indeed, the influence of the 19th Century Cu mine at Tomnadashan, which closed in 1862 (Bainbridge, 1970), can perhaps be seen in the elevated Cu concentration of 98 mg kg^{-1} at 21–22 cm (dated at ca. 1840–1855) in the eastern core (Fig. 3d). Moorbath (1962) reported $^{206}Pb/^{207}Pb$ ratios of 1.145 ± 0.003 for Tomnadashan and 1.130 ± 0.003 for nearby Ardtalnaig. Future work, including the determination of $^{206}Pb/^{207}Pb$ ratios for sections of long sediment cores from the central and eastern portions of the loch and for stream sediments from both the western (Tyndrum) end and southern shore of the loch, should help to shed further light on the specific events and geographical origins of the elevated concentrations of Pb found in Loch Tay sediments. These, along with the results for the other elements, especially As, will also help to serve as a benchmark for the heavy metal status of the loch should the proposed Au mining at Cononish, near Tyndrum, commence in 1996.

Acknowledgements

We thank E.K. Brechin, C.L. Bryant, E. Cartmell, D. Kesterton, S.E. Hutchison, M. McCartney, R.H.H. Pearson, J.J.A. Poole, C. Robertson, T.M. Shimmield and the Firbush Field Centre for assistance in various phases of this work.

References

Bainbridge, J.W., 1970. A nineteenth-century copper working: Tomnadashan, Lochtayside. Ind. Archaeol., 7: 60–74.

British Geological Survey, 1990. Regional Geochemical Atlas series: Argyll.

Bryant, C.L., Farmer, J.G., MacKenzie, A.B., Bailey-Watts, A.E. and Kirika, A., 1991. The biogeochemistry of heavy metals in an acidified Scottish freshwater loch. In: J.G. Farmer (Editor), Proceedings of the Eighth International Conference on Heavy Metals in the Environment. CEP, Edinburgh, Vol. 1, pp. 347–350.

Bryant, C.L., Farmer, J.G., MacKenzie, A.B., Bailey-Watts, A.E. and Kirika, A., 1993. Distribution and behaviour of radiocaesium in Scottish freshwater loch sediments. Environ. Geochem. Health, 15: 153–161.

Craig, G.Y., 1965. The Geology of Scotland. Oliver and Boyd, Edinburgh, p. 524.

Farmer, J.G., 1991. The perturbation of historical pollution records in aquatic sediments. Environ. Geochem. Health, 13: 76–83.

Farmer, J.G., 1994. Environmental change and the chemical record in Loch Lomond sediments. Hydrobiologia, 290: 39–49.

Farmer, J.G. and Lovell, M.A., 1986. Natural enrichment of arsenic in Loch Lomond sediments. Geochim. Cosmochim. Acta, 50: 2059–2067.

Farmer, J.G., MacKenzie, A.B., Sugden, C.L., Bryant, C.L., Eades, L.J., Bailey-Watts, A.E. and Kirika, A., 1993. The history of environmental lead pollution in Scotland. In: R.J. Allan and J.O. Nriagu (Editors), Proceedings of the Ninth International Conference on Heavy Metals in the Environment. CEP, Edinburgh, Vol. 2, pp. 211–214.

Farmer, J.G., Eades, L.J., MacKenzie, A.B., Kirika, A. and Bailey-Watts, A.E., 1996. Stable lead isotope record of lead pollutionin Loch Lomond sediments of since 1630 A.D. Environ. Sci. Technol., 30: 3080–3083.

Johnson, L.R. and Farmer, J.G., 1987. Arsenic mobility and speciation in the sediments of Scottish inland and coastal waters. In: Proceedings of the Sixth International Conference on Heavy Metals in the Environment. CEP, Edinburgh, Vol. 2, pp. 218–222.

Mackereth, F.J.H., 1969. A short core sampler for sub-aqueous deposits. Limnol. Oceanogr., 14: 145–151.

Maitland, P.S. and Smith, I.R., 1987. The River Tay: ecological changes from source to estuary. Proc. R. Soc. Edinburgh, 92B: 373–392.

Moorbath, S., 1962. Lead isotope abundance studies on mineral occurrences in the British Isles and their geological significance. Philos. Trans. R. Soc. London A, 254: 295–360.

Murray, J. and Pullar, L., 1910. Bathymetrical Survey of the Freshwater Lochs of Scotland. Challenger Office, Edinburgh, Vol. 2, pp. 53–147.

Ohnstad, F.R. and Jones, J.G., 1982. The Jenkin Surface-Mud Sampler User Manual. Freshwater Biological Association Occasional Publication No. 15.

Plant, J.A., Breward, N., Simpson, P.R. and Slater, D., 1990. Regional geochemistry and the identification of metallogenic provinces: examples from lead–zinc–barium, tin–uranium and gold deposits. J. Geochem. Explor., 39: 195–224.

Sugden, C.L., Farmer, J.G. and MacKenzie, A.B., 1991a. Lead and $^{206}Pb/^{207}Pb$ profiles in ^{210}Pb-dated ombrotrophic peat cores from Scotland. In: J.G. Farmer (Editor), Proceedings of the Eighth International Conference on Heavy Metals in the Environment. CEP, Edinburgh, Vol. 1, pp. 90–93.

Sugden, C.L., Farmer, J.G. and MacKenzie, A.B., 1991b. Isotopic characterisation of lead inputs and behaviour in recent Scottish freshwater loch sediments. In: J.G. Farmer (Editor), Proceedings of the Eighth International Conference on Heavy Metals in the Environment. CEP, Edinburgh, Vol. 1, pp. 511–514.

Sugden, C.L., Farmer, J.G. and MacKenzie, A.B., 1993. Isotopic ratios of lead in contemporary environmental material from Scotland. Environ. Geochem. Health, 15: 59–65.

Viczian, M., Lasztity, A. and Barnes, R.M., 1990. Identification of potential environmental sources of childhood lead poisoning by inductively coupled plasma mass spectrometry. J. Anal. At. Spectrom., 5: 293–300.

Whittow, J.B., 1979. The Grampian Highlands. In: P. Hall (Editor), Geology and Scenery in Scotland. Pelican Books, Middlesex, pp. 170–193.

Wilson, G.V., 1921. In: The Lead, Zinc, Copper and Nickel Ores of Scotland. Mem. Geol. Surv. G.B. Miner. Resour., 17: 93–106.

Papers that seek to integrate geological, geochemical and geophysical methods of exploration are particularly welcome. Given the many links between exploration and environmental geochemistry, the journal encourages the exchange of concepts and data; in particular, to develop mineral resources while protecting the environment. Submission of Letters to the Editor is encouraged. This provides a means of commenting on papers that have been published in this journal.

Publication information
Journal of Geochemical Exploration (ISSN 0375-6742). For 1997 volumes 59–61 are scheduled for publication. Subscription prices are available upon request from the publisher. Subscriptions are accepted on a prepaid basis only and are entered on a calendar year basis. Issues are sent by surface mail except to the following countries where air delivery via SAL is ensured: Argentina, Australia, Brazil, Canada, Hong Kong, India, Israel, Japan, Malaysia, Mexico, New Zealand, Pakistan, PR China, Singapore, South Africa, South Korea, Taiwan, Thailand, USA. For all other countries airmail rates are available upon request. Claims for missing issues must be made within six months of our publication (mailing) date. For orders, claims, product enquiries (no manuscript enquiries) please contact the Customer Support Department at the Regional Sales Office nearest to you:

New York, Elsevier Science, P.O. Box 945, New York, NY 10159-0945, USA. Tel: (+1) 212-633-3730, [Toll Free number for North American Customers: 1-888-4ES-INFO (437-4636)], Fax: (+1) 212-633-3680, E-mail: usinfo-f@elsevier.com
Amsterdam, Elsevier Science, P.O. Box 211, 1000 AE Amsterdam, The Netherlands. Tel: (+31) 20-485-3757, Fax: (+31) 20-485-3432, E-mail: nlinfo-f@elsevier.nl
Tokyo, Elsevier Science, 9-15, Higashi-Azabu 1-chome, Minato-ku, Tokyo 106, Japan. Tel: (+81) 3-5561-5033, Fax: (+81) 3-5561-5047, E-mail: kyf04035@niftyserve.or.jp
Singapore, Elsevier Science, No. 1 Temasek Avenue, #17-01 Millenia Tower, Singapore 039192. Tel: (+65) 434-3727, Fax: (+65) 337-2230, E-mail: asiainfo@elsevier.com.sg

US mailing notice – *Journal of Geochemical Exploration* (ISSN 0375-6742) is published monthly, except in the months of April, June, July, August and September, by Elsevier Science B.V. (Molenwerf 1, P.O. Box 211, 1000 AE Amsterdam). Annual subscription price in the USA US$ 1139 (valid in North, Central and South America), including air speed delivery. Periodicals postage paid at Jamaica, NY 11431.
USA POSTMASTERS: Send address changes to *Journal of Geochemical Exploration,* Publications Expediting, Inc., 200 Meacham Avenue, Elmont, NY 11003.
Airfreight and mailing in the USA by Publications Expediting.

NOTE TO CONTRIBUTORS

A detailed Guide for Authors is available upon request. A short version is included at the back of each volume.

Submission of manuscripts
Three copies should be submitted to: Dr. Eion M. Cameron, Derry Laboratory, Department of Geology, University of Ottawa, Ottawa, K1N 6N5, Ont., Canada. Australian contributors may submit directly to: Dr. C.R.M. Butt, CSIRO, Private Bag P.O., Wembley, W.A. 6014, Australia. Contributors in biogeochemistry and geobotany may submit to: Prof. R.R. Brooks, Department of Chemistry, Biochemistry and Biophysics, Massey University, Palmerston North. New Zealand.
The indication of a fax and e-mail number on submission of the manuscript could assist in speeding communications. The fax number for the Amsterdam office is +31-20-4852696.
Authors in Japan please note: Upon request, Elsevier Science Japan will provide authors with a list of people who can check and improve the English of their paper (*before submission*). Please contact our Tokyo office: Elsevier Science Japan, 1-9-15 Higashi Azabu, Minato-ku, Tokyo 106, Tel. +81 3 5561 5032; Fax +81 3 5561 5045.
Submission of an article is understood to imply that the article is original and unpublished and is not being considered for publication elsewhere.

 0375-6742/97/$17.00

♾ The paper used in this publication meets the requirements of ANSI/NISO Z39.48-1992 (Permanence of Paper).

PRINTED IN THE NETHERLANDS

Stable Lead Isotope Record of Lead Pollution in Loch Lomond Sediments since 1630 A.D.

John G. Farmer and Lorna J. Eades

Department of Chemistry, The University of Edinburgh, Edinburgh EH9 3JJ, Scotland, U.K.

Angus B. MacKenzie

Scottish Universities Research and Reactor Centre, East Kilbride, Glasgow G75 0QF, Scotland, U.K.

Alex Kirika and Tony E. Bailey-Watts

Natural Environment Research Council Institute of Freshwater Ecology, Bush Estate, Penicuik, Midlothian EH26 0QB, Scotland, U.K.

ENVIRONMENTAL® SCIENCE & TECHNOLOGY

Reprinted from
Volume 30, Number 10, Pages 3080–3083

Environ. Sci. Technol. 1996, 30, 3080–3083

Stable Lead Isotope Record of Lead Pollution in Loch Lomond Sediments since 1630 A.D.

JOHN G. FARMER* AND LORNA J. EADES

Department of Chemistry, The University of Edinburgh, Edinburgh EH9 3JJ, Scotland, U.K.

ANGUS B. MACKENZIE

Scottish Universities Research and Reactor Centre, East Kilbride, Glasgow G75 0QF, Scotland, U.K.

ALEX KIRIKA AND TONY E. BAILEY-WATTS

Natural Environment Research Council Institute of Freshwater Ecology, Bush Estate, Penicuik, Midlothian EH26 0QB, Scotland, U.K.

Stable lead isotope data can yield information on the geochemical origins of lead and on its relative contributions from sources such as coal burning, mining, smelting, and car-exhaust emissions. This extremely detailed $^{206}Pb/^{207}Pb$ profile for dated bottom sediments in Loch Lomond, Scotland, shows the trends clearly related to the varying nature and extent of anthropogenic lead inputs after 1630. In particular, a significant decline in the $^{206}Pb/^{207}Pb$ ratio of excess lead during 1929–1991 is attributable to the introduction and use of (^{206}Pb-depleted) leaded petrol since the 1920s. This accounts, however, for just 24–53% of the excess lead deposited since 1929 and ≤19% of the total excess lead inventory. Deposition of lead from industrial (and domestic) activities has predominated overall and, on an annual basis, until at least the mid-1950s.

Introduction

Comparatively few of the many records of environmental lead pollution derived from dated aquatic sediments, peat bogs, ice cores, and corals have been accompanied by stable lead isotope data (*1–13*). Characteristic abundances of the four stable isotopes of lead (primordial ^{204}Pb and radiogenic ^{206}Pb, ^{207}Pb, and ^{208}Pb) in different materials (e.g., coal, petrol additives) afford the opportunity of source apportionment. For example, the $^{206}Pb/^{207}Pb$ isotopic ratio of leaded petrol in the U.K. today is 1.06–1.09, reflecting the mix of Australian ore ($^{206}Pb/^{207}Pb = 1.04$) with British Columbian ore ($^{206}Pb/^{207}Pb = 1.16$), whereas that for British lead ore used in the production of domestic water pipes during the 19th and early 20th Centuries is typically 1.16–1.18, similar to the 1.16–1.19 value for Scottish coal (*14*). In view of the finding in our preliminary work on sediment (*7*) and peat (*6*) in Scotland that the introduction of leaded petrol in the late 1920s could be detected through a reduction in the $^{206}Pb/^{207}Pb$ ratio of deposited anthropogenic lead from a late 19th/early 20th Century value of ~1.17, we investigated the $^{206}Pb/^{207}Pb$ historical record in much greater detail. We chose sediments, for their vastly superior time resolution via feasible slicing of very thin sections (~3 mm), from the southern basin of Loch Lomond (Figure 1), the site of much of our previous work (*15*) on environmental change.

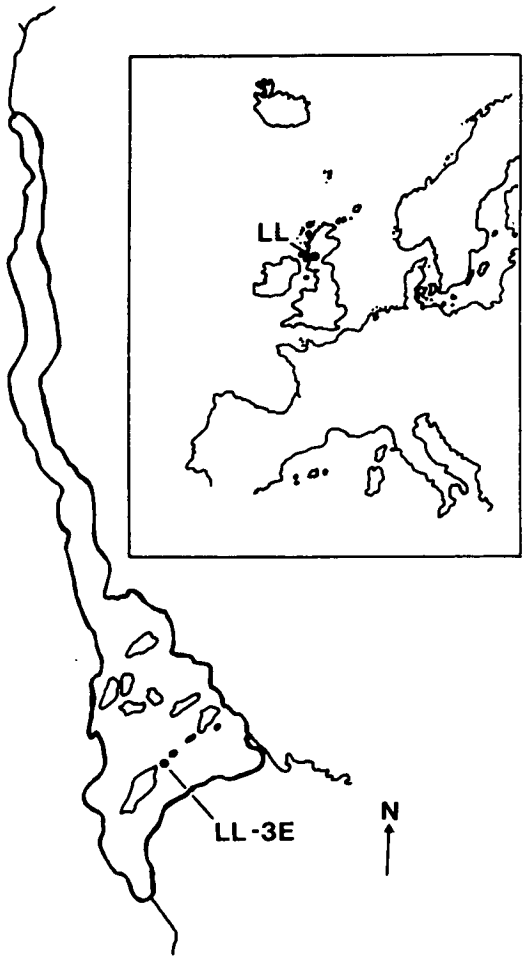

FIGURE 1. Sediment core sampling site in the southern basin of Loch Lomond, Scotland, on the northwestern fringe of Europe.

Methods

Sampling. An 80-cm-long mini-Mackereth core (LL-3E) and a 14.4-cm-long Jenkin core were collected on November 26, 1991, at a water depth of 18 m in Loch Lomond (56°–56°19′ N, 4°30′–4°43′ W), 30 km to the northwest of Glasgow and situated on the fringe of the densely populated and formerly heavily industrialized west-central belt of Scotland (Figure 1). Both of these devices, a piston corer and a gravity corer, are designed to minimize disturbance of the sediment (*16, 17*). The sampling site shown is at OS grid ref. NS 391 884 in the southern basin of Loch Lomond, where the oxygen saturation of the water never falls below 78% (*18*). Core LL-3E was sliced into sections (0.3 cm thick to a depth

* Corresponding author e-mail address: JGFarmer@ed.ac.uk; telephone: 0131 650 4757; fax: 0131 650 4743.

S0013-936X(96)00162-9 CCC: $12.00

of 30 cm, then 2 cm to a depth of 50 cm, and 5 cm to a depth of 80 cm), which were dried at 35–40 °C and finely ground prior to chemical pretreatment.

Analysis. Aliquots of the 116 dried sections from the core were digested for several hours in hot mixed acid (0.3–0.5 g of sediment, 20 cm^3 of 8 M HNO_3, 10 cm^3 of 11.6 M HCl, filtration, further 5–10 cm^3 aliquots of 11.6 M HCl until brown fumes of NO_2 driven off) prior to preparation (in 1 M HCl) for determination of lead by flame atomic absorption spectrometry (Unicam SP-9 800) and in hot nitric acid (0.1 g of sediment, 30 cm^3 of 8 M HNO_3) prior to preparation (in 2% v/v HNO_3) for analysis by inductively coupled plasma-mass spectrometry (VG Plasmaquad PQ1 or Plasmaquad PQ2) for $^{206}Pb/^{207}Pb$ (*14*). Precision ($\pm 1\sigma$) was typically ±3% for duplicate lead analysis and ±0.004 for $^{206}Pb/^{207}Pb$ ratios in the range of 1.127–1.180. The mean $^{206}Pb/^{207}Pb$ ratio for the reference material IAEA SL-1, lake sediment, was 1.214 ± 0.006 ($n = 34$), in agreement with the 1.214 ± 0.012 value of Viczian et al. (*19*).

Radiocaesium from nuclear weapons testing in the 1950s and 1960s (^{137}Cs) and from the Chernobyl nuclear reactor accident in 1986 (^{134}Cs, ^{137}Cs) was determined in the 48 0.3-cm-thick sections of the Jenkin core by γ-spectrometry (Canberra intrinsic Ge detector) (*20, 21*). The sediment samples were too small for satisfactory determination of the naturally occurring ^{210}Pb radionuclide. Thus, we used the relative positions of the two main ^{137}Cs peaks (taken to correspond to the major deposition from the atmosphere in 1963 and 1986) to derive a sedimentation rate of 30.9 ± 1.3 mg cm^{-2} yr^{-1}. Detailed discussion of the radiocaesium data is presented elsewhere (*21*).

The use of radiocaesium concentration profiles to establish sedimentation rates in freshwater lake sediments is well established, and the chronologies derived have been validated by repeated sampling over an extended time period and by close agreement between radiocaesium derived-chronologies and those obtained independently by ^{210}Pb dating (*22, 23*). Such agreement was also observed in the present case with the accumulation rate derived from the radiocaesium distribution being in excellent agreement with the value, obtained from ^{210}Pb dating of a core from a nearby site, of 32 ± 4 mg cm^{-2} yr^{-1} (*20*). The accumulation rate will be subject to an uncertainty arising from the finite thickness of the sampling increment and, potentially, broadening of the peaks in radiocaesium concentration as a consequence of bioturbation. While some broadening was observed, the peaks were nevertheless well resolved and the maxima were well defined, indicating that the effects of bioturbation on the chronology are probably negligible. An extrapolated sedimentation rate of 30.9 mg cm^{-2} yr^{-1} was used along with the cumulative weight (g cm^{-2}) for each depth to date the sections of the mini-Mackereth core LL-3E and thus derive the chronology. Assuming a constant sedimentation rate, we estimate an uncertainty of no more than ±5% in the age of each section.

Results and Discussion

The lead concentration and $^{206}Pb/^{207}Pb$ ratio were constant below 28.5 cm, at 15 ± 4 mg kg^{-1} and 1.174 ± 0.002, respectively (Figure 2). Above 28.5 cm the lead concentration increased, especially above 18 cm, reaching a maximum of 158 mg kg^{-1} at 6.45 cm before declining to 65–81 mg kg^{-1} in the uppermost 2.4 cm. The $^{206}P/^{207}Pb$ ratio declined above 10.5 cm from values of ~1.17 to a minimum of 1.127

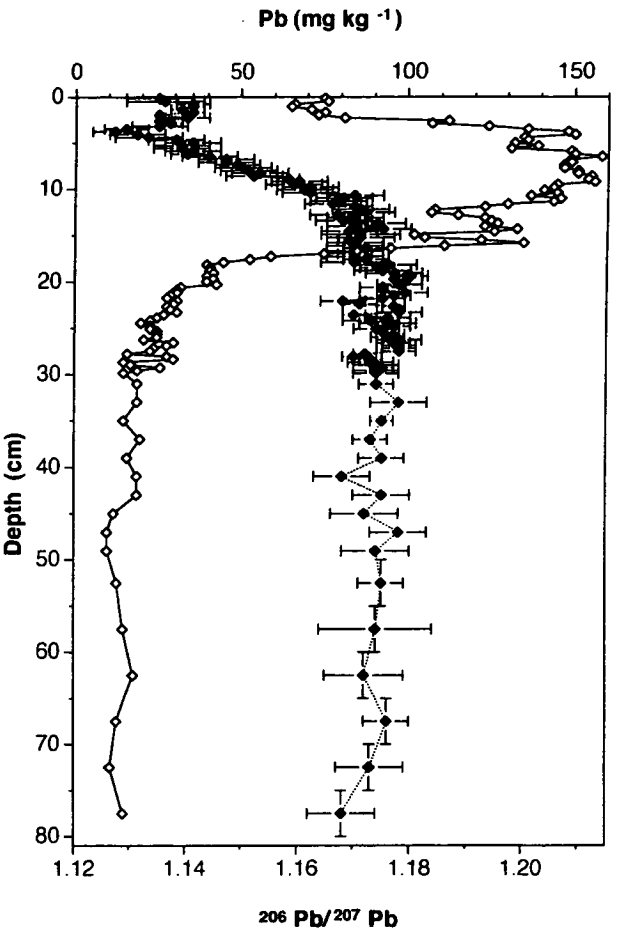

FIGURE 2. Lead concentrations (◇) and $^{206}Pb/^{207}Pb$ ratios (◆) in sections of the Loch Lomond sediment core LL-3E (mini-Mackereth) collected on November 26, 1991.

at 3.75 cm followed by an increase to 1.135–1.141 in the top 3.3 cm.

For each of the 95 sections above 28.5 cm, the lead concentration and $^{206}Pb/^{207}Pb$ ratio were corrected with background values to derive an excess lead concentration with an associated $^{206}Pb/^{207}Pb$ ratio, representing anthropogenic input of lead. Using the value of 1.174 for the $^{206}Pb/^{207}Pb$ ratio below 28.5 cm, the $^{206}Pb/^{207}Pb$ ratio of the excess lead for each section was calculated from the formula:

$$^{206}Pb/^{207}Pb_{excess} = [(Pb_{meas} \times {}^{206}Pb/^{207}Pb_{meas}) - (15 \times 1.174)]/(Pb_{meas} - 15)$$

The excess lead concentration (mg kg^{-1}) was then multiplied by the sedimentation rate of 0.309 kg m^{-2} yr^{-1} to yield the excess lead flux (mg m^{-2} yr^{-1}), plotted along with the corresponding excess $^{206}Pb/^{207}Pb$ ratio against the calendar year in Figure 3.

Three key periods can be identified for the excess $^{206}Pb/^{207}Pb$ ratio. (i) From the mid-17th to early 19th Century (1634–1817), it was fairly constant at 1.178 ± 0.006, during which time the flux slowly increased but never exceeded 8.7 mg m^{-2} yr^{-1}. The total excess lead deposited during this period was 0.84 g m^{-2}, 13% of the inventory for the core of 6.36 g m^{-2}. (ii) From 1817–1929 the ratio was very steady at 1.169 ± 0.002 despite, as the Industrial Revolution flourished, a dramatic increase in flux, which was always ≥25 mg m^{-2} yr^{-1} after 1847 and peaked at 40.5 mg m^{-2} yr^{-1} in 1925. The total excess lead deposited during 1817–1929

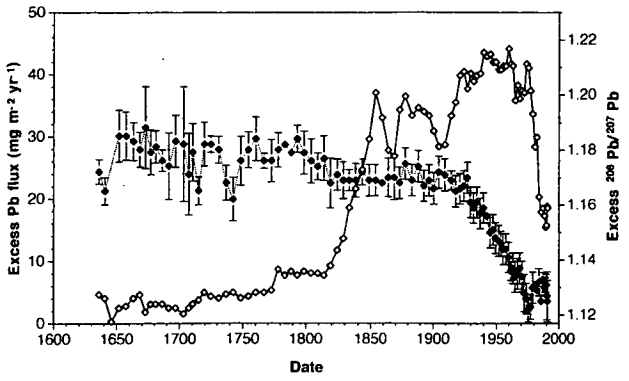

FIGURE 3. Excess (i.e., anthropogenic) lead fluxes (◇) and associated $^{206}Pb/^{207}Pb$ ratios (◆) at Loch Lomond site LL-3E vs calendar year (1634–1991).

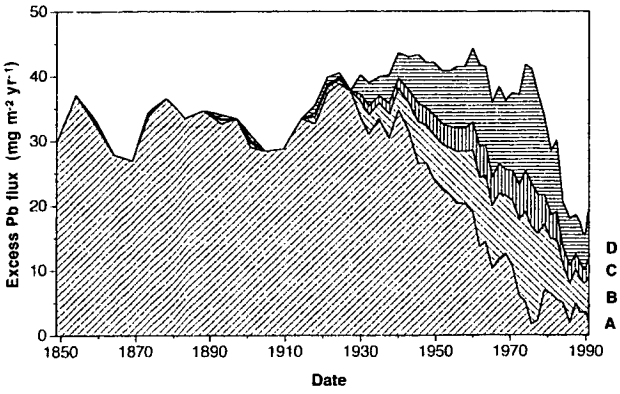

FIGURE 4. Plot from 1850 to 1991 of the contributions of "industrial" lead and of "petrol" lead to the flux of excess lead at Loch Lomond site LL-3E for three scenarios based on petrol $^{206}Pb/^{207}Pb = 1.06, 1.09,$ or 1.12 (see text). A represents the industrial lead flux, and B + C + D represents the petrol lead flux when the $^{206}Pb/^{207}Pb$ ratio of petrol is taken as 1.12. A + B represents the industrial lead flux and C + D represents the petrol lead flux when the $^{206}Pb/^{207}Pb$ ratio of petrol is 1.09. A + B + C represents the industrial lead flux and D represents the petrol lead flux when the $^{206}Pb/^{207}Pb$ ratio of petrol is 1.06.

was 3.23 g m^{-2}, 51% of the core inventory. (iii) From 1929, soon after the introduction of leaded petrol (*24*), the isotopic ratio decreased steadily to 1.122 by the mid-1970s, although the flux of lead remained at ≥35 mg m^{-2} yr^{-1}, peaking at 44.2 mg m^{-2} yr^{-1} in 1960, and was still as high as 41.7 mg m^{-2} yr^{-1} in 1974. Thereafter, at the same time as steps were taken to reduce the lead content of petrol in the U.K. (*25*), the ratio increased slightly to 1.125–1.133 as the flux fell steeply to 15.4–18.8 mg m^{-2} yr^{-1} by 1985–1991. Overall, the excess lead deposited from 1929 to 1991 was 2.29 g m^{-2}, 36% of the core inventory.

Source Apportionment. We deduce that the shift in the $^{206}Pb/^{207}Pb$ ratio of excess lead occurring in 1929, after more than a century of stability, was due to the introduction of leaded petrol with a low $^{206}Pb/^{207}Pb$ value. Direct information on the $^{206}Pb/^{207}Pb$ ratio of petrol in the U.K. for the period since 1929 is not available, but our measurements since 1989 show a range of 1.06–1.09 with a mean of 1.071 ± 0.010 (n = 18), in good agreement with Delves and Campbell (*26*). In view of the possible use at times of imported tetraalkyllead from the United States and contributions to atmospheric lead over the U.K. from car-exhaust emissions in parts of continental Europe with higher $^{206}Pb/^{207}Pb$ ratios (*27*), we have taken 1.12 as a plausible upper limit for petrol-derived atmospheric lead. Figure 4 shows the outcome for relative contributions of "industrial" lead ($^{206}Pb/^{207}Pb$ = 1.169) and of "petrol" lead to the flux of excess lead for three scenarios based on petrol $^{206}Pb/^{207}Pb$ = 1.06, 1.09, or 1.12 since 1929. The percentage of petrol contribution to the excess lead flux for each section is calculated using the formula:

$$Pb_{petrol}(\%) = [(1.169 - {}^{206}Pb/{}^{207}Pb_{excess}) \times 100]/(1.169 - {}^{206}Pb/{}^{207}Pb_{petrol})$$

At 1.06 (D), petrol lead accounts for 40% of the excess lead in 1991 (at 1.071, 45%) and 24% of that deposited from 1929 to 1991; at 1.09 (C + D), petrol lead accounts for 56% in 1991 and 33% from 1929 to 1991; at 1.12 (B + C + D), petrol lead accounts for 90% in 1991 and 53% from 1929 to 1991. For the latter scenario, petrol lead replaced industrial lead as the major contributor in 1955. The maxima for both relative and absolute contributions by petrol lead occurred in 1976, with 43% (17.7 mg m^{-2} yr^{-1}), 59% (24.5 mg m^{-2} yr^{-1}), and 96% (39.4 mg m^{-2} yr^{-1}) for $^{206}Pb/^{207}Pb$ ratios of 1.06, 1.09, and 1.12, respectively. According to Department of Trade and Industry statistics (1975–1992) (*28*), estimated emissions of lead from petrol-engined road vehicles in the U.K. peaked in 1976. Overall, these trends are consistent with (i) the decline of heavy industry and major reduction in the use of coal as a fuel in the U.K. since the mid-20th Century and (ii) the corresponding increase over the same time period of the number of vehicles in use.

Petrol lead has thus contributed up to 53% of the anthropogenic lead deposited in Loch Lomond sediments since its introduction in the 1920s, but this amounts to only 19% of the total excess lead inventory in the sediments. The apparent presence pre-1929 of petrol lead contributions can, in part, be attributed to the uncertainty in the chronology and the limited influence of bioturbation, but could also perhaps be due to the use or release of a very small amount of ^{206}Pb-depleted lead in other activities. Industrial (and domestic) lead emission and deposition, especially at the high fluxes sustained in the 120 years prior to the onset of a steady decrease (in any of the three scenarios) in 1940 (Figure 4), has dominated the history of lead accumulation in Loch Lomond sediments. Just under 50% of the lead inventory in these sediments was deposited prior to 1900, long before the advent of increasingly strict U.K. environmental controls such as the Clean Air Acts in 1956 and 1968 and legislation in the 1980s to reduce and phase out the use of lead in petrol. This early deposition underlines the importance of taking past human activities into account in assessing the long-term burden, fate, and impact of lead in the wider environmental context (*29, 30*).

Acknowledgments

We thank T. M. Shimmield and K. McKay (Scottish Universities Research and Reactor Centre) for their technical expertise in ICP-MS analysis; C. Robertson (SURRC) for help with γ-spectrometry analysis; and R. McMath, R. Tippett (Glasgow University Field Station), C. L. Bryant, and C. L. Sugden (University of Edinburgh) for assistance with fieldwork arrangements and sampling.

Literature Cited

(1) Hamilton, E. I.; Clifton, R. J. *Estuarine Coastal Mar. Sci.* **1979**, *8*, 271–278.

(2) Shirahata, H.; Elias, R. W.; Patterson, C. C.; Koide, M. *Geochim. Cosmochim. Acta* **1980**, *44*, 149−162.
(3) Ng, A.; Patterson, C. C. *Geochim. Cosmochim. Acta* **1982**, *46*, 2307−2321.
(4) Petit, D.; Mennesier, J. P.; Lamberts, L. *Atmos. Environ.* **1984**, *18*, 1189−1193.
(5) Shen, G. T.; Boyle, E. A. *Earth Planet. Sci. Lett.* **1987**, *82*, 289−304.
(6) Sugden, C. L.; Farmer, J. G.; MacKenzie, A. B. *Proceedings of the Eighth International Conference on Heavy Metals in the Environment*; CEP: Edinburgh, 1991; Vol. 1, pp 90−93.
(7) Sugden, C. L.; Farmer, J. G.; MacKenzie, A. B. *Proceedings of the Eighth International Conference on Heavy Metals in the Environment*; CEP: Edinburgh, 1991; Vol. 1, pp 511−514.
(8) Keinonen, M. *Sci. Total Environ.* **1992**, *113*, 251−268.
(9) Rosman, K. J. R.; Chisholm, W.; Boutron, C. F.; Candelone, J. P.; Gorlach, U. *Nature* **1993**, *362*, 333−335.
(10) Ritson, P. I.; Esser, B. K.; Niemeyer, S.; Flegal, A. R. *Geochim. Cosmochim. Acta* **1994**, *58*, 3297−3305.
(11) Graney, J. R.; Halliday, A. N.; Keeler, G. J.; Nriagu, J. O.; Robbins, J. A.; Norton, S. A. *Geochim. Cosmochim. Acta* **1995**, *59*, 1715−1728.
(12) Gobeil, C.; Johnson, W. K.; MacDonald, R. W.; Wong, C. S. *Environ. Sci. Technol.* **1995**, *29*, 193−201.
(13) Croudace, I. W.; Cundy, A. B. *Environ. Sci. Technol.* **1995**, *29*, 1288−1296.
(14) Sugden, C. L.; Farmer, J. G.; MacKenzie, A. B. *Environ. Geochem. Health* **1993**, *15*, 59−65.
(15) Farmer, J. G. *Hydrobiologia* **1994**, *290*, 39−49.
(16) Mackereth, F. J. H. *Limnol. Oceanogr.* **1969**, *14*, 145−151.
(17) Ohnstad, F. R.; Jones, J. G. *The Jenkin Surface-Mud Sampler User Manual*; Freshwater Biological Association Occasional Publication 15, 1982.
(18) Maulood, B. K.; Boney, A. D. *Hydrobiologia* **1980**, *71*, 239−259.
(19) Viczian, M.; Lasztity, A.; Barnes, R. M. *J. Anal. At. Spectrom.* **1990**, *5*, 293−300.
(20) Bryant, C. L.; Farmer, J. G.; MacKenzie, A. B.; Bailey-Watts, A. E.; Kirika, A. *Environ. Geochem. Health* **1993**, *15*, 153−161.
(21) Eades, L. J.; Farmer, J. G.; MacKenzie, A. B.; Kirika, A.; Bailey-Watts, A. E. *J. Environ. Radioact.*, in press.
(22) Pennington, W.; Cambray, R. S.; Eakins, J. D.; Harkness, D. D. *Freshwater Biol.* **1976**, *6*, 317−331.
(23) Bonnett, P. J. P.; Cambray, R. S. *Hydrobiologia* **1991**, *214*, 63−70.
(24) Nriagu, J. O. *Proceedings of the Seventh International Conference on Heavy Metals in the Environment*; CEP: Edinburgh, 1989; Vol. 2, pp 361−366.
(25) *Lead in the Environment*; Royal Commission on Environmental Pollution, Ninth Report; HMSO: London, 1983.
(26) Delves, H. T.; Campbell, M. J. *Environ. Geochem. Health* **1993**, *15*, 75−84.
(27) Hopper, J. F.; Ross, H. B.; Sturges, W. T.; Barrie, L. A. *Tellus* **1991**, *43B*, 45−60.
(28) *Digest of Environmental Protection and Water Statistics No. 15*; Department of the Environment; HMSO: London, 1993.
(29) Bacon, J. R.; Berrow, M. L.; Shand, C. A. *Int. J. Environ. Anal. Chem.* **1992**, *46*, 71−76.
(30) Bacon, J. R.; Berrow, M. L.; Shand, C. A. *Int. J. Environ. Anal. Chem.* **1995**, *59*, 253−264.

Received for review February 22, 1996. Revised manuscript received May 29, 1996. Accepted May 31, 1996.[⊗]

ES960162O

[⊗] Abstract published in *Advance ACS Abstracts*, August 1, 1996.